181 C
DR-1780

MASTER

ORNL-4555
UC-70 — Waste Disposal and Processing

PROJECT SALT VAULT: A DEMONSTRATION OF THE DISPOSAL OF HIGH-ACTIVITY SOLIDIFIED WASTES IN UNDERGROUND SALT MINES

R. L. Bradshaw
W. C. McClain

Editors

THIS DOCUMENT CONFIRMED AS
UNCLASSIFIED
DIVISION OF CLASSIFICATION
BY O H Kahn / aoml
DATE 4/22/71



OAK RIDGE NATIONAL LABORATORY
operated by
UNION CARBIDE CORPORATION
for the
U.S. ATOMIC ENERGY COMMISSION

DISTRIBUTION OF THIS DOCUMENT IS UNLIMITED

P9368

Printed in the United States of America. Available from
National Technical Information Service
U.S. Department of Commerce
5285 Port Royal Road, Springfield, Virginia 22151
Price: Printed Copy $6.00; Microfiche $0.95

This report was prepared as an account of work sponsored by the United States Government. Neither the United States nor the United States Atomic Energy Commission, nor any of their employees, nor any of their contractors, subcontractors, or their employees, makes any warranty, express or implied, or assumes any legal liability or responsibility for the accuracy, completeness or usefulness of any information, apparatus, product or process disclosed, or represents that its use would not infringe privately owned rights.

DISCLAIMER

This report was prepared as an account of work sponsored by an agency of the United States Government. Neither the United States Government nor any agency Thereof, nor any of their employees, makes any warranty, express or implied, or assumes any legal liability or responsibility for the accuracy, completeness, or usefulness of any information, apparatus, product, or process disclosed, or represents that its use would not infringe privately owned rights. Reference herein to any specific commercial product, process, or service by trade name, trademark, manufacturer, or otherwise does not necessarily constitute or imply its endorsement, recommendation, or favoring by the United States Government or any agency thereof. The views and opinions of authors expressed herein do not necessarily state or reflect those of the United States Government or any agency thereof.

DISCLAIMER

Portions of this document may be illegible in electronic image products. Images are produced from the best available original document.

ORNL-4555
UC-70 — Waste Disposal and Processing

Contract No. W-7405-eng-26

ORNL--4555

A80002691

HEALTH PHYSICS DIVISION

PROJECT SALT VAULT: A DEMONSTRATION OF THE DISPOSAL OF HIGH-ACTIVITY SOLIDIFIED WASTES IN UNDERGROUND SALT MINES

R. L. Bradshaw and W. C. McClain
Editors

This report was prepared as an account of work sponsored by the United States Government. Neither the United States nor the United States Atomic Energy Commission, nor any of their employees, nor any of their contractors, subcontractors, or their employees, makes any warranty, express or implied, or assumes any legal liability or responsibility for the accuracy, completeness or usefulness of any information, apparatus, product or process disclosed, or represents that its use would not infringe privately owned rights.

APRIL 1971

OAK RIDGE NATIONAL LABORATORY
Oak Ridge, Tennessee
operated by
UNION CARBIDE CORPORATION
for the
U. S. ATOMIC ENERGY COMMISSION

DISTRIBUTION OF THIS DOCUMENT IS UNLIMITED

RICHARD LOUIS BRADSHAW

(1928–1971)

The research and development program on disposal of radioactive waste in natural salt formations began about 1957 and culminated with Project Salt Vault (1965–1967). Lou Bradshaw was associated with the program beginning in 1959, and his leadership in the design, operation, and especially in the analysis of the experimental results of Project Salt Vault was largely responsible for its success. This report, which summarizes the entire program, reflects his contribution on almost every page, and it is respectfully dedicated to his memory.

Contents

Preface xi

1. Introduction 1
   1.1 Background Material 1
   1.2 Development of Need and Concept for Demonstration Experiment 2

2. Summary of Previous Pertinent Studies 3
   2.1 Heat Transfer Properties 3
      2.1.1 In Situ Tests at Slightly Elevated Temperature 3
      2.1.2 In Situ Tests at High Temperature 4
   2.2 Trapped Moisture Effects 4
   2.3 Radiation Effects on Structural Properties 7
      2.3.1 Stress-Strain Determinations 7
      2.3.2 Creep Studies 7
      2.3.3 Anticipated Effects on Waste Disposal 8
   2.4 Gamma Radiation Shielding Properties 10
   2.5 Mine Stability Studies 10
      2.5.1 Ambient Temperature 10
      2.5.2 Effects of Elevated Temperature 10
   2.6 Economics of Solids Disposal in Salt 11
   2.7 Summary and Conclusions 12

3. Preliminary Design of Experiment 13
   3.1 Objectives and General Description 13
   3.2 Selection of Mine and Radiation Source 13
   3.3 Calculation of Fuel Assembly Temperatures 16
      3.3.1 In the Hot Cell 16
      3.3.2 In the Shipping Cask 17
      3.3.3 In the Salt Mine 17
   3.4 Radiation Dose Calculation 18
   3.5 Experimental Layout in Mine 19
      3.5.1 Consideration of Use of Existing Mine Space 19
      3.5.2 Alternative Layouts in Specially Mined Areas 20
      3.5.3 Layout Selected for the Test 20
   3.6 Salt Temperature Patterns in Arrays 21
   3.7 Experimental Instrumentation 22
   3.8 Conclusions 23

4. Field and Laboratory Studies Preliminary to Project Salt Vault 24
   4.1 Plastic Flow 24
      4.1.1 Heated Model Room 24
      4.1.2 U.S. Bureau of Mines Gage Tests 27
      4.1.3 Trial Installation of Gage Types in Hutchinson 29

4.1.4 Results of Convergence Measurements and Correlation with Laboratory Creep-Test Data ... 30
4.2 Prototype Hole Liner Test ... 37
4.3 Corrosion Studies ... 40
4.3.1 Field ... 40
4.3.2 Laboratory ... 41
4.4 Radiolytic Chlorine Production Studies ... 43
4.5 Dosimeter Development ... 45
4.5.1 Glass Rod Dosimeters ... 45
4.5.2 Chemical Dosimeters ... 47

5. Geology and Description of the Lyons Mine ... 49
5.1 Geology of Lyons Mine ... 49
5.1.1 Regional Setting ... 49
5.1.2 General Stratigraphy of the Salt Section ... 50
5.1.3 Detailed Lithology of the Ceiling in the Experimental Area ... 53
5.1.4 Mineralogical Analysis of the Salt Section ... 54
5.2 History of the Lyons Mine ... 55
5.3 Description of Lyons Mine at Start of Preparation for Project Salt Vault Experiment ... 55
5.3.1 Shaft and Collar ... 55
5.3.2 Hoist ... 55
5.3.3 Headframe ... 56
5.3.4 Mine Ventilation ... 56
5.3.5 Underground Workings ... 56
5.3.6 Electrical System ... 56
5.3.7 Hoist House ... 57
5.3.8 Summary ... 58

6. Mine Renovation and Preparation of Experimental Area ... 59
6.1 Renovations at Mine Topside ... 59
6.1.1 Headframe ... 59
6.1.2 Hoist ... 60
6.1.3 Hoist House Renovation ... 60
6.1.4 Electrical System ... 60
6.2 Waste Charging Shaft ... 61
6.2.1 Location ... 61
6.2.2 Design ... 61
6.2.3 Installation ... 61
6.3 Mine Level Preparation ... 61
6.3.1 Mining Machinery ... 61
6.3.2 Mine Cleanup ... 62
6.3.3 Ventilation ... 62
6.3.4 "Old Workings" Rock Mechanics Gages ... 62
6.4 Excavation and Preparation of the Experimental Area ... 62
6.4.1 Ramp ... 63
6.4.2 Salt Disposal Areas ... 63
6.4.3 Excavation Procedure and Progress ... 64
6.4.4 Drilling ... 65
6.5 Summary ... 66

7. Design and Fabrication of Equipment ... 67
7.1 Fuel Assembly Canister ... 67
7.2 Shipping Cask ... 69

7.3 Waste Charging Facility 72
7.4 Underground Transporter 74
7.5 Storage Hole Liners 76
7.6 Heated Pillar Equipment 77
7.6.1 Heaters 77
7.6.2 Modified Heaters 77
7.6.3 Thermocouples 77
7.6.4 Power Supply 77
7.7 Instrumentation 78
7.7.1 Thermocouples, Cables, and Recorders 78
7.7.2 Power System 79
7.7.3 Off-Gas System 80
7.7.4 Radiation Detection Systems 82
7.7.5 Alarm System 83
7.7.6 Dosimetry 83
7.8 Summary 84
Appendix 7A. Shielding Calculations 84
Appendix 7B. Project Salt Vault Remote Alarm System 85
Description of System 85
Discussion of System 87
Alarm Interpretation 88
Alarm System Malfunctions 90

8. Installation of Experimental Equipment 92
8.1 Waste Charging Facility 92
8.2 Underground Transporter 92
8.3 Power Distribution System 92
8.3.1 Surface Power 93
8.3.2 Underground Power 93
8.4 Array Hole Liners 93
8.5 Pillar Heaters 94
8.6 Instrumentation 94
8.6.1 Temperature Recording System 94
8.6.2 Power Control System 95
8.6.3 Off-Gas System 95
8.6.4 Radiation Detection System 96
8.6.5 Alarm System 96
8.7 Equipment Check Out 97
8.7.1 Cold Check Out (and Resulting Modifications) 97
8.7.2 Cobalt Check Out (and Resulting Modifications) 98
8.8 Summary 98

9. Hazards Analysis 99
9.1 Introduction 99
9.1.1 Individual and Total Fission Product Activity 99
9.1.2 Heat Generation 99
9.1.3 Idaho Operations, Canisters, and Fuel Shipments 104
9.2 Evaluation of Cask Design 104
9.2.1 Compliance with Structural Criteria Cited in Sections 72.32, 72.33, 72.34, Code of Federal Regulations, Title 10, Part 72 104
9.2.2 Resistance of the Cask to Fire – Sections 72.31(*c*) and 72.34(*b*) 104
9.2.3 Shielding Against Ionizing Radiation – Section 72.35 106
9.2.4 Criticality – Section 72.37 107
9.2.5 Removal of Decay Heat – Section 72.38 108

9.3 Evaluation of Shipping Hazards 109
9.4 Analysis of Transfer Operations in Project Salt Vault 110
9.4.1 Topside Transfer Procedures 110
9.4.2 Transporter Loading at Shaft Bottom 112
9.4.3 Transporter Unloading at Shaft Bottom 112
9.4.4 Transfer Operations at Mine Level 112
9.5 Fission Product Containment 113
9.6 Evaluation of Accidents 113
9.6.1 At the Ground Surface 114
9.6.2 In the Waste Charging Shaft 115
9.6.3 Loading the Transporter at the Waste Shaft 116
9.6.4 During Transport in the Transporter 117
9.6.5 Loading or Unloading Storage Holes 118
9.7 Accident Categories 119
9.7.1 Type I Accident 120
9.7.2 Type II Accident (Maximum Credible Accident) 121
9.8 Conclusions 123

10. Operating Experience 124
10.1 Main Radioactive and Electrical Arrays, Rooms 1 and 4 124
10.1.1 Operation Prior to Startup 124
10.1.2 Official Startup 125
10.2 Canister Handling 125
10.2.1 First Canister Handling 125
10.2.2 Changeout of Canisters, June 1966 125
10.2.3 Changeout of Canisters, November 1966 126
10.2.4 Removal of Fuel Element Canisters 126
10.2.5 Results of Canister Handling Operations 126
10.3 Pillar-Heater Experiment 126
10.4 Routine Operation 127
10.4.1 Data Collection 127
10.4.2 Alarm System 127
10.4.3 Servicing 127
10.5 Nonroutine Activities 128
10.5.1 Roof Bolting Program 128
10.5.2 Condensate Collection 128
10.5.3 Correction of Heat Losses 128
10.5.4 Materials Testing 129
10.6 Power Shutoff, Cooldown, and Closeout 130
10.6.1 Dismantling, Inspection, and Disposal of Experimental Equipment 130
10.6.2 Metallurgical Examination of Pillar and SWCT Heaters 130
10.7 Summary 132
Appendix 10A. Operating Procedures for Project Salt Vault, Revision O 135

11. Results and Analysis 161
11.1 Radiation 161
11.1.1 Source Activity 161
11.1.2 Absorbed Dose in Salt 162
11.1.3 Radiolytic Gas Production 163
11.1.4 Miscellaneous Effects 164
11.2 Moisture 164
11.2.1 Cavity Migration 164
11.2.2 Off-Gas Condensate 167

11.2.3 Corrosion Effects on Hardware ... 169
11.2.4 Further Studies on Moisture ... 170
11.2.5 Water Migration into Future Disposal Holes ... 170
11.3 Temperature ... 172
11.3.1 Power Input ... 172
11.3.2 Array Rooms ... 173
11.3.3 Heated Pillar ... 180
11.3.4 Modified Pillar Heaters ... 187
11.3.5 Effects of Salt, Sand, and Air Backfill ... 188
11.3.6 Simulated Waste Container Test ... 189
11.4 Rock Deformation and Mine Stability ... 191
11.4.1 Description of Gage Types ... 191
11.4.2 Design of Gage Layouts ... 197
11.4.3 Movements Resulting from Experiment Area Excavation ... 200
11.4.4 Situation in Experimental Area Prior to Heating ... 208
11.4.5 Movements Induced by Heat in Array Experiment – Rooms 1 and 4 ... 209
11.4.6 Movements Induced by Room 5 Experiment ... 230
11.4.7 Movements Induced by Heated Pillar Experiment ... 236
11.4.8 Deformation of Entire Experimental Area and the Rest of the Mine ... 249

12. Laboratory Pillar Model Experiments ... 257
12.1 Summary of Previous Work ... 257
12.2 Preliminary Investigations ... 258
12.2.1 Sample Preparation and Test Procedure ... 258
12.2.2 Simulation of Mine Pillars in Scale Models ... 259
12.2.3 Size of Model Specimens ... 261
12.3 Results of Model Pillar Tests ... 261
12.3.1 Effect of Load ... 262
12.3.2 Effect of Temperature ... 263
12.3.3 Effect of Temperature Elevation after Initial Loading ... 265
12.3.4 Effect of Shale Partings ... 270
12.3.5 Effect of Pillar Shapes ... 272
12.3.6 Comparisons of Salt from Various Localities ... 275
12.3.7 Reproducibility of Results ... 277
12.3.8 Ultimate Strength ... 278
12.3.9 Mechanisms of Deformation ... 278
12.3.10 Long-Term Creep ... 282
12.4 Discussion of Results ... 282
12.4.1 Relationship of Load, Temperature, and Time ... 282
12.4.2 Relationship to Actual Mine Conditions ... 284
12.5 Summary and Conclusions ... 287

13. Analysis of Combined Effects ... 291
13.1 Theoretical Analysis ... 291
13.1.1 Rheological Properties of Rock Salt ... 292
13.1.2 Creep in Salt Pillars ... 293
13.1.3 The Mining Horizon as an Incompatability in an Infinite Elastic Body ... 294
13.1.4 Temperature Changes and Thermal Stresses ... 298
13.2 Description of the Computer Program ... 299
13.2.1 Basic Setup ... 299
13.2.2 Computation at Each Time Step ... 300
13.2.3 Input Data ... 301

13.3 Comparison of Computer Model with Experimental Area 302
13.3.1 Basis of Comparison 302
13.3.2 Computer Simulation of Experimental Area 304
13.3.3 Discussion 309
13.3.4 Extrapolation of Computer Model to Waste Disposal Facility Design Problems 310
Appendix 13 A. FORTRAN Listing of Computer Program 312

14. Summary and Conclusions 317
14.1 Background 317
14.2 Previous Studies 318
14.3 Preliminary Design of Project Salt Vault 318
14.4 Studies Preliminary to Main Experiment 320
14.5 Geology and Description of Lyons Mine 322
14.6 Mine Renovation and Preparation 323
14.7 Design and Fabrication of Equipment 324
14.7.1 Fuel Assembly Canisters 324
14.7.2 Shipping Cask 325
14.7.3 Waste-Charging Facility 325
14.7.4 Underground Transporter 325
14.7.5 Storage Holes 325
14.7.6 Heated Pillar Equipment 325
14.7.7 Instrumentation 327
14.8 Installation of Experimental Experiment 328
14.9 Hazards Analysis 330
14.10 Operating Experience 333
14.11 Results and Analysis 336
14.11.1 Radiation 336
14.11.2 Moisture 337
14.11.3 Temperature 338
14.11.4 Rock Deformation and Mine Stability 340
14.12 Laboratory Pillar Model Experiments 348
14.13 Analysis of Combined Effects 351
14.14 Conclusion 355

Preface

SCOPE AND OBJECTIVES

The primary purpose of this report is to document in one volume (as completely as practical) the background, design, installation, operation, and conclusions derived from Project Salt Vault. Project Salt Vault was a demonstration of the disposal of high-level solidified radioactive wastes in a salt mine in Lyons, Kansas. Associated with the demonstration were several necessary side experiments.

In order to be complete, the significant results of the earlier studies are also included. In many cases only the major results are included, but a fairly complete list of references to reports covering the original work is given.

Much of this material has not been published previously.

ORGANIZATION OF REPORT

The first two chapters deal with the early work which led up to the demonstration.

Chapters 3 and 4 describe the early experiments and the preliminary design of the demonstration.

Chapters 5 and 6 deal with the geology of the mine and general area and with the renovations and preparations required for the demonstration.

Chapters 7 and 8 describe the design, fabrication, and installation of equipment required for the demonstration and associated experiments.

Chapter 9 is a safety evaluation of the demonstration.

The operating experience is detailed in Chap. 10, and the results and analyses are discussed in Chap. 11.

The remaining chapters deal with relations between the results of the demonstration and associated experiments, laboratory pillar model studies, and computer simulation of mine behavior.

ORNL PERSONNEL MOST DIRECTLY INVOLVED

The authors of the references in this report are those individuals who were most active in the work prior to the initiation of studies relating to the demonstration. There were others, both at ORNL and at other institutions, who made both direct and indirect contributions to the background of knowledge at ORNL. Unfortunately, it would be impractical to try to list them all.

At the time of the feasibility study of the demonstration (mentioned in Chap. 1), those in the Health Physics and Chemical Technology Divisions who made major contributions were J. O. Blomeke, W. J. Boegly, Jr., R. L. Bradshaw, F. M. Empson, F. L. Parker, J. J. Perona, and W. F. Schaffer. During the preliminary design stages, essentially the same personnel were involved.

During the design, fabrication, and installation stages, many more persons at ORNL were involved, and the following list includes those who made major contributions. Due to the lapse of time, the Editors have no doubt overlooked some individuals, and to them we apologize. Those listed below are Health Physics Division personnel unless otherwise stated: W. J. Boegly, Jr., R. L. Bradshaw, D. W. Brown (Carbide Purchasing), Don Dunning (Chemical Technology), F. M. Empson, M. B. Herskovitz (Instrumentation and Controls), T. W. Hodge, B. L. Houser, F. K. Koon (Carbide Purchasing), Hisashi Kubota (Analytical Chemistry), T. F. Lomenick, W. C. McClain, F. L. Parker, W. F. Schaffer (Chemical Technology), R. C. Sexton (Plant and Equipment), J. A. Steed (General Engineering and Construction), and E. G. Struxness.

During the operating period those who were involved essentially full time (for extended periods) were: Boegly, Bradshaw, Empson, Hodge, Houser, and McClain. Most of the others who were listed as participating in design, fabrication, and installation were also involved to various extents during the operating period. In addition, others not listed previously are C. R. Guinn, D. G. Noe, and H. J. Wyrick.

The persons responsible for preparation of the data for analysis and for the writing of the various chapters of this report are generally indicated by the names which appear with the chapter headings. Others who

have played a major role in this phase are Joe Marie Davis, T. W. Hodge, D. W. Phifer, and H. J. Wyrick.

Many other individuals in the above-named ORNL divisions and in other divisions also made significant contributions to the success of the operation.

OTHER PERSONS AND ORGANIZATIONS

Again, this section cannot list all who were involved, and to those whom we miss we apologize.

The Carey Salt Company of Hutchinson, Kansas, provided the mine, the mine development and operating crew and supervisor, administrative support in Kansas, and the enthusiastic support of both management and employees.

The Stearns-Roger Corporation conducted a thorough inspection of the premises and submitted a detailed report on required renovations to the Lyons facility.

Many subcontractors, who did excellent jobs, were involved in the preparation of the mine facility, but due to the number, only one will be mentioned: the Sterling Drilling Company (of Sterling, Kansas) which drilled and installed the 19.1-in.-OD waste shaft to very exacting specifications.

The Stowers Machinery Corporation of Knoxville, Tennessee, contracted to provide the underground transporter; they in turn secured the services of the Athey Products Corporation of Chicago to fabricate the trailer.

The AEC's Y-12 Plant was involved in modification of the shipping carrier and other major fabrication.

The Topographic Division of the U.S. Geological Survey established bench marks on the surface and in the mine and established the relationship between surface and underground points.

The U.S. Bureau of Mines participated in a comparative study of various types of stress or stress-change meters. They also provided general advice, as well as periodic mine-safety inspections and reports.

Professor E. L. J. Potts, head of the Mining Engineering Department of the University of Newcastle, England, acted as a consultant on the mining and rock mechanics aspects of the project. In addition, his department supplied a large portion of our rock mechanics instrumentation.

A. M. Starfield, School of Mineral and Metallurgical Engineering of the University of Minnesota, made the theoretical analysis and wrote the basic computer program for the interpretation of the deformational behavior of the experimental area under the combined influences of stress, heat, thermal gradients, and time (Chap. 13).

The people of the city of Lyons, especially as represented by both the official and service organizations, contributed in many ways by their general cooperative spirit.

The project was funded by the AEC's Division of Reactor Development and Technology, Environmental and Sanitary Engineering Branch.

1. Introduction

R. L. Bradshaw

1.1 BACKGROUND MATERIAL

In September 1955, at the request of the U.S. Atomic Energy Commission, a committee of geologists and geophysicists was established by the National Academy of Sciences–National Research Council to consider the disposal of high-level radioactive wastes in geologic structures within the continental United States. This committee proposed storage in natural salt formations as the most promising method for the future.[1] As a result of the recommendations of the committee, study was begun on the problems of disposal of high-level radioactive waste in salt.

Some of the advantages of natural salt formations as repositories for radioactive wastes are:

1. Salt is essentially impermeable due to its plastic properties.
2. Salt is widely distributed and abundant, underlying about 500,000 square miles in the United States and with known reserves greater than 6×10^{13} tons.[2,3]
3. The cost of developing space is relatively low.[4,5]
4. The thermal conductivity of salt is good (2.5 Btu hr^{-1} ft^{-1} $°F^{-1}$ at 200°F).[6]
5. Salt formations in the United States are located in areas of low seismicity.
6. The compressive strength of salt is similar to that of concrete about 3000 psi.

Early ORNL investigations were aimed at the disposal of liquid waste.[7-11] This approach was prompted by the fact that the high-level wastes being produced under the technology existing at that time were relatively dilute liquids. Processes for reduction of the liquid fuel-reprocessing wastes to solids had been proposed but were in an early stage of development. Therefore, the initial program was designed to secure answers to the following questions: (1) To what degree will the structural properties of salt be altered by heat and radiation? (2) Will there be interactions between waste and salt? (3) Can gaseous reaction products be handled?

The liquid waste investigations and experiments were encouraging, but there remained a number of unsolved problems unique to liquid waste disposal. Cavity alteration, due to evaporation-condensation processes and localized movement of solution through shale bands and gas-pocket cavities, occurred. While chemical conditions could be controlled to prevent formation of

[1] Committee on Waste Disposal, Division of Earth Sciences, *Disposal of Radioactive Wastes on Land,* National Academy of Sciences–National Research Council Publication 519, April 1957, p. 6.

[2] W. B. Lang, *Annotated Bibliography of Salt Deposits in the United States,* Geological Survey Bulletin 1019-J (1957).

[3] *Mineral Resources of the United States,* Public Affairs Press (1958), p. 180.

[4] A. E. Inman, *Salt, an Industrial Potential for Kansas,* University of Kansas Research Foundation (1951), p. 22.

[5] Research and Coordinating Committee, Interstate Oil Compact Commission, *Underground Storage of Liquid Petroleum Hydrocarbons in the United States* (April 1956), p. 2.

[6] Francis Birch and H. Clark, "The Thermal Conductivity of Rocks and Its Dependence on Temperature and Composition," *Am. J. Sci.* 238, 552 (1940).

[7] F. L. Parker, L. Hemphill, and Julian Crowell, *Status Report on Waste Disposal in Natural Salt Formation,* ORNL-2560 (August 1958).

[8] F. L. Parker (ed.), *Status Report on Waste Disposal in Natural Salt Formations: II,* ORNL-2700 (April 1959).

[9] F. M. Empson (ed.), *Status Report on Waste Disposal in Natural Salt Formations: III,* ORNL-3053 (July 1961).

[10] F. L. Parker, W. J. Boegly, Jr., R. L. Bradshaw, F. M. Empson, L. Hemphill, E. G. Struxness, and T. Tamura, "Disposal of Radioactive Wastes in Natural Salt," *Disposal of Radioactive Wastes* 2, 365–86 (1960), IAEA, Vienna, 1960.

[11] W. J. Boegly, Jr., R. L. Bradshaw, F. M. Empson, and F. L. Parker, "Disposal of Radioactive Wastes in Natural Salt–Field Experiments," *Proc. Fifteenth Industrial Waste Conf., May 3–5, 1960,* pp. 577–90, Purdue University, Lafayette, Indiana, March 1961.

chlorine and nitrosyl chloride, radiolytic reactions producing hydrogen and oxygen were not controlled. There were promising leads on these problems, but it was not possible to say that the problems of disposal of liquid waste in salt had been solved.

While the liquid waste investigations were in progress, the fuel-reprocessing business and the nature of the expected waste underwent a radical change. The volume of waste produced per ton of uranium was reduced from about 800 to 40–50 gal/ton. Concurrently, an accelerated program aimed at reduction of this concentrated liquid to a solid was begun by AEC contractors. There was a demonstration plant, for conversion to a granular solid by calcination in a fluidized bed, under test at the National Reactor Test Station near Idaho Falls, Idaho, and a demonstration program got under way at Hanford, utilizing ORNL, Brookhaven, and Hanford processes to convert liquid wastes to solids. It was expected that the first "pots" of solidified waste would be produced in the late 1960's. Therefore the ORNL program shifted to studies of ultimate disposal of packaged dry solid waste.

Many of the studies completed in connection with disposal of liquid wastes were directly applicable to disposal of solids. For example, in the case of studies of the structural and thermal properties of salt, the chief difference from the standpoint of the solid waste characteristics would be the much higher allowable salt temperatures. A summary of the pertinent studies is included in Chap. 2.

1.2 DEVELOPMENT OF NEED AND CONCEPT FOR DEMONSTRATION EXPERIMENT

In December 1961 the National Academy of Sciences–National Research Council Committee on Geologic Aspects of Radioactive Waste Disposal met at the Savannah River Plant, near Augusta, Georgia, to discuss progress made since the 1955 meeting and to make recommendations regarding future work.

The meeting was attended by approximately 40 guests and observers representing the U.S. Atomic Energy Commission, the Du Pont Company, the Corps of Engineers, the U.S. Geological Survey, the Oak Ridge National Laboratory, and other interested contractors.

The committee's conclusions and recommendations regarding the studies were:

> The consensus of the Committee discussion was that experience both in the field and in the laboratory on disposal of wastes in salt have been very productive, well conceived, and that plans for the future are very promising. The Committee noted that the interpretations relating to disposal in salt are by the very nature of salt deposits capable of being extrapolated to a considerable degree from one deposit to another. . . .
>
> The Committee suggests that, in investigating the plastic flow of salt, experiments be designed on the assumption that the volume of salt changes only by thermal expansion and that the movement takes place by a shortening and thickening of the column of salt under load.
>
> The Committee strongly recommends that the effect of storing dry packaged radioactive wastes in a salt deposit be tested, and urges the Atomic Energy Commission to consider using, at an early date, Federally controlled land in the Hutchinson area.[12]

Following this meeting the AEC requested that the Health Physics and Chemical Technology Divisions of ORNL consider the possibility of testing or demonstrating the disposal of high-level radioactive solids in a salt mine, using whatever radiation sources might be available. Consequently several sources were considered, with the final choice being irradiated fuel assemblies from the Engineering Test Reactor (ETR) at the Idaho plant. In July of 1962 the preliminary feasibility study was completed, and a document, "Feasibility Study of the Use of Irradiated Fuel Elements to Simulate Solidified High Level Radioactive Waste Storage in Salt Formations," was transmitted to the AEC in Washington, D.C. This study led to the general conclusion that it was feasible to use irradiated fuel elements to establish the practicality of using salt for waste disposal by the time significant quantities of calcined wastes would be produced.

As a result of a review of the scope of the demonstration as conceived in the feasibility study, it was concluded that, for a relatively small additional cost, the scope could be extended to yield much additional information which would be valuable in the design of an actual disposal facility. After further discussions with Laboratory management and AEC officials, it was decided in early 1963 to extend the scope to include design and fabrication of prototype waste-handling equipment and to obtain additional information on the effect of elevated temperatures on the creep and plastic flow of salt.

---

[12] William Thurston, Secretary, Minutes of the Meeting of December 7–8, 1961, National Academy of Sciences–National Research Council, Division of Earth Sciences, Committee on Geologic Aspects of Radioactive Waste Disposal Advisory to the U.S. Atomic Energy Commission.

2. Summary of Previous Pertinent Studies

R. L. Bradshaw

2.1 HEAT TRANSFER PROPERTIES

For disposal of high-level radioactive waste in salt deposits, it is necessary to predict the waste temperature rise that will occur due to the heat generated by fission product decay. The allowable rise will be limited by the boiling point for liquid wastes and by the decomposition temperature for solid wastes. A further limit on temperature rise may be imposed by the effects of increased temperature on the structural properties of salt.

Birch and Clark have measured the temperature dependence of the thermal conductivity and diffusivity of single natural halite (NaCl) crystals.[1] This relationship is shown in Fig. 2.1. Results of measurements made by the U.S. Geological Survey with rock salt taken from the Carey Salt Company's Hutchinson, Kansas, mine are in substantial agreement with those of Birch and Clark for the single crystals.[2]

A comparison of conductivities at room temperature of two Hutchinson samples, one unirradiated and one irradiated to an exposure dose of 5×10^8 R, showed less than 10% drop due to radiation.

2.1.1 In Situ Tests at Slightly Elevated Temperatures

Several in situ tests were run in the Hutchinson mine in which actual temperature rise measurements were compared with approximate theoretical calculations based on the Birch and Clark values. Typical of the correlations was that obtained with a $7\frac{1}{2}$-ft cube of simulated liquid waste, shown in Fig. 2.2. It may be seen that there is good agreement for times up to about 20 days. Beyond 20 days the measured values are lower than the theoretical due to increased heat losses through the floor. (The calculations assumed an infinite salt medium.) The thermal conductivity and diffusivity of the salt in place, calculated from the thermal data of the tests, were 2.6 Btu hr^{-1} ft^{-1} $°F^{-1}$ and 0.10 ft^2/hr respectively. By comparison, the Birch and Clark values for single salt crystals at 60°C, the peak salt temperature reached in the experiment, are 2.8 Btu hr^{-1} ft^{-1} $°F^{-1}$ and 0.10 ft^2/hr respectively.

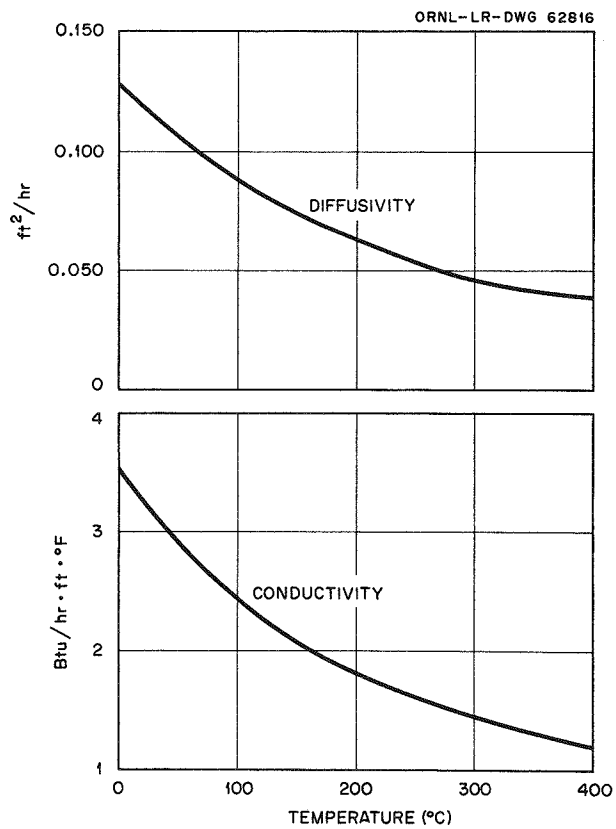


Fig. 2.1. Thermal Properties of Halite (Adapted from Birch and Clark, ref. 1).

[1] Francis Birch and H. Clark, "The Thermal Conductivity of Rocks and Its Dependence on Temperature and Composition," *Am. J. Sci.* 238, 529–58, 613–35 (1940).

[2] W. A. Schneider, H. Hughes, and E. C. Robertson, *Thermal Conductivity to 300°C of Natural Salt, Technical Letter: Special Projects-2,* USGS, Denver, Colo. (Apr. 20, 1962).

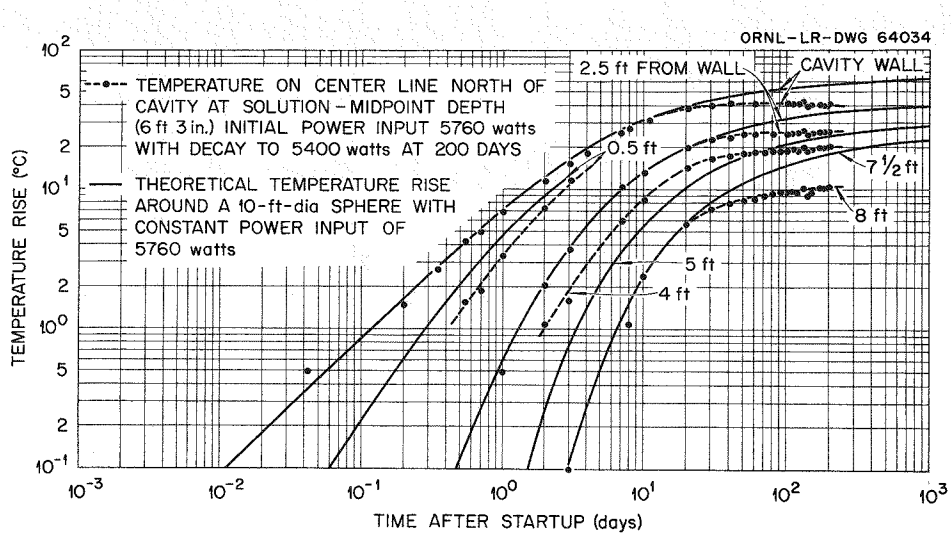


Fig. 2.2. Comparison of Temperature Rise in 7½-ft-Cube Acid Waste Experiment with Theoretical Values for 10-ft-diam Sphere.

2.1.2 In Situ Tests at High Temperature

Several tests were carried out using 4-ft-long, 6-in.-diam cylindrical heat sources in 10-in.-diam holes, 10 ft deep. Heat transfer properties at salt temperatures up to about 350°C were investigated. Again, the agreement with the Birch and Clark single-crystal values was good. This relatively close agreement lends confidence to theoretical calculations of temperature rise based on single-crystal values.

It may be seen from Fig. 2.1 that both the conductivity and diffusivity decrease rather sharply with increasing temperature, while the theoretical equations assume constant thermal properties. To be conservative, the theoretical calculations should include values for the thermal properties at the highest temperatures which may be reached in a particular case. It was felt that this might impose an unduly severe restriction since, in some cases, only the salt in contact with the waste or waste container will ever reach this peak temperature, while salt at greater distances will be at much lower temperatures. The results obtained with an equation for a uniformly heated slab of salt (with a vertical extent of a few feet and infinite horizontal extent) in contact with an infinite salt medium indicate that this need not be a serious concern, since the peak temperature rise is not a strong function of the conductivity and diffusivity. For example, the peak temperature rise in the slab calculated with the 100°C salt conductivity and diffusivity constants was only 18% less than that calculated with the 300°C salt thermal properties, even though the conductivity was 70% greater and the diffusivity 90% greater than at 300°C. This apparent paradox obtains because the heat capacity remains nearly constant over the designated temperature range although salt conductivity and diffusivity change appreciably. In addition, the heat-generation rate of radioactive waste is always decreasing, and thus a steady-state condition is never achieved.

2.2 TRAPPED MOISTURE EFFECTS

In most bedded salt there is moisture trapped along the grain boundaries and in so-called "negative crystal" cavities within the crystals. In mine-run salt from Hutchinson, there are numerous brine-filled negative-crystal cavities less than $\frac{1}{16}$ in. in size. Most of these roughly cubical cavities are completely filled with brine, but a few of them contain small vapor bubbles. Figure 2.3 is a photomicrograph showing several small vapor bubbles floating in brine-filled negative crystals. Schneider *et al.* report that nearly spherical pores a few tens of microns in diameter are distributed uniformly on all the grain boundaries.[3]

In order to determine the effect of temperature on salt, 1- to 2-lb samples were heated to temperatures up to 400°C.[4] Salt from the Hutchinson mine was used in

[3] W. A. Schneider, H. Hughes, and E. C. Robertson, *Thermal Conductivity to 300°C of Natural Salt, Technical Letter: Special Projects-2,* USGS, Denver, Colo. (Apr. 20, 1962), p. 4.

[4] Studies performed by Hisashi Kubota of the Analytical Chemistry Division.

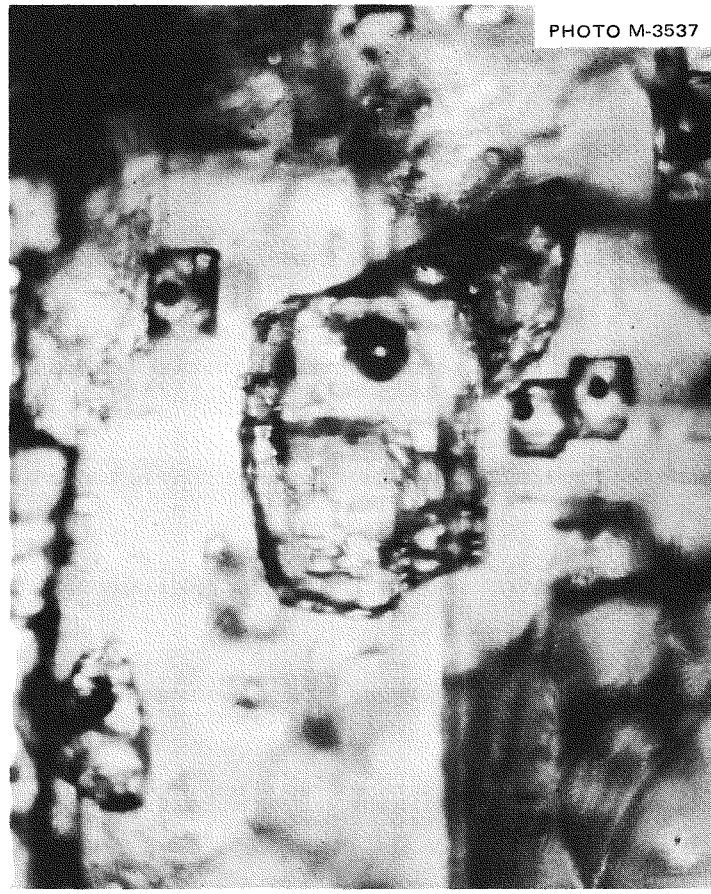


Fig. 2.3. Vapor Bubbles in Salt.

the initial study. It was found that the salt fractured with considerable violence when heated to around 280°C. With one sample the explosion was violent enough to lift the door of the muffle furnace, as well as to rupture the wire basket used to contain the sample. Each explosion resulted in the release of a cloud of steam and took place at about the same temperature regardless of the rate of heating.

Quantitative measurement of the amount of water released and more detailed observations of the effect of temperature on Hutchinson and Lyons salt were carried out by heating the salt in a "bomb." The moisture released was swept into a tared absorption bottle and weighed. When the salt was heated, there was initially a large disintegration at a temperature above 250°C, followed by lesser events at random temperature increases up to the upper limit of heating. Nearly all of the water was released during the initial large fracture. The heating process reduced the original salt mass into particles which varied in size from fine powder to centimeter-size crystals.

The moisture content results are shown in Table 2.1. There appears to be a significant difference in the moisture content between the samples from the Hutchinson and Lyons mines. (However, see Sect. 11.2.4.3 for more recent results.) The sample showing the greatest moisture content was a clear crystal from the Hutchinson mine containing several visible inclusions of water. The variation in the water content is apparently due to the random distribution and size of these inclusions throughout the salt.

Three possible mechanisms for the fracturing were advanced: (1) unequal thermal expansion along the crystal axis, (2) chemical reactions such as the combustion of organics, and (3) the pressure effects of brine inclusions. Consideration of the effects discussed in the following paragraph indicated mechanism 3 to be the prime one. The salt from a given site "exploded" at

Table 2.1. Moisture Release of Salt from the Hutchinson and Lyons Mines

Source	Weight of Sample (g)	Water Released Weight (%)
Hutchinson	702	0.127
	763	0.182
	467	0.293
	530	0.150
		Av 0.188
	153[a]	1.08[a]
Lyons	1327	0.090
	667	0.048
	714	0.100
	709	0.082
		Av 0.080

[a]Clear crystal, not typical.

nearly the same temperature regardless of the rate of heating. Even a very slow rate of heating, which could have the effect of annealing some of the strains in the crystals, did not alter the temperature at which the first disintegration occurred. Analysis of the gases produced showed a trace of carbon dioxide which was of a magnitude far below that which would be produced by a reaction capable of causing the observed phenomenon. The vapor pressure of water rises sharply from 1 atm at 100°C to 15 atm at 200°C, 38 atm at 250°C, and 84 atm at 300°C. Even more important, pressures of several hundred atmospheres could be built up in those cavities which do not contain vapor bubbles (since the thermal expansion of brine is considerably greater than that of the salt) if the cavity wall does not yield. In tests of several small samples (about ½ in. and smaller sizes), negative-crystal cavities were observed to undergo permanent volume expansion upon heating. The permanent increase in cavity volume was proportional to temperature, amounting to about 7½% at 225°C. These considerations, along with the observed release of steam, led to the conclusion that the greatest single cause of the disintegration process was the pressure of the heated brine.

In Table 2.2 are shown the shattering (fracturing) temperatures for salt samples taken from various locations. It is of interest that bedded salt from all but one of the locations shattered at temperatures between 250 and 380°C, while none of the dome salt was affected at temperatures up to 400°C. (No negative crystals could be found in the dome salt samples.)

A few samples of Hutchinson salt which were irradiated to exposure doses of 5×10^8 R or greater fractured between 260 and 320°C. It was thus concluded that radiation will have little effect on fracturing temperatures. This result is in line with the results of previous tests which have shown that the radiolytic process in a confined saturated salt solution will attain a steady-state pressure of about 10 atm, a pressure that is well below the pressures that may be produced by volumetric expansion of the brine at the fracturing temperature.

Table 2.2. Thermal Stability of Salt

Location	Number of Samples Tested	Fracturing Temperature (°C)	Salt Type
Hutchinson, Kansas	30	260–320	Bedded
Lyons, Kansas	8	285–320	Bedded
Fairport Harbor, Ohio	2	380	Bedded
Retsof, New York	2	*a*	Bedded
Detroit, Michigan (International)	2	290	Bedded
Cheshire, England	1	250	Bedded
d'Alsace, France			
NaCl	2	240–280	Bedded
KCl	1	*a*	Bedded
Winnfield, Louisiana	2	*a*	Dome
Grand Saline, Texas	2	*a*	Dome
Weeks Island, Louisiana	2	*a*	Dome

[a]Indicates that the salt did not fracture up to 400°C.

In the high-temperature in situ tests mentioned in the previous section (10-in.-diam holes, 10 ft deep), salt shattering was observed to occur when the salt at the periphery of the heated hole reached a temperature of about 280°C. As the 280°C front moved away from the hole, salt continued to fracture, releasing the trapped water. Some 190 ml of water was actually collected during a test in a pillar from a fractured-salt volume estimated to be 1.8 ft^3. More than 190 ml was actually released by the shattering, but it was not possible to get an accurate estimate of the amount not collected.

The sudden release of large quantities of water in an actual waste disposal operation may be undesirable. Thus, from the standpoint of water release, a conservative upper allowable temperature for salt is about 200°C. As discussed in Sect. 11.2, water migration at 200°C is not expected to be a major concern in an actual waste disposal facility. Even if temperatures exceed 200°C immediately around the waste containers, the volume of water is relatively small and will not cause concern.

2.3 RADIATION EFFECTS ON STRUCTURAL PROPERTIES

Uniaxial compression testing was carried out at the Oak Ridge National Laboratory to evaluate the effects of ionizing radiation on the physical properties of rock salt from two formations. Bedded salt was secured from the Carey Salt Company mine at Hutchinson, Kansas, and dome salt from the mine of the Morton Salt Company at Grand Saline, Texas. The test work was carried out by B. D. Gunter.[5] The test specimens were 2-in. cubes prepared from large blocks removed from the respective mines by hand drilling. The test cubes were accurately machined to assure the application of a uniform force between parallel plane surfaces. No standard test procedures have been established for rock salt, and these physical property tests were run without the use of end friction reducers.

The machined specimens were irradiated in the ^{60}Co storage facility of the Isotopes Division at Oak Ridge National Laboratory. Approximately 200,000 Ci of ^{60}Co were stored in the facility at the time of irradiation, giving a gamma field of 3.2×10^6 R/hr. The temperature inside the chamber was approximately 70°C.

[5] B. D. Gunter and F. L. Parker, *The Physical Properties of Rock Salt as Influenced by Gamma Rays,* ORNL-3027 (March 1961).

2.3.1 Stress-Strain Determinations

The definition of terms used in this study is as follows. The peak of the stress-strain curve is compressive strength. The 0.2% offset yield strength is determined by passing a line parallel to the elastic portion of the curve through a strain of 0.2% of the sample reference length. (Although salt may not have any truly elastic region, in this study the portion of the stress-strain curve from 0 to 0.2% strain was assumed to be linearly elastic.) The point of intersection of this line with the stress-strain curve is the yield strength. The apparent elastic limit is the point at which the rate of deformation is 50% greater than the initial rate. The modulus of elasticity is the slope of the elastic portion of the curve.

Stress-strain curves were obtained for three samples each of dome salt, bedded salt with force applied perpendicular to the planes of stratification, and bedded salt where the force was applied parallel to the planes of stratification at radiation exposure doses of 0, 10^6, 10^7, 10^8, and 5×10^8 R at room temperature. In addition, similar tests were run at 200°C with radiation exposures of 0 and 5×10^8 R. Table 2.3 presents the physical properties of rock salt as determined for the conditions outlined above. Figure 2.4, the stress-strain curves for force applied perpendicular to the bedding planes at room temperature, is typical of the curves obtained in the tests.

The results of these measurements may be summarized as follows:

1. The compressive strength of the unirradiated dome salt at room temperature is higher than that of the bedded salt.
2. The compressive strength of rock salt exposed to 5×10^8 R at room temperature is, without exception, less than the compressive strength of unirradiated rock salt (about 10 to 20% less for bedded salt, and 30 to 40% less for dome salt). On the basis of statistical evaluation, the observed differences are probably real.
3. At 200°C and exposure doses of 5×10^8 R, there is little difference between the strengths of bedded and dome salt.
4. Without exception, the modulus of elasticity is greater for exposures of 5×10^8 R than for unirradiated specimens.

2.3.2 Creep Studies

In addition to the static tests, the creep rate resulting from the application of a constant load of 2500 psi for

Table 2.3. Physical Properties of Rock Salt[a]

Type of Salt	Exposure Dose (R)	Compressive Strength (psi)	Yield Strength (psi)	Apparent Elastic Limit (psi)	Modulus of Elasticity (psi)
					$\times 10^6$
		At 20°C			
Bedded parallel[b]	0	4200 ± 500	2500 ± 300	1900 ± 300	0.35 ± 0.06
	10^6	4500 ± 500	2500 ± 150	1900 ± 200	0.32 ± 0.06
	10^7	4600 ± 400	2700 ± 250	2100 ± 200	0.35 ± 0.02
	10^8	4600 ± 150	3400 ± 250	2800 ± 200	0.36 ± 0.09
	5×10^8	3500 ± 50	2700 ± 200	2000 ± 300	0.39 ± 0.07
Bedded perpendicular[c]	0	4000 ± 400	2300 ± 300	1700 ± 200	0.36 ± 0.17
	10^6	3800 ± 500	1800 ± 250	1400 ± 250	0.35 ± 0.10
	10^7	4100 ± 400	2300 ± 500	1800 ± 500	0.38 ± 0.04
	10^8	4000 ± 400	2400 ± 500	1900 ± 300	0.38 ± 0.06
	5×10^8	3500 ± 400	2400 ± 300	1900 ± 250	0.37 ± 0.11
Dome	0	5600 ± 100	2900 ± 150	2000 ± 100	0.50 ± 0.05
	10^6	5300 ± 100	2900 ± 150	2000 ± 300	0.51 ± 0.12
	10^7	5100 ± 200	3000 ± 100	2100 ± 300	0.62 ± 0.06
	10^8	4100 ± 200	2700 ± 100	1800 ± 200	0.48 ± 0.04
	5×10^8	3600 ± 500	2600 ± 200	1900 ± 50	0.59 ± 0.12
		At 200°C			
Bedded parallel	0	3900 ± 200	1600 ± 200	1400 ± 100	0.09 ± 0.01
	5×10^8	3400 ± 400	1900 ± 250	1800 ± 250	0.12 ± 0.02
Bedded perpendicular[d]	0	3600 ± 100	1600 ± 100	1500 ± 150	0.11 ± 0.01
	5×10^8	3300 ± 400	2100 ± 150	1800 ± 100	0.13 ± 0.01
Dome	0	3600 ± 500	1900 ± 150	1600 ± 200	0.14 ± 0.01
	5×10^8	3100 ± 300	2300 ± 150	1800 ± 200	0.16 ± 0.01

[a] All results have been rounded off to the nearest 100 psi and the standard deviation to the nearest 50 psi.

[b] Bedded salt, force applied parallel to the planes of stratification.

[c] Bedded salt, force applied perpendicular to the planes of stratification.

[d] Two samples only tested.

100 min was measured. After the initial rise due to elastic compression, the strain increases slowly with time. As in the stress-strain tests for compressive strength, the dome salt is strongest, that is, shows the least creep, or greatest creep strength. The bedded salt loaded parallel to stratification is next strongest, and the bedded salt loaded perpendicular to stratification shows the maximum creep.

The creep curves for bedded salt loaded perpendicular to stratification are shown in Fig. 2.5. The irradiated salt which received 5×10^8 R had the greatest creep strength, as shown by less creep. When the load was applied parallel to the planes of stratification, the creep curves almost coincide, but the strain is slightly greater for irradiated salt. In the creep tests of dome salt the irradiated material again shows less creep, though the difference is not great.

2.3.3 Anticipated Effects on Waste Disposal

In connection with the program of studies on disposal of calcined radioactive waste solids, calculations have been made of the dose resulting from placing waste "pots" in the floor. Integrated salt doses as high as $5 \times$

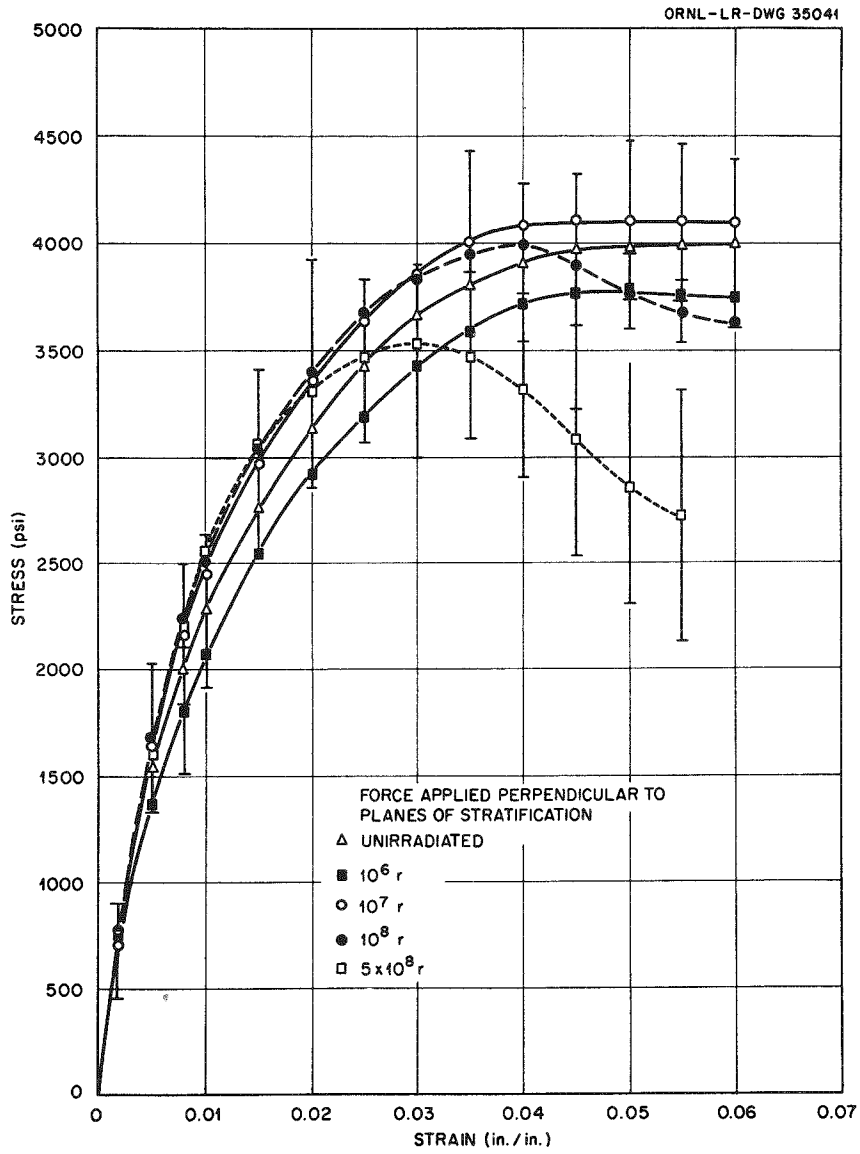


Fig. 2.4. Compression Test of Bedded Salt at Room Temperature.

10^8 rads would not accumulate at distances of more than 1 ft from the waste containers. Since the floor does not have to support the overburden pressure and the dose reaching the pillars is insignificant, radiation would not be expected to affect the structural stability of the rooms.

In addition, many of the physical property changes which take place upon irradiation at ambient temperatures may be partially annealed at the temperatures involved in a waste disposal operation. For example, white crystalline reagent-grade sodium chloride changes color with increased doses of irradiation. At 10^6 rads it is light tan; it progressively deepens to brown and finally to a dark blue-black at about 5×10^8 rads. When salt is irradiated at elevated temperatures, the resultant color depends on which process is faster – the accumulation or the annealing of the color centers. At 160°C, accumulation predominates, and the salt becomes colored; but at 250°C the annealing process predominates, and the salt remains white.

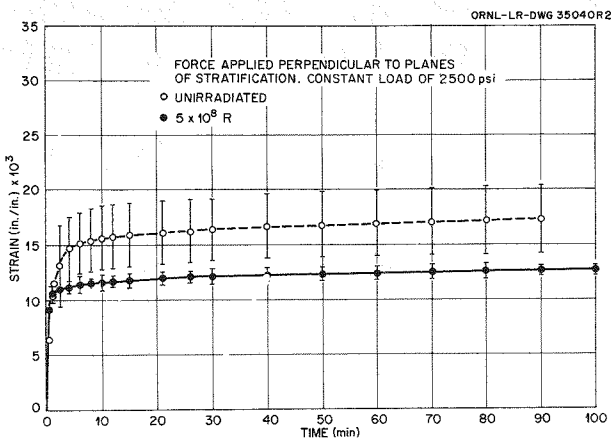


Fig. 2.5. Creep Test of Bedded Salt at Room Temperature.

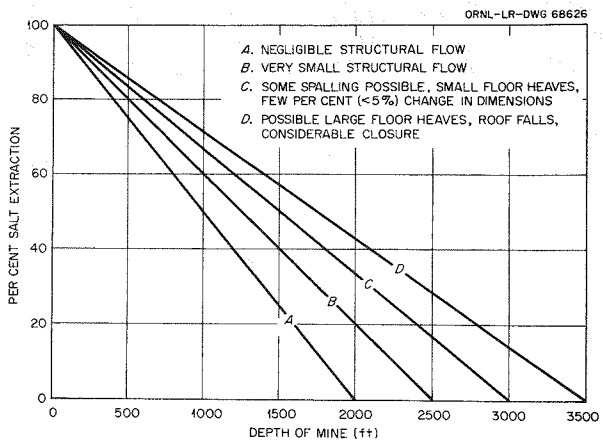


Fig. 2.6. Effect of Percent Salt Extraction and Depth on Structural Stability of Mine Opening.

2.4 GAMMA RADIATION SHIELDING PROPERTIES

Rock salt, with a specific gravity of about 2.16, is equivalent in weight to a light concrete. In addition, the atomic numbers of sodium and chlorine, 11 and 17, respectively, are close to those of the major constituents of concrete. It would thus be anticipated that rock salt should serve as an absorber of gamma radiation essentially as efficiently as concrete of the same density. Two-, four-, and six-inch-thick slabs of concrete (specific gravity, 2.18) and rock salt gave essentially identical shielding factors for the two materials when placed between a radium gamma source and a detector. Since radium emits a broad spectrum of gamma energies, it is felt that this is sufficient confirmation to permit shielding calculations to be based on the well-known properties of concrete.

Calculations have been made which indicate that about 5 ft of solid salt (or 7½ ft of crushed salt, assuming one-third voids) over the tops of the waste containers will provide sufficient shielding to permit unlimited access to a mine room whose floor has been filled with the most radioactive waste solids anticipated in the future.

2.5 MINE STABILITY STUDIES

2.5.1 Ambient Temperature

In the consideration of radioactive waste disposal into salt, it is desirable to be able to predict the allowable salt extraction as a function of depth.

Table 2.4 is a compilation of mine stability data and observations from a number of sources. The structural conditions of the mines (or specific areas in the mines) are described, and pertinent data with regard to depth, extraction, and calculated pillar load are listed. It should be noted that the observations were not all made by the same individual, and criteria may not be the same in every case. The calculated pillar loads are based on 1 psi per foot of overburden.

Figure 2.6 is a generalization based on the data shown in Table 2.4. The designations of the boundary lines are derived from the last column of the table. By use of this figure, the basic criteria for creating waste disposal space, or for mining operations, might be established. For example, if only a negligible amount of structural flow can be tolerated, the maximum allowable pillar load is 2000 psi, and operation to the left of curve A of the figure must be maintained. On the other hand, if some spalling and a few percent closure of the rooms can be tolerated, the pillar load can be increased to 3000 psi, and operation can be anywhere to the left of curve C. In the first case (negligible flow) it may be seen from the figure that the stability criterion cannot be met at depths greater than 2000 ft. It may also be seen that any extraction of salt at depths greater than 3500 ft will produce large structural flows. Also, floor heaves and roof falls are greatly dependent on the presence and exact location of shale bands in the floor and roof.

2.5.2 Effects of Elevated Temperatures

Elevation of the temperature was expected to have considerable effect on the structural flow rate. Based on an extrapolation of such meager laboratory results as existed at that time for elevated temperatures, it was anticipated that creep rates in mine pillars would be

Table 2.4. Salt Structural Stability Conditions in Various Mines

Mine Number	Depth (ft)	Percent Extraction	Room Height (ft)	Calculated Pillar Load (psi)	Structural Conditions
1	990	75	9	4000	Flow reported.
2A	645	80	6–12	3200	Early mining; stable but some spalling.
2B	645	75	12	2600	Current mining; less spalling; approximately 0.5% vertical closure.
3A	1020	75	9–14	4100	Early mining; large floor heaves and roof falls from shale partings.
3B	1020	65	9–14	2900	Approximately 1940; small floor heaves above shale parting.
4A	970	70		3200	Some flow reported.
4B	970	64		2700	No trouble reported.
5	700	estd 77		3000	Vertical closure, 4%.
6	840	75	8–9	3400	Large floor heaves and roof falls from shale parting.
7	1100	65		3100	Generally good; only one small roof fall.
8A	1100	75		4400	Approximately 1920; large floor heaves, roof falls, and heavy spalling.
8B	1050	30–47		1500–2000	Current mining; no spalling or heaving.

accelerated over the ambient temperature rates by a factor of about 4 to 8 at 100°C and by a factor of 30 to 100 at 200°C. However, in most cases, pillars would probably never reach 200°C, and calculations indicate that it would take several years for the temperatures in and under the pillars to approach the maximum values.

2.6 ECONOMICS OF SOLIDS DISPOSAL IN SALT

In order to determine which variables are important contributors to the cost of storage of radioactive solids in salt mines, a preliminary conceptual design was developed and some approximate cost figures calculated.[6] Even though these early cost figures were based on approximate calculations because of the uncertainty of predicting the thermal effects, later calculations generally produced similar results. Although it is out of chronological sequence (the report having been issued after the completion of Project Salt Vault), the results of the later and more accurate study will be reported in this section.[7]

In the conceptual design the waste container shipping cask is removed from a rail car and carried into a hot cell which encloses the top of the waste shaft. Waste containers are then unloaded into a storage area, from which they are lowered down the shaft into a motorized carrier at the working level of the mine. The carrier moves to the current disposal area, lowers the container into a hole in the floor, and backfills the hole with fine crushed salt. Concurrently with this operation, salt is being mined in another corridor.

A mine with gross area of 1 square mile was assumed to be served by one set of shafts and to be developed

[6] R. L. Bradshaw, W. J. Boegly, Jr., F. M. Empson, H. Kubota, F. L. Parker, J. J. Perona, and E. G. Struxness, "Ultimate Storage of High-Level Waste Solids and Liquids in Salt Formations," *Treatment and Storage of High-Level Radioactive Wastes*, International Atomic Energy Agency, Vienna, 1963, pp. 153–75.

[7] R. L. Bradshaw, J. O. Blomeke, J. J. Perona, and W. J. Boegly, Jr., *Evaluation of Ultimate Disposal Methods for Liquid and Solid Radioactive Wastes: VI. Disposal of Solid Wastes in Salt Formations*, ORNL-3358 (Rev) (March 1969).

one quadrant at a time. The operation would be conducted so that the salt mining was completely isolated from the disposal operations. Disposal operations personnel and equipment would use the mining shaft for ingress and egress, however.

Ventilating air would come down a compartment in the mining shaft, a portion being split off into the disposal tunnel. The disposal tunnel air would travel completely around the quadrant and exit up the waste shaft. The air would be drawn from the shaft, through the hot cell, through an absolute filter, and up a 200-ft stack.

The disposal operations would start at the most remote point of each quadrant and work back toward the shaft in order to assure that ventilating air would never pass a filled storage area before it reached the current working area. The criteria of isolation and ventilation require that a double tunnel be driven completely around the quadrant and that the initial row of rooms be excavated before disposal operations start.

The net yearly space requirements were calculated for storage of various waste combinations for a 15,000-MW(e) nuclear power economy (a level which should be reached by the early 1970's). The gross requirements are dependent on the allowable salt extraction for a specified stability condition. If no fission product heat were involved, then the extraction as a function of depth based on observations of existing mines would be adequate. With the presence of heat, the dimensional changes of the rooms due to thermal expansion and plastic flow must also be considered.

Cost figures were calculated for disposal at a depth of 1000 ft. The life of the mine was found to range from about 12½ years for wastes aged 1 year at the time of burial to about 70 years for wastes aged 30 years at burial. Total costs ranged from 3×10^{-3} mill/kWhr(e) with 30-year-cooled wastes to 19×10^{-3} mill/kWhr(e) for 1-year-cooled wastes (using present worth considerations at 4% interest). The cost of removal of salt was 50 to 80% of the total costs. Of the remaining costs, only operating costs appeared to be appreciably more important than the others.

2.7 SUMMARY AND CONCLUSIONS

The following major conclusions were drawn from the studies discussed in this chapter.

1. In situ heat transfer properties of rock salt are sufficiently close to the values determined in the laboratory that confidence can be placed in theoretical heat transfer calculations.
2. Most bedded salt contains trapped moisture which is released at temperatures above about 250°C.
3. Radiation exposure doses of 5×10^{8} R produce some change in structural properties, but the effect on mine stability should be negligible.
4. Rock salt is approximately equivalent to concrete as a gamma radiation shield.
5. Stability of a waste disposal mine at ambient temperature can be predicted from observed conditions in existing salt mines.
6. Elevated temperatures will cause accelerated creep, but the exact effects on structural stability could not yet be predicted accurately.
7. Preliminary estimates of the cost of a large-scale disposal operation in salt [about 0.01 mill/kWhr(e)] show that such an operation is economically compatible with competitive nuclear power.

3. Preliminary Design of Experiment

R. L. Bradshaw

3.1 OBJECTIVES AND GENERAL DESCRIPTION

The engineering and scientific objectives of Project Salt Vault were:[1] (1) demonstration of waste-handling equipment and techniques; (2) determination of possible gross effects of radiation (up to 10^9 rads) on hole closure, floor uplift, salt-shattering temperature, etc., in an area where salt temperatures were in the range of 100 to 200°C; (3) determination of possible radiolytic production of chlorine; and (4) collection of information on creep and plastic flow of salt at elevated temperatures which could be used later in the design of an actual disposal facility.

The demonstration was carried out in the Lyons, Kansas, mine of the Carey Salt Company using 14 irradiated Engineering Test Reactor (ETR) fuel assemblies contained in seven cans. These cans were placed in a circular array of holes in the floor with one can in the center and the other six cans located peripherally on 5-ft centers. To increase the radiation dose received by the salt, the assemblies were exchanged for freshly irradiated assemblies at six-month intervals over the course of two years. All fuel assemblies were returned to the Idaho Chemical Processing Plant (ICPP) for recovery of the unfissioned fuel.

An identical array using electrical heaters only was operated as a control to determine the combined effect of radiation and heat on the salt characteristics. In addition, one rib pillar was heated with a number of electrical heaters placed in the floor around its base to yield information on the creep and plastic flow of salt at elevated temperatures.

A schematic cross section of the demonstration is shown in Fig. 3.1, and the plan of the demonstration site is shown in Fig. 3.2. As originally conceived,[1] the assemblies, after canning in Idaho, would be shipped by rail in an existing cask, especially modified for this purpose. At Lyons the cask would be removed from a rail car standing on an existing spur and upended over a cased vertical shaft extending to the mine working area, approximately 1000 ft below. The assemblies would be lowered one at a time through the shaft and into a movable shielded cask mounted on a fuel assembly transporter. The transporter would move to the experimental area, where the cask would be positioned and lowered over the designated hole in the floor of the mine. The can would then be lowered through the bottom of the cask into place. The holes, approximately 10 in. in diameter by 12 ft deep, would have suitable liners. Lead or uranium shields placed in the top of the holes would serve as biological shielding while the cans were in place.

To meet the objectives of the experiment, it was necessary to expose a reasonably large mass of salt to radiation dosages and temperatures comparable with those anticipated in an actual disposal operation. The particular geometrical configuration chosen for this experiment would expose a circular area about 12 to 14 ft in diameter to the desired temperatures and radiation dosages. The 5-ft spacing is about as small as will likely be used in an actual disposal operation, and the dose midway between any two containers will be due almost entirely to those two containers. An outer ring of 12 additional cans would, of course, increase the area affected; however, the benefits to be gained from a larger test were not believed to justify the added expense and complexity.

3.2 SELECTION OF MINE AND RADIATION SOURCE

Several alternative sites considered for the operation of the demonstration were the Project Gnome site in

[1] R. L. Bradshaw, J. J. Perona, and J. O. Blomeke, *Demonstration Disposal of High Level Radioactive Solids in Lyons, Kansas, Salt Mines: Background and Preliminary Design of Experimental Aspects*, ORNL-TM-734 (Jan. 10, 1964).

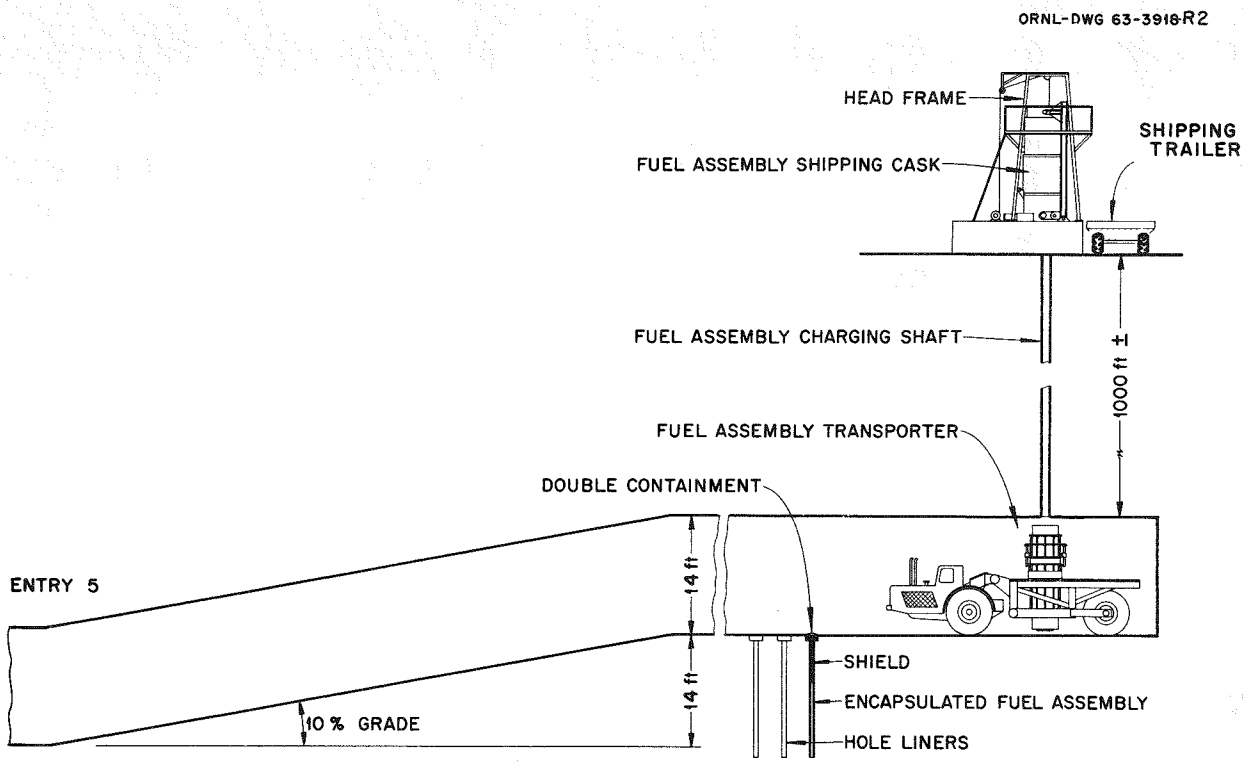


Fig. 3.1. Schematic Cross Section of Demonstration.

New Mexico, the Hutchinson Naval Air Station, and the Carey Salt Company's Hutchinson mine.

The Hutchinson mine was ruled out by the Carey Company. The Naval Air Station was ruled out by the fact that the use of this site would require the development of a complete mine installation, including a shaft and hoisting equipment.

The Gnome site had the advantages of being located on Government-owned land and having mine space available for immediate use. The disadvantages of the Gnome site were the very poor quality of the salt, so that it would not be representative of the salt formations which most likely would be used as a permanent facility, its inconvenience with regard to transportation facilities, and possible conflicts in schedule with the Plowshare program. The remoteness of the Gnome site was both an advantage and a disadvantage.

The Lyons mine has the advantages of location, rail connections, and favorable public relations background at both state and local levels.

The decision to use irradiated reactor fuel assemblies in this experiment, rather than actual calcined wastes or separated fission product sources, was based on considerations of availability, cost, and radiation characteristics. Selection of the ETR fuel was made from considerations of the operating cycle of the reactor, the number of assemblies which would be required to charge seven holes in the demonstration, and the dimensions of the assemblies. From the standpoint of allowable element temperature, power reactor elements would have been preferable, but uncertainties in availability led to the selection of the ETR fuel assembly as the best overall choice.

The fluidized-bed waste calciner facility (WCF) at the National Reactor Testing Station (NRTS) was considered and ruled out as a source of waste for the test. Operation of the WCF with radioactive waste was expected to begin the latter part of 1963, and possibly by the end of 1964 the systems could have been debugged and flushed out with the hottest waste (200-day decayed) which the plant is designed to handle. By the time the waste could be canned and placed in the mine, it would have decayed about one year. A 6-in. by 6-ft-long cylinder of WCF waste would have a heat generation rate of about 140 W at one year's decay and 41 W at two years' decay. This compares with 750 W at 90 days and 74 W at $1\frac{1}{4}$ years for two ETR assemblies in a 5-in. cylinder about 7 ft long. In addition to the fact that the WCF waste would result in lower dose rates than ETR assemblies, there

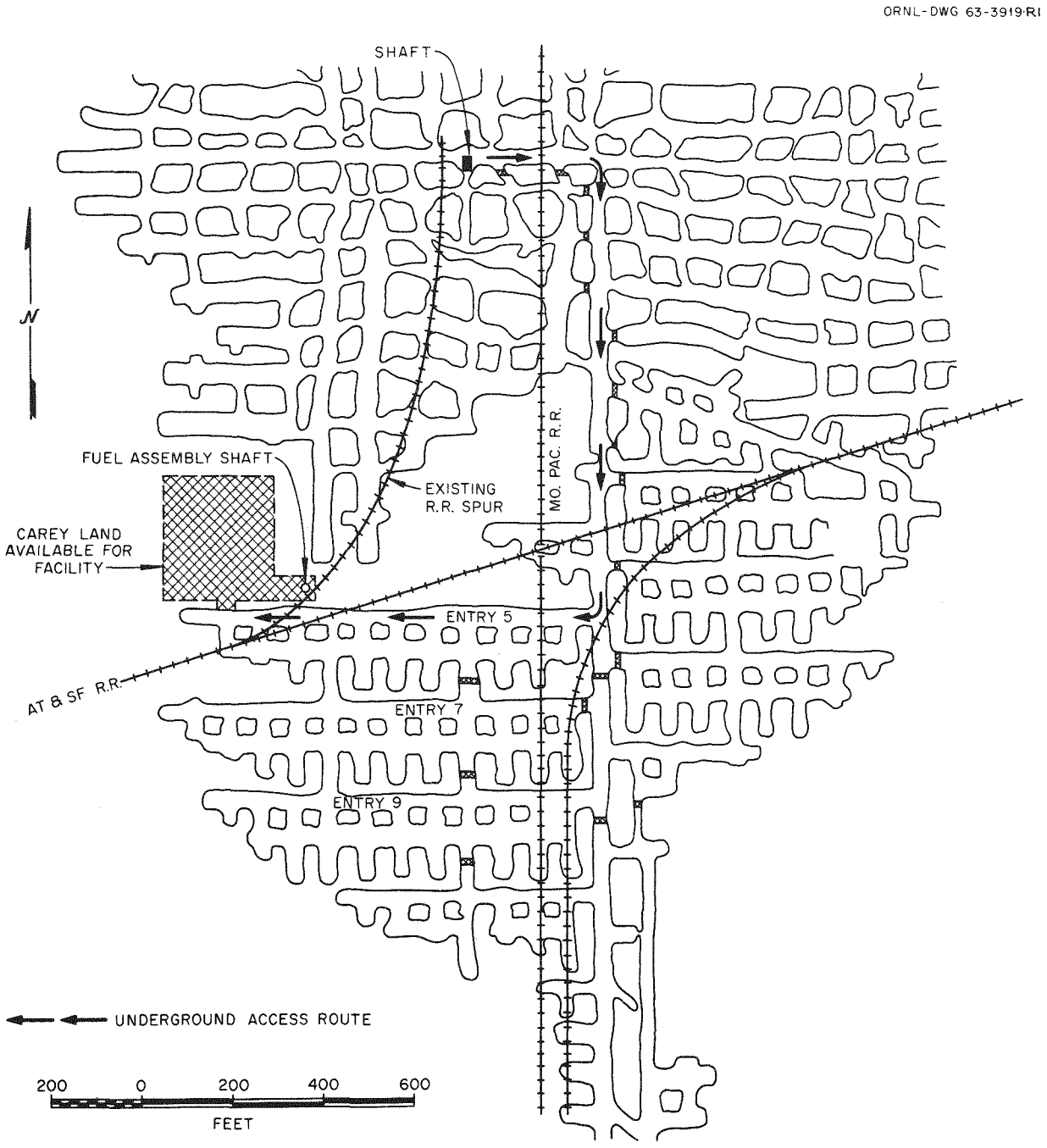


Fig. 3.2. Demonstration Site in Newly Mined Area, Lyons, Kansas.

was no hot-cell facility available at the WCF to fill the cans.

Cylinders of solidified waste from the pilot plant at Hanford were ruled out, primarily on the basis of the projected schedule. It seemed probable that the first seven pots would not have been produced before January 1967, and these pots might not be available for experimental storage in any event. The heat generation rate of a 6-in. pot filled to a level of 6 ft was expected to be about 810 W at one year's decay and 260 W at two years' decay.

Of the power reactor fuel assemblies, the Yankee Atomic appeared to be the most favorable, except for its dimensions. The overall assembly dimensions are about 11 in. across the diagonal by 12 ft long. The heat generation rate of an assembly would be about 1070 W at six months' decay (about the earliest that it could be canned and moved to the mine), 470 W at one year, and 175 W at two years. However, the uncertainty of availability of enough assemblies to fill seven cans from any given power reactor within any given time period, coupled with the fact that hot-cell facilities for canning were not generally available at the reactor, led to the elimination of power reactor fuel assemblies.

The use of various isotopes was ruled out on the basis that they did not appear to offer any appreciable cost advantages and they had the disadvantage of not presenting the wide gamma energy spectrum which could be obtained with fuel assemblies. For example, to obtain the same peak gamma dose to the salt as would be obtained from the ETR assemblies (assuming four sets of assemblies during the two-year period) would require about 200,000 Ci of ^{60}Co. The projected inventory price (the price to AEC users) of ^{60}Co by the end of 1964 was expected to be about \$0.40 to \$0.60 per curie, or about \$100,000 for 200,000 Ci.[2] However, as the design of the handling equipment and fuel assembly containers proceeded, it became apparent that there could be a number of problems incidental to use of the assemblies which might be simplified or eliminated by the use of ^{60}Co. Consequently, ^{60}Co was considered as a possible attractive alternative should later complications in the use of fuel assemblies develop.

The ETR had an average thermal flux of about 1.5×10^{14} and a cycle time of about six weeks. A typical reactor cycle might average about 20 full-power days out of 23 operating days, followed by a one- to three-week shutdown for reloading, etc. Thus it was possible to obtain assemblies at almost any time desired. The dimensions of the assembly were also convenient (3 in. square by 36 in. long), and the only major disadvantage (one which it shared with most test reactors) was that it was relatively low-melting aluminum-base fuel.

If the fuel assembly temperature was to be kept below 900°F (melting point of aluminum is 1220°F), the earliest that the assembly could be canned would be about 60 days out of the reactor, as explained further in the next section. This meant that it would be 90 days decayed before it was placed in the salt mine.

3.3 CALCULATION OF FUEL ASSEMBLY TEMPERATURES

3.3.1 In the Hot Cell

The system consists of two ETR fuel assemblies in a 5-in.-OD stainless steel pipe sealed at the ends. The heat generated in the fuel is transmitted to the pipe wall and then to the ambient air in the hot cell. The heat flux through the pipe surface as a function of time since reactor discharge was as follows:

Time (days)	Flux (Btu hr^{-1} ft^{-2})
7	3250
20	1610
45	737
90	325

These fluxes were obtained using the heat generation rate curve in Fig. 3.3. (For comparison purposes, a heat generation curve is also shown for a hypothetical 6-in. acid Purex calciner pot ca. 1975.) Calculated fuel assembly temperatures varied from 1740°F at 7 days to 650°F at 90 days (Fig. 3.4). The earliest age for canning with a reasonable margin of safety appeared to be about 60 days, when the fuel assembly temperature would reach 850°F and the can surface 300°F.

Can temperatures were calculated using combined convection and radiation heat transfer coefficients for steel pipe.[3] Combined coefficients ranged from 5.70 to 2.35 Btu hr^{-1} ft^{-2} $°F^{-1}$ as the pipe temperatures varied from 665 to 220°F.

Temperature differences between the fuel assembly surface and the can wall were calculated using emissivities of 0.1 for the aluminum fuel assembly and 0.55 for the stainless steel can, which gave an *F*-factor of

[2] F. N. Case, Isotopes Division, personal communication, May 16, 1964.

[3] W. H. McAdams, *Heat Transmission*, 3d ed., Table 7.2, p. 179, McGraw-Hill, New York, 1954.

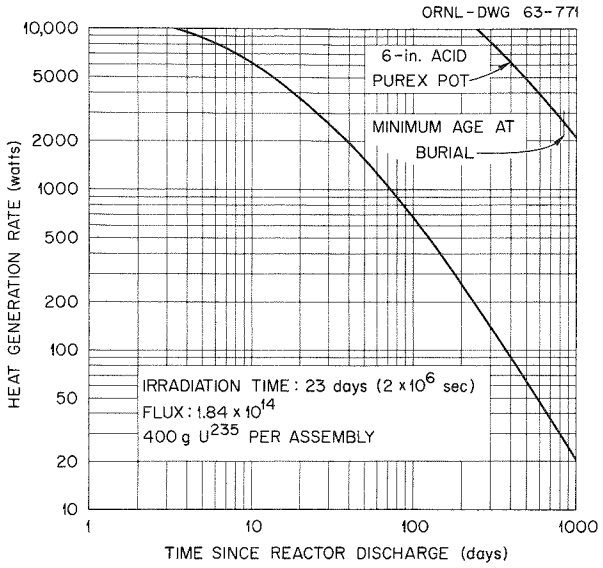


Fig. 3.3. Heat Generation for Stack of Two ETR Assemblies.

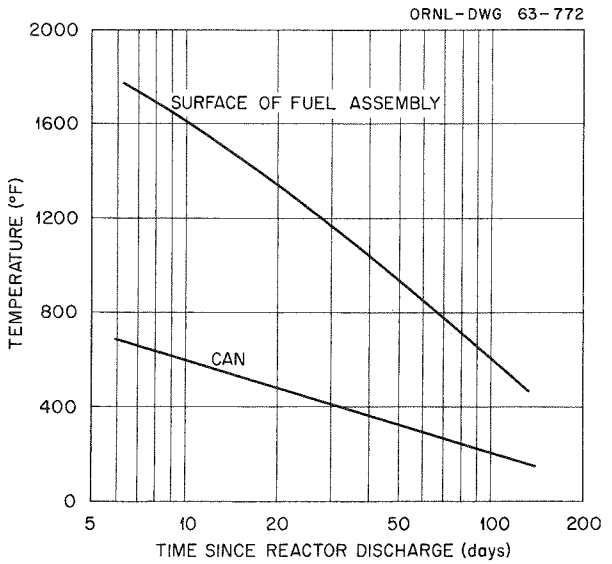


Fig. 3.4. ETR Fuel Assembly Temperatures in Hot Cell.

0.095. Convection coefficients for the enclosed air layer were calculated using a plot[4] of the ratio of a combined convection and conduction coefficient to the conduction coefficient as a function of the Grashof number. Heat fluxes between the fuel assembly and the can (based on the fuel assembly surface area of 3.0 ft^2) are listed as follows:

[4]M. Jakob, *Heat Transfer*, p. 538, Wiley, New York, 1949.

Time Since Reactor Discharge (days)	Fuel Assembly Temperature (°F)	Radiant Heat Flux (Btu hr^{-1} ft^{-2})	Convection and Conduction Flux (Btu hr^{-1} ft^{-2})
7	1740	3530	724
20	1350	1590	520
45	970	609	351
90	650	218	207

Temperature gradients through the fuel assembly would be negligible (on the order of 10°F difference between interior and exterior plates), because of the excellent thermal conductivity and adequate cross-sectional area available for conduction to the side plates.

3.3.2 In the Shipping Cask

If the first fuel assembly was canned at 60 days, the seven cans could be ready for shipping 75 days after reactor discharge. The system would then consist of a canned fuel assembly in a tube surrounded by water at 100°F. (The shipping cask was water cooled with forced circulation.) The gap between the can wall and the cask tube wall was assumed to be about ¼ in. Both the can and tube were stainless steel with emissivities of 0.55, giving an F factor for radiant heat transfer of 0.38. Conduction, convection, and radiation were taken into account through this second air gap using the same methods as before. The calculated temperatures were:

	Temperature (°F)	Radiant Flux (Btu hr^{-1} ft^{-2})	Convection and Conduction Flux (Btu hr^{-1} ft^{-2})
Cask tube	100		
Can	345	200	213
Fuel assembly surface	810	352	189

At 75 days the heat generated in the cask from the 14 fuel assemblies would be about 22,600 Btu/hr. If the water coolant would undergo a 20°F temperature rise in passing through the cask, a flow rate of 2.2 gpm would be sufficient. The water inventory in the cask would weigh about 200 lb and the lead about 20 tons, so that if circulation stopped, the water would be heated to the boiling point in about 2 to 4 hr, and about 10 hr would be required to evaporate the water.

3.3.3 In the Salt Mine

It was thought that the shielding on the transporter in the mine might be made of lead shot, resulting in a

shield with a thermal conductivity poorer by a factor of 75 than solid lead.[5] Although the heat capacity of the cask would prevent melting of the lead for 10 to 20 hr, a cooling system would be desirable if lead shot were to be used.

The fuel assembly can would be lowered into a hole in the floor of the mine containing a second or outer can to keep the salt from freezing the inner can in the hole. The outer can (stainless steel) would have heaters attached to permit more heat to be transferred to the salt than was emitted by the fuel alone. For temperature calculations the outer can was assumed to have an outside diameter of 6.25 in. and the hole in salt a diameter of 10 in.

If the shipping cask could be loaded at 75 days, the cylinders would be in place in the mine 90 days after reactor discharge. The emissivity of the salt was taken to be 0.9, giving an F factor for the last air gap of 0.41. Calculated temperatures and heat fluxes, assuming 1600 W total heat generation rate per can (both decay and electrical heat), were as follows:

	Temperature (°F)	Radiant Flux (Btu hr^{-1} ft^{-2})	Convection and Conduction Flux (Btu hr^{-1} ft^{-2})
Salt	400 (assumed)	312	36
Outer can	540		
Inner can	625	258	67
Fuel assembly surfaces	875	295	132

It thus appeared that the fuel assemblies could be canned at 60 days decay, shipped at 75 days, and placed in the mine at 90 days without exceeding a temperature of 900°F in the assembly.

3.4 RADIATION DOSE CALCULATIONS

The final radiation dose calculations could not be made until the irradiation history of the actual assemblies was known; but, based on preliminary calculations, it appeared that the peak radiation dose to the salt with two 90-day-decayed ETR assemblies in a can would be about 3×10^8 rads, accumulated over a two-year period. Since laboratory tests had indicated little change in physical properties at 10^8 rads but a significant (about 10%) drop in compressive strength at 5×10^8 rads, it was desirable to achieve radiation doses near 10^9 rads in this experiment, if practical. Changing the assemblies three times during the course of the two-year test (four sets of assemblies, total) would increase the peak dose to about 8×10^8 rads. At the same time this would give additional experience with the operation of the handling equipment.

These preliminary calculations were made with a shielding code on an IBM-7090 computer.[6] No mass attenuation coefficients, energy absorption coefficients, or buildup factors were available for salt, but since its density (135 lb/ft^3) is about the same as that of concrete, it was believed that the shielding and energy absorption properties would be about the same as concrete. Thus concrete was assumed as the medium in the dose calculations. The shielding code also gave dose rates in units of rems per hour, but since the energy absorption coefficients in tissue for gamma energies from 0.15 to 3 MeV are within 10% of those for concrete, it was believed that the calculations were sufficiently accurate.

Figure 3.5 shows the radiation dose expected during the two-year period from the ETR assemblies if placed in the mine after 90 days' decay (curve A) and from changeout of four sets of 90-day-decayed assemblies (curve B). Shown for comparison is the radiation dose which might be expected from a 6-in.-diam by 10-ft-long pot calciner cylinder containing a hypothetical acid Purex waste of the future. Curve C is the radiation dose from the calciner pot which would be accumulated in a two-year period following burial at the earliest possible age (2.3 years). Curve D shows the radiation dose which would accumulate over a period of 286 years. (After 300 years, little additional radiation dose would accumulate.) It should be pointed out that the assumed Purex waste was from fuel with a burnup of 10,000 MWd per metric ton of 2%-enriched uranium and was considerably "hotter" than any being produced currently. (The calciner cylinder would contain about 15 kg of fission products, while the two ETR assemblies, with about 15% burnup of 93%-enriched uranium, would only contain about 0.12 kg.) The hypothetical Purex pot at two years' decay was about an order of magnitude hotter than anticipated in a two-year-decayed pot from the ORNL pot calciner pilot plant at Hanford.

From curve B in Fig. 3.5 it may be seen that, at distances of more than a foot from the fuel assembly

[5] W. H. McAdams, *Heat Transmission*, 3d ed., p. 290, McGraw-Hill, New York, 1954.

[6] E. D. Arnold and B. F. Maskewitz, *SDC: A Shielding Design Code for Fuel Handling Facilities*, ORNL-TM-124 (Jan. 25, 1962).

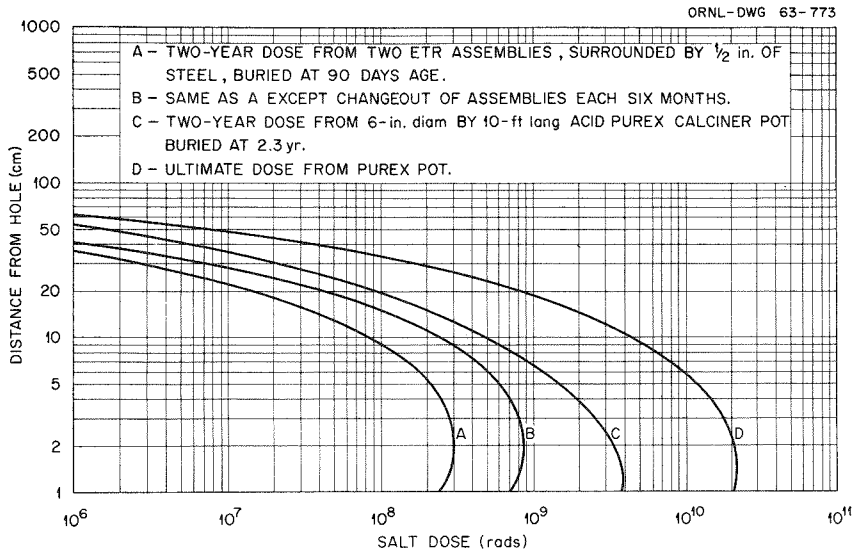


Fig. 3.5. Estimated Radiation Dose to Salt from ETR Assemblies and Acid Purex Calciner Pot.

cans, the dose accumulated over the two-year period would be less than 10^7 rads. Since the cans are spaced 5 ft on centers, the contributions from the other six cans to the dose near any one can will be negligible. Isodose surfaces in the regions of accumulated dose greater than 10^6 rads are thus essentially circular cylinders around the individual fuel assembly cans.

Calculations for a 50-ft-wide room full of 6-in.-diam calciner pots of acid Purex waste, spaced 5 ft on centers, have indicated that the radiation dose in air at the center of the room would be less than 0.3 mR/hr if there is 6 ft of solid salt above the pots. Thus with the fuel assemblies (which are less radioactive) it would only be necessary to provide shielding in and near the top of the holes to keep personnel exposure levels within acceptable limits.

3.5 EXPERIMENTAL LAYOUT IN MINE

3.5.1 Consideration of Use of Existing Mine Space

From the standpoint of the economics of an actual disposal operation in an abandoned mine, it would probably be cheaper to use existing mine space for the disposal of the waste, rather than using it to store excess salt, *provided it could be shown that the use of existing space for disposal did not significantly reduce the safety of the operation.* At the time of this consideration it was not possible to predict the structural safety of a mine in general, or the Lyons mine in particular, under temperature conditions which would prevail in a disposal operation. Further, in the Lyons mine, and in practically all existing bedded salt mines, there is considerable shale (containing a few percent water) in the floor. All available corrosion data indicated that stainless steel waste containers would corrode rapidly in the presence of salt and water, possibly to failure in a matter of a few months. It was also reasonably certain, on the basis of existing experimental data, that water from the shale would migrate to the surface of the floor,[7] and that, possibly, this water which had been in contact with the corroded waste cans would contain some radioactivity.

In an actual operation in an existing mine floor it may be possible to cope with mine instability and water problems, but at the time it was not apparent what measures would have to be taken and, thus, what cost should be assessed for such measures.

If the fuel assembly demonstration were run in the existing floor of the Lyons mine, some information could be obtained on the behavior of such an area for possible use as a disposal operation. However, to get definitive information would require significant heating of at least one pillar, and, in view of the structural instabilities which were already manifest in this mine, the primary objectives of the demonstration could be jeopardized. Some information could be gained, of course, on the migration of shale-borne water, but

[7] F. L. Parker and R. E. Blanco, *Waste Treatment and Disposal Progress Report for November-December 1962, and January 1963*, ORNL-TM-516, p. 96 (June 12, 1963).

migration of such water to the floor surface had already been domonstrated in electrical-heater tests in the Hutchinson mine.[7]

Another consideration involved was the choice of the particular mining pattern in the existing mine. The major portion of the mined area, while generally similar to the modified-checkerboard pattern common in current practice, had no repeating pattern; thus, it would be difficult to say that one had chosen a representative area in which to run the demonstration.

It was thus concluded that the demonstration should be run in the periphery of the mine, with the fuel cans located in the relatively pure salt stratum which was originally mined, thus minimizing the water problem and also allowing use of the most desirable experimental layout.

3.5.2 Alternative Layouts in Specially Mined Areas

Since the demonstration array of seven fuel assembly cans was to be operated in the floor, where stresses due to mining (and thus salt flow) are minimum, the possibility of introducing stresses in the vicinity of the array using flat jacks installed in the floor around the array or by jacking between floor and ceiling was considered. It was concluded that this method would not produce data which could be interpreted in terms of conditions which might exist in an actual operation.

An experimental pattern was considered in which a central square pillar would be surrounded by four heated arrays (the radioactive array, the nonradioactive duplicate array, and two simple heater arrays) and four additional square pillars (plan I).[1] This pattern would yield information on both primary (radiation) and secondary (salt flow) objectives but had the disadvantage that salt flows could be of such nature and magnitude as to jeopardize the primary objectives by forcing the premature removal of the fuel assemblies.

A second pattern (plan II),[1] consisting of a single rib pillar with the radioactive and duplicate arrays adjacent, was considered. This pattern would minimize the possibility of interference with the changeout of the fuel assemblies but would not be likely to yield much information on salt flow.

3.5.3 Layout Selected for the Test

A third plan (plan III) was finally chosen which incorporated the best features of plans I and II and eliminated most of their disadvantages (Fig. 3.6). In this plan there would be four rooms, two 30 ft wide and two 40 ft wide. All rooms would be 60 ft long and connected by a corridor. The center pillar would be 20 ft wide and the other two would be 30 ft wide.

If the 30-ft rooms and pillars were a repeating pattern, the extraction ratio would be 50%; and if the 40-ft rooms and 20-ft pillars were repeating, the extraction would be 67%. With these extraction ratios at ambient temperature, the end rooms should show negligible salt flow and the center rooms should not show enough flow to produce roof falls or noticeable floor heaves.

The radioactive and duplicate arrays would be contained in the end rooms, and the center pillar would be heated by means of 22 heaters. The calculated temperature-rise pattern in the floor at the heater center plane (9 ft below floor level) after about 1½ years' operation (12,800 hr) of the 22 heaters (1546 W per heater) is shown in Fig. 3.7 (the calculation assumes an infinite salt medium). It may be noted that the major portion of the pillar base would experience temperature rises in excess of 70°C. It may also be seen that the temperature rise in the center of the floor in the end rooms would be negligible, and thus the heating of the center pillars should not have any thermal effect on the radioactive and duplicate arrays. These arrays, however,

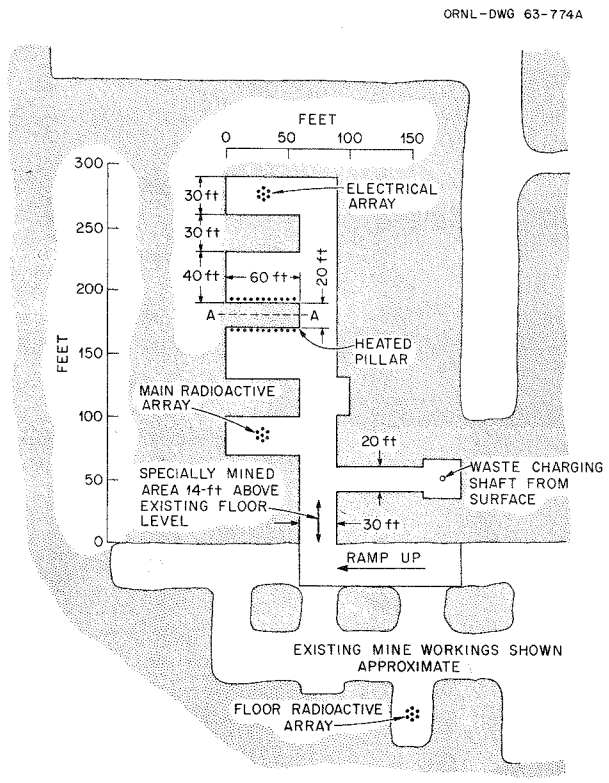


Fig. 3.6. Proposed Layout for Hot Demonstration Area Room and Pillar Pattern, Plan III.

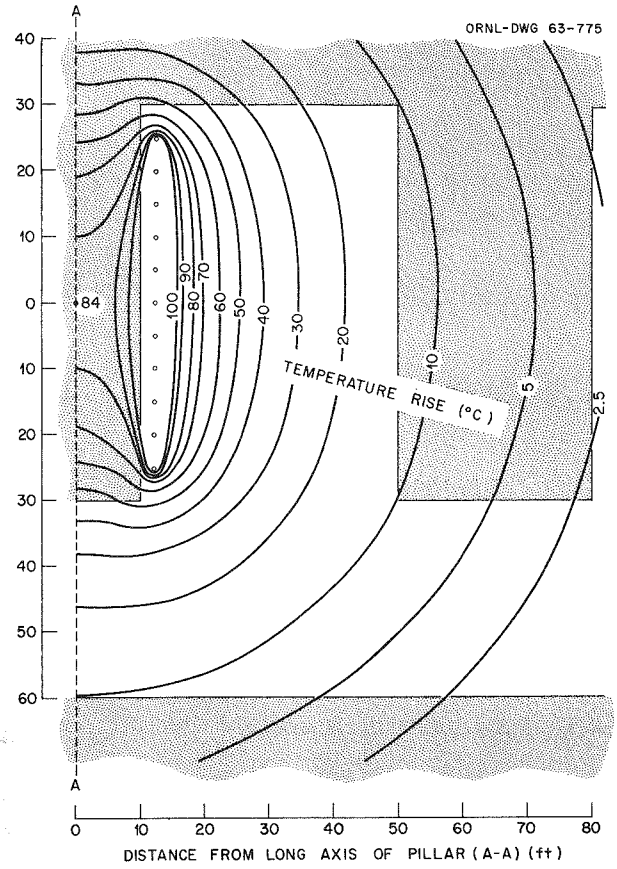


Fig. 3.7. Nine Feet Below Floor Level; Temperature Rise Isotherms After 1½ Years' Operation of 22 Heaters at Base of Pillar (1546 W per Heater), Plan III.

would contribute to heating of the two 30-ft-wide pillars.

The power supply and heaters for the center pillar would be designed so that the heat input could be doubled, thus doubling the center-pillar temperature rises, if desired.

The advantages of this plan over either of the previous plans were: (1) The area containing the fuel assemblies should be relatively stable even if considerable flow and/or roof falls took place in and around the center pillar (thus changeout of the fuel assemblies would not be interfered with). (2) One pillar could be heated sufficiently to produce significant load transfer and salt flows. (3) The mining pattern is essentially that envisioned for a disposal facility in which space is created specifically for waste storage, and thus the flows and load transfers, and the rates at which they take place, would be useful empirical information in the design of a production facility.

Figure 3.6 also shows a third seven-can heater array which was to be installed in the existing floor of the mine. The fuel assemblies which would be removed from the main test array at the end of each six-month period would be placed in this array so that a radiation dose of the order of 10^8 rads could be delivered to the salt-shale mixture in the floor. In this way the possibility of using existing mine space rather than new excavations for waste disposal could be investigated.

3.6 SALT TEMPERATURE PATTERNS IN ARRAYS

Based on an examination of the apparent thermal properties of salt as determined from the liquid cavity and cylindrical heater tests, it appeared that theoretical calculations based on the 100°C properties should be sufficiently accurate for use in the design of the experiment. In regions where the temperature is of the order of 200°C, the theoretical predictions were expected to be around 10% low, and for regions of temperatures well below 100°C, the predictions may be high.

A peak salt temperature of 200°C has been used as the limiting temperature in the study of the economics of salt disposal. This value is well below the point at which shattering of the salt has been found to take place (see Sect. 2.2). Since the amount of salt which must be mined is a direct function of the peak allowable temperature, 200°C would appear to be a logical peak salt temperature.

Calculations were made assuming seven heat sources, 6 ft long, arranged in a hexagonal array with 5-ft-on-centers spacing of the sources. Thermal conductivity and diffusivity of salt at 100°C were used.[8] Constant heat generation rate was assumed, and it was found that the salt temperature rise at the periphery of the center heater hole will be within 95% of the steady-state value after 12,800 hr (about 1½ years). No allowance was made for the fact that salt has been removed to create the rooms.

In order to achieve 180°C rise after 1½ years' operation of the heaters, it was found that the heat generation rate should be 1546 W per heater. Figure 3.8 shows the temperature rise curves for the horizontal planes at the center of the heaters and 6, 12, and 18 ft from the ends of the heaters. The curves are for radials running out between two peripheral heaters and thus correspond to minimum temperature curves. A radial running through the center of a peripheral heater would

[8] Francis Birch and H. Clark, "The Thermal Conductivity of Rocks and Its Dependence on Temperature and Composition," *Am. J. Sci.* **238**, 529–58, 613–35 (1940).

show a discontinuity at 5 ft from the center of the array and would be somewhat higher in temperature from about 3 ft on out to 10 or 15 ft.

The vertical cross section through the center of the seven-can array is shown in Fig. 3.9, along with the temperature contours after 1½ years' operation.

Figure 3.10 shows a plan view with temperature contours at a depth of 9 ft below the floor (midplane of the array). The isotherms are shown as circles in this figure, but there would actually be some ripples on the contours as they pass peripheral heaters.

Figure 3.11 shows isotherms at floor level for the same conditions as Fig. 3.10.

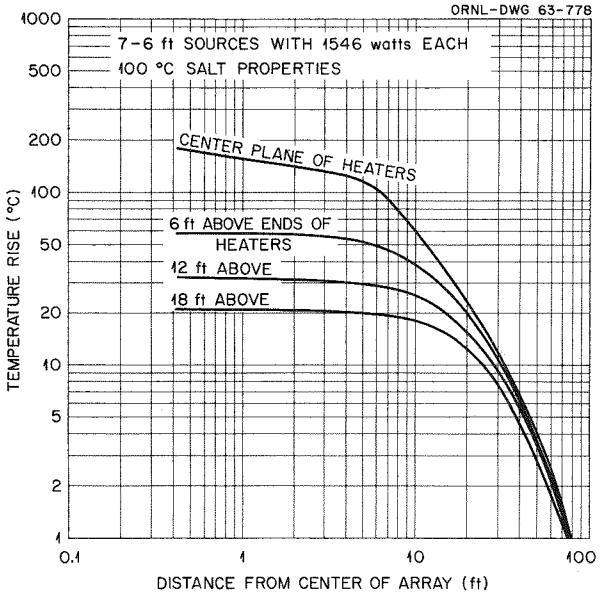


Fig. 3.8. Temperature Rise Profile in Demonstration Array Along Radial Between Peripheral Heaters After 1½ Years.

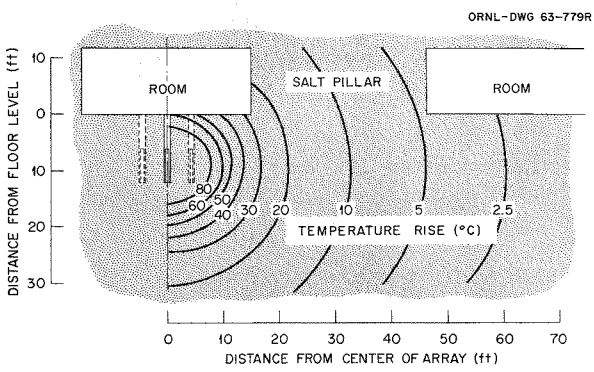


Fig. 3.9. Temperature Rise Isotherms After 1½ Years' Operation of One Array (Seven Cans, 1546 W per Can, 100°C Thermal Properties of Salt). Vertical cross section.

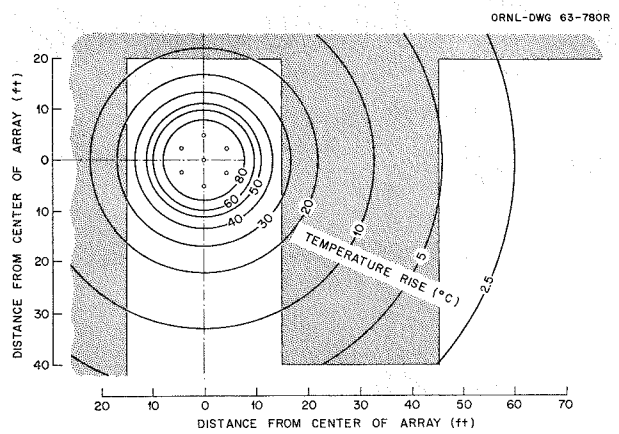


Fig. 3.10. Nine Feet Below Floor Level; Temperature Rise Isotherms After 1½ Years' Operation of One Array (Seven Cans, 1546 W per Can, 100°C Thermal Properties of Salt).

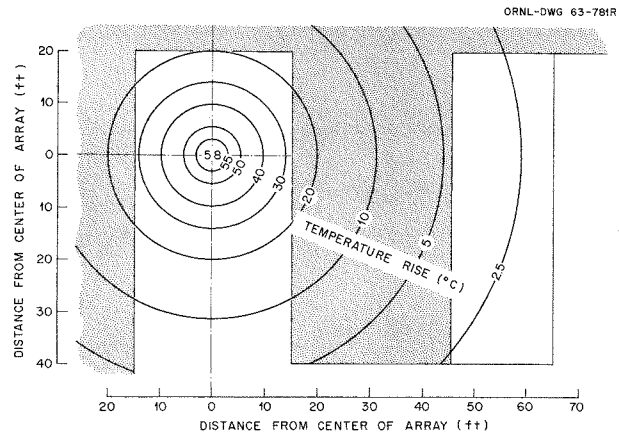


Fig. 3.11. Floor Level Temperature Rise Isotherms After 1½ Years' Operation of One Array (Seven Cans, 1546 W per Can, 100°C Thermal Properties of Salt).

3.7 EXPERIMENTAL INSTRUMENTATION

Details of the instrumentation were not completely worked out, but experimental measurements which were to be made included salt temperatures, salt radiation dose, radiolytic gas production, thermal expansions of floor and pillars, and stress and stress changes in pillars and other parts of the formation.

It appeared desirable to have a total of about 400 thermocouples, based on 13 thermocouple holes each containing 5 thermocouples located in and around each of the seven-can arrays plus 40 thermocouple holes associated with the center pillar. These 40 holes would be located in the center pillar, in the floor around and beneath the pillar, and in the formation at the back of the room.

The method for measuring radiation dose had not been selected, but chemical dosimeters appeared to have certain advantages. Several measuring points in the salt would be required.

Theoretically, it was possible that some radiolytically produced chlorine could be released into the array holes, although laboratory results indicated that the amount would be very small. Thus it was planned to sample and analyze the gas from the annulus between the salt and the outer can in some of the radioactive array holes. Gas from some of the holes in the duplicate array would also be sampled as a control.

Thermal expansion of the floor in and near the arrays would be measured by means of leveling points related to a bench mark located elsewhere in the mine. Floor-to-ceiling movement would be measured by a portable strain gage. In addition, thermal expansion, along with creep and plastic flow of the pillars, floor, roof, and end walls, would be measured by both surface and internal strain gages. These gages would be installed as soon as possible after excavation so that background creep rates could be obtained. A first approximation of the number of strain gages required was 300 external and 150 internal gages.

Stress meters were being investigated, and, if relatively cheap gages proved to be suitable, probably 100 or more would be installed. In any event, it was anticipated that some stress determinations would be made before and during the course of the experiment so that the flow data could be more readily interpreted.

The holes in both radioactive and duplicate arrays would have an annulus between the outer can (hole liner) and the salt wall. The annulus would be left free so that comparative measurements of hole closure could be made between the radioactive and duplicate arrays and so that salt shattering could be detected, should it occur. Also, this annulus would ensure that the salt could not flow against the liner and possibly freeze the fuel assembly cans in place.

3.8 CONCLUSIONS

Project Salt Vault was part of the development program designed to determine the requirements for safe and economical disposal of radioactive wastes in rock salt formations. The salt flow data obtained in this demonstration experiment, when combined with the results of theoretical work and model studies on the structural stability of rock salt at elevated temperature and pressure, should provide the technical basis for the design of an actual disposal facility.

4. Field and Laboratory Studies Preliminary to Project Salt Vault

R. L. Bradshaw

Several studies which were pertinent to the demonstration were either already under way prior to, or were initiated and run concurrently with, the design and preparation phases of the demonstration. These studies are discussed in this chapter.

4.1 PLASTIC FLOW

4.1.1 Heated Model Room

It is expected that holes in the floors of mined openings will be used for ultimate disposal of high-level radioactive solids in salt. Therefore, the effect of elevated temperatures on the deformational properties of salt will significantly affect the structural behavior of the mine rooms and pillars.

Under certain limited conditions, theoretical solutions exist for stress distributions around cylindrical openings in an elastic medium and for plastic closure of cylindrical openings at elevated temperatures. However, for rectangular openings the only theoretical solutions known to exist are those for the stress distributions in an elastic medium around openings with rounded corners.

Even in the case of cylindrical openings it was not known how well the theoretical solutions would predict thermally induced deformations in an actual salt formation, where some of the assumptions made in the theoretical solutions may not be valid. Thus, to obtain empirical data, both cylindrical and rectangular openings needed to be heated. Since the electrical energy requirements for heating an actual mine room are extremely high, studies of this nature are best carried out on scale-model openings.

To study the effect of temperature on a rectangular room of proportions similar to a mine room, an opening 8 ft wide by 9½ ft deep by 2 ft high was created in the face of a very large pillar in the Carey Salt Company mine in Hutchinson, Kansas. Immediately after the opening was created, electrical transducer-type strain gages capable of operating at 200°C were installed to measure floor-to-ceiling convergence, movement of the floor, and convergence of the side walls.

After the gages were installed (June 15, 1962), background creep-closure data were collected for a period of 214 days. The gages were then temporarily removed (February 11, 1963) to permit the installation of heaters, which were turned on March 18, 1963, and which operated until August 10, 1964.

The heating system consisted of ten tubular heaters with diameters of 0.44 in. and active lengths of 7 ft, located inside the cavity. Heater power was controlled by a thermostat (exposed to the cavity air but shielded from radiant heat) set for 170°C.

Two radiant-heat-shielded thermocouples monitored the cavity air temperature. Six thermocouples were installed in the cavity surfaces with the junctions recessed ½ in. into the salt. A total of 24 thermocouples were installed in the salt structure around the room at distances of 6 in. to 8 ft from the cavity. Six thermocouples, in two series, were located 1½, 5, and 8½ ft from the front of the room; all the other thermocouples were in the plane 5 ft from the front of the room.

4.1.1.1 Background Data. – Figure 4.1 shows the floor-to-ceiling movement which took place in the cavity at the various gage locations after it was excavated and before the heating system was installed. To excavate the cavity, an undercutter was used to slice into the wall; the resulting salt slab was then broken off and removed. (The undercutter was turned on its side to make the vertical cuts.) As soon as the slab was removed, the strain gages were installed; the total elapsed time was three days from the first cut to the first set of gage readings (zero time on Fig. 4.1).

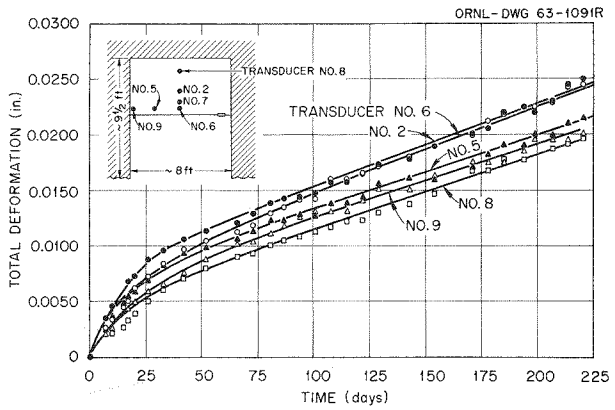


Fig. 4.1. Floor-to-Ceiling Movement at Ambient Temperature and Plan View of Model Room Containing Strain Transducers.

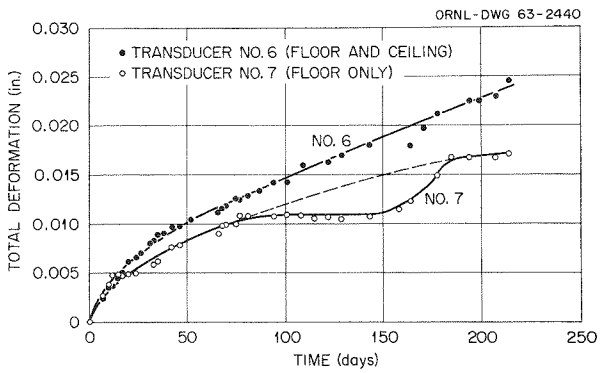


Fig. 4.2. Deformation at Ambient Temperature.

The initial deformation rates were high, but they decreased rapidly as the salt flowed to relieve the stress concentrations produced by the creation of the cavity. During the period of rapidly decreasing flow rates (about 50 days), the gages near the wall (Nos. 8 and 9) indicated slower floor-to-ceiling convergence than those in the middle of the room (Nos. 2, 5, and 6). This might be interpreted as a beam deflection of the ceiling, except for the fact that the floor-only gage in the center of the room (No. 7) indicated that floor movement accounted for about three-fourths of the total deformation (see Fig. 4.2). The floor-only gage apparently had a tendency to stick, as indicated by the flat portion in the middle of the curve (Fig. 4.2).

After the initial transients, all of the gages indicated steady deformation rates, decreasing only slightly with time. The rates of movement for the final 114 days of the background period are shown in Table 4.1. The unit deformation rates (in. in.$^{-1}$ day^{-1}) were obtained by dividing total rates by the height of the room.

As may be noted from Table 4.1, the floor-to-ceiling deformation rates near the walls (gages 8 and 9) were nearly as large as those in the center of the room. It has also been observed in the measurements made in various locations in the mine that after the initial transient period in the first few months after the opening was created, the floor-to-ceiling convergence rate near the pillars was almost as large as that in the center of the openings. In comparison, the deformation rates of Hutchinson mine openings, ranging from about 2 to 30 years in age and from 6 to 12 ft in height, fall within the range of 2×10^{-6} to 7×10^{-6} in. in.$^{-1}$ day^{-1}.

The floor-only gage (No. 7) indicated that the floor was rising a little faster than the ceiling was falling. The wall-to-wall gage (No. 3) was inadvertently connected so that it measured wall-to-wall movement plus floor movement near the wall. Since there was no floor-only gage near the wall, the readings cannot be readily interpreted; thus the data from this gage are not shown.

Table 4.1. Heated-Room Transducers – Background Closure Data

Gage No.	Cumulative Deformation (in.)		Rate of Movement, Final 114 Days	
	100 Days	214 Days	in./day	in. in.$^{-1}$ day^{-1}
			$\times 10^{-5}$	$\times 10^{-6}$
2	0.0153	0.0239	7.5	3.1
5	0.0132	0.0209	6.8	2.8
6	0.0146	0.0236	7.9	3.3
8	0.0113	0.0192	6.9	2.9
9	0.0124	0.0201	6.8	2.8
7[a]	0.0120	0.0173	4.6	1.9

[a]Based on idealized curve in Fig. 4.2.

4.1.1.2 Heating Phase. – The heating phase began on March 18, 1963, with a power input of 11 kW. The average power input decreased to about 9 kW by 40 days as the salt heated up.

Temperature-rise isotherms around the center of the cavity after 32 days of operation are shown in Fig. 4.3. As shown by the temperature increases ½ in. into the salt around the perimeter of the cavity, the heating was reasonably uniform, although the floor and walls were somewhat cooler than the ceiling. Temperatures were beginning to approach equilibrium, and thus the cavity deformation due to thermal expansion also should have

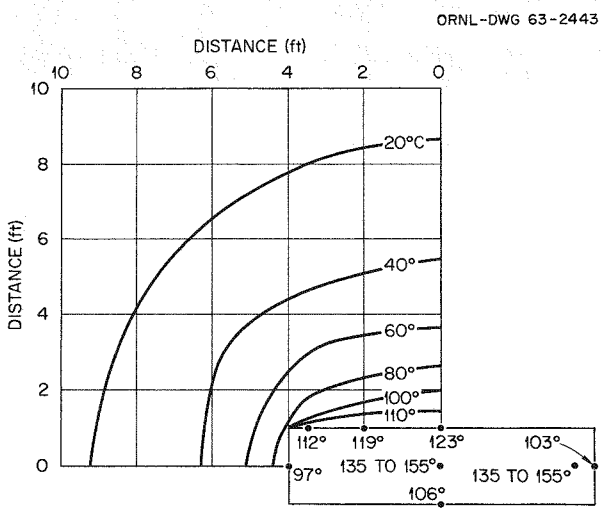


Fig. 4.3. Heated Room Temperature-Rise Isotherms After 32 Days of Operation.

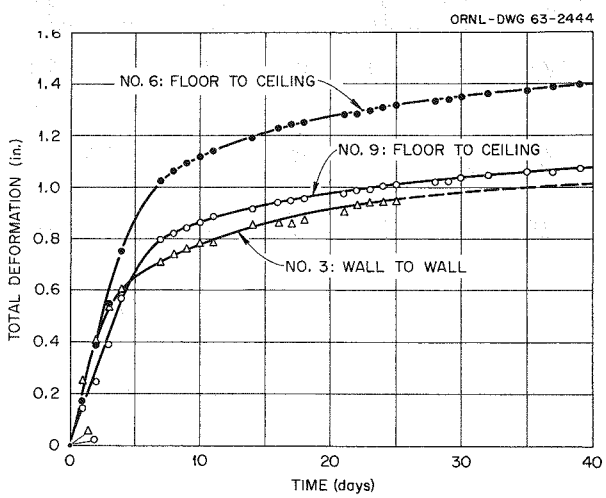


Fig. 4.4. Deformation During Heating – Heated Room Experiment.

been approaching equilibrium. (After 32 days temperatures 8 ft away from the cavity had already reached about 90% of maximum.)

Figure 4.4 shows the cavity deformations which took place during the first 40 days of heating. The cumulative deformation from wall to wall (~1 in.), gage No. 3, was about the same as that from floor to ceiling near the wall, gage No. 9, and only about two-thirds as great as the floor-to-ceiling movement in the center of the room (~1½ in.), gage No. 6. Gage No. 6 is typical of the other floor-to-ceiling gages, which are not shown.

Deformation rates for the period from 30 to 40 days are shown in Table 4.2. The floor-to-ceiling rates appear to be about the same throughout the cavity except next to the wall (gage No. 9). Comparing the deformation rates with those of the background period (Table 4.1), it is seen that the cavity was closing at a rate two orders of magnitude greater than before heating. Even at this accelerated rate it would take 12 years for the cavity to close completely. However, it must be remembered that this is, in effect, an isolated cavity and does not represent the behavior expected with a series of adjacent openings, as in a mine operation.

After about 50 days of heating, strain gages suddenly showed an apparent increase in the rate of convergence of the floor and ceiling. Investigation showed this to be due to bowing of the pipes supporting the strain gage anchor bracket. This bracket was located in the haulageway, outside the cavity. Heat from the cavity was causing a vertical expansion of the haulageway floor, compressing the pipes between floor and ceiling. To correct for bowing of the pipes, a reference gage measuring the movement of the bracket toward the cavity was attached to the anchor bracket. The reference gage was installed after 93 days of heating. This gage indicated that movement of the bracket was

Table 4.2. Closure of the Cavity During Heating

Gage No.	Cumulative Deformation (in.)		Rate of Movement in Units of 10^{-6} in. in.$^{-1}$ day^{-1}				
	At 215 Days	At 511 Days	Prior to Heating	During Heating			
				30 to 40 Days	40 to 115 Days	115 to 215 Days	215 to 460 Days
2	1.64	1.79	3.1	210	100	42	32
5	1.66	1.85	2.8	210	100	17	28
6	1.66	1.87	3.3	210	100	29	25
8	1.47	1.68	2.9	210	100	17	27
9	1.25	1.45	2.8	170	80	13	24

somewhat erratic, and a slip joint was installed on the support pipes. This was done after 150 days of operation and appears to have corrected the difficulty; however, the closure rates determined for the period from 115 to 215 days (Table 4.2) are not believed to be reliable, due to this difficulty.

After installation of the correction gage and the slip joints, the cavity closure rates as indicated by the strain gages should be correct; but in order to get the total cumulative closure, it was necessary to extrapolate the deformation curves from 50 to 93 days. The corrected cumulative deformations, as indicated by the floor-to-ceiling gages at the end of 215 and 511 days of heating, are shown in Table 4.2. Shown in the right-hand column are the deformation rates during the period from 215 to 460 days. (During this period the rates remained essentially constant. During the period from 460 to 511 days there was a malfunction in the heating system, and the heating phase was terminated after 511 days.) Also shown for comparison purposes are earlier rates and the rates before heating. It may be noted that the final closure rates are about one order of magnitude higher than the closure rates before heating.

The heating phase has shown that elevating the wall temperature of an isolated cavity by about 120°C (about 20°C rise at a distance of 9 ft from the cavity) resulted in a rapid reduction of about 5% in cavity dimensions, followed by a rapid decrease in closure rate. However, after more than a year at elevated temperature, the rate was still ten times higher than at ambient temperature. The effect appears to be approximately equivalent to that which would be obtained by doubling the load on the salt pillar.

4.1.1.3 Cooling Phase. – The power was turned off after 511 days of heated operation (August 10, 1964), but transducer readings were taken until January 16, 1967. All temperatures were back to within about 10°C of ambient by three weeks after shutdown and to within 2 to 3°C of ambient by the end of 1964.

During the first month or so after termination of the heating phase, the transducers indicated a recovery of cavity dimensions of around 0.1 to 0.2 in. or about 10%. This could be recovery of elastic thermal expansion of salt into the cavity, but calculations of the thermal expansion of steel indicate that it more likely represents the recovery of the thermal expansion of the steel cables attached from the transducer cores inside the cavity to the anchor bracket located outside the cavity. This being the case, the cumulative deformations shown in Table 4.2 should also be reduced by about 0.1 to 0.2 in.

After the salt temperature had returned to ambient (1965 and 1966), the transducer readings indicated little or no movement taking place inside the cavity. However, by this time the readings were becoming somewhat erratic, perhaps due to the length of time the transducers and readout unit had been exposed to the salt environment. About the only conclusion that can be drawn is that cavity closure rates after the termination of heating were probably less than they were immediately prior to heating.

4.1.2 United States Bureau of Mines Gage Tests

The Applied Physics Laboratory of the U.S. Bureau of Mines did considerable development work in connection with the Disposal in Salt Project on stress gages for use in salt to measure the magnitude and direction of the principal stresses.[1] Several types of gages were studied, since the problems of measuring the stress in salt are such that it was felt that no one gage could provide all the information desired, to the accuracy required. As a result, four gages or measurement methods were tested simultaneously by APL at the Carey mine, Hutchinson. These gages or methods are:

1. A solid-inclusion-type gage designed to permit the simultaneous measurement of the components of stress in three mutually perpendicular directions, referred to as a 3D gage.
2. An oil-filled hydraulic cell (BPC) designed for measuring the component of stress in the direction normal to the plane of the cell.
3. Photoelastic borehole gages developed by A. Roberts (Sheffield, England).
4. The borehole deformation gage (BDG). This gage and procedure had already been developed. The only question remaining was whether this method would work satisfactorily in salt at the depth of either the Hutchinson or Lyons mine.

Because of the uncertainties in the field response of the gages listed above, each gage or method was tested in a biaxially loaded in situ block of salt. The loading was accomplished with large flat jacks placed on four sides of a 5-ft cube of salt. The flat jacks were approximately 48 by 60 in. Four flat jacks were grouted into slots cut to form four faces of the 5-ft cube. The installation was made in a face of a dead-end

[1] C. K. Quan, *Tests of Instruments for Measuring Stress and Strain in Salt, Hutchinson Mine, Carey Salt Company, July–August 1963*, Report No. E-50.1, USBM, Applied Physics Laboratory, College Park, Md. (Sept. 15, 1964).

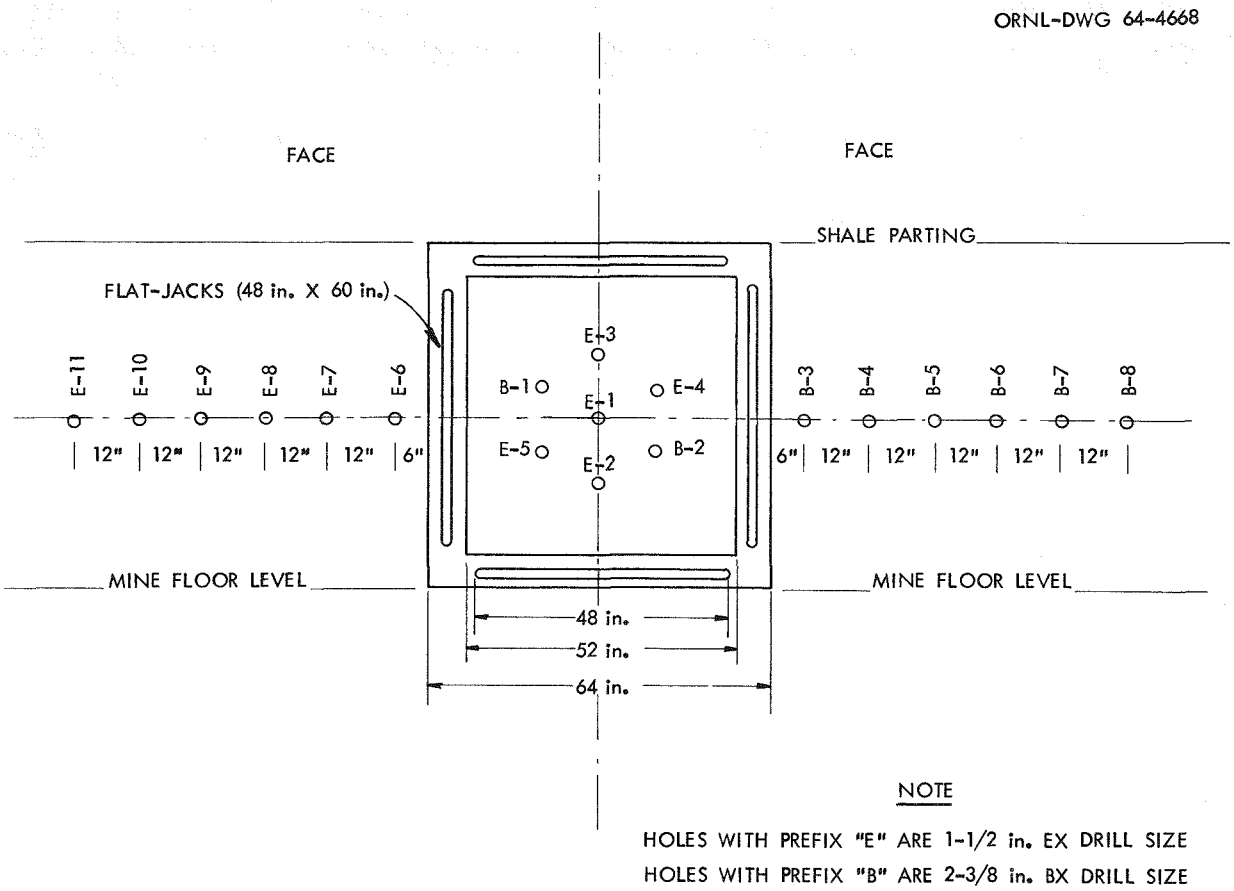


Fig. 4.5. Flat Jack and Gage Installation, Carey Salt Mine, Hutchinson, Kansas.

entry in the Hutchinson mine, Fig. 4.5. Borehole pressure cells with Bourdon gages attached were grouted into holes B-1 through B-8. A photoelastic plug gage was installed in hole E-4. Borehole deformation gages installed in holes E-1, E-2, E-7, and E-8 were used to measure the change of borehole diameter occurring during the slot cutting. Three-dimensional stress gages were installed in holes E-3 and E-5. In July and August 1963, pressures were applied to the 4-ft by 5-ft flat jacks, thus creating controlled biaxial loadings of the salt block. The responses of the various pressure- and strain-sensing devices were determined by the pressure cyclings.

Incidental to the gage development work, it was determined by APL that it should be possible to ascertain the vertical component of stress by consideration of static equilibrium conditions surrounding the flat-jack area or, for that matter, in the proximity of any underground opening cut after the installation of a properly oriented row of gages. The gage installation in the proximity of the flat-jack block was such that it should be possible to make a determination of the vertical stress by this procedure.

Near the end of the test series, one of the flat jacks developed a leak, thus terminating part of the test. Pressure was maintained on the remaining pair of jacks, and the gage readings were taken periodically until the end of January 1964.

Results[1] seemed to indicate that the salt was isotropic, with a modulus of elasticity of about 4×10^6 psi. Responses of the gages were linear for loads up to 1000 psi. Plastic deformation was indicated under a biaxial hydrostatic pressure of about 1200 psi.

4.1.2.1 3D Gage Results. – With the 3D gage there was incomplete agreement between observed and theoretical values. These discrepancies probably indicate an inadequacy of plane-stress theory to describe the behavior of the gage and/or the salt. The 3D gage is probably more effective as a strain meter than a stress meter.[1]

4.1.2.2 BPC Results. – Separate calibration of the borehole pressure cells may be required for different ranges of applied load.

Only about 10 to 40% of the vertical force applied by the horizontal pressure cells (flat jacks) was distributed to the BPC's outside the block. Part of the remainder was probably distributed to the zone behind the block.

It can be said that a properly calibrated borehole pressure cell would serve effectively as a pressure monitor within the elastic range of the salt. When the elastic limit (about 1000 psi) is exceeded, however, an analysis of BPC data must include a consideration of plastic flow of the medium.[1]

4.1.2.3 Photoelastic Gage. – Results of this series of tests indicated that the usefulness of the photoelastic stress meter in salt is limited.[1]

4.1.2.4 BDG Results. – As a strain measuring device, the BDG was quite effective in salt. Within the elastic range the gage responses were generally linear. Under high hydrostatic loads the analysis was complicated by plastic flow.

With known calibration the BDG can be used to determine the modulus of elasticity of the test medium.[1]

4.1.3 Trial Installation of Gage Types in Hutchinson

A test installation of a Potts-type stress meter (SM-36) and a strain gage (1-A-N) was made in a pillar (station 11) in the Hutchinson mine about January 1964. (These instruments are described in Sect. 11.4.1 of this report.) This type of stress meter has been used in salt mines by Professor Potts, and while it does not yield absolute values for stress or changes, it gives a qualitative indication of stress changes. The stress meter and the wire-type strain gage were installed in the center of a pillar whose fourth face was still attached to the salt formation. Since the gages were installed, the pillar has been cut free and the mine periphery progressively extended. Under these conditions it would be expected that the pillar stress should increase with time. The stress meter readings have, indeed, indicated that the stress in the pillar is increasing (Fig. 4.6). The strain gage generally showed pillar transverse expansion rates decreasing with time (up to about 250 days in Fig. 4.6). This is not necessarily inconsistent with an increasing stress, since the normal decrease in expansion rate could be more rapid than the increase due to the rising stress produced by retreat of the periphery.

At 244 days on Fig. 4.6, a third type of gage labeled T-2 (a pipe-type gage described in Chap. 11) was installed. This gage is anchored in the roof and floor, next to the pillar on the same side of the pillar that the transverse expansion gage is installed, and measures floor-to-ceiling convergence.

From Fig. 4.6, it may be seen that the vertical convergence of the pillar is just about equal to the total

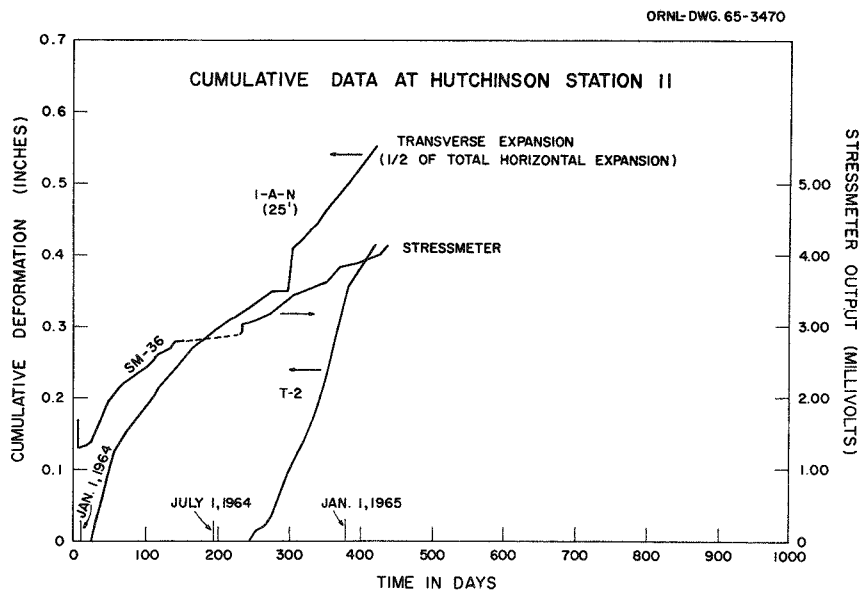


Fig. 4.6. Cumulative Data at Hutchinson Station 11.

transverse expansion, a phenomenon which has been observed at most of the other stations where there are horizontal convergence gages. For example, the vertical convergence next to the pillar, as measured by T2 over the period from 244 to 421 days, is about 0.41 in. Over this same period the transverse expansion gage (1-A-N) indicated 0.55 – 0.33 = 0.22 in. expansion from the center of the pillar to the edge, or 0.44 in. total expansion. (The apparent bad point at 298 days on 1-A-N is believed to be due to a reading error.) SM-36 and 1-A-N were installed during the height of the salt production season at a time when the pillar was still attached to the west wall. The rapid rise in stress meter output and transverse expansion during the winter of 1964 may be noted in Fig. 4.6. Also note the decrease in the rate of change during the summer (when production is minimum), followed by the rapid increase during the period from about October 1964 up to the middle of February 1965 (the end of the curves). It should be pointed out that the stress meter output can continue to increase even when the pillar stress is not increasing. However, an increase in the *rate of change of output* indicates an almost certain load increase.

The general conclusion to be drawn from this test gage installation is that the *rate of change* of readings of all these types of gage is indicative of changing loads on mine pillars, but none of the three is directly capable of indicating quantitative stress levels. The pipe-type convergence gage is easiest and cheapest to install and gives the most precise readings. On the other hand, it is only capable of being used external to pillars, whereas the other types can provide information on internal behavior of pillars and rib sides.

4.1.4 Results of Convergence Measurements and Correlation with Laboratory Creep-Test Data

To be able to predict the effects of elevated temperature (due to heat generated by decay of radioactive wastes) on creep and mine stability, an understanding of creep effects at ambient temperature is necessary.

S. Serata in 1959 suggested that creep rates (or closure rates) of mined openings always decrease with time.[2] In 1959 both ORNL and Serata (then at the University of Texas) installed several vertical and horizontal convergence measuring stations in the Carey Salt Company's mine at Hutchinson. Since that time ORNL has added additional stations at the Carey mines in both Hutchinson and Lyons. These stations were designed to determine the effects of both age of the opening and pillar stress on creep rates. Data from these stations tended to indicate that Serata's hypothesis of steadily decreasing vertical convergence was correct, at least for the pillar stress levels encountered in the Kansas mines. In March 1963 Serata indicated that he had successfully extrapolated creep data from laboratory pillar models to creep rates in mined openings.[3]

4.1.4.1 Pillar Model Test Results. – L. Obert, of the Applied Physics Laboratory of the U.S. Bureau of Mines, developed a somewhat different technique for performing creep tests on pillar models. At our request the Applied Physics Laboratory carried out 1000-hr creep tests on model pillars which they machined from 6-in.-diam cores of Lyons mine salt. Steel restraining rings were epoxied around the upper and lower ends of the specimens, and then the centers of the specimens were ground out to form the pillar and surrounding roof and floor (see Chap. 12). The model pillars had a diameter-to-height ratio of 4, and tests were run with average pillar stresses of 4, 5, 6, 7, 8, 10, and 12 thousand psi. Vertical shortening of the pillars, as a function of time and stress, was measured by means of dial gages mounted between the steel restraining rings.

In the 12,000 psi test, flow was rapid, and the pillar was considered to have failed due to excessive flow; however, there was no evidence of catastrophic (sudden or brittle) failure. The 10,000-psi model exceeded 20% deformation before the 1000 hr of the test was completed.

Based on the cumulative deformation curves supplied to us by Obert, we prepared Fig. 4.7 showing the creep rates as a function of time, obtained by taking the tangents to Obert's curves at the indicated times. Data from these curves can be fitted by an equation of the form:

$$\dot{\epsilon} = B\sigma^m t^n ,$$

where

$\dot{\epsilon}$ = strain rate (vertical convergence, μin. in.$^{-1}$ day^{-1}),

B = a constant (dependent on units of $\dot{\epsilon}$),

σ = average pillar stress (psi),

m = slope of $\dot{\epsilon}$ vs σ on a log-log plot (positive),

t = time (hr),

n = slope of $\dot{\epsilon}$ vs t on a log-log plot (negative).

[2] S. Serata and E. F. Gloyna, *Development of Design Principle for Disposal into Underground Salt Cavities,* chap. 10, Technical Report to the Atomic Energy Commission, Dept. of Civil Engineering, Sanitary Engineering Research Laboratory, Univ. of Texas, January 1959.

[3] S. Serata, Dept. of Civil Engineering, Michigan State Univ., personal communication, March 1963.

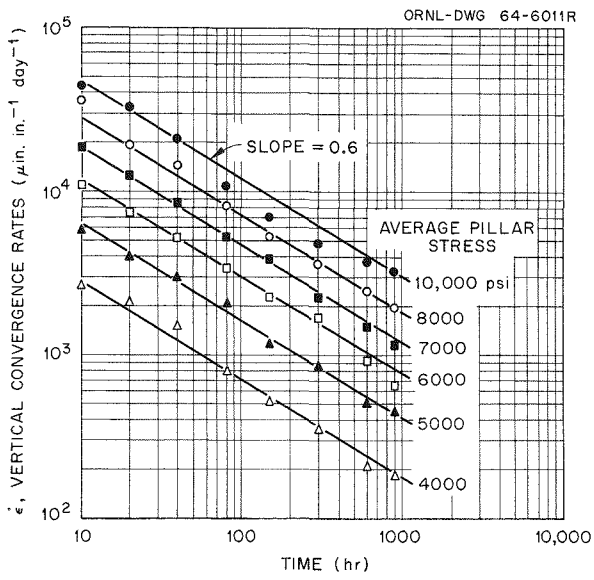


Fig. 4.7. Creep Rate Data on Lyons Pillar Models (USBM Tests).

A reasonable fit was obtained with:

$$\dot{\epsilon} = 9 \times 10^{-8}\, \sigma^{3.1} t^{-0.6} .$$

The exponent of the stress dependent term (σ^m) is in reasonable agreement with those obtained by the USBM with salt and similar rocks from other localities. The 0.6 slope obtained for the time function appears to be significantly different from the range of 0.8 to 1 (obtained from unpublished data of USBM and S. Serata) for salt from a different locality. However, extrapolation of the above equation out to periods up to 70 years (in excess of 600,000 hr) produces predicted creep rates which agree reasonably well with those actually measured in the Hutchinson and Lyons mines, whereas agreement was poor when compared with extrapolation of the data from models made from salt from the other localities. It thus appears that the creep behavior of the Lyons and Hutchinson salt is somewhat different from that of salt from some other formations and that data from one mine should not be presumed to be representative of that from mines in different salt formations (see Sect. 12.3.6). For a discussion of reproducibility of results on samples from the same mine, see Sect. 12.3.7.

4.1.4.2 Correlation of Vertical Convergence Measurements with Pillar Model Tests. – Tables 4.3 and 4.4 show the results of vertical and horizontal convergence measurements in the Hutchinson and Lyons mines respectively. Figures 4.8 and 4.9 show the locations of the measuring stations. Horizontal closure rates (in inches per year) in the Hutchinson mine are believed to be subject to about +0.02 in. error due to use of a less accurate type of gage installation than that used for the

Table 4.3. Creep Measurements in the Hutchinson Mine[a]

Hutchinson Station No.	Approximate Age of Opening (years)	Total Closure Rate (in./year)			Average Pillar Height (in.)	Vertical Closure Rate (Next to Pillar) (μin. in.$^{-1}$ day^{-1})	$\frac{\Delta \text{ Horizontal}}{\Delta \text{ Vertical}}$
		Vertical		Horizontal			
		Next to Pillar	Center of Room	Center of Pillar			
1	1.6	0.19	0.23	0.06 ± 0.02	130	4.0	0.3 ± 0.1
2	7.3	0.10	0.11	0.07 ± 0.02	121	2.4	0.7 ± 0.2
3	10.3	0.16	0.17	0.18 ± 0.02	122	3.5	1.1 ± 0.1
4[b]	28	0.04	0.05	0.02 ± 0.02	96	1.6	0.5 ± 0.5
5[c]	40	0.02	0.03	0.02 ± 0.02	160	0.3	1.0 ± 1.0
6	16	0.25	0.26	0.17 ± 0.02	118	5.7	0.7 ± 0.1
7	11.3	0.14	0.15	0.11 ± 0.02	119	3.2	0.8 ± 0.1
8	No longer in existence						
9[b]	40	0.02			160	0.4	
10[b]	40	0.01			160	0.2	

[a]Data as of September 1963.
[b]Stations located in rib pillar panels.
[c]Station located in an airway.

Table 4.4. Creep Measurements in the Lyons Mine[a]

Lyons Station No.	Approximate Age of Opening (years)	Total Closure Rate (in./year)		Approximate Vertical Gage Length (in.)[c]	Vertical Closure Rate (μin. in.$^{-1}$ day^{-1})	$\frac{\Delta \text{Horizontal}}{\Delta \text{Vertical}}$
		Vertical[b]	Horizontal			
1	70	0.20	0.23	204	2.7	1.1
7	70	0.22	0.20	204	2.9	0.9
8[d]	70	0.52	0.20	186	7.6	
9[d]	70	0.37	0.19	96	10.4	
10	70	0.22		204	2.9	
13	60	0.17		204	2.3	
14	30	0.25		144	4.7	
15	30	0.14		144	2.6	
16	30	0.19		174	3.0	
20	30	0.08		120	1.8	
24	30	0.10	0.10	186	1.4	1.0
33	30	0.08	0.08	186	1.2	1.0
E7R8-T1 (center of opening)	30	0.06		108	1.5	
E7R8-T2 (next to pillar)	30	0.05		108	1.3	

[a]Data as of September 1963.

[b]Due to rounded openings most gages are in the center of the openings.

[c]Also assumed to be the effective pillar height.

[d]Vertical gages 8 and 9 are anchored in sagging roof slabs.

other measurements. For the other measurements (both horizontal and vertical) anchors are set approximately 18 in. into the salt, and readings are taken with a dial gage which reads to 0.001 in.; however, other variables, such as minor seasonal variations in mine air temperature, reduce the accuracy of the results to perhaps ±0.005 in./year.

Figure 4.10 shows the cumulative deformation at the various Hutchinson gaging stations. The T-2 gages are located next to the pillars, and the T-1 gages are in the center of the room (passage between pillars). (In this context, "center of room" will refer to midway between pillars rather than in the center of an intersection, unless otherwise stated.) The north panel was currently being worked, and the working face was to the west of the location shown for station 11. Most of the gages were installed on or after April 2, 1962. Of those shown in Fig. 4.10, the exception is station 8. Station 8 was installed about 900 days before the beginning of the period covered in Fig. 4.10, during which time a cumulative deformation (floor-to-ceiling convergence) of about 0.39 in. took place. During this time the gage station was located very near the western and southern boundaries of the north panel, and mining was taking place along the eastern boundary. Somewhere around zero time on Fig. 4.10, mining was moved to the western boundary, thus producing the rapid increase in deformation at station 8.

Hutchinson station 1-T1 was installed soon after the area was mined, but 1-T2 was not installed until about 3½ months later. All of the other gages shown in Fig. 4.10 were installed in areas which were excavated at least six years previously, except for station 11-T2, which was installed about nine months after three sides of the pillar at this location were excavated. By the time the 11-T2 gage was installed, the fourth side of the pillar had been cut free for some time. It may be noticed that at all of the stations which had both T1 and T2 gages the rate of closure at the center of the room is only slightly greater than next to the pillar, with the exception of station 1, where there is a more significant difference. The behavior of station 1 (greater movement in the center of the room) indicates a possible parting separation, although the separation rate (difference between rates in the center of the room and next to the pillar) is less than 0.1 in./year. It should be

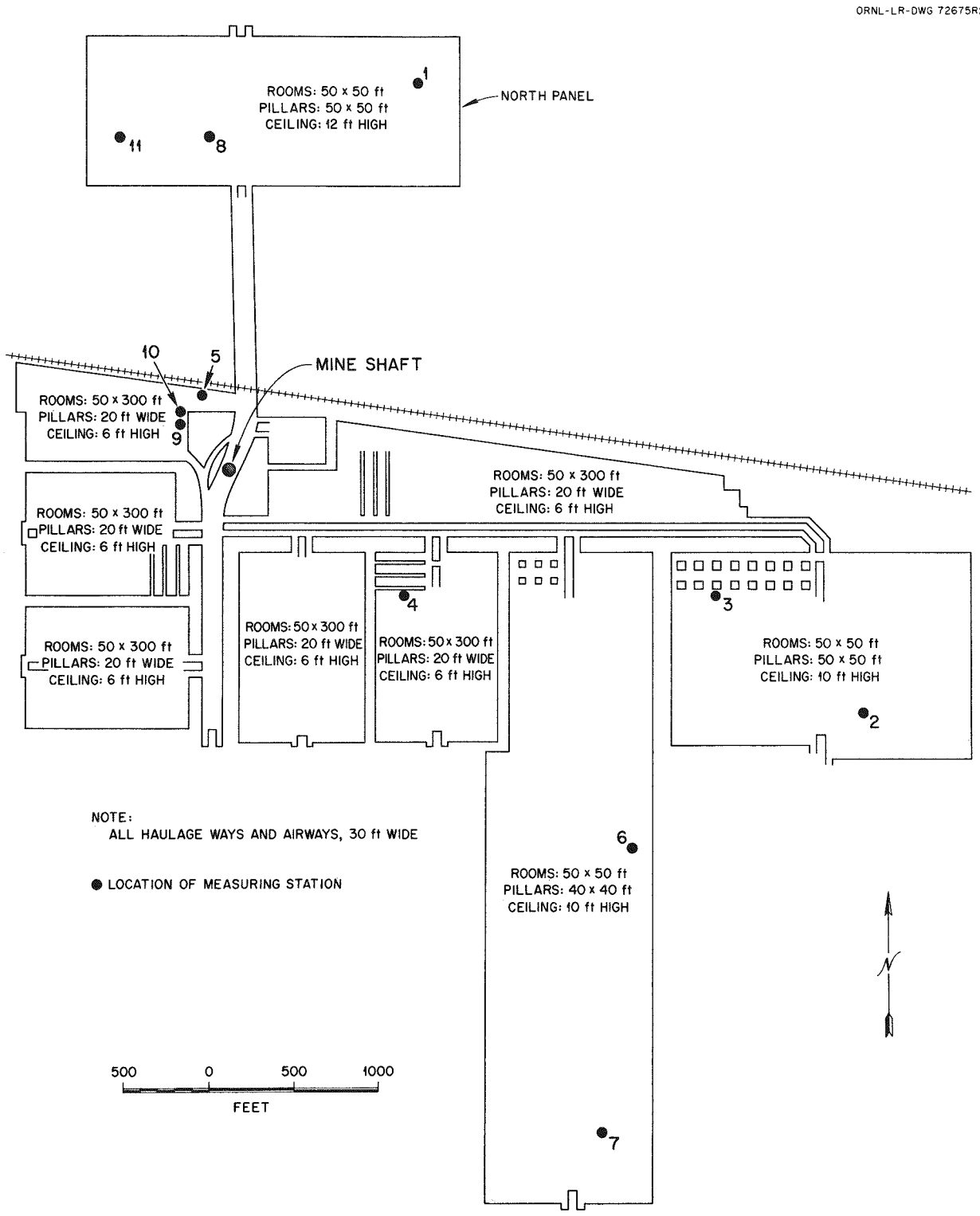


Fig. 4.8. Plan of Hutchinson Mine Showing Locations of Convergence Measuring Stations.

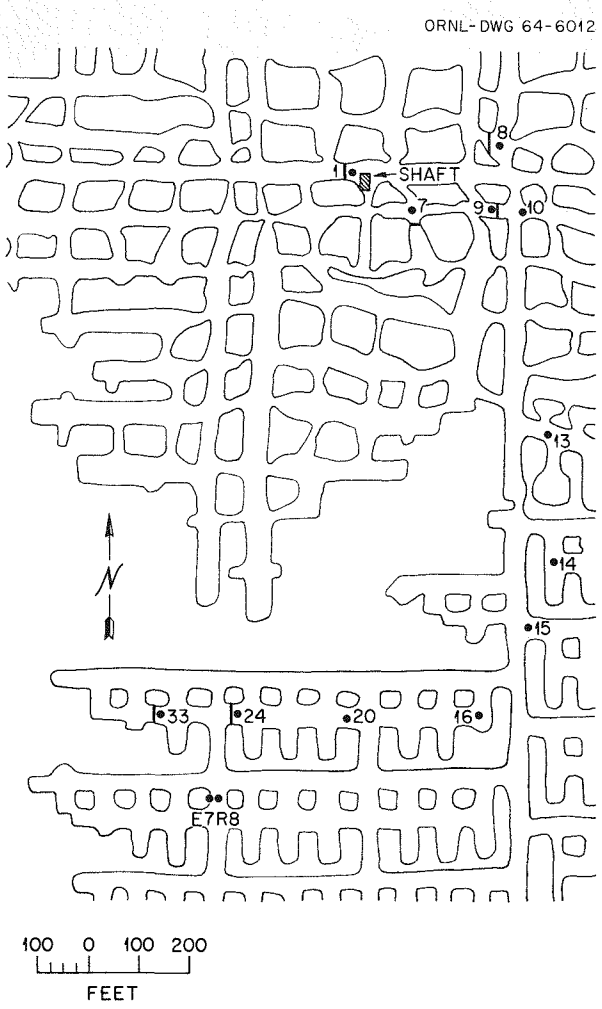


Fig. 4.9. Partial Plan of Lyons Mine Showing Locations of Convergence Measuring Stations.

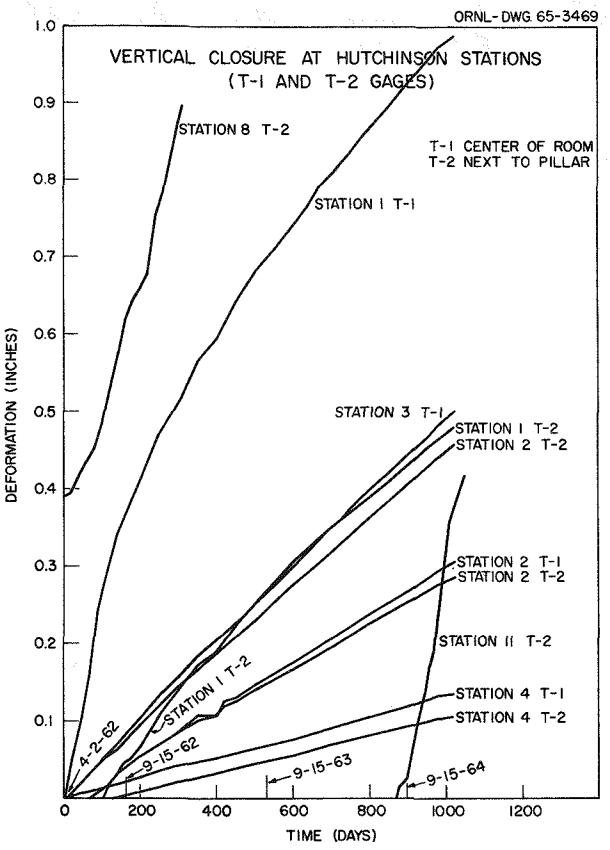


Fig. 4.10. Vertical Closure at Hutchinson Stations (T-1 and T-2 Gages).

noted that in discussion of the gage measurements it is basically the movement between gage anchor points which is measured. In the Hutchinson mine the roof anchors are set at points which are about 1½ to 2 ft into the ceiling, and thus separations at partings below this level would not be indicated. Partings are not generally left this close to the ceiling, however. The floor anchors are set just above the anhydrite layer which lies from about ½ to 1½ ft below the floor.

Figure 4.11 compares the vertical convergence rates in both the Hutchinson and Lyons mines (Tables 4.3 and 4.4 plus additional data) with the convergence rates predicted by the empirical equation derived from the pillar model tests. After an opening is about ten years old, approximately two years of data are necessary to establish two points of sufficient accuracy on the convergence rate vs time plots, due to the slow decrease in rate of closure. Thus each of the points for Hutchinson stations 2, 3, and 7 is the rate established by taking the total deformation for a period of one year, converting it to the proper units, and plotting it as the rate at mid year. Only one point is shown for the older stations since, for example, in a 30-year-old opening about five years of data would be required to produce two significant points. Most of the gaging stations in the Hutchinson mine are located near the boundaries of the mined-out area, and thus the adjacent pillars would not be expected to be supporting the calculated dead weight of the overburden, as should be the case if the pillars were in the center of a very large panel of rooms. That this is true (at least for openings up to a few years of age) is shown in Fig. 4.11 by the behavior of Hutchinson station 8. A short time after the excavation in the area of station 8, mining was discontinued on the west side and shifted to the east

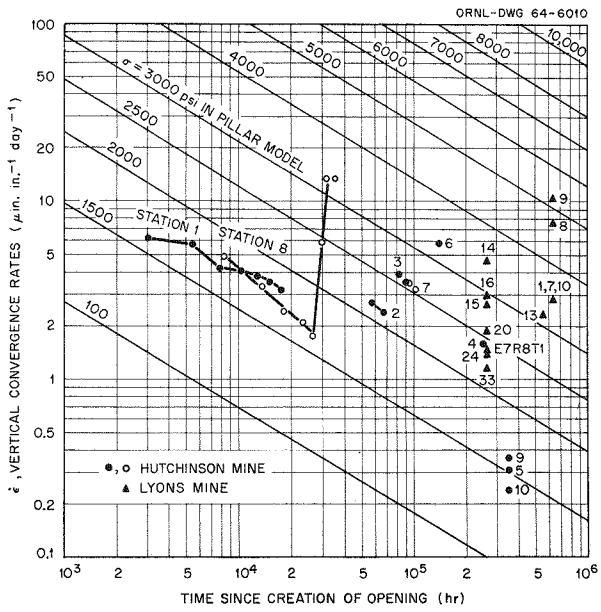


Fig. 4.11. Measured Mine Convergence Rates Superimposed on Plots of Equation Derived from Model Tests.

side of the north panel. When the opening at station 8 was about three years old, the apparent stress in the pillar was about 1700 psi (see Table 4.5 as well as Fig. 4.11). At this time, mining was resumed near station 8, and the western boundary was extended. The rapid rise in vertical convergence rate indicates that the pillar had not been fully loaded after the initial mining; however, it should not be assumed that the load increased to more than 3000 psi (as might be inferred from Fig. 4.11). With the incremental load added some three years after the opening was created, the time scale would have to be shifted to take into account the fact that the creep due to the incremental load essentially begins at a new zero on the time scale. With the points plotted, as shown, as a function of time after the original loading (initial creation of the opening), the convergence rate would have been expected to show a more rapid decrease as the pillar stabilized under its new load. Unfortunately, the gaging station had to be removed before this stage was reached.

In general the stations located nearest the centers of large mined-out areas tend to approach the stress calculated by assuming an infinitely large mined area (see Table 4.5). Hutchinson station 6, for example, while located near the eastern boundary, is in the center of a panel which is very long in the north-south direction, and the stress value obtained from Fig. 4.11

Table 4.5. Pillar Stresses Estimated by Different Methods

Station No.	Pillar Stress		
	Calculated from Dead Weight of Overburden	Calculated from Pillar Model Extrapolation	Measured by USBM[a] (Stress Relief Method)
	Hutchinson		
1	3000[b]	1800	
2	2900[b]	2100	
3	3000[b]	2600	
4	2500[b]	2400	
5	2200[c]	1500	
6	3800[b]	3300	
7	3950[b]	2600	
8	2600[c]	1700	1600
9	2200[c]	1600	1300
10	2200[c]	1400	1300
	Lyons		
1	2500[b]	3400	
7	2500[b]	3400	
8[d]	2500[b]	4700	
9[d]	2500[b]	5200	
10	2500[b]	3400	
13	2500[b]	3200	
14	2900[e]	3400	
15	2900[e]	2800	
16	2500[b]	3000	
20	2500[b]	2600	
24	2500[b]	2400	
33	2500[b]	2200	
E7R8-T1	2500[b]	2400	

[a] L. Obert, *Stress Determinations and Borehole Deformation Studies,* Report APRL, E 40.1, USBM, Applied Physics Research Laboratory, College Park, Md.

[b] Based on actual measurement of room and pillar areas.

[c] Based on nominal extraction ratio in the whole panel of rooms.

[d] Anchored in sagging roof slab.

[e] Based on estimated extraction ratio.

approaches the calculated value. On the other hand, Hutchinson stations 5, 9, and 10, located near a northern boundary as well as the large irregular pillar left around the mine shaft, indicate stresses considerably below the calculated values.

It is unfortunate that none of the Hutchinson stations are located near the centers of the large panels. The reason for this omission is that, since it was necessary that some of the stations be located near the periphery

in order not to interfere with the mining, it was felt that a better comparison of the effects of age and extraction ratio on creep rates could be made if all stations were similarly located.

Lyons stations 1 through 13 are located in the area around the shaft (no large shaft pillar was left in this mine), where the mining pattern was very irregular and the extraction ratio may not be too accurate. Therefore, the calculated pillar loads for these stations (Table 4.5) may also be inaccurate. The vertical convergence rates at stations 8 and 9 are anomalous, and the anomaly is definitely known to be due to a parting separation and resultant ceiling sag. Stations 16 through 33 are progressively nearer a western boundary, and the convergence rates seem to reflect this fact, although it is believed that there may be some ceiling sag contributing to the convergence at 16 and possibly at 20.

Referring again to Table 4.5, it should be noted that stress measurements made in the Hutchinson mine by the USBM (using stress relief techniques)[4,5] tend to confirm the general validity of the pillar model extrapolations. The 1300-psi figure was measured one pillar away from stations 9 and 10, and the 1600 psi was measured in a pillar near station 8 soon after station 8 was installed.

4.1.4.3 Relationships Between Vertical and Horizontal Convergence Rates. – If it is assumed that the shortening of a pillar in a mine is similar to squeezing a parallelepiped body between two parallel plates, that the pillar volume displaced in the vertical direction is redistributed by equal expansion on all sides of the pillar, and that the change in height is small compared with the original height, it can be shown that, for a rectangular pillar of height H, width W, and length $L = nW$, the change in width (ΔW) is related to the change in height (ΔH) by:

$$\frac{\Delta W}{\Delta H} = \frac{n}{n+1}\left(\frac{W}{H}\right).$$

For a round pillar (of diameter D) under the same assumptions, the relationship is:

$$\frac{\Delta D}{\Delta H} = \frac{1}{2}\frac{D}{H}.$$

Thus *if it is assumed that expansion is equal on all sides of a pillar* (round, square, or rectangular), and since Hutchinson pillars are square and most pillars in Lyons are roughly square or at most 2:1 rectangular, it would be expected that the measured ratio of horizontal to vertical convergence (Δ horizontal/Δ vertical) should be between $\frac{1}{2}$ and $\frac{2}{3}$ times the width-to-height ratio.

If it is assumed that horizontal expansion is directly proportional to the horizontal dimension, it can be shown that:

$$\frac{\Delta W}{\Delta H} = \frac{1}{2}\left(\frac{W}{H}\right)$$

and

$$\frac{\Delta L}{\Delta H} = \frac{n}{2}\left(\frac{W}{H}\right).$$

If pillars are not round or square, the results are dependent upon the direction in which the horizontal convergence is measured. If convergence is measured between the long sides of two rectangular pillars, the measured value is ΔW, and Δ horizontal/Δ vertical is thus $\frac{1}{2} \times (W/H)$. If convergence is measured between short sides, the measured value is ΔL ($= n\ \Delta W$), and Δ horizontal/Δ vertical is $(n/2) \times (W/H)$. For the case of a pillar with $L = 2W$, the ratio of the measured values Δ horizontal/Δ vertical would equal W/H. If the convergence is measured between a long and a short side, the measured ratio (Δ horizontal/Δ vertical) would thus be $[(1+n)/4] \times (W/H)$, or $(\frac{3}{4}) \times (W/H)$ for the case where $L = 2W$.

Thus it would appear that if horizontal expansion volume is equal to vertical contraction volume (assuming uniform shortening throughout a pillar), then no matter whether the pillar is round or rectangular with long dimensions up to twice the short dimension, no matter which sides of the pillars the convergence measurements are made between, and no matter whether horizontal expansion is uniform all around or is greatest in the direction of the longer dimension, the measured ratio of horizontal convergence to vertical convergence should lie between $\frac{1}{2}(W/H)$ and W/H, where W is the short dimension and H is the height.

The foregoing assumes, of course, that convergence measurements are not influenced by ceiling sags due to parting separation or by pillar spalling. It also assumes that the horizontal expansion of the pillars is uniform over the vertical extent of the pillars. This last assumption is an oversimplification. However, if the

[4] L. Obert, *Stress Determinations and Borehole Deformation Studies,* Report APRL, E-40.1, U.S. Bureau of Mines, Applied Physics Laboratory, College Park, Md.

[5] L. Obert, "In Situ Determination of Stress in Rock," *Mining Engineering,* August 1962, pp. 51–58.

horizontal expansion is nonuniform in the vertical plane, it is to be expected that the greater expansion would take place at the vertical center of the pillar.[6] Under these conditions the horizontal measurements reported here would tend to be on the high side, since the horizontal gages are located at the vertical centers.

In the Hutchinson mine the pillars are very nearly square, and W/H ratios at our measuring stations run from about 3.7 to 4.7. The data also indicate that there is little or no parting separation, since the closure rates near the pillar and in the center of the room are nearly equal. Thus it would be expected that measured Δ horizontal/Δ vertical should be about 2. However, at all the Hutchinson stations the measured ratio (last column, Table 4.3) is less than, or approximately equal to, unity.

In the Lyons mine the Δ horizontal/Δ vertical ratio would be expected to range up to about 3. Instead, at stations which do not show evidence of parting separation, the ratio is approximately unity (last column, Table 4.4). Thus the behavior in the Lyons and Hutchinson mines is similar in that horizontal expansions of the pillars do not seem to be great enough to account for the apparent shortening of the pillars.

There are a number of possible explanations for this apparent anomaly. One plausible explanation is that part of the pillar volume expands into the room via the floor and roof, thus contributing to the vertical closure. If this is true, then the existing data indicate that the expansion is such that after the first couple of years it produces a nearly uniform vertical convergence all the way across the room. A point which tends to support this hypothesis is the fact that parallelepiped samples compressed uniaxially do not behave in the same manner (as regards creep rates) as do pillar models (with the same relative pillar dimensions as the parallelepiped samples) that include the roof, floor, and surrounding opening, with restraining rings simulating the center of the surrounding opening by restricting the horizontal flow of the roof and floor. There appears to be some flow of salt at the junctions between the pillar and the floor and roof.

4.1.4.4 Conclusions. – Laboratory pillar model tests of 1000 hr duration run at several different values of average pillar stress appear to be sufficient to allow the development of an empirical equation which can be used to predict vertical closure rates in salt mine openings up to several years old.

Vertical convergence rates have been shown to continue to decrease with time in openings up to 12 years old where the pillar stress is well below the ultimate strength. Accumulation of data at individual stations in older openings is not sufficient to determine with certainty if the closure rates are still decreasing after several decades, but the data from the collective stations seem to indicate that rates are still decreasing after 70 years.

4.2 PROTOTYPE HOLE LINER TEST

In order to check out techniques, a prototype test was operated in the same room in which the secondary radioactive array was to be located. A vertical cross section of the prototype hole-liner installation is shown in Fig. 4.12.

Drilling of the 16-in.-diam upper portion and 12-in.-diam bottom portion of the hole was begun in April 1964, and the upper portion of the liner was grouted into position. After the grout had set, auxiliaries and ancillary equipment were installed, and operation of phase I (without a fuel canister, but with a metal plate closing the hole where the top of the canister should be) was started on June 2. There was some uplift of the floor (a few tenths of an inch as the salt temperature at the periphery of the hole approached 200°C), and the first ten days of operation produced approximately 1 liter of water (released from shale interbedded with salt in the floor) in the off-gas condensate trap. This water became progressively more concentrated in stainless steel corrosion products, primarily from corrosion of the stainless steel condenser.

Operation throughout the duration of phase I of the test proceeded without significant incident. The test was terminated on July 20, 1964, after running 48 days.

When the liner was opened, the prototype canister was placed in it without difficulty. From this test and other observations, it was concluded that there had been essentially no temperature distortion of the lower part of the liner.

When the lower part of the liner was removed, it was found to have a bright red oxide film on all welds and a little corrosion at those places where water had dripped back from the off-gas and caliper ports. The main body of the lower liner, however, was completely unaffected and practically indistinguishable from its original state.

A total of 30 pins were shot into the floor around the prototype hole liner for periodic measurement of floor

[6] J. D. Snyder and L. F. Dellwig, "Plastic Flowage of Salt in Mines at Hutchinson and Lyons, Kansas," *State Geological Survey of Kansas, Bulletin 152, Part 2,* University of Kansas Publications, Lawrence, Kan. (1961).

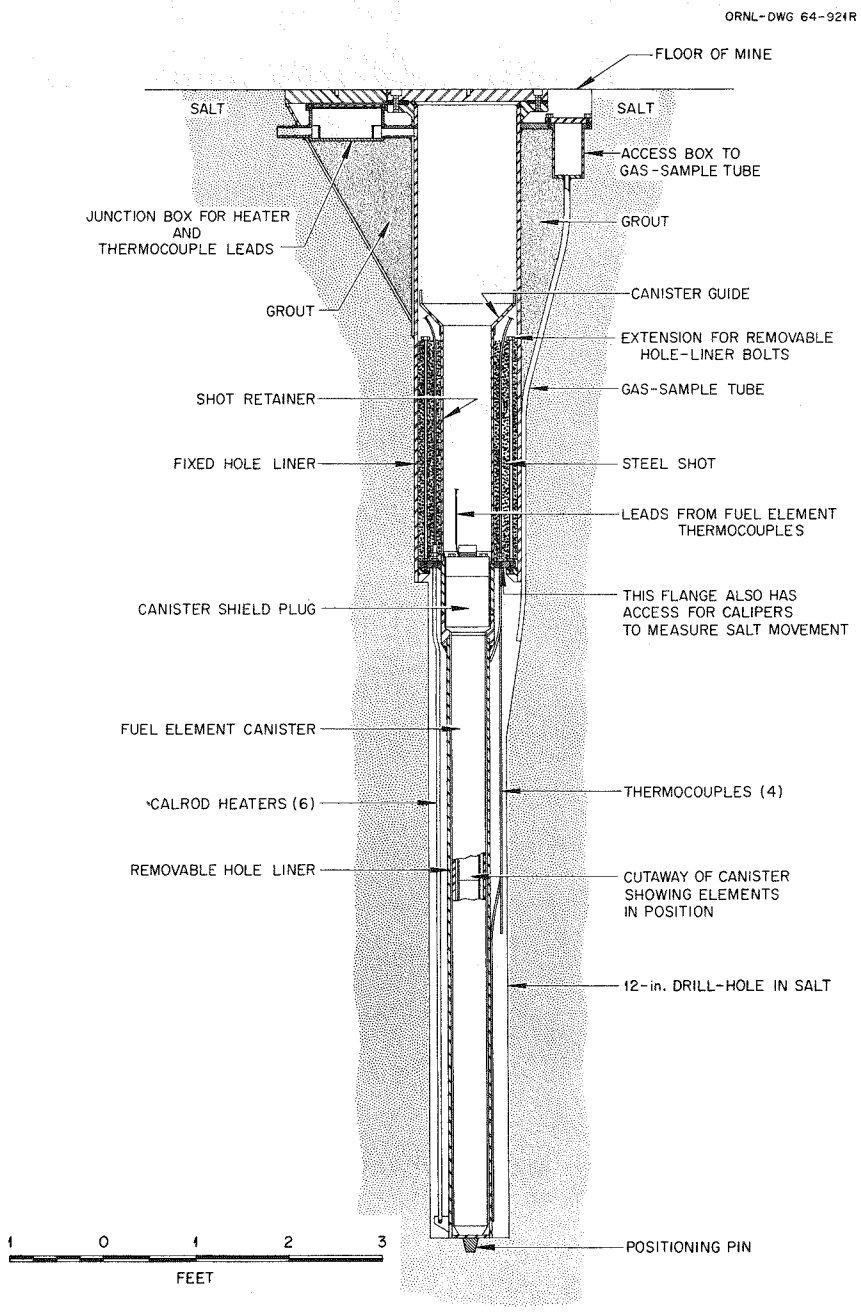


Fig. 4.12. Prototype Hole-Liner Installation.

uplift. Figure 4.13 illustrates the areal extent and shape of the maximum measured uplift by contours (on July 20, 1964, just before turning off the heat).

The conclusions which could be drawn from the floor leveling part of the prototype test were:

1. that standard leveling techniques would provide a sufficient accuracy (about 0.002 ft) and a satisfactory method of measurement in the demonstration;
2. that the magnitude of total uplift was of the order which was anticipated (about $\frac{1}{2}$ in.);
3. that the floor leveling results, in conjunction with the temperature measurements, would provide a valuable adjunct to the investigation of the thermal-plastic properties of salt.

The room containing the prototype hole liner was also instrumented with rock mechanics gages in order to gain some insight into the type of behavior to be expected from the experimental arrays. This instrumentation consisted of borehole extensometer stations (internal strain gages) in the roof, floor, and both pillars.

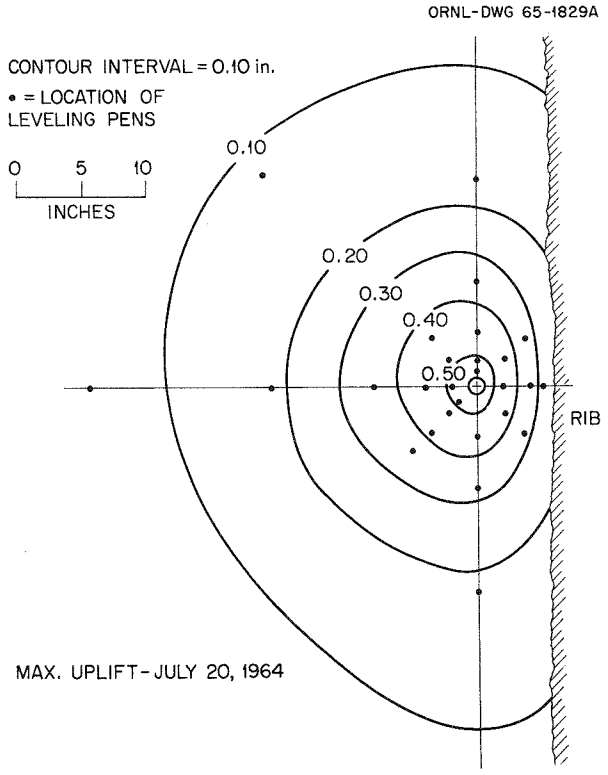


Fig. 4.13. Prototype Test Phase I – Floor Uplift Contours. In inches.

The results of the two horizontal stations are shown in Fig. 4.14 on a time-vs-deformation plot. A comparison of the two stations, P-2-W (Fig. 4.14*a*) and P-5-E (Fig. 4.14*b*), indicates that the extensometer stations will be very sensitive to changes induced by heating. The strain rate at P-2-W was approximately twice that at P-5-E, and there was a significant decrease in strain rate when the heaters were turned off.

Most of the movement taking place at the floor station was probably induced by heat, and a sizable portion of it was recovered when the heaters were turned off. By contrast, very little movement took place at the roof station, indicating that the roof was not sagging appreciably. Figure 4.15 illustrates the movements of the floor and roof anchors relative to each other. This was constructed by assuming that the anchor 22 ft above the roof (U-1) did not move and by comparing the movements of all other anchors with it (by using convergence results). It is interesting to note that the anchor located 20 ft below the floor (D-1) showed essentially no movement.

The annulus between the nominal 12-in.-diam hole (actually about $12\frac{1}{4}$ in. in diameter) and the outside of the lower liner was measured during the test by using a specially designed tube caliper. This instrument read to $\frac{1}{16}$ in. and had an estimated accuracy of about $\frac{1}{16}$ in. Its primary purpose was to monitor the closure of the salt hole in order to avoid damage to the liner. The radial hole closure measured with the caliper during phase I was between $\frac{1}{4}$ and $\frac{1}{2}$ in., which agrees with a

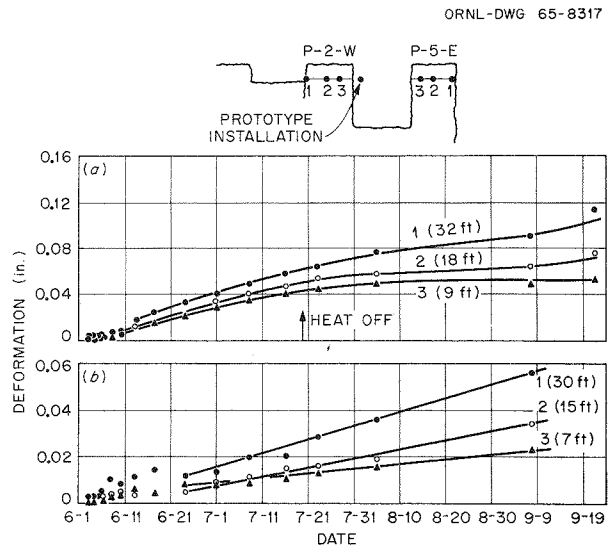


Fig. 4.14. Prototype Test Phase I – Rock Mechanics Gage Results, Stations P-2-W and P-5-E.

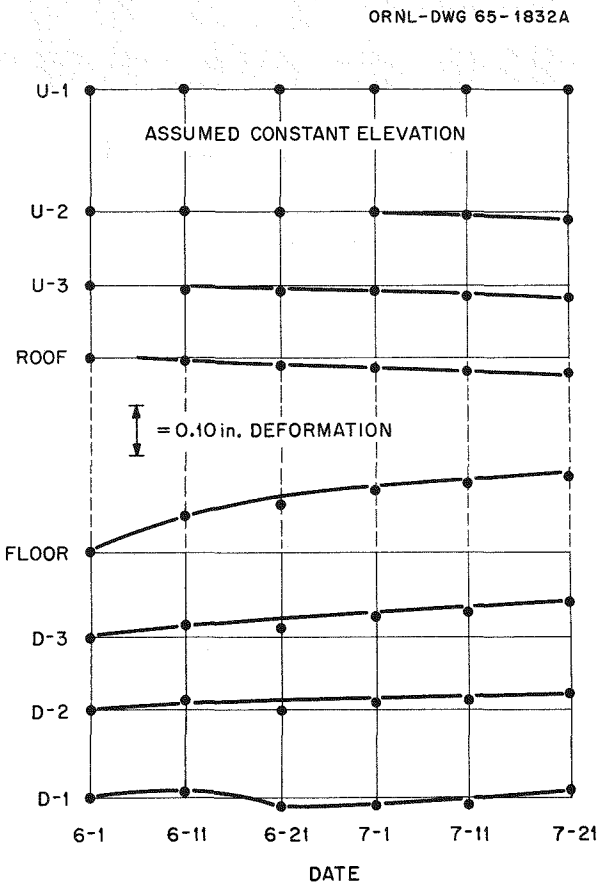


Fig. 4.15. Prototype Test Phase I – Relative Vertical Movements at Center of Room.

measured diameter of 11.5 in. after the liner was removed (approximately ¾ in. decrease in diameter).

The temperature at the periphery of the 12-in.-diam hole was about 200°C, and temperatures in excess of 100°C extended out to about 2 ft from the center of the hole. As in previous tests the floor uplift does not appear to be linearly related to the depth-integrated temperature rise.

During the operation of phase I, about 2½ liters of condensate was collected. Most of this condensate was heavily laden with stainless steel corrosion products, which came primarily from the condenser tube. For phase II a nickel condenser was installed, and the remainder of the equipment was put back together as before.

Phase II operation began on November 9, 1964, and lasted for about 100 days, during which time about two-thirds of a liter of condensate was collected. Examination of the hole liner indicated little change from the conditions at the end of phase I.

Phase III operation began on January 26, 1965, and lasted for about 50 days. The off-gas system was not operated during this phase, except for about 1 hr near the middle of the test, during which time about 40 ml of condensate was collected. The purpose of this test was to simulate an actual disposal in the floor of an existing mine in a bedded deposit. During the operation there were indications of some refluxing of water in the caliper guide tube, off-gas line, dosimeter hole, etc., as had been anticipated. When the lower liner was pulled for inspection at the end of phase III, the bottom 1 to 2 in. of the liner remained frozen in the bottom of the hole. The break was sharp and appeared to have taken place before the end of the test, since almost the entire area of the break had an oxide coating. There was salt on the liner and other evidence of splashing up to a distance of about 4 to 6 in. from the bottom.

Such an occurrence would not be anticipated in the demonstration itself due to several reasons: (1) little water should be present in the main radioactive array; (2) the off-gas system will be operated continuously on both the arrays; (3) the end of the liner will not be in contact with the salt, and, thus there should be no axial stress on the liner, such as was produced in the prototype due to the flow of salt into the bottom of the hole; and (4) the liners will be made of 304L steel instead of 304 as was the case with the prototype.

The bottom foot of the lower liner was cut off, and a new section made of 304L steel was welded on. The bottom of the hole was then deepened to avoid contact with the liner, and phase IV was started on June 2, 1965. During phase IV, there was no air flushing of the hole.

Phase IV of the Hole Liner Prototype Experiment was terminated on July 19, 1965, after 47 days of operation without off-gas purge. The new bottom section of the lower liner, made at ORNL (type 304L stainless steel) and attached by the Lyons Manufacturing Company, appeared to be in good condition, although there was a bright red coating on the bottom 3 in. The off-gas system was operated for 45 min just before shutdown, producing about 50 ml of condensate.

4.3 CORROSION STUDIES

4.3.1 Field

A number of thermocouple failures occurred during the high-temperature heat experiments (Sect. 2.1) as a result of scaling and corrosion of the type 304 stainless steel sheath. When the large heaters (304L) were removed from the structure, they were also heavily

scaled, with the greatest attack on those heaters exposed to the highest temperature.

Thermocouples attached to the wall heater were found by metallography to have lost as much as 0.007 in. of the original 0.018 in. thickness by scaling. Heavy intergranular attack also completely penetrated the sheath. This resulted from exposure to approximately 600°C for 33 days. Thermocouples in the salt at 6 in. out from the heater showed much less scaling, but complete penetration due to stress corrosion cracking was observed. At 12 in. out from the heater, there was a small amount of scaling on the thermocouples. The temperature reached approximately 225°C at 6 in. and 190°C at 12 in. out from the heater.

The wall heater that operated at temperatures up to 690°C for 33 days was very heavily scaled, and intergranular attack to 0.045 in. was observed. Significantly, carbide precipitation was also observed at grain boundaries throughout the heater wall, serving to accelerate the intergranular attack. The floor heater that reached a maximum of 590°C in 33 days was less heavily scaled, and intergranular attack penetrated only 0.002 in. Precipitated carbides were present at the grain boundaries. The array heater in the floor had still less scale on the surface after 28 days of operation at a maximum temperature of 435°C, and intergranular attack penetrated only to 0.0015 in. No carbide precipitation was observed in the array heater sheath. Table 4.6 presents these data. Since carbides may be expected to precipitate in type 304L stainless steel in the range of 800 to 1600°F (426 to 870°C), the long period of operation of the wall and floor heaters within this temperature range provided ideal conditions for carbide precipitation. The array heater operated at the very lower limit of carbide precipitation, and no precipitation was observed. This indicates that calcination operations and storage of calcined waste containers should be carefully controlled to minimize the time stainless steel containers are in the temperature range of carbide precipitation.

4.3.2 Laboratory

A sodium chloride–moist air atmosphere or sodium chloride in the presence of moisture at a high temperature is very severe service for most construction materials. Type 304 stainless steel thermocouple sheaths used in the single-heater and array experiments (described above) showed severe scaling and stress corrosion in areas where the temperature reached ~175°C. The relatively thin-wall (0.018 in.) sheath of the thermocouples was completely penetrated in a number of cases. Consequently, a series of laboratory tests were run to determine which materials might be suitable for use in Project Salt Vault.

Construction materials tested include stainless steel (types 304L, 310, and 347), Hastelloy C, Haynes alloy No. 25, titanium, carbon steel, aluminum, nickel, Monel, Inconel, Ni-o-nel, and protective coatings designed to allow use of a cheaper material, such as carbon steel, as the base metal. Corrosion testing was performed by the corrosion group of the Reactor Chemistry Division.

The test environment consisted of ground natural salt (or reagent salt plus contaminants present in Kansas rock salt) in air and contained in sealed quartz tubes. These quartz tubes, containing the welded coupons and ground reagents in air, were placed in a furnace maintained at the test temperature. Tests performed under these conditions covered a period of 30 days (720 hr).

Tables 4.7 and 4.8 present the results of corrosion tests at 300 and 500°C. Titanium and carbon steel were eliminated from the 500°C tests and 1100 aluminum from both 300 and 500°C tests because rapid attack was observed in earlier, aborted tests.

The data presented in these tables show that in natural salt all the materials (types 304L and 310 stainless steel, Hastelloy C, and Haynes alloy No. 25) exhibit satisfactorily low corrosion rates at 500°C. At 300°C the type 310 stainless steel and the carbon steel

Table 4.6. Corrosion of Type 304L Stainless Steel Heater Cans

Location	Maximum Temperature (°C)	Duration (days)	Scaling	Intergranular Penetration	Carbide Precipitation
Wall	690	33	Severe	0.045	Yes
Floor	590	33	Moderate	0.002	Yes
Array	435	28	Slight	0.0015	No

Table 4.7. Corrosion in Salt

Medium	Penetration (mils/yr)[a]					
	Type 304L Stainless Steel	Type 310 Stainless Steel	Hastelloy C	Haynes Alloy No. 25	Ti-45A	Carbon Steel
Natural NaCl	0.4	0.2[b]	0.1	0.1	0	2.0[b]
Reagent-grade NaCl	0.2	0.1	<0.1	0.1	0	1.6[b]
99.5% NaCl–0.5% H_2O	0.5[b]	0.3[b]	0.1	0.1[b]	0.1	1.5[b]
99.75% NaCl–0.25% $MgCl_2$	0.8	0.4[b]	0.1	0.2	0.1	3.5[b]
95% NaCl–5% $CaSO_4$	0.6[b]	0.2[b]	0.1	0.1[b]	0	1.9[b]
94.25% NaCl–0.5% H_2O–0.25% $MgCl_2$–5% $CaSO_4$	0.4	0.3	0.1	0.1[b]	0.1	3.8[b]

[a]Exposure at 300°C for 720 hr.
[b]Pitting attack.

Table 4.8. Corrosion in Salt

Medium	Penetration (mils/yr)[a]			
	Type 304L Stainless Steel	Type 310 Stainless Steel	Hastelloy C	Haynes Alloy No. 25
Natural NaCl	0.5	0.1	0.1	0.2
Reagent-grade NaCl	0.3	0.5[b]	0.1	0.1
99.5% NaCl–0.5% H_2O	0.6	0.4	0	0.1
99.75% NaCl–0.25% $MgCl_2$	0.5	0.4[b]	0.5	0.3
95% NaCl–5% $CaSO_4$	0.4[b]	0.3[b]	<0.1	0.1
94.25% NaCl–0.5% H_2O–0.25% $MgCl_2$–5% $CaSO_4$	0.7	0.2	0.1	0.1

[a]Exposure at 500°C for 720 hr.
[b]Pitting attack.

have low corrosion rates but show pitting. On the basis of these data, type 304L stainless steel appeared to be the most economical and satisfactory material for use in natural salt at both 300 and 500°C. Hastelloy C, Haynes alloy No. 25, and titanium would also be satisfactory at 300°C, but undesirable because they are more expensive and more difficult to fabricate. Because of the unpredictable nature of pitting corrosion, any material which develops significant pitting is considered unsuitable.

The materials discussed above were also tested at 200°C. Tests of the additional materials (type 347 stainless steel, nickel, Monel, Inconel, and Ni-o-nel) and a test of the corrosion of type 304L stainless steel in a cobalt gamma-radiation field were also run. The test of 304L stainless steel in contact with salt in a ^{60}Co

gamma-radiation field indicated that gamma radiation should have no effect on the corrosion rate. The results of the 200°C tests may be found in a report by W. E. Clark *et al.*[7] Based on these tests, it was decided to use 304L stainless steel for all critical components in Project Salt Vault where contact with salt could cause problems.

4.4 RADIOLYTIC CHLORINE PRODUCTION STUDIES

The storage of high-level wastes in salt formations will expose the surrounding salt to radiation, and the dose in the immediate proximity of the packaged wastes is expected to be as high as 10^{10} rads. While it is known that radiation will cause some damage to alkali halides, there has been no definitive work to prove or disprove the release of free halogen from sodium chloride. The only work found in the literature that seems to be related to this problem is that of Epstein,[8] who gives quantitative data on the amount of oxidizing substance (presumably chlorine) formed in solid potassium chloride upon exposure to high levels of gamma or beta radiation. Epstein could not detect any chlorine in the gas phase with certainty; thus he placed an upper limit of 0.5% of the total oxidizing power generated within the solids which escapes to the gas phase. The oxidizing power stored within the crystalline solid was determined by dissolving the solid in water and determining the oxidizing equivalent against potassium iodide or *o*-tolidine. Values of *G* (number of molecules produced per 100 eV of energy absorbed) are given which decrease with dose – from 1.47×10^{-2} at 2×10^{7} rads to 5.1×10^{-4} at 3.27×10^{9} rads.

Chemically pure sodium chloride was gamma irradiated at the steady-state temperature (35 to 60°C) of a 10,000-Ci ^{60}Co source, as well as at temperatures up to 250°C. No release of chlorine to the vapor phase was detected by gas chromatography or by chemical methods in the irradiations performed at 35 to 60°C with doses up to 8×10^{9} rads and at 250°C with 3×10^{8} rads. The *G* values for the production of oxidizing power generated in the solid decreased with dose.

White crystalline sodium chloride changes color with increased doses of irradiation. At 10^{6} rads it is light tan; it progressively deepens to brown and finally to a dark blue-black at about 5×10^{8} rads. Color produced by irradiation can be annealed. The annealing process is temperature dependent and is essentially complete in a few hours at 250°C, but it requires nearly a week at 190°C. When salt is irradiated at elevated temperatures, the resultant color depends on which process is faster – the accumulation or the annealing of the color centers. For example, at 160°C, accumulation predominates, and the salt becomes colored; but at 250°C the annealing process predominates, and the salt remains white. As a result, the salt irradiated at 250°C still retains oxidizing power even though it shows no apparent change in color. (However, the residual oxidizing power is several orders of magnitude less than for salt irradiated at ambient temperature.)

The *G* values obtained by the irradiation at 35 to 60°C were used to calculate the oxidizing power that would be produced in the salt surrounding a hypothetical waste container of the future. These values are given in Table 4.9. The *G* values used for the higher dose rates were obtained by extrapolation. The temperature of the zones receiving doses of 10^{8} rads and greater is expected to be about 200°C, and the *G* values for these zones would be expected to be lower than those used in the table.

The calculated time rate of production is shown in Table 4.10. This table (as was Table 4.9) was based on a Purex-type waste in a 6-in.-diam can that had been cooled 2 years before burial.

The studies indicated that the release of chlorine from irradiated salt will be negligible from the standpoint of a short-term storage. It was not possible to determine whether long-term (several years) storage and irradiation would result in the release of up to 2 moles of free chlorine from the salt surrounding the waste containers.

The previously discussed studies were limited to reagent-grade salt of +20 mesh size. Since the salt surrounding disposal containers will consist of massive rock salt as well as fine pieces of mined or otherwise crushed material, the effect of particle size on the extent of radiolysis was investigated. Finely ground salt (−100 mesh) was found to produce more oxidizer per unit weight than the unground material. Part of the ground powder was annealed at 500°C for 24 hr before irradiation in an effort to remove strains introduced by the grinding. There was a slight drop in oxidizer content as a result of this annealing; however, the amount of oxidizer found was still substantially higher than that of

---

[7] W. E. Clark, D. N. Hess, P. D. Neumann, L. Rice, and J. L. English, *Laboratory Development of Processes for Fixation of High-Level Radioactive Wastes in Glassy Solids. (4) Corrosion Studies on Candidate Materials of Construction,* ORNL-3816 (August 1967).

[8] L. M. Epstein, *Formation of Chemically-Free Halogen by Radiolysis of Potassium Chloride,* WERL-0100, Westinghouse Electrical Corp. Research Laboratories, Pittsburgh, Pa. (June 1962).

Table 4.9. Yield of Oxidizing Agent with Dose

Dose (rads)	G	Moles of Oxidizing Substance (per gram of salt)	Mass of Salt Radiated (g)	Total Moles of Oxidizing Agent Produced
10^6	9×10^{-3}	9×10^{-9}	1.4×10^7	0.2
10^7	3.7×10^{-3}	3.7×10^{-8}	6.8×10^6	0.4
10^8	1.4×10^{-3}	1.4×10^{-7}	3.6×10^6	0.3
10^9	7×10^{-4}	7×10^{-7}	1.5×10^6	1.0
1.2×10^{10}	2×10^{-4}	4×10^{-6}	2.9×10^5	0.7

Table 4.10. Probable Rate of Formation of Chlorine in Solid NaCl

Time After Burial	Dose	Percent of Total Chlorine Produced
20 days	8.6×10^6	8.5
40 days	1.7×10^7	11.0
80 days	3.4×10^7	14.0
160 days	6.9×10^7	17.0
320 days	1.4×10^8	21.0
1.75 yr	3.8×10^8	30.0
3.5 yr	7.5×10^8	38.0
7 yr	1.5×10^9	49.0
14 yr	3×10^9	63.0
28 yr	6×10^9	80.0

Table 4.11. *G*(Oxidizer) in Salt as a Function of Particle Size and Annealing

	Dose (rads)			
	3.2×10^6	10^7	3.8×10^8	10^9
	$\times 10^{-3}$	$\times 10^{-3}$	$\times 10^{-3}$	$\times 10^{-3}$
CP crystals (+20 mesh)	47	6.8	2	1.1
−100 mesh (ground)	147	37		
−100 mesh (annealed 24 hr at 500°C)			6	
−100 mesh (annealed 100 hr at 500°C)			2.9	
Synthetic crystals (+2 mm)			2.1	
Synthetic crystals (−100 mesh)			2.3	

the unground salt. This suggested that surface effects might be involved.

Crystals of salt were grown from saturated salt solutions in two sizes. Precipitation with alcohol gave a product of −100 mesh which was carefully rid of alcohol by vacuum desiccation. Large crystals at least 2 to 3 mm to a side were grown by slow evaporation of saturated salt solution over a period of three months. Irradiation of these crystals gave the same radiolysis rate as that of the unground sample. Further annealing of ground material was then carried out, and the rate of radiolysis was found to approach that of the unground material after over 100 hr of annealing at 500°C. The *G* values for oxidizer production for the different conditions are shown in Table 4.11. It was concluded that radiolysis takes place within the crystal itself and is quite independent of surface effects.

It should be pointed out that the *G* values were obtained by dissolving the salt samples, and, even though grinding or crushing of salt appears to produce

higher G values, it would not be expected that any appreciable chlorine would be released under field conditions in a waste disposal operation.

Under some conditions, water may be released to the disposal holes from either shale strata or halite. Thus radiolysis of salt solutions is another possible hazard that was considered. Laboratory studies show that production of chlorine takes place in acid chloride solutions with chloride concentrations greater than 1.4 M; however, no serious problems from this mode of radiolysis would be anticipated since the samples of water collected from the mine were slightly on the basic side.

4.5 DOSIMETER DEVELOPMENT

For the demonstration disposal of high-level radioactive wastes in a salt mine, a dosimeter was required to measure the gamma dose being delivered to the salt surrounding the radioactive material. The requirements which had to be met by the dosimeter were:

1. have a reasonably accurate response to dose rates as high as 10^5 rads/hr and integrated doses as high as 10^5 rads,
2. be insensitive to temperature to 200°C or have a known response over the temperature range,
3. be able to withstand contact with the salt during the exposure period,
4. have a reasonably flat energy response for energies above about 0.1 MeV,
5. be limited in size to a maximum of about 0.8 in. in diameter and 2 in. in length and be capable of being inserted through a 2-in.-diam by 10-ft-long hole.

Ionization chamber instruments were first considered as potential dosimeters; however, it appeared that if the chamber were remote from the electronics, the connecting cable itself would act as an ionization chamber, and the 200°C appeared to rule out the possibility of placing the electronics in the probe. Thermoluminescent dosimeters were ruled out because of the temperature. The two most promising types seemed to be the silver-activated metaphosphate glass rods and the glass-encapsulated ferrous sulfate dosimeters. Both types were investigated and found to be practical.

4.5.1 Glass Rod Dosimeters[9]

Three glass fluorod types (all 1 × 6 mm) were tried: Toshiba II, Bausch and Lomb high Z, and Bausch and Lomb low Z. The Toshiba II rods were quickly eliminated, since they were found to lose their radiation-induced photoluminescence rapidly at 250°C. Both low-Z and high-Z Bausch and Lomb rods were found to be usable, but it was concluded that the low-Z rods were better suited for the application for the following reasons:

1. The response of the low-Z rods is less dependent on the gamma energy.
2. The low-Z rods have a greater sensitivity to radiation.
3. Low-Z rods are reported to be less susceptible to chipping, thereby assuring more reliable readings.

4.5.1.1 Procedure. – A Turner model 111 instrument was used in this study. Due to certain peculiarities in the instrument, no two instruments are likely to read the same on a given rod, although if the instruments are working properly, the shapes of their response curves should be about the same. In order to establish if our instrument was performing properly, it was compared with points taken from the published curves of two other investigators. The data from all three sources were normalized at a dose of 5×10^3 rads. The agreement was quite good.

The procedure used in this study was essentially the standard procedure for use of glass rod dosimeters. Generally, three rods were exposed for each test condition. Rods were not read until at least 24 hr after exposure to allow for buildup of the fluorescence. All irradiations were performed in either of two ^{60}Co facilities, which delivered dose rates of 2.3×10^3 and 2.3×10^4 rads/min respectively. All of the irradiations at elevated temperature and a few of the ambient temperature exposures were carried out with the glass rods inside a miniature electric furnace which was placed in the cobalt facility. The presence of the furnace reduced the dose rates to 1.8×10^3 and 1.8×10^4 rads/min respectively. Calibration of the dose rates delivered by the cobalt facilities was by means of the ferrous sulfate dosimeter. Exposure times ranged from 1 min up to about 1 hr.

Since the bare glass rods have an energy response characteristic which increases very sharply below about 0.3 MeV, peaking at about 0.04 MeV, it was necessary to place the rods in a shield to flatten the response curve. The shield chosen consists of 0.030 in. of tantalum and 0.015 in. of Teflon. This shield used with

[9] R. L. Bradshaw, W. L. Beck, H. W. Dickson, and W. F. Hanson, "High Dose Response of Glass Rod Dosimeters Irradiated at Temperatures up to 250°C," *Health Phys.* **13**, 910–15 (1967).

the Bausch and Lomb low-Z rods produces a response curve which peaks at about 0.25 MeV with a value about 1.3 times that at 1 MeV. The minimum response is about 0.3 of that at 1 MeV, occurring at 0.07 MeV. Since generally less than 10% of the dose at any point in salt is from gammas below 0.25 MeV, this response appeared to be adequate for our purposes, and all of our exposures were made using this shield.

4.5.1.2 Results. – Figure 4.16 shows the results obtained for irradiations carried out at ambient temperature, 150°C, and 200°C. When the irradiations were carried out at the elevated temperatures (open circles and triangles), the response as read by the fluorometer was greater by about a factor of 2 than the response for ambient temperature irradiation (solid dots). The curves are such that the calibrations would be usable up to about 10^5 rads. However, if one were to use the ambient temperature curve to estimate the dose which was received at some unknown irradiation temperature up to 200°C, the estimate could be off by a factor of 4 at doses approaching 10^5 rads.

There was reason to believe that a postirradiation heat treatment would improve the response at high doses and reduce the effect of variation in irradiation temperature; so the same rods which were used to obtain the data in Fig. 4.16 were heated for 1 hr at 325°C and then read again. These results are shown in Fig. 4.17. The 150 and 200°C irradiation temperature curves (open circles and triangles) now appear to coincide and to be much closer to the curve for the ambient temperature irradiation than before. If one were to use this ambient temperature curve to estimate the dose received at some unknown irradiation temperature up to 200°C, the estimate would not be more than about 50% off at doses as high as 10^5 rads, and less than that at lower doses. Thus it is not necessary to know the irradiation temperature as exactly, or to control it as precisely, when the postirradiation heat treatment is used. Another point which should be noted is that now the calibration is usable up to about 3×10^5 rads.

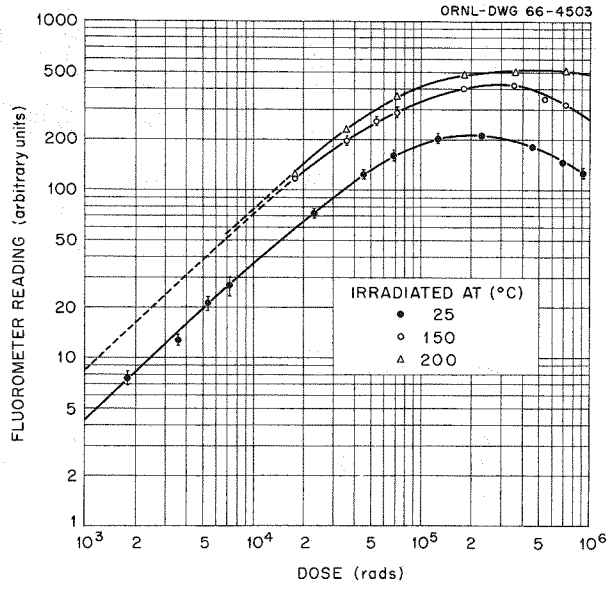


Fig. 4.16. Response of Bausch and Lomb Low-Z Rods Before Heat Treatment.

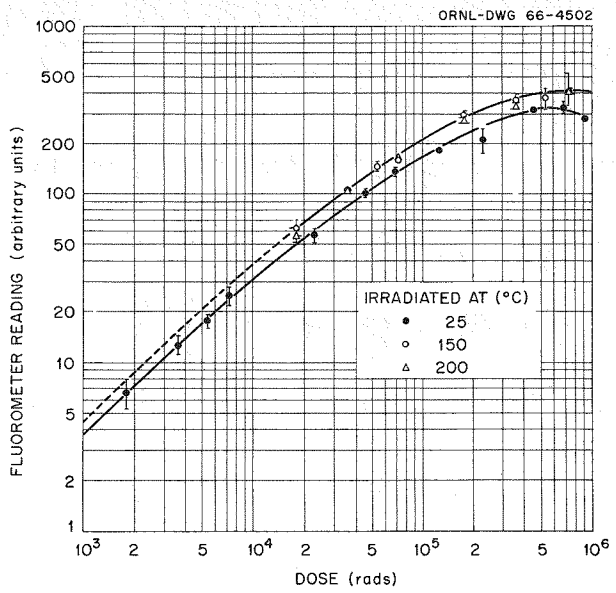


Fig. 4.17. Response of Bausch and Lomb Low-Z Rods After Heat Treatment for 1 hr at 325°C.

A heating test was run to determine if the photoluminescence in rods irradiated under the different temperature and dose conditions could be erased and the rods reused. One hour at 450°C was found to be totally inadequate, but 1 hr at 500°C reduced about 80% of the rods to background readings. Probably a small increase in the erasure temperature would erase most of the photoluminescence in the remaining rods.

The reused rods irradiated at 200 and 250°C showed about the same response as the new rods at 200°C. The sensitivity of the rods exposed at ambient temperature appeared to have been reduced by about 25% by the annealing process. It has been suggested that this reduced sensitivity is due to a surface reaction on the rod during the annealing period and that this effect can be minimized by annealing in an inert atmosphere.

(Attix[10] has found as much as 50% variation in sensitivity between different batches of rods. It thus

[10] F. H. Attix, *Present Status of Dosimetry by Radiophotoluminescence and Thermoluminescence Methods*, NRL-6145 (1964).

appears that it is important to check the calibration of each batch of rods.)

These reused rods were given the postirradiation heat treatment of 325°C for 1 hr and read again. Generally it appears that the photoluminescence in rods can be erased and the rods reused without the necessity of determining a new calibration curve if they are given the postirradiation heat treatment. It also appears that there is little difference in the response between rods irradiated at 200 and 250°C.

Another point which should be considered is fading of the fluorescence with time. Over a five-month period, eight of our reused rods which were not postirradiation heat treated gained an average of 7% in reading. Over this same period of time, ten rods which were heat treated (four reused and six new ones) lost an average of about 14% in reading; however, the reused rods lost less than the new rods, and the rods exposed at ambient temperature lost less than those exposed at elevated temperature. Thus it appears that the long-term stability of the readings of rods stored at ambient temperature is somewhat dependent upon the postirradiation heat treatment, the temperature at which the irradiation took place, and whether the rods are new or have been reused. This would suggest that the length of time which the rods were held at an elevated exposure temperature might be an important consideration. Although the studies reported herein have not indicated any significant effect for exposures varying from 1 min up to about 1 hr, long exposure period results could be significantly different.

4.5.1.3 Conclusions. – Bausch and Lomb low-*Z* glass rod dosimeters with postirradiation heat treatment are usable at doses up to about 3×10^5 rads and exposure temperatures up to 250°C.

Postirradiation heat treatment of 1 hr at 325°C produces a calibration curve which is essentially the same for exposure temperatures from 150 to 250°C. The calibration curve for exposures at 25°C is about 25% lower than the elevated temperature curve. (Temperatures between 25 and 150°C were not investigated.)

The photoluminescence of exposed rods can be erased by holding them at 500°C for 1 hr. Of the rods so treated, 80% were reduced to background readings. These rods can then be reused with the same postirradiation heat treatment calibration curve with somewhat less accuracy than new rods.

The long-term stability of readings depends on several variables, including the exposure temperature and the postirradiation heat treatment.

The length of the exposure period does not appear to be important for periods from 1 min up to 1 hr; however, there is some indication that it may be important for long exposures at elevated temperatures.

4.5.2 Chemical Dosimeters[11]

Ferrous sulfate solution, which shows relatively flat response to radiation with energies between 0.1 and 2 MeV, and ceric sulfate solution are the two reagents most commonly used in chemical dosimetry. The former has been reported to be reliable up to 72°C and the latter up to 90°C. The *G* value of the ferrous solution is reported to increase linearly with temperature, while there is considerable discrepancy in the reported temperature response of the ceric system, whose *G* value is claimed to increase, decrease, or remain relatively unchanged with temperature. Since these solutions will boil and evaporate at temperatures above 100°C, it was necessary to keep them enclosed in sealed containers for this work. Thus contamination or interference by the salt atmosphere of the mine did not have to be considered. The size of the vessel required to contain the 1 ml of dosimetric solution was well within the size limit specified for the field setup.

The small change in response with increasing temperature of the two chemical dosimeters that were considered was encouraging because it indicated that there was little change in the fundamental radiolytic processes with temperature, at least up to the upper limits reported. The possible use of either of these dosimeters up to a temperature as high as 250°C was investigated, and the results are reported here. The ^{60}Co facilities used were the same as those for the glass rods.

4.5.2.1 Effect of Temperature on Dosimetry Solutions. – First of all, the stability of each solution at temperatures up to 250°C was established by sealed-tube tests. Ceric sulfate solution heated to 150°C showed slight fading in color. Heating above 200°C caused the precipitation of a light yellow and amorphous material which was presumably cerous hydroxide. Increasing the acidity to 3 *N* from the usual 0.8 *N* prevented this precipitation; however, ceric ions still were reduced, with corresponding loss in color of the solution. Solid ceric sulfate is known to decompose at 196°C, and it is evident that ceric sulfate in solution also undergoes decomposition in the same temperature region.

---

[11] H. Kubota, "Gamma Dosimetry at 150–250°C with Deaerated Ferrous Sulphate Solution," *J. Inorg. Nucl. Chem.* 28, 3053–56 (1966).

Air-saturated ferrous sulfate solution was put through a similar test. The absorbance of each solution at 305 mμ increased by 0.2 to 0.4 absorbance unit when heated to 150, 200, or 250°C. This increase was found to result from the oxidation of iron(II) by air and varied with the volume of air above the solution.

Deaerated ferrous sulfate solutions put through the same heating test showed either no change or loss in absorption. It was concluded that the loss in absorption was due to impurities on the walls of the irradiation tube, since careful cleaning of the tubes with hot perchloric acid followed by steaming with water distilled from an acid dichromate solution eliminated this negative effect. Thus it was established that deaerated ferrous sulfate solution was stable up to the maximum temperature specified, and any changes in optical absorbance would be due solely to radiation effects.

4.5.2.2 Deaerated Ferrous Sulfate Dosimetry at Room Temperature. – Ferrous sulfate dosimetry solution (0.002 *M* $FeSO_4$, 0.001 *M* NaCl dissolved in water specially prepared for irradiation purposes) was deaerated by several techniques including bubbling with purified argon, neon, or nitrogen and vacuum degassing with alternate freeze and thaw. When deaeration was essentially complete, the tube containing the solution was sealed. This tube was then irradiated for a given time at room temperature, and the change in absorbance of the dosimeter solution was compared with that of air-saturated solution which had been exposed in the same position for the same duration. The *G* values were calculated [using air-saturated $G(Fe^{3+})$ = 15.6 and molar absorbance of Fe^{3+} at 25°C = 2240] and ranged from 5.7 to 8.4. It was found that dosimetry solution adhering to the tube walls at the point where the seal was made was decomposed by the heat of the sealing flame to cause negative error. This was eliminated in the vacuum technique coupled with alternate freeze and thaw by passing argon into the tube prior to that stage to prevent the melting solution from surging up the tube. The *G* value at 25°C with this technique averaged 8.07 ± 0.07.

4.5.2.3 Deaerated Ferrous Sulfate Dosimetry at High Temperature. – Deaerated ferrous sulfate solution sealed in glass tubes was heated to 150, 200, or 250°C and irradiated for prescribed periods. The irradiation was carried out in a furnace placed within a ^{60}Co source. The tube was then removed and cooled, and the absorbance of its contents at 350 mμ was determined on a Cary spectrophotometer. The results of irradiations at three temperatures are shown in Fig. 4.18.

Figure 4.18 shows a linear relation between absorbance and dose up to 60,000 rads, after which the

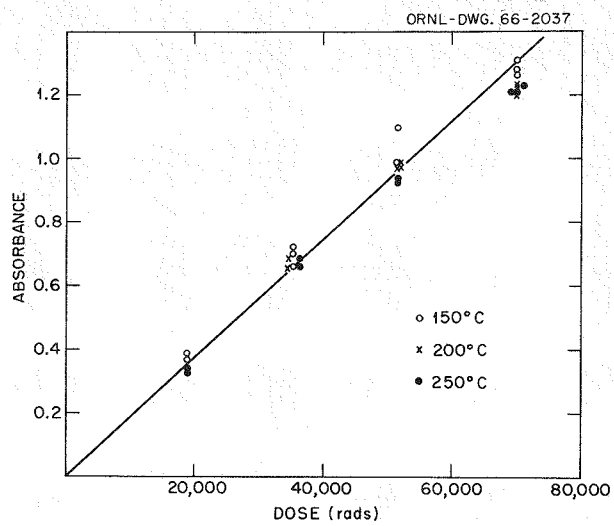


Fig. 4.18. Response of Deaerated Ferrous Sulfate Dosimeter at Elevated Temperatures.

relation begins to fall off, and 10,000 to 60,000 rads is the range that is being monitored at the demonstration. There is a slight variation in the responses at 150, 200, and 250°C, but the readings all come within the standard deviation for each temperature. The assumption was made, therefore, that the mean *G* value of 8.1 which was derived from the slope of the best-fitting line for the readings at the three temperatures would apply over this entire temperature range. The standard deviation is 6%.

Faulty cleaning of tubes appears as a negative bias, while incomplete deaeration and contamination of the solution will cause positive bias. There is no way to check this type of interference beforehand, and the only remedy is the use of great care in preparing the dosimeters.

Some of the factors which need to be considered in evaluating the temperature effect on the reactions taking place in these solutions are discussed by Hochanadel and Ghormley.[12] Their results indicate that the oxidation of deaerated ferrous sulfate has a positive temperature coefficient, so that the *G* value goes up with increasing temperature. If this trend can be extrapolated to above 100°C, then the *G* values should be higher than the 25°C value, which is reported to be 8.2 and found to be 8.1 in this study. There is apparently some negative temperature factor which becomes important above 100°C to cause the dosimeter response to remain at the ambient temperature level.

[12] C. J. Hochanadel and J. A. Ghormley, *Radiation Res.* **16**, 653 (1962).

5. Geology and Description of the Lyons Mine

T. F. Lomenick F. M. Empson

This chapter serves primarily to introduce the Lyons mine, the site selected for the demonstration experiment. This is accomplished by a discussion of (1) the geology of the area, including considerable information which was developed much later, (2) a brief history of the mine, and (3) a general description of conditions at the mine at the beginning of preparations for the experiment.

5.1 GEOLOGY OF LYONS MINE

The Lyons mine of the Carey Salt Company is located in Rice County, Kansas, near the city of Lyons (Fig. 5.1, taken from ref. 1). The mine was opened in 1890 and closed in 1948. During this period approximately 100 acres were mined out. The salt was mined by the room-and-pillar method, with salt extraction varying from about 60 to 70%. The floor of the mine lies a little over 1000 ft below the land surface, which is about 1700 ft above sea level.

5.1.1 Regional Setting

The Hutchinson salt member of the Wellington formation underlies central and southcentral Kansas

[1] J. M. Jewett and W. H. Schoewe, *Kansas Mineral Resources for Wartime Industries*, Kansas Geological Survey Bull. 41, pt. 3, pp. 73–180, 1942.

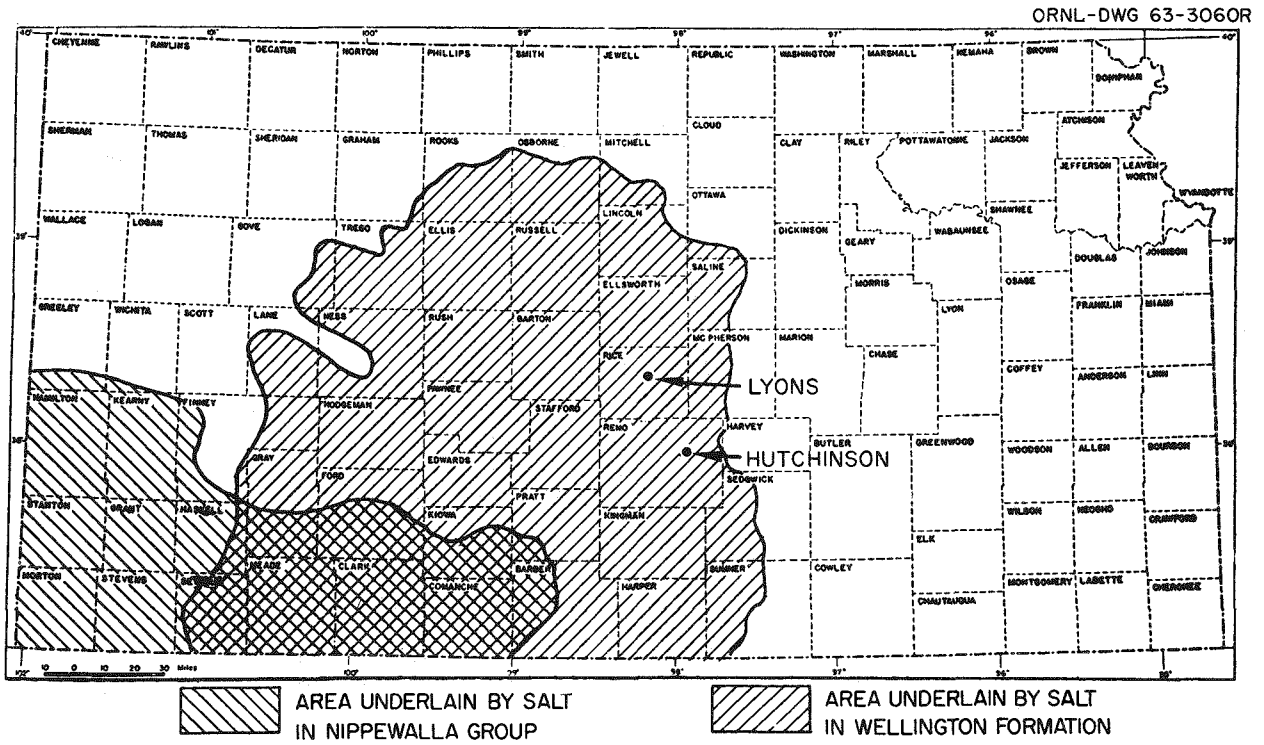


Fig. 5.1. Area Underlain by Deposits of Rock Salt in Kansas.

and extends southward into Oklahoma (see Fig. 5.1). The member is an integral part of the gently westward-dipping Permian-Pennsylvanian sedimentary rocks that underlie much of Kansas and crop out in the eastern third of the state. The salt is not present along this outcrop, probably because it has been dissolved by groundwater and surface water; however, it is present down the dip to the west. The eastern edge of the salt body lies approximately 400 ft below the land surface, but near its western edge in Kansas it is found at a depth of more than 1500 ft. Thicknesses of the unit range up to as much as 400 ft in Kansas. In general the Hutchinson consists of a complex mixture of salt, anhydrite, and shale, with salt being the predominant fraction throughout most of its extent in Kansas.[2,3]

It is generally agreed that large salt beds such as the Hutchinson were formed as a result of the evaporation of seawater. During the Permian period a relict sea covered a large part of what is now the state of Kansas. The sea was partially cut off from the ocean to the southwest by an uplift of mountains across present-day southwestern Oklahoma.[4] As water vaporized in the evaporation basin, it was replaced by the lateral flow of sea water through the inlet to the southwest. When the brine became saturated, salts were deposited. Periodic inflows of clay and silt to the basin from streams draining the surrounding land masses resulted in the deposition of shale beds in the sequence. As the evaporites and associated sediments were deposited, the basin underwent intermittent downwarping. This allowed a relatively thick sequence of evaporites to be deposited in a comparatively shallow basin. The Mediterranean Sea is an example of a modern evaporation basin. Here more water is removed through evaporation than is added by the sum of rainfall and runoff from the surrounding land. A net water inflow from the Atlantic Ocean through the Strait of Gibraltar compensates for the volume deficit in the Mediterranean.

5.1.2 General Stratigraphy of the Salt Section

At the Lyons mine the Hutchinson salt member consists of about 300 ft of nearly flat-lying beds of salt, shale, and anhydrite, with salt comprising about 60% of the sequence. The mine was operated in the lower part of the member. Within the mined unit, 1- to 6-in. layers of relatively pure sodium chloride are separated by clay and shale laminae that are usually less than 1 mm thick. These laminae constitute the major impurity in the salt and are characteristic of most bedded salt deposits. Shale beds, several inches thick and separated by about 15 to 18 ft of salt, lie above and below the mined unit and thus limit the vertical extent of mining. The mine floor was usually cut within a few inches of the underlying shale bed, while the roof is normally several feet below the overlying shale bed. The least contaminated salt, and thus the source of most of the production in the mine, lies in a 9-ft-thick section that extends from the top of the shale below the floor upward to a thin shale parting, approximately $\frac{1}{16}$ in. thick. Another prominent shale parting lies about $3\frac{1}{2}$ ft above the 9-ft roof. In some parts of the mine, this section was also mined. However, the additional excavation has resulted in a weak roof that buckles and fractures and frequently allows a 3-ft section of overlying impure salt to fall.

Two 2-in.-diam, 30-ft-deep core holes were drilled in the floor of the mine in entry 9 (Fig. 5.2), while two cores approximately 20 ft in length were obtained from the roof of the mine at the same locations. These cores, along with the log of a third hole drilled previously in entry 7 (ref. 5), were used to construct a geologic cross section of a portion of the salt section from the northwest end of entry 7 to the southwest end of entry 9 (Fig. 5.3).

Considerable quantities of shale and some anhydrite are included in the salt section from the floor down to a depth of about 115 in. in entry 9 and to a depth of approximately 135 in. in entry 7 of the mine. The shale, which is noncalcareous and greenish gray to black, commonly occurs in beds 1 in. to as much as 15 in. thick that usually contain a few crystals of clear to orange halite and some stringers of fine-grained anhydrite. As seen in Fig. 5.3, these beds thicken and thin considerably over relatively short distances. Frequently the beds grade, both laterally and vertically, into salt that contains many pods and irregularly shaped lenses of shale. This unit of the section is underlain by about 80 to 125 in. of relatively pure salt. The salt consists essentially of medium to coarsely crystalline clear to brownish halite that contains disseminated blebs and

[2] Lee Wallace, *Stratigraphy and Structural Development of the Salina Basin Area,* Kansas State Geological Survey Bull. 121, p. 167, 1956.

[3] W. G. Pierce and E. I. Rich, *Summary of Rock Salt Deposits in the United States as Possible Sites for Radioactive Waste Materials,* U.S. Geological Survey Bull. 1148, pp. 38–41, 1962.

[4] William H. Twenhofel, *Treatise on Sedimentation,* 2d ed., p. 505, Dover Publications, New York, 1961.

[5] William B. Heroy, *Lithology of the Salt Section in the Mine of the Carey Salt Company, Lyons, Kansas,* Technical Report No. 62–9, The Geotechnical Corporation (June 1962).

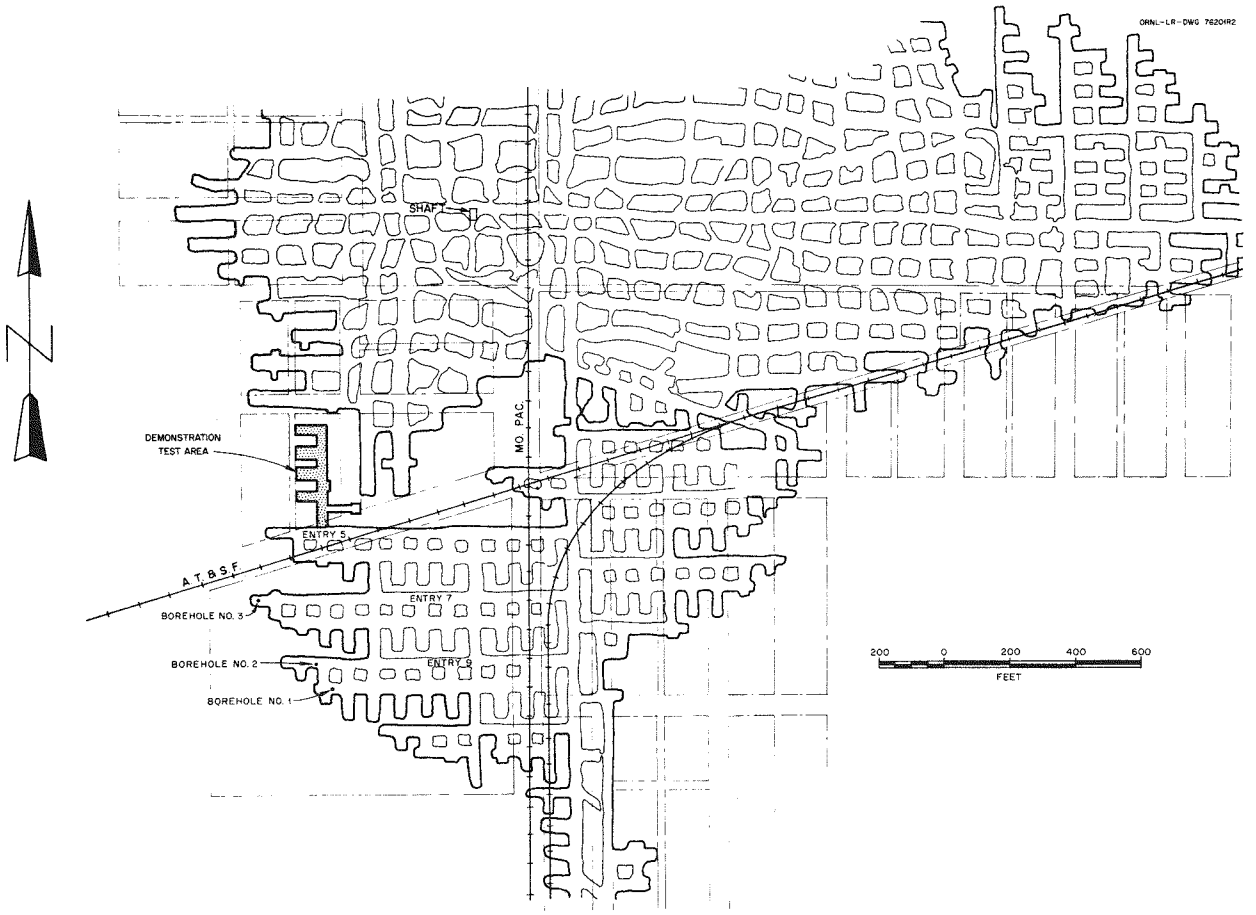


Fig. 5.2. Map of Part of Mine of the Carey Salt Company, Lyons, Kansas, Showing Location of Boreholes and Experimental Area.

inclusions of dark-colored clay that, in places, gives the salt a dark smoky appearance.

A second zone of interbedded salt, shale, and anhydrite about 40 to 50 in. thick lies beneath the relatively pure salt sequence. The shale and anhydrite are similar to the beds described higher in the section, but the shale beds are thinner, and a larger amount of anhydrite in the form of layers and lenses is present. For the remaining part of the section in entry 9, which was cored to a depth of about 360 in. below the mine floor, the cores show a relatively pure salt sequence like that described above. In entry 7 the same salt is interbedded with thick shale and anhydrite beds at a depth of about 360 in. It is likely that the same thick shale and anhydrite unit would have been intercepted in entry 9 had the drilling proceeded a few feet deeper.

The sediments above the ceiling of the mine, up to 250 in., consist of a relatively pure salt sequence that is interbedded with four separate shale zones. These shales, like those below the mine floor, are greenish gray to black and frequently contain lenses and crystals of clear to orange halite and stringers and lenses of anhydrite. The thickest of the shale beds lies at a minimum distance of about 20 in. above the present roof of the mine. (In the experimental area excavation, this shale bed lies about $2\frac{1}{2}$ ft above the mine floor.) The bed was observed to be about 12 in. thick in borehole 2, entry 9, but it had thinned to about 3 in. in the core from entry 7 of the mine. The other shale zones, as shown in Fig. 5.3, lie between about 130 and 230 in. above the roof. (The shale bed at about 180 to 200 in. comprises the ceiling in the newly mined test area.) The salt from the ceiling cores is composed mainly of medium- to coarse-grained clear to brownish halite crystals that contain, in places, many blebs and irregularly shaped masses of clay that give the material a

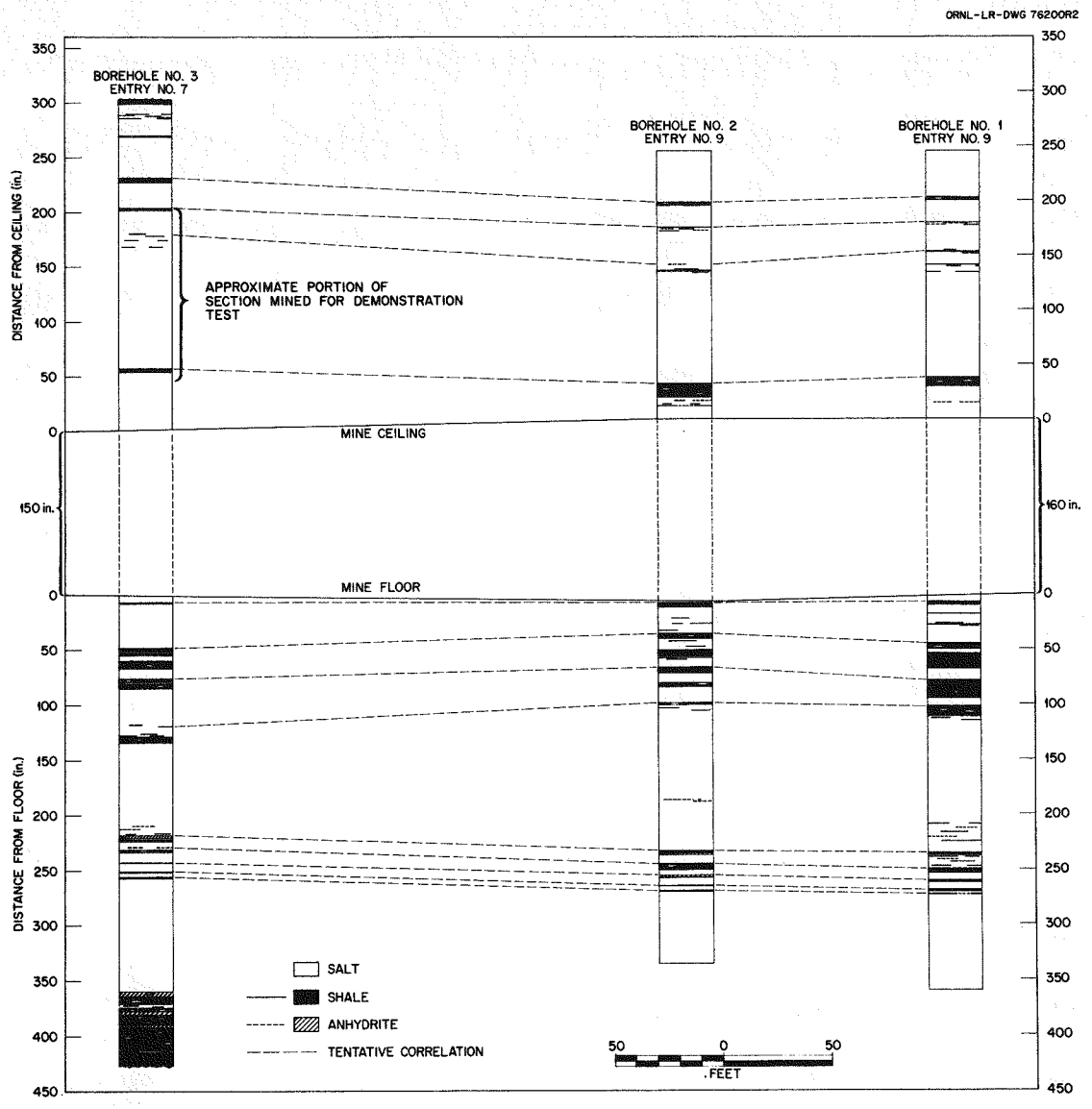


Fig. 5.3. Generalized Geologic Cross Section of a Portion of the Hutchinson Salt Member of the Wellington Formation in the Lyons Mine.

smoky appearance. In addition, from about 70 in. above the mine roof to the end of the cored section, the salt contains many scattered blebs of an orange- to red-colored microcrystalline mineral that has been identified as polyhalite.

In summary, the salt unit that has been mined in the Lyons mine consists of relatively pure salt that contains minor inclusions of clay and shale. The first 115 to 135 in. of the section below the floor in the westernmost portion of entries 7 and 9 contains between 20 and 40% shale. The shale is present in beds that vary greatly in thickness over relatively short distances and may grade vertically and laterally into zones of salt that contain many pods and irregularly shaped lenses of shale and anhydrite. A second shaly zone approximately 40 to 50 in. thick is present, generally from about 220 to 235 in. below the floor. Four separate shaly zones occur in the first 250 in. of section above the mine roof. The thickest shale bed lies at a minimum distance of about 20 in. above the ceiling of the mine, while the other less prominent zones of shale lie between about 130 and 230 in. above the roof. These zones are usually only a

few inches thick and contain, in addition to shale, lenses and stringers of anhydrite and salt.

The newly mined experimental area lies at a level of about 14½ ft above the preexisting mine floor and extends upward a distance of about 15½ ft to a thin shale parting at the roof (Fig. 5.3). The floor of the newly mined area is composed predominantly of rock salt, while a thin shale parting marks the roof. A prominent shale bed that varies from a few inches to more than 1 ft in thickness lies approximately 2½ ft above the floor. Two easily distinguishable shale beds that are about ⅛ to ¼ in. in thickness are also observed in the test area at distances of about 12 ft above the floor. The salt in the excavation area contains numerous blebs of polyhalite that are commonly concentrated along bedding, giving the salt a banded appearance.

5.1.3 Detailed Lithology of the Ceiling in the Experimental Area

Because of the importance of the ceiling within the experimental area in maintaining mine stability, a series of ten cores ranging from 3.5 to 11 ft in length were

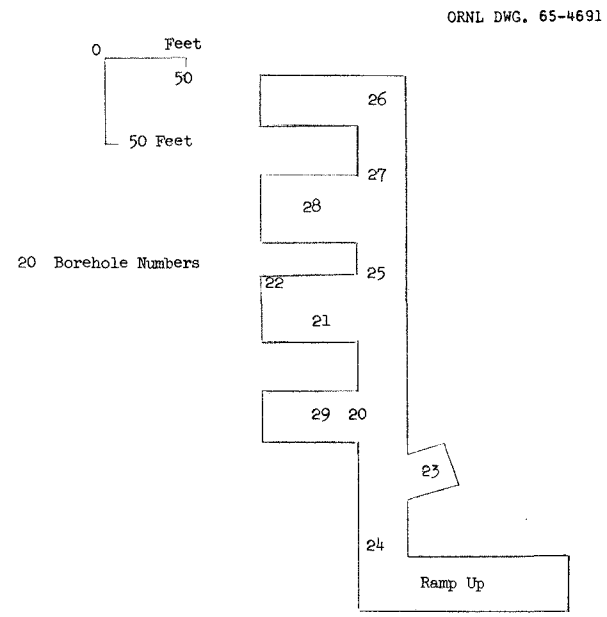


Fig. 5.4. Location of Boreholes in the Ceiling of the Experimental Area.

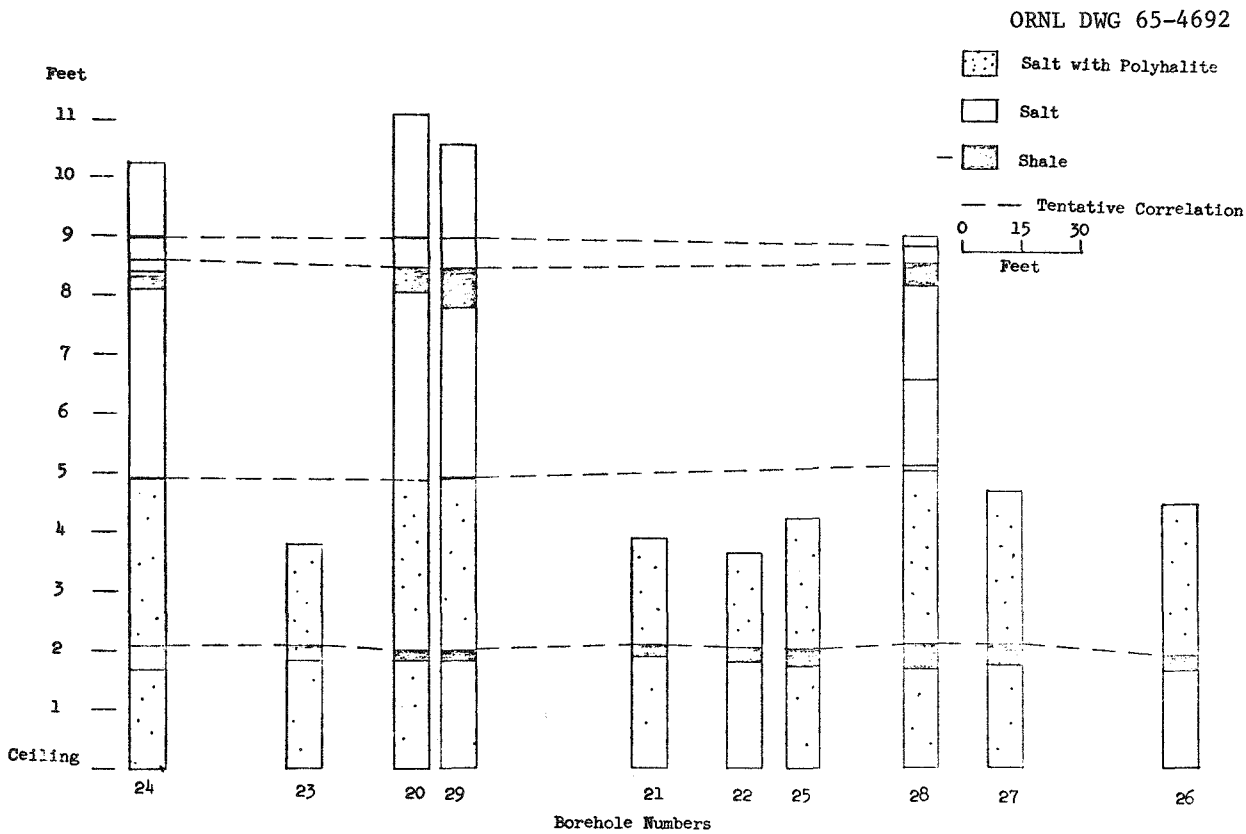


Fig. 5.5. Generalized Cross Section Through a Portion of the Roof in the Experimental Area.

taken in the roof of the experimental area of the mine to define the lithology of the salt section more specifically. The locations of these holes are shown in Fig. 5.4. From the cores a generalized cross section of the first 11 ft of roof in the experimental area has been prepared (Fig. 5.5). In general the salt is medium to coarsely crystalline and contains inclusions of shale, clay, polyhalite, and, occasionally, anhydrite. The shale, clay, and polyhalite inclusions tend to be concentrated along lines or zones that are parallel to bedding, thus giving the salt a characteristic banded appearance. With an increase in the amounts of shale or clay inclusions, banded salt grades into salt with thin shale partings. Shale or clay partings that are intermediate between banded salt and distinct shale beds may be referred to as "marginal" shale partings. Distinct shale beds varying from $1/16$ to 6 in. in thickness occur at distances of about 2, 5, $8\frac{1}{2}$, and 9 ft above the present ceiling, while several "marginal" shale partings occur principally within the section of salt 2 to 5 ft above the ceiling.

From the ceiling to the first shale bed at about 2 ft, the salt grades from almost clear halite, which is in a few places somewhat friable and also contains a few blebs of polyhalite, to smoky or banded salt that contains numerous clay blebs. The first shale bed, which begins a little less than 2 ft above the ceiling, varies from 2 to 5 in. in thickness over the experimental area and contains interbedded anhydrite stringers and lenses as well as some halite crystals. Generally the shale makes a sharp straight-line contact with the overlying salt, but the contact with the underlying salt is more irregular and undulating. Above this shale bed and up to about 5 ft the salt contains varying amounts of polyhalite, which gives the salt a characteristic orange to reddish color. In several places the concentration of clay or shale along bedding is great enough so that banded salt grades into salt having "marginal" shale partings. The shale parting at 5 ft is generally $1/16$ in. or less in thickness. From 5 ft to 11 ft the salt column, which contains some shale, polyhalite, and anhydrite impurities, is interrupted by shale beds at about $8\frac{1}{2}$ and 9 ft. The shale bed at $8\frac{1}{2}$ ft is as much as 6 in. thick and contains anhydrite stringers as well as a few large halite crystals, while the shale at 9 ft is only about $\frac{1}{2}$ in. thick and is essentially all shale.

It is generally agreed that small amounts of impurities, such as shale, clay, polyhalite, and anhydrite, tend to strengthen rock salt. However, when clay or shale inclusions become very heavily concentrated along planes parallel to bedding and there is a continuous film, or nearly so, of clay or shale between crystal faces, there is a reduction in the cohesion of the salt aggregate, and partings tend to develop. Of course the thicker the shale bed, the more pronounced is the parting. In the Lyons mine, where shale beds occur interbedded with salt beds, it is observed that separations occur in the roof at contacts between shale beds and salt. These separations develop initially at the first thick shale bed above the ceiling, and, as deformation proceeds, separations occur at shale beds higher in the section and then perhaps at the "marginal" shale partings in the original separated portion.

The first prominent shale bed above the ceiling in the experimental area lies about 2 ft above the roof (Fig. 5.5), and, from the core drilling, it was observed that a separation has developed at this point. It is expected that eventually separations may occur at the 5-, $8\frac{1}{2}$-, and 9-ft shale beds and perhaps at some of the marginal shale partings between the 2- and 5-ft beds.

5.1.4 Mineralogical Analysis of the Salt Section

A detailed mineralogical study has been completed of the salt section extending from 30 ft below the floor of the old mine workings to 10 ft above the ceiling in the demonstration site, a total thickness of 75 ft. The section was prepared through examination of numerous exposures in the rooms and haulageways of the old mine workings and the demonstration area, as well as from the cores of several holes that were drilled in the roofs and floors of these areas. X-ray diffraction was the principal means used to identify mineral species. Halite is by far the predominant evaporite in the sequence, while anhydrite and polyhalite are prominent in a few localities. Traces of gypsum, dolomite, and calcite were also identified. Illite and montmorillonite are the principal clay constituents, while quartz is also abundant in the interbedded shales. In general, the salt consists of layers of halite up to several inches in thickness that contain clay as thin laminae or blebs that tend to be concentrated parallel to bedding, thus giving the salt a banded appearance.

In that part of the section below the floor of the old mine workings, halite beds up to several feet in thickness are separated by shale layers that may be as much as 6 in. thick. A few thin anhydrite layers are usually present along with the shale. The 9-ft-thick portion of salt of the old mine workings contains the purest salt in the section examined, although a few blebs or very thin laminae of clay occur with the halite.

In the demonstration area the salt section contains several prominent shale layers, the lowermost of which is several feet thick in some places. Polyhalite blebs are distinguishable in this part of the section, and in some

places they are concentrated so heavily along bedding that the salt takes on a dark red banded appearance. Anhydrite blebs are commonly associated with the polyhalite. The salt in the roof of the experimental or demonstration area is, in general, quite similar to the salt immediately below it.

5.2 HISTORY OF THE LYONS MINE

The Lyons mine of the Carey Salt Company was opened in 1890 by sinking an 8- by 16-ft rectangular shaft to a depth of 1024 ft. The original developer was the Lyons Rock Salt Company, which was succeeded by a series of owners until the mine was closed in 1948. The Carey Salt Company purchased the property in 1939 and has retained ownership since that time.

Information on the mine facilities and equipment during early years of operation is not available. However, it is known that a fire destroyed the timber headhouse and processing plant in 1916, with some damage to the upper section of the wood-lined shaft. The headhouse was rebuilt, again as a timber structure, incorporating the headframe and mill in one building. At about the same time a new steam hoist was installed. During World War II two new hoist drums were installed.

When the mine was closed in 1948, the steam hoist was converted to electric drive, and the headframe and mill were scrapped. A light-duty headframe, fabricated from steel pipe, was installed to permit access to the mine. All production equipment was removed from the mine.

Tenants were secured for parts of the mine on two occasions. One firm made an unsuccessful attempt to raise chickens to broiler size under the relatively constant temperature and humidity conditions of the mine. This operation was terminated early in 1960. In 1960–61, the Armour Packing Company carried out experimental feeding of two lots of steers underground. Controls from the same herds were fed in pens on the surface. There was no use of the mine following these experiments until the beginning of preparations for Project Salt Vault.

The Lyons mine shaft is timber lined throughout its depth except for a few feet at the top, and appreciable quantities of groundwater have leaked into the shaft and into the mine. Water rings are installed at 300 ft below the surface to divert the water into a sump for pumping to the surface. At times large quantities of water dripped to the mine level and were pumped into a low area in the mine (in and around entry 2 south and west room – Fig. 11.41). The resulting solution and recrystallization under undisturbed conditions over many years resulted in the formation of exceptionally large crystals of sodium chloride over a large area in the mine. This brine was eventually pumped to the surface a few years before the initiation of Project Salt Valult.

5.3 DESCRIPTION OF LYONS MINE AT START OF PREPARATION FOR PROJECT SALT VAULT EXPERIMENT

The Lyons mine was in relatively good condition, considering its age and history, at the time preparations for Project Salt Vault began in 1963. Access to the mine had been maintained, and essential equipment was operable. However, the facility was not in condition for regular work underground, and hoisting equipment was not adequate to handle the expected loads. The following information on the condition of specific areas and components was taken largely from a mine evaluation report by Stearns-Roger Corporation, which in turn was based on two inspections of the mine, one on March 6 and the second during the week of March 18, 1963.

5.3.1 Shaft and Collar

Access to the mine is through a single rectangular shaft, approximately 8 by 16 ft, divided into two hoisting compartments, 5 ft 9 in. by 6 ft 9 in., and a ventilating compartment, 3 ft 0 in. by 6 ft 9 in. Except for a few feet at the collar, the shaft is lined for its full depth of 1024 ft with 4-in.-thick longleaf yellow pine, which has required only slight repair since installation when the shaft was sunk in 1890. A small part of the lining near the top was replaced after the fire in 1916. In 1951 the lining between the 680- and 780-ft levels was replaced because of damage in the form of inward bowing due to formation pressure. Wetted areas of the timber lining were soft to approximately 2 in. from the surface and solid for the remainder of the thickness. The dry areas were sound under about ¼ to ½ in. of soft surface. Shaft condition was generally good, with only minor repairs to guides, corner strips, the water rings, and inspection openings considered necessary. No escape way or ladder had ever been provided in the shaft to allow escape in case the hoist became inoperative or in case of damage to the shaft.

The shaft collar was of unknown competence, and replacement was considered desirable.

5.3.2 Hoist

The main frame of the mine hoist is part of the steam-driven unit furnished by the Litchfield Foundry

and Machine Company to Bevis Rock Salt Company in 1919. Two new cable drums, 8 ft 0 in. in diameter by 2 ft 9 in. wide, the north one with a 9-in.-wide brake drum attached, were installed in 1944. The drums are grooved for 1⅛-in.-diam rope with a capacity of 1145 ft in two layers of 26 wraps each. The drums were in good condition. A post brake was installed to provide a braking force of 22,000 lb with a 100-lb pull. The cable drums are mounted on a 9-in.-diam shaft.

The hoist was changed from steam drive to electric when the mine was shut down in 1948. A 150-hp, 350-rpm wound-rotor electric motor was installed, with a pinion mounted on the motor shaft driving a gear bolted to the south cable drum. Gears are 1.5 diametral pitch, 14½-deg pressure angle, and 12-in. face width. The pinion is 9.33 in. pitch diameter with 14 teeth, and the driven gear is 117.33 pitch diameter with 176 teeth. The large gear was not new when installed but was found to be sound when inspected in 1963. The pinion and gear required realignment in order to secure full face contact.

A Welch safety controller was installed to drive from the hoist shaft. Only minor repairs were needed on the controller.

A single cage designed for approximately a 1-ton load was installed in the shaft. The hoisting rope was 1⅛ in. in diameter, 6 × 19 improved plow steel, installed new in 1955. The exposed section of cable was somewhat corroded.

5.3.3 Headframe

The headframe, installed in 1955 following the scrapping of the timber mill and headframe, was fabricated of steel pipe. External corrosion was obvious, and it was suspected that corrosion was also present on the inner surfaces. The headframe was not considered suitable for further use.

5.3.4 Mine Ventilation

Mine ventilation was provided by a small (about 10 hp) industrial fan on the surface discharging down the airshaft. Two open fans were installed underground as boosters. Air control stoppings and brattices were in a deteriorated condition, and underground ventilation was minimal.

5.3.5 Underground Workings

Figure 5.2 is a plan of a large part, but not all, of the underground workings of the Lyons mine. The conditions of the workings vary with their age and with the mining practice at the time various sections were mined. Figure 5.6 is an example of conditions in part of the mine.

In general, areas near the shaft and to the north, west, and immediately south of the shaft were mined during the early years of operation. During this period, extraction was undesirably high, and an arched roof was used. The high extraction ratio resulted in rapid movement, and a thin section of salt remaining at the top of the arch fell away from the shale parting above. In large areas the floor is covered with the roof slab.

In later years the mining practice was changed to open entries and rooms which are rectangular in section, about 10 ft in height. This left a roof slab about 7 ft thick below the first major shale parting at 17 ft above the floor. Areas mined in this way have been exceptionally stable.

It will be noted also that the mining pattern is much more regular in the areas to the east and south of the shaft. This is a result of improved surveying and mine layout.

During World War II the demand for increased production under conditions of limited supply of labor and material resulted in "high topping" the roof slab in some areas, leaving a thin roof slab below the 17-ft parting, similar to that during early years. Only rooms and cross cuts were treated in this way; entries and haulageways were left with the original roof intact.

In general the underground areas of the Lyons mine were in good condition considering the age and long inactivity of the mine.

5.3.6 Electrical System

The Kansas Power and Light Company system terminated at the Carey Salt Company mine with three 50-kVA transformers connected to deliver power at 2300 V. The 2300-V feeder connected to a 2300-V main circuit breaker in the hoist house. Additional 2300-V breakers were in use for the mine feeder, the hoist feeder, and a 20-kVA station service transformer. The 20-kVA station service bank powered the 10-hp ventilating fan and a three-phase motor at the water sump 300 ft down the shaft.

In addition, a 7½-kVA transformer for surface lighting was connected to the 2300-V feeder ahead of the main breaker. These 2300-V breakers were originally installed as part of the power-generating system, consisting of two turbine generators. Five additional breakers were in place but unused, although some were connected on one side. These oil-filled circuit breakers were of 1920 vintage. Condition of the breakers,

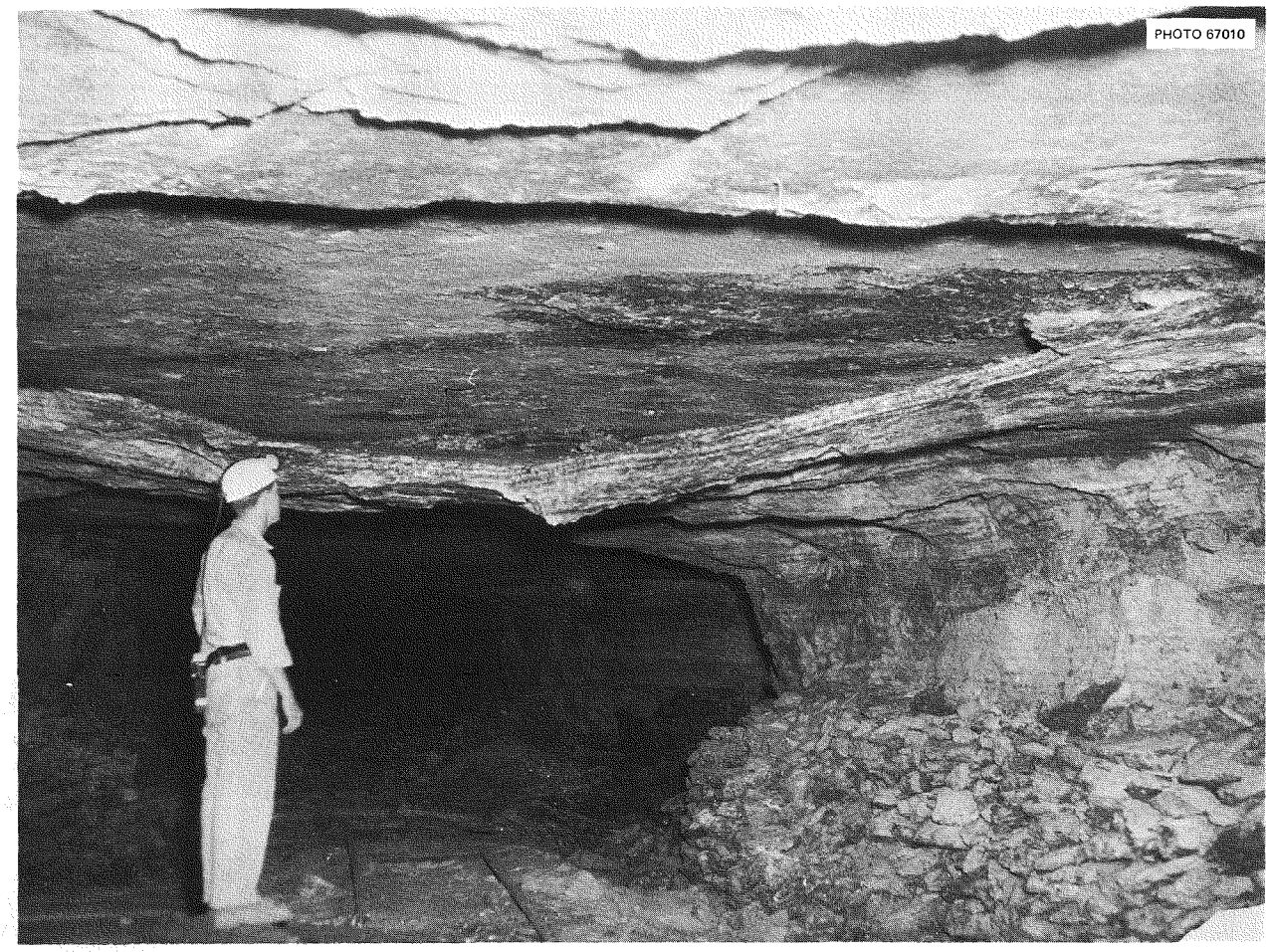


Fig. 5.6. Area in Lyons Mine.

switchboard, and wiring was extremely poor. The wiring for the 20-kVA station service bank was also in poor condition.

The electrical components of the hoist drive were in good condition. The 350-rpm, 150-hp wound-rotor induction motor, in use at Lyons since 1949, was in good condition. The drum controller was in good shape, and the secondary grid resistors were in satisfactory condition. The reversing contactor, while old, was serviceable and required only minor repair.

The mine feeder cable was a three-conductor No. 6 3-kV Anaconda parkway cable, about 1200 ft long. It was installed in 1935. The cable is installed in the main shaft supported by wooden cleats. It had failed in 1962 at a point about 500 ft down the shaft, and the splice installed at the time of the failure was still in service. Three-conductor cable with splices continued to a point about 300 ft beyond the shaft bottom and furnished lighting current. The cable continued about 700 ft to another 20-kVA transformer which powered two booster fans and furnished lighting. About 800 ft of three single-conductor No. 8 5-kV street lighting wires were in place to a third 20-kVA transformer bank not in use. Lighting circuits consisted of various types of wire, copper and aluminum, attached to the roof.

The mine was equipped with a magneto telephone system with instruments in the hoist house, at the shaft bottom, and at points about 800 and 1500 ft down the Missouri Pacific (Mo.P.) entry. Signals for hoist operation were with a magneto bell at top and bottom.

5.3.7 Hoist House

The hoist house was a two-room brick building, which had been allowed to deteriorate badly. One room housed the hoist drums, motor, grid resistors, and drum

controller. The second room contained the switch gear and reversing contactor. The wooden floor was in poor condition, as was the roof. The mortar was badly eroded, and brick had fallen out in many places. Doors and windows were in poor condition. No sanitary facilities were available, and only minimal heating was installed.

5.3.8 Summary

Although the Lyons mine was considered to be in good condition and probably the best readily available site for the demonstration experiment, a considerable amount of repair, replacement, renovation, and cleanup was required before beginning installation of the experimental equipment proper.

6. Mine Renovation and Preparation of Experimental Area

F. M. Empson W. C. McClain

This chapter describes the sizable portion of preparatory work at the Lyons mine which does not fit under the heading "Installation of Experimental Equipment" (Chap. 8). Table 6.1 gives a brief outline of this work and when it was performed. The distinction between preparation and installation is somewhat arbitrary and is based largely on whether hardware described in the next chapter ("Design and Fabrication of Equipment") was involved or not. Various items in the table will be discussed in detail in the following sections.

6.1 RENOVATIONS AT MINE TOPSIDE

6.1.1 Headframe

One of the first jobs to be undertaken was the construction of a new shaft collar and a headframe to replace the existing inadequate structure. Both the shaft collar and the headframe were constructed to the design and specifications supplied by Stearns-Roger Corporation. The collar work included a concrete pad and foundations and a new poured concrete collar on the shaft to a depth of 12 ft. The 14,000-lb-capacity structural steel headframe was of fairly typical design, 60 ft high overall with dual 8-ft-diam sheave wheels. Although no provisions were made for hoisting salt to the surface, the dual sheave wheels permitted hoisting in both compartments or the use of a counterweight in one compartment. All structural members of the headframe were assembled using high-tensile-strength bolts in order to facilitate its dismantling and removal should that ever be desired. The headframe (shown under construction in Fig. 6.1) was enclosed with asbestos-coated sheet metal (Galbestos) to prevent icing during cold weather.

Table 6.1. Schedule of Mine Renovation and Experimental Preparation

June 15, 1963, to Nov. 7, 1963	Preliminary work both underground and around shaft at topside.
Nov. 7, 1963, to Mar. 23, 1964	Construction of new shaft collar and headframe and renovation of mine hoist. All access to underground areas denied.
Mar. 23, 1964, to June 17, 1964	Limited underground work (mostly surveying, gage hole drilling, and preparation of prototype hole liner experiment). Mining equipment disassembled.
May 25, 1964, to June 17, 1964	Transfer mining equipment underground and reassemble.
June 2, 1964	Start of prototype hole liner experiment (see Sect. 4.2).
June 17, 1964, to July 9, 1964	Installation of 19-in.-diam waste shaft.
June 17, 1964, to July 31, 1964	Cleanup of entries and access ways in mine.
July 9, 1964, to Oct. 13, 1964	Structural and interior renovation of hoist house.
July 15, 1964, to Aug. 29, 1964	Construction of ramp up to experimental area level from mine level.
Sept. 2, 1964, to Mar. 25, 1965	Excavation of experimental area.
Nov. 24, 1964, to Nov. 4, 1965	Drilling in experimental area (including room 5) for gages, thermocouples, heaters, hole liners, etc.

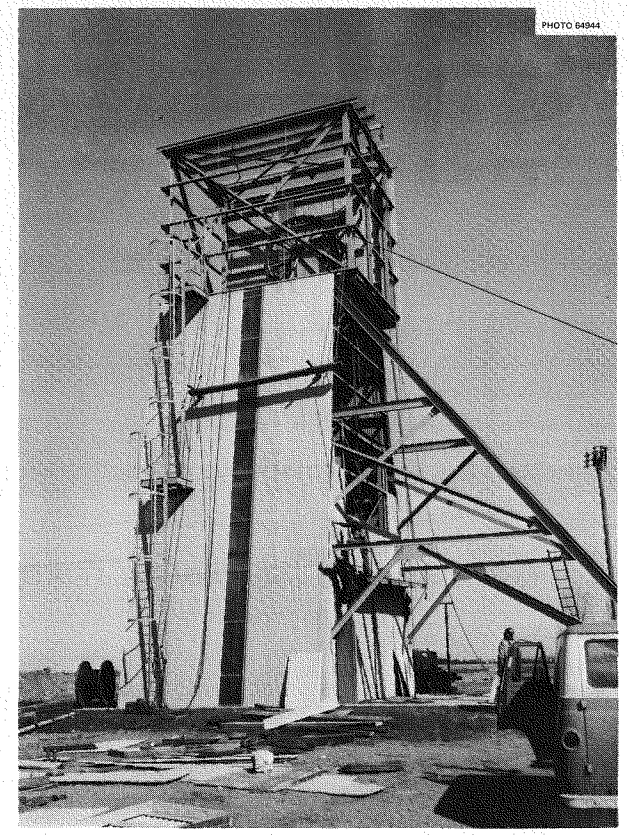


Fig. 6.1. New Headframe Under Construction.

6.1.2 Hoist

No basic repairs were necessary in the electric drive and control of the hoist. The secondary grid resistors were relocated from the operating floor to the basement. The drum controller contacts were cleaned and adjusted. The reversing contactor was relocated during renovation of the hoist house. Chattering relays and contacts were cleaned up or replaced.

Plans to replace the rotor of the hoist motor were not carried out when it was concluded that the spare rotor was in poorer condition than the original. The pinion was replaced and the motor-pinion assembly aligned to secure full contact of the gear teeth.

The 9-in.-diam shaft on which the two cable drums, driven gear, and brake of the hoist were mounted was found to deflect about $\frac{1}{4}$ in. in operation, even without a hoist load. Ultrasonic examination of the shaft showed it to be sound. A detailed analysis of the stresses in the shaft led to a decision to install a pillow block bearing between the two cable drums. This bearing eliminated the shaft deflection.

The Welch safety controller was overhauled and minor adjustments made. Safety guards were installed around all moving parts and electrical controls of the hoisting machinery.

As a part of the hoist renovation, the entire length of the mine shaft was closely inspected, timbers renailed where necessary, minor repairs to the water rings made, and new yellow pine guides installed. A new man cage was installed in one hoisting compartment and a counterweight box in the other. The hoisting rope in both compartments was replaced with new $1\frac{1}{2}$-in.-diam 6 X 25 improved plow steel rope.

6.1.3 Hoist House Renovation

The existing hoist house was rehabilitated to provide adequate quarters for the hoist operator and an office area for supervisory personnel. A new roof was installed, and the exterior brick walls were repaired and covered with sprayed concrete. A new dormer was installed in the roof to conform to the changed slope of the hoisting cable. Inside, the wooden floor was replaced with concrete and, in the area around the hoist controls, with steel grating. The mine hoist switchgear was relocated in a partitioned-off area in the old turbine room section of the building, and the remaining portion of that room was converted to office space. Washroom facilities and a gas-fired heating system were installed, and the building was painted inside and out.

6.1.4 Electrical System

The Kansas Power and Light Company installed a bank of three 150-kVA transformers to supply power to the project at a nominal 2300 V. New line was installed to a terminal pole at the hoist house and through new entry fixtures into the switchgear.

Four new adjustable main circuit breakers of 400 A maximum capacity were installed in the building. They provided switching and protection for the main service for the hoist, for the other surface facilities, and for the main mine feeder. A new 112.5-kVA, 2300/480-V transformer bank for surface station service was installed, and the hoist house was completely rewired with a 208/115-V four-wire system. New lighting was installed in the hoist house and in the mine yard. A 3-kVA, 480/240-V transformer was installed to supply power for a sump pump at the water rings in the shaft.

A new feeder cable into the mine, three-conductor No. 4 with 5-kV insulation and an integral ground (Super Coronol Geoprene), was installed in the shaft suspended by wooden cleats attached to the shaft lining.

6.2 WASTE CHARGING SHAFT

6.2.1 Location

It was desired to drill the waste-charging shaft into solid salt at the center of what would later become a room off the corridor in the experimental area. In order to locate this shaft, the Topographic Division of the U.S. Geological Survey carried out an accurate survey of the surface and underground, including shaft plumbing to tie the surveys together. Two independent surveys were made, one in December 1962 and the other in May 1964, which agreed well. Based on these surveys, a point was marked on the surface about 1100 ft southwest of the mine shaft and directly above the desired location of the shaft.

6.2.2 Design

In designing the waste shaft facility, it was considered desirable to have the maximum diameter available within the limitations imposed by project financing. While the canisters to be handled in the demonstration were only about 6 in. in diameter, it would be advantageous to have a larger diameter shaft in case it should become possible to dispose of actual pots of calcined waste. Standard oil field casing, 20 in. OD and 0.438 in. wall thickness with inside diameter of 19.1 in., was chosen on the basis of availability of casing and cost of the completed shaft.

Another important factor in the design of the shaft was that of double casing at the top to assure sealing of the casings into the structure in such a way that groundwater could not reach the salt formation. This was accomplished by first drilling a 32-in.-diam hole to 300 ft and cementing 26-in.-OD surface pipe for the entire 300 ft. No water-bearing formations are present below 300 ft, and the bottom of the 26-in. casing is cemented in an impermeable shale which continues to the salt.

The remainder of the hole was drilled at 24 in. diameter, and the 20-in. casing was cemented from the surface to a depth of approximately 1040 ft.

6.2.3 Installation

By far the most rigorous specification to be met by the drilling contractor was that the shaft must not deviate from vertical at any point by more than 1°. In other words, the entire length of the shaft had to lie within a slender cone described by the starting point at the surface and a circle of 17 ft radius at the mine level. The successful bidder (Sterling Drilling Company) elected to drill an 8¾-in.-diam pilot hole and check plumbness with a down-hole drill stem device (accurate to ±¼°) every 100 ft. When these surveys indicated a maximum deviation of ¼°, the hole was reamed to size. An accurate survey of the shaft using gyroscopic instruments (Sperry-Sun Company) indicated a total deviation of 2.53 ft to the northwest.

The centralized well casings were cemented in place using salt-saturated cement. (Drilling mud was also made up with brine to prevent solution enlargement of the hole in the salt section.) After completion and dewatering of the cased shaft, a 20-ft-long, 16-in.-diam mandrel was run in and out as a final test for collapsed segments of casing and for doglegs.

6.3 MINE LEVEL PREPARATION

A very minimum amount of maintenance had been carried on underground during the period between closing of the mine in 1948 and preparations for Project Salt Vault beginning in 1963. Therefore, a substantial part of the effort in preparation for Project Salt Vault consisted in cleaning up the main entries and access ways and restoring the services required for underground operations, especially power and ventilation.

6.3.1 Mining Machinery

Since all of the mining machinery had been removed from the Lyons mine, it was necessary to procure and install underground all of the equipment needed for the excavation of the experimental area. The basic elements of this equipment consisted of a used loading machine, Joy Manufacturing Company model 18HR-1H, with a rated capacity of 5 tons/min, and two used Joy trailing-cable shuttle cars, model 60-5-7, with a capacity of 285 ft^3 (about 12 tons), which were purchased. Other equipment, supplied by the Carey Salt Company on a rental basis, consisted of post-mounted drills (Jeffrey A-6) for blast hole drilling, a Goodman short-wall undercutter fitted with a 10-ft bar, and a 50-hp three-drum tugger hoist for stacking the salt underground.

Except for the shuttle cars, all this mining machinery was electrically powered with 480-V three-phase alternating current. The shuttle cars used 250-V direct current. A used General Electric motor-generator set, consisting of a 190-hp 2300-V three-phase synchronous motor driving a 100-kW, 250-V direct-current generator, was purchased to drive the shuttle cars.

It was necessary to disassemble both the loader and the shuttle cars in order to lower them into the mine.

Since this is a common problem in transferring equipment into shaft mines, such equipment is usually constructed so that it can be readily disassembled in pieces small enough to be handled in a normal shaft. This was true in the case of Project Salt Vault, except that it was necessary to section the shuttle car chassis and weld them back together after transfer into the mine.

6.3.2 Mine Cleanup

Since no regular cleanup of the underground workings had been done for many years, the first task to be undertaken after reassembly of the mining machinery was the removal of spalling walls, sagging roofs, and floor heaves along the access route from the main shaft to the experimental area (Fig. 5.2).

This cleanup was carried out in several steps. The first section was the main east entry from the shaft about 300 ft to the Missouri Pacific (Mo.P.) entry. This was one of the first areas opened in the original development of the mine. Included in this area was a high-pressure pump used for pumping shaft water leakage to the surface and a small pump for transferring leakage water collected in the sump to a holding tank west of the shaft. Narrow-gage tracks were still in place from the shaft to the east and then south. The trackage was removed, and the pumps were relocated west of the shaft. Then the roof was drilled and shot down to apparently stable strata. The waste rock was dumped in an unused area east of the Mo.P. entry.

Considerable spalling had occurred at the intersection of the main east and Mo.P. entries, along with roof falling away to the 17-ft parting. This intersection was squared up and widened somewhat. From this point southward the trackage was removed from the Mo.P. entry, and overhanging slabs were taken down. At the old mine office and generator room, where the section of the entry changed from arched (fallen to 17 ft) to about 8 ft, it was necessary only to scale spalled material from the walls and small pieces from the roof. The floor slab was missing due to heavy traffic during mining and solution during cattle feeding experiments.

Entry 5 from the Mo.P. entry west to the area of the demonstration was also mined to the 8-ft roof. This roof was stable, although slight separation could be detected in holes drilled upward. The floor slab had heaved throughout the length of the entry and was taken up to secure an even surface. In rooms 7, 8, and 9 and entry 5A in that area, it was necessary to clear the roof to 17 ft in order to secure a stable, safe roof and sufficient headroom to perform the operations required by the demonstration. The roof was poor in these areas because of "high topping" operations.

6.3.3 Ventilation

A new 3-ft-diam by 2-ft double-inlet nonreversible blowing fan was installed over the air compartment of the main shaft. The installation was designed to operate at 650 rpm with a 40-hp motor and deliver 30,000 cfm at 3.5 in. H_2O gage. The fan discharged through a Y connection into two 36-in.-diam fabric ducts which extended below the water rings at approximately 300 ft down the shaft.

Underground, existing stoppings were repaired where possible and new brattices installed where needed to direct the air flow through the workings to the area of the experiment and back to the main shaft. An existing fan installed in the air path downstream from the demonstration served as a booster.

A second fan was installed as part of the facility at the top of the waste shaft, which aided in the ventilation of the dead-end experimental area. This auxiliary ventilation system is described in Sects. 7.3, 8.1, and 9.4.1.

6.3.4 "Old Workings" Rock Mechanics Gages

A detailed description of the various types of rock mechanics gages installed throughout the existing mine area of the Lyons mine, including installation technique, is given in Sect. 11.4.1. A few of these gages had been installed in the summer of 1962. Most of the gages in the general vicinity of the main shaft were installed during the period prior to erection of the new headframe. By far the major portion of gage hole drilling and gage installation was carried out during the mine cleanup period. This installation included all of the instruments in the old workings surrounding the experimental area (Fig. 11.41), most of the gages in entries 5 and 7 south and east of the experimental area, and some of the gages in the main shaft area.

6.4 EXCAVATION AND PREPARATION OF THE EXPERIMENTAL AREA

The experimental area was located in the area to the north of entry 5 and west of the No. 2 south entry of the old workings, as shown in Fig. 5.2. It was located at an elevation of approximately 14 ft above the original mine floor, necessitating construction of a ramp for access.

6.4.1 Ramp

Construction of the ramp was accomplished by shooting down the roof over entry 5. A part of the roof material served as the ramp, and the surplus was hauled away. The original mining procedure gave a sloping roof of approximately the same slope as the floor. When this inclined roof gave some indication of separation at shale partings, it was squared up to the same elevation as the experimental area roof. The ramp was approximately 140 ft long, rising 14 ft in that distance (10% grade). The surface was smoothed with the Joy loader and by shuttle car traffic, followed by wetting down. This produced a durable surface which served throughout the demonstration. Figure 6.2 shows the ramp and the transporter.

6.4.2 Salt Disposal Areas

All of the salt from the excavation of the experimental area and the clearing of existing rooms (rooms 7, 8, and 9) at entries 5 and 5A (Fig. 11.41) was disposed of underground. In general, the available space in entries 5, 5A, 7, and 7A was used for this purpose. Specifically, the salt was stacked in rooms 2 to 6, entry 5A; rooms 3 to 7 and 9 to 12, entry 7A; and in entry 7, west of room 8. Entries 5 and 7, east of room 8, were used for haulage.

Two different methods were used for stacking the salt. In the "ramp building" method, the floor of the room was gradually built up until the shuttle car could no longer enter. With this method, it was possible to fill to within 3 to 4 ft of the ceiling. In the second method

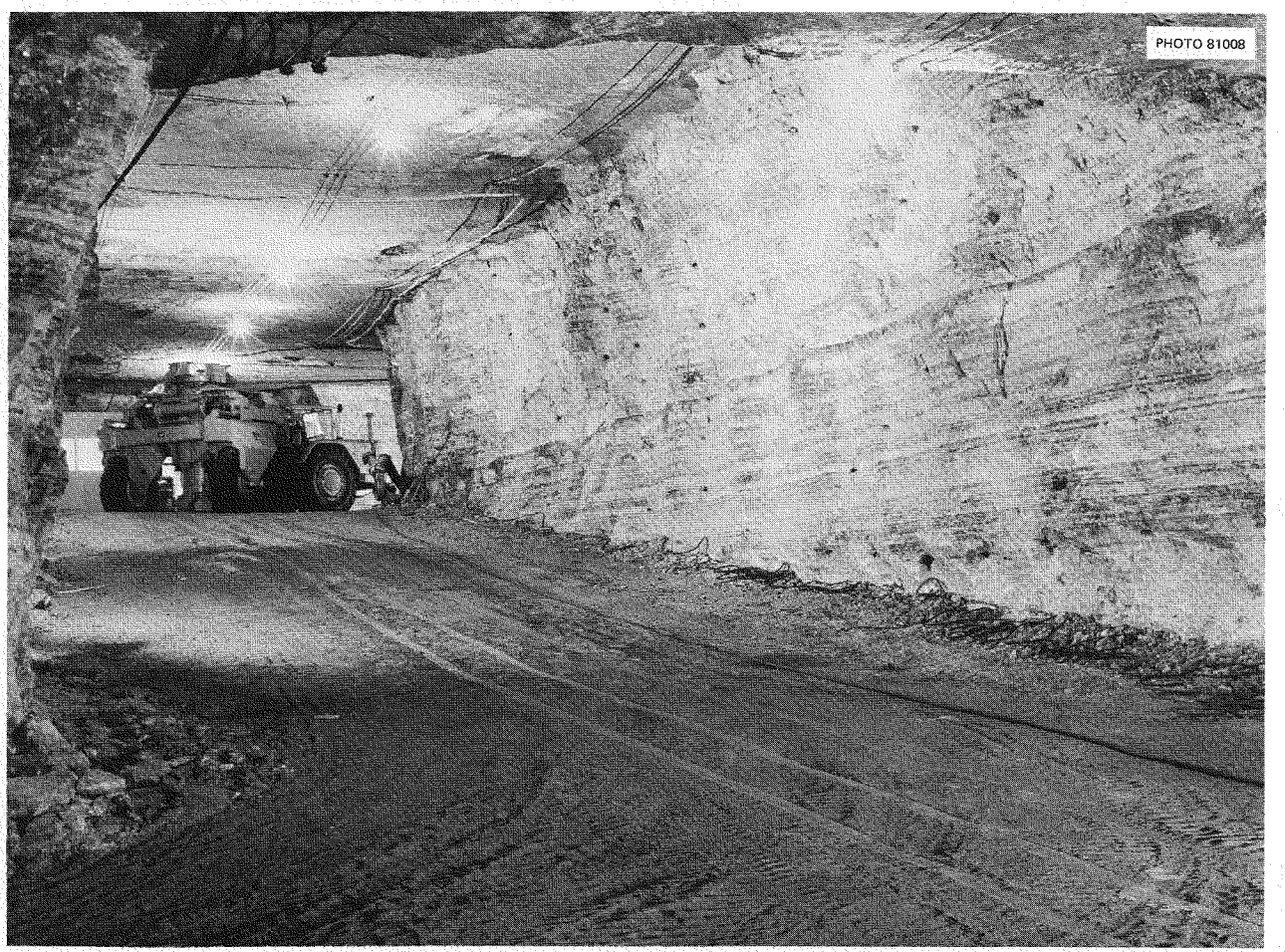


Fig. 6.2. View of Ramp Up to Experimental Area Showing Underground Transporter and Experimental Control Room.

the three-drum tugger hoist, mounted in the entry, was used in conjunction with a scraper blade to drag the salt into the room. This method permitted filling a room to within 2 to 3 ft of the ceiling.

6.4.3 Excavation Procedure and Progress

The procedure used for excavating the experimental area was similar to that used in the Carey operations at the Hutchinson mine and throughout the industry. In this procedure the face is first undercut to a depth of approximately 10 ft and a straight pattern of blast holes drilled to an equivalent depth in the material above. The holes are then charged with explosive (40% dynamite in this case) and detonated electrically using time-delay caps in such a way that progressively higher layers of salt are broken loose. The broken salt is then loaded onto the shuttle cars with the Joy gathering-arm-type loader.

During the initial part of the mining of the experimental area, this procedure was modified to make the advance in two stages. The first shot was to a height of about 10 ft, leaving about 4 ft of salt in the roof. This was then later removed by "high topping," that is, by drilling vertically into the roof and shooting the slab down with relatively small charges. This technique was adopted because it permitted use of a 10-ft-long post for the blast hole drill rather than one 14 ft long, thereby considerably improving its efficiency.

The progress made in the excavation of the experimental area is shown in Fig. 6.3, where the date indicates when that portion of the material was shot.

On January 20, 1965, the full-height excavation had progressed just past the mouth of experimental room 3, and the bottom excavation extended about 40 ft beyond that point in the experimental entry. During loading operations under the temporary roof, a thin (about 4 in. thick) slab of salt fell from the roof, killing one man and seriously injuring a second. Normal procedure required scaling the roof and ribs following every shot before entering the area. Repeated efforts to break loose this thin seam were unsuccessful. As a part of the investigation of the accident, a complete inspection of the mine was carried out by the Health and Safety Laboratory, U.S. Bureau of Mines, in February 1965, with reinspection September 1965 and October 1966. Following the accident, the mining method was modified to discontinue the "high topping" and shoot the full height of 14 ft. This slightly less efficient procedure was used for the remaining excavation.

The last mining in the experimental area was the excavation of the salt around and behind the waste

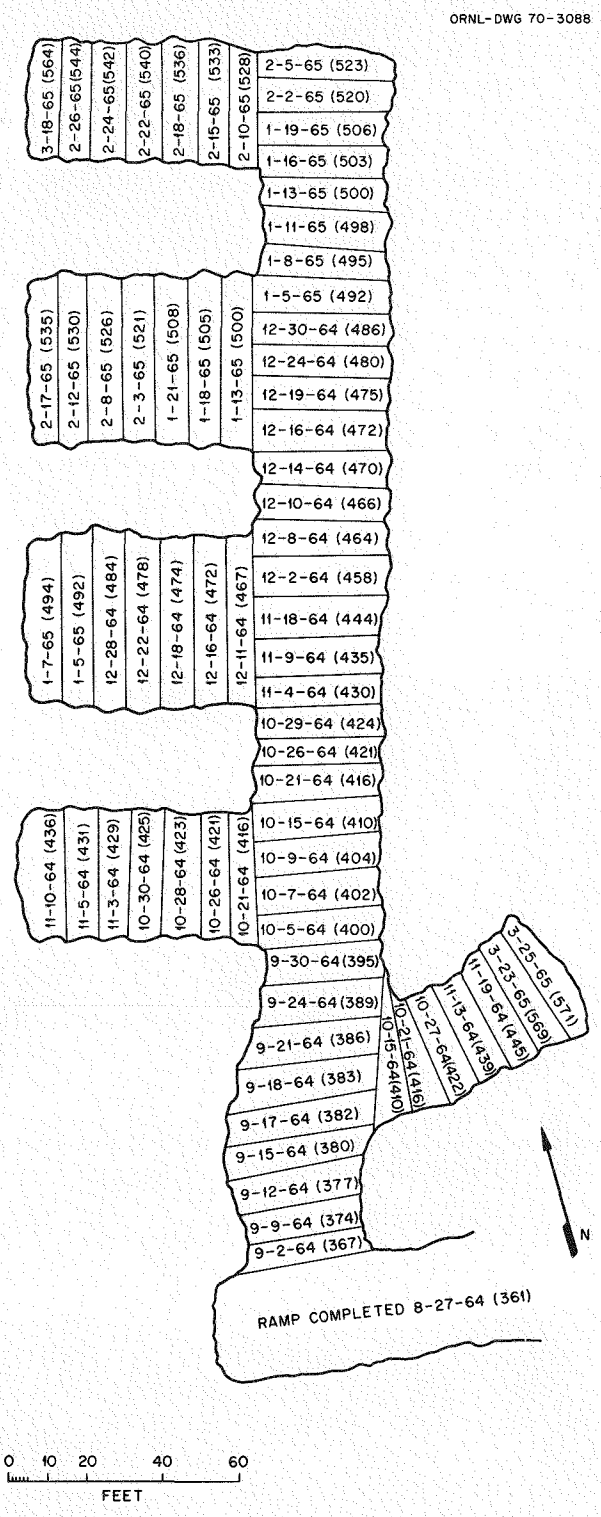


Fig. 6.3. Detail of Experimental Area Showing Dates of Excavation.

shaft. Previous mining had exposed this shaft at a location about 9 in. from its anticipated position. This error represents the cumulative error in the surface and underground surveys (including the difficult shaft plumbing) *and* in the precise hole deviation survey.

Figure 6.3 also shows the exact configuration of the finished newly excavated experimental area. The irregular nature of the walls due to overbreak in the blasting operations is normal and was expected. Slight modifications to the planned widths of the rooms and pillars were necessary in the course of the mining in order to correct excessive overbreak and in an effort to maintain the symmetry of the area. The nominal widths of the actual rooms and pillars are compared with the original design widths in Table 6.2.

The floor of the experimental area was that left by the undercutter. Normally this would be a slight downward incline about 10 ft long, followed by about a 3- to 6-in. step-up. Each incline represents one pass with the undercutter. Throughout most of the experimental area this type of floor was obtained and was acceptable. However, in both rooms 1 and 4, the cutter break steps were much higher than usual, and in room 4 the undercutter had been allowed to drift vertically in making several cuts, so that the floor was very uneven. Furthermore, the stratigraphic elevation of the floor in room 1 was about 18 in. lower than that in room 4. Since a flat level area was required in room 1 for placing the underground transporter shield against the hole liners (see Sect. 7.4), the floor produced by the undercutter was considered unsatisfactory. Consequently a square area 28 ft on a side at the center of room 1 was leveled to $\pm 1/4$ in. using hand-held pneumatic picks. This area can be seen in Fig. 8.3. A similar area was leveled to $\pm 1/2$ in. in room 4 at a stratigraphic elevation approximately 14 in. above the floor in room 1. The two main array experiments were placed in these leveled areas.

Table 6.2. Comparison of Design and Actual Widths of Rooms and Pillars in Experimental Area

	Design Width (ft)	Actual Average Width (ft)
Room 1	30	32
Pillar 1-2	30	27
Room 2	40	44
Pillar 2-3	20	23
Room 3	40	44
Pillar 3-4	30	29
Room 4	30	31

6.4.4 Drilling

A large amount of drilling was required in the experimental area for the installation of rock mechanics gages, thermocouples, array hole liners, heaters, and geologic cores. All of this drilling as well as most of the gage holes in the old workings – some at depths up to 150 ft – was carried out with a Sprague and Henwood model 325 underground core drill. The drill was mounted on a $3\frac{1}{2}$-in.-diam steel post and was operable through a full 360°. The drill was powered by a reciprocating compressed-air motor, and air was also used as the drilling fluid. The extremely dusty condition created by air drilling was alleviated by inserting the drill rod through one half of a paper powder box over the top of the hole and using an industrial vacuum cleaner to remove most of the drilling air and salt dust from inside the box.

As soon as the excavation of room 1 was completed, the drill was moved, and drilling on the rock mechanics instrumentation network started. By the time these holes had been drilled, excavation in room 2 was finished, and gage hole drilling started there. This procedure was followed throughout the excavation of the experimental area in an effort to install the rock mechanics gages as soon as possible after completion of mining.

After all of the gage holes were drilled and the gages installed, the drill was returned to room 1 for drilling of the array holes, thermocouple holes, and dosimeter holes. Drilling in room 4 was then completed, followed by rooms 2 and 3. After completion of all drilling in the experimental area, drilling was started in experimental room 5 in the existing mine (previously room 9, entry 5) as permitted by manpower availability. The details of these various holes are given below.

1. Stress meter holes, $1\frac{7}{8}$ in. in diameter, were drilled using AX size pilot-type plug bits. In some cases these holes were reamed to 3 in. in diameter (NX) to within a few feet of the stress meter location in order to have a larger diameter hole in which to insert the necessary tools. Maximum length of hole in the experimental area was 45 ft.
2. Extensometer holes were drilled to $1^{11}/_{16}$ in. in diameter using an EX size pilot bit set to slight oversize. Holes were drilled vertically up and down a maximum distance of 25 ft and horizontally up to 70 ft.

3. Borehole leveling gage holes were drilled $2\frac{3}{8}$ in. in diameter using a special plug bit. Care was exercised on these holes to produce a horizontal hole so that the backlighted target at the bottom of the hole could be seen through the level.
4. Thermocouple holes were drilled $1\frac{3}{16}$ in. in diameter using SP size core bits, although no attempt was made to recover the core. Thermocouple holes, especially those near the array holes, were drilled with great care in order to produce a truly vertical hole. This was considered necessary in order to assure that the thermocouple junction was located at its design point, so that the temperature readings could be correctly interpreted.
5. Array holes were drilled in three operations. The first step was the drilling of a pilot hole to 13 to 14 ft depth with an AX pilot-type plug bit. This hole was drilled very carefully to ensure plumbness. A 16-in. masonry-type diamond coring bit fitted with a concentric 1.9-in.-OD pipe to follow the pilot hole was used to drill a hole 5 ft 3 in. deep. A 12-in. masonry diamond bit modified in the same way as the 16-in. bit was then used to drill the remaining 7 ft 5 in. These large-diameter holes exceeded the normal capacity of the drill. The 12-in. holes required constant throttling of the air motor and adjustment of speed and feed on the drill. Drilling of the 16-in.-diam holes might be described as "worrying" the hole down. The fact that two days were required for drilling each array hole (12 ft 8 in. deep) is indicative of the overload.
6. Twenty-two pillar heater holes were drilled to a depth of about $12\frac{1}{2}$ ft at the base of the center pillar of the experimental area. Two of these (for the modified pillar heaters) were 8 in. in diameter, and the remainder were 6 in. in diameter. Masonry-type diamond coring bits without pilot holes were used in both cases. These holes were drilled without any difficulties related to the limited capacity of the drill.
7. Two dosimeter holes were required in both room 1 and room 5. On each of these holes, it was desired to have their center line tangent to the 12-in.-diam section of an array hole at a point exactly 8.85 ft below the floor. The setup of the drill on these holes was quite complicated and usually required about a half day. Subterfuges such as plumb-bob protractors mounted on the drill rod clamped in the drill and sighting through the drill rod with a transit were employed. In room 1 both holes struck the target point within $\frac{1}{2}$ in. In room 5, deflection of the post mounting and (probably) deviation of the hole due to the shales present caused the holes to miss the target point by about 2 in. (One of these holes was unusable because it would have produced a direct radiation beam and was subsequently backfilled.) These holes were completed with a 5-ft-long, $1\,1\frac{1}{16}$-in.-diam lower section and a 5.25-ft-long, 4-in.-diam upper section.

6.5 SUMMARY

The work described in this chapter represented a significant portion of the total effort in Project Salt Vault, even though none of it was directly associated with the hardware aspects of the equipment. In addition to the various subcontractors (for the headframe, waste-charging shaft, hoist house renovation, etc.), an average of 12 men were employed underground for approximately one year. This personnel included: two men who operated the diamond drill, two men involved with various experimental aspects (prototype hole liner experiment, rock mechanics gage installation, etc.), three in supervisory capacities (two ORNL and one Carey), and the remainder making up the mining crew. During this period about 20,000 tons of salt was excavated from the experimental area, in addition to the many thousands of tons moved in the mine cleanup operations; 7000 ft of small diameter (less than 6 in.) hole was drilled for instrumentation, most of it under rigorous directional control, and about 1600 ft of large diameter hole (6 in. and greater), including the waste shaft, was completed. An approximate estimate of the average drilling rate for the small-diameter holes is 40 ft/day.

In addition to this, a large amount of support work (both for the mining and the experimental operations) was completed. Most of this work consisted in such activities as temporary installation and later removal of power, compressed air, and lighting services. Perhaps it is sufficient to say that it was accomplished.

7. Design and Fabrication of Equipment

W. J. Boegly, Jr. W. F. Schaffer R. L. Bradshaw

Major operations in Project Salt Vault requiring special equipment were:

1. Encapsulation of the fuel assemblies. Special containers were designed to receive the fuel that was loaded at the National Reactor Testing Station in Idaho.
2. Modification of a cask for cross-country shipment. A cask used earlier for the Sodium Reactor Experiment (SRE) fuel shipments required extensive alteration for this project.
3. Waste charging facility at the surface. This operation was unique in that hot cells were not used for the transfer of the fuel from the shipping cask at the surface to the mine level and into holes in the mine floor.
4. Underground transfer. A full-scale prototype machine was developed for the underground transfer of radioactive materials.
5. Storage in salt. Special provisions were required to ensure removal of the radioactive materials at the conclusion of the demonstration.
6. Heated-pillar experiment. Special heaters, power supply, and instrumentation were required.
7. Instrumentation. The entire operation required heaters, power supplies, thermocouples, recorders, off-gas systems, radiation detection systems, etc.

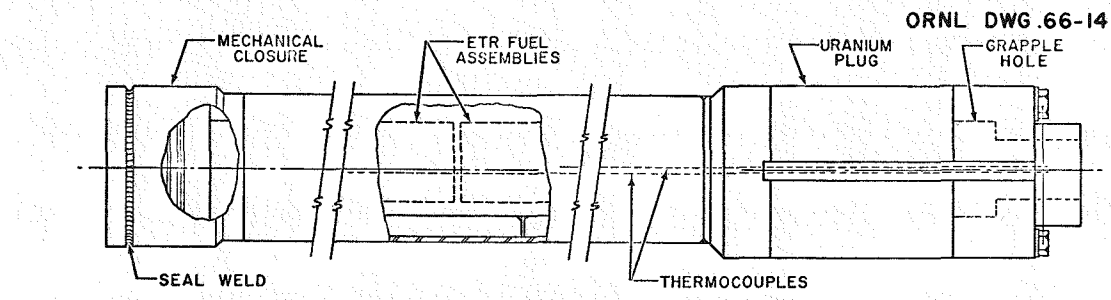
7.1 FUEL ASSEMBLY CANISTER

Selection of the ETR fuel assemblies as the sources for irradiating and heating the salt fixed the minimum size of the fuel container. The fuel assembly canisters (cans) were approximately 5 in. in diameter by about $7\frac{1}{2}$ ft long and were designed to hold two ETR fuel assemblies end to end in a shock-resistant and hermetically sealed container. To ensure safe fuel element temperatures, thermocouples had to be located between the center plates of each of the two assemblies. Shipping and storage specifications required that the containers for the assemblies be hermetically sealed. The walls of the container needed to be as thin as practical to maximize the radiation dose to the salt, yet strong enough to withstand the pressure buildup that might occur as a result of (1) release of fission product gases from a leaky assembly or (2) an increase in the temperature of the gases in the event of loss of coolant during loading and shipment. The body of the canister was fabricated of $4\frac{3}{4}$-in.-OD, 0.120-in.-wall 304L stainless steel tubing.

Figure 7.1 shows a view of the assembled canister and fuel assemblies; the line drawing is a diagrammatic cutaway view of the canister showing important features of the design. The head of the canister provided a recessed cavity (grapple hole) for connecting the hoisting cable, a spool for retaining the thermocouple lead wires during loading and transfer operations, and a biological shield (uranium plug). The body is the container for the fuel assemblies and provided a union of the thermocouple and fuel assemblies. The closure provided a mechanically strong joint by virtue of deep screw threads and incorporates two effective gas seals.

Figure 7.2 shows the several subassemblies of the head of the canister. Incorporation of the thermocouples so that they terminated in the central region of both the upper and lower fuel assemblies caused many problems. Four stainless-steel-sheathed thermocouples (including two spares), 62 mils in diameter, were first connected to flexible wire leads and potted to form a hermetically sealed junction. The thermocouple sheaths then were brazed to a circular disk in an induction furnace. The ends of the thermocouples were fed through holes in the top plug of the canister, and the disk assembly was attached by seal welding to the plug.[1] This procedure was necessary to minimize the

[1] W. F. Schaffer, Jr., *et al.*, "Project Salt Vault: Design and Demonstration of Equipment," pp. 685–706 in *Proc. Intern. Symp. on Solidification and Long-Term Storage of Highly Radioactive Wastes, Richland, Wash., Feb. 15-18, 1966*, CONF-660208 (November 1966).



CROSS SECTION OF PROJECT SALT VAULT CANISTER



CANISTER ASSEMBLY



Fig. 7.1. ETR Fuel Assemblies and PSV Canister.

ORNL PHOTO 69690-A

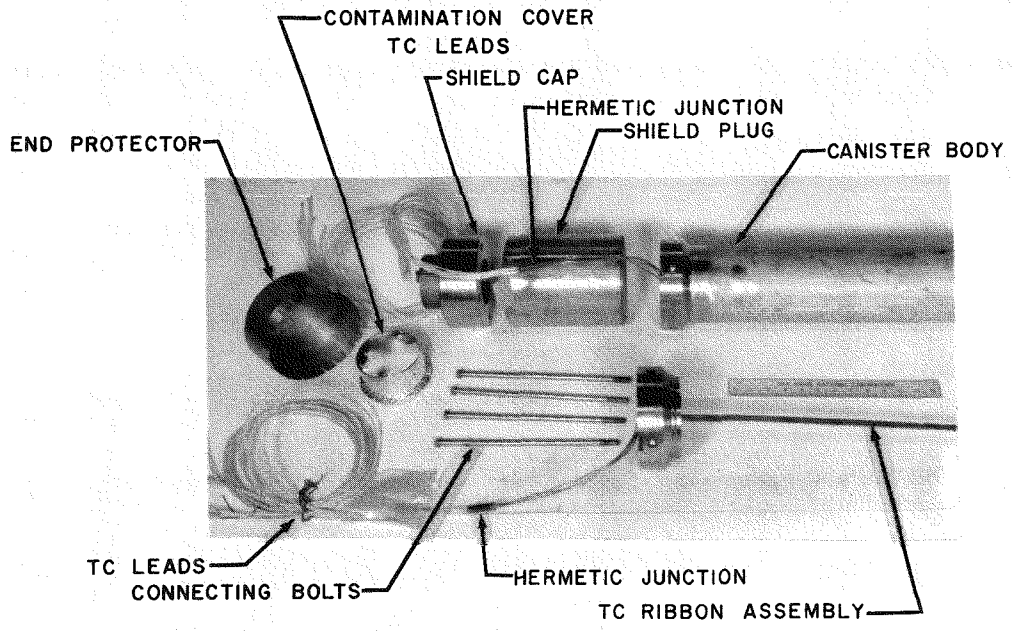


Fig. 7.2. Canister Head Subassemblies.

amount of heat applied to the thermocouple assembly and to avoid damage to the thermocouples. The free ends of the thermocouples were then placed in a jig, separated by a $\frac{1}{4}$-in.-wide flat shim stock, and joined together by brazing the sheaths to the shims to form a flat ribbon assembly with a maximum thickness of 70 mils. Since the fuel plate separation was only 100 mils and since allowance for fuel plate warpage or distortion was necessary, the tolerance on the thermocouple ribbon had to be carefully controlled. A removable tongue was provided, on the end of the ribbon, which extended beyond the closure end of the canister to provide a means of inserting the thermocouple ribbon between the fuel plates. After the fuel assemblies were in place, the notched section of the tongue was broken off. The flexible leads on the thermocouples were wound on a spool on the top of the canister body and retained by a sheet-metal spring slip, which was removed after the canister was in the storage hole. Spring bumpers in the head assembly compensated for tolerances in the length of the cut fuel assemblies, thereby reducing the shock loads in transit and preventing possible damage to the thermocouple assembly.[1] Tracks were provided in the canister body to align the fuel assembly with the thermocouple assembly.

The canister body was provided with a shielded end (the top) so that when the canister was in place in the storage hole in the mine, direct connection of the thermocouples and the instrument leads could be made without remote operations. Depleted uranium was chosen as the material for the shield to minimize the length of the canister and, in turn, the length and the weight of the shipping cask. To prevent oxidation at elevated temperatures, the uranium was hermetically sealed in a thin-walled stainless steel can. The top of the canister was joined to the body by bolts so that the uranium shield plug could be salvaged and reused on subsequent loadings. The uranium plugs were tested for leaks by purging the assemblies with helium and sealing off the gas lines. Then several plugs were temperature cycled in a furnace up to 800°F as a further leak test. The uranium plug was larger in diameter than the main body of the canister, to provide an offset to minimize radiation streaming in the storage holes.

A dependable seal closure for the canister was evolved after a number of designs were developed, including fabrication and testing of the more promising ones. The end closure design actually incorporated two types of seals, a line contact tapered-plug mechanical seal and a seal weld, either of which was capable of hermetically sealing the canister to a leak rate of $<1 \times 10^{-8}$ std cc of helium per minute. The plug was designed as a nonrotating part to prevent galling of the sealing surfaces. The mechanical seal design was tested by temperature cycling a prototype closure to 800°F and allowing it to cool to room temperature. The closures and other subassemblies of all production units were tested by helium leak-check methods at various stages during fabrication to ensure the integrity of the system. The end closure was contained in one unit to simplify hot-cell procedures. Just before the closure was installed, the canister was purged with helium. The assembly was seated by using an impact wrench. After seal welding was accomplished, the canister was placed in a cylindrical tank (in the hot cell), which was first evacuated and then connected to a helium leak detector to test the container for leakage before it was loaded into the shipping cask.

7.2 SHIPPING CASK

Figure 7.3 is a diagrammatic cross section of the shipping cask and shows the canisters in position in the rotary magazine.[1] The magazine served a dual purpose: as an indexing mechanism to allow loading or unloading of one canister at a time, and as a heat exchanger to remove the decay heat, amounting to approximately 23,000 Btu/hr, from the cask. The structural framework of the magazine was constructed, for the most part, from pipes terminating in headers at both ends. Cooling water entered and left through concentric pipes at one end of the magazine. Heat was removed, mainly, by radiation from the canister to the pipe walls; water circulating through the pipes carried the heat to an external radiator, which is described later. Close tolerances between the canister shield plugs and the storage cavities of the magazine prevented the use of a cylindrical stiffening shell on the magazine. Curved plates welded to the outer pipe circle, together with radial sheet metal supports welded between the inner and outer pipe circles, gave rigidity to the structure and also allowed maximum utilization of the cask cavity. The clearance between the magazine and the internal cavity of the cask, as well as between the canister shield plug and the cavity, was approximately $\frac{1}{16}$ in.

Figure 7.4 shows a longitudinal cross section of the cask, as well as the modifications that were made. These include the water-cooled magazine just described, a new shorter spool piece, and supplementary external cast-steel shielding, which brought the total shielding to 10 in. lead equivalent. The shipping weight of the cask was 28 tons.

A standard GM model 5033-7101 three-cylinder diesel engine having a displacement of 159 in.^{3} and

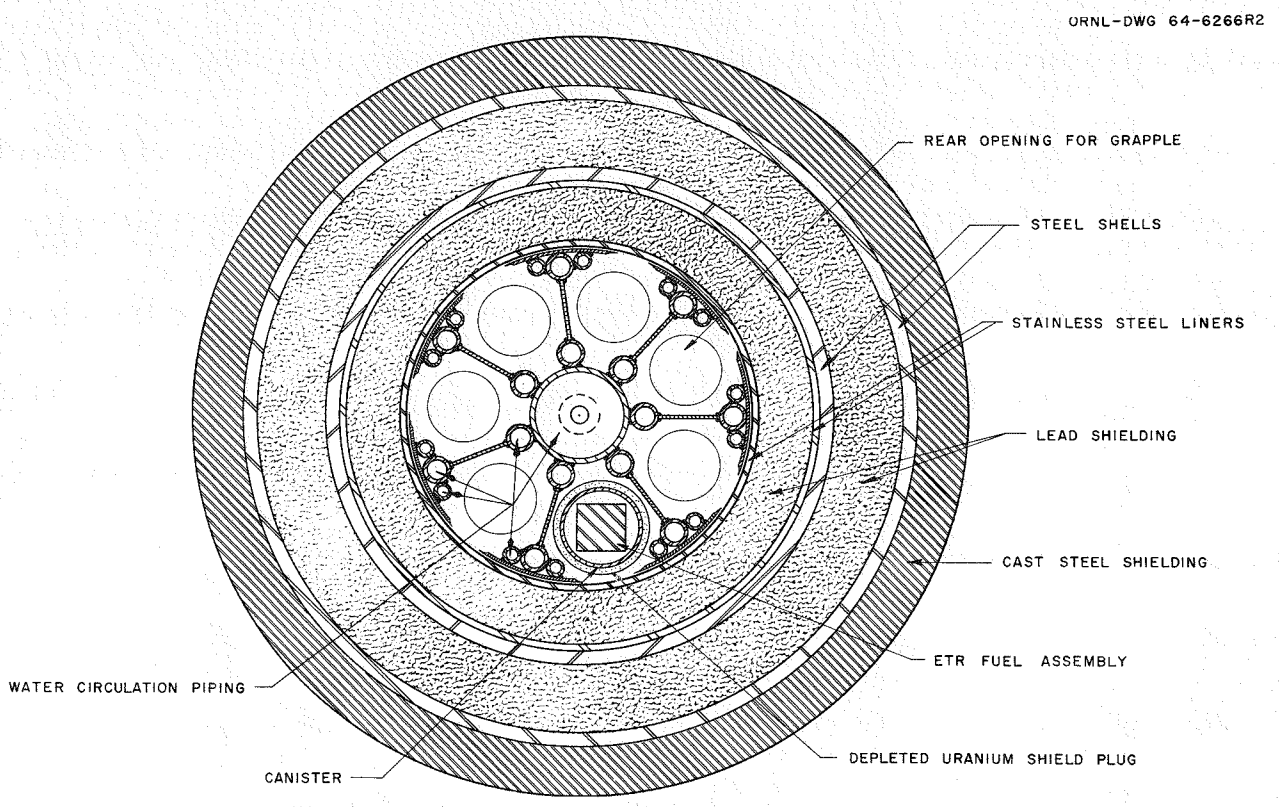


Fig. 7.3. Diagrammatic Transverse Cross Section Through Center Section of Shipping Cask Showing Position of Canister in Rotary Water-Cooled Magazine.

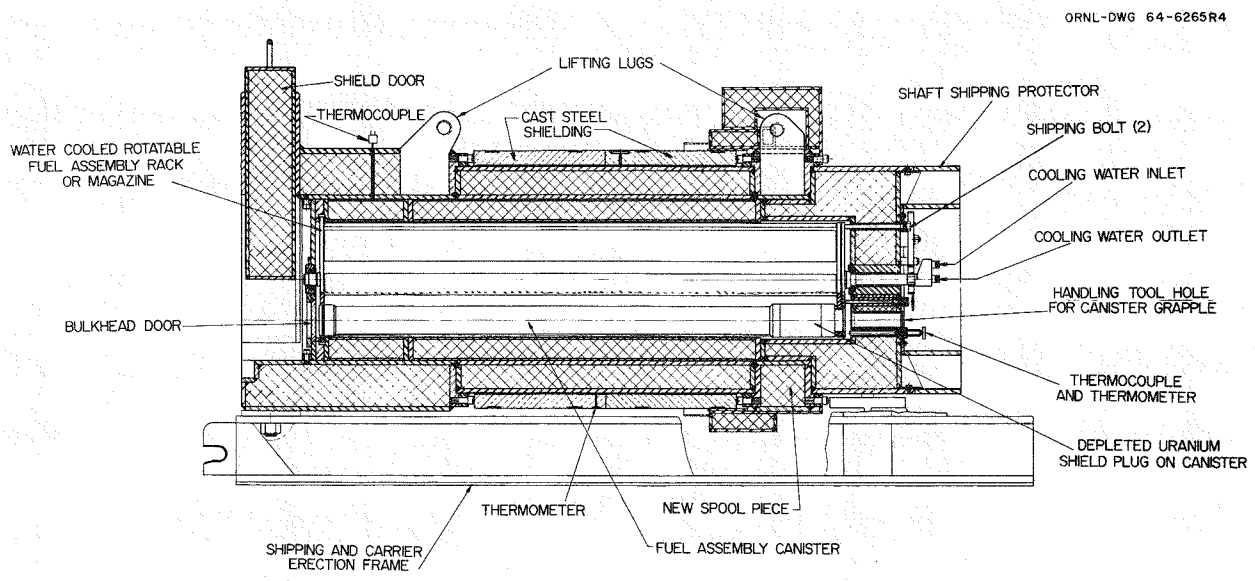


Fig. 7.4. Diagrammatic Longitudinal Cross Section of Shipping Cask.

equipped with an auxiliary water pump and an oversized radiator provided for the heat dissipation from the cask. The cask was analyzed in accordance with the requirements of the Code of Federal Regulations, Title 10, Part 72, and was approved for the shipments, based on this analysis, without reservation. To verify the heat transfer calculations, a series of tests was made by using dummy fuel assembly cans containing electrical heaters to simulate the radioactive decay heat of the fuel assemblies. Tests were conducted for extended periods, with the cooling system operating until a steady-state condition was achieved at 1 kW of power input per canister position; the canisters reached a maximum temperature of 225°C (437°F). Tests were also run with the cooling system disconnected, as well as with the coolant lines cut, to simulate a broken line. The highest temperature reached on the outside of the canister was 400°C (752°F) after 24 hr without cooling. The temperature of the inner liner of the cask at that time was about 260°C (500°F), well below the melting point of lead (632°F).

Calculations indicated that the cask should be able to withstand a sustained fire at a temperature of 1850°F from 45 to 60 min without serious shield or canister damage (see Sect. 9.2.2). Fire-retardant or intumescent paint on the exterior surface of the cask was used to retard the transfer of heat into the cask.

Shipment of the cask from Idaho to Lyons, Kansas, was originally planned for railway transport. Reduction of the number of handling operations at Idaho, a shorter shipping time, safety and continuous control enroute, convenience of unloading at Kansas, and a lower cost led to the decision to ship the cask by truck. The Tri-State Transit Company of Joplin, Missouri, specialists in shipping radioactive materials, offered the use of a special heavy-duty truck trailer (Fig. 7.5) for the shipment. Only minor modifications to the trailer were required to carry the cask and coolant system.

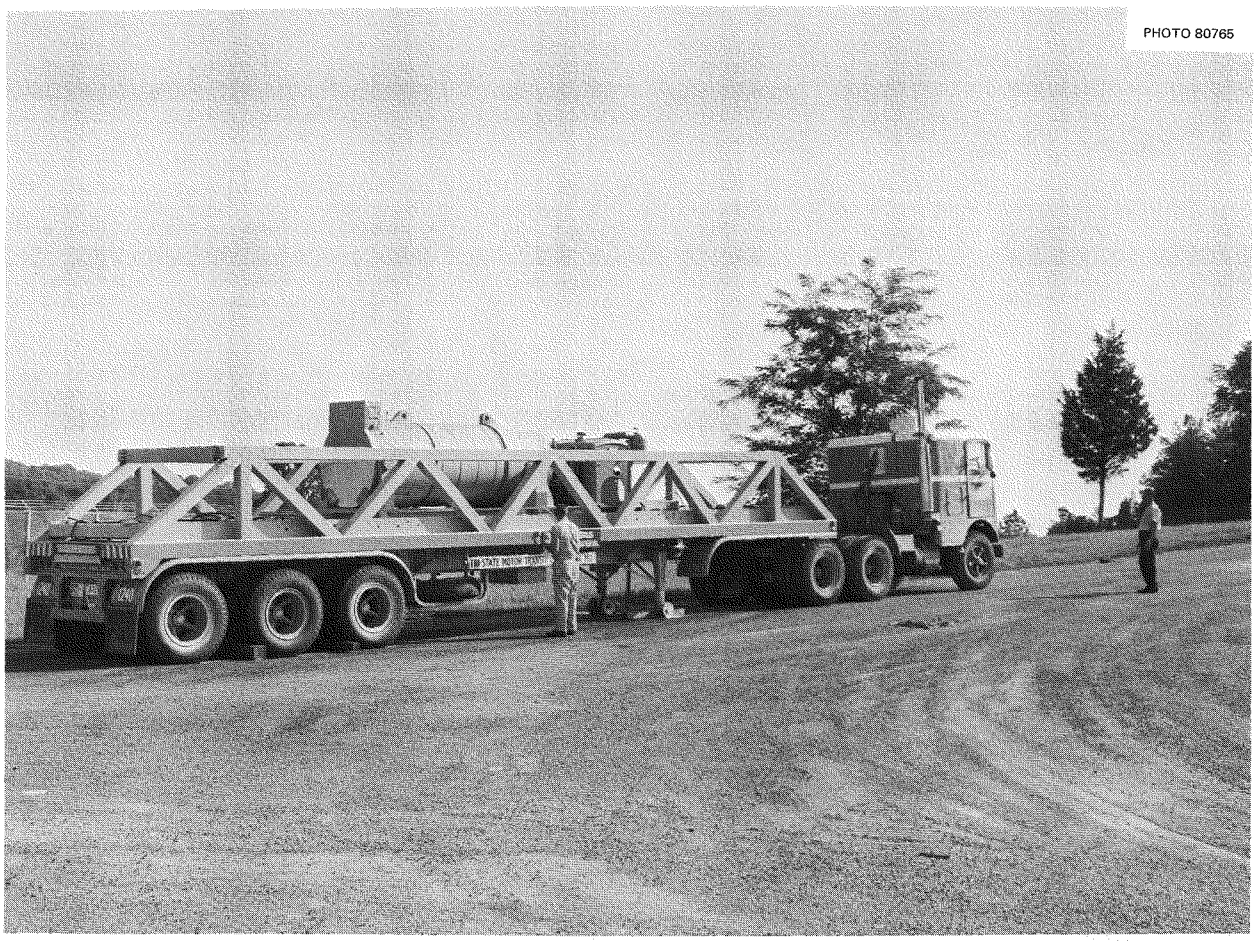


Fig. 7.5. Shipping Cask Mounted on Special Reinforced Truck Bed.



Fig. 7.6. Shipping Cask Being Erected over Waste Shaft.

The cask was secured to a heavy steel shipping frame, which also served as an erection frame at the Lyons mine in Kansas. The shipping frame was simply secured to the truck frame by bolts; no steel cable or chain tie-downs were used. The frame was designed to take shock loads up to 10*g* during the shipment.

A 35-ton mobile crane was used to lift the cask from the shipping trailer at Kansas. The cask was moved by the crane to a position proximate to the hole, and the lugs in the forward end of the shipping frame were engaged in pivots integral with the charging-hole structure. The crane was then used to elevate the cask to approximately 40°. At this time, hydraulic cylinders were attached to lifting pivots on the shipping frame (Fig. 7.6). The hydraulic cylinders were retracted and lifted the cask safely to a vertical position over the hole.

7.3 WASTE CHARGING FACILITY

The waste charging facility at the mine provided biological shielding during unloading and a means of erecting the cask (from its horizontal shipping position to the vertical position) for unloading the canisters into the mine. At Lyons it was planned to erect the carrier over the waste shaft and lower the canisters to the mine level without the use of an expensive hot cell. Detailed study of this portion of the experiment led to the design of a heavily shielded remote-operation facility that would meet the required safety criteria.

The canister handling facility was located atop the 19.1-in.-ID waste shaft and consisted of a concrete work platform and biological shield, a ventilation system, headframe, hoist, and protective enclosure. A schematic view of the facility is shown in Fig. 7.7. The hoist, designed in accordance with applicable state codes for the hoisting of men and materials, was equipped with standard mine safety auxiliaries such as independent dual brakes and a depth indicator. The facility was equipped to handle the fuel element canisters and to remove personnel from the mine in case of an emergency in the main hoisting shaft.

The concrete work platform and shield was designed to provide a minimum of 5 ft of concrete shielding, or its equivalent, for any position of the canister in the waste shaft. This amount of shielding was calculated to reduce the radiation levels during transfers to less than 25 mR/hr (see Appendix 7A), with the exception of one position at which the dose rate was about 75 mR/hr. The appurtenances necessary to assist in erecting the carrier and to operate the main carrier and bulkhead doors were installed as an integral part of the work platform.

To prevent contamination of the mine air in the access tunnels should an accidental release of radioactivity from a canister occur, arrangements were made for a special air flow pattern. A fan powered by a 10-hp electric motor was installed at the surface to exhaust all air entering the experimental area up the shaft. In order to install the fan in such a way as to not interfere with the canister transfers, an underground bypass ventilation duct was installed from the waste shaft to the fan installation. Concern over oxygen depletion in the experimental area should a fire occur in the mine dictated that the fan be installed so that air flow in the waste shaft could be reversed. The specifications for the fan installation called for 5000 cfm at a pressure drop of $7\frac{1}{2}$ in. H_2O gage.

The upper part of the steel-cased waste charging shaft (see Fig. 7.7) contained the 19.1-in.-ID bypass ventilation duct, a transition section to reduce any pendulum action in the canister at the top of the shaft (this section also assisted in guiding the canister into the carrier), and a safety door to prevent accidental release of canisters or other items down the waste shaft. The

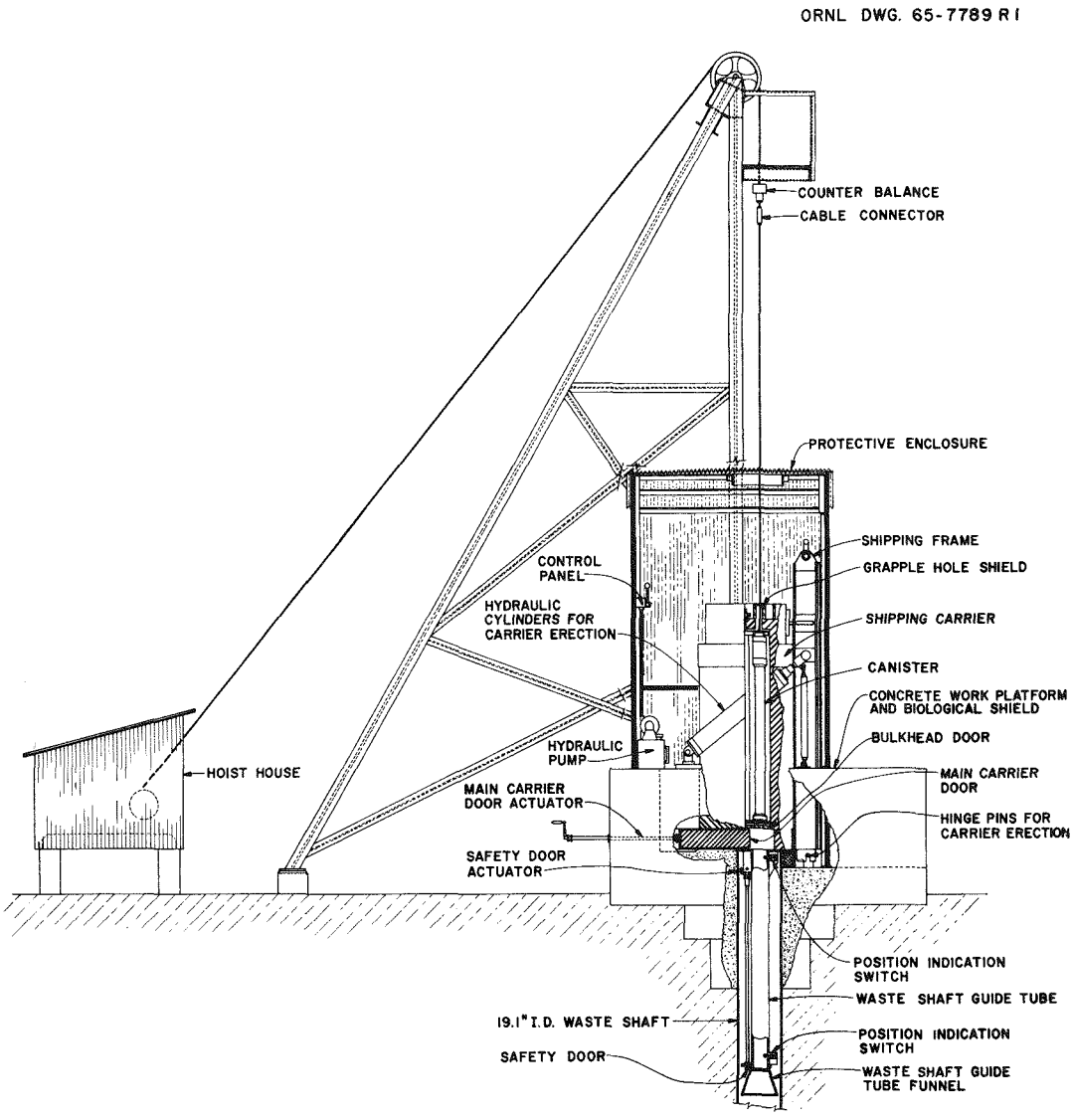


Fig. 7.7. Waste Charging Facility Showing Shipping Carrier in Erected Position.

safety door was operated by means of a hand lever located at the side of the waste shaft facility.

Hoisting of the canisters was controlled by a central control panel located within the topside facility. A series of limit switches located in the upper section of the waste shaft, in the underground transporter, and on the hoist were used both to locate the canister in the waste shaft and to control the hoisting or lowering operation. In addition to the limit switches, the cable was color coded to indicate relative locations in the waste shaft.

The headframe at the waste charging facility was designed for a 2000-lb load and was 40 ft high. The protective enclosure was provided for convenience in transferring canisters in wet or cold weather. The hoist was a specially designed unit having a capacity of 1 ton. This hoist was unique in that it provided for three hoisting speeds:

1. a slow inching speed of $1\frac{1}{4}$ fpm, which was used when the canister was being accurately positioned in the shipping carrier or the underground transporter;
2. a medium speed of 33 fpm, which was used in the upper and lower ends of the waste shaft;
3. a high speed of 100 fpm, which was used during most of the lowering distance in the shaft.

These ranges of speed were required because of tolerances in the carriers and to prevent the possibility of a canister being lodged in some of the safety and locating devices installed at the top and bottom of the waste shaft.

In case of an accident to the main shaft or hoist, or a fire in the mine, the topside facility and hoist were designed to provide safe emergency hoisting of personnel in the waste charging shaft. An auxiliary emergency cage was stored at the topside facility for this purpose. This cage could be connected to the hoist cable and would allow one man at a time to be removed from the mine. It would be necessary, however, to remove the carrier from the top of the waste shaft if this means of egress was required. The cage was equipped with a self-engaging brake system which would activate in the event of a cable break.

7.4 UNDERGROUND TRANSPORTER

To provide the flexibility necessary for an actual disposal operation, a highly maneuverable transporter was developed. A number of alternative transportation systems were considered, including overhead rail and trolleys and rail-type transportation. Rough cost estimates indicated that it would be cheaper to use a self-powered vehicle to provide flexibility within the mine.

Subcontracting the fabrication of the vehicle to an outside manufacturer experienced in the building of heavy construction vehicles seemed desirable and expedient. Thus the shield and vehicle functions were designed at ORNL, but the procurement and fabrication were handled on a fixed-price contract. The Stowers Machinery Corporation of Knoxville, Tennessee, was the successful bidder. The services of the Athey Products Corporation of Chicago were employed by Stowers for the fabrication of the trailer; later, the shield was also subcontracted to the same company.

Figure 7.8 shows the actual transporter in the mine. The procurement specification included the design, fabrication, and testing of a standard two-wheel rubber-tired diesel-powered tractor and a special two-wheel rubber-tired trailer with a power-positioned steel-cased lead shield. The contractor was responsible for determining that the tractor had adequate power for the work to be performed, including auxiliary power systems for the trailer requirements, and coupling of the tractor and trailer for the required load and maneuverability. The specifications required that the unit negotiate a 10% grade at a speed of at least 1 mph with a fully loaded trailer. The unit supplied had a rated brake horsepower of 250 at 1900 rpm. The vehicle had to be able to turn in a 25-ft-wide corridor without backing or scraping the walls. It had to be sufficiently maneuverable to spot the shield within 1 ft of any fixed point on the floor of the mine. The shield indexing system was required to provide movement along three axes and to position the shield to $\pm 1/16$ in. of any predetermined point within the range of the indexing system. The carrier had to withstand a minimum shock force of 10*g*, such as could occur in the collision of the tractor and trailer with a rigid body, in forward or reverse direction, without the shield breaking free from the bridge or other structural members in such an impact. Another requirement was that the transporter should not overturn in the event of failure of a tire, an axle, or a wheel. Finally, the complete unit had to be capable of being disassembled into subassemblies small enough to pass down the mine shaft. Restrictions on size were dictated by the available shaft area, which was approximately $4\frac{1}{2} \times 6$ ft. Restrictions on weight were dictated by the head frame, which was limited to 7 tons. Final inspection for acceptance was performed in the mine at Lyons, Kansas.

The complete assembly, less the tractor, weighs about 80,000 lb. (The tractor weighs about 22,000 lb.) The shield itself weighs approximately 50,000 lb and therefore could not be constructed in the manner normally used for casks of this size. The top door assembly of the cask was removable. The steel shell and the lower door-frame assembly was one-piece welded construction. The bulk of the weight was, of course, represented by the lead shielding. To minimize costs, facilitate assembly, and minimize radiation leakage, uncased lead rings of a chevron-type cross section were designed. All the rings were identical, except for the top and bottom ones, and each weighed approximately 900 lb. Their loading proved to be easier than expected, and none were damaged in shipping or handling or in loading into the cask. The transporter handled surprisingly well, and with very little practice one could maneuver the cask into any area desired. The unit could be spotted in any fixed position more closely than the specification required. The index system provided positioning anywhere within a 3-ft-square area, and the cask could be stopped precisely where desired. The cask could be elevated to the ceiling of the mine to receive the canister and could be lowered to the floor of the mine to discharge the canister. All shield motions were actuated by small hydraulic motors. The operation of both the upper and lower doors, as well as that of the winch, was remotely controlled. The remote control panel was provided with operating lights, to indicate

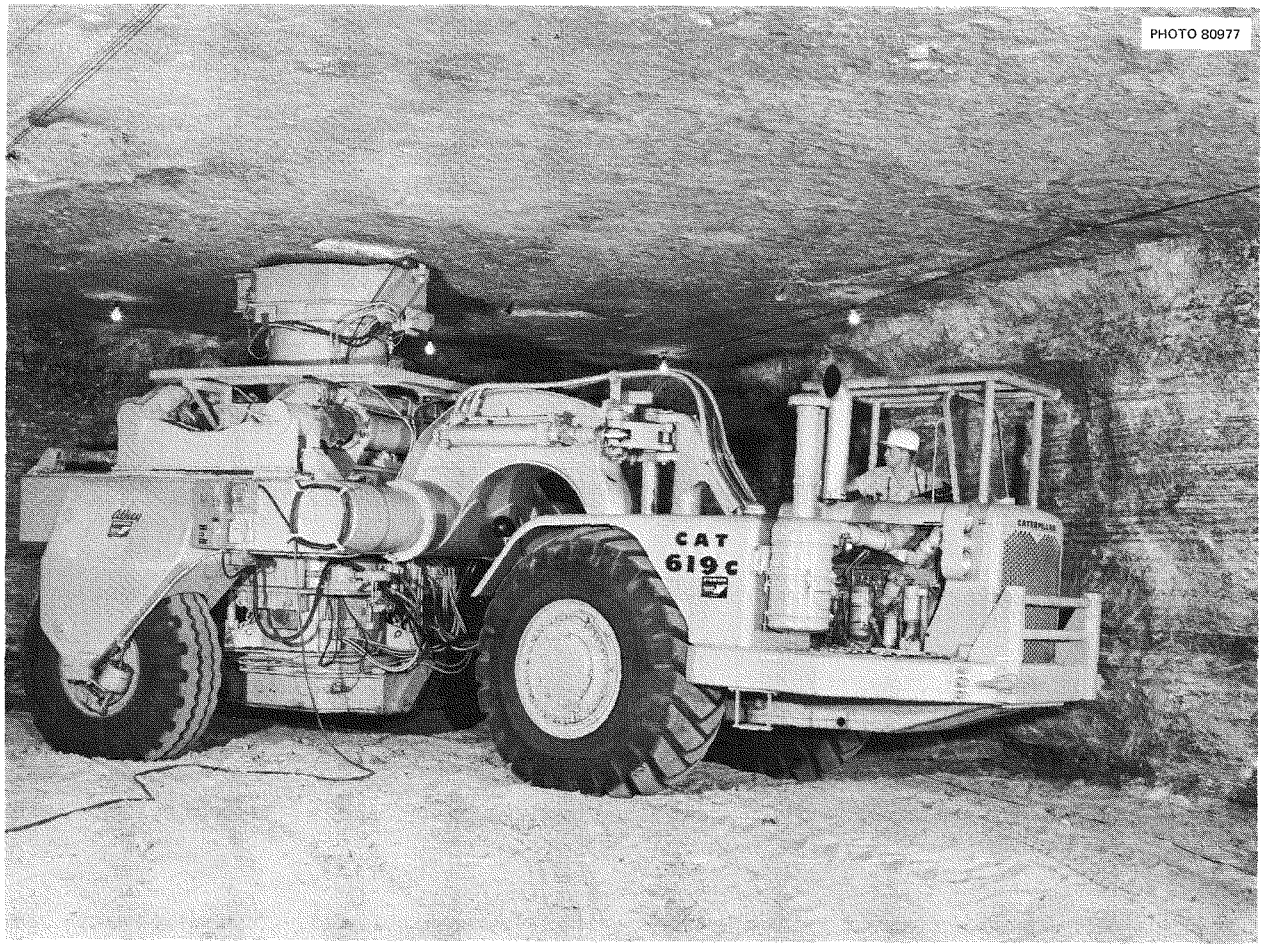


Fig. 7.8. Underground Transporter.

door positions and critical positions of the canister, and with a footage counter for the winch, to indicate the length of cable released. The indexing of the shield was directly controlled from the tractor cab. The shield provided approximately 9 in. of lead-equivalent shielding and had an internal cavity 15 in. in diameter by 9 ft long. This size was chosen because it was compatible with early calcined waste containers at Hanford and was within the power capability of the tractor used. For purposes of this demonstration, an insert tube was placed in the cavity to retain the canister in the vertical position. The body of the tube was made of 6-in. sched 10 stainless steel pipe.

Appropriate safety devices installed on the cask and trailer included safety chains to prevent accidental lowering of the shield during transport, locking pins on both cask doors, and a hydraulic interlock to prevent operation of any of the cask- or door-opening hydraulic systems unless the trailer brakes were locked. In addition, the cask operations were controlled by an electrically driven hydraulic pump located on the tractor. This motor was not connected unless the tractor was in the correct operating position.

The area provided underground for the transfers at the bottom of the waste shaft consisted of a room mined from the corridor in the experimental area to the waste shaft (see Fig. 3.6). The transporter was backed into this room and positioned under the waste shaft. A special funnel and shield assembly was installed on the top of the transporter shield to assist in centering the canister at the bottom of the waste shaft. Installed inside the transporter shield was a guide tube assembly equipped with limit switches to indicate the location of the canister. During waste transfers there were no personnel in the transfer room, and all operations were carried out remotely.

Shielding calculations (see Appendix 7A) indicated that the radiation fields in the transfer room would not exceed 14 mR/hr until the canister was within 3 ft of the bottom of the waste shaft. When the canister passed this point and until it was completely within the shield of the transporter radiation fields as high as 93 mR/hr would occur. The maximum calculated radiation field with the canister in the transporter shield and the doors closed was 37 mR/hr at contact with the shield.

7.5 STORAGE HOLE LINERS

Figure 7.9 shows a cross section of a storage hole and the various auxiliaries required. For an actual disposal operation, these auxiliaries would not be necessary. A hole would be drilled in the floor; then crushed salt would be dumped in to provide shielding. The salt charging mechanism could be incorporated on the transporter so that the salt could be fed into the hole upon completion of the loading operation. Since space in the Lyons mine was only rented from the Carey Salt Company, it was necessary to provide additional features to guarantee that the canned fuel assemblies could be withdrawn from the mine at the end of the operation.

The upper part of the storage hole consisted of a 16-in. hole drilled to a depth of 5 ft 3 in., followed by a 12-in. hole drilled to a total depth of 12 ft 8 in. Into this hole was inserted a metal liner used to provide containment and to ensure that the canisters could be removed at the conclusion of the experiment. The liner was made in two sections: the upper liner was carbon steel well casing, 14 in. OD, 0.514 in. wall, grade N-80, 5 ft 1 in. long, capable of withstanding an external pressure of 3500 psi. This upper liner was grouted into the salt, and the lower liner section was bolted to the fixed upper section and was removable. The lower section was designed as a thinner-wall vessel to allow maximum radiation dose to the salt. For maximum corrosion resistance the lower liner section was made of 304L stainless steel tubing, 6 in. OD by $\frac{1}{4}$ in. wall, 6 ft $4\frac{1}{4}$ in. long. To avoid the problem of collapse pressure, an annular space was provided between the salt and the lower liner section. Movement of the salt inward toward the liner was measured by special calipers. If the movement of the salt was sufficient to endanger the integrity of the system, it would be necessary to withdraw the canister and the liner and to overbore the hole and reinstall the equipment. Auxiliary heaters were provided to supplement the heat lost as the radioactive decay heat rate diminished. Provisions were made for monitoring the off-gas from the annular cavity. When

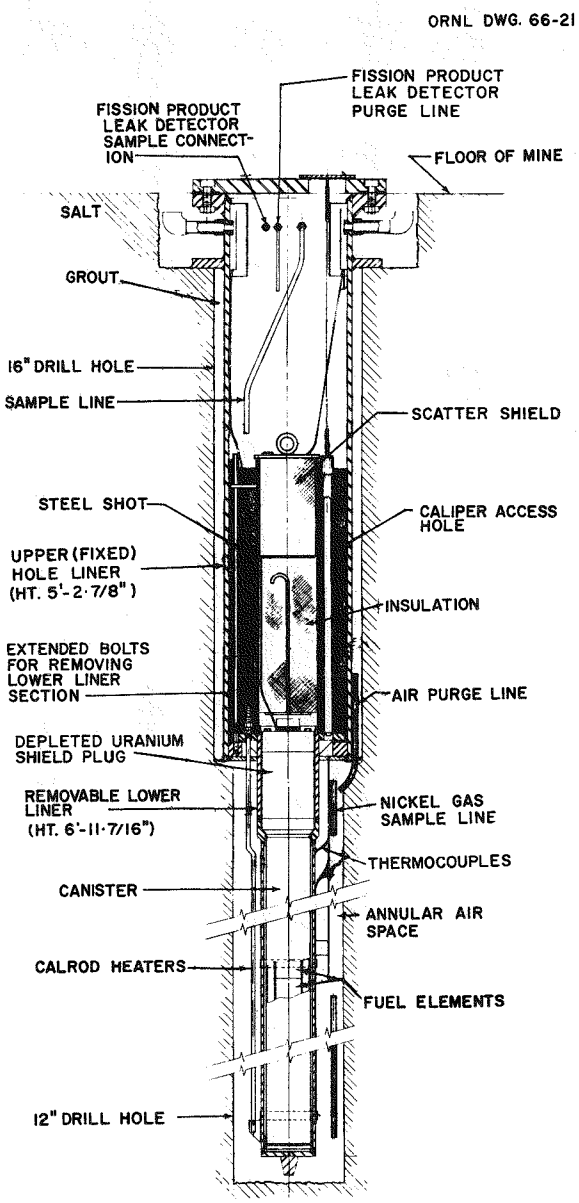


Fig. 7.9. Cross Section Through Main Array Hole.

the canister was in place, the radiation field was reduced to a level that was acceptable for connecting the thermocouples to the instruments. A supplementary shield (scatter shield, Fig. 7.9) reduced the background radiation so that it was negligible at the surface of the floor. The maximum radiation air dose in the upper liner section with the canister in place was calculated to be 54 mR/hr (at the top of the grapple tube).

The upper liner section was sealed with a gasketed steel cover to provide containment and to allow the

transporter wheels to roll over the holes. The cover also prevented foreign objects from falling into the liner.

7.6 HEATED PILLAR EQUIPMENT

The heated-pillar test was designed to obtain additional information on the thermomechanical properties of salt in situ under transient temperature conditions. In this test a nominally 20-ft-wide pillar between the two center rooms of the experimental area was heated by a total of 33 kW of electrical power applied to 22 heaters in the floor along the base of the pillar. The locations of the heaters with respect to the actual pillar is shown in Fig. 11.43. The heaters were located approximately 2 ft from the base of the pillar.

7.6.1 Heaters

Twenty of the twenty-two heaters were of the same design, and two were known as "modified pillar heaters." The regular heaters were contained in a 4-in. sched 40 carbon steel pipe 13 ft long, with three 2-in.-long, $\frac{1}{2}$-in.-diam legs on the bottom. Each of the standard pipes contained an assembly of two U-shaped heater elements with Incoloy sheaths similar to Chromalox type TI-15648 with heated lengths of about $12\frac{1}{2}$ ft (before bending). The bent length was about 6 ft, and the bottom of the U was about 4 in. from the bottom of the pipe. (These same heater elements were used for the electrical array heaters in order to minimize the number of spares required for the operation.) The upper region of the pipes (a section about $6\frac{1}{2}$ ft long above the top of the heater element assembly) was filled with glass fiber insulation to minimize convective heat transfer up the pipe.

7.6.2 Modified Heaters

The two modified heaters were designed to yield additional information about the durability of carbon steel and 304L stainless steel in the salt environment at elevated temperatures. One was made of 4-in. sched 40 carbon steel pipe, and the other 304L steel, but the overall length was only 7 ft, instead of 13 ft as for the regular heaters. Also, the top was welded shut, the electrical leads were brought up through a conduit, and a "standpipe" extending down into the sealed heated zone was brought up and connected to a pressure gage. (Each standpipe was of the same material as its respective heater pipe.) The heated zone and pressure pipe were flushed with dry nitrogen at ambient temperature and then sealed, so that as the temperature went up, a pressure would build up, and leaks in the heater pipe could be detected by a pressure loss.

Three nickel tubes ($\frac{1}{8}$-in. sched 40 pipe) were strapped on the outside of each of the heater pipes. Each tube had welded to its bottom end a 2-in.-long section of $\frac{3}{8}$-in. sched 40 pipe with $\frac{5}{32}$-in. perforations spaced on $\frac{3}{8}$-in. centers. These three perforated sections were located at the bottom, middle, and top of the heater pipe. A fourth tube was located in the crushed salt about 3 ft above the pipe. By pressurizing these tubes and measuring the flow, information could be obtained about the degree to which the salt had sealed around the pipe.

The heater elements in the modified pillar heaters were not quite identical to the elements in the regular heaters, but were close enough in ratings for our purposes. Each element had a rating of 5 kW at 480 W, was 164 in. long, $\frac{5}{16}$ in. in diameter, and 156 in. in heated length (resistance calculated to be about 46.1 Ω, compared with about 46.5 Ω for the regular heaters).

7.6.3 Thermocouples

Ten regular heaters plus the carbon steel modified heater were installed in room 2, with numbering starting at the back of the room and running to the front. Number 6 (the center) heater was the modified one. Heaters 1, 4, 7, 9, and 11 had Chromel-Alumel thermocouples located in the air inside the pipe and on the outside of the pipe at about 3 ft up from the bottom (i.e., in the center of the heated zone). Number 6 had Chromel-Alumel thermocouples located on the outside of the heater pipe at the top, middle, and bottom (about 6, 9, and 12 ft below floor level). Twelve of these were recorded, and the 13th was read manually using a portable potentiometer with the trade name Minimite.

In room 3, heater numbering was the same, with the 304L heater being in hole 6. Heaters 2 and 8 had iron-constantan thermocouples in the air inside the pipe and on the outside of the pipe at the center of the heated zone, while heater 6 had thermocouples on the outside of the pipe at the top, middle, and bottom. All of these iron-constantan thermocouples were read manually.

7.6.4 Power Supply

The power supply for the heated-pillar experiment consisted of a three-phase feeder connected through a 225-A circuit breaker to an automatic voltage regulator with a rated output of 70 kVA (in order that, if desirable, pillar heater power could be raised to 66 kW).

This in turn fed into a three-phase open-delta adjustable-voltage autotransformer with manual pushbutton motor drive (rated 67.9 kVA).

Individual elements in the heaters were connected in parallel, and then two heaters were connected in parallel to 30-A double-pole circuit breakers located on the end of the center pillar. Loads were approximately evenly distributed between the three phases.

At the main power control panel, electrically located between the adjustable autotransformer and the load, were an ammeter, a voltmeter, and a recording wattmeter (normally connected for 50 kW full scale). Power was controlled by adjusting the autotransformer. The voltmeter and ammeter gave a rough check on the performance of the wattmeter.

7.7 INSTRUMENTATION

This section describes the instrumentation exclusive of that connected with the rock deformation and mine stability, which is described in Sect. 11.4.

7.7.1 Thermocouples, Cables, and Recorders

7.7.1.1 Recorded Thermocouples. – There were 393 thermocouples that were automatically recorded at regular intervals. To accomplish this, several multipoint recorders were used: one 12-point, five 24-point, and two 144-point loggers. On the loggers only 132 points were available for recording temperatures, the other 12 being used to indicate which bank of thermocouples was being recorded at any given time. Table 7.1 shows the pertinent data regarding these recorders. It will be noted that only logger F was for iron-constantan thermocouples. All of the others were calibrated for Chromel-Alumel thermocouples.

In addition to the recorded thermocouples, there were others which were read with a portable potentiometer called a Minimite. These nonrecorded thermocouples are discussed later.

The recorder A thermocouples were all located in or on the pillar heater pipes in room 2 and are discussed in Sect. 7.6.

Recorder B thermocouples were located between the plates of the ETR fuel assemblies in each of the radioactive arrays. Since there were only 12 points available per array, and 14 fuel assemblies, two of the fuel assemblies were not monitored (the coolest one in each of two cans, as determined from the irradiation history). Recorder B had a high-temperature sensor switch which was set normally at 500°C so that the

Table 7.1. Recorder Tabulation

Recorder Designation	Recorder Location	Function	No. of Points	Type Couple	Temperature Range (°C)
A	Pillar between rooms 1 and 2	Heater temperature, pillar heaters	12	C/A[a]	0–800
B	Pillar between rooms 1 and 2	Fuel elements, main and floor arrays	24 (12 per array)	C/A	0–800
C	Pillar between rooms 1 and 2	Heater control (salt 1½ ft from center of hole)	24 (7 per array, 3 not used)	C/A	0–250
G	Main control room	Liner, air, salt periphery, room 1	24	C/A	0–400
H	Main control room	Liner, air, salt periphery, room 4	24	C/A	0–400
J	Main control room	Liner, air, salt periphery, room 5	24	C/A	0–400
E	Main control room	Salt temperature, three arrays	132 (44 per array)	C/A	0–250
F	Main control room	Salt temperature, pillar experiment	132	I/C[b]	0–250
	Total number of recorded points		393		

[a]Chromel-Alumel.
[b]Iron-constantan.

auxiliary heater power to the hole liners would be shut off if any fuel assembly temperatures got that high (in practice, this temperature was never approached).

Recorder C monitored the salt temperature 9 ft below floor level (the center plane of the heat sources) at 1½ ft from the center of each of the array holes. By comparing these temperatures between holes in the same array and between corresponding holes in the three arrays (with due regard to the later start time for the floor array), judgments could be made regarding the uniformity of power input and variations between the arrays.

Recorders G, H, and J performed identical functions for the three arrays. Temperatures of all seven hole liners at 9 ft below floor level were recorded, along with those at 6 and 12 ft on liner IV (the center hole). Also, the salt temperature at the periphery of each of the holes at 9 ft depth and the temperatures at 6 and 12 ft depth for hole IV were recorded. The remaining six recorder points were used to record the air temperature in the annulus between the liner and the hole in all except hole VII.

Logger E recorded 44 salt temperatures at points in and around each array. Thermocouple depths were usually 1, 5, 9, 13, and 17 ft below floor level, but not all depths were used at all locations. Thermocouples were generally located so that it was possible to construct isotherms in three dimensions.

Logger F recorded salt temperatures in room 2, in the south, west, and north walls of the room, under the north pillar (pillar 2-3), and in the floor. Depths in the floor were again usually 1, 5, 9, 13, and 17 ft.

Thermocouples on the outside of the hole liners in the arrays, at the walls of the array holes, and in and on the pillar heaters had 304L stainless steel sheaths. Most other thermocouples were made from thermocouple extension cable and protected by jackets of Teflon if the temperature was expected to exceed 100°C, or polyethylene if lower maximum temperatures were anticipated. (Prior tests during operation of the prototype indicated no significant difference in temperature reading if a metal-sheathed thermocouple were placed in a plastic jacket.)

Each individual thermocouple terminated in a standard male-type connector which plugged into a female connector on the end of an individual extension cable. These cables were generally gathered into bundles for routing to the junction boxes located on the walls of the rooms. From the junction boxes the signals were carried to the recorders by multiconductor plastic-sheathed extension cables. These cables ranged in length from 80 to 450 ft. Fifteen of the cables each contained pairs for 24 thermocouples, and the remaining five cables contained 12 pairs each.

7.7.1.2 Manually Read Thermocouples. – The remainder of the thermocouples were read periodically with a portable potentiometer called a Minimite. This instrument could be read with a repeatability of about ±1°F, but its accuracy depended to some extent upon the ambient temperature. In practice, with ambient temperature variations and operator error, variations of up to about ±5°F were not unusual.

There were about 152 thermocouples which were read with this instrument. Rooms 1 and 5 each had 49, which included the fuel assembly thermocouples not recorded automatically (each fuel assembly had a spare thermocouple), thermocouples inside the upper portion of the hole liners, thermocouples on the off-gas pipes and tubes leading to the master sampling and metering station, and some thermocouples located out in the salt. Room 4 was the same as rooms 1 and 5, but without the fuel assembly thermocouples, giving it a total of 33. Room 2 had four, with three of these in the end of pillar 1-2 and the fourth 12 ft below floor level on heater 6. Room 3 had 17, measuring salt temperatures in floor and pillars and in and on the heater pipes.

In addition to the thermocouples (which totaled about 545), there were also a few dial-type thermometers used for miscellaneous measurements.

7.7.2 Power System

Figure 7.10 is a simplified block diagram of the power circuit for the array and pillar heaters. The main mine supply comes in at 2400 V three phase, and the experiment was operated from a 150-kVA transformer bank.

The pillar heater supply system is described in Sect. 7.6.

The three arrays were fed through a 125-A circuit breaker and open-delta automatic voltage regulator rated at 45 kVA. Each individual array was then supplied with three-phase regulated voltage through a 40-A fuse and switch box. Individual heaters in each array were supplied through double-pole 15-A breakers, and each heater had its own adjustable autotransformer and ammeter.

Each of the radioactive array hole liners had two sets of three heater elements installed on the outside to supplement the radioactive decay heat and to allow the total power input (radioactive plus electrical) to be maintained at a constant level as the radioactive heat decreased with time. Only one set of three heater elements was used, the second set being a spare. The

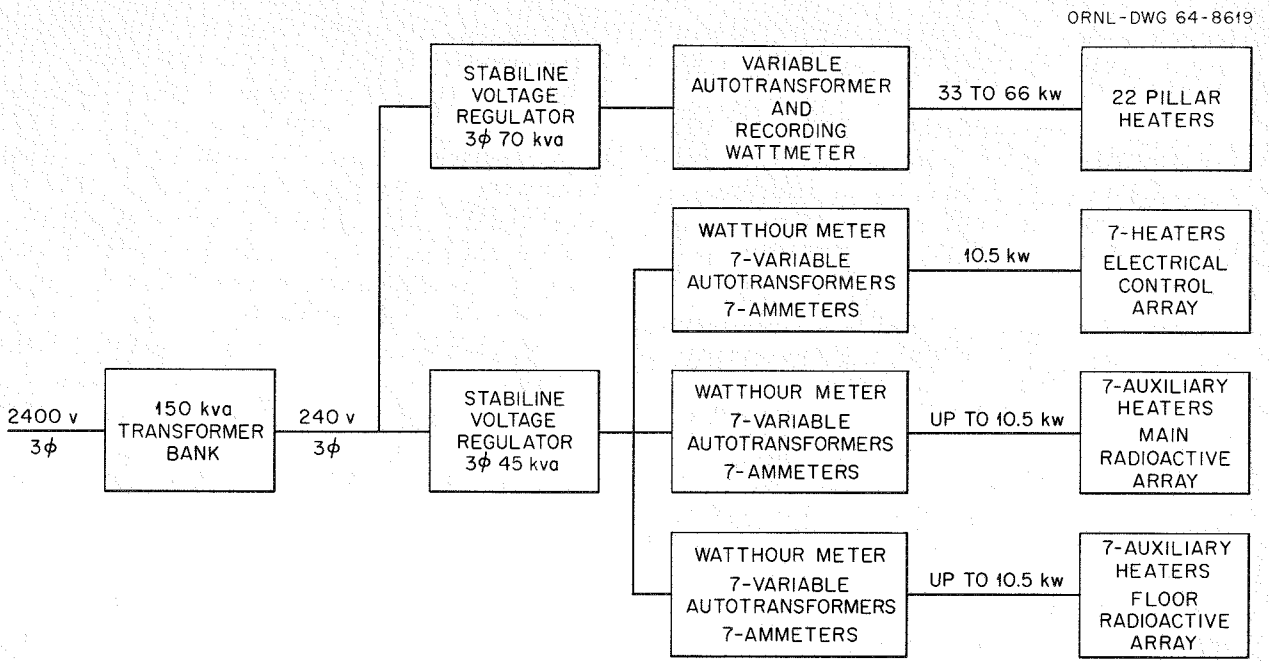


Fig. 7.10. Simplified Block Diagram of Power Circuit for Array and Pillar Heaters.

three elements in each set were connected in parallel. Each element was 0.375 in. in diameter, with a heated length of 149½ in., an overall length of 180 in., an Incoloy sheath, and an electrical rating of 4950 W at 480 V.

The electrical array heater elements were located inside the liners (two units connected in parallel) and were identical to the pillar heater elements described earlier.

The power to individual heaters in the radioactive arrays was adjusted to give the desired total power by means of the ammeter readings and the adjustable transformer scale settings. In addition, the total electrical power to each array was monitored by watt-hour meters. (Figure 8.2 shows the power control panel for the experiment.) The desired electrical power input at any given time was determined from the calculated fission product decay heat, based on the knowledge of the irradiation history of each fuel assembly in each hole.

7.7.3 Off-Gas System

The off-gas system was used only on the arrays and was designed primarily to detect chlorine or other reaction products which might be produced by irradiation and/or elevated temperatures. Each array hole liner had an inlet tube (with a particle filter) which extended down to the top of the annulus between the salt and the lower section of the hole liner. The off-gas outlet line extended from near the bottom of the annulus, up through the steel shielding shot in the upper liner (with appropriate bends to minimize radiation beams), and out the side of the liner, where it tied into a Teflon tube which ran (in a bundle with the other six tubes) over to the wall, where individual flowmeters, sampling ports, and throttle valves were contained in a box with a transparent window (see Fig. 7.11).

Originally, the outlet lines were coated with an electrical heating material so that all portions of the lines could be maintained at temperatures in excess of 100°C to prevent any condensate collection. However, these heater coatings failed at the points where the power supply leads were connected, in both the main radioactive array and the electrical array. Since quantities of water expected to be liberated in these arrays were small, it was decided to operate without the heaters. For the floor radioactive array, where large quantities of water were anticipated, the pipes were wrapped with a ribbon-type heater, which performed satisfactorily.

Before installation the off-gas pipes (made of nickel) were heat treated with fluorine so they would not react with chlorine, should any be released.

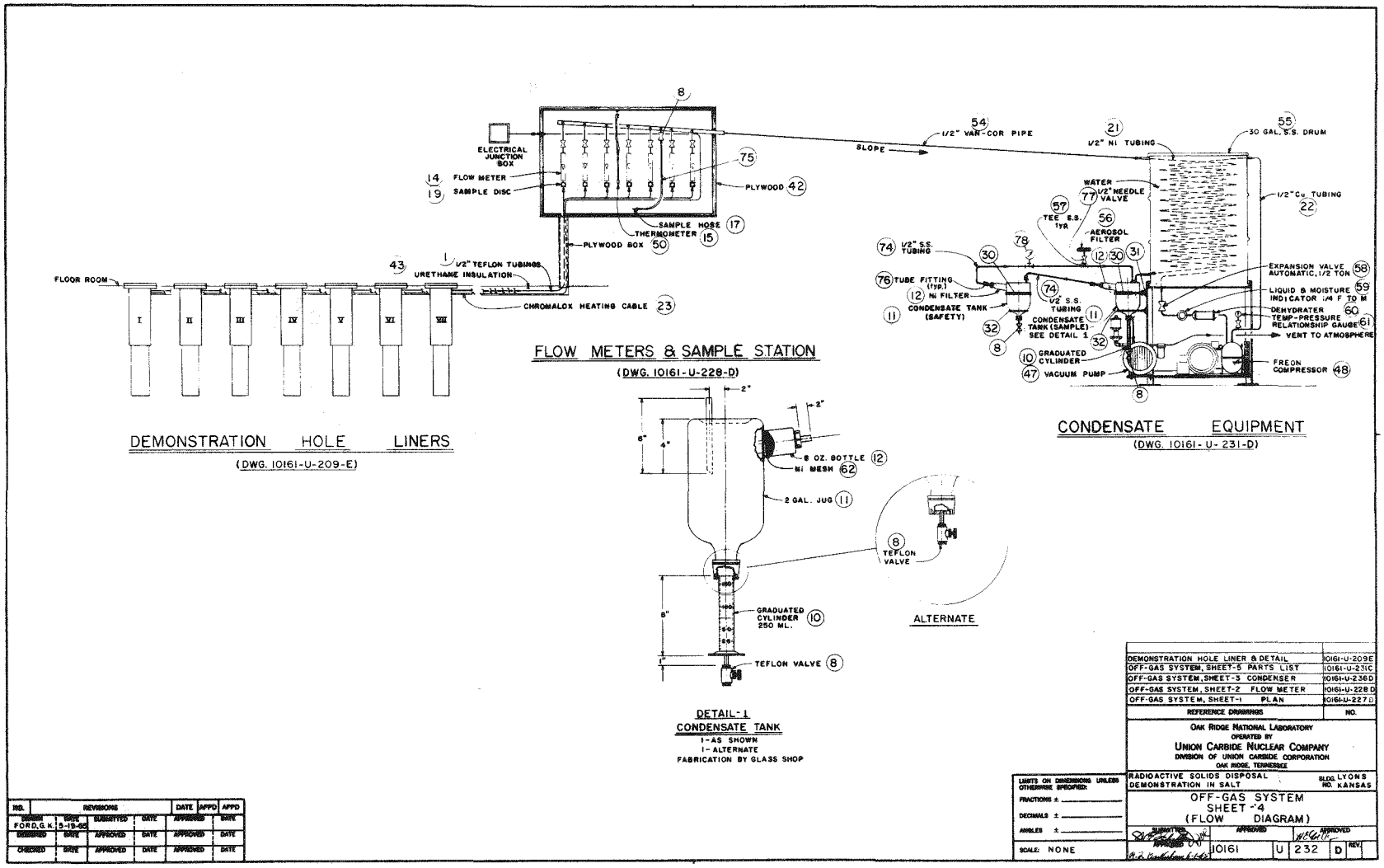


Fig. 7.11. Flow Diagram – Off-Gas System.

The Teflon tube bundle contained copper-sheathed flexible-tube heaters which were used to maintain the off-gas above 100°C. Heaters were also contained in the flowmeter boxes. Inside the flowmeter boxes the off-gas lines joined a manifold, and the line from it (polyvinyl chloride) sloped down to a nickel condenser, which drained into a water trap (polyethylene). A vacuum pump was used to maintain an air flow rate of about 7 liters/min per array hole. The nickel condenser coil was contained in a water drum, which also had a copper coil connected to a refrigeration unit. The refrigeration units were not normally operated, since the off-gas temperature was down to ambient by the time it emerged from the condenser anyway.

Periodically, Mine Safety Appliance and/or Drager chlorine detector tubes were used to sample the individual off-gas lines at the sampling points in the wall boxes (Fig. 7.11). Also, at other times special sampling apparatus was connected to individual lines for non-routine analysis.

7.7.4 Radiation Detection Systems

The radiation detection system (also called the purge system) was primarily designed to detect and contain any possible leaks in the fuel assembly canisters. (Such a leak would have required a breach in the fuel element cladding plus a leak in the canister.) In addition to this system, a continuous air monitor was located in front of the main underground control room and was used with an extension hose to monitor near the underground transporter during canister transfer operations.

In each radioactive array hole, the upper liner (which was in communication with the canister) contained an inlet port with particle filter and solenoid shutoff valve, and an outlet port, also with shutoff valve (see Fig. 7.12). These outlet ports were fed into a common silicone rubber and/or polyethylene tubing which then led into an activated coconut-charcoal trap which contained two thin-wall G-M tubes inside a modified lead counter pig. From there the line led into a second counter pig containing a chamber with an end-window G-M tube. A purge pump, rotameter, and valve system were adjusted to draw about 1 liter/min through each of the hole liners and into the trap and counter system.

Normally the G-M tubes in the charcoal traps were read periodically with a portable G-M survey meter. The end-window tube was connected to an alarming-type count-rate meter in the underground control room which would (if the reading exceeded the alarm set point) cut off the purge pump, close the port solenoids on the hole liners, cut off all auxiliary electrical heater power, and transmit an alarm to the appropriate places.

All components of this system were designed in the fail-safe mode. If, for example, the purge air flows were to fail (due to pump or other trouble) the system would automatically shut down and sound the alarm.

The reason for using the end-window tube in the chamber after the charcoal trap is that if any radioactive material were to escape the liner and get as far as the detection system, it would almost certainly be xenon or krypton, and the end-window tube would be more sensitive than a thin-wall tube to the krypton beta emission.

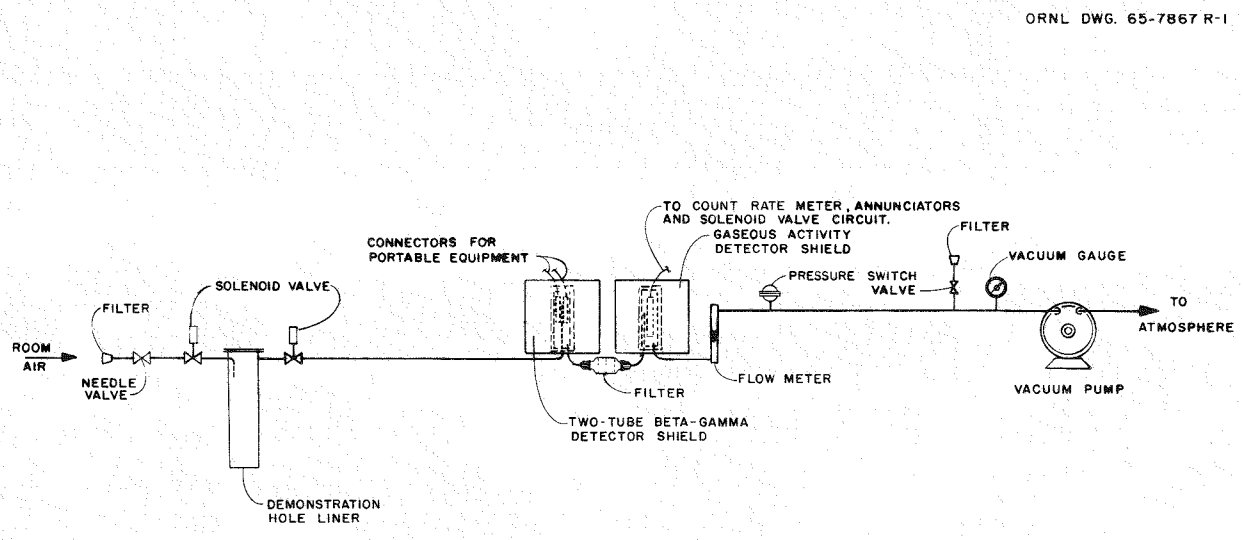


Fig. 7.12. Flow Diagram – Radiation Detection System.

7.7.5 Alarm System

The alarm system covered not only possible radioactivity leakage but a number of other conditions.

Although there were other items monitored, such as thermocouple failure, there were four conditions of prime concern to the experiment which were included in an extensive monitoring and alarming system. These were: (1) radioactivity leakage from one of the fuel assembly containers, (2) excessive fuel element temperatures, (3) rapid sag of a layer of salt in the roof of the experimental area, and (4) auxiliary electrical power failure to one of the arrays. The reason for concern with the first two is obvious. The third, a rapid rate of sag of the 2-ft-thick layer of salt in the roof, could indicate an impending roof fall. The fourth item was not concerned with safety, but with the fact that the power input to the main array and that to the electrical control array had to be maintained as nearly equal as possible in order to determine any gross effects due to radiation. Therefore, if trouble was experienced with one array, the other should be shut down also, and the trouble corrected as soon as possible.

These four items were monitored and telemetered to the surface and to the operators' houses by the system described in Appendix 7B. (Some of the system deficiencies are described in Chap. 10 on operating experience.)

It may be noted in Appendix 7B in the section "Alarm System Malfunctions" that there were certain conditions which could make the system inoperative and which would not be readily apparent. It was therefore necessary to make periodic tests of all units by triggering the primary alarm-condition detection units. The original concept had called for a completely fail-safe system, but this was abandoned (due to the time and expense involved in developing such a system) in favor of the use of as many existing components as possible. While this proved adequate for the demonstration, it would not be in an actual waste disposal facility.

7.7.6 Dosimetry

Both the ferrous sulfate dosimeter and the Bausch and Lomb low-Z glass rod dosimeters proved to be usable at temperatures up to 250°C (see Sect. 4.5). Both types required batch calibrations, both cost about 50¢ per dosimeter, and both required about the same amount of time for preparation and reading. There is essentially no time limit between the time of irradiation and reading of either dosimeter, so readings could be done either in the field or at ORNL. The chemical dosimeter required a colorimeter for readout, while the glass rod required an oven plus a fluorometer. Both types were subject to fairly large variations, so that more than one dosimeter per measurement was desirable. The glass fluorods were smaller and thus more closely represent the dose at a point. Based on the above considerations, the following system was designed for measurement of dose to the salt in the arrays.

Each array had two holes (stepped diameter for shielding purposes), drilled tangent to the storage holes at an angle of 25° from the vertical, for insertion of rods containing the dosimeters. These dosimeter holes were associated with array holes I and IV. The rod design allowed the insertion of six chemical dosimeters and 18 glass fluorods in each dosimeter hole. It was also planned to use thermocouple hole 19, which was located 18 in. from hole I, to position three fluorods. A full set of dosimetry measurements for an array consisted of, in each of two holes, three fluorods and two chemical dosimeters measuring the radiation incident on the salt; three fluorods with ½ in. of salt shielding; three fluorods plus one chemical dosimeter each with 1, 2, 4, and 8 in. of salt shielding; and three fluorods with 18 in. of salt shielding. (These salt thicknesses were nominal, due to variations in the dosimeter holes.) This amounted to 12 chemical and 39 fluorod dosimeters per array for each complete set of measurements.

The following procedure was used as a design basis. At startup time a complete set of measurements would be taken as soon as time permitted. Thereafter, once per month a set of incident radiation measurements would be taken, and complete sets at the middle and end of the period with each set of fuel assemblies.

In order to smooth the energy response of the glass rods, they were exposed in shields, as described in Sect. 4.5. The dosimeter holder rod was about 10 ft long, and the exact dimensions were tailored for each of the exposure holes after the holes had been drilled and measured. In room 1 the holes came very close to the desired position, but in room 5 one hole intercepted the array hole at an angle which would have produced a direct beam from the fuel assembly container, and the other hole was barely tangent to the array hole. (The difficulties with hole alignment in room 5 were related to the higher ceiling, which required the drill to be mounted on a much longer post. Flexure and twisting of this post resulted in a hole which deviated considerably from the desired alignment.) Therefore, one hole had to be plugged, and the other one was used for incident dose measurement only.

The upper 5 ft of each exposure rod was made of 3½-in.-OD nickel tube, filled with steel shot for shielding purposes. The bottom 5 ft was 1½-in.-OD thin-wall Monel tube filled with a solid salt plug, except for the places where the tube and salt were perforated to receive the dosimeters. Due to difficulty in filling the tubing with molten salt, the salt plugs were machined from salt cores.

Because the dosimeters had to be located with different thicknesses of salt between them and the wall of the array holes, they could not all be located at the vertical center of the fuel assembly canister. In room 1, the incident dose and the ½ in. of salt shielding position were within about 2 in. of the center, but the 1 in. of salt shielding position was located about 8 in. above center, the 2 in. of salt about 11 in. up, the 4 in. about 17 in. up, and the 8 in. of salt about 27 in. above canister center. This meant that the accuracy of the dose measurements would vary somewhat with position.

7.8 SUMMARY

The work described in this chapter involved many individuals in a number of divisions at ORNL as well as at other plants, contractors, suppliers, etc. The number of man-hours involved cannot be estimated, but it is probably considerably larger than that represented by the other phases of Project Salt Vault described in other chapters of this report.

It is not possible to describe in detail the specifications and fabrication procedures for most of the equipment, but an attempt has been made to make the general design criteria as clear as possible.

More details are on record in a series of drawings on file with the General Engineering and Construction Division of ORNL. The Engineering Job Number on these drawings is 10161. By function, the numbers of drawings are: 6 civil; 17 electrical; 11 heating, ventilation, and air conditioning; 29 instrumentation; 91 mechanical; 21 structural; 13 conceptual; 10 Stearns-Roger; 5 Stanspec Company; and 566 Athey Products Corporations drawings showing details and all parts of the underground transport trailer.

APPENDIX 7A. Shielding Calculations

The shielding calculations for this report were performed with a special shielding code on an IBM-7090 computer.[2] For purposes of these calculations the fuel assemblies were converted into a cylindrical source of equal volume having the same radioactivity and irradiation history. This source has a radius of 6.3 cm and a length of 190 cm. The resulting nine energy groups and source strengths were obtained by using the Phoebe code[3] and are shown in Table 7A.1.

Table 7A.1. Canister Source Strength

Group	Source Strength (photons/sec)	Group Energy (MeV)
1	1.8480×10^{15}	0.300
2	3.6780×10^{15}	0.630
3	1.239×10^{15}	1.100
4	2.570×10^{14}	1.550
5	1.184×10^{13}	1.990
6	2.720×10^{13}	2.380
7	2.838×10^{12}	2.750
8	1.253×10^{12}	3.250
9	7.164×10^{11}	3.700
Total	7.0658×10^{15}	

The calculations were made by considering the amount of shielding present at the top, middle, and bottom of the source. The amount of shielding for each canister position was then calculated by using the average shield thickness and ray lengths from the three points. No mass attenuation coefficients, energy absorption coefficients, or buildup factors are available for salt, but since its density (135 lb/ft^3) is about the same as that of concrete, it is believed that the shielding properties will be about the same as for concrete. Thus for the calculations in which salt was a part of the shielding, concrete was used in equivalent thickness.

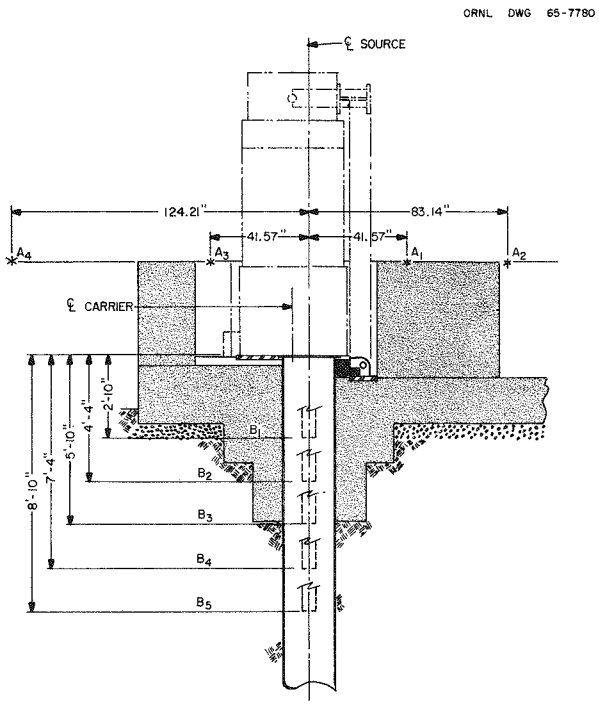
Dose calculations were performed at three different locations: the topside facility, at the bottom of the waste shaft, and at the storage hole. At each location the dose was calculated at multiple points for different positions of the canister. The results of these calculations are shown in Figs. 7A.1–7A.3. The highest dose rates occur when the canister is being lowered from the transporter into the storage hole. However, during this time the area would be evacuated.

As a part of the preoperational checkout of the equipment and facilities prior to the first delivery of fuel assemblies, a cobalt shielding checkout was performed to verify the shielding calculations and to observe any beams or areas where more shielding might be required. Corrective action was taken at that time.

---

[2] E. D. Arnold and B. F. Maskewitz, *SDC: A Shielding Design Code for Fuel Handling Facilities,* ORNL-TM-124 (Jan. 25, 1962) and ORNL-3041 (March 1966).

[3] E. D. Arnold, *Phoebe – A Code for Calculating Beta and Gamma Activity and Spectra for ^{235}U Fission Products,* ORNL-3931 (July 1966).



LOCATION OF CANISTER	RADIATION DOSE (mr/hr) Point A_1	Point A_2	Point A_3	Point A_4
B_1. Bottom of Canister 2'-10" into Waste Shaft	3	< 1	< 1	< 1
B_2. Bottom of Canister 4'-4" into Waste Shaft	73	< 1	< 1	< 1
B_3. Bottom of Canister 5'-10" into Waste Shaft	1	< 1	< 1	< 1
B_4. Bottom of Canister 7'-4" into Waste Shaft	24	< 1	< 1	< 1
B_5. Bottom of Canister 8'-10" into Waste Shaft	< 1	< 1	< 1	< 1

Fig. 7A.1. Radiation Dose at Topside Facility During Canister Transfer Operations.

APPENDIX 7B. Project Salt Vault Remote Alarm System

Description of System

Figure 7B.1 shows in functional form all of the alarm circuits which were telemetered to the hoist house. These diagrams should be referred to in connection with the discussions which follow.

The primary activation for the "hi-temp on recorder B" (fuel element temperature) alarm was a pair of contacts on a microswitch which was actuated by the "bull wheel" on the recorder. These contacts opened when the indicated temperature exceeded the set point. The "radiation – room 1" contacts were in a relay in the ratemeter unit located in the control room. This relay was actuated by the set-point contact on the ratemeter panel meter. The panel meter contact was of the lock-in type, and the reset button on the ratemeter had to be pushed to deactivate. "Radiation – room 5" functioned the same as that for room 1. "Radiation – CAM" (continuous air monitor) also functioned the same way. The "power failure" contacts were on a relay in the power panel at pillar 1-2. Contacts opened if power to the arrays failed for any reason (blown fuse, shutdown signal from radiation detection system, etc.). The "plastic flow" (ceiling sag) contacts were in relays in the transducer-readout units in the control room. The relay was actuated by set-point contacts on the panel meter. The contact was locking as on the ratemeters, and the reset button had to be pushed to deactivate.

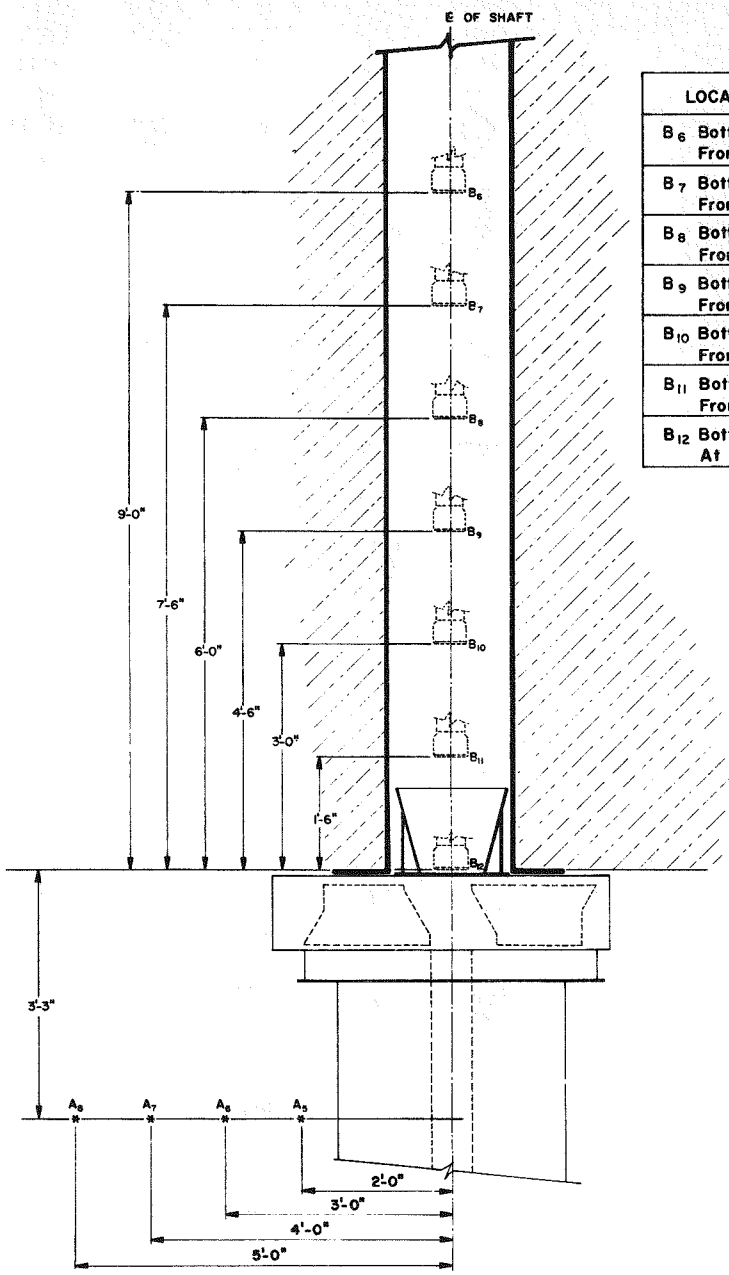
The ceiling-sag transducer consisted of a potentiometer housing anchored to the ceiling, with spring-loaded sliders attached to a wire that was anchored above the bed separation about 2 ft up into the roof. The set point on the panel meter could be set to actuate on as little as 0.05 in. movement.

The Tel-Alarm units in Fig. 7B.1 are essentially a source of 115 V ac energizing a relay through the normally closed (primary) contacts on the sensing units just described. When the relay is energized, the retransmit contact in the Tel-Alarm unit is closed. When the primary contacts open, the relay opens, the red light comes on, and a latching circuit keeps the relay open even if the primary contacts close again. (Not shown in Fig. 7B.1 are the relay contacts for the Tel-Alarm lights.) All control room Tel-Alarms had a common reset button. Pushing the reset opened the latching circuit and permitted the red light to go off and the retransmit contacts to close (if the trouble had been cleared up so that the primary contacts were reclosed). In series with the reset button was another pair of contacts, which were closed when the G.E. relay was energized with 115 V ac.

There were five circuits (ten wires or five telephone pairs) in use from the control room to the hoist house. These were: (1) hi-temp rec. B (fuel elements), (2) radiation (three in series), (3) power failure, (4) plastic flow (two in series), and (5) remote reset.

The hoist house Tel-Alarms were the same as those below ground except that they had individual reset buttons. The retransmit contacts for "hi-temp," "radiation," and "power failure" were in series and connected by telephone line with unit 1 at the No. 1 operator's house. The remote reset box had a source of 24 V dc which energized a relay to keep the contacts on the reset circuit to the mine closed, and also to keep the contacts closed to the "power failure" reset circuit. Pushing the reset button on this box thus reset the hoist house "power failure," as well as all the control room

ORNL DWG 65 07781



LOCATION OF CANISTER	RADIATION DOSE (mr/hr)			
	Point A_5	Point A_6	Point A_7	Point A_8
B_6 Bottom Of Canister 9'-0" From Shaft Bottom	<1	<1	<1	<1
B_7 Bottom Of Canister 7'-6" From Shaft Bottom	<1	<1	<1	<1
B_8 Bottom Of Canister 6'-0" From Shaft Bottom	<1	<1	<1	<1
B_9 Bottom Of Canister 4'-6" From Shaft Bottom	<1	<1	<1	<1
B_{10} Bottom Of Canister 3'-0" From Shaft Bottom	<1	<1	13.7	2.7
B_{11} Bottom Of Canister 1'-6" From Shaft Bottom	<1	<1	1.7	9.3
B_{12} Bottom Of Canister 0" At Shaft Bottom	<1	10.7	17.3	18.5

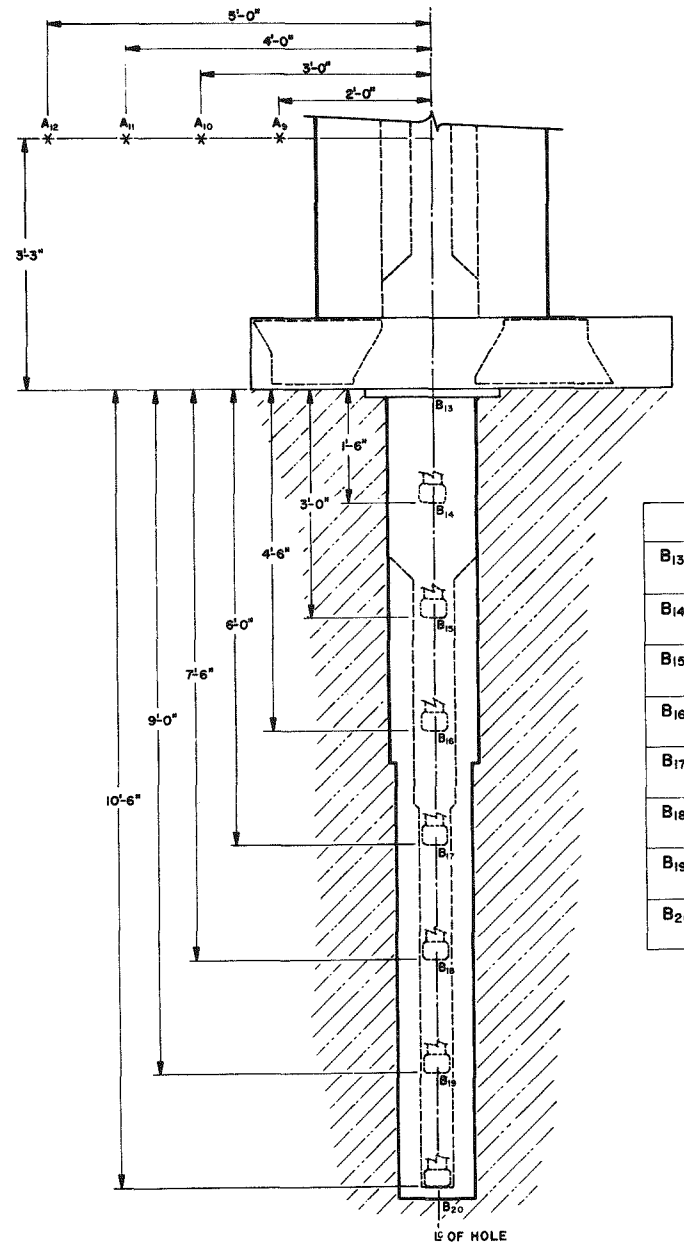
Fig. 7A.2. Calculated Radiation Dose During Lowering and Raising of Canister from Waste Shaft into Underground Transporter.

Tel-Alarm units. In series with this reset button were similar buttons at the operators' houses.

At the No. 1 operator's house there was the equivalent of a Tel-Alarm unit except that the relay and power supply were 24 V dc, the horn took the place of one of the lights, and there was a "test" button. One important difference was that there was no latching circuit, so that if the hoist house retransmit contacts reclosed, the alarm shut off by itself.

The system at the No. 2 operator's house was functionally identical to that at the No. 1 house, although there were some differences in the internal circuit. (The units were interchangeable, however, should the need arise.)

ORNL DWG 65-7782



LOCATION OF CANISTER	RADIATION DOSE (mr/hr) Point A_9	Point A_{10}	Point A_{11}	Point A_{12}
B_{13} Bottom Of Canister 0" Into Storage Hole	72	31	30	31
B_{14} Bottom Of Canister 1'-6" Into Storage Hole	90	85	23	39
B_{15} Bottom Of Canister 3'-0" Into Storage Hole	72	30	110	85
B_{16} Bottom Of Canister 4'-6" Into Storage Hole	<1	5.6	5	99
B_{17} Bottom Of Canister 6'-0" Into Storage Hole	<1	<1	122	70
B_{18} Bottom Of Canister 7'-6" Into Storage Hole	<1	<1	4	16
B_{19} Bottom Of Canister 9'-0" Into Storage Hole	<i	<1	14.5	4
B_{20} Bottom Of Canister 10'-6" Into Storage Hole	<1	<1	1	<1

Fig. 7A.3. Calculated Radiation Dose During Transfer of Canisters from Transporter to Storage Holes in Mine.

The unit at the sheriff's office (a backup unit in case both operators had to be away from home at the same time) was also functionally the same except that there was no remote reset circuit. Also, there was no retransmit contact, so the unit could not be used interchangeably with the other units. It could be used, however, at the No. 2 house with the reset phone-pair jumpered across.

Discussion of System

The system as shown could be modified to include other alarms or to omit some merely by connecting in the proper retransmit contacts or putting jumpers across them as the case may be.

Pushing the remote reset at an operator's house reset only the power failure unit in the hoist house. Thus

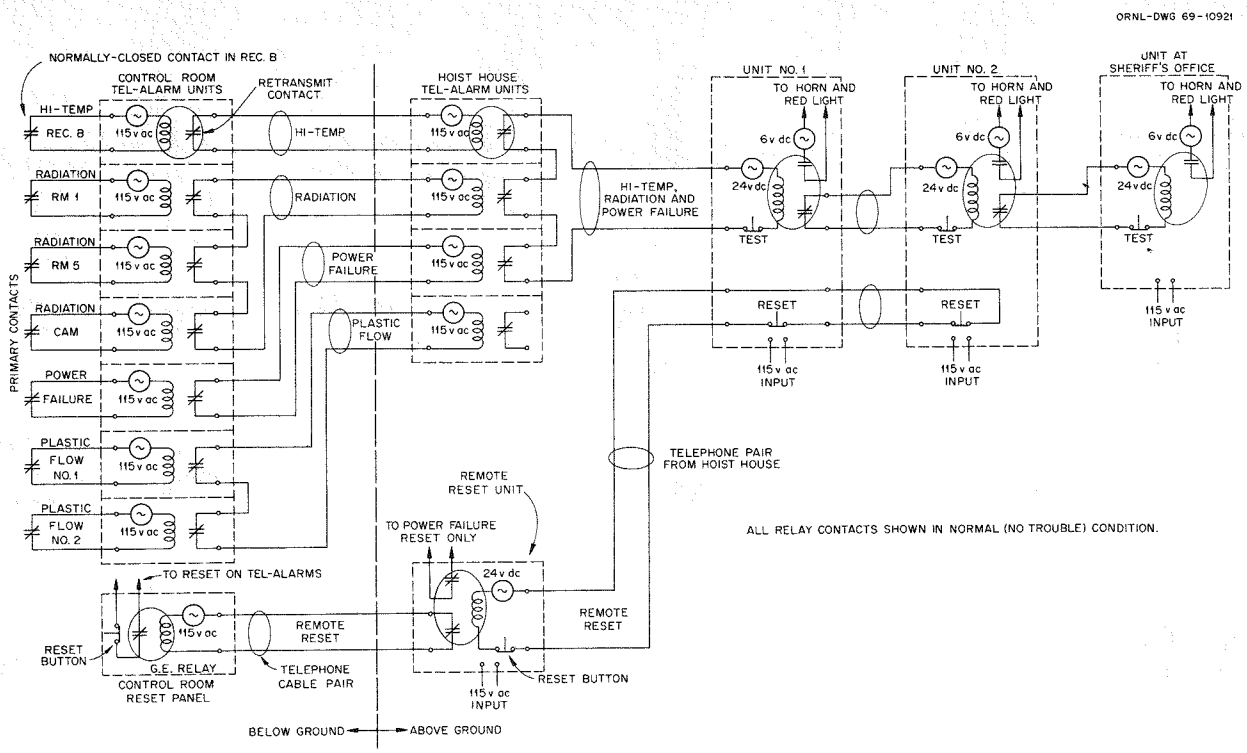


Fig. 7B.1. Remote Alarm System Functional Diagram.

only a temporary power failure (self-correcting) would result in a signal which could be cleared up by the operator's reset button.

Pushing the remote reset button on the box in the hoist house would clear up all of the control room Tel-Alarms (if the primary contacts were not still open), following which the whole system could be cleared by pushing the individual reset buttons on the hoist house Tel-Alarm panel. If the system did clear in this manner, it meant that the trouble was temporary (such as a momentary drop in power feeder voltage), and there was no need to go underground.

Alarm Interpretation

1. *Condition:* Momentary (self-correcting) alarm at the sheriff's office.
   Causes: Voltage sag on the 115-V ac circuit at the sheriff's office; momentary open circuit on the system anywhere on the telephone line or in either operator's house (e.g., "test" button pushed by either operator).
   Action: No action required.
2. *Condition:* Momentary (self-correcting) alarm at the No. 2 house.
   Causes: Voltage sag on the 115-V ac circuit at the No. 2 house; momentary open circuit in the system anywhere from the No. 2 house to the hoist house (e.g., unit 1 "test" button being pushed.)
   Action: No action required.
3. *Condition:* Momentary (self-correcting) alarm at the No. 1 house.
   Causes: Momentary open circuit in the system between the No. 1 house and the hoist house (e.g., operations in telephone central station).
   Action: No action required.
4. *Condition:* Alarm at either operator's house which clears when reset is pushed.
   Causes: Temporary power failure on mine feeder circuit.
   Action: No further action required. (This condition was not likely, due to the probability of the hoist house Tel-Alarm units also being actuated by the power failure.)
5. *Condition:* Alarm at operator's house which did *not* clear with reset.
   Causes: Possible trouble.
   Action: Go to hoist house, and make further checks.

6. *Condition:* One or more alarm signs on hoist house Tel-Alarm panel which cleared after remote reset and then the individual reset buttons were pushed.
   Causes: Temporary trouble such as momentary power failure (or voltage sag).
   Action: No further action required.
7. *Condition:* "Plastic flow" alarm alone which would not reset by pushing remote reset and then "plastic flow" reset.
   Causes: Failure in transducer readout unit; broken transducer anchor wire, or failure of transducer or cable (such as an open circuit) which would let the readout unit hit the lower limit contact; ceiling sag having reached the alarm set point.
   Action: Proceed underground with caution, and make visual inspection of ramp roof before proceeding to the control room. At the control room, check and record the other transducer readings, make analysis of situation, determine probable cause of alarm, and take such steps as seem necessary.
8. *Condition:* "Power failure" alarm alone which would not reset by pushing remote reset and then "power failure" reset.
   Causes: Failure somewhere in the electrical system to one or more of the arrays.
   Action: Proceed to the power panel at pillar 1-2, and *momentarily* push reset button at top of main array panel. If array-power lights at the top of this panel come back on and remain on when reset button is released, the shutdown was spurious, and all panel ammeter readings, etc., should be checked (and recorded) to make sure that the system is OK before leaving.
9. *Condition:* "Radiation" alarm alone which would not reset by pushing remote reset and then "radiation" reset.
   Causes: Failure somewhere in the "radiation" alarm system; continuous air monitor ratemeter having hit alarm set point.
   Action: Make sure that the waste-shaft fan is running in the upcast direction, and then proceed underground. Under normal operating conditions (i.e., not during a fuel-assembly can transfer period) it would be practically impossible for the CAM to detect activity coming from the arrays without the radiation detection system also alarming and causing shutdown of array power. Alarm of the CAM may be caused by buildup of radon and thoron daughters during periods of inversion topside or during periods of reduced mine ventilation. Alarm may also be caused by spurious electrical discharges within the CAM circuit itself. These spurious discharges will show as pips on the recorder chart.
10. *Condition:* "Hi-temp" alarm alone which would not reset by pushing remote reset and then "hi-temp" reset.
    Causes: Failure somewhere in the "hi-temp" alarm circuit.
    Action: "Hi-temp" should cause a shutdown of array power, and thus there should also be a "power failure" alarm if a high fuel element temperature has actually occurred. Proceed underground, and determine the cause of trouble. Since this is the most critical variable (fuel element temperature) in the whole operation, no time should be lost in making sure that fuel element temperatures are safe (i.e., that the alarm really is spurious) and in repairing the alarm system.
11. *Condition:* Both "hi-temp" and "power failure" alarms would not reset by pushing remote reset and then the individual reset buttons.
    Causes: Shutdown of array power due to high temperature indication on recorder B (fuel element temperature).
    Action: Proceed underground, and determine the cause of the apparent or actual excessive fuel element temperature. Take such actions as indicated by the results of the inspection.
12. *Condition:* Both "radiation" and "power failure" alarms would not reset by pushing remote reset and then the individual reset buttons.
    Causes: Shutdown of array power due to radiation detection system ratemeter hitting the alarm set point.
    Action: Make sure that the waste-shaft fan is running in the upcast direction, and proceed down entry 5. Listen for CAM alarm (it may be heard from beyond the bottom of the ramp). If CAM is also alarming, don gas masks with both particle and gas filters (or a Chemox type) before proceeding up to the control room with cutie pie in hand. If the CAM is alarming it might mean some catastrophic occurrence such as an explosion (*very* highly improbable) of a fuel assembly can. More likely it would indicate a coincident spurious alarm condition of the CAM with a possibly real leak indication on the radiation detection system.

    If the CAM is *not* alarming, proceed to the control room, and inspect the radiation detection system ratemeter recorder chart. If the leak (in a fuel element can) is real, there will probably be a slow increase of reading on the chart up to the

point at which the alram was set off. From this point on, the reading should level off and perhaps decrease, since the alarm actuation shuts off the power to the liner solenoid valves, and thus the radiation detection system should not be drawing any air through the liners. Only the rare gases, primarily ^{85}Kr, should pass through the charcoal trap and filter to be read by the radiation detection system. The gas detection chamber has a sensitivity of about 250 counts/min for an ^{85}Kr concentration of about 100 times the continuous exposure MPC_a. Thus the alarm should be actuated (and the liners sealed off) long before a hazardous concentration exists in the experimental area, even with no ventilation. After checking the recorder, etc., proceed to the room in question, and check for activity in the filter between the counter pigs, in the charcoal trap, and in the lines leading to the hole liners. Contact ORNL.

13. *Condition:* "Radiation," "power failure," and "hi-temp" alarms would not reset by pushing remote reset and then the individual reset buttons.
    Causes: Leak in fuel assembly can caused by excessive temperature.
    Action: Proceed as in condition 12 and then as in condition 11.
14. *Condition:* Any other combination of alarms (e.g., "radiation" and "plastic flow") which will not reset by pushing remote reset and then the individual reset buttons.
    Causes: Possible alarm circuit failure coincident with real trouble in one or more other circuits.
    Action: Treat as real troubles, and proceed as warranted until true situation is ascertained.

Alarm System Malfunctions

1. *Condition:* Alarm at sheriff's office but not at unit 1 or unit 2.
   Causes: Malfunction of sheriff's office unit; open circuit on telephone line between sheriff's office and the No. 2 house.
2. *Condition:* Alarm at sheriff's office and the No. 2 house but not at the No. 1 house.
   Causes: Malfunction of No. 2 system; open circuit on telephone line between the No. 2 house and the No. 1 house.
3. *Condition:* Alarm at sheriff's office and at both operator's houses but not at hoist house.
   Causes: Malfunction of the No. 1 system; open circuit on telephone line to hoist house; malfunction of one of the Tel-Alarm units in hoist house.
4. *Condition:* Alarm on one hoist house Tel-Alarm unit and at all remote units, but not on corresponding Tel-Alarm unit in control room.
   Causes: Malfunction of Tel-Alarm unit in hoist house; open circuit on telephone pair between hoist house and control room.
5. *Condition:* Alarm on one control room Tel-Alarm unit (and on corresponding remote units) but no alarm condition actually existing.
   Causes: Malfunction in the Tel-Alarm unit; open in the circuit to the primary contacts; malfunction in the alarm-condition detection system.
6. *Condition:* True alarm condition on one control room Tel-Alarm unit but no transmission of signal above ground.
   Causes: Malfunction of control room Tel-Alarm unit; short circuit on telephone pair between control room and hoist house; malfunction of Tel-Alarm unit in hoist house.
7. *Condition:* True alarm condition on one hoist house Tel-Alarm unit but no transmission of signal to operators' houses.
   Causes: Malfunction of hoist house Tel-Alarm unit; short circuit on telephone pair between hoist house and the No. 1 house; malfunction of No. 1 system.
8. *Condition:* True alarm condition on No. 1 system but no transmission to the No. 2 house.
   Causes: Malfunction of No. 1 system; short circuit on telephone line to the No. 2 house; malfunction of No. 2 system.
9. *Condition:* True alarm condition on the No. 2 system but no transmission to sheriff's office.
   Causes: Malfunction of No. 2 system; short circuit on telephone line to sheriff's office; malfunction of sheriff's office unit.
10. *Condition:* Pushing remote reset button in hoist house did not clear units in control room.
    Causes: Malfunction of hoist house remote reset unit; short circuit on remote reset telephone pair between hoist house and control room; malfunction of control room reset unit.
11. *Condition:* Reset button at the No. 1 house will not clear "power failure" unit in hoist house.
    Causes: Malfunction of hoist house remote reset unit; short circuit on remote reset telephone pair between the No. 1 house and hoist house.
12. *Condition:* Reset button at the No. 2 house will not clear system, but the No. 1 unit's reset will.
    Causes: Short circuit in remote reset circuit between the No. 2 house and the No. 1 house.

13. *Condition:* One Tel-Alarm dim light (normal no-trouble condition) burns brighter than normal.
    Causes: The other bulb in the Tel-Alarm unit is burned out.
14. *Condition:* All Tel-Alarm dim lights in control room off and "power failure" dim light in hoist house off.
    Causes: Open circuits on remote reset line somewhere between hoist house and the No. 2 unit's house; malfunction of hoist house remote reset unit.
15. *Condition:* All Tel-Alarm dim lights in control room off but "power failure" dim light in hoist house on.
    Causes: Open circuit on remote reset line between hoist house and control room; malfunction in control room remote reset unit.

8. Installation of Experimental Equipment

F. M. Empson W. C. McClain

In this chapter the installation of the experimental equipment – the hardware described in the previous chapter – is discussed. Most of this work was done between June 1, 1965, and the start of the experiment in November 1965.

8.1 WASTE CHARGING FACILITY

The facility at the top of the waste charging shaft for handling the shipping cask and lowering the canisters into the mine was constructed primarily by subcontractors. (Work began on March 2, 1965.) The largest contract was for grading and leveling the area around the shaft and constructing the shielding (involving 33½ yd of concrete and 1300 lb of reinforcing steel), headframe, shelter, paving, and security fence. Following this, the installation of various services and auxiliary equipment was undertaken, including:

1. construction of a 45-kVA power line from the main shaft area to the waste shaft,
2. installation of wiring for power and for lighting in the waste-shaft area,
3. foundations and a shelter for the winch,
4. foundations for a 5000-cfm ventilating fan,
5. ductwork for the 5000-cfm ventilating fan,
6. installation of the hydraulic system for erection of the shipping cask,
7. installation of the 2500-lb capacity winch,
8. installation of the 5000-cfm ventilating fan.

8.2 UNDERGROUND TRANSPORTER

The contract for the underground transporter (Fig. 7.8) specified that it be delivered underground at the Lyons mine. Therefore, the disassembly, transfer into the mine, and reassembly were the responsibilities of the Stowers Machinery Corporation, Knoxville, Tennessee. The machine was received at the mine fully assembled (except for the lead shield rings) on a railroad flatcar. Since size and weight limitations of the main shaft at Lyons had been incorporated in the design of the various components of the machine, no particular difficulties were experienced in the disassembly-reassembly phase of the transfer. The Carey Salt Company personnel supervised the rigging of large components under the counterweight box in the shaft, and smaller pieces were lowered on the cage. Mine personnel with other equipment (shuttle cars) also assisted in moving components from the shaft bottom to the experimental area.

Reassembly of the transporter was carried out in room 7, entry 5A (Fig. 11.41), with the aid of a large portable A-frame gantry. It was also necessary to excavate a 4-ft-deep hole in the floor to obtain the headroom required for installation of the lead shielding rings. The disassembly-reassembly job (including installation of the lead rings) occupied a three-man Stowers crew for a total of five weeks. Final acceptance testing was deferred about a month, pending construction of the 10% grade ramp up to the experimental area.

Performance of the transporter in the mine exceeded expectations. The 10% grade could be negotiated with ease. The shield could be spotted to within a couple of inches of a predetermined point without difficulty, using the tractor alone, whereas the design requirement had been to within 1 ft. Even during normal maneuvering within the fairly restrictive underground passages, the transporter with its 25-ton shield was found to be nimble, responsive to the controls, and stable.

8.3 POWER DISTRIBUTION SYSTEM

Incoming power was received from Kansas Power and Light Company at 2300 V and divided into four separate circuits – three on the surface and the fourth supplying power for the underground operations.

8.3.1 Surface Power

One surface power circuit supplied power at the waste charging facility for the winch, hydraulic system, and lighting. A 2300-V three-phase line supplied a bank of three 15-kVA, 2300/440-V transformers at the site.

The other three circuits supplied power through new switchgear in the hoist house (the main breaker was set at 150 A). One of these supplied power to the 150-hp hoist motor at 2300 V. (The breaker was set at 40 A.)

A second circuit (known as the surface feeder and set at 40 A) fed a bank of three 37.5-kVA transformers connected 2300/440 V. The 440-V three-phase 40-hp main ventilation fan was powered by this bank, while hoist house lighting and utility power were supplied through a 15-kVA, 440/208–120-V transformer. A 3-kVA, 440/220-V three-phase transformer was installed to drive the pump at the shaft water collection rings 300 ft below the surface.

The third circuit was set for 85 A as the mine feeder.

8.3.2 Underground Power

The underground power system was supplied at 2300 V by a feeder cable, three-conductor No. 4 with 5-kV insulation and an integral ground, installed in the counterweight compartment (north) of the main shaft. This cable was continuous from the main switchgear to a point about 300 ft east of the shaft bottom. At this location the wire configuration changed to three No. 4 conductors, attached to the mine roof, and the ground became a separate No. 8 bare copper wire.

A 10-kVA, 2300/220-V three-phase dry-type transformer was also installed at this point. It supplied power for pumps removing water from the shaft sump and for pumping the collected water to the surface, as well as supplying lighting and utility current in that part of the mine.

A 15-kVA, 2300/220-V three-phase dry-type transformer was located at the old mine office, about 700 ft along the Mo.P. entry. This transformer supplied power to a $7\frac{1}{2}$-hp booster fan located in entry 10 off the Mo.P. entry. It also supplied lighting along the Mo.P. entry and entry 5 to the experimental area.

The 2300-V three-phase line terminated at a substation in entry 5 at room 7. Three 50-kVA, 2400/480/240-V dry-type transformers were installed as a source of power for mining operations, for experiment requirements, and for lighting. During mining operations the transformers were connected for 480 V output to operate the undercutter, shot-hole drills, air compressor, and the Joy model 18HR-1H loader. Hookup was changed to 240 V output at completion of mining operations.

At that time three separate 240-V three-phase systems were installed from this underground substation. The first system, constructed of 3/0 copper, served the regulated power supplies for the main array heaters in rooms 1, 4, and 5 and for the pillar heaters in rooms 2 and 3. Also connected to this system were four receptacles for the hydraulic power on the transporter. These receptacles were located in the waste-shaft room, room 1, room 5, and the parking area in room 7, entry 5A. The second system, constructed of 4/0 aluminum, supplied service power to the control room, to the experimental power control panel, and to all accessory experimental equipment, including off-gas systems, local ventilating fans, and instruments. The third system, constructed of No. 8 copper wire, supplied general lighting throughout the experimental area.

In all of the systems the loads were distributed among the phases. In general, the main power supply lines in all three systems were attached to the mine roof using insulators and $\frac{1}{4}$-in. pins shot into the salt (Ramset). These main feeder lines were tapped where necessary, and drop lines were brought down the walls of the room to a circuit breaker mounted on the wall, again with Ramset pins.

Although there was no 480-V power available for operation of most of the mining machinery, the shuttle cars were employed for hauling materials using 250-V dc supplied by the motor-generator set operating on 2300 V and connected just ahead of the transformers at the substation. The dc output was delivered to a 4/0 aluminum bus which extended to within about 600 ft of the shaft bottom. This bus, equipped with connection stations along its length, permitted operation of the shuttle cars from the shaft bottom throughout the experimental area.

8.4 ARRAY HOLE LINERS

The hole liners for the arrays in rooms 1, 4, and 5, described in Sect. 7.5, were fabricated at ORNL and shipped to the mine disassembled, that is, without the connecting power leads, off-gas lines, thermocouple leads, etc. The first step in their installation was placing the "wall of hole" thermocouples. These were the thermocouples designed to be in salt but as near as possible to the wall of the array hole at a depth of 9 ft below the floor. (Three thermocouples at 6, 9, and 12 ft below the floor were used at the center hole of each array.) These $\frac{1}{8}$-in.-diam stainless-steel-sheathed thermocouples were installed by first drilling a $\frac{1}{8}$-in. hole

about 1 in. deep horizontally into the wall of the 12-in.-diam array hole using an ordinary ½-in. electric drill taped on the end of a piece of ¾-in. pipe. (Many drill bits were broken before this technique was perfected.) A sharp bend was then placed in the thermocouple about ¾ in. from the end, and this "hook" fished into the small hole and tapped in with light rod. The snug fit prevented the thermocouple from falling out. These wall thermocouples had to be installed prior to the upper hole liner sections, because they were brought up outside of the liner through the grout.

The upper sections of the array hole liners were then grouted into the 5-ft-3-in.-deep, 16-in.-diam upper portion of the hole with "salt-crete" grout. This grout was made in the ordinary way except that crushed and graded salt (size "fine" – about ⅛ in.) was used instead of sand, and brine was used instead of fresh water. The most important part of the hole liner installation was to assure that the liners were plumb and concentric in the hole and even with the floor. This was facilitated by the dummy flange 2½ in. below the top of the liner, which supported the liner on the shelf chipped in the salt (Fig. 7.9). Final positioning was accomplished by placing the lower liner into the hole and matching a centering jig attached to its bottom end with the AX pilot hole in the bottom of the 12-in.-diam hole. The lower liner was then removed and the upper section grouted. The remainder of the hole liner installation was simply to attach the various connections (described in Sects. 7.5 and 7.7), bolt the lower section in place, and assemble the steel shot shield above it (Fig. 7.9).

8.5 PILLAR HEATERS

The 22 heaters for the pillar-heater experiment were installed in holes along the base of the pillar between rooms 2 and 3. In each room a row of 11 heaters, spaced at 5-ft intervals, was placed 2 ft out from the pillar's edge. They were therefore on two parallel lines 27 ft apart. The holes were numbered from the back of each room, and the two "modified" pillar heaters (see Sect. 7.6.2) were placed in hole 6. The heaters were installed so that all were at the same elevation. This was accomplished by backfilling the holes with crushed salt to the proper depth.

Thermocouples were installed in the field both on the outside and inside of some (but not all) of the pillar heater pipes. Thermocouples inside the heaters were supported between heater elements with sheet metal clips, while those on the outside were attached with hose clamps. Installation of the heater pipes was simply a matter of lowering them into the hole. Heater 7 in room 2 was backfilled with dry quartz sand. Heaters 6 and 8 in room 3 and heater 6 in room 2 were backfilled with crushed salt. All other heaters were not backfilled, but glass fiber insulation was placed in the upper portion of the annulus between the heater and the hole to prevent excessive convective heat losses.

8.6 INSTRUMENTATION

A major part of the equipment installation effort, especially by mine personnel, was involved in what may be classed as instrumentation. This work, except that involving the rock mechanics gages, which is discussed elsewhere (Sects. 6.3.4, 6.4.4, and 11.4.1), is described in the following sections. Much of the instrumentation, especially for power control, temperature recording, and the alarm system, was centrally located at: (1) the control room, a 12 × 20 ft wooden frame building located at the top of the ramp to house the instruments, and (2) the power control panel located in the corridor between rooms 2 and 3.

8.6.1 Temperature Recording System

8.6.1.1 Thermocouples. – All thermocouples were fabricated before delivery to the mine; that is, they were received with the male connector plugs attached and with the junctions formed at the proper lengths. Thermocouples which were attached directly to heaters or otherwise exposed to temperatures in excess of 150°C (for example, the "wall of hole" thermocouples discussed above) were sheathed in swaged stainless steel. All other thermocouples were unsheathed and insulated with glass fiber fabric. Thermocouples to be installed in holes in the salt were first encased in ¼-in. plastic tubes or wells (Teflon or polyethylene depending on the maximum temperature expected). Where several thermocouples were installed in one well, it was sometimes necessary to use a lubricant such as talc to facilitate the passage of the bundle of thermocouples.

After the Teflon tube or well had been placed in the 1 3/16-in. holes, the annular space around the wells was backfilled with dry quartz sand. For the vertical holes in the floor, the sand was simply poured in. For the horizontal holes, it was necessary to pneumatically place the sand backfill using a ½-in.-diam plastic tube and compressed air.

8.6.1.2 Cables and Leads. – For those few thermocouples which were to be read manually with the portable Minimite instrument, the male connector plug was left exposed. The connections between the re-

corded thermocouples and the appropriate recorder or logger were completed by running duplex leads from the thermocouple connector plug to junction boxes mounted on the walls of the rooms. From the junction boxes, 12- and 24-pair cables carried the signals to the recorders. The cables, junction boxes, and leads were all cut to length, wired, and assembled when received at the mine. Routing of the leads and cables was handled in several different ways. In rooms 2, 3, and 4, where operation of the transporter was not expected and the use of shuttle cars would be minimal, the leads were bundled and placed in the "cutter breaks" in the floor. In rooms 1 and 5, where the underground transporter would be operated for the fuel element canister change-outs, the thermocouple leads were bundled and placed in small trenches chipped into the floor, and covered with steel plates. These trenches were laid out so as to minimize possible interference from the power leads going to the heater. The cables leading from the junction boxes to the recorders were hung on the walls of the rooms and placed in trenches in the floor and backfilled with crushed salt in the corridor. Where the cables crossed the mouth of the waste shaft room, steel covers were also installed on the trenches. Even though the cables and leads were precut to length, their exact location was determined in the field with the criteria of maximum protection from physical damage and electrical interference, and the most expeditious installation.

8.6.1.3 Recorders. – Temperatures were recorded on standard Honeywell potentiometric-type recorders and loggers which were mounted in modular steel panels. The only completely new instrument was one of the two 132-point loggers, which was assembled in the mine by Honeywell personnel. The other recorders had been used previously and repaired and/or modified as required at ORNL. The steel panels had to be prewired and preassembled (except for the recorders) before delivery to the mine. Assembly of the recorders into the panels and hookup with the cables was carried out by mine personnel under supervision of the ORNL Instrumentation and Controls Division. Final calibration and adjustment of all recorders were performed by Honeywell personnel. Figure 8.1 shows one of the temperature loggers as installed in the control rooms.

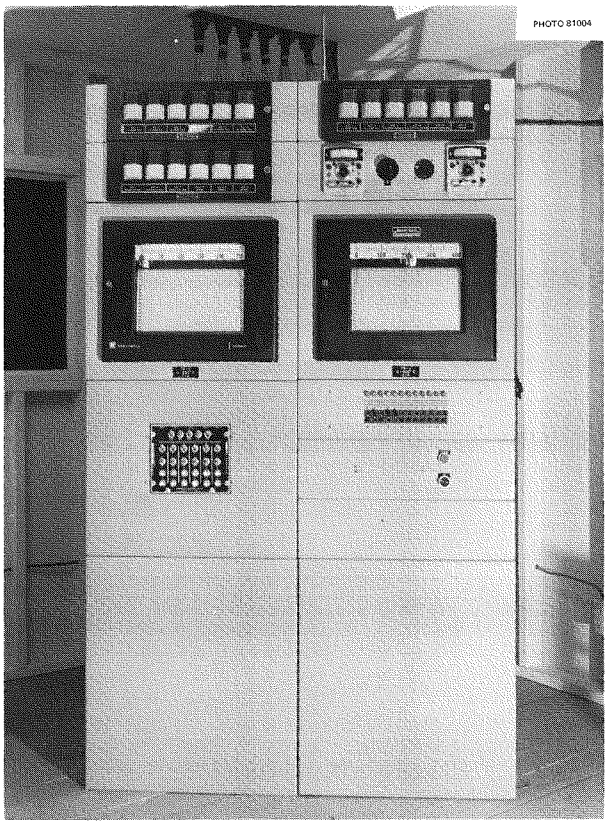


Fig. 8.1. Photo of Installed Temperature Logger in Control Room.

8.6.2 Power Control System

The equipment and instruments for the control of the power to the heaters in the three main arrays and the pillar-heater experiment were mounted in modular steel panels, each prewired and preassembled before delivery to the mine. Installation therefore consisted in mounting the panels and making the necessary connections to the power distribution system and between the various panels. The installed panel is shown in Fig. 8.2, where the first panel (from left to right) contains the voltage regulators for the array heater power; the next three contain the ammeters, autotransformers, and watt-hour meters for the room 5, room 4, and room 1 arrays respectively; and the fifth panel contains the fuel element and array heater temperature recorders. On the far right is the equipment for the heated-pillar experiment.

8.6.3 Off-Gas System

The major components of the off-gas system were also preassembled prior to delivery to the mine (see Sect. 7.7.3.). Installation consisted in mounting the various parts (rotameter box, vacuum pump, condenser, etc.) at convenient places and hooking them together. In all three rooms (the off-gas system applied only to the arrays, not the pillar heaters) the bundle of Teflon off-gas tubes was placed in a small trench, along with

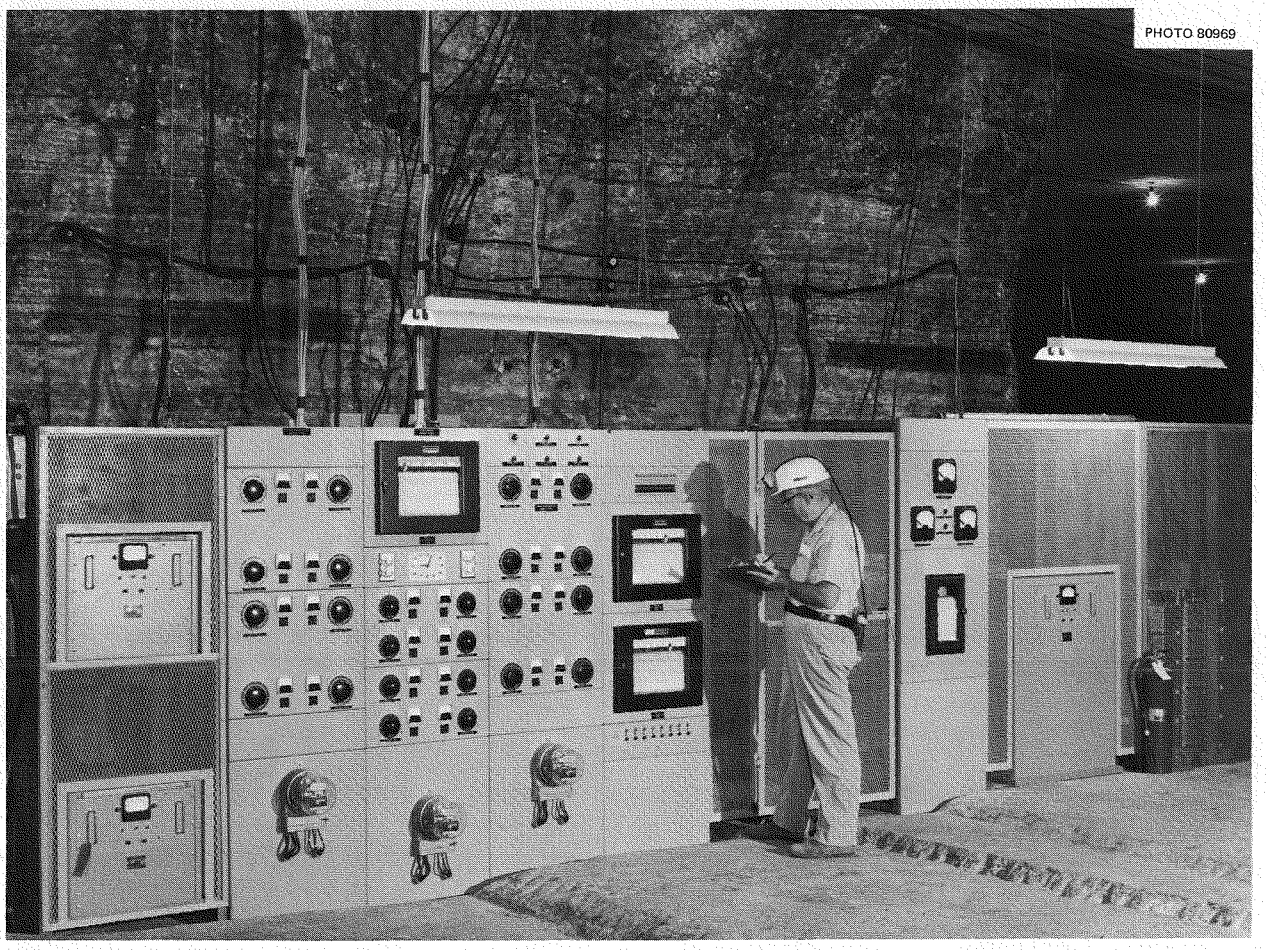


Fig. 8.2. Photo Showing Completed Power Control Panel.

the heater power leads, and covered with steel plate. Figure 8.3 shows room 1 during installation of the off-gas system.

8.6.4 Radiation Detection System

The radiation detection system was installed in rooms 1 and 5 only. Again, the installation was primarily a matter of locating, mounting, and connecting the prefabricated components. The common plastic tube and the solenoid control lead wires leading from the hole liners were placed in the steel-plate-covered trench with the off-gas tube bundle.

A continuous air monitor (CAM) was also used to continuously sample the air at the top of the ramp throughout the operation of the experiment. An extension hose permitted the use of this instrument at more remote and specific points during the canister handling operations.

8.6.5 Alarm System

The function and various modes of operation of the alarm system are described in Sect. 7.7.5. Since the various components of the system had been fabricated in the preassembled panels, installation at the mine was largely a matter of connecting and checking the system. The various alarm signals were carried from the experimental area to the unit in the hoist house through a 25-pair telephone cable installed by Southwestern Bell Company down the main shaft and to the control room. One circuit on the cable was also used for communication between the waste handling facility and the underground area during the canister handling operations. One circuit was also used for an extension of the regular business telephone to the control room. It is interesting to note that the telephone company considered this as a "basement extension" and billed it accordingly.

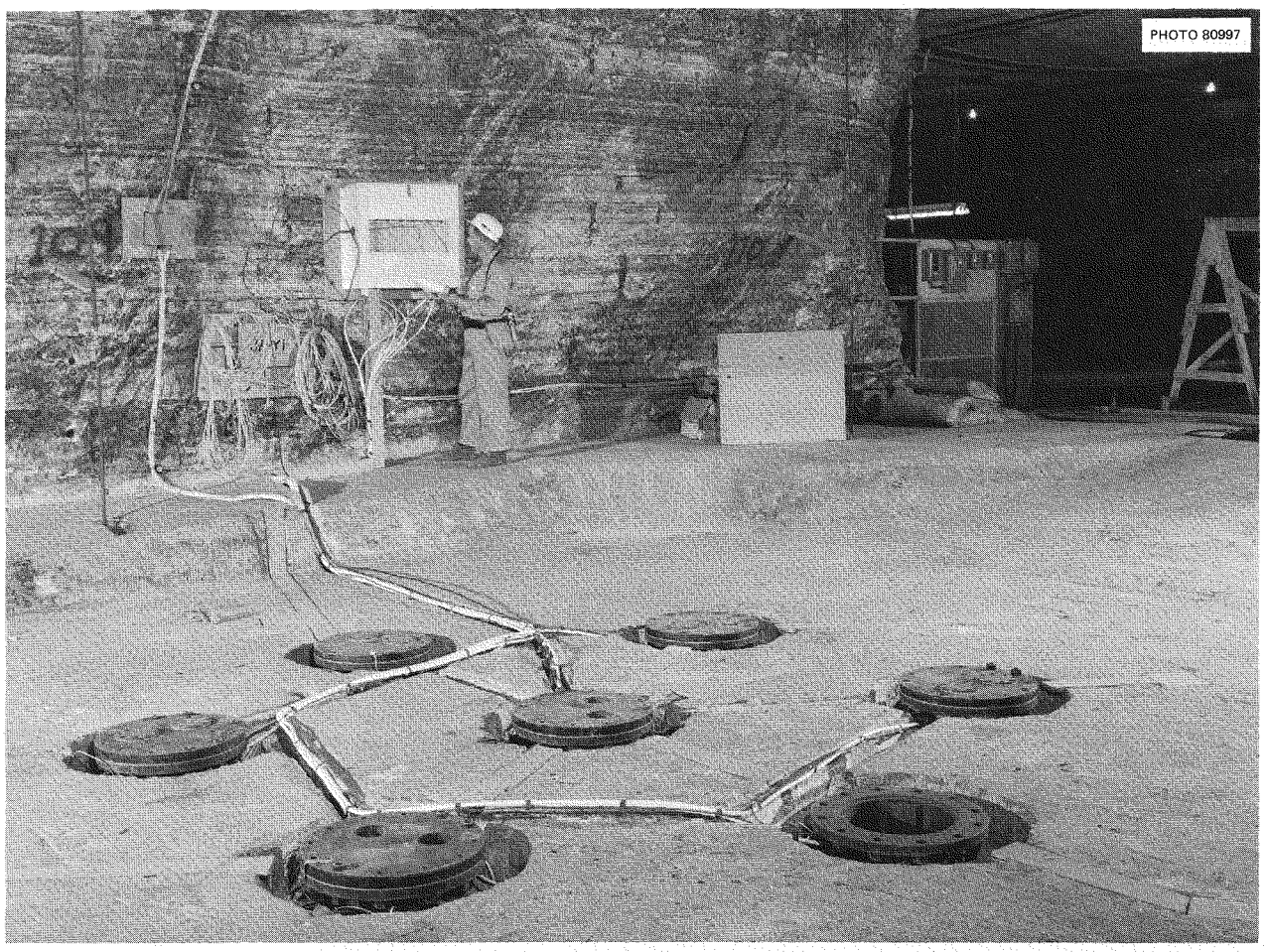


Fig. 8.3. Photo of Array in Room 1 Under Construction, Showing the Off-Gas Tube Bundle and Its Trench.

The alarm system signals were transmitted from the hoist house alarm unit to the three remote signaling units located at the operators' houses and the sheriff's office on existing telephone lines.

8.7 EQUIPMENT CHECKOUT

It was possible to check out most of the experimental equipment by some method, usually no more complicated than turning it on and seeing if it operated correctly. However, this was not true of the canister handling equipment, which was, of course, the most critical for the success of the experiment. Therefore two periods of intensive testing were scheduled which would duplicate, as nearly as possible, the actual fuel element canister handling operations. These two tests were called "cold checkout," which was intended to check and debug the mechanical functioning of the equipment, and the "cobalt checkout," which would provide additional testing and experience with the mechanical equipment and check all of the shielding facilities.

8.7.1 Cold Checkout (and Resulting Modifications)

For the cold checkout, several empty canisters were shipped to the mine in the shielded shipping cask. (Another empty canister was already in the mine.) The cask was erected over the waste shaft and the various handling operations carried out. At first the various subprocedures (such as moving a canister in and out of an array hole or in and out of the shipping cask) were run through several times. Finally, these procedures were put together, and several complete canister handling cycles were carried out, from shipping cask to array hole and return.

No basic deficiencies in the equipment or its design were encountered in the checkout, but a few normal

and expected mechanical "bugs" were turned up. Some of the most important of these were:

1. The hydraulic cask erection mechanism was inadequately anchored to the concrete shielding and pulled out in trial operation. Deeper anchors and a steel plate to spread the stress corrected the problem.
2. The electric clutch on the waste charging facility winch was improperly wired (apparently at the factory). This caused a cable to be broken and a canister to drop on the safety door (see Sect. 7.3) when the "up" button was inadvertently pushed while the canister was in the cask with the cable attached. This problem was easily corrected.
3. A number of solenoid-operated hydraulic valves on the underground transporter malfunctioned and were subsequently replaced.
4. The slight deviation of the waste shaft from vertical resulted in the canister sliding down the side of the shaft and catching on the upper edges of the guidance funnel mounted in the transporter top door. A spring steel deflector was attached to the interior wall of the waste shaft near the bottom so as to deflect the canister to the center of the shaft. This deflector helped but did not completely eliminate this problem. Occasionally a canister would hang up on either the deflector or the guide funnel for a brief period and then drop into the transporter shield. The position-indicating signal lights in the transporter guide tube permitted recognition of these cases, which could then be readily corrected.
5. Positioning of the underground transporter shield over the array holes by use of a plumb bob was found to be inadequate, probably due to minor lack of symmetry in the shield and trailer assembly. A plywood template matching the bottom door and centered on the array hole liner was devised and found to give satisfactory location of the shield.

8.7.2 Colbalt Checkout (and Resulting Modification)

In the cobalt checkout, two canisters were loaded with 500 Ci of ^{60}Co each, in the form of five 100-Ci capsules distributed along the length of the canister. These were then loaded into the shipping cask and sent by truck to Lyons using the procedures planned for the fuel element shipments. A detailed survey of the shipping cask when received at Lyons revealed a fanlike beam of radiation, 30 to 60 mR/hr, at a joint in the outer wall of the cask. Examination of the design indicated that earlier modifications of the cask which had added shielding had resulted in a "window" of several inches of steel in the lead. This was corrected by installing a girdle of lead, contained in a steel jacket, around this joint.

The cask was then erected and the canister lowered into the mine and deposited in the array holes. The detailed procedural checklist to be used for the change-outs (see Appendix 10A) was followed, and a close examination of the radiation field was made at every stage as a check on the shielding.

Only a few very minor mechanical "bugs" were discovered, and these were quickly corrected. However, two significant shielding deficiencies were found. The first of these was at the mating of the top of the transporter shield and the bottom of the waste shaft. Apparently the loose salt that had been backfilled into the waste shaft room, to enable the transporter shield to reach the ceiling and mating surface, had compacted unevenly. Two concrete pads at equal elevations were installed for the transporter wheels, which not only reduced the radiation leakage to an acceptable figure but prevented any possibility of an occurrence of this problem.

The second shielding problem occurred at the hole liners. When the cobalt canisters were placed in the array holes and the holes buttoned up, the field through the top of the liner was higher than desirable. When several thicknesses of lead sheet were placed over the shot retainer ring, the field was reduced to an acceptable level. For operation, stainless steel plugs or "scatter shields" filled with steel shot were designed and fabricated. The scatter shields fitted loosely into the shot retainer tube and contained an S-curve hole for the thermocouple leads from the canister in the lower liner. With the scatter shields in place, it was possible to work in the upper liner without receiving a significant radiation dose. When the liners were buttoned up, maximum radiation fields were generally less than 10 mR/hr immediately above the hole.

8.8 SUMMARY

The work described in this chapter covered a period of about six months and involved a mine crew of nine men, in addition to the ORNL personnel at the site, some permanently and others temporarily assigned to direct particular aspects of the installation. This total, of course, does not include the effort devoted to shop fabrication of the experimental equipment or the work supplied under subcontract. The installation and check-out of equipment brought preparations for the experiment to completion.

9. Hazards Analysis

W. J. Boegly, Jr. W. F. Schaffer

9.1 INTRODUCTION

The decision to use irradiated reactor fuel assemblies in the demonstration rather than actual calcined wastes or separated fission product sources was based on considerations of availability, cost, and radiation characteristics. Selection of the ETR fuel was based on the operating cycle of the reactor, the number of assemblies which would be required to charge the seven holes in the demonstration, and the dimensions of the assemblies. From the standpoint of allowable element temperature, power reactor elements rather than research reactor elements, because of their sheath materials, would have been preferable, but uncertainties in availability and reactor cycle time led to the selection of the ETR fuel assembly as the best overall choice.

The ETR has an average thermal flux of about 1.5×10^{14} and a cycle time of about six weeks.[1] A typical reactor cycle might average the equivalent of about 20 full-power days out of 23 operating days. The assemblies to be selected would be those with the highest burnup that could be safely canned at from 60 to 75 days out of the reactor. The following irradiation history was assumed to be representative of the assemblies to be selected for the demonstration.

Irradiation time	23 days (2×10^6 sec)
Thermal neutron flux	1.84×10^{14} neutrons cm^{-2} sec^{-1}

The unirradiated ETR fuel assembly originally contained 400 g of ^{235}U (1.025×10^{24} atoms). Since each fuel assembly canister contained two assemblies, all calculations were performed on the assumption that two assemblies or 2.05×10^{24} atoms of ^{235}U were present initially. The fission product concentrations and heat generation were obtained using published curves.[2]

9.1.1 Individual and Total Fission Product Activity

The total radioactivity present as a function of time was calculated, and the results are shown in Fig. 9.1. At 80 days out of the reactor, the fuel canisters would be at the Lyons mine ready for transfer underground. At this time each canister would contain 240,000 Ci, and the total surface carrier loading would be about 1.7×10^6 Ci. Six months later, at the time of transfer from the main array to the floor array (time out of the reactor, about 270 days), the radioactivity per canister would have decayed to 52,000 Ci. When the fuel canister finally would be removed from the mine and returned to the surface carrier (about 450 days), the radioactivity would have decreased to 24,000 Ci.

Results of the calculations for individual fission products of interest, because of their hazard potentials, are shown in Figs. 9.2 (half-life less than one month) and 9.3 (half-life greater than one month).

9.1.2 Heat Generation

Figure 9.4 shows the calculated heat generated by fission product decay for each fuel canister as a function of time out of the reactor. Approximately 780 W of fission product power would be produced when the canisters were placed in the mine; this would decrease to about 170 W by the time the canisters were transferred from the main to the floor array. At the time the canisters would be removed from the mine for shipment back to Idaho, the heat generation would be about 74 W.

Also shown in Fig. 9.4 is the fraction of the total power that would be due to gamma decay. Most of this heat would be generated within the fuel assembly and hole liner (up to 90%).

---

[1] R. L. Bradshaw, J. J. Perona, and J. O. Blomeke, *Demonstration Disposal of High-Level Radioactive Solids in Lyons, Kansas, Salt Mine: Background and Preliminary Design of Experimental Aspects*, ORNL-TM-734 (Jan. 10, 1964).

[2] J. O. Blomeke and Mary F. Todd, *Uranium-235 Fission-Product Production as a Function of Thermal Neutron Flux, Irradiation Time, and Decay Time*, ORNL-2127, Part I, Vols. 1 and 2 (Aug. 19, 1957).

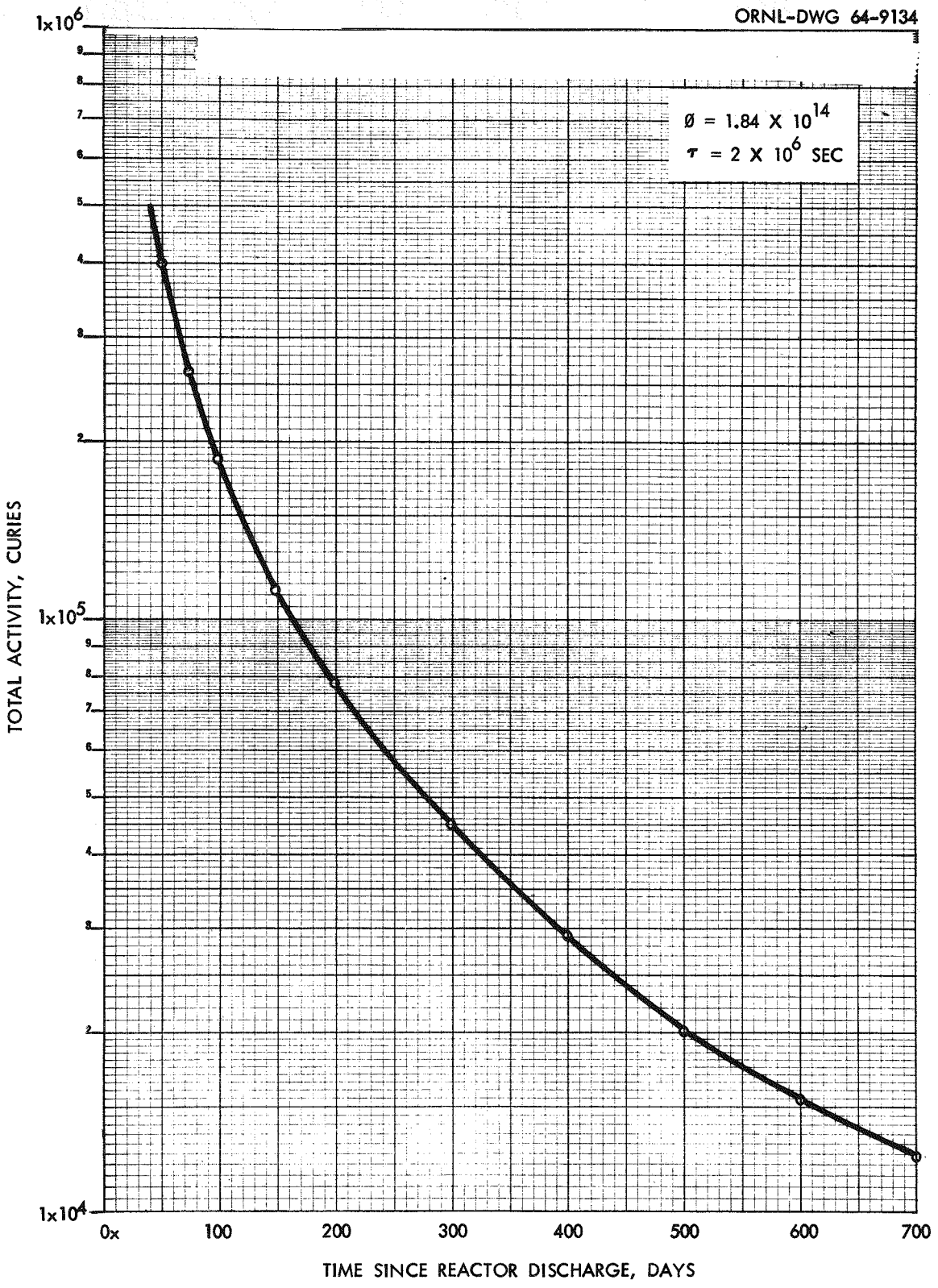


Fig. 9.1. Total Fission Product Activity for One Canister.

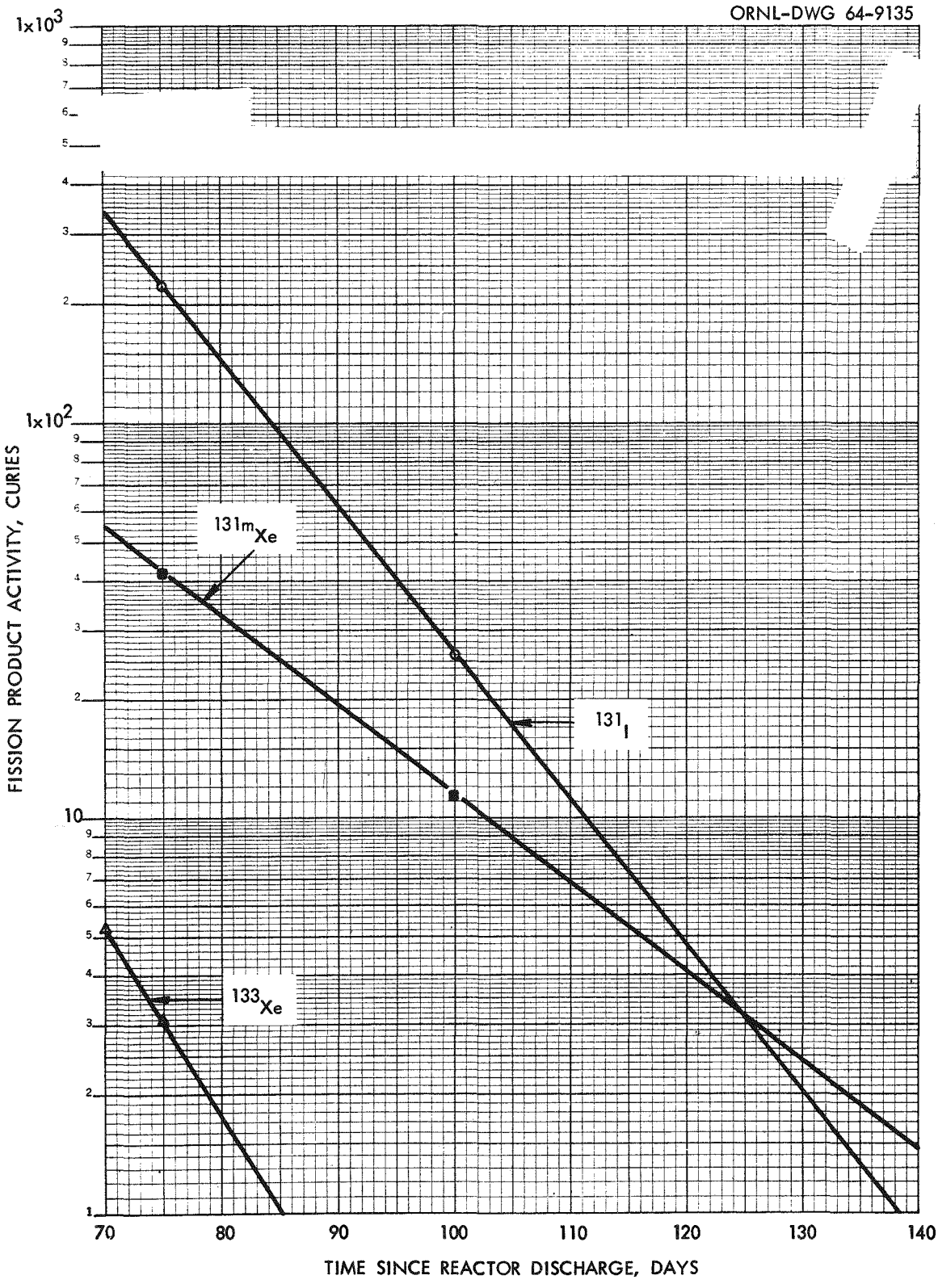


Fig. 9.2. Fission Product Concentration per Canister, Half-Life Less than One Month.

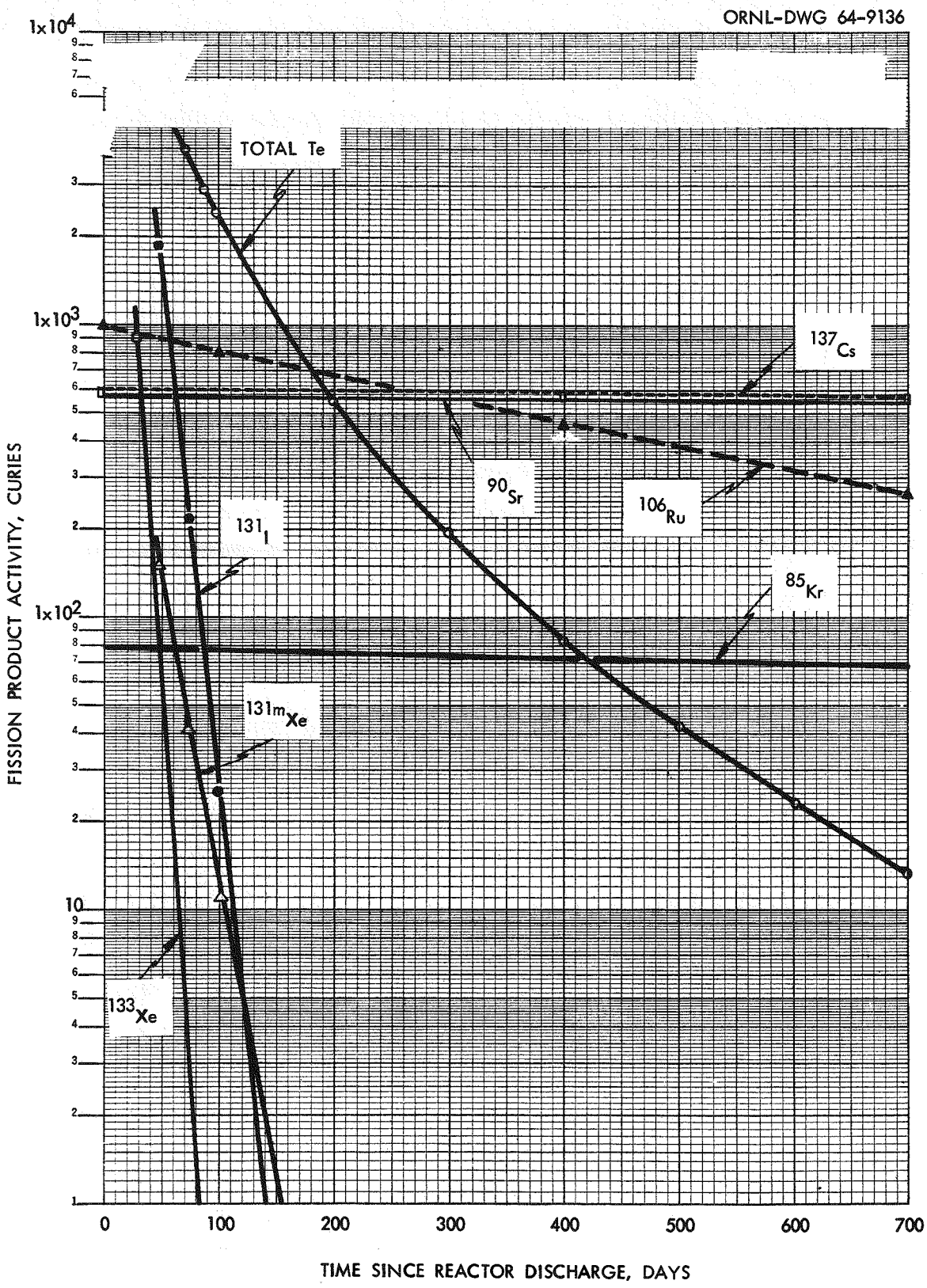


Fig. 9.3. Fission Product Concentration per Canister, Half-Life Greater than One Month.

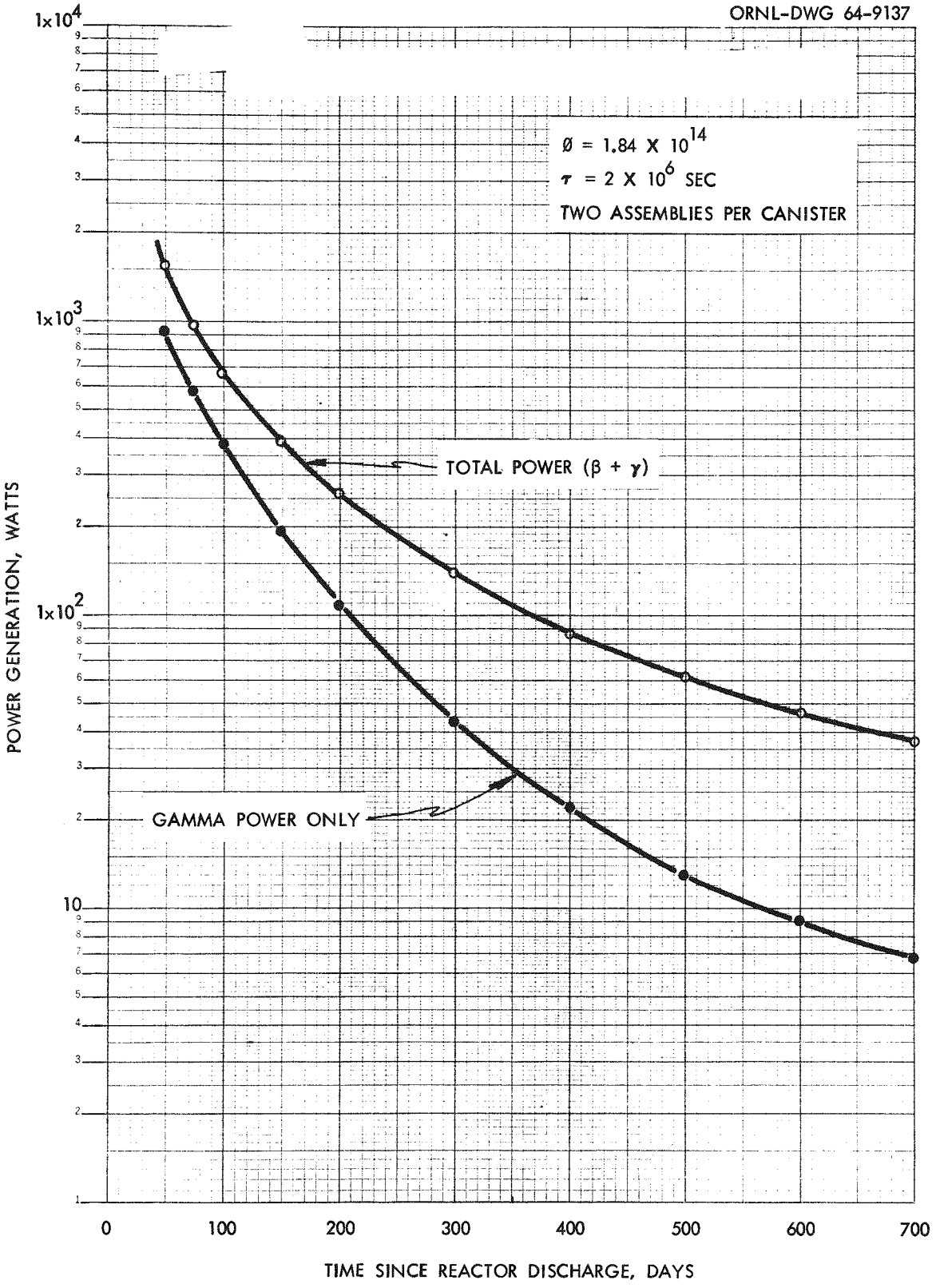


Fig. 9.4. Total and Gamma Heat Generation per Canister.

9.1.3 Idaho Operations, Canisters, and Fuel Shipments

In order to deliver the fuel assemblies to the mine at 80 days out of the reactor, it was assumed that the carrier would leave Idaho after about 75 days to allow time for shipping contingencies and transfers. The estimated travel time between Idaho and Lyons, Kansas, was 2 days.

Table 9.1 shows the proposed shipments and the cooling times for each of the six shipping cycles of the waste carrier. Four of the Idaho-to-Lyons shipments would be with 75- and 90-day-cooled assemblies, four Lyons-to-Idaho shipments would be with 455- to 470-day-cooled assemblies, and four would be with the carrier empty. (In the actual operation only three sets of fuel assemblies were used. The actual shipment schedules are shown in Table 10.1.)

Basically, the 14 fuel assemblies (at from 60 to 75 days out of the reactor) would be transferred from the ETR canal to the hot-cell facilities, where the fuel would be loaded into the canisters. After loading, mechanical sealing, seal welding, and helium leak testing, the fuel canisters would be loaded into the shipping carrier and the carrier and its shipping rack transferred to a special heavy duty trailer. When this operation was complete, the truck would be routed to Lyons, Kansas. Responsibility for the fuel canning, seal welding, carrier loading, and shipping was assumed by the Phillips Petroleum Company.

9.2 EVALUATION OF CASK DESIGN

9.2.1 Compliance with Structural Criteria Cited in Sections 72.32, 72.33, 72.34, Code of Federal Regulations, Title 10, Part 72

Structural details of the cask, magazine, shipping frame, and canister were analyzed. The results of this analysis are summarized in Tables 9.2–9.5. A portion of the calculations was based on preliminary design-modification drawings; later the cask was reduced approximately 35 in. in length by replacing the intermediate spool subassembly with a similar but shorter one (see note at bottom of Table 9.2). These calculations were not corrected, since the preliminary design met all requirements of this section, and the changes only reduce the values of the maximum stresses shown.

The regulations [Sect. 72.32(*b*) and (*c*)] pertaining to stresses encountered in a 15-ft free fall were interpreted for the purpose of calculations as a force of 60 times the weight of the loaded cask. The regulation [Sect. 72.34(*a*)] pertaining to a force equal to 30 times the weight of the loaded cask applied over a 6-in.-diam area was calculated similarly. Scale tests conducted at ORNL led to a semiempirical method for determining the results of a penetration drop.

9.2.2 Resistance of the Cask to Fire – Sections 72.31(*c*) and 72.34(*b*)

Two methods were used for calculating the ability of the cask to withstand the effects of a fire. Depending

Table 9.1. Schedule of Shipments

Transfer No.	Projected Dates	From	Destination	Contents of Carrier	Approximate Fuel Decay (days)
1A	Nov. 1, 1965	NRTS, Idaho	Lyons, Kansas	7 canisters	75–90
B	Apr. 15, 1966	Lyons, Kansas	NRTS, Idaho	Empty	
2A	May 1, 1966	NRTS, Idaho	Lyons, Kansas	7 canisters	75–90
B	Oct. 15, 1966	Lyons, Kansas	NRTS, Idaho	Empty	
3A	Nov. 1, 1966	NRTS, Idaho	Lyons, Kansas	7 canisters	75–90
B	Nov. 15, 1966	Lyons, Kansas	NRTS, Idaho	7 canisters	455–470
4A	May 1, 1967	NRTS, Idaho	Lyons, Kansas	7 canisters	75–90
B	May 15, 1967	Lyons, Kansas	NRTS, Idaho	7 canisters	455–470
5A	May 30, 1967	NRTS, Idaho	Lyons, Kansas	Empty	
B	Nov. 1, 1967	Lyons, Kansas	NRTS, Idaho	7 canisters	455–470
6A	Nov. 15, 1967	NRTS, Idaho	Lyons, Kansas	Empty	
B	May 1, 1968	Lyons, Kansas	NRTS, Idaho	7 canisters	455–470

Table 9.2 Summary of Load Conditions and Stress of Cask

10-CFR-72 Section No.	Load Condition	Load Application	Resulting Maximum Stress (psi)	Limiting Stress (psi)
72.32(*a*)	10 times weight of loaded cask	As uniformly loaded beam supported at ends[a]	7,256	33,000
72.32(*b*)	60 times weight of loaded cask	On cylindrical shell (uniformly along side)	24,100	75,000
		On shielding ring retaining bands	41,400	75,000
		On center portion of cask (neglecting strength from shielding rings)	72,525	75,000
		On bolts holding cask together	93,500	141,000
		Uniformly applied on shaft end	23,500	75,000
		Uniformly applied on lid end	93,200	140,000
72.32(*d*)	20 psi internal pressure	On cylindrical shell	520	35,000
		On end plate	8,320	35,000
72.34(*a*)	60 times weight of loaded cask applied over 6-in.-diam circular area	On cylindrical shell	73,700	75,000
		Applied to lid (front end)	69,500	75,000
72.34(*f*)	6 times weight of lid	On lid-lifting ring	20,113	33,000

[a]Calculations are based on the cask supported at lifting trunnions which were 115 in. apart on the original design-modification drawings and located a short distance from either end. The revised length of carrier is approximately 114 in. (less shaft shipping protector), or slightly less than the distance used for the calculation, and therefore the resulting maximum stress values are high.

Table 9.3. Summary of Load Conditions and Stresses for Magazine – Section 72.33(*a*)

Load Conditions	Calculated Deflection (in.)	Resulting Maximum Stress (psi)	Limiting Stress (psi)
Entire shaft as a simple beam		364	21,500 at 1000°F
One outer section as a fixed-end beam, loaded by two canisters		<2150	21,500 at 1000°F
Center section as a fixed-end beam, loaded by three canisters		603	21,500 at 1000°F
Curved plate considered as a cantilever, loaded by ½ weight of canister	0.002	3500	21,500 at 1000°F

Table 9.4. Summary of Load Conditions and Stresses for Canister – Section 72.33(*c*)

Load Condition	Load Application	Resulting Maximum Stress (psi)	Limiting Stress (psi)
60 times weight of shield plug	As column loaded on end	4195	70,000
	As simple beam, uniformly loaded	2576	70,000
150 psig internal pressure	On cylindrical body	2819	13,500 at 1000°F
	On end closure (threads)	411	6,750

Table 9.5. Summary of Load Conditions and Stresses for Shipping Rack – Section 72.34(*d*)

Load Condition	Load Application	Resulting Maximum Stress (psi)	Limiting Stress (psi)
10 times weight of loaded cask	Force directed toward side on:		
	Sect. "A-A" (Figs. A.11 and A.12, Appendix A)[a]	27,000	33,000
	Sect. "B-B" (Figs. A.12 and A.13, Appendix A)	32,400	33,000
	Sect. "C-C" (Fig. A.13, Appendix A)	30,000	33,000
	Load on front supports (Figs. A.15 and A.16, Appendix A)	32,000	33,000
	Bolts securing shipping rack and cask to trailer	72,000	75,000
	Force directed to rear on:		
	Support section "C-C" (Fig. A.12, Appendix A)	26,000	33,000
	Support section "B-B" (Fig. A.12, Appendix A)	25,800	33,000
	Force through two side beams and ½-in. base plate (Fig. A.14, Appendix A)	31,000	33,000
	Force on tie-down shaft	22,200	24,500

[a]Figures in Appendix A of a report given special distribution: W. F. Schaffer, Jr., *Evaluation of Project Vault Cask for Conformance with Code of Federal Regulations Title 10, Part 72,* ORNL-CF-64-12-8 (Dec. 9, 1964).

upon the assumptions made, the time required for the exterior surface of the lead to reach its melting point ranged from 18 to 72 min. The controlling factor in the second method of calculation was the size and number of air gaps in the path of the heat flow. A gap of 0.020 in. between the outer steel shell and the surface of the lead casting was assumed and was considered conservative for castings of this size with current lead foundry techniques. Based on the calculations, the time required for the exterior surface of the lead to reach its melting point was between 32 and 58 min when the steel shell is at a fire temperature of 1850°F. The use of fire-retardant or intumescent paint on the exterior surfaces of the cask would retard the transfer of heat to the steel shell so that it would take an additional 10 to 20 min before the shell reached the temperature of melting lead.

The cask was coated with intumescent paint before use because of the excellent fire-retardant properties and low cost of application. Based on the calculations, paint test data, and engineering judgment, it was estimated that the cask should be able to withstand a fire of from 45 to 60 min without serious shield damage and certainly without release of any radioactive materials to the environment.

9.2.3 Shielding Against Ionizing Radiation – Section 72.35

Fission product gamma-activity calculations for the ETR fuel assemblies were made with the PHOEBE code,[3] which provides a machine method of calculation for beta and gamma activities from ^{235}U-produced fission products for any given set of irradiation and decay-time conditions. The activities obtained were then used as the source strengths for the shielding calculations. Shield thickness and direct-dose determinations were made with the SDC (Shielding Design Code) shielding code.[4] Exposure rates and/or required shield thickness for a large number of configurations and shielding materials could be used in the code. As many as 12 gamma groups could be used to express the source energy spectrum. Gamma leakage and gamma

[3]W. F. Schaffer, Jr., *et al.*, "Project Salt Vault: Design and Demonstration of Equipment," pp. 685–706 in *Proc. Intern. Symp. on Solidification and Long-Term Storage of Highly Radioactive Wastes, Richland, Wash., Feb. 15–18, 1966,* CONF-660208 (November 1966).

[4]E. D. Arnold and B. F. Maskewitz, *SDC: A Shielding Design Code for Fuel Handling Facilities,* ORNL-TM-124 (Jan. 25, 1962) and ORNL-3041 (March 1966).

scattering calculations were determined by hand calculations according to standard methods.[5]

The calculations indicated that the ICC regulations could be met without difficulty. In most cases the radiation exposures are probably overestimated between 20 and 200%. The results of the calculations are given in Table 9.6.

9.2.4 Criticality – Section 72.37

It was necessary that the fuel element array be subcritical in the normal condition, even if the sealed canisters became filled with water. Furthermore, it was necessary that the configuration be subcritical in the event of a collision that might involve loss of all the cooling water, dislodgement of the canisters such that they could be located anywhere within a 5-in.-ID by 19½-in.-OD by 7.5-ft-long annular cylinder within the cask, or loss of coolant and fuel meltdown in the event of a fire. The following experimental data may be used to analyze the problem.[6]

1. A slab array more than 3 ft long containing two rows of BSF-ORR (Bulk Shielding Facility – Oak Ridge Research Reactor) fuel elements (each 168 to 200 g ^{235}U, 3 in. square by 24 in. active length) with water moderation and reflection and with the elements spaced for minimum critical mass was found to be subcritical.
2. Extrapolation to an infinite system indicated that an infinite horizontal planar array of vertical BSF-ORR fuel elements one element high spaced (in water) so that the elements are more than 2 in. apart would be subcritical.
3. The minimum critical number of BSF-ORR fuel assemblies was 13 to 15 (corresponding to a minimum mass of 2.5 kg of ^{235}U in a 2-ft active height). The minimum mass was obtained, as expected, at an $H/^{235}U$ atomic ratio of about 370.

Using the data from item 3 above, it may be shown that 14 ETR fuel assemblies arranged so that they are effectively 7 fuel assemblies 6 ft long cannot be made critical under any conditions of water moderation and reflection. The ETR assemblies are very similar to the ORR assemblies that were used in the criticality experiments. Both assemblies are made of the same materials, have a 3 × 3 in. cross section, and have a free volume of approximately 59%. The primary difference is that the ETR and ORR assemblies have 133 and 100 g of ^{235}U per foot of active length respectively. Assuming that the array of ORR fuel assemblies having minimum critical mass contains 2.5 kg of ^{235}U at an $H/^{235}U$ ratio of 370, the dimensions of the array would approximate a cylinder of diameter 10.45 in. and height 24 in. Such a cylinder, if fully reflected with water, would have a geometric buckling of approximately 0.0155 cm^{-2}. The comparable array of seven 6-ft-long ETR fuel assemblies at the conditions for minimum critical mass (an $H/^{235}U$ ratio of 370) would approximate a cylinder of diameter 8.37 in. and height 6 ft. The geometric buckling of this cylinder, assuming full water reflection, would be approximately 0.0182 cm^{-2}. By comparison, since the buckling was larger than the critical buckling, it was concluded that seven 6-ft-long ETR fuel assemblies cannot be critical under any conditions of water moderation and reflection.

An analysis similar to that above could be made to show that the array of BSF-ORR assemblies in item 1 above is more reactive than any possible annular array of seven 6-ft-long ETR assemblies.[7] Using the data in item 2, it could be shown that the normal 3-in. spacing between ETR elements is sufficient to assure that many more than seven 6-ft-long assemblies are required for criticality.

All of these considerations assumed that the ETR fuel assemblies were arrayed in a large pool of water. An array of intact ETR fuel assemblies would have even

Table 9.6. Estimated Radiation Exposures from Cask with 75-day-cooled Fuel Assemblies

	At Any Accessible Surface (mR/hr)	At 1 m from Source (mR/hr)
ICC regulation	200	10
Project Salt Vault shipping cask		
Central surface, part 22	<40	<10
Flange region, parts 3 and 22	<30	<8
Intermediate spool, part 3	<15	<4
Rear surface, end spool, part 2	Negligible	Negligible
Shield door	<50	~10

[5]Theodore Rockwell III (ed.), *Reactor Shielding Design Manual*, TID-7004 (March 1956).

[6]E. P. Blizard, *Neutron Phys. Div. Ann. Progr. Rept. Sept. 1, 1958*, ORNL-2609, (October 1958).

[7]J. K. Fox *et al.*, *Critical Data for Annular Cylinders Containing ^{235}U Solutions*, ORNL-2367 (February 1958).

less reactivity in any possible array in the Project Salt Vault carrier under practical conditions. Factors that would cause the reactivity of the array to be lower are as follows:

1. the neutron poisons in the cask cavity structural materials;
2. lower ^{235}U content, and fission product poisons present in irradiated elements;
3. the assumption that all of the canisters would not become flooded and that some of the assemblies would remain dry.

It can also be shown[8] that the reactivity will decrease upon loss of water from the carrier. In the event of a fuel meltdown with consolidation of the fuel and aluminum into a solid mass, the minimum critical mass would be more than four times the mass in 14 MTR elements, even if the solid mass were subsequently to become flooded with water.

9.2.5 Removal of Decay Heat – Section 72.38

During normal shipping conditions the bulk of the heat would be removed by the circulating cooling water in the canister magazine. The cooling water was to be supplied by a system consisting of a radiator, fan, and circulating pump on a diesel engine. This system was selected because it was simple, reliable, and economical. A diesel motor fitted with an oversize radiator and dual inlet and outlet nozzles to provide a net cooling capacity of 1900 Btu/min at 125°F maximum ambient air temperature was specified based on data obtained from equipment manufacturers. The unit purchased had greater cooling capacity than specified; it should have a cooling capability of at least 4350 Btu/min when running at 1800 rpm under full load. The diesel was equipped with an auxiliary water pump which was used solely for circulating the water between the cask and the radiator. A schematic diagram of the cooling system is shown in Fig. 9.5. The magazine inlet cooling water temperature was not known at this time and for the purposes of heat calculations was assumed to be 150°F.

Heat transfer calculations were made to obtain estimates of the temperatures which might be reached in strategic locations in the cask under the following conditions:

1. without coolant circulating,
2. with forced cooling,
3. including the maximum effect of solar heating.

Calculated temperatures were within acceptable limits, although it was not known how valid some of the assumptions used in the calculations were, and under the loss-of-coolant conditions the fuel assembly temperatures approached the melting point of the aluminum cladding. Therefore, a series of tests was run using dummy canisters. Some of the results of these tests were presented in Sect. 7.2.

[8] H. C. Paxton, *Critical Masses, Volumes, Cylinders and Slabs of ^{235}U Solutions and Metal-Water Mixtures,* LAMS-2415, pp. 8–11 (May 1960).

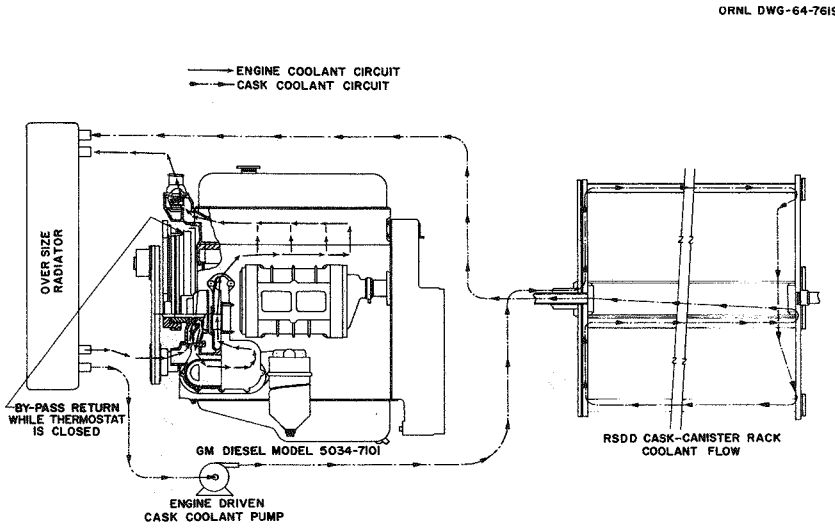


Fig. 9.5. Schematic Diagram of Project Salt Vault Cask Cooling System.

In the loss-of-coolant-circulation test, the simulated fuel assembly canisters reached 400°C (752°F) after 24 hr. The calculated value for maximum canister temperature with no coolant present was 673°F, at which time the fuel assembly temperature would be 1016°F. Thus it may be assumed that fuel assembly temperatures would not become critical in the event of a complete loss of cooling motor for a period approaching 24 hr.

9.3 EVALUATION OF SHIPPING HAZARDS

The analyses of the cask showed that structural integrity was guaranteed under normal shipping and severe collision conditions, that the external radiation exposure would be reduced to less than 10 mR/hr at 1 m from the surface, that a configuration which would allow a critical mass to develop was not possible, that the cooling system would remove sufficient decay heat to prevent melting of the fuel elements under normal operating conditions, and that release of radioactivity to the environment in any credible accident was highly improbable.

The containment design was unusual for shipping casks in that complete radioactive material containment was assured by a hermetically sealed fuel element container. Only sound fuel elements were canned for use in the demonstration, and under normal conditions fission gases would be retained by the fuel element cladding. In a severe collision, when the integrity of the cladding could be lost by impact damage or high temperature, the canister would retain gaseous as well as volatile fission products.

The volume of all radioactive and nonradioactive fission gases and volatile fission products which could be released would be about 20% of the total gas volume, the remainder being air (or helium) which was contained in the canister at the time it was sealed. If it was assumed that air at 25°C and 1 atm was contained in the canister (neglecting the volume occupied by the fuel assembly), the pressure at 700°C would be about 4 atm or 60 lb, a value well below the design pressure (see Table 9.4).

The maximum credible accident was considered to be one in which the cask was involved in a sustained fire and loss of shielding resulted from a rupture in the steel shell of the cask and the release of molten lead.

Engineering design was used to prevent the maximum credible accident from occurring. The cask and shipping rack were normally handled and were stress analyzed as an integral unit. When the unit was secured to the truck by bolts, for practical purposes the cask, shipping rack, and trailer could be considered as one body for accident analysis. The trailer body was a rugged structure with bridge-truss side-frame construction, able to sustain severe damage while acting as a crash frame for the cask and shipping rack. A stress analysis of the trailer was not made, but it was probable that the trailer and truck would separate on severe impact. Energy absorbed by the truck and trailer should reduce the impact loading on the cask to values it could withstand with minimal damage.

In a severe collision, damage to the cooling system would be possible. The loss of coolant would not be disastrous and should not result in damage to the fuel elements if corrective action was taken. If the normal system could not be restored to operation, adapter fittings were provided which would allow the connection of a standard ¾-in. garden or industrial water hose to be connected to provide cooling water. Since the cooling water did not circulate through or over the fuel elements or even over the canisters, contamination of the discharge water would not be possible, and disposal of the waste cooling water would present no problem. In the unlikely event that the inlet and outlet water nozzles are both damaged (since either one could be used to supply cooling water in an emergency), one or both of the shipping bolts could be removed to provide access to emergency nozzle connections for ¾-in. hose to supply water directly to the inner cavity of the cask in an amount sufficient to ensure that the fuel elements did not melt. Radiation exposures from the end of the cask would not be increased by removal of the shipping bolts. Slight contamination of the water might be possible by using this strictly emergency system, but certainly not enough to present a serious health hazard. The water inventory in the magazine would be about 21 gal; if it is assumed that up to half the water would be lost due to line rupture, the remaining water would reach the boiling point in 2 to 2½ hr. From 7 to 12 hr would be required to vaporize the remaining water, depending upon the amount initially lost. It was possible that some of the water would be pushed out of the rack by escaping steam, thus shortening the time to a few hours. The piping was designed so that normally the water must boil to escape.

If the cask was involved in a fire after a collision, the fuel for the fire could come from the following sources:

1. diesel-motor cooling system	Max 43 gal
2. diesel-tractor	Max 100 gal
3. tires from trailer	20 units
4. a tank truck or railroad tank car	10,000 gal

In a severe collision, it was possible that a fire would result. If another source (item 4) of fuel was not

involved, a maximum fuel supply of 143 gal would be available for the fire. Although some or all the tires could also burn, their location relative to the cask (at extreme ends of the trailer and below a metal trailer deck) should prevent extreme temperatures near the cask. If it is assumed that the total fuel supply (1 and 2) would be placed in an optimum location under the projected area of the cask, a pool approximately 6 in. deep would result. Burning rates for fuel have been measured from $\frac{1}{4}$ to $\frac{1}{6}$ in./min. Assuming a rate of $\frac{1}{5}$ in./min, the burning time for the fuel would be about 30 min. Both the truck bed and shipping rack were provided with drain holes, and retention of fuel in a vulnerable region is difficult to postulate even if the fuel were deliberately placed in such a location. Estimates of the time required for the lead to reach the melting point at the surface of the cask indicate that the cask should be safe for at least 45 min (see Sect. 9.2.2). The cask would suffer little, if any, fire damage unless an additional source of fuel (4) were added.

If an additional source of fuel (4) were involved, one might postulate that the cask could be involved in a 1-hr fire, although the probability of the fire being near enough to transfer maximum heat to the cask was considered extremely low. Fire has been found to occur in all types of collisions about 1% of the time, and in overturns about 2% of the time. These data were obtained from the Bureau of Motor Carriers of the Interstate Commerce Commission and cover a four-year period (1956–1960) with a total of 111,120 reportable accidents by 2500 large motor carriers in more than 30.5 billion vehicle miles of intercity travel. (A reportable accident was one from which there results a death or injury or property damage of $100 or more.)

The accident rate per 10 million miles for typical carriers of radioactive materials was 36.26 ± 1 accident. The rate in the western region of the states, in which the PSV route lies, was lower than the all-region average: only 28.55 per 10 million miles.

The maximum likelihood estimate of accident rates for carriers of radioactive materials was 28.55 per 10 million miles of travel in the western region. Overturns amount to only 9% of the total.[9]

The most pessimistic evaluation of fire frequency can be made from the preceding data for all types of collisions: 1% of maximum accident rate, or 0.0286 fires per million miles; and for overturn accidents: 9% of maximum accident rate times the 2% which result in fires, or 0.0051 fire per million miles.

An overturn accident in which the trailer and/or cask would be thrown in a ditch where fuel could collect to provide a 1-hr fire is still less probable. In other accidents in which fire might occur, the fuel would normally spread out over a greater area, and the duration and intensity of the fire would be reduced. However, to be conservative, assume that a 1-hr fire could occur at a frequency rate of 0.0286 fire per million vehicle miles. The total number of trips involving shipment of radioactive materials was to be 8, the miles per trip 1100, for a total of 8800 miles for the period of the demonstration. Thus the probability of a collision involving fire (using the most conservative assumptions) would be extremely small, and the maximum likelihood of a fire only

$$\frac{8.8 \times 10^{3} \times 28.6 \times 10^{-3}}{1 \times 10^{6}} = 252 \times 10^{-6}$$

for the total demonstration.

9.4 ANALYSIS OF TRANSFER OPERATIONS IN PROJECT SALT VAULT

9.4.1 Topside Transfer Procedures

Three types of transfer procedures would be carried out at the waste charging facility. The first type, carrier unloading only, would be required for the first two fuel assembly shipments (transfers 1 and 2, Table 9.1). The canisters in these two shipments would be used to load the main and floor radioactive arrays. For the next two transfers (3 and 4, Table 9.1), a procedure involving simultaneous unloading and loading would be required. These transfers would be used to move canisters from the main array to the floor array, with the canisters from the floor array being returned to the surface carrier. Finally, the last two transfers would require a carrier loading procedure only and would be required to remove all canisters from the mine. (As mentioned previously, only three sets of canisters were actually used, thus eliminating transfer 4.)

Listed in Appendix A of Chap. 10 are the detailed operations required for each of the three types of transfers.

All transfer operations were to be controlled by the supervisor in the waste charging facility. A detailed checklist would be used throughout all transfers to ensure that operations were kept in sequence. One health physicist would be available at all times for

[9] Accident Data NYO-9771, The John Hopkins University, "Statistical Analysis of the Frequency and Severity of Accidents to Potential Highway Carriers of Highly Radioactive Materials," by F. F. Leimkuhler, M. J. Karson, and J. T. Thompson.

routine monitoring when required, both at the top and the bottom of the waste shaft.

In order to carry out these transfers without the need for hot cells or remote-handling equipment, a special handling tool (grapple) was designed. This grapple would be connected to the canister while it was in the shipping carrier and would remain attached to the canister until it was located in the storage hole in the mine. The grapple is shown in Fig. 9.6. Basically, the grapple contained four lifting lugs which would extend out from the grapple body by a cam action and be engaged in a recessed cavity in the canister head. A special locking tool would be used to activate the grapple. The tool would be inserted in the top of the grapple, pushed down, and rotated, engaging a bayonet-type lock which would prevent accidental release of the lifting lugs. Later, when the canister was in the storage hole, the locking tool would again be used to disengage the bayonet lock and retract the lifting lugs. Connected to the grapple would be a 20-ft length of $\frac{1}{4}$-in.-diam 6 X 37 strand wire rope.

When the transfer operations at the topside facility were completed, the carrier would be returned to a horizontal position. This operation is required so that the waste shaft would not be blocked and, as a result, not be available for emergency use. With the exception of transfers 3 and 4 (in this case the carrier would be loaded with fuel assemblies removed from the mine and would be shipped back to Idaho) the carrier would be stored at the topside facility. Storage could be on the charging pad or adjacent to the waste charging facility.

After the carrier was returned to a horizontal position, a metal plate would be placed over the open top of the waste shaft and locked, sealing the waste shaft. This would allow the bypass ventilation duct to be tied into the experimental area ventilation system. The bypass ventilation duct led to a 5000-cfm fan at the base of a 20-ft stack.

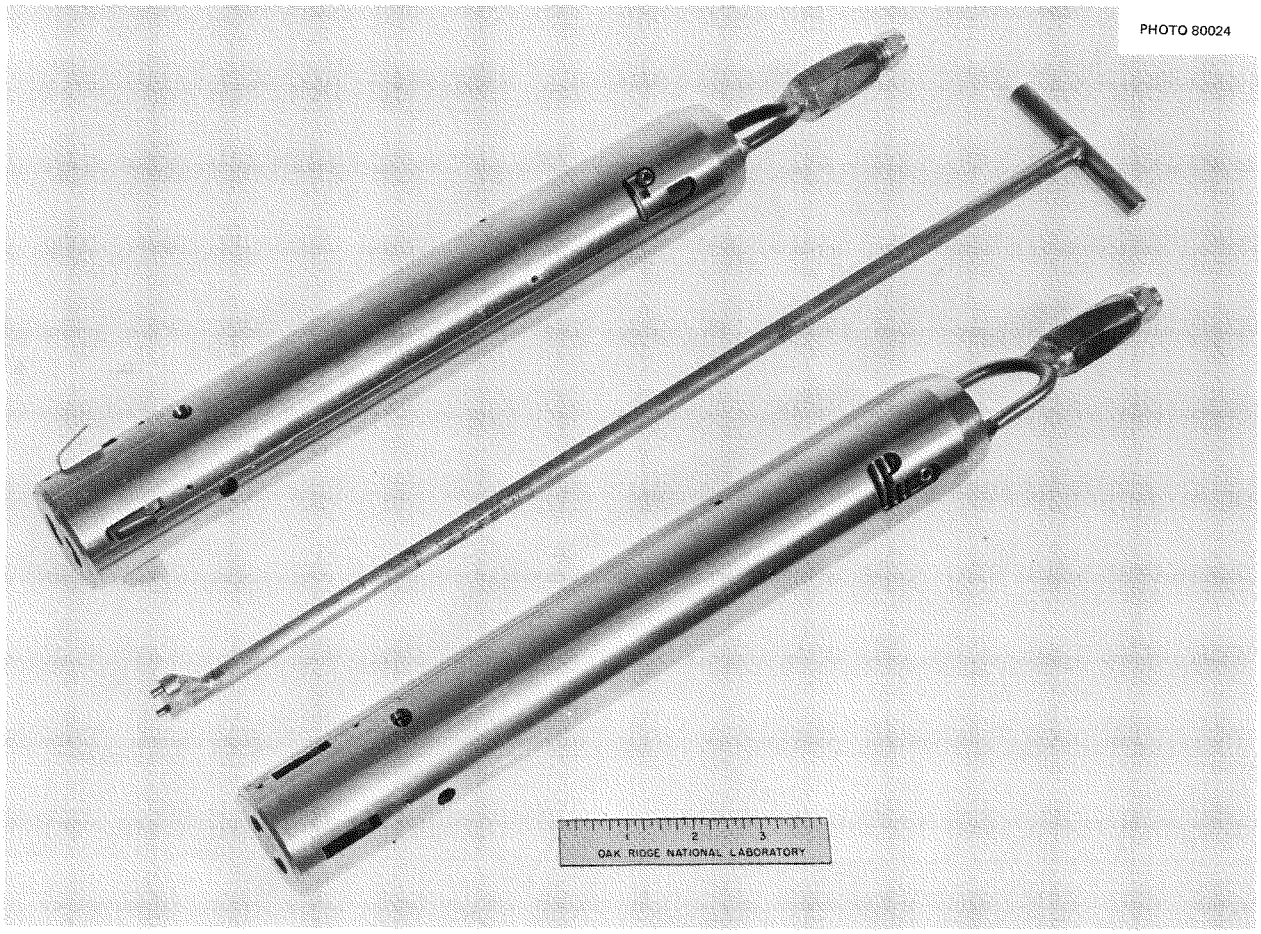


Fig. 9.6. Grapple Used in Handling Fuel Canisters.

9.4.2 Transporter Loading at Shaft Bottom

The transporter would be driven by its own power to a location directly under the waste shaft and the cask raised until the cable door assembly and the upper funnel and shield were in contact with the waste shaft. When this was achieved and all operations of the doors checked, the upper shield doors would be opened, and the control box would be moved outside the shaft room. All personnel in the area would then be evacuated and air flow up the waste shaft shut off.

A detailed outline of the operations required when lowering the canister into the transporter shield is given in Chap. 10. Basically, the canister would be lowered into the transporter shield and the doors closed remotely until a $\frac{3}{8}$-in. gap was left between the doors. At this point, after radiation monitoring, the waste shaft area would be entered, the transporter shield and canister lowered, and the $\frac{1}{4}$-in. hoist cable placed in the slot provided in the door. After this the door would be manually closed completely. The shield would then be made ready for transportation.

9.4.3 Transporter Unloading at Shaft Bottom

The basic steps in unloading the transporter are the reverse of those used in loading. Personnel would be required in the area until the grapple cable had been removed from the winch drum and attached to the main hoist cable and some of the slack in the main cable had been taken up so that the cask could be raised vertically until it was in contact with the bottom of the waste shaft. When this had been completed, all personnel would leave the area, and the air flow would be shut off. The balance of the operations would then be carried out remotely.

9.4.4 Transfer Operations at Mine Level

Transfer operations below ground consisted in filling the main array, transferring canisters from the main array to the floor array, and unloading the floor array. Table 9.7 shows the types of transfer operations required for each of the six transfers in Table 9.1. The sequence of canister transfers for the third and the fourth transfer is shown diagrammatically in Fig. 9.7. (In the actual operation transfer No. 4 was omitted.) It can be seen from this figure that a storage hole was required to temporarily hold one canister prior to these operations. This storage hole would be installed as a duplicate of the array storage holes with the exception that no heaters would be attached. (During actual operation the procedure was changed so that the storage hole was not required, see Sect. 10.2.3.)

Table 9.7. Mine-Level Transfers During the Demonstration

Transfer No.	Transfers Required		
	To Main Array	From Main Array to Floor Array	From Floor Array
1	Yes	No	No
2	Yes	Yes	No
3	Yes	Yes	Yes
4	Yes	Yes	Yes
5	No	Yes	Yes
6	No	No	Yes

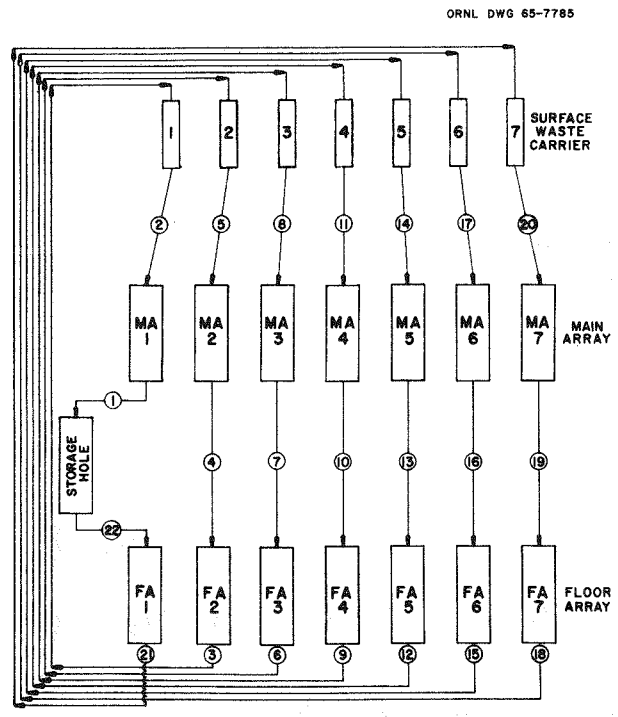


Fig. 9.7. Transfer Cycles – Third and Fourth Fuel Changeout (Second Changeout, Same But No Fuel Removal).

Although the transfer operations for each shipment were different, the handling procedures could be broken down into two basic operations: (1) loading the transporter cask from the array or storage holes and (2) unloading the transporter cask to the array or storage holes.

The rooms containing the radioactive arrays would be sealed off from the rest of the mine by brattice cloth curtains to reduce air flow and serve as a form of containment barrier to the release of activity to the mine workings. It would be necessary to open these

curtains to allow the transporter access to the storage rooms and to allow the diesel exhaust fumes to escape. However, when the tractor was not operating the curtains would be closed.

9.5 FISSION PRODUCT CONTAINMENT

The Engineering Test Reactor fuel assembly is composed of 19 uranium-aluminum alloy fuel plates clad with a 6061 aluminum alloy. The melting point of the alloy cladding is in the range of 1080 to 1200°F. As long as the assembly is not subjected to temperatures in excess of these figures, or cladding mechanically damaged, during the irradiation period, it is assumed that the cladding on the core material constitutes the first containment barrier. Assemblies having cladding leaks reported during any portion of their irradiation history would not be used in Project Salt Vault.

During removal of the end boxes from the fuel assemblies, the assemblies were to be trimmed to a length approximately $\frac{1}{8}$ in. from the active core of the assemblies. It is possible that a release of fission product gases could occur during the trimming operation if pinholes or small cracks were exposed during the cutting operation. All cut assemblies were to be submerged in water and monitored to detect any possible cladding leaks. (The Idaho hot cell operating personnel reported that submerging the assemblies in water and observing any bubbles produced is the most sensitive detection method for cladding leaks.) Only fuel assemblies showing no leaks after cutting would be used.

Design of the fuel assembly canister was based on the necessity for providing secondary containment by the canister. The canister as designed provided containment by means of both a mechanical closure and a seal weld. If, during any portion of the shipment from Idaho to Lyons or the experiment, the fuel assembly cladding temperature were allowed to exceed its melting point, the canisters would still provide containment. Thus, during fuel shipments and whenever canisters were being transferred from the surface into the mine, two containment barriers would be provided.

When the canister is inserted into the array storage hole, a third containment barrier would be provided by the gasketed upper flange. However, due to the large number of penetrations in the upper liner section (for thermocouple leads, power leads, and off-gas lines) 100% tertiary containment for the entire storage period could not be guaranteed. Therefore a gas purge system was installed which pulled air into the upper liner and vented it through a charcoal trap, filter, and monitoring system before release (see Sect. 7.7.4). Air inlet and outlet lines were provided in the top part of the hole liner. The inlet line was fitted with a gas mask filter cartridge followed by a needle valve and an open-when-energized solenoid valve. A slow air flow (about 1 liter/min) was maintained through the hole liner and into a series of shielded chambers containing: a filter, a charcoal bed and detector, and a G-M detector in a flow-through chamber. All seven of the hole liners in each array were tied into the same monitor through a manifold. Each liner outlet line was also provided with an open-when-energized solenoid valve. In the event of a leak, the first nuclide likely to reach the monitoring system would be the ^{85}Kr, which would pass through the filter and charcoal bed, but would be detected in the flow-through chamber. Particulate releases would be trapped on the filter paper, and ^{131}I would be adsorbed by the charcoal bed. The system was designed so that activity in the flow-through chamber would cut off the liner air flow, close the solenoid valves, cut off the power to the auxiliary heaters, and activate an alarm signal.

To prevent contamination of the mine air, a special air flow pattern was provided in which air was pulled from the main mine air flow into the experimental area and released up the waste shaft. Thus, if any radioactivity were accidentally released, it would not contaminate the mine access corridors or the main mine shaft.

9.6 EVALUATION OF ACCIDENTS

In the operation of Project Salt Vault, transfers and handling of the fuel assembly canisters were planned to take place at the ground surface (waste charging facility) and below ground at the mine level. The below-ground transfers would take place at the bottom of the waste charging shaft and at the storage holes. In addition the canisters would be moved in the underground transporter from one storage hole in the main radioactive array to another hole in room 5. The types of accidents that could occur are described in detail for each location.

Because of the handling procedures planned for Project Salt Vault, it was not possible for an accident to occur in the mine which would involve more than one fuel assembly canister (two ETR fuel assemblies). Canisters were to be handled one at a time, and each handling cycle had to be completed before the next canister would be moved. Table 9.8 shows the calculated fission product inventory for one canister at various times out of the reactor. The fission products of

Table 9.8. Fission Product Concentrations in One Canister at Various Times Out of the Reactor

Fission Product	Concentration (Ci)		
	75 Days	270 Days	455 Days
^{131}I	220	<1	<1
^{85}Kr	78	75	72
^{133}Xe	3	<1	<1
^{131m}Xe	42	<1	<1
^{90}Sr	570	560	550
^{137}Cs	610	600	590
Total Te	3700	250	58

major concern were the gaseous fission products (^{85}Kr, ^{131m}Xe, ^{131}I, and ^{133}Xe). Once the fuel assemblies had been out of the reactor for about 140 days (or about 50 days in the mine) only ^{85}Kr remained in significant amounts. The ^{90}Sr and ^{137}Cs would present problems only if the fuel assemblies were melted or raised to temperatures at which these fission products would be volatilized.

9.6.1 At the Ground Surface

Operations performed at the waste charging facility are briefly described in Sect. 9.4.1. Detailed procedures are described in Appendix A of Chap. 10. During normal operations accidents could result from laxness in following operational procedures or from equipment malfunction that would result in the accidental release of a canister down the waste shaft, shearing of the canister tube by the carrier doors, or the physical dropping of a canister down the waste shaft, shearing of the canister tube by the carrier doors, or the physical dropping of the shipping cask during erection or lowering from the vertical position required for canister loading or unloading. Engineering design and safety devices were used to reduce the probability of any of these possible accidents.

9.6.1.1 Accidental Release of Canister into Waste Shaft. – The canister could be released into the waste shaft at an unexpected time by opening both the bulkhead door on the shipping cask and the safety door in the shaft before the grapple was connected to the canister; by failure of the grapple; by breakage of the hoist gearing, cable, or connector; or by a physical failure of the upper part of the canister containing the grapple recess cavity. The methods used to eliminate these accidents and the associated safety factors are described in this section.

As previously described, the grapple engaged the canister head recess cavity with four lifting lugs that are forced out of the grapple body. In order to activate the grapple, the lifting lugs had to be in the recess cavity; otherwise, rotation of the locking tool would not be possible. As a result, there had to be a positive indication that the grapple was correctly inserted and held prior to opening the bulkhead door.

With the shipping cask in erected position, the main carrier shield door would be opened. At this point the canister would be held in the cask by the bulkhead door. The grapple hole shield plug is removed from the cask, and the grapple is inserted and locked, and a load check is made to ensure that it is engaged. When this procedure is completed, the bulkhead door would be opened. Thus the canister would be held by the grapple, which is connected to the hoist cable at this time. To back up this system a safety door is installed in the waste shaft to prevent the canister being lowered or falling any farther than about 8 ft down the waste shaft. After the canister is lowered to about this depth, the safety door would be opened and the canister lowered the balance of the way down the waste shaft.

A detailed operation checklist would be followed to ensure proper operational sequences (see Appendix A of Chap. 10). Position-indicating switches were installed as a part of the safety door and guide assembly to indicate the position of the canister in the upper 10 ft of the waste charging shaft.

In reloading the shipping cask with canisters brought from the mine level, a reverse procedure would be required, but the safety equipment would function in a similar manner. The bulkhead door and the shaft safety door would remain open until the canister was within 8 ft of the top of the waste shaft. At this point the canister would be raised slowly until the limit switches and cable markings indicate the canister has passed the safety door. The safety door would then be closed, preventing the canister from dropping the full depth of the shaft. Using slow hoisting speed, guide tube position switches, and cable markings, the canister would finally be lifted into the shipping cask. At this point the bulkhead door would be closed (door position indicated by a built-in position indicator), the grapple would be removed, and the magazine in the cask would be rotated into a new position for loading or unloading.

9.6.1.2 Accidental Shearing of the Canister by the Bulkhead Door or the Waste Shaft Safety Door. – The possibility of shearing a canister by the door assemblies is minimized by the use of position-indicator switches in the guide tube assembly and by cable markings. The main hoist is equipped with a device to show the

location of the canister in the waste shaft, and the control of hoisting speed would be based on this unit. When the canister is within 50 ft of the top of the shaft, the hoist speed would be reduced from 100 to 33 fpm; it would continue at this speed until the canister is within 15 ft of the top, at which time the hoist would be stopped and switched to slow inching speed (1.25 fpm). At this speed the canister would be slowly raised into the guide tube and then into the shipping cask. Limit switches would indicate when the canister had passed the safety door. In the case of the bulkhead door, however, more accurate positioning would be required, since there is only about ½ in. of free space inside the carrier when the bulkhead door is closed. Slow inching speed would be used, and cable marking and visual observation of the grapple would show when the canister was correctly positioned and the door should be closed.

Since both the safety door and bulkhead door have very little mass and both would be operated manually, a positive feel of the force required to open or close the doors should be acquired by the operators. Any additional increase in force required to operate a door would be immediately sensed by the operator. Therefore, the probability of any damage of the canister by the two doors was considered very remote.

During lowering of the canister, the doors would be opened to release the canister and not closed until the cable was brought back up through the cask.

9.6.1.3 Damage to Canister by Dropping Shipping Cask During Erection or Lowering. – The possibility existed that the cask could be dropped during erection over the waste charging shaft. This could occur due to cable failure on the crane raising the carrier or to a failure in the hydraulic system that completes the erection procedure.

The hydraulic system for elevating the cask uses two hydraulic cylinders, each of which alone is capable of handling the erection loads. The hydraulic piping was designed with check valves and flow-limiting valves that would not allow rapid movement of the cask in either direction should the electrical power to the hydraulic pump fail. Even if a hydraulic line were to break at any point, the carrier would not drop abruptly because of the cushioning action built in at each end of the hydraulic cylinders.

Since all carrier doors would be closed and the carrier was designed to handle shock loadings, as required by the Federal shipping regulations, it is not possible that the cask or the canisters would be ruptured. The most probable result of such an accident would be a jamming of the rotating magazine, or the cask doors, such that the canisters could not be removed. In this case the cask would have to be returned to Idaho for unloading and repair.

9.6.1.4 Fuel Meltdown in the Waste Carrier. – After the shipping cask is erected over the waste charging shaft, the water cooling system used during the shipment from Idaho to Lyons would be reconnected to the carrier water lines to remove decay heat. Failure of this system and the resulting time interval required to produce excessive fuel element temperatures is described in Sect. 9.2.5. If failure of the cooling system should occur, sufficient water would be available near the waste charging facility to provide an adequate emergency supply until the diesel system could be repaired, so that no fuel meltdown would occur.

9.6.2 In the Waste Charging Shaft

Major accidents that might occur in the waste charging shaft included: failure of the hoist cable, power failure to the hoist, grapple failure, or fuel meltdown. A summary of preventative measures to overcome these possible accidents is given in the following sections.

Due to the large diameter of the waste charging shaft (19.1 in. ID) and the size of the canister (approximately 5.6 in. maximum diameter), there was no possibility that the canister could be wedged in the shaft. The shaft as drilled (bottom of shaft is displaced 2.56 ft horizontally from top) was essentially vertical and contained no doglegs or bends of sufficient angle to impair free movement of the canister in the shaft. This was tested by running a mandrel which was 16 in. in diameter by 20 ft long up and down the cased shaft.

9.6.2.1 Breaking of Hoist Cable During Lowering or Raising of Canister in Waste Shaft. – The cable on the waste shaft hoist is ⅜-in.-diam, 19 X 7 strand improved plow steel nonrotating wire rope. The breaking strength of this rope is 5.59 tons (11,200 lb). The rope safety factor (ratio of the breaking strength to the load plus weight of reeled-out cable) is 25. A safety factor of 6 is required by the Kansas Mining Code.

In order to simplify the handling procedures at the bottom of the waste shaft, a 25-ft-long section of ¼-in. cable was connected to the end of the main cable. This section of cable is disconnected from the main cable after the canister is located inside the underground transporter, and the ¼-in. cable is reconnected to the transporter winch. This procedure eliminated the need to disconnect the grapple from the canister inside the transporter. The ¼-in. cable is a 6 X 37 strand improved plow steel wire rope having a breaking

strength of 5568 lb. The safety factor for this cable is 27.

The cable safety factors show that the possibility of breaking the hoist cable would be very remote. It would be possible, however, to break the cable if the load were caught as it is pulled from the transporter into the waste shaft, or as it leaves the waste shaft and enters the shipping cask, since a 2000-lb hoist (required code safety factor of 5 in design or about a 10,000-lb load required to stall hoist) could exert more force than the 1/4-in. cable could resist. This possibility was minimized by the installation of a slip-type clutch in the drive train of the hoist. This clutch is set to slip at a load capacity of 1000 lb or less and should prevent overloading of the cable.

As the cable wore, it would be inspected, as required in the mining code, for broken strands, strand elongation, and flattening and replaced when necessary. The hoist would also be inspected as required to maintain all safety systems in operating condition.

9.6.2.2 Power Failure to Hoist. – In case of a power failure to the hoist during the raising or lowering of a canister, a self-actuating safety brake would operate which could stop the canister in less than 1 ft from the point at which the power failure occurred. This brake could only be released when the power failure is corrected or an alternate power source is connected. The brake is located on the main gear train.

If power failure were to occur, the main problem would be that the canister could not be moved from its location in the waste shaft until power to the hoist was resumed.

9.6.2.3 Failure of Grapple. – The grapple used to handle the canisters is positive locking and could only be disengaged by using a special handling tool. Calculations indicated that the weakest part of the grapple assembly was the weld holding the cable loop to the grapple body (strength equal to 6*g* or 1200 lb). Since this part was the weakest section, all welds were inspected by radiography for flaws. Although it would have been possible to increase the strength of this connection, it was felt that the safety factor of six times the weight of the canister was sufficient and in line with those on the hoist and hoisting cable. The four steel lugs which held the canister when the grapple was engaged were capable of withstanding a 10*g* force before failure.

Due to the safety devices built into the hoist (slip clutch) there existed only one manner in which a force of 6*g* could be produced. This would be due to a rapid deceleration of the canister, such as would be produced by a power failure and subsequent automatic braking of the hoist. Calculations showed that with the canister being lowered at its maximum speed (100 fpm) the canister would have to come to a complete stop within 0.11 in. to produce a 6*g* force. The braking on the hoist would not be able to produce a complete stop within this distance. As a result, inertial forces could not be produced which would cause structural failure of the grapple.

9.6.2.4 Fuel Meltdown in Waste Shaft. – If for any reason, such as power failure, the canister were left hanging in the waste shaft for an extended period of time, the heat generation from the fuel assemblies would not be capable of producing melting temperatures. It was calculated that the maximum fuel assembly temperature (for all seven canisters in the shipping cask) with no coolant would not exceed 1016°F, which is below the melting point of the aluminum cladding. Since this calculation was based on seven canisters in a carrier at 75 days cooling, there is no reason to expect a single canister at 90 days cooling to overheat while in the waste shaft for an unlimited period of time.

Since transfers in the waste shaft would normally be made with no air flow in the waste shaft, it would be possible to bring air up the waste shaft to cool a canister if it were desired to keep the canister at as low a temperature as possible.

9.6.3 Loading the Transporter at the Waste Shaft

At the bottom of the waste shaft, canisters would be loaded into the underground transporter for transfer into the storage holes. During these operations a number of accidents (described below) could occur that could lead to a release of radioactivity to the experimental areas. Additional safety components were designed and installed to prevent these accidents from occurring.

9.6.3.1 Shearing of Canister by the Transporter Shield Doors. – Since visual observation of the location of the canister in the underground transporter shield was not possible because of positioning of the shield against the ceiling during loading, devices were installed to indicate the location of the canister in the shield. These devices consisted of position-indicating switches on the guide tube located inside the transporter shield. The position switches were actuated by the canister and showed the position of the canister by means of red and green indicator lights. In addition to this system the hoist operator at the topside facility had the depth indicator on the hoist and the cable color coding to indicate canister location. By using these devices and the detailed operational procedures, the possibility of shear-

ing the canister by closing the shield doors was very remote. The locations of these position switches are shown in Fig. 9.8.

9.6.3.2 Shearing of the Hoist Cable by the Transporter Shield Doors. – Since the grapple and its cable are connected to the canister at all times to continue the handling operations and, further, since no provisions are made to allow disconnecting or reconnecting the grapple at any point other than in the storage hole (which was done to simplify procedures and eliminate the need for special remote tools), it was essential that the $\frac{1}{4}$-in. cable fastened to the grapple not be sheared at any point in the transfer operations. The upper transporter shield door is equipped with a groove to allow the cable to protrude from the shield when the doors are closed. This groove is in the center of the doors, and as a result the cable had to be accurately located in this groove prior to closing the doors. This could be done by closing the main doors until a $\frac{3}{8}$-in. gap was left between the doors, and the cable would then be manually fitted in the slot. The doors are prevented from closing on the cable by steel blocks fastened to the waste shaft funnel, which had to be removed before the doors could be closed. This procedure, plus the inner guide tube on the transporter shield, ensured that the canister cable would not be sheared by the doors.

9.6.3.3 Meltdown of Fuel Assemblies in Transporter Shield. – Since it was shown that the seven canisters when contained in the shipping cask would not melt on loss of cooling water, it would not be possible for one canister contained in the transporter shield to generate sufficient heat to produce fuel meltdown. (There are fewer air gaps, and the surface area for heat dissipation in the transporter is greater than that per can in the cask.)

9.6.4 During Transport in the Transporter

9.6.4.1 Physical Damage to Canister During Transport. – Since the mine floor is not perfectly flat and since the transporter must move up and down the ramp, there is a remote possibility that the canister could be damaged by impact with the side walls of the shield. In order to reduce this action a guide tube 6 in. in diameter was installed inside the shield. Thus the canister would be limited in the amount of movement within the shield during transport, and as a result no damage should occur to the canister.

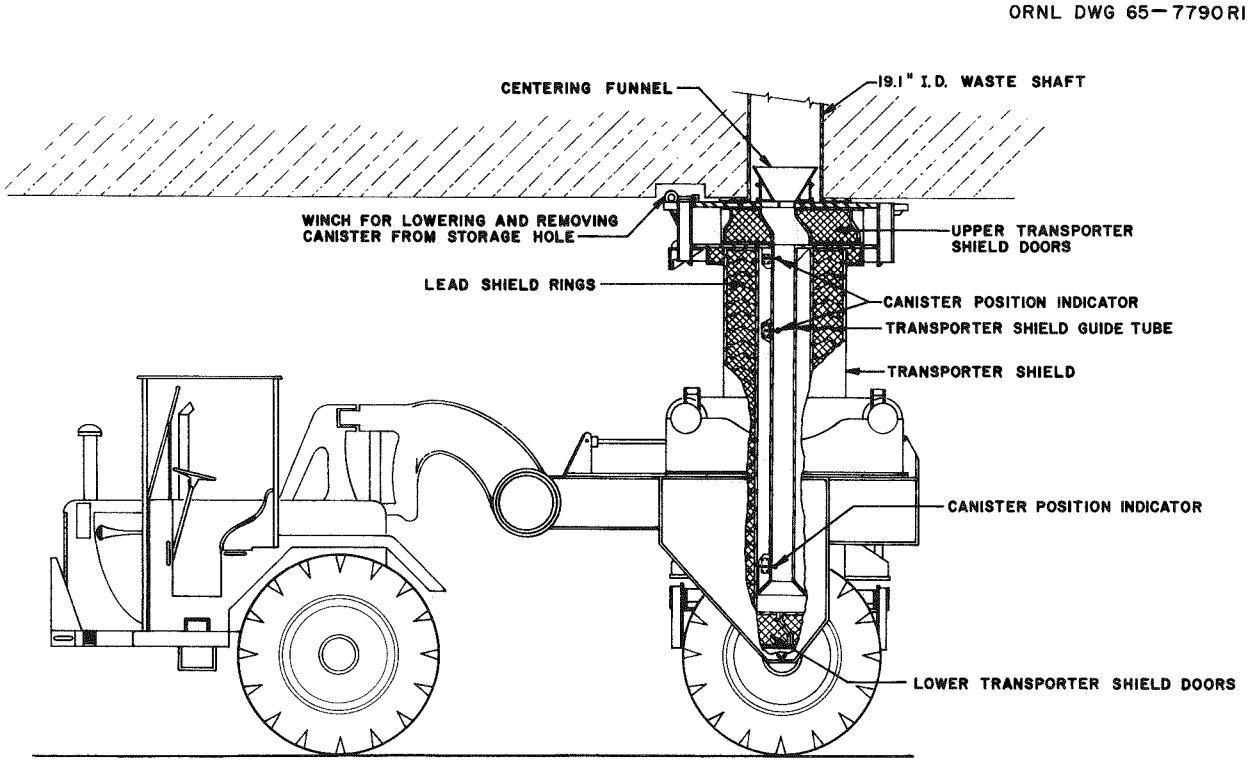


Fig. 9.8. Cross-Section Drawing of Underground Transporter in Loading Position.

9.6.4.2 Accidental Dropping of the Canister or the Shield During Transport. – In order to prevent accidents of this type from occurring, an interlock system was provided in the shield controls to prevent movement of the shield or opening of the shield doors unless the trailer brakes were locked. A manual lock has to be set on each of the four doors before the transporter can be moved, and a key lock also has to be unlocked on the control box before the doors can be opened. Even in the case of an accidental operation of the shield controls during transit, no possibility exists that the cask could move or the doors open. As a further safety measure, large chains are connected to the shield from the transporter trailer frame to hold and prevent vertical movement of the shield. These chains have to be removed before the shield can be lowered.

9.6.4.3 Mechanical Failure of Transporter Brakes. – If the transporter brakes were to fail when the transporter is in motion, damage to the transporter and shield could result. Normal mine speeds would be low (about 10 mph); however, if the brake failure should occur while the transporter is driving down the 10% grade ramp, speeds in excess of this could result. Since the ramp terminates in a right-angle turn and since sufficient headroom is not available for the transporter if it should not make the turn, it is possible that the 10 *g* design force on the transporter could be exceeded. The major damage resulting from this type of accident could be the physical tearing of the transporter shield from the trailer and demolition of the tractor unit. Damage to the canister resulting from such a collision should not be severe and should not result in the release of radioactivity because of the cushioning effect of the guide tube in the shield and the inherent strength of the canister. The major problem resulting from such an accident would be the operations required to repair the transporter and unload the canister from the shield.

9.6.5 Loading or Unloading Storage Holes

The final step in the handling procedures would be the loading of the canisters into the storage holes in the mine floor. This operation would be performed by the winch located on the transporter, consisting in lowering or raising the canister into or out of the storage hole. The hole liner is equipped with a guide funnel to assist in inserting the canister into the lower liner section. During the operations required to pull the canister from the liner, the limit switches in the transporter guide tube would be used to determine the position of the canister in the shield prior to closing the lower shield door.

As described in Sect. 9.5, the hole liner is equipped with a purge system and monitoring assembly to determine if any radioactivity has been released from the canister. Thus no radioactivity should be released when the hole liner flange is removed for canister transfers.

In general, other than the possibility of a canister leak, the number of accidents which could occur when the canister is being inserted or removed from the hole liner is very small; furthermore, accidents are protected against by the safety features for transporter loading described previously. There are, however, two types of accidents that could occur in the hole liner which would not be possible at any other time during the operation of Project Salt Vault. These accidents are the melting of fuel and the binding of a canister in the liner, preventing canister removal.

9.6.5.1 Fuel Meltdown in the Storage Holes. – Since a major part of the data to be collected in Project Salt Vault is concerned with the combined effects of heat and radiation on the plastic flow of salt and mine stability, it is essential that the salt be raised to as high a temperature as would be anticipated in an actual disposal operation. Because of the relatively rapid decrease in the heat generation rate with time (see Fig. 9.4) of the ETR fuel assemblies, supplementary electric power is needed to provide an essentially constant total power input. A constant heat generation rate was desirable to simplify the confirmation of the thermal calculations and analysis of the plastic flow data. The supplementary electric heat was to be supplied by tubular heaters located on the outside of the hole liner. If for some reason the power controls on these heaters should fail, it might be possible to supply sufficient heat to melt the fuel assemblies. In order to prevent this from occurring, four thermocouples in each canister were located between the fuel plates in the fuel assemblies, and these thermocouples would be connected to a recorder equipped with high-temperature alarms and relays to shut off all external heat should the fuel assemblies exceed a predetermined temperature. Additional thermocouples were located on the hole liner which would give backup confirmation if high temperatures were achieved. In order to ensure that the operators of the experiment would be aware of the high-fuel-element-temperature alarm, the signal from the annunciation system had to be transmitted to the topside mine office and directly to the operators' residences.

9.6.5.2 Seizing of the Canister in the Hole Liner. – As the salt is heated around the hole liner, it would be

expected to expand and flow radially into the storage hole, decreasing the hole diameter. It might be possible for sufficient flow to occur that the salt would come into contact with the hole liners and produce sufficient pressure to collapse the liner, thereby preventing removal of the canister from the storage hole. In order to prevent this action, an annular space was left between the salt and the hole liner, and the width of this annulus would be measured periodically with a special hole caliper. If the salt should flow close enough to the hole liner that contact with the liner might be possible, the canister would be removed from the storage hole and temporarily kept in the transporter. The transporter would be moved away from the hole, and the lower liner section would be unbolted and removed and the hole reamed out. The lower liner could then be replaced, followed by the canister. If the canister for some other reason should seize in the lower liner and become nonremovable, the guide tube could be removed from the transporter and the entire assembly of canister and lower liner hoisted into the transporter. The combination of lower liner and canister would require a special carrier for the return to Idaho.

9.7 ACCIDENT CATEGORIES

The previous section describes the accidents which could occur during the operation of Project Salt Vault and indicates the engineering safeguards that were designed into the waste-handling equipment to reduce the probability of such accidents. However, even with the engineering safeguards and detailed checklists, there still remained the possibility that a mishap could occur that would ultimately lead to a release of radioactivity from the fuel assembly canister. This release could be due to a number of unrelated occurrences (such as a cladding failure in the ETR assembly followed by a subsequent leak in the canister), or to one event such as a drop or impact to the canister. In general, because the ETR fuel assemblies are fabricated from an aluminum-uranium alloy completely clad with aluminum, the amount of radioactivity released would depend on the number of plates which were ruptured or damaged.

Fuel assembly meltdown would not be possible while a single canister was being transferred in the experiment (see Sect. 9.6), and the only possible place where meltdown could occur would be in the storage hole in the mine floor, where additional heat was supplied by electrical heaters. Because of this possibility, the storage hole was made leak-tight, and a purge system was installed to detect and contain any potential activity released. As a further safeguard, control systems were provided (see Sect. 9.6) to shut down electrical power to the auxiliary heaters should the fuel assembly temperature exceed a safe level.

The fission products of concern in a typical canister at 75 days, 270 days (time of fuel transfer from the main array to the floor array), and 455 days (time at which assemblies would be removed from the mine) are given in Table 9.8. If an assumption is made that the burnup in each fuel plate is the same, there are 38 fuel plates (19 per assembly) that would contain the activities listed in Table 9.8. Dividing the various activities by the number of fuel plates gives an average product concentration per plate. Table 9.9 gives the fission product activity for various numbers of fuel plates at 75 days out of the reactor.

Using these values and assuming that a potential accident can be described in terms of the number of plates ruptured, the following release categories can be defined for Project Salt Vault:

I. Type I accident – an accident or release due to cladding failure on one fuel plate.

II. Type II accident – an accident or release due to impact or dropping of the canister. This accident category is assumed to result in the breakage of up to 19 fuel plates (one ETR assembly).

In addition to the number of plates which could be broken, the two categories of accidents can be described by the location in which they might occur. A type I accident could occur anywhere in the handling or storage operation, since it is the result of an initial cladding failure of the fuel assembly followed by a

Table 9.9. Average Concentration of Fission Products in Various Numbers of ETR Fuel Plates

Fission Product	Concentration (Ci)				
	1 Plate	10 Plates	19 Plates	30 Plates	38 Plates
^{131}I	6	58	110	174	220
^{85}Kr	2	21	39	62	78
^{131m}Xe	1	11	21	33	42
^{133}Xe	0.1	0.8	1.5	2.3	3.0
^{90}Sr	15	150	285	450	570
^{137}Cs	16	161	305	483	610

failure of the canister and would not necessarily require impact to produce. A type II accident, however, is not possible during the handling operations at mine level. The movements of the canister during these stages of the experiment would be slow, and there would be no possibilities of long drops or severe impact that would result in this amount of damage. This type of accident would occur in the waste shaft and would result in the release of activity up the waste shaft to the atmosphere.

9.7.1 Type I Accident

A type I accident (a "leaky fuel assembly") could not occur unless the integrity of the canister was also lost. The exact causative agent for producing such a failure in the canister cannot be predicted; however, such things as corrosion, minor physical damage, or inadequate welds are possible. The canister is constructed of 304 stainless steel, which is judged to be satisfactory for corrosion resistance under the conditions anticipated, since the canister would not be in direct contact with salt. (304L is expected to have greater corrosion resistance in contact with moist salt.) Furthermore, the canister would be inspected for defects at every stage in the fabrication process and subjected to a helium leak check after loading. The canister would be protected from direct exposure to the salt by the hole liner, and the air inlet to the liner (for the fission product detection system) has a filter to exclude salt dust.

Because of these precautions, the probability of a failure in canister integrity during the early stages of the experiment should be small, but it increases with length of time in the mine. As a result, the only gaseous fission product of concern would be the ^{85}Kr, since the ^{131}I would have decayed to less than 1 Ci per canister after 150 days out of the reactor.

The degree of severity of a canister leak would depend on the position of the canister when the leak occurs. If a leak occurs while the canister is located in the storage holes, the release would be detected by the hole liner purge system, and corrective action could be taken without the release of any activity to the mine atmosphere. If the leak were to occur when the canister is in the underground transporter, it would be detected by the air monitoring equipment, and the canister and the transporter could be isolated either in the storage rooms or the waste shaft room. These rooms are equipped to have minimum air flow, and the transporter could be stored in these areas until corrective action could be taken. The same holds true for a leak occurring when the canister is in the waste shaft. In this case the air flow in the shaft would be essentially zero, and the activity could be contained in the shaft. In no case, because of the system employed for ventilating the experimental area, could the activity be released to the main mine air, resulting in contamination of the mine access tunnels or the main access shaft. Remedial actions that would be taken would depend on the location of the canister when the leak occurs, but in general they would probably consist in allowing a decay period for shorter-lived fission products if they are present, followed by either a slow and controlled release of the activity up the waste shaft or collection and containment of the gases.

The activity released by the failure of one fuel plate (not by melting) was assumed to be 100% of the rare gases and 0.1% of the ^{131}I present. Because the failure of the fuel plate would probably not expose all of the core material, and further because the canister leak would probably be from a relatively small hole, it is felt that these assumptions on activity release are conservative.

Based on the above assumptions, 0.006 Ci of ^{131}I, 2 Ci of ^{85}Kr, and 1 Ci of ^{131m}Xe could be released into a mine storage room (see Table 9.9). The storage room dimensions are 60 by 30 by 14 ft (a volume of 25,200 ft^3, or 7.1×10^8 cm^3). The ^{131}I concentration in this volume would be 8.4×10^{-6} $\mu Ci/cm^3$, the ^{85}Kr concentration would be 2.8×10^{-3} $\mu Ci/cm^3$, and the ^{131m}Xe would be 1.4×10^{-3} $\mu Ci/cm^3$, assuming the fission products are uniformly distributed throughout the air in the room.

The exposure doses from the assumed concentrations of ^{131}I, ^{85}Kr, and ^{131m}Xe were calculated using the following relationships.[10] Internal exposure to the thyroid due to inhalation of the ^{131}I was calculated from the relationship that 1 μCi of ^{131}I inhaled will deliver a dose of 1.48 rems to the thyroid, and the number of microcuries inhaled is determined by the following equation:

$$I = B\bar{Q}t\,, \tag{9.1}$$

where

I = the number of microcuries inhaled,

B = the breathing rate (assumed to be 5×10^{-4} m^3/sec),

$\bar{Q}$ = the average concentration in the room ($\mu Ci/m^3$), and

[10] T. J. Burnett, "Reactors, Hazard vs Power Level," *Nucl. Sci. Eng.* **2**, 382–93 (1957).

t = the time during which the inhalation took place (sec).

For the concentration of ^{131}I in the room (8.4×10^{-6} $\mu Ci/cm^3$), it was found that the maximum permissible exposure for a 13-week period (8 rems) would be received by the thyroid if the individual were to remain in the room for 21.3 min. Since the room would be evacuated when the release of ^{131}I is detected, only a small fraction of this dose would be received. If for any reason it is necessary to reenter the room, the time interval would be restricted to less than the 21 min. The dose to the thyroid received by an individual who is in the room for 1 min would be 375 millirems, which is below the allowable value for one week.

In the case of released fission product gases, the dose was calculated on the basis of the external whole-body exposure from submersion within the cloud using the following relationship:[10]

$$Z = 2.6 \times 10^{-7} E_s \bar{Q} t , \qquad (9.2)$$

where

Z = the submersion dose (rems),

E_s = the effective energy of the fission product radiation,

$\bar{Q}$ = the average concentration within the cloud ($\mu Ci/m^3$),

t = the exposure time (sec).

For the ^{85}Kr released (2.8×10^{-3} $\mu Ci/cm^3$, or $2.8 \times 10^{+3}$ $\mu Ci/m^3$) the submersion dose would be 10.5 millirems/min, and the allowable time in the room to accumulate 100 millirems would be 9.5 min. In the case of the ^{131m}Xe (concentration of $1.4 \times 10^{+3}$ $\mu Ci/m^3$) the submersion dose would be 3.5 millirems for each minute of exposure; this would allow a maximum of 28.7 min in the room to accumulate 100 millirems.

Therefore the release of activity from a type I accident in the mine would not produce conditions in the mine that could not be tolerated. Limits would have to be placed on the amount of time that could be spent in the room, but in the case of ^{131}I, after waiting eight days, the exposure time could be doubled because of decay of the radioiodine. The fission gases could be bled slowly out to the waste shaft without causing hazards in the mine or at the surface. If the type I accident were to occur in the waste shaft, the iodine would probably be trapped on the surface of the waste shaft (approximately 5000 ft^2 of metal surface), and the release of 3 Ci of ^{85}Kr and ^{131m}Xe to the atmosphere would not cause any greater hazards than those produced in the mine room.

9.7.2 Type II Accident (Maximum Credible Accident)

A type II accident is one in which the canister and the fuel assemblies are both extensively damaged at the same time. The exact causative agent for such an accident is not known, but it could result from dropping or some other type of impact. Due to the handling procedures and equipment design, this type of accident could only occur in the waste charging shaft. As a result the activity would be released to the atmosphere.

Depending on the amount of impact, varying degrees of damage to the fuel assemblies could result. However, it is assumed that the maximum amount of damage would be the rupture of one-half of the total number of fuel plates in the canister (19 plates ruptured). This assumption is thought to be very conservative because of the design and construction of the ETR assembly (basically a square with inner plates) and the fact that breaks in the plates would only expose a relatively small amount of the metallic alloy core material.

No information was available on the release of fission products from broken or damaged ETR fuel assemblies in air. Parker[11] estimated that considerably less than 1% of the ^{131}I would be released at temperatures below melting. For this study a release of 0.1% of the ^{131}I and 100% of the fission product gases was assumed. Based on these releases and the amount of fission products available in 19 fuel plates, the following quantities of radioactivity would be released: 39 Ci of ^{85}Kr, 21 Ci of ^{131m}Xe, and 0.11 Ci of ^{131}I. No cesium or strontium was assumed to be released, since melting would not occur.

The hazard associated with the release of the fission product activity to the atmosphere was calculated using Sutton's theory for an instantaneous point source. For this case at or near ground level the following relation can be used:[12]

$$\int x \, dt = \frac{2Q}{\pi C_y C_z \mu x^{2-n}} . \qquad (9.3)$$

[11] G. W. Parker, ORNL, personal communication (Sept. 1, 1965).

[12] J. R. Beattie, *An Assessment of Environmental Hazards from Fission Product Releases*, British Report AHSB (s) R. 64 (1963).

In this equation Q is the activity released, Ci; $\int x\,dt$ is the time integral of the concentration (x) expressed as Ci-sec/m^3; μ is the wind speed, m/sec; and C_y, C_z, and n are Sutton's parameters. Using the relationships between C_z and σ_z and between C_y and σ_y reported by Gifford,[13] the equation can be converted into

$$\int x\,dt = \frac{Q}{\pi\sigma_y\sigma_z\mu}, \tag{9.4}$$

where σ_y and σ_z are dispersion coefficients based on meteorological observations. Values of σ_y and σ_z are presented in Fig. 5.1 of ORNL-3441.[14]

For the case of inhalation exposure, the following relation was used:

$$I = B\int x\,dt\,, \tag{9.5}$$

where I is the activity inhaled, μCi; B is the breathing rate, m^3/sec; and $\int x\,dt$ is the time integral of the concentration (expressed as μCi-sec/m^3). The number of microcuries inhaled, I, was then used to calculate the exposure dose to the critical organ (see type I accident discussion). In this calculation the man was assumed to remain at a fixed point while the cloud passed.

Surface contamination resulting from cloud deposition was calculated using the formula

$$S = V_g\int x\,dt\,, \tag{9.6}$$

where S is the surface concentration, Ci/m^2, and V_g is the deposition velocity, m/sec (see ref. 14 for a more detailed description of V_g). When using the above formula, no reduction is made in the cloud concentration to allow for material that has already settled out of the cloud. As a result the ground concentrations reported will be larger than those that would actually occur. The value of V_g that was used to determine the ground concentration for ^{131}I was 0.01 m/sec.

External exposure doses received from the fission product gases in the over-passing cloud were calculated using the same procedure that was used for calculating the submersion dose in the mine room (type I accident). In the case of the atmospheric release, the quantity $\overline{Q}t$ was replaced with $\int x\,dt$ (time integral of the concentration).

Weather Bureau information for Wichita, Kansas (nearest station to Lyons, approximately 80 miles to the southeast), indicated that the average wind speed was 13 mph and that the prevailing direction was from the south. For this study, calculations for atmospheric release were performed using two meteorological categories: condition D (cloudy to partly cloudy with wind speed of 6 m/sec) and condition F (inversion with wind speed of 2 m/sec).

The results of the calculations of the ground contamination and inhalation dose due to the release of 0.11 Ci of ^{131}I to the atmosphere in a type II accident are presented in Figs. 9.9 and 9.10. Release of this activity on a cloudy or partly cloudy day with the average wind speed equal to 13 mph (a type D condition) would produce an inhalation dose of 125 millirems to an individual standing 100 m away (Fig. 9.10). This is considerably below the permissible dose

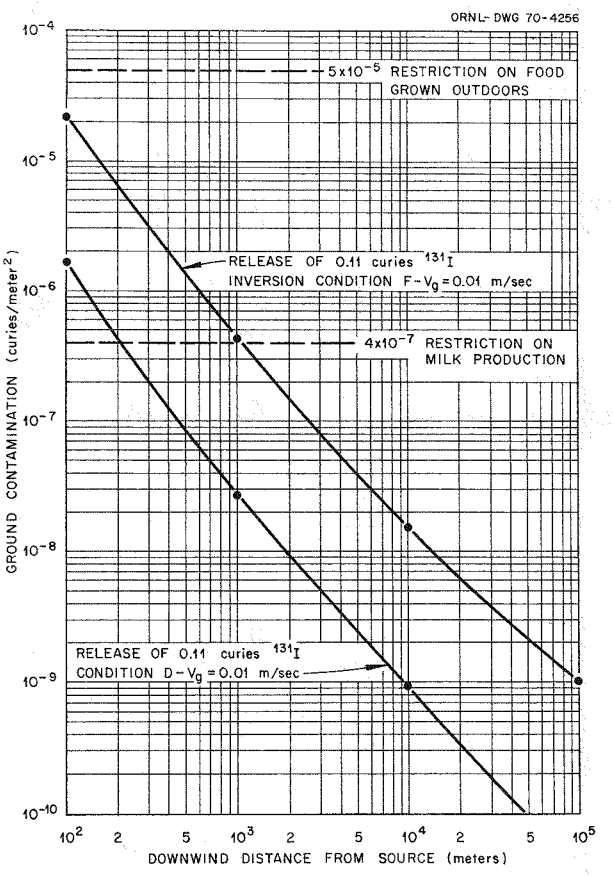


Fig. 9.9. Ground Contamination Resulting from Iodine Release – Type II Accident.

[13] F. A. Gifford, Jr., "Atmospheric Dispersion Calculations Using the Generalized Gaussian Plume Model," *Nucl. Safety* **2**, 56–59 (December 1960).

[14] C. E. Guthrie and J. P. Nichols, *Theoretical Possibilities and Consequences of Major Accidents in U^{235} and Pu^{239} Fuel Fabrication and Radioisotope Processing Plants*, ORNL-3441 (April 1964).

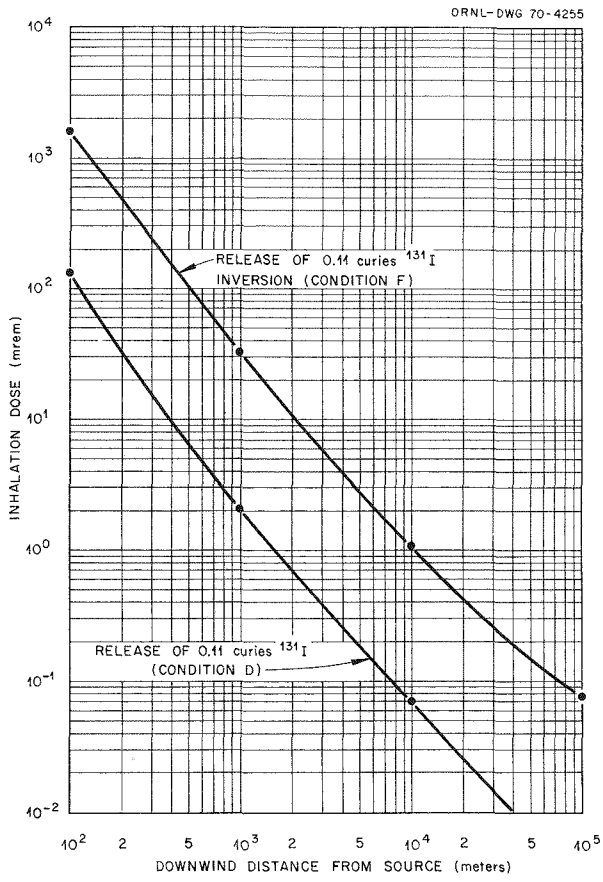


Fig. 9.10. Thyroid Dose at Various Distances from Source – Type II Accident.

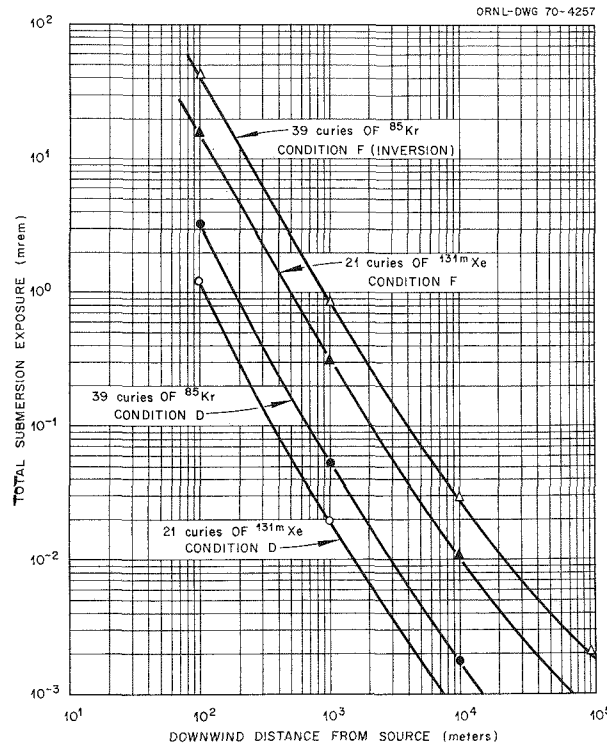


Fig. 9.11. Submersion Exposure from Released Fission Product Gases.

to the thyroid for a 13-week period. In the case of the inversion, dose to the thyroid would be 1.6 rems, which is below the permissible dose to the thyroid for a 13-week period. Figure 9.9 presents the data on ground contamination resulting from the release of radioiodine. For either of the assumed meteorological conditions there would be no restriction on food production at distances greater than 100 m. If the activity were released during an inversion condition, milk produced on land located less than 1050 m could not be consumed. However, the restriction on land from 100 to 1000 m could be lifted after about 30 days.

Exposures due to submersion in the ^{85}Kr and ^{131m}Xe released from the waste shaft are shown in Fig. 9.11. At 100 m, in the worst condition (an inversion) the total whole-body dose would be 42 millirems due to the ^{85}Kr and 16 millirems due to the ^{131m}Xe. Both of these dosages are within permissible limits.

Thus the release of the assumed fission products would not produce conditions at the surface which could not be handled. In fact, since the material would be released initially in the waste shaft, the time at which the material could be released to the atmosphere could be controlled, and as a result the optimum weather conditions (wind speed and meteorological condition) could be selected to result in minimum hazard conditions.

9.8 CONCLUSIONS

Two documents, one an evaluation of the Project Salt Vault shipping cask by W. F. Schaffer, Jr., and the other a hazards report on Project Salt Vault by W. J. Boegly, Jr., were the source for most of the material in this chapter. These documents were presented to the ORNL Radiochemical Plants Committee prior to a meeting of PSV personnel with the Committee on September 21, 1965. At this meeting the project was reviewed for conformance with ORNL radiation safety policy.

In a report to ORNL management, the Committee commended the PSV personnel for the thoroughness of their safety analysis and plans for operation, and recommended approval of the operation.

10. Operating Experience

F. M. Empson B. L. Houser

This chapter recounts the events of the operating period of the project. Although most of the results concerning temperature, rock deformation, off-gas, etc., and their analysis appear in Chap. 11, this chapter does contain some important "results" of the demonstration. These are related principally to the performance of and experience with the equipment for handling the fuel element canisters.

A schedule of the more significant activities during this period is given in Table 10.1. Various items in this table are discussed in the following sections, but not necessarily in chronological order.

10.1 MAIN RADIOACTIVE AND ELECTRICAL ARRAYS, ROOMS 1 AND 4

10.1.1 Operation Prior to Startup

A few days prior to startup of the array experiments in rooms 1 and 4, all of the experimental equipment was operated for a brief period at design levels of power input in order to make final adjustments and in general to shake down the various components.

For this shakedown all instruments were first read; then the radiation detection and off-gas systems were put into operation and checked. Power to the electrical heaters was then turned on (at a level of 1500 W per hole), and final checks were made of the multiple interlocks and alarm system. As soon as the "control temperature" thermocouples (located 9 ft below the floor and 1½ ft from the center lines of the holes) showed a noticeable temperature rise, in about 3 hr, the power was turned off. A period of about one day was allowed for cooling to ambient temperature before starting the experiment.

All components worked well during this period, with the exception of the off-gas tube heaters on the hole liners. These were plated-on heaters, and failure

Table 10.1. Schedule of Operation of Experiment

Nov. 15, 1965	Official startup; power turned on in rooms 1 and 4.
Nov. 17, 1965–Nov. 19, 1965	Fuel element canisters installed in room 1.
Dec. 1, 1965–April 19, 1966	Room 5 experimental equipment installed, hooked up, and checked out.
Mar. 8, 1966–Apr. 17, 1966	Roof bolt test in room 3.
Apr. 28, 1966–July 19, 1966	Install, torque, and retorque roof bolts throughout entire experimental area.
June 6, 1966	Room 5 startup (power on).
June 8, 1966–June 15, 1966	Changeout of fuel element canisters, room 1 to room 5; new canisters from Idaho into room 1.
June 22, 1966–Nov. 11, 1966	Operated modified pillar heater in hole 6, room 2.
Sept. 22, 1966–Jan. 6, 1967	Glass fiber insulation boards on floors of rooms 1, 4, and 5.
Oct. 11, 1966–Oct. 13, 1966	Fuel element canisters removed from room 5 for shipment to Idaho.
Oct. 31, 1966–Nov. 10, 1966	Changeout of fuel element canisters, room 1 to room 5; new canisters from Idaho into room 1.
Nov. 14, 1966	Start heated-pillar experiment; 33 kw power input.
Jan. 23, 1967	Increased power to array heaters in rooms 1, 4, and 5 by 40%.
Mar. 2, 1967–July 14, 1967	Intermittent work on installation and hookup of simulated waste can tests (SWCT).
July 17, 1967–Dec. 20, 1967	Operation of SWCT.
June 5, 1967	Termination of array experiment in room 5 (power off).
June 14, 1967	Termination of array experiments in rooms 1 and 4 (power off).
June 5, 1967–Jan. 31, 1968	Collection of cooldown data, dismantling inspection, and disposal of experimental equipment.
June 12, 1967–June 14, 1967	Fuel element canisters removed from room 5 for shipment to Idaho.
June 26, 1967–June 27, 1967	Fuel element canisters removed from room 1 for shipment to Idaho.
Oct. 9, 1967	Termination of pillar-heater experiment (power off).

occurred where the electrical leads were attached to the plating. Some of the tubes were replaced after failure, and others were not. These tube heaters were not operated during the experiment, since it was felt that the flow of heated air would maintain their temperature high enough to prevent moisture condensation until the air got up to the heated off-gas tubing in the trenches in the floor.

10.1.2 Official Startup

Since an initial period of intensive gage reading at the start of the experiment (involving 24-hr activity) was considered desirable, the array experiments were started and operated for the first two days using electrical heat only. At the end of this period, the fuel element canisters were installed. A special procedure for this startup was adopted as follows:

1. All rock mechanics gages and floor leveling pins were read.
2. All thermocouples were read, including those on recording instruments and those read with the portable pyrometer.
3. The radiation detection system and alarm system were placed in operation and checked for function.
4. The air annulus off-gas system was placed in operation and left on. This included the tube-bundle heaters.
5. The off-gas was checked for chlorine content.
6. The array power trip circuitry was checked for operability.
7. All array holes were calipered.
8. Power supplies were checked for 230-V output, and the array hole heaters were placed in operation at 1500 W per hole.
9. The dosimeter holder was tested by inserting it into the slanting dosimeter holes.
10. Temperatures were read at intervals of 1, 2, 4, 8, and 16 hr after the startup, then twice the second day, then daily for the first two weeks.
11. Rock mechanics gages and floor leveling pins were read, and holes were calipered twice during the first week of operation as permitted by other activities.

10.2 CANISTER HANDLING

On the third day following startup, the first fuel element canisters were transferred from the shipping cask to the main radioactive array in room 1. This transfer and the others discussed below were carried out using the detailed procedure and checklist included as Appendix 10A. This procedure included removal of the canisters from the erected shipping cask through to their final placement in an array hole.

Handling of the canisters required a crew of 8 to 11 people, depending on which phase of the transfer procedure was being carried out. The full complement of personnel included:

1. General supervisor – responsible for the entire operation and in continuous communication with both the waste charging facility and the underground;
2. At topside waste charging facility:
   a) Supervisor in charge of operations,
   b) Hoist operator,
   c) Health physics surveyor,
   d) Helper;
3. At mine level:
   a) Mine level supervisor in charge of underground operations,
   b) Transporter operator and helper,
   c) Health physics surveyor,
   d) Two additional helpers to open and close holes and control the movement of other personnel not involved in the transfer.

At various times the same person performed the duties of two. For example, the general supervisor was frequently the underground supervisor as well, and the hoist operator usually acted as health physics surveyor at the topside waste charging facility.

10.2.1 First Canister Handling

The first handling of fuel element canisters consisted in receiving the fully loaded shipping cask from Idaho and transferring the seven canisters into the room 1 array. This was accomplished over a three-day period. The electrical heaters on each individual liner were turned off while the hole was opened and, upon completion of the transfer, restarted at a reduced level so that total thermal power (electrical plus radioactive decay) was maintained at 1500 W. All seven canisters were transferred without difficulty except for one in position 7 of the shipping cask, which stuck slightly in the cask, apparently due to a small piece of tape on its outside surface.

10.2.2 Changeout of Canisters, June 1966

Equipment in experimental room 5 was identical to that in room 1 and was started in the same way.

Following the various checks, all systems were turned on temporarily for shakedown. After allowing a period for all temperatures to return to ambient, the experiment was started (June 6, 1966) and closely monitored for two days. During the next two days the seven canisters from room 1 were moved to room 5 using the last portion of the checklist (Appendix 10A) and a slightly modified inverted procedure for the placement portion of the operation.

The lower liner section of the center hole in room 1 was pulled for inspection and found to be in very good shape. This was after six months of operation at temperatures approaching 200°C. There appeared to be no corrosion of the liner but a considerable deposit of fine white salt crystals on the side of the hole. No residual radioactivity was found on any of the liners in room 1.

By this time the shipping cask, containing seven canisters with fresh fuel elements, had arrived and was erected over the waste shaft. These canisters were transferred to the room 1 array using the same procedure as that used for the first canister handling operations. The only difficulty experienced was with the fuel element thermocouple leads. These leads are wound around a small spool at the top of the canister and must be unwound and retrieved manually after the canister is in place but before the scatter shield is installed. In several cases these leads could be retrieved only with difficulty, and in one case only one pair (of four) could be retrieved. The time required for this work in the radiation field at and in the upper liner produced the highest radiation doses experienced in the entire operation (see Sect. 10.2.5).

10.2.3 Changeout of Canisters, November 1966

This changeout of fuel element canisters was carried out in a manner somewhat different than the original plans. These plans called for receiving the full shipping cask and moving new ones to room 1, those in room 1 to room 5, and those in room 5 back up the waste shaft and into the shipping cask (see Fig. 9.7). Instead the original canisters, which had been in the mine a year and in the room 5 array for the last six months, were removed and returned to Idaho. There canisters containing new fuel elements were loaded into the shipping cask, and it then was returned to Lyons. In the meantime the canisters in room 1 were moved to the then empty holes in room 5. (This eliminated the need for the storage hole shown in Fig. 9.7.) When the new canisters were received, they were installed in the array holes in room 1. All of these transfers were carried out using the appropriate procedure and checklists. Minor difficulties were experienced with the hydraulic system of the underground transporter. This was corrected during the period following the changeout.

10.2.4 Removal of Fuel Element Canisters

Although initial plans called for four sets of fuel element canisters and continuous operation for two years, the design objective of 10^9 rads peak dose to the salt in room 1 was attained with only three sets of canisters and operation for about 19 months. Therefore, it was decided to terminate this portion of the demonstration experiment. Electrical power to rooms 1, 4, and 5 was turned off on June 5, 1967. (See Sect. 10.6 for discussion of operation during this "cooling period.")

Commencing a week after power shutoff, the fuel element canisters were removed from room 5, loaded into the shipping cask, and returned to Idaho. The cask was returned to Lyons empty, and the canisters were removed from room 1 on June 26 and 27, 1967. These transfers were completed without incident.

10.2.5 Results of Canister Handling Operations

Over the 19-month course of this part of the project, 21 canisters containing about 200,000 Ci of activity each (when received at the mine) were handled, 14 of them on three occasions and the other 7 twice. All handling operations were completed without incident and with only very minor mechanical problems. Quarterly radiation doses to the personnel in Kansas exceeded 50 mrem only during the one period when difficulties (described above) were experienced with retrieval of the thermocouple leads. This was in spite of the fact that all of the transfers were accomplished without the aid of hot cells. One of the major objectives of the demonstration experiment was to demonstrate the techniques and equipment for handling waste containers in an underground environment. Project Salt Vault experience toward achieving this objective can be considered an unqualified success.

10.3 PILLAR-HEATER EXPERIMENT

The second major experiment in Project Salt Vault was the extensive heating of the small pillar between rooms 2 and 3 in the experimental area. This was accomplished with 22 heaters in the floor along the two sides of the pillar. Two of these heaters, the "modified pillar heaters," were also involved in a subsidiary experiment described in Sect. 10.5.4.

Startup of the pillar-heater experiment (November 14, 1966) was much simpler than the arrays experiment. Startup procedure consisted in reading all gages, roof-bolt load cells, and thermocouples for background; turning on the power at 1500 W each or a total of 33 kW; and reading these instruments at fairly frequent intervals during the early period of rapid heating. Other aspects of the experiment are discussed in sections that follow.

10.4 ROUTINE OPERATIONS

During the operation phase of the experiment, and not counting startup, cooldown, and canister changeout periods, activities of the seven-man underground operating crew were about equally divided between routine scheduled activities and nonroutine special items. These nonroutine activities are discussed in the next section.

10.4.1 Data Collection

The reading and recording of data from the many gages and instruments throughout the experimental area and elsewhere in the mine constituted one of the major activities of Project Salt Vault. After initial periods, when rates of change stabilized at nearly constant levels, it was possible to schedule these readings by taking into account the sensitivity of the instrument, the importance of the measurement, and the expected rate of change. The routine readings and their approximate frequency are given below:

1. Experimental area rock deformation instruments (410 gages), read every other week.
2. Old workings rock deformation instruments (119 gages), read every other week.
3. Recorded thermocouple temperatures read from chart (390 points), read twice weekly.
4. Manually read thermocouples (160 points), read twice weekly.
5. Floor uplift points by leveling, including a level traverse brought in from bench marks outside the experimental area (262 points), read every other week.
6. Calipering of the annulus between the lower liners and the wall of the holes in the array rooms (about 35 measurements), read every other week.
7. Sample of gas from each array hole tested for chlorine (21 measurements), made weekly.
8. Electric power levels checked, recorded, and adjusted, weekly, if necessary.
9. Dosimeter measurements in two holes in room 1 and one in room 5, two or three times during each six-month period.

10.4.2 Alarm System

Throughout the radioactive portion of the experiment no releases of activity occurred. However, alarms due to malfunctions of the system were such a regular (but unscheduled) occurrence that discussion of the system's deficiencies is considered worthwhile.

During the 19-month period, a total of 20 alarms occurred which required trips into the mine during off-duty hours, and at least nine additional alarms required trips to the mine office or the sheriff's office. Nearly all these false alarms were due to one of two types of malfunction: (1) extreme sensitivity of the system to minor variations in line voltage and (2) failure of a transistorized input module in the count rate meter. In the first type, any temporary drop in line voltage, which might only cause the lights to dim briefly, usually resulted in activation of one or more alarms by tripping the relays within the Tel-Alarm units. In some cases, all alarms at the mine surface unit would be activated but would clear when reset. Usually, however, either the radiation alarm or the high-temperature alarm in addition to the power failure alarm would have to be reset at the underground panel. In the second type of malfunction, trouble in the count rate meter would nearly always cause a false radiation alarm. The transistorized module in the input circuit of the rate meter was the usual source of the trouble. Typically these plug-in units failed within two or three months, although many failed in a much shorter period.

10.4.3 Servicing

In addition to routine servicing and maintenance of the experimental equipment and instruments which do not justify detailed discussion, there were several items of routine servicing which were related to the more unusual aspects of this demonstration experiment. The first of these was the servicing of ordinary mine equipment, which was necessary because the experiment was conducted 1000 ft underground. This included twice-monthly checks of the hoisting equipment and its associated safety devices, and weekly servicing of the mine lamps carried by the underground crew. The second was the routine scaling of the roof and walls in all regularly traveled portions of the mine. Here, it should be mentioned that the thermally accelerated deformation of the center (heated) pillar in the experimental area required extensive scaling of the pillar after

about six months of operation – much earlier than would have been expected under ordinary mining conditions. The third item was the monthly servicing and "exercising" of the underground transporter.

10.5 NONROUTINE ACTIVITIES

Nonroutine activities during the operational period included relatively small subsidiary experiments which were either planned beforehand or added to the experimental plan in order to elucidate other results, or unexpected activities resulting from the operation of the experiment. The first of these was the installation of the experimental equipment in room 5. This was identical to the installation in room 1 but was carried out after the startup.

10.5.1 Roof Bolting Program

The roof condition which made the roof bolt program necessary is described in Sect. 11.4.5.6, along with the sequence of operations.

The trial installation of 37 roof bolts in room 3 was carried out by the regular mine crew. Later, when the decision was made to proceed with the installation of roof bolts throughout the experimental area, arrangements were made to secure a separate three-man crew for this work. They performed the drilling, bolt installation, and torquing. Retorquing subsequent to that performed during the two-month bolt installation period was again done by the regular mine crew.

Approximately 1600 bolts of high-strength steel 4 ft long by $\frac{3}{4}$ in. diameter were installed on 4-ft centers in a triangular pattern. The first 100 bolts were manufactured by Bethlehem Steel Company and the remainder by Armco Steel Corporation. The bolts were identical except for differences in the bolt head and bearing plate design. The former 100 used a domed plate and washer, while the latter used a bearing plate with a washer surface pressed in. It was found to be desirable to grease the surfaces between the bearing plate and the bolt head. This lubrication made it possible to secure the desired bolt loading at a torque of 125 to 150 ft-lb. Bethlehem type K-3 expansion shell anchors were used on all bolts.

Three dozen load cells were installed under selected bolt heads with leads running to a central location in each room. Some preliminary testing as to the desirable length of leads to minimize stray pickup of noise resulting from proximity to power lines was also performed. It was determined that the lead cable should be no longer than 40 ft for tolerable readings and that service lines affected the readings very little. Two instruments, Baldwin-Lima-Hamilton SR4 type N and type 120C strain gage indicators, were used for simultaneous readings until sufficient data were accumulated for correlation of the instruments. The type 120C was continued in use and the type N discarded.

Soon after installation and after several load cell readings had been taken, U.S. Bureau of Mines personnel checked the bolts for load-carrying capacities. They reported that the bolts would elongate at 20,000 lb load and pull from the shell anchorage at 24,000 lb.

10.5.2 Condensate Collection

Several special experiments were carried out in an effort to accurately measure the rate at which moisture was entering the array holes due to the migration of brine inclusions in the salt (see Sect. 11.2). The difficulty with these measurements was due to the moisture already in the mine air (40 to 60% relative humidity) and the low rate of moisture production from the salt in the array holes. These special experiments included the use of Drierite columns in the off-gas lines; cold traps using ice and brine, dry ice, and liquid nitrogen; and one series of experiments (the most successful) where dry nitrogen gas was swept through the hole and off-gas system.

10.5.3 Correction of Heat Losses

One objective of the array experiments was to heat the largest possible volume of salt to a temperature approaching 200°C without running the risk of developing excessive temperatures within the fuel elements. After about six months of operation of the arrays, it was determined that heat losses from the floor of the array rooms were sufficient to appreciably distort the isotherms (see Sect. 11.3). To reduce these heat losses to the ventilation air and thus increase the peak salt temperature, leveled areas around the arrays in rooms 1, 4, and 5 were covered with 1-in.-thick glass fiber insulation boards, beginning September 22, 1966. By December it was obvious that these measures were ineffective in increasing the peak temperature, although temperatures in the upper half of the array were increased. Therefore, the glass fiber insulation was removed, and on January 23, 1967, the total power (electrical and decay) to all three arrays was increased by 40% (from 1500 to 2100 W per hole). The effects of this increase in power will be seen in all the temperature results and most of the rock deformation measurements discussed in the next chapter. (This power boost achieved the desired effects.)

10.5.4 Materials Testing

The "modified pillar heater" portion of the experiment was included to comparatively evaluate the qualities of stainless steel and carbon steel as waste container materials when in contact with salt at elevated temperatures. When the stainless steel heater assembly lost pressure after several months operation, this portion of the experiment was expanded by the addition of the "simulated waste container test" (SWCT). Operation of these two experiments is discussed below.

10.5.4.1 Modified Pillar Heater Test. – The two modified pillar heaters (see Sect 7.6.2) were of identical design except that one was carbon steel while the other was 304L stainless steel.

The carbon steel modified pillar heater in room 2 was started on June 22, 1966, at a nominal power of 3 kW (the recorder indicated 2.8 kW) and operated until termination of the heated-pillar test on October 9, 1967. Power input was reduced to 1.5 kW on November 14, 1966, when the heated-pillar test was started. The pressurized system remained tight throughout the test period. The hole was backfilled with crushed salt around and over the heater in the same way as in an actual disposal operation. When the heater was removed from the hole, the surfaces exposed to the salt were covered with a general coating of rust.

The second modified pillar heater, fabricated of 304L stainless steel, was started on November 14, 1966, along with the other 20 open pillar heaters. This heater lost pressure in about three months, although the heating elements did not fail. The heater functioned satisfactorily for the duration of the test. When this heater was removed from the hole, the pressure loss was found to be due to severe corrosion of the $\frac{1}{2}$-in. sched 40 pipe connecting the pressurized section of the heater. The heater container itself was still pressure tight, although metallurgical examination of the can revealed that stress corrosion cracking had penetrated about half the wall thickness.

10.5.4.2 Simulated Waste Container Test (SWCT). – The objective of this test was to obtain additional data on the effect of moisture on stainless steel and carbon steel containers in the relatively pure salt in the floor of the experimental area and in the interbedded salt and shale in the original mine floor. The test utilized six heaters, three of 304L stainless steel and three of carbon steel. Two of each, containing two heating elements, were located in the original mine floor in a square array of 10-in.-diam by 12-ft-deep holes about 50 ft from the room 5 (floor) array. One of each containing three heating elements was located in the corridor of the experimental area near the electrical (room 4) array. These heaters were fabricated of 6-in. sched 40 pipe, with electrical heaters installed in a sealed section about 6 ft long. An open extension of the heater can, equipped with a gasketed cover plate, served as a terminal box for heater leads, which were conducted to the floor through a plastic tube. A pressure connection was made to the floor level through a $\frac{1}{4}$-in. steel tube.

The two heaters in the corridor of the experimental area were located in similar holes with the bottom 12 ft below the floor. Those in the original mine floor were located approximately 1 ft higher in order to place the center of the heated section at the same elevation as a major shale seam. The holes were backfilled with crushed salt after placing the heaters.

Design of the SWCT called for a power input of 4.3 kW per can, with a possible increase of the power in the two experimental area cans to 8 kW per can. It was expected that 4.3 kW would give a temperature of about 200°C after several months for the wall of the hole in which the can was located. However, it was not possible to follow through on this design because of difficulty with the heaters. The main difficulty was loss of heaters due to shorting or failure of heater terminals resulting from leakage of moisture into the enclosed, but not sealed, end section containing the terminals. In addition, leaks occurred in the pressure connections to the floor, and some thermocouples malfunctioned.

In the experimental area the salt wall temperature for the mild steel heater reached approximately 200°C before one heater element failed after about 100 hr operation. A second heater failed during the course of the test, leaving only one in operation. All elements in the stainless steel heater continued in operation throughout the test. The can reached a maximum temperature of about 320°C and a salt wall temperature of 240°C before leveling off at about 220°C can wall temperature and 190°C salt temperature.

The four heaters in the original mine floor operated even more erratically. Both stainless steel heaters failed within two months of startup and only one of the two elements in one of the other two heaters remained in operation to the end of the test (after about five months). Again heater failures were due to corrosion from water leakage into the terminal housing or to mechanical failure of connections. Maximum can temperatures were in the range of 360 to 400°C; maximum salt wall temperatures were 245 to 300°C.

10.6 POWER SHUTOFF, COOLDOWN, AND CLOSEOUT

Special procedures were adopted for obtaining frequent readings on both the thermocouple network and the rock mechanics instruments during the rapid cooling period following power shutoff of the major experiments. For both the arrays and pillar heating experiments, this procedure included reading all instruments immediately prior to shutoff; reading temperatures at 1, 2, 4, 8, and 16 hr, followed by daily readings for about a week; and reading rock deformation gages, floor leveling, roof-bolt load cells, etc., as frequently as possible but at least every other day for the first week. This accelerated reading schedule was followed for only one week, and readings thereafter reverted to the regular operating schedule.

10.6.1 Dismantling, Inspection, and Disposal of Experimental Equipment

Dismantling of equipment began as soon as possible after termination of each part of the demonstration. In some cases it was necessary to make modifications in order to continue other experiments. For example, after the array operation ceased, wiring was changed to utilize the regulated power supply and the watt-hour meter from one array to power the SWCT array in the original mine floor. The remainder of the array equipment was available for disassembly. As cooling continued, off-gas and radiation monitoring equipment was removed. Other facilities were likewise removed upon completion of the pillar heater experiment and the SWCT. A major portion of the service lines and some equipment were left installed and on a standby basis primarily for lighting and ventilation of the mine. Data taking and maintenance services continued on a routine, but less frequent, basis. A portion of the dismantled equipment and materials was declared surplus and sold after removal from the mine.

Inspection of facilities involved liners from array holes, the salt wall of the holes, pillar heaters, and, in particular, the two modified heaters and the simulated waste container cans. The liners and holes used for the radioactive arrays were checked for contamination, cleaned, and inspected for deterioration – corrosion, pitting, discoloration, plastic flow, recrystallization, or other physical changes. The simulated waste container cans were given the same inspection except for cleaning and checking for contamination. The pillar heaters were similarly inspected, and three regular pillar heaters, two modified pillar heaters, and four simulated waste container heaters were returned to ORNL for thorough inspection and analysis (see Sect. 10.6.2).

Removal of the heaters and SWCT cans was most difficult. A redrilling around the modified heaters and SWCT cans was necessary, and additional dissolution of salt in the lower section of the holes (using fresh water) to relieve them from their original test hole was effective.

10.6.2 Metallurgical Examination of Pillar and SWCT Heaters

Examination of the modified pillar heaters and of the SWCT heaters revealed gross cracking both in the 304L stainless steel pillar heater (operated in the pure salt of the experimental area) and in one of the 304L SWCT heaters.[1] Also, the 304L $\frac{3}{4}$- and $\frac{1}{4}$-in. pipes used on the modified pillar heater as electrical conduit and for a pressure connection to the floor were severely corroded. The cracking and severe corrosion were in those parts of the heaters which were cooler and on which water may have condensed. Figure 10.1 shows the crack in the cold section of the modified pillar heater. A similar crack was observed in one of the SWCT heaters. The lower section of the heater, to the left of the weld in the picture, and the similar section of the SWCT were pressurized with air during the investigation and showed no loss of pressure in more than 72 hr. Metallographic examination of the 304L stainless steel modified pillar heater revealed the cracking to be due to stress corrosion. Transgranular cracks were found in a metallographic sample removed from the center of the sealed heated portion of the heater assembly as well as in the cool portion. Although the sealed heated portion had held air pressure, more than half of the wall thickness was penetrated by the cracks. Also, pits as great as 0.14 mm (Fig. 10.2) deep were observed at the center of the heated portion. Figure 10.3 shows a stress corrosion crack penetrating about half the wall thickness.

Metallographic examination of the carbon steel modified pillar heater showed a corroded outer surface but no evidence of penetration. There was apparently little, if any, loss of wall thickness to corrosion. Measurement of a section taken 40 in. below the top of the sealed heated portion indicated a thickness of 0.239 in. as compared with a nominal wall thickness of 0.237 in. for 4-in. sched 40 pipe.

---

[1] T. M. Kegley and F. M. Empson, *Examination of Modified Pillar and Simulated Waste Container Test Heaters,* ORNL-TM-2422 (January 1969).

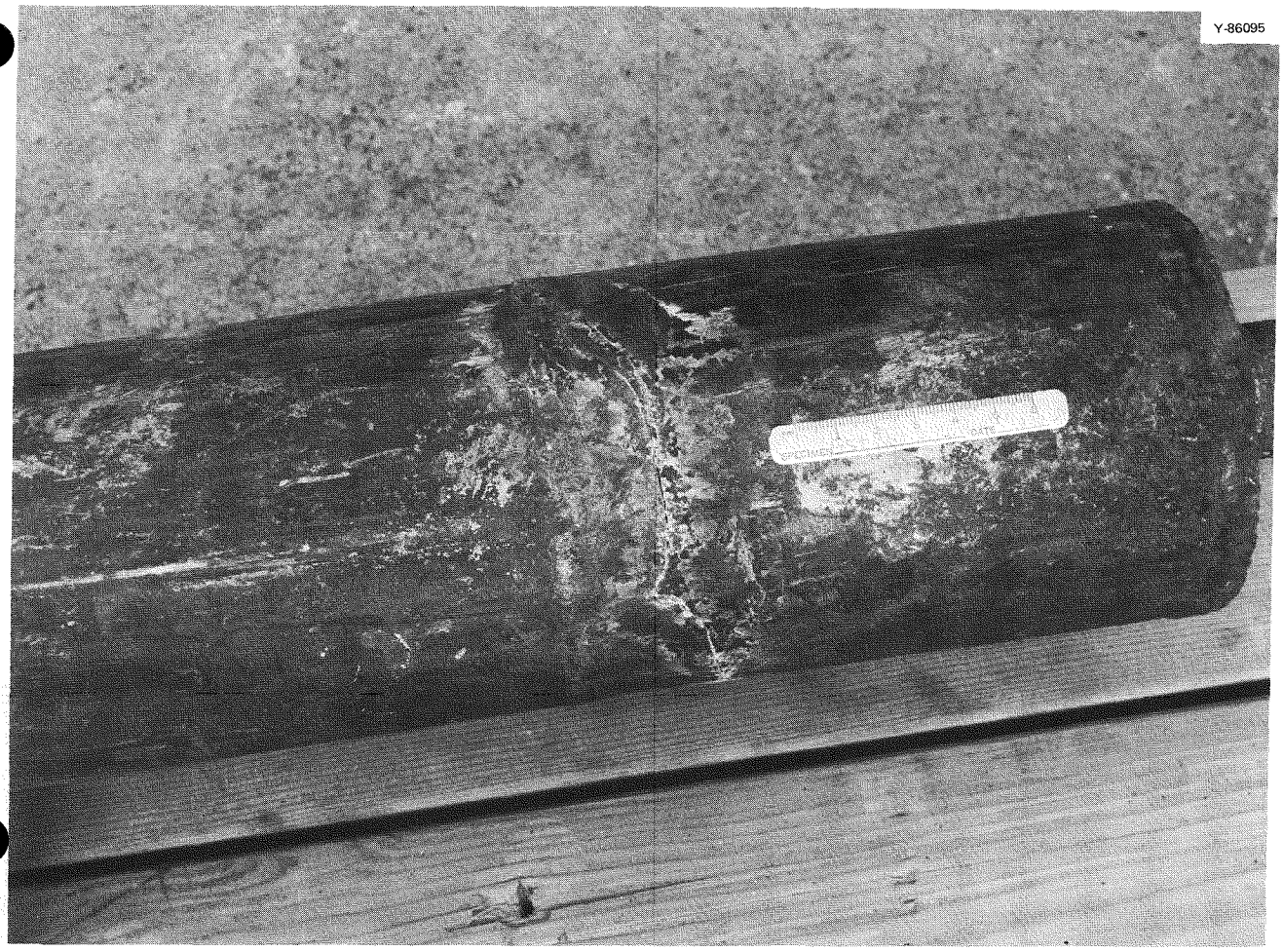


Fig. 10.1. Crack in the Cold Section of the Stainless Steel Modified Pillar Heater.

Metallographic examination of the 304L stainless steel SWCT heater from the original mine floor also revealed transgranular stress corrosion cracks. The sample of the heated portion taken 2 ft below the top of the heated section contained cracks penetrating half of the wall thickness and pits as great as 0.4 mm deep. Cracks almost completely penetrating the wall were found in the pressurized section near the cool end of the heater.

Figure 10.4 shows some of the cracks that occurred in the heated section of the stainless steel SWCT in the original floor. Two cracks may be seen partially penetrating the 0.280-in. wall thickness of the heater.

Five conditions must be satisfied for stress corrosion to occur in austenitic stainless steel:[2]

1. The steel must be in a state of tensile stress.
2. Liquid-phase water must be present.
3. An elevated temperature is necessary. The minimum temperature is frequently stated to be 50°C.
4. The water must contain chlorides.
5. Oxygen must be present. Concentrations on the order of parts per million are sufficient.

All the above conditions existed in the experimental operation of the modified pillar heaters and the SWCT heaters. The first condition is always present in practice, since stainless steel parts are stressed in some way during fabrication. The second condition will probably occur during either the heating or cooling part of the operation. The third, fourth, and fifth conditions are inherent in the waste-disposal operation and are unavoidable (see Sect. 11.2.3). The second condition,

[2]T. Marshall, *Corrosion* **14**, 61 (March 1958).



Fig. 10.2. Corrosion Pits 0.14 mm Deep at the Center of the Heated Portion of the 304L Stainless Steel Modified Pillar Heater.

presence of a liquid water phase, may have been the principal factor in the occurrence of stress corrosion in the modified pillar heater and the SWCT heaters.

10.7 SUMMARY

In general, the operational phase of the Project Salt Vault experiment was successfully completed, with many minor problems but without anything even approaching the major difficulties which could have been expected in an experiment of this size and complexity. The demonstration of the canister handling equipment and techniques was especially successful.

The operational period covered in this chapter, including the dismantling and removal of most of the experimental equipment, ran from November 15, 1965, to January 31, 1968. Throughout this period, the underground operating crew consisted of seven men including two resident supervisors from ORNL. Supplementary personnel from ORNL, including a health physics surveyor, were employed at all of the canister changeout periods. Three additional men were used in roof bolt installation.

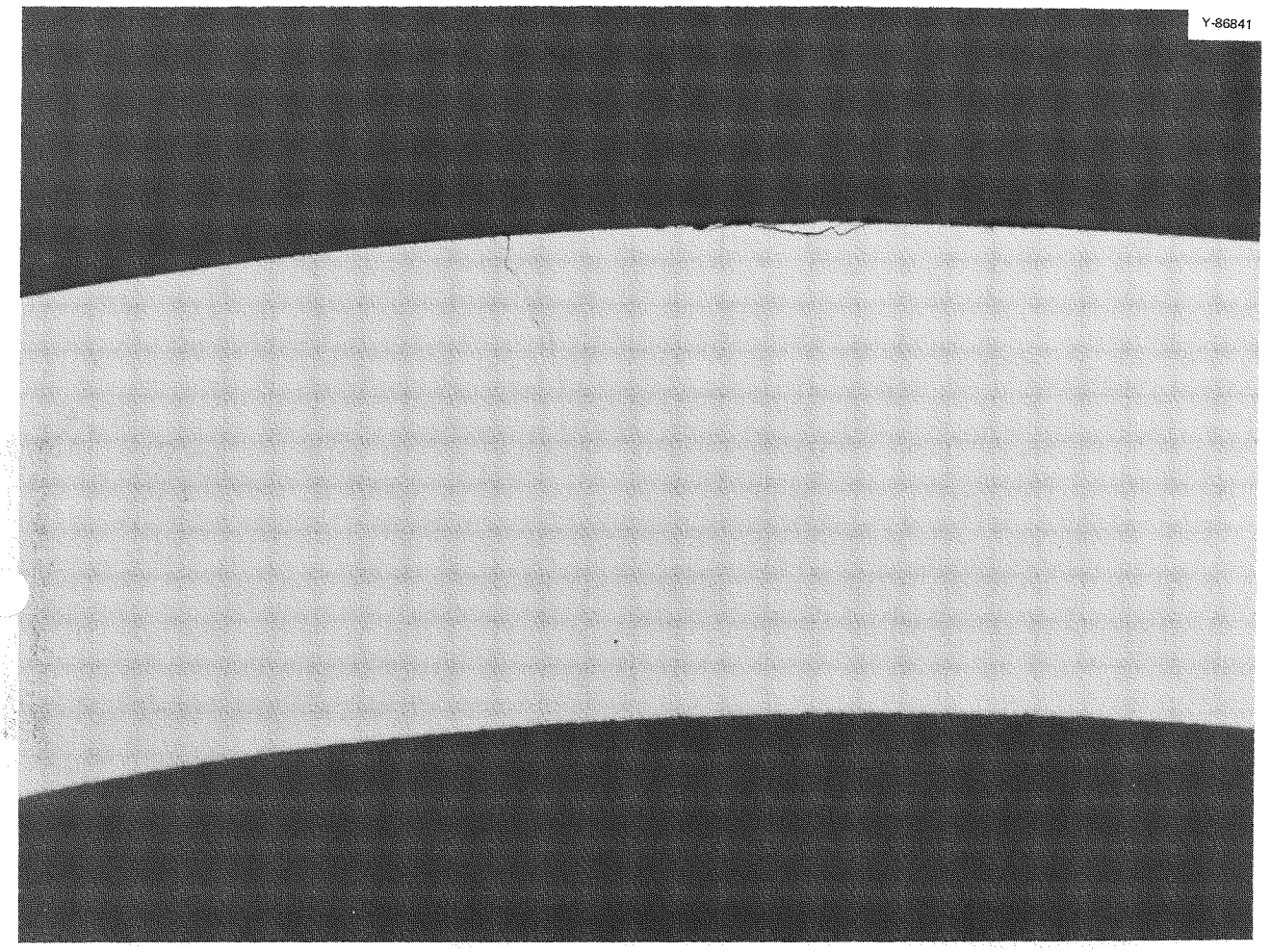


Fig. 10.3. Stress Corrosion Cracking, with Penetration About Half the Wall Thickness of the Stainless Steel Modified Pillar Heater.

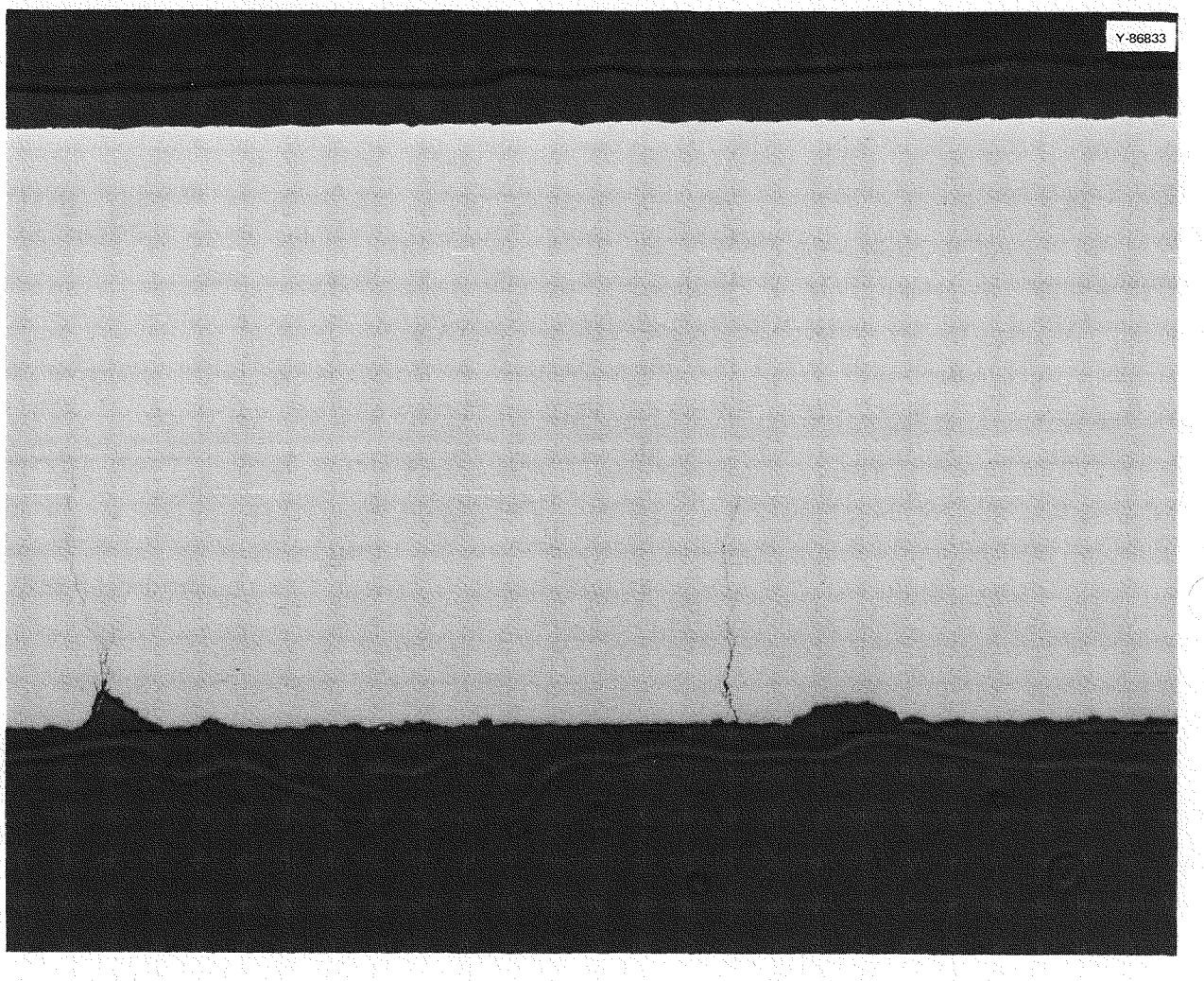


Fig. 10.4. Stress Corrosion Cracks in the Heated Section of the Stainless Steel SWCT Heater Operated in the Original Mine Floor.

APPENDIX 10A. Operating Procedures for Project Sault Vault, Revision 0

Prepared by W. F. Schaffer, Jr.
Chemical Technology Division

October 1, 1965
Revised October 20, 1965
Second Revision, May 12, 1966
Third Revision, July 28, 1966

Canister Position Color Code

W = White

R = Red

B = Blue

G = Green

Y = Yellow

W - 2 in. Band Close Loading Shield

WRWR - Upper Limit Switch AMB → Red

WY - Bottom Limit Switch AMB → Red

Red Light On - Door Open

WGWG - Can out of Guidance Tube

R - 8 ft Long Band - Can in Shaft

Y - Band at 100, 200, 300, 400 ft Down Shaft

BYB - 500 ft Down Shaft

B - Band at 600, 700, 800, 900 ft Down Shaft

R - 10 ft Long - 10 ft Above Top of Funnel

W - 2 in. Band Following R Band - Top of Funnel

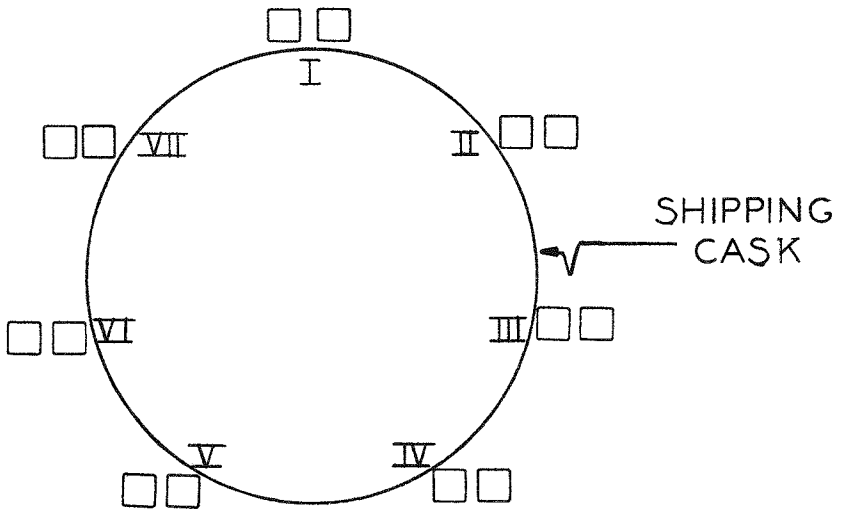
G - Transporter Shield Upper Limit Switch

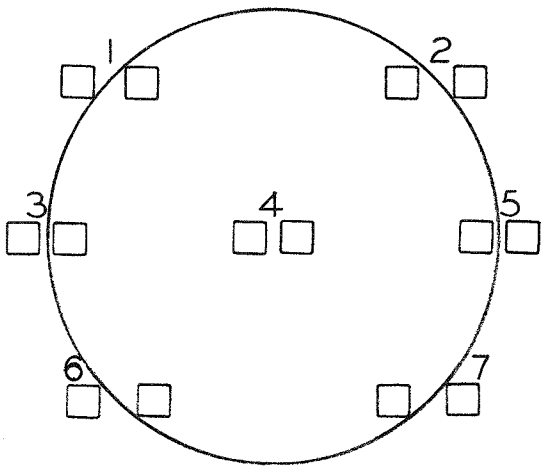
GY - Transporter Shield Lower Limit Switch

W - 2 in. Band { Bottom of Band - On Door Shield
Top of Band + 2 in. Slack for Door Closure

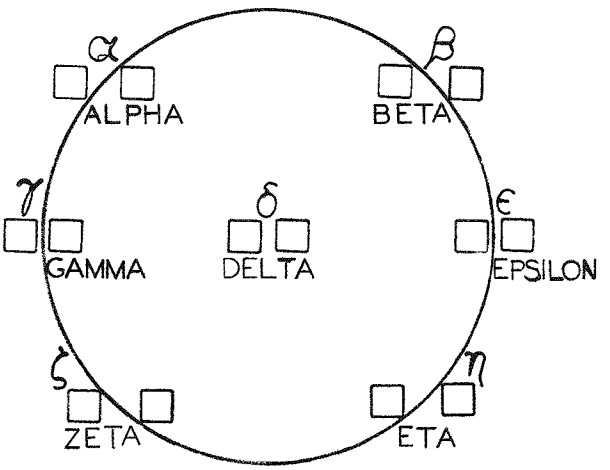
Y - +2 ft Mark

WY - +18 ft





MAIN ARRAY



FLOOR ARRAY

1. Show position at each time.

2. Numbers are position holes.

3. Canisters have Roman numbers plus subscripts 1, 2, 3, and 4 for each of the changeouts respectively.

4. Left space is for condition at beginning of transfer, right space for position at end of transfer.

A. WASTE CHARGING FACILITY - PREOPERATIONAL CHECK

Supervisor _____ Date _____
Surveyor _____
Other _____
_____
_____

		Initial Below
1.	Check the operating area for surface contamination.	
	Clean if necessary	
2.	Clean the operating area free of mud, dirt, waste paper, and other trash.	
3.	Repaint the area proximate to waste charging shaft as necessary to prepare area for possible future decontamination.	
4.	Check the condition of the hoist controls and cable, slip clutch, sheave wheel, footage counter, counter-weight, connector, and canister handling tool.	
5.	Lubricate hoist and sheave wheel.	
	Repair or replace the defective components.	
6.	Check the condition and operation of the waste shaft ventilation system.	
	Lubricate fan and motor bearings.	
7.	Remove the locks and cover from the waste charging shaft.	
8.	Install guidance tube in waste shaft.	
9.	Remove the pipe cap cover on the pipe sleeve for the guidance tube safety door control shaft.	
	Install safety door control shaft.	
	Check the operation of the cask-charging door control.	
	Check the operation of the three limit switches in the guidance tube and monitoring lights on panel.	
10.	Turn the operating lever to open guidance tube safety door.	

W = White G = Green
R = Red Y = Yellow
B = Blue

	Initial Below
11. Check the operation of the hoist using the dummy canister as a load.	
Using the INCH speed control of the hoist lower the dummy load into the guidance tube and observe monitoring lights.	
Lower dummy load to mine level, testing both the SLOW and FAST SPEED operation.	
Check condition of the cable during hoisting operation.	
Check on the condition of the color coding on the cable.	
Repair color coding as necessary.	
Return the dummy load to surface using footage indicator and color coding to determine the position of the load at all times.	
Use the INCH speed for reentry into the guidance tube.	
Make note of all defects or malfunctions in the system.	
Initiate the steps necessary for repair.	
Recheck the complete system if any repairs have been made.	
12. Check cask pivot lugs for damage or excessive wear.	
13. Replace waste charging shaft cover and locks.	
Remove control shaft for the guidance tube safety door, and replace pipe cap cover.	

SHIPPING CASK - OPERATIONS AFTER ARRIVAL IN LYONS

Supervisor _____ Date _____
Surveyor _____
Other _____
_____
_____

	Initial or Record Data - Time
1. Examine shipment for damage en route; Check cask and tool box seals.	
2. Examine driver's record (log book) of shipment en route to determine if any unusual conditions were encountered which might affect the integrity of the shipment.	
Record temperatures of the two cask dial thermometers.	
Record temperatures indicated by the three thermocouples in the cab (tractor) monitor.	
Examine the cooling system for leaks.	
Record flow through the cask.	
Refuel diesel at this time if necessary; record fuel consumption.	
3. Check cask for external contamination; record results of smears.	
Record external radiation readings.	
4. If the shipment is determined to be in good condition after making the preceding checks, move tractor and trailer to the waste charging area and spot trailer in position for unloading the cask from the trailer.	

	Initial or Record Data - Time
5. Spot crane in position for unloading the cask from the trailer.	
6. Remove the eight shipping-frame-trailer securing nuts and bolts. (As soon as practical all nuts and bolts should be examined carefully for any wear or damage. Cotter keys should be discarded and replaced by a new set for the return shipment. Any questionable nuts and bolts should also be replaced.)	
7. Attach sling between the crane and the cask.	
8. Unlock and remove the waste shaft cover.	
Install safety door control shaft.	
9. Remove fire retardant front panel.	
Remove the two shield door securing bolts.	
10. Disconnect the water cooling lines from the cask. (Diesel should be kept in operation.) ATTACH DISCONNECTS WITH PRESSURE RELIEF VALVES TO BOTH THE INLET AND OUTLET COOLANT NOZZLES.	
11. Lift the cask and shipping rack to clear the trailer, and lower and swing into position to engage the pivot pins on the waste shaft pad.	
12. Relocate trailer to position adjacent to waste charging facility.	
Remove disconnects with pressure relief valves from cask.	
Attach coolant jumper hoses between cask and diesel cooling system.	
13. Remove the steel protective cover from operating door handwheel.	
14. Start pump in hydraulic elevating system.	
15. Remove sling from cask and attach to rear lifting lugs on shipping rack.	
Elevate the cask to approximately 45°.	

	Initial or Record Data - Time
16. Using the hydraulic controls, lower the hydraulic erection cylinders until one of the clevis ends of the piston rods is aligned with the mating hole in the shipping frame.	
Adjust elevation as necessary with the chain fall and leveling jack.	
Lubricate and insert the securing pin; lock in place with the hand set screw.	
Repeat the operation for the opposite side of the shipping frame.	
Elevate the cask using the hydraulic erection system.	
Raise the crane hook to follow the movement of the cask until the cask is past the c.g. point. (The sling and crane hook must be removed before vertical position is reached because of building interferences.)	
17. Disconnect coolant jumper lines from cask; install disconnects with pressure relief valves.	
Continue to elevate cask until it is in vertical position.	
Stop hydraulic pump.	
18. Reconnect coolant jumper lines to cask.	
CAUTION: STEPS 10 THROUGH 12 AND 17 AND 18 MUST BE TIMED NOT TO EXCEED 20 MIN TO PREVENT EXCESSIVE HEATING OR BOILING OF COOLANT. IF A DELAY IS ENCOUNTERED, THE COOLING LINES SHOULD BE REATTACHED AND THE COOLANT CIRCULATED FOR APPROXIMATELY 5 MIN OR UNTIL COOLANT REACHES NORMAL TEMPERATURE.	
19. Place the rear concrete shield block in position.	
20. Extend the shield door operator into the shield door frame; lower door pin into hole in frame to connect operator to door.	
21. Slowly open shield door and monitor the area for any change in radiation level.	

C. WASTE CHARGING FACILITY - CASK UNLOADING PROCEDURE

(SHIPPING CASK IN VERTICAL POSITION OVER WASTE CHARGING SHAFT)

Surface Supervisor _____ Date _____
Hoist Operator _____
Surveyor _____
Other _____
_____
_____

Initial or Record Data - Time

1. Remove the magazine shipping bolts.

   Check for contamination; record smears.

2. Remove the canister handling tool access plug.

   Check for contamination; record smears and radiation level.

3. Assemble the unloading shield to access hole.

   Check movement of the sliding shield block.

   Remove the index plug and install the index pin.

Canister Position No.						
1	2	3	4	5	6	7

   Rotate the magazine to No. 1 position or other position desired by lifting index pin and using the wrench on the hexagonal nut located on the small drive gear on the rear of the cask.

   RECORD POSITION NUMBER OF CANISTER IN CASK.

4. Set the safety door handle to "CLOSE" position, indicator light should be AMBER.

5. Puncture the aluminum foil cover on the canister and insert and lock the canister handling tool (grapple) using special locking tool.

   NOTE POSITION OF TOOL ENGAGEMENT HOLES BEFORE AND AFTER LOCKING GRAPPLE.

Slide the counterweight up on the cable to allow space to open the slide on the cable connector.

Attach the ball end of the grapple cable to the cable connector.

Close the slide and move the counterweight to a position directly above the connector.

6. Raise hoist at "SLOW" and then "INCH" to remove slack in hoist cable,and check engagement of the grapple in canister. Winch man keeps hand on cable for control.

7. Wait for "GREEN" clearance from mine control point before proceeding further. SEE STEP D.10

8. On "GREEN" clearance from Mine Control, acknowledge "GREEN" here, if steps 1 through 6 are complete.

   Open the cask operating door by pressing in on the operating handle and revolving the crank until the indicator rod indicates the door is in open position.

9. (Unloading shield is in "OPEN" position and locked by the index pin.) Using the "INCH" speed, jog hoist "DOWN" button until grapple and grapple cable connector just clear the cavity in the unloading shield. Color coded. ~3 in. 2 in. W Band.

   Stop the hoist at this point.

   Move the unloading shield to "CLOSE" position and lock.

10. Continue lowering at "INCH" speed.

    Note passage of the canister into the guidance tube by indicator lights. Change from AMBER to RED. Hits upper limit switch. WRWR.

Color band on cable will also indicate position of canister in guidance tube.

STOP the hoist when lower indicator light changes from "AMBER" to "RED". (The bottom of canister is just above the safety door at this time). Color Code WY.

Record or Record Data - Time						
Canister Position No.						
1	2	3	4	5	6	7
Color Code						

11. Turn the safety door handle to "OPEN" position, Indicator light should be "RED".

12. Continue lowering at "INCH" speed until the main cable connector is above the shield block by 1/64 to 1/8-in.

    "STOP" the hoist at this position

    Pull the index pin and move the unloading shield to "OPEN" position and lock.

13. Still at "INCH" speed, continue lowering until the connector passes into the shield and the hoist counterweight is seated in the shield cavity. Color Code WGWG - Can out of guidance tube.

14. Change hoist speed to "SLOW" for the next 20 ft., note distance by color code. Color code R - 8-ft -long band can in shaft, Y band at 100, 200, 300 and 400 ft. Color code BYB - 500 ft in shaft, B band at 600, 700, 800, 900 ft in shaft.

    "HIGH" speed range of the hoist can now be used to lower the canister until the canister is within approximately 10 ft of the bottom of the shaft as indicated by the cable footage indicator and color code. Color code R - 10 ft long - 10 in. above top of funnel.

    "STOP" hoist when this depth is reached.

15. Surface Supervisor contacts Mine Level Supervisor and transfers hoist command to Mine Level using the telephone control.

    Sequence of operations continues under Transporter Loading Procedures, SEE STEP D. 11.

16. Required after STEP D. 13.

In co-ordination with underground procedure C.

a. Bottom of canister at top of funnel. 10 in. R 2 in. W.
b. Upper microswitch No. 1 trips.
c. Lower microswitch No. 2 trips.
d. Bottom of canister on lower shield doors.
e. Ditto + 2 in. Close top shield door.
f. Ditto + 2 ft.
g. Ditto + 18 ft.
h. Raise cable till flush with shaft.

Initial or Record Data - Time						
Canister Position No.						
1	2	3	4	5	6	7
Color Code						
Color Code						
Additional Color Codes						

D. TRANSPORTER LOADING PROCEDURES

Mine Level Supervisor _____ Date _____
Transporter _____
Surveyor _____
Other _____
_____
_____

Initial or Record Data - Time						
Canister Position No.						
1	2	3	4	5	6	7

Waste Receiving Room

1. Back the transporter into waste receiving room and position the trailer so the shield is approximately under the center of the waste charging shaft.

   (The diesel motor in the tractor is now shut down and power for hydraulic operation of the shield is supplied by electrical power.)

2. Release manual latches on the upper doors of the shield. Lights off on remote control.

   Turn the console switch to remote panel control.

   Open the upper doors. (Front door should open first.)

3. Test the operation of the shield guidance tube position switches and indicator lights.

   Return the switch to "console" position.

   Release safety carry chains.

   Shut off fan.

4. Lower shield and place centering funnel in position on top of transporter shield. (Note: the funnel can be placed in only one position on the shield by virtue of the index blocks.)

   Attach funnel to shield by clamps.

5. Raise the shield to a position close to the ceiling and reposition the shield in the horizontal plane as necessary to allow the entry of the centering funnel in the waste charging shaft. Watch safety chains.

   Raise the shield to the ceiling. Check to see that there are no gaps at ceiling.

Waste Receiving Room

6. Turn console switch to "remote" control position.

   Move the remote control box to the "control" point.

7. Clear personnel from the receiving room.

Control Point

8. Check remote control panel lights by pressing "test" button.

9. Mine Level Supervisor contacts the surface by phone and informs the Surface Supervisor that the area is "GREEN" (operation is ready to go).

10. Wait for the signal from the Surface Supervisor transferring hoist command to Mine Level. (The canister is approximately 10 ft above the bottom of shaft.) SEE STEP C. 15.

    NOTE: ALL HOIST OPERATIONS WITH CANISTER AT MINE LEVEL ARE CONDUCTED USING "INCH" SPEED OF HOIST.

11. Instruct Surface Supervisor to lower canister.

12. Inform Surface Supervisor when upper microswitch No. 1 trips circuit by calling out "No. 1 contacted." (The bottom of the canister is now about 8 1/2 ft above the bottom of the shield cavity.)

13. Inform the Surface Supervisor when lower MICROSWITCH NO. 2 trips the circuit by calling out "No. 2 contacted." (The bottom of the canister is now about 1 ft above the bottom of the shield cavity.) Middle limit switch is not pertinent to this operation.

    This is the command to the Surface Supervisor to STOP hoist and take cable readings by the footage indicator or color coding.

Initial or Record Data - Time						
Canister Position No.						
1	2	3	4	5	6	7

14. The Surface Supervisor shall inform the Mine Level Supervisor that the cable reading has been made. (The canister is now roughly 14 ± 1/2 in. from the bottom of the cask.)

    If all conditions are "GREEN" the command by the Surface Supervisor should be given to lower the canister the final distance and STOP hoist. (The canister should be resting on the lower shield doors with just enough slack to allow the cable to follow the curved slot in the doors when they are closed without lifting the canister. See 16 e.) Color code - top of 2 in. W band.

    Surface give 2 in. for slack. Turn on power.

15. Press top door "CLOSE" button; a green light for each door indicates the doors are closed. (Rear door should close first.)

    Release button.

16. Instruct Surface Supervisor to release two additional feet of cable. See C.16f. Color code - Y band.

    Waste Receiving Room

17. Proceed to the waste receiving room with radiation survey meters and check the radiation level.

    Record level.

    If the level is within the permissible tolerance, proceed with step 19.

    Return remote control box to the immediate vicinity of the transporter.

    Return control to tractor.

Initial or Record Data - Time						
Canister Position No.						
1	2	3	4	5	6	7
mr/hr						
1	2	3	4	5	6	7

18. Lower the shield and move shield to one side to clear cable connector.

19. Instruct the Surface Supervisor to lower additional cable 18 ft until the connector is within reach of a man on the top of the transporter. Color code WY band.

    Disconnect the 1/4-in. cable from the cable connector and remove centering funnel from the transporter. SEE C.16g. Raise cable connector till flush with pipe. Check funnel for contamination.

20. (One of the two top doors is not fully closed by approximately 3/8 in. by design in order to avoid crushing the cable.)

    Place the cable in its groove in the forward door.

    Lock top back door. Close the front top door the remaining distance by use of a ratchet wrench on the shaft end of the door operator.

    Manually lock front top door.

    Return power to remote console.

21. Attach the ball end of the 1/4-in. cable to the winch drum.

    Take up the surplus cable so as to leave the canister resting on bottom door.

    Return power to cab console.

22. Center the shield in the trailer and attach the safety chains to the shield.

23. Lock out the trailer controls using the key switch.

    The keys should be retained by the Mine Level Supervisor.

Initial or Record Data - Time						
Canister Position No.						
1	2	3	4	5	6	7

24. Unplug the electrical connector from wall plug and spool cable on the holder on the transporter.

    Spool cable from remote control box on its rack and hook the remote control box on the trailer.

25. Move the transporter to room 1 for the charging operation.

Room 1 (or Room 5)

26. Increase range on count rate meter.

27. Check purge flow.

28. Check to see if funnels are in array hole.

29. Back the transporter into room 1 over one of the previously certified storage holes.

30. Reduce power on appropriate hole to level indicated on curve. Connect the hydraulic power system to the electrical supply source.

30A. Remove the shield safety chains.

31. Position the shield over one of the empty storage holes using from plate centering system and lower the shield to floor level.

32. Raise can about 1 in.

    Reset selsyn to zero.

33. Release the lower door manual locks.

34. Turn switch to remote operation system.

35. Move to control point.

    Clear personnel from the demonstration area.

Initial or Record Data - Time						
Canister Position No.						
1	2	3	4	5	6	7

Hole No.						
1	2	3	4	5	6	7

Control Point	Initial or Record Data - Time						
	Canister Position No.						
	1	2	3	4	5	6	7
36. Check lights.							
Turn power on.							
37. Push lower door "OPEN" button. (Rear door should open first.)							
RED lights indicate when both doors are open.							
38. Push winch "DOWN" button.							
Indicator lights on the remote control panel indicate the relative position of the canister.							
(When the lower limit switch red light goes out, the bottom of the canister is already engaged in the liner centering tube and approximately 7 ft from the bottom of the hole liner.							
Run 26.6 units on the selsyn and continue lowering till selsyn shows slack. (Selsyn runs counter clockwise to 3.4 on second rotation.)							
STOP winch at this point.							
39. Proceed to room 1 with the radiation survey meters and check the radiation level.							
Record levels.							
If within permissible tolerance, proceed with step 36. Return radiation detection system ratemeter to normal range.							
Return control to room 1 (or room 5).							
40. Push winch "DOWN" button to spool remainder of cable from drum.							
Disconnect cable from winch.							
Return power to console.							
41. Elevate shield to carry position while monitoring the opening between floor and shield for abnormal radiation.							
42. Reposition shield horizontally to clear hole liner.							

43. Release grapple with special tool and remove the grapple from the canister.

    Lift the grapple from hole.

    Put power to remote console.

44. Partially open one of the upper doors and drop cable through the shield.

    Coil cable and return cable-grapple assembly to receiving room.

    Close and lock upper door.

45. Push lower doors "CLOSE" button. (Front door should close first.)

    When GREEN lights indicate that the doors are closed, manually lock both lower doors.

    Return power to console.

46. Center shield, secure shield safety chains. Take up cable and move transporter to waste receiving rooms and reposition the shield under the shaft as previously.

    Remove funnels. Check grapple and funnels for contamination.

    Connect TC's.

Waste Receiving Room

47. Open manual top door latches; push the upper door "OPEN" button until RED lights indicate that both doors are open.

48. Reconnect cable-grapple assembly to the surface hoisting cable.

49. Signal the Surface Supervisor to withdraw the cable from the shaft.

50. Prepare the transporter to receive the next load as covered by steps 1 through 10.

Initial or Record Data - Time						
Canister Position No.						
1	2	3	4	5	6	7

E. CANISTER REMOVAL PROCEDURE - ROOM 1

Supervisor _____ Date _____
Transporter _____
Surveyor _____
Other _____
_____

1. Remove flange cover from hole liner.
2. Survey region for radiation level.

   Record readings.
3. Open hole and remove scatter shield from center guide tube. Place template on flange.
4. Back transporter into room and position shield approximately over the storage hole.
5. Stop diesel engine.
6. Mine Level Supervisor opens key lock to control panel.
7. Connect electrical power cable for hydraulic system operation to the power source and start electric motor.
8. Remove shield safety chain pins.
9. Reposition shield to side of floor array hole above the salt floor at carry position, about 6 in.
10. Turn switch to remote control panel.

    Release manual door locks on upper and lower doors.

    Press door "OPEN" buttons to open both upper and lower doors.

INITIAL OR RECORD DATA-TIME						
CANISTER-POSITION NO.						
1	2	3	4	5	6	7
HOLE NO.				MR/HR		

Retain ball end of cable above upper doors and lower grapple through shield.

Insert grapple into the canister recess.

Using the grapple tool, engage and lock the grapple to the canister.

Coil TC leads in can.

Place cable in forward door groove and press upper doors "CLOSE" button.

Set and lock manual door latches on upper doors.

11. Switch to the console panel and position shield over the hole liner using the template alignment system.

12. Lower the shield until it is against the template.

Switch to the remote panel.

Connect ball end of cable to winch drum.

Push winch "UP" button and spool cable on winch until it is taut.

Set selsyn footage counter to zero.

13. Increase range on radiation detection count ratemeter.

14. Carry remote control console to control point.

15. Clear all personnel from room 1 area and retire to control point.

Control Point

16. Push winch "UP" button and spool about 15 ft of cable on winch.

Selsyn will turn clockwise, and dial indicator should show 26.25 revolutions. This is 11.25 on second rotation.

Initial or Record Data - Time						
Canister Position No.						
1	2	3	4	5	6	7

Watch selsyn dial for any slippage indicating some hangup in transporter shield. Final location should be approximately 0.5 units past middle limit switch.

16A. Return radiation detection count rate system to more sensitive scale.

17. Press lower door "CLOSE" button and wait until lights indicate that the doors are closed.

18. Proceed to room 1 with radiation survey equipment and determine whether or not the area is safe for operation.

19. Move remote control panel to room 1 (or room 5).

Set and lock manual door latches on the two lower doors.

20. Push winch "DOWN" button, until cable tension is released (about 0.60 revolution).

Return power to console.

21. Elevate shield, position in transport position, and attach safety carry chains.

Return power to remote console.

22. Disconnect electrical power supply for hydraulic system.

23. Mine Level Supervisor locks control panel and removes key.

24. Start diesel motor and move transporter to waste receiving room.

25. Back transporter into position under the waste charging shaft.

26. "OPEN" key lock and turn switch to remote control console.

27. Stop diesel engine.

28. Remove safety carry chains.

Initial or Record Data - Time						
Canister Position No.						
1	2	3	4	5	6	7

29. Press winch "DOWN" button, spool cable from winch drum,and disconnect ball connector.

30. Attach ball-end connection of 1/4-in. cable to connector on main hoist cable.

31. Contact Surface Supervisor and advise him to take up slack in cable (slow + jog).

    (The cable length was predetermined during the cold runs and is controlled by utilizing the footage counter and by color coding.)

32. Center and elevate shield under and against waste charging hole. (The shield top plate should be tightly butted against the ceiling plate at the bottom of the waste charging shaft at this time.) Safety chains may kink. Keep them loose.

33. Release manual latches on top doors.

    Ratchet top doors 1/2 turn open.

34. Turn key lock on console to remote position.

35. Move remote control console to control point.

36. Clear all personnel from the demonstration area.

37. Press top doors "OPEN" button until lights indicate that both doors are open.

    Mine Level Supervisor should contact Surface Supervisor and inform him that operation is "GREEN."

    (This indicates the operation is ready to go and the shield is in position for removal of the canister from the mine level into the shipping cask.)

Initial Or Record Data - Time						
Array Position No.						
1	2	3	4	5	6	7

F. WASTE CHARGING FACILITY - CASK LOADING PROCEDURES

(THE PROCEDURE ASSUMES THAT THE SHIPPING CASK IS IN A VERTICAL POSITION READY TO RECEIVE THE CANISTER AND CABLE AT MINE LEVEL)

Supervisor _____ Date _____
Hoist _____
Surveyor _____
Other _____
_____
_____

1. a. On the signal "GREEN" from the Mine Level Supervisor, the Surface Supervisor acknowledges the signal and indicates whether or not conditions are "GREEN" on the surface.

   b. If conditions are "GREEN" at both points, the command is given to the hoist operator to start hoisting.

   c. The hoist should be started and maintained in the "INCH" speed until the canister has entered the waste charging shaft.

   d. The Mine Level Supervisor will advise the Surface Supervisor when the canister clears the lower and top position switches in the transporter shield - upper switch 8 1/2 ft above bottom shield cavity and lower switch 1 ft above bottom shield cavity.

   (Verification of signals is obtained by cable color codes.) YG clears lower limit switch. G clears upper limit switch.

2. When the information is transmitted to the surface that the canister has cleared the shield by virtue of tripping the last position switch, the Surface Supervisor is free to change from "INCH" to "SLOW" AND "FAST" speed hoisting of the canister; that is, light changes from green to red to green.

Initial Or Record Data - Time						
Canister Position No.						
1	2	3	4	5	6	7

(The approximate position of the canister in the waste charging shaft should be monitored at all times using the footage counter on the main hoist and by color coding of the cable.

The Surface Supervisor should also relay information to the mine as to the relative position of the canister.)

3. When the canister is within about 27 ft of the surface as indicated by the color coding of the cable red or the footage counter, the Surface Supervisor instructs the hoist operator to switch to slow speed operation. Switch to "INCH" speed at 6 in. of red cable - color coded.

4. The Surface Level Supervisor should carefully observe when the cable connector starts lifting the counterweight from its position on the unloading shield.

   Eight feet of red cable is color code which will indicate approach of connector.

   The hoist is stopped at this point and controlled by jogging the "INCH" button until the connector is above the unloading shield by approximately 1/64 to 1/8 in.

5. Move the unloading shield block from "OPEN" position to "CLOSE" position and continue hoisting operation at "INCH" speed.

6. (The next point of observation for hoisting control is when the canister enters the guidance tube. The light on the lower position switch will change from amber to red when the canister enters the guidance tube.)

   When the upper limit switch trips, the hoist operation must be stopped by command from the Surface Supervisor to the hoist operator.

   Color code on cable will verify canister position.

Initial Or Record Data – Time						
Canister Position No.						
1	2	3	4	5	6	7
Color Code 900 B 400 Y 800 B 300 Y 700 B 200 Y 600 B 100 Y 500 BYB						
Color Code						
Color Code						

7. The Surface Supervisor instructs an operator to close the guidance tube safety door.

   The light on the indicator panel will switch from red to amber when this operation is completed.

8. The operation of hoisting is now continued at "INCH" speed.

   Closely observe the indicator panel until the upper position light changes from RED to AMBER.

   (At this point the canister head is approximately 18 in. from the top of the carrier magazine.

   The cable is color coded to designate this position.

9. Continue hoisting until the color coding indicates that the grapple is entering the hole in the rear of the shield.

10. The unloading shield is now moved from "CLOSE" position to "OPEN" position.

11. The hoist "INCH UP" button must be jogged carefully until the canister is fully withdrawn into the shield as noted by the color coding.

12. The Surface Supervisor instructs an operator to close the cask operating door.

    The operator will report back to the Surface Supervisor when this has been done.

    (An indicator built into the operating handle will indicate that the door is fully closed.)

    THE SURFACE SUPERVISOR SHALL VERIFY THAT DOOR IS CLOSED BY OBSERVING THE POSITION OF THE OPERATING SCREW IN RESPECT TO THE DOOR HANDWHEEL.

Initial Or Record Data - Time						
Canister Position No.						
1	2	3	4	5	6	7
Color Code						
Color Code						
Color Code						

Initial or Record Data - Time						
Canister Position No.						
1	2	3	4	5	6	7

13. The Surface Supervisor shall then give the command to the hoist operator to lower the hoist approximately 1 ft.

14. The grapple tool is inserted through the unloading shield and the grapple is disengaged from the canister and withdrawn from the shield.

15. The magazine index pin is released and the magazine is rotated to the next receiving position. The position number of the canister must be noted at this time.

11. Results and Analysis

R. L. Bradshaw W. C. McClain

This chapter covers the results and analysis of the experimental aspects of Project Salt Vault. Typical, but selected data are presented to illustrate the behavior of the various phenomena under investigation. With, or following, the various data presentations, there is usually some interpretation as to the meaning or implications of the results. In a few instances data have been included primarily for purposes of record, with little or no interpretation included. In other cases data and/or interpretations have been discussed in other sections of the report, and references to these previous sections are included.

11.1 RADIATION

This section covers all aspects of the radiation problems associated with the ETR fuel assemblies except those relating to personnel exposure, which are covered in Chap. 10, "Operating Experience."

11.1.1 Source Activity

The nominal ETR assembly irradiation history is discussed in Sects. 3.2 and 9.1. This nominal history was 23 days (2×10^6 sec) irradiation at a flux of 1.84×10^{14}. Four hundred grams of ^{235}U per assembly was assumed. The calculated earliest age for canning this nominal fuel assembly was 60 days after discharge from the reactor, based on a maximum fuel assembly temperature of about 850°F in the hot cell. This meant that shipment could be made by 75 days after reactor discharge, and the cans could be in the mine by 90 days. At 90 days the nominal radioactive heat generation would be about 750 W per canister (two ETR fuel assemblies). The supplementary heat (in the air gap between the salt and the hole liner) was assumed sufficient to bring the total up to 1600 W per canister. Under these conditions the fuel assembly temperatures were calculated to be about 875°F, an acceptable value.

It was thus assumed that the nominal fuel assemblies would be placed in the mine at 90 days out of the reactor. It was further assumed (as explained in Sect. 3.4) that four sets of fuel assemblies would be used (each for six months) in the main array in order to boost the peak dose to the salt to near 10^9 rads during a two-year operating period.

Of the first set of fuel assemblies (from ETR cycle 73) five of the seven canisters had calculated heat generation rates of about 620 W at 90 days, while the other two canisters were generating about 590 W. The canisters were not placed in the mine until the assemblies were 107 to 109 days out of the reactor (November 17–19, 1965), so the dose to the salt from the first set of assemblies should be somewhat less than that from a nominal run. Figure 11.1 shows the theoretical relationship between total heat generation rate (beta plus gamma), gamma power, and radiation dose to the salt for the nominal canisters and those with ETR cycle 73 fuel assemblies.

The second set of fuel assemblies (from ETR cycle 78) was transferred into the main array on June 13–15, 1966, when they were 105 to 107 days out of the reactor. However, due to a higher average burnup, these fuel assemblies were much more radioactive than the first set (as well as a nominal set), having a heat generation of about 780 W at the time of placement in the mine.

On June 8–9 the first set of fuel assemblies had been transferred from room 1 to room 5. On October 11–13, 1966, this first set of canisters was removed for return to Idaho. On October 31–November 1 the second set of canisters was moved from room 1 to room 5.

The third (and final) set of canisters (from ETR cycle 82) was transferred into room 1 on November 7–10, 1966, when the fuel assemblies were 84 to 87 days out of the reactor and canister heat generation rate was about 800 W. This set of assemblies was removed from room 1 on June 26–27, 1967, for return to Idaho.

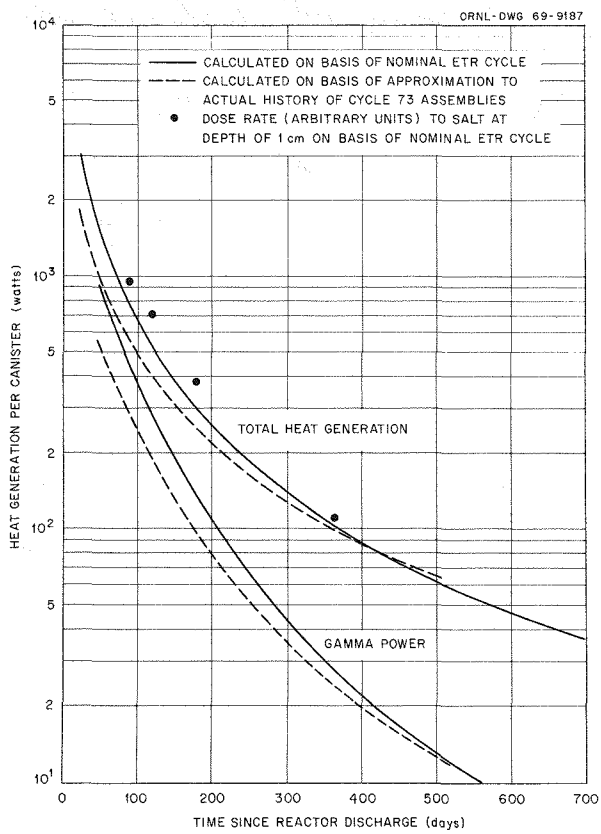


Fig. 11.1. Heat Generation per Canister – Nominal and Cycle 73 Assemblies.

Thus three sets of fuel assemblies were used in room 1, covering a total period of about 19 months. Room 5 was exposed only to the first two sets of assemblies, for a total period of about 11½ months. A total of about 4,000,000 Ci of fission product activity in 21 containers each having an average of about 200,000 Ci was transferred to the mine and then back to the NRTS by the end of the test.

11.1.2 Absorbed Dose in Salt

Dose measurements in the salt were made in room 1 four times during the period that the first set of fuel assemblies was in place, three times during the residence of the second set of assemblies, and six times with the third set of assemblies. Measurements were not always made at all locations on the dosimeter holder. Generally, the chemical dosimeter measurements confirmed the glass-rod values, but the chemical dosimeters were bad occasionally, or the tubes were broken, so the glass-rod data were used for the integrated dose calculations.

The peak absorbed radiation dose to the salt in the main array (room 1) at the junction between the two ETR fuel assemblies was about 3.7×10^8 rads as of November 1, 1966. By May 1967 the total was about 5.3×10^8 rads. Generally, the accuracy of the dose measurements themselves is believed to be within about 20%. However, the point at which the measurements of the incident dose to the salt were made (the junction between the assemblies) was such as to produce dose values which were lower than the average incident salt dose (over the 6-ft length of the tandem fuel assemblies) by about a factor of 1.4 and lower than the peak dose by a factor of about 1.9. The reason for this may be seen in Fig. 11.2, which shows the actual dose distribution measured along the outside of an array hole liner along a line which is about 4¼ in. from the center of the liner. The measurements appear reasonable, since the power in the lower fuel assembly was reported by ETR operations to be about 14% lower than in the upper assembly. For comparison purposes the normal incident salt dose (corrected to 4¼ in. from the center of the liner on the basis of cylindrical geometry) is also shown in Fig. 11.2.

It should be noted that the measured doses for salt depths up to about 5 cm would also be expected to be

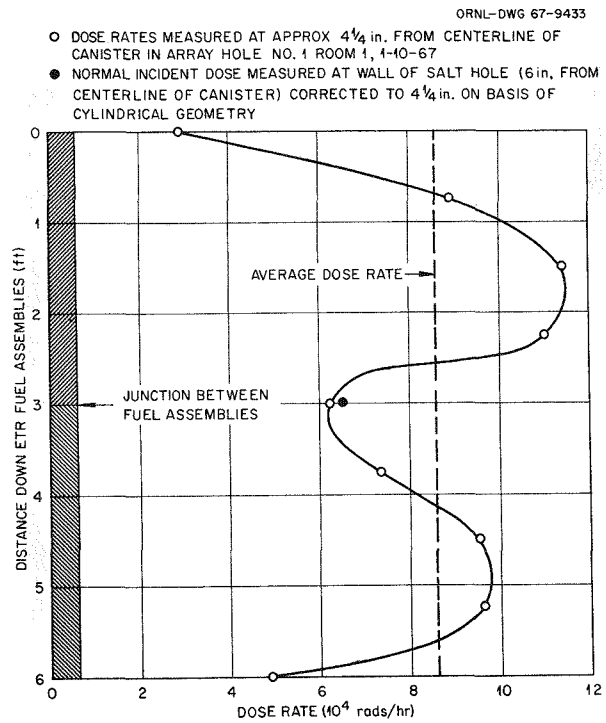


Fig. 11.2. Dose Rate Distribution Along ETR Fuel Assembly Canister.

lower than the maximum, due to the fact that all of the dosimeters, except the incident, were located at varying distances above or below the junction of the two fuel assemblies. The 10- and 20-cm dosimeters were located near the points of maximum dose and thus should be approximately correct. (These doses will be discussed later.)

If the fourth set of fuel assemblies is assumed to be identical to the third, the total dose at the junction of the fuel assemblies would have been about 6.8×10^8 rads after two years of operation. On the other hand, the original goal of achieving a peak dose of at least 5×10^8 rads had been met by May of 1967. This 5×10^8 minimum was based on the fact that at 10^8 rads there was no indication of any change in the physical properties of salt, while at 5×10^8 there was an indication of a small change in such properties as the compressive strength (see Sect. 2.3). On the other hand, a hypothetical Acid Purex solid waste of the future would deliver a calculated peak dose of about 4×10^9 rads in two years, and more than 10^{10} rads ultimately (see Fig. 3.5). It would be impractical to attempt to reach these levels until actual waste solids become available. In any case, only the first few inches of salt adjacent to the containers would be exposed to such levels.

In view of the fact that both field and laboratory studies confirmed that the radiation effects on salt do not appear to have any detrimental effects for waste disposal, there did not appear to be any need for bringing in the fourth set of fuel assemblies. The approximately 30% increase in total dose which would accrue with the fourth set of fuel assemblies would be unlikely to produce any new results. For example, even if the salt around the waste containers were to lose all its structural strength, the extent of the damaged zone (even for the future wastes) would not be enough that it should have any significant effect on mine stability. Therefore it was decided to terminate the radioactive tests with the third set of fuel assemblies, and they were removed from the room 1 array at the end of June 1967.

The radiation doses accumulated in the salt are shown in Fig. 11.3. The curve determined by the solid circles shows the originally calculated theoretical two-year dose based on ETR fuel having nominal irradiation. It was expected that, because of the buildup factor, the peak dose to the salt would be about 7×10^8 to 8×10^8 rads at a salt depth of $2\frac{1}{2}$ cm. The curve with upright triangles, based on the actual measurements, indicates that the peak dose after about 19 months of operation in the mine was approximately 5.5×10^8

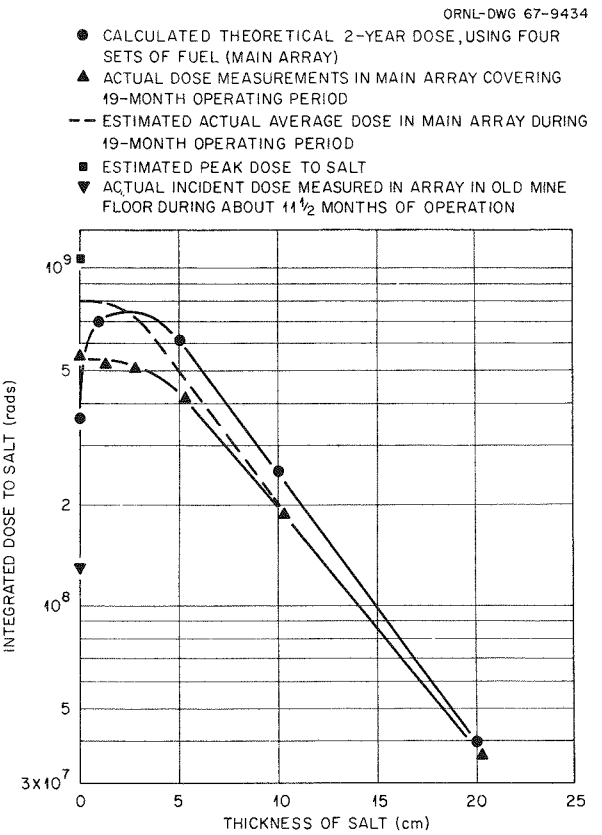


Fig. 11.3. Comparison of Measured and Calculated Doses to Salt.

rads and occurred at the wall of the hole. The estimated actual average dose to the salt over the length of the hole is shown by the dashed line and was about 8×10^8 rads for reasons explained above. The estimated peak salt dose is shown by the square and was about 10^9 rads. The measured dose at the wall of the hole in the array in the old mine floor (room 5), which received the ETR fuel after it had remained about six months in the main array in the experimental area, was slightly more than 10^8 rads, as shown by the inverted triangle. The average dose over the length of the hole in room 5 would be higher.

11.1.3 Radiolytic Gas Production

Dose dropped off very rapidly with distance out into the salt, with doses at 6 in. into the salt being a little less than 10^8 rads. Therefore, in each of the seven main array holes, a volume of about 14 ft^3 of salt was exposed to doses ranging from 10^8 to 10^9 rads. In addition, temperatures at the periphery of the array holes ranged up to about 200°C.

Theoretical studies indicate that some free chlorine should be produced within the salt structure at these dose levels; however, the elevated temperatures tend to have the reverse effect (i.e., anneal some of the radiolytic effects).

On several occasions the chlorine indicator tubes (which were also sensitive to other substances) indicated the presence in the off-gas of small quantities of some material which reacted with the tubes. The first instance was in early March of 1966 with hole IV of room 1 indicating about 0.1 ppm.

The next instance was in early February 1967 after the power input to the arrays had been boosted. In this instance all holes in both rooms 1 and 5 gave indications. The room 1 holes indicated values of around 1 ppm, with the room 5 holes indicating less than 0.5 ppm. (Flow rates were about 7 liters/min per array hole.) These indications started after temperatures at the walls of the holes exceeded about 175°C, and it is of interest to note that they were roughly proportional to the fuel assembly dose rates, that is, more in room 1 where the dose rate was much higher. Indications continued until the shutdown of the arrays at the end of June 1967. However, the levels decreased with time to about 0.2 to 0.3 ppm in room 1 and 0 to 0.1 ppm in room 5, again suggesting a dose rate dependence. During this period there was one instance in which a positive reading at the minimum detectable level was obtained in room 4 (the electrical control array), but this was probably an erroneous reading.

Chlorine production due to radiolysis of rock salt is possible; however, this production is favored at low temperature and not above 175°C, from which temperature region the annealing process becomes more important than the radiolytic process.

When the array-hole off-gas was run through cold traps and the contents of these traps were analyzed for chlorine, the results were negative. When the contents of the cold trap were run over a gas chromatographic column, a relatively strong peak indicative of a hydrocarbon was found. After several unsuccessful attempts, this fraction was analyzed mass spectrometrically. Peaks corresponding to fragments with mass-to-charge ratios (m/e) of 41, 42, and 43 were found. These results indicate that a compound like methyl ethyl ketone was present.

It seems most likely that this organic material was a remnant of an organic peroxide that was formed by radiolysis. It is believed that the elevated temperature was responsible for the release of organic material which was then converted to a peroxide by the radiation. The peroxide was stable enough to react with the chlorine detector but decayed in time to form some residual organic compound. It was thus concluded that no free chlorine had been released from the salt.

The presence of small quantities of such an organic peroxide is not expected to be of any consequence in an actual waste disposal operation.

11.1.4 Miscellaneous Effects

In Sect. 11.1.2 the anticipated effects of radiation on the structural properties of salt are discussed. Comparisons of both temperature and rock mechanics data between rooms 1, 4, and 5 do not indicate any significant differences which could be attributable to radiation.

One effect which may be due to radiation was an apparent increased sensitivity of the radioactive array to the release of trapped moisture when there was a power shutdown. (This subject is covered in Sect. 11.2.2.) This is believed to be due to radiation hardening of the surface layer of salt, thus producing a more brittle material.

11.2 MOISTURE

A discussion of previous studies on the effects of moisture trapped in "negative crystals" (brine-filled cavities) is contained in Sect. 2.2. With salt temperatures below about 250°C, no significant effects were expected from this moisture in rooms 1 and 4. In room 5, where there was appreciable shale (which was known to release water at temperatures above 100°C), considerable water was expected in the off-gas.

11.2.1 Cavity Migration

In the demonstration it was found that small quantities of brine trapped in so-called "negative crystals" or brine-filled cavities tend to migrate toward a heat source. This water posed no problem in the demonstration, since it was removed by the off-gas system; but, in order to determine the approximate water inflow rates which might be expected in an actual disposal operation, a theoretical study was made, along with a few experimental measurements.

11.2.1.1 Theoretical Aspects. – Previous theory on the migration of liquid inclusions in ice crystals by Hoekstra *et al.*[1] and later modified by Seidensticker[2]

[1] P. Hoekstra, T. F. Osterkamp, and W. F. Weeks, "The Migration of Liquid Inclusions in Single Ice Crystals," *J. Geophys. Res.* 70(20), 5035 (1965).

[2] R. G. Seidensticker, "Comment on Paper by P. Hoekstra, T. E. Osterkamp, and W. F. Weeks," *J. Geophys. Res.* 71(8), 2180 (1966).

was found applicable to the migration of negative crystals in rock salt. In this case the cavity contains saturated NaCl solution (along with other salts normally associated with evaporite deposits, which we assumed could be neglected as a first approximation). The driving force for the migration of brine cavities through rock salt under the influence of a temperature gradient is considered to be the difference in solubility between the warm and colder sides of the brine cavity and the resulting diffusion of dissolved salt ions from one side to the other. The flux of solute J may be described by

$$J = cv\,, \tag{11.1}$$

where

c = NaCl concentration (g/cm^3),

v = rate of NaCl diffusion (cm/sec),

J = flux (g/cm^3 × cm/sec) or (cm^2/sec × g cm^{-3} cm^{-1}).

From Fick's law,

$$J = -D\frac{dc}{dx}, \tag{11.2}$$

where

D = diffusion coefficient of NaCl in H_2O (cm^2/sec),

$\frac{dc}{dx}$ = concentration gradient (g cm^{-3} cm^{-1}).

Rearranging and expressing the diffusion rate as a function of absolute temperature, we obtain:

$$v(T) = -\frac{D(T)}{c(T)}\frac{dc}{dT}\frac{dT}{dx}, \tag{11.3}$$

where

T = absolute temperature,

$\frac{dc}{dT}$ = concentration gradient as a function of temperature,

$\frac{dT}{dx}$ = the temperature gradient.

Expression (11.3) is negative, because migration is up gradient.

However, Seidensticker showed that the rate of diffusion of solute is not equal to the rate of migration of the cavity. His argument is based on the fact that the solid and liquid have different densities and different thermal gradients. Assuming that the cavities are spherical, the correction factors are

$$\frac{G_l}{G_s} = \frac{3K_s}{2K_s + K_l} \quad \text{and} \quad \frac{\rho_l}{\rho_s}, \tag{11.4}$$

where

G_l = thermal gradient of the saturated solution,

K_l = thermal conductivity of the saturated solution,

ρ_l = density of the saturated solution,

G_s = thermal gradient of the solid,

K_s = thermal conductivity of the solid,

ρ_s = density of the solid.

The final expression for the rate of migration of negative crystals in rock salt then becomes

$$v(T) = -\frac{D(T)}{c(T)}\frac{dc}{dT}\frac{dT}{dx}\frac{3K_s}{2K_s + K_l}\frac{\rho_l}{\rho_s}. \tag{11.5}$$

Published data on the solubility of NaCl from 0 to 350°C (ref. 3) and thermal conductivity data on saturated NaCl solutions from 10 to 150°C (ref. 4) were used. Above 150°C the thermal conductivity of water was used, since both curves follow each other closely.[5,6] Thermal conductivity data on solid NaCl from 0 to 400°C as published by Birch and Clark[7] were used. The correction factor for the difference in thermal gradients was approximated as a linear function of temperature up to 300°C. Also, the densities for both solid NaCl from 0 to 50°C and saturated NaCl solutions[3] from 0 to 107°C are approximately linear functions of temperature and were extrapolated linearly to higher temperatures.

Diffusion coefficients were calculated using the Stokes-Einstein model:[8]

$$D(T) = \frac{kT}{6\pi\eta r}, \tag{11.6}$$

---

[3] D. W. Kaufmann, *Sodium Chloride*, 743 pp., Reinhold, New York, 1960.

[4] Walter Unterberg, "Thermal Properties of Salt Solutions," *Brit. Chem. Eng.* **11**, 494–95 (June 1966).

[5] W. R. Gambill, "Predict Thermal Conductivity – I," *Chem. Eng.* **64**(2), 238 (February 1957).

[6] W. R. Gambill, "Physical Properties of Water," *Chem. Eng.* **66**(7), 139–40 (Apr. 6, 1959).

[7] Francis Birch and Harry Clark, "The Thermal Conductivity of Rocks and Its Dependence upon Temperature and Composition," *Am. J. Sci.* **238**(8), 529–58 (August 1940).

[8] R. A. Robinson and R. H. Stokes, *Electrolyte Solutions*, 2d ed., p. 12, Eq. 1.7, Academic, New York, 1959.

where

D = diffusion coefficient,

k = Boltzmann's constant,

T = temperature (°K),

η = viscosity of water (g cm^{-1} sec^{-1}),

r = molecular radius.

In our case we used the mean ionic radius of Na^+ and Cl^-, ½(0.95 A + 1.81 A).[3] The diffusion coefficient D proved to be nearly exponential with temperature because of the dependence of viscosity on temperature from 0 to 300°C (refs. 6, 9). As a check on the validity of using this method for calculating D for a saturated NaCl solution, the value calculated for 18°C was 1.46×10^{-5}, which compares favorably with the value 1.54×10^{-5} given by Kaufmann (ref. 3, p. 612).

Theoretical calculations were made with the aid of a computer program in which the solubility of NaCl and the viscosity of water were interpolated by Lagrange's method using quadratics. Lagrange's method was also used to find the slope of the solubility curve.[10]

The most important characteristic of the theoretical model is that the cavity migration rate is a function of temperature and is directly proportional to temperature gradient, both of which can be measured directly from the NaCl crystal.

11.2.1.2 Experimental Aspects. – Specimens consisted of relatively pure salt crystals from the Carey Salt Company mine at Hutchinson, Kansas; the crystals were about 2½ cm on a side, containing brine cavities between 2 and 10 mm in maximum dimension. Thirty-one rate measurements (on 12 separate cavities) were obtained, covering the temperature range of 75 to 244°C, with gradients ranging from 4 to 34 C°/cm. Migration periods varied from 20 to 358 hr, and the observed distances of migration ranged from 0.8 to 8 mm (ref. 11).

For salt temperatures above 100°C, the crystals were placed on a hot plate. In those cases where the hot plate was not enclosed in a temperature chamber, the four vertical sides were insulated with asbestos tape, but the top was left exposed. Insulation was not used below 100°C or on experiments where the hot plate was enclosed in a temperature chamber.

Six type K thermocouples, three on each of two opposite sides, were placed in 3-mm-deep, 0.8-mm-diam horizontal holes drilled 1 cm apart along the vertical sides of the specimens. Temperatures were recorded on a strip-chart recorder. Specimen temperatures were controlled by a variable autotransformer connected to the hot plate. The smaller gradients at the higher temperatures (around 200°C) were obtained by placing the experimental setup in the temperature chamber, where ambient temperatures could be controlled. For salt temperatures around 100°C or less, a knife-blade heater was used to migrate brine cavities in a horizontal direction; it was interesting to note that cavity migration in a horizontal direction behaved the same as migration in a vertical direction.

Measurements on migration were made with a comparator to within about 0.1 mm. The initial position of the negative crystal face nearest to the heat source was marked with a scalpel on the surface of the salt crystal. Measurements were made between the scalpel mark and the final position of the negative crystal face nearest to the heat source. Migrations were usually in the order of millimeters over a period of a day or two; however, at temperatures below 100°C cavities were migrated for about two weeks. Temperatures were read from the thermocouple nearest to the cavity or were taken as the average of the two nearest thermocouples, both on the same side, if the cavity happened to be about halfway between the two. Since the thermocouples were 1 cm apart, temperature gradients were taken to be the difference between the two nearest thermocouples, both on the same side. Since salt crystals can be shattered by thermal shock, temperatures on cold salt crystals were raised slowly over a period of about 30 min. Cooling was accomplished over a period of 30 min by turning the power off, but for experiments in the temperature chamber, the fan was left on, and the chamber door was pulled open about a centimeter.

11.2.1.3 Results. – The main objective of the experiment was to compare the results with the diffusion model and to attempt to obtain agreement at least within an order of magnitude. Although the experimental work was not done with high precision, and even though the experimental setup was rather simple, the results were adequate. The experimental data (see Fig. 11.4) agree with theoretical calculations (the curve of Fig. 11.4) within the anticipated range.

The salt crystals maintained steady-state temperatures within about 5°C; and, although the temperature

---

[9] N. A. Lange, *Handbook of Chemistry*, 8th ed., Handbook Publishers, Inc., Sandusky, Ohio, 1952.

[10] The computer program was developed and run by Florentino Sanchez, an Oak Ridge Associated Universities Summer Student Trainee. Essentially all of the experimental measurements were also performed by him.

[11] R. L. Bradshaw and Florentino Sanchez, "Migration of Brine Cavities in Rock Salt," *J. Geophys. Res.* 74(17), 4209–12 (1969).

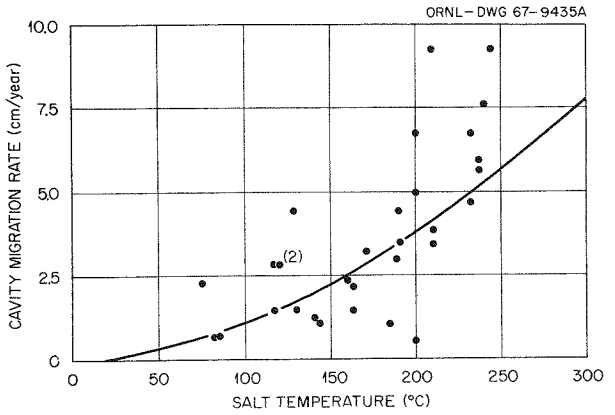


Fig. 11.4. Comparison of Theoretical and Experimental Migration Rates of Brine-Filled Cavities in Rock Salt.

gradients were not reproducible from one test to the next, almost identical gradients along two opposite sides were obtained. However, the gradients were by no means constant with respect to the position along the sides. Therefore, at a given position along a side, the temperature gradient in the salt could only be estimated from the thermocouple readings. Another factor to be considered in comparing results is that cavities sometimes increased in volume due to creep expansions, while the diffusion model does not include the effects of change in shape or volume.

Using the migration rates indicated by the theoretical curve of Fig. 11.4, calculations were made to determine what might be expected in an actual disposal facility (see Sect. 11.2.5). They were based on the temperature-vs-time and -distance relationships for a typical high-level future solidified-waste disposal facility. Assuming about ½% by volume of water in the salt, one might expect a total inflow per waste container disposal hole of perhaps 2 to 10 liters, taking place over a period of 20 to 30 years after burial of the waste. The peak inflow rate would occur at around one year after burial and be somewhere in the range of 200 ml to 1 liter per year per hole. This corresponds to about ½ to 3 ml/day per hole, a range similar to that estimated in the demonstration waste container holes. This water inflow rate would be expected to taper off and approach zero after 20 to 30 years. Other considerations indicate that such volumes and inflow rates will be tolerable in a disposal facility.

11.2.2 Off-Gas Condensate

As mentioned in previous sections, each of the three arrays was equipped with an off-gas condensate collection system (see Sect. 7.7.3). In rooms 1 and 4, where the salt in the floor around the array holes was relatively pure, little condensate was anticipated. In room 5, in the old mine floor, where there was considerable shale, moisture collection was anticipated when the temperatures reached about 100°C, since the shale was known to contain several percent moisture which would be released at temperatures above 100°C.

As discussed in Sect. 11.2.1, the brine cavities in the salt migrated toward a heat source and tended to slowly release small amounts of moisture into the array holes. This had not been anticipated, but would not have been of any concern in the demonstration because the off-gas system would not allow any water to accumulate in the array holes anyway.

Another phenomenon which had not been anticipated was the release of some of the trapped moisture when there was a power shutdown. When power inside the hole was shut down, the off-gas flow produced a slight drop in wall temperatures, and thereby a reversal of the temperature gradient. That is, whereas under normal conditions the inner wall of the hole has the highest temperature, after a few minutes of power outage the inner wall temperature was lower than at some point out in the salt. It is believed that the result was a reduction of the tangential compressive stress at the inner wall of the hole, thus allowing the trapped water (under considerable pressure due to the elevated temperature) to break free. As mentioned in Sect. 11.1.4, the salt in the irradiated holes would be more brittle and would be expected to be more prone to rupture than the unirradiated salt.

In an actual disposal operation, there would be no air annulus and no air flow. Also, with the heat being supplied by radiation alone, there would be no such thing as a power shutdown and thus no reason for a reversal of the thermal gradient. (The relatively slow decay of the radioactive source would not produce a gradient reversal either.) Therefore this phenomenon would not be anticipated in an actual facility.

11.2.2.1 Condensate Collection in Rooms 1 and 4 Before Shutdown. – In Fig. 11.5 is shown the condensate collection during the operating period for each of the three arrays. The curves start at the beginning of heated operation for each array. In room 1 the first measurable condensate was collected some four months after startup. There had been power outages of short duration prior to this time, but apparently there was no outage of any significant duration associated with this first collection. With essentially all of the other condensate collections there was a power outage, although not all such temporary power outages pro-

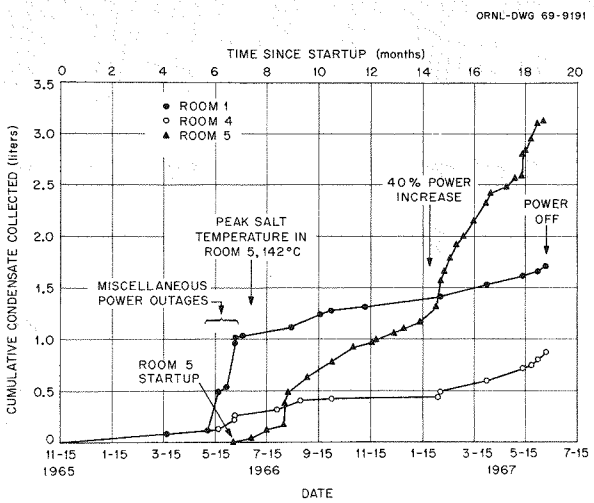


Fig. 11.5. Condensate Collection Before Shutdown.

duced collections. Frequently, if an outage occurred soon after one in which a substantial amount of condensate was collected, there would not be any collection.

By about the middle of June 1967 (shortly before shutdown) the total condensate collection in room 1 was about 1.7 liters, and in room 4 it was about 0.8 liter. (A possible reason for the greater collection in the radioactive array, radiation hardening of the salt, was discussed in Sects. 11.1.4 and 11.2.2.)

Several attempts were made to determine if water was migrating into the holes during the periods between the sporadic collections. These included the use of Drierite columns and the determination of the dew point by means of the refrigeration units on the condenser systems. However, due to the fact that the mine air normally ran about 40 to 60% relative humidity (a rough average moisture content of about 11 g/m^3) these methods were unsuccessful. Several tests using dry nitrogen gave the most reliable estimates, although even these were good only for upper limit values. The best test was performed in room 1 on January 19–20, 1967 (about 70 days since there had been any condensate collection). In this test there was a 1-hr sweep of dry nitrogen through hole IV at 7 liters/min. This should produce more than three volume changes of the gas in the hole (greater than 95% removal of the original gas, if complete mixing is assumed), so that a negligible amount of water vapor (less than 0.1 ml) should remain in the hole. After this the hole was closed off for 24 hr to permit the diffusion of water from the salt into the hole. Then nitrogen at a flow rate of 2.1 liters/min for about $3\frac{1}{2}$ hr was passed through the hole and into a system of traps at a temperature ranging from about 0 to 5°F. About $\frac{1}{2}$ ml of liquid was collected in the traps. This meant that, if the nitrogen was *absolutely* dry when it entered the hole, it picked up enough moisture in the hole to become saturated at around 12°F. If that was the case, then the total emission of water from the salt into the hole during the 24-hr period was no more than 1 ml. On the other hand, a test on the nitrogen alone (without its passing through the array hole) produced some traces of condensate at similar temperatures. (This was in spite of the fact that the nitrogen supplier said that the dew point should be below −20°F.) Thus it must be concluded that the water collected from the array hole after the 24-hr period of no off-gas flow may not have come from the salt at all, so that the maximum inflow rate from the salt at that time must have been between 0 and 1 ml/day.

It is now possible to estimate the minimum and maximum probable water inflows into the array holes. In room 1 the total condensate collected to shutdown was 1710 ml (from the seven holes) over a period of about 572 days, or about 0.43 ml/day per hole. In room 4 the corresponding figure was 0.22 ml/day per hole. These would be the minimum figures. Now if this amount of moisture was collected, the off-gas air at the condenser exit must have been 100% saturated during the collecting period. A reasonable assumption based on field observations is that the off-gas was saturated for an average of about 10 hr during each significant collection period. Based on the estimate of 39 g/hr (for the entire array) to bring the mine air up to 100% relative humidity and 16 collection periods in room 1, this would (when added to the 0.43 ml/day) bring the water emission up to 1.98 ml/day per hole. The corresponding number for room 4 would be 1.77 ml/day. These figures assume that no water came out between condensate collection periods. If we now add the maximum estimate of water inflow determined from the nitrogen tests, the minimum and maximum estimates of daily inflow rates lie between about 0.4 and 3.0 ml/day per array hole for room 1 and 0.2 to 2.8 ml/day per hole for room 4. These rates are about what would be calculated from the theoretical migration rates of brine cavities, as discussed in Sect. 11.2.1.3.

11.2.2.2 Condensate Collection in Room 5 Before Shutdown. – As may be seen from Fig. 11.5, the behavior in room 5 was somewhat different than in the other two arrays. This was expected, as explained previously (Sect. 11.2.2). Condensate collection began when the peak salt temperature was about 142°C (only about three weeks after startup), although probably

some water was being removed by the off-gas before the first condensate collection occurred.

Based on the total water collected before shutdown (about 3.1 liters) and assuming that the off-gas air was saturated at least 10% of the time, the minimum emission rate would be about 10 ml/hole per day. At the other extreme, if it is assumed that the off-gas air was saturated at all times, the emission rate would be about 93 ml/day per hole. The true situation probably falls somewhere between these two limits.

In the case of the room 5 condensate, although some collections took place after power outages, they did not generally depend on an outage occurring.

11.2.2.3 Condensate Collection After Shutdown. – The total condensate collections in all three arrays (pre and post shutdown) are shown in Fig. 11.6. The most noticeable phenomenon is that the amount of water collected in the first two days after shutdown of all three arrays is about an order of magnitude greater than that collected during the whole prior period of operation. The final total collection was about 11 liters in room 1, about 12½ liters in room 4, and 35 liters in room 5. The previously postulated mechanism (reverse thermal gradient) might possibly account for rooms 1 and 4, but it does not appear to be adequate to explain the behavior in room 5, where most of the water was believed to come from the interbedded shale.

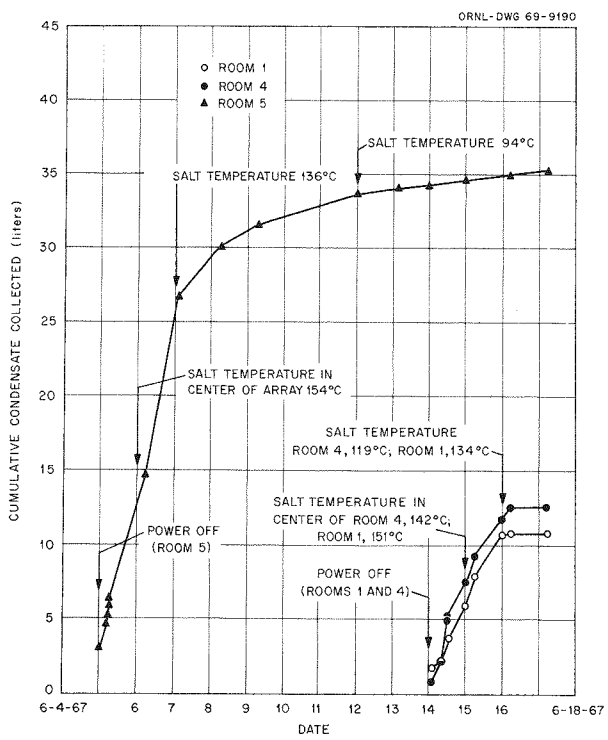


Fig. 11.6. Total Condensate Collection Including Post Shutdown.

A probable explanation for room 5 is that some of this water originated with a source of cattle urine (considerably modified by time and passage through shale) which was discovered in drilling holes for the SWCT cans in front of room 5 during March of 1967 (see Table 10.1). In one of these holes (which was abandoned and the SWCT location moved), more than 100 gal of liquid (determined by laboratory tests to have originally been urine from cattle which were housed in the mine several years earlier) was removed by early June. However, since neither the rapid cool-down phase nor waste cans in the original mine floor are expected in an actual disposal operation, this phenomenon is of only passing interest.

11.2.3 Corrosion Effects on Hardware

The effects of the water in the salt (and in the shale in the case of some of the SWCT tests) on the modified pillar heaters and the simulated waste container (SWCT) heaters has been described in Sect. 10.6.2. The general conclusions which follow from these results are described below.

The field tests indicated that once the migrating brine reaches the crushed salt backfilling the hole, the water moves upward and condenses in the colder regions above the waste containers. Under some conditions, since the upper regions of the waste containers may not be completely full of waste, the upper ends of the containers may be located temporarily in the condensation zone. If this is the case, stress corrosion cracking of these portions of stainless steel containers may occur. If the containers are of mild steel, only generalized rusting would be expected, and container integrity should be maintained for an indefinite period of years. Even if the containers do perforate, this should not produce any serious problem in a disposal facility, since there should be little or no gas in the containers; and, even if there is, the 7 to 8 ft of crushed salt above the containers would be expected to act as a filter and adsorber for the released material. As an additional safeguard, the anticipated operating procedure is that ventilating air will never come in contact with personnel after it passes a filled storage room; container failure would not be anticipated during the relatively short period of operation in an individual room (typically, about one month). Provision would also be made to route the ventilating air through an air-cleaning system and up a stack in the event of an activity release.

In the PSV arrays, hole liner corrosion would not be indicative of the effects to be expected in an actual

disposal operation, since the liners were not in contact with the salt, and the off-gas systems kept the moisture from accumulating in the air annulus. For the record, however, the 304L stainless steel lower liner sections in both rooms 1 and 5 were essentially unaffected, although they were spotted with evaporated salt from the bursting brine-filled cavities. In room 4, where the liners were carbon steel, they were very rusty on the outside but showed no signs of penetration.

The Incoloy-sheathed heaters on the outside of the hole liners in the radioactive array (which probably operated at temperatures up to about 400°C) were also apparently unaffected by the moisture and salt atmosphere. There were no tubular-heater failures at all during any of the operations, except for the case of the SWCT's where water got into the terminal compartments.

11.2.4 Further Studies on Moisture

11.2.4.1 Volume of Salt Represented by Water Release. – It is of interest to calculate the volume of salt required in order to account for all the water which was collected in the off-gas system and which may have been released if the maximum values calculated in Sect. 11.2.2 are assumed. The calculated maximum values were 25.3 liters for room 1 and 28.1 liters for room 4 during the entire period, including shutdown. (Quite likely, the actual values were somewhat less than these estimated maximums.) As determined from a section of 12-in.-diam core taken from room 1, the average water content of the salt around the lower sections of the array liners was about 0.53% by volume. From a core taken from a SWCT hole in front of room 4, the estimated average water content of the salt around the lower sections of the room 4 liners was about 0.46%. We will thus assume an average of about 0.5% by volume for the two arrays. With an average maximum water emission of 26.7 liters per array, this represents a salt volume of 5340 liters per array. Assuming that equal amounts of water came from each hole, this is 763 liters of salt per hole, or 26.9 ft^3. If all this water came from a 7-ft-long annular cylinder around the hole, the diameter of the cylinder would be about 2.43 ft (the ID is 1 ft). That is, all of the original water out to a distance of about 8.6 in. from the wall of the hole could account for the maximum estimated emission during the entire test period, including shutdown.

11.2.4.2 Water Content of Salt After Shutdown. – After the arrays were shut down and the salt had cooled off, a series of 12-ft-deep cores were taken in room 1, and moisture determinations were made (by heating samples to 625°C). Cores were taken midway between array holes IV (the center hole) and I, 6 in. out beyond hole I wall, and $1\frac{1}{2}$ and $2\frac{1}{2}$ ft beyond hole I. Cores were also taken on a line running from hole IV midway between holes I and III at distances from hole IV of $\frac{1}{2}$, $1\frac{1}{2}$, $2\frac{1}{2}$, $3\frac{1}{2}$, $4\frac{1}{2}$, $5\frac{1}{2}$, $7\frac{1}{2}$, and $9\frac{1}{2}$ ft. In six of these holes, three to five samples about 6 in. long, selected as representative of the full 12-ft depth, were tested for moisture content. In the other six holes, the 6-in. sections centered around 9 ft depth were tested. A total of 31 samples was tested.

The depth-averaged (over the 12 ft) water content of the four holes which were at least 2 ft from the wall of any array hole was about 0.50%, or essentially the same as the estimated water content of the salt prior to the demonstration. The depth-averaged water content of the two holes which were only 6 in. away from an array hole was only 0.31%. The 9-ft-depth (center plane of heat source) average water content in all of the holes was also about 0.31%.

11.2.4.3 Further Comments on Water Content of Salt from Various Mines. – In Sect. 2.2 the results of tests of water content (or shattering temperature) of salt from different mines, when heated to about 400°C, were given. Table 2.1 listed the water content of Hutchinson and Lyons salt in weight percent. Converted to volume percent, the Hutchinson salt averaged about 0.4% but the Lyons salt only about 0.2%. The more recent tests have taken the salt up to 625°C instead of only 400°C, but little additional water is released above 400°C, so this does not account for the apparent discrepancy in water content between the early and more recent Lyons salt tests. The answer probably lies in the fact that the samples used for the early Lyons salt water content were obtained before the start of operations in the mine, when there was limited means for acquiring samples. Therefore the samples were taken from chunks of salt which had fallen from the original mine roof and which may have been in a stratum with lower than average water content.

On the salt from the Retsof and Detroit mines of the International Salt Company, the original tests were only on shattering temperature (Table 2.2). (Retsof salt did not shatter up to 400°C and was thus presumed to be essentially free of trapped moisture.) Some of this salt was still available, and two samples from each mine were tested up to 625°C. The Retsof salt showed about 0.06 vol % water, while the Detroit salt had about 0.9%.

11.2.5 Water Migration into Future Disposal Holes

In Sect. 11.2.1 the theoretical migration rate of brine cavities was developed, and Fig. 11.4 showed the theoretical rate as a function of temperature for a

temperature gradient of 1°C/cm. The migration rate is directly proportional to temperature gradient, so rates may be obtained by multiplying by the gradient in question. By examination of some plots of temperature gradients around isolated cylinders at times from about 6 to 25 hr, it would appear that even for very young wastes (less than 3 years old) it would be practically impossible to get temperature gradients of more than 10°C/cm in salt around a can 6 in. or more in diameter.

In order to get an approximate upper limit estimate for the water inflow rates, the best available data were from one of the cases calculated by the computer code for the infinite array of line sources in the economic study report.[1,2] This calculation used the 300°C salt thermal properties, $3\frac{1}{3}$-year-age waste, and spacing between cans about $9\frac{1}{2}$ ft (a = 5 ft). Temperatures as a function of time were calculated for distances from the center of the line source of $\frac{1}{4}$, $\frac{1}{2}$, 1, and 5 ft for times of 100 hr up to about 36 years. Using a heat generation rate of 5660 Btu/hr per 6-in.-diam pot, the temperature rises would thus be as shown in Fig. 11.7 as a function of time from 100 hr to 27.4 years, about the time of the peak temperature. Adding in 20°C ambient, the peak salt temperature would be about 380°C. This is because a should be about $7\frac{1}{2}$ ft rather than 5 ft in order to limit the peak temperature to 200°C. Nevertheless, this will serve as an indication of the upper limit to brine cavity migration rates which might be expected in an actual disposal operation.

Table 11.1 shows very approximate brine cavity migration data calculated from Figs. 11.7 and 11.4. Figure 11.8 was then plotted from the data of Table 11.1; it shows the migration rates as a function of time at the wall of the hole (5 in.) and at 12 in. from the center of the can. These curves assume that water migrates into a region as fast as it migrates out, but from the table and Fig. 11.8 this is obviously not so, even when cylindrical geometry is taken into account. If spherical geometry were to apply, then the rates in Fig. 11.8 would come closer to being correct as a function of time. At any rate, they can be assumed to represent upper limit values (based on the theoretical curve of Fig. 11.4), and it is seen that the maximum water inflow would be expected to occur about one year after the waste is buried. The linear rate is about 4 in./year, maximum, representing about $1\frac{1}{3}$ liters of water per year (assuming $\frac{1}{2}$% by volume water in salt). This rate falls with time, approaching zero at around 20 to 30 years after burial. Very roughly, the first 5 years would produce a total inflow of about 6 liters/hole; the next 5 years, about 5 liters/hole; 10 to 15 years, about 3 liters/hole; and 15 to 20 years, about 1 liter/hole. Total inflow would thus be around 15 liters/hole. These numbers have been calculated conservatively, so they may be too high by at least a factor of 2, but probably not by an order of magnitude. One might then expect a total inflow per hole of something like 2 to 10 liters, taking place over a period of 20 to 30 years. The peak inflow rate might occur at around one year after burial

[1,2] R. L. Bradshaw, J. J. Perona, J. O. Blomeke, and W. J. Boegly, Jr., *Evaluation of Ultimate Disposal Methods for Liquid and Solid Wastes VI. Disposal of Solid Wastes in Salt Formations*, ORNL-3358 (Rev.) (March 1969).

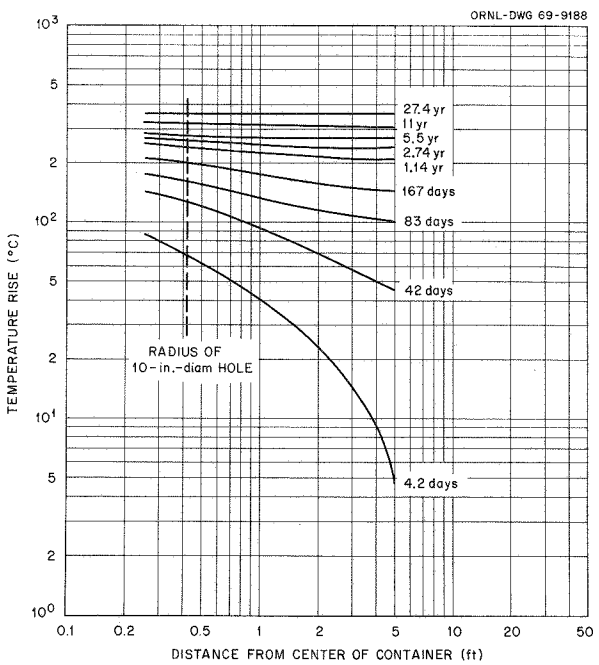


Fig. 11.7. Temperature Rise Around 6-in.-Diam Acid Purex Pot.

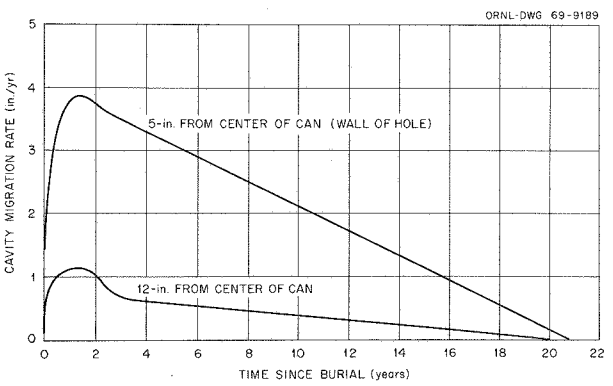


Fig. 11.8. Brine Cavity Migration Rate for 6-in.-Diam Acid Purex Pot.

Table 11.1. Approximate Calculation of Brine Cavity Migration Rates for 6-in. Acidic Purex Pot with a = 5 ft

From runs 4 and 5 of infinite array calculations

Incremental Period (year)	Time After Burial	Gradient (°C/cm)	Temperature (°C)	Migration Rate at 1°C/cm (in./year)	Migration Rate (in./year)	Migration During Incremental Period (in.)	Total Migration (in.)
			Distance = 0.417 ft (5 in.)[a]				
0.01	4.2 days (0.01 year)	3.0	9	0.36	1.08	0.011	0.011
0.10	42 days (0.11 year)	2.6	148	0.86	2.24	0.224	0.23
0.12	83 days (0.23 year)	2.3	175	1.18	2.72	0.326	0.56
0.23	167 days (0.46 year)	2.0	220	1.64	3.28	0.754	1.31
0.68	1.14 years	1.6	260	2.40	3.84	2.61	3.92
1.60	2.74 years	1.3	280	2.74	3.56	5.70	9.62
2.74	5.48 years	1.0	300	3.08	3.08	8.44	18.06
5.5	11 years	0.5	340	3.78	1.89	10.4	28.46
16.4	27.4 years	~0	380				
			Distance = 1 ft[b]				
0.01	0.01 year	1.0	61	0.17	0.17	0.002	0.002
0.10	0.11 year	1.3	113	0.53	0.69	0.069	0.07
0.12	0.23 year	0.9	153	0.91	0.82	0.099	0.17
0.23	0.46 year	0.7	195	1.43	1.00	0.230	0.40
0.68	1.14 years	0.5	250	2.25	1.13	0.770	1.17
1.60	2.74 years	0.3	270	2.58	0.72	1.15	2.32
2.74	5.48 years	0.2	290	2.90	0.58	1.59	3.91
5.5	11 years	0.1	325	3.52	0.35	1.92	5.83
16.4	27.4 years	~0	375				

[a]Volume of NaCl in 1-in. cylindrical annulus = 2.40 ft^3; volume of H_2O in 1-in. annulus = 340 ml (@ ½%).
[b]Volume of NaCl in 1-in. cylindrical annulus = 5.35 ft^3; volume of H_2O in 1-in. annulus = 752 ml.

and be somewhere in the range of about 200 ml to 1 liter/year per hole. This corresponds to about ½ to 3 ml/day per hole, a value similar to that estimated in the demonstration.

11.3 TEMPERATURE

This section covers the temperatures associated with all of the various phases of the demonstration, including the three arrays, the heated pillar, and the simulated waste container tests. Salt temperatures, heater temperatures, and other temperatures of interest are discussed.

11.3.1 Power Input

In the arrays the total power input was nominally 10½ kW, including both electrical and radioactive decay heat. (Previous temperature calculations had assumed up to 11.2 kW per array to be conservative.) Both the main radioactive and electrical control arrays (rooms 1 and 4) were started on November 15, 1965. As the fuel assembly cans were inserted, the electrical power was cut back to maintain a constant total power input. The heat generation of the fuel assemblies is discussed in Sect. 11.1.1, and no further discussion is necessary here, except to note that electrical power was increased periodically as the radioactive power decreased.

During operation with the first set of fuel assemblies (until early June 1966), the average power over the period was 10.9 kW in room 1 and 10.6 kW in room 4 (see Fig. 11.9).

With the second and third sets of assemblies, the average power in all three arrays was about 10.9 kW for the approximately eight-month period up to the time of the power boost. On January 24, 1967, the power was increased about 40% in order to get the peak salt temperatures up to around 200°C. (The original power level had been chosen on the basis of very conservative calculations in order to ensure that no excessive temperatures would be reached.) During the remainder of the operating period (to June 1967), room 1 averaged 14.9 kW; room 4, 15.1 kW; and room 5, 14.4 kW.

The carbon steel modified pillar heater in room 2 was started on June 22, 1966, at a nominal power input of

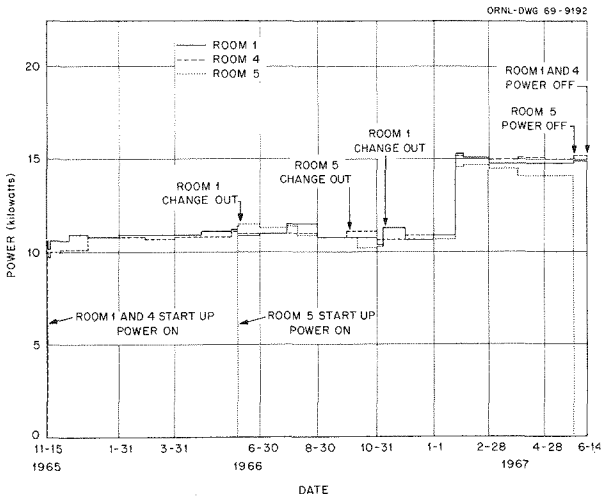


Fig. 11.9. Array Power Input.

3 kW and operated at this level until November 11, 1966. The average power input over this period, as indicated by the recording wattmeter, was 2.8 kW.

On November 14, 1966, all pillar heaters (22 including the modified heaters) were started at a nominal power input of 1.5 kW per heater (33 kW total). The wattmeter indicated that this average level was fairly well maintained until shutdown on October 9, 1967. There were, however, minor variations and a few brief periods of power failure.

Due to the difficulties experienced with the simulated waste container heaters (SWCT), as discussed in Sect. 10.5.4.2, power inputs to the SWCT heaters were erratic. The original design had called for an initial power input of 4.3 kW per can. (All SWCT heaters were started on July 17, 1967.) For heater 1 (mild steel) in the Experimental Entry, the power was about 4.7 kW for the first 100 hr, then there was a period of failure, and from about 160 to 1300 hr the power was about 3.3 kW. It then operated at 1.6 kW until it was raised to 3.2 kW at about 2700 hr and operated at this level until shutdown on December 20, 1967 (about 3740 hr). Heater 2 (stainless steel) in the Experimental Area operated at about 4.7 kW (with some interruptions) for about 550 hr and at about 3.1 kW from then until the end of the test on December 20, 1967.

Number 1 SWCT heater (mild steel) in entry 5A operated at about 3.2 kW for about 50 hr; it was then boosted to 4.3 kW until trouble was experienced at about 95 hr. Power was applied again at around 170 hr, and the heater operated at about 1.6 kW until shutdown on December 12, 1967. Entry 5A heater 2 (stainless steel) operated at 4.7 kW for the first 100 hr, was restarted at this level at about 170 hr, and failed at about 300 hr. Heater 3 (stainless steel) operated for about 100 hr at 4.8 kW, was restarted at about 1.6 kW at around 170 hr, and failed at about 1440 hr. Heater 4 (mild steel) operated at 4.8 kW for 100 hr, was restarted at 4.8 kW at about 170 hr, had the power reduced to 3.3 kW at about 300 hr, and failed at about 1900 hr.

As discussed in Sect. 10.5.4.2 of this report, the heater failures were due to water entering the terminal compartments and causing short circuits. Some thermocouple failures were also caused by this water.

11.3.2 Array Rooms

Power to the arrays in rooms 1 and 4 was started on November 15, 1965, and finally shut down on June 14, 1967. Array room 5 was started on June 6, 1966, and shut down on June 5, 1967. The power was increased 40% for all three arrays on January 23, 1967.

11.3.2.1 Temperature Profiles. – The temperature contours in the horizontal plane 9 ft below floor level (the center of the heat sources) just before shutdown are shown in Figs. 11.10–11.12. Temperatures are given in °C, and the ambient salt temperature was about 23°C before the start of operations. Contour temperatures are shown on the contours; they are 35, 50, 75, 100, 125, 150, and 165°. The temperatures shown next to the array holes are the maximum salt temperatures at the walls of the holes. The temperatures listed by the solid dots are measured temperatures in the thermocouple holes at these points.

The 165°C contour for room 1 is slightly smaller than for room 4. The other contours are not significantly different. On the other hand, the room 5 contours out to 100°C are larger than those for room 4. Salt wall temperatures in the center holes of rooms 1 and 4 are not significantly different, but the center hole temperature in room 5 is different, even though the room 5 power was about 4 to 5% lower than room 4. The average array hole wall maximum temperatures for both rooms 1 and 5 (179 and 186°C respectively) were greater than for room 4 (166°C).

The differences between rooms 1 and 4 are not considered to be significant, and thus it appears that the radiation in room 1 did not have any appreciable effect on heat transfer in the salt. The higher temperatures in room 5 are almost certainly associated with the poorer heat transfer characteristics of the 25 to 30% shale and anhydrite interbedded with the salt over the 12-ft depth of the array holes (see Table 11.2).

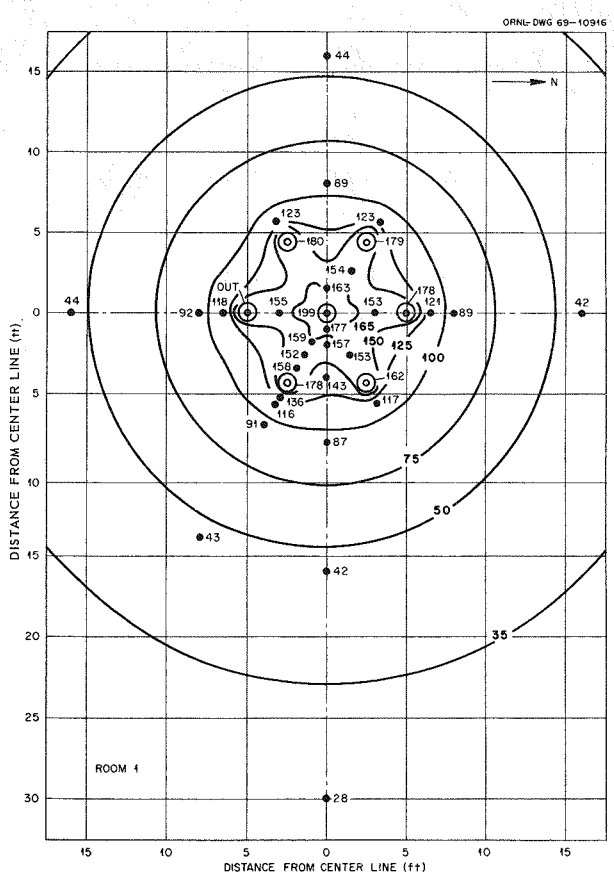


Fig. 11.10. Temperature Contours in Horizontal Plane 9 ft Below Floor – Room 1.

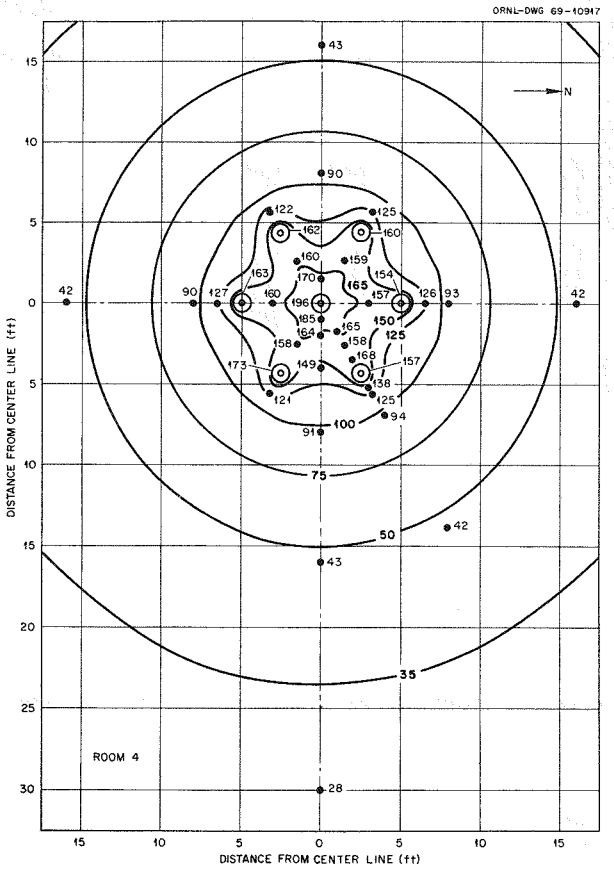


Fig. 11.11. Temperature Contours in Horizontal Plane 9 ft Below Floor – Room 4.

These horizontal temperature contours at 9 ft depth may be compared with the theoretical calculations in the preliminary design of the experiment. Figure 3.10 is the comparable figure, except that it shows temperature *rises*. Also the theoretical calculation assumed an infinite salt medium; that is, the rooms were filled with solid salt. As will be seen presently, the heat losses to the room air were considerably greater than if the salt had been solid (and the in-place heat dissipating properties of the salt also appear to have been somewhat better than the 100°C values assumed in the calculations). Consequently, it was necessary to raise the power per array hole from a nominal 1500 to 2100 W in order to get the peak salt temperature to about 200°C at the center of the arrays. After this power boost, the room 1 80°C rise contour was approximately 15 ft in diameter, as was the theoretical contour. However, the 30° rise contour was only about 29 ft in diameter compared with 33 ft for the theoretical.

Figure 11.13 shows the vertical temperature contours (at the end of the operating period) in room 1 through the center in the east-west direction (that is, midway between peripheral cans). Here may be seen the effect of the greater heat loss to the room than would be the case if the room were filled with solid salt. For example, the 50°C contour intersects the floor (9 ft above the center of the heat sources) at about 4 ft from the center of the array, while the corresponding point beneath the array (18 ft depth) is about 10 ft from the center. Again, the 100°C contour intercepts the center of the array about 5 ft above the center of the heat sources, while the bottom of the contour is about 7 ft below the center of the sources. Thus the temperature gradients are considerably higher above the center of the array than they are below, indicating a more rapid heat loss upward into the room than would have been the case if the room contained solid salt. Contours for the other two arrays at the end of the test were similar.

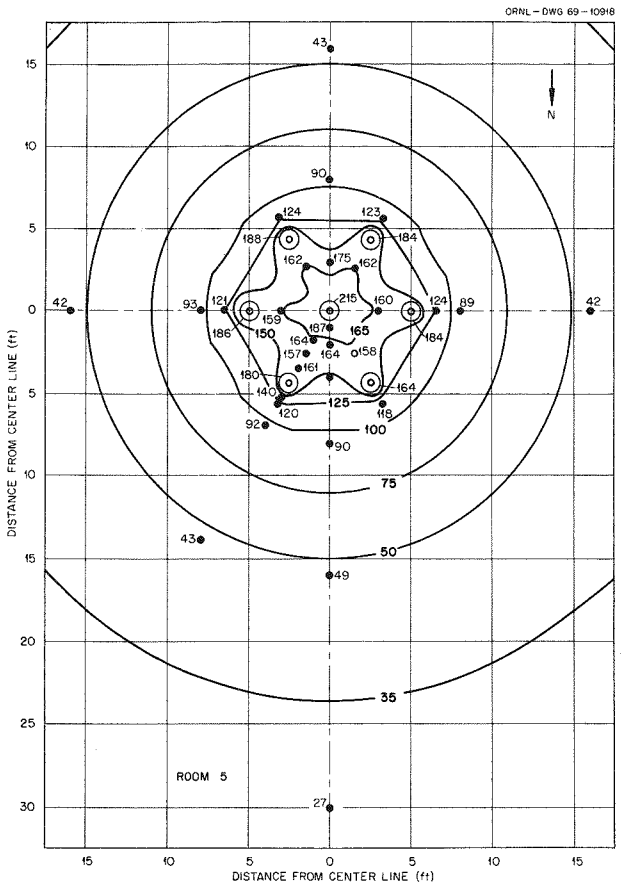


Fig. 11.12. Temperature Contours in Horizontal Plane 9 ft Below Floor – Room 5.

This vertical contour plot may be compared with the early theoretical prediction in Fig. 3.9. At 9 ft depth, the theoretical 50°C rise contour extended about 12 ft from the center of the array while that in room 1 was about 10 ft. The theoretical 80°C rise contour extended about 8 ft, while the room 1 contour was only about 7 ft out.

The vertical temperature contours through the room 1 array on the north-south center line may be seen in Fig. 11.14, which shows the maximum temperatures through rooms 1, 2, and half of 3 (the remainder of room 3 and room 4 would be mirror images of rooms 2 and 1). Actually, room 1 data are from June 1967, while room 2 and 3 data are for early October 1967; however, room 2 and 3 temperatures were not much lower in June, except for those points which were most remote from the heaters. The effect of the rooms on heat transfer can be most vividly seen in this figure. If it were not for heat loss to circulating air in the rooms, the contours in rooms 2 and 3 should be symmetrical above and below a line 9 ft below floor level.

Table 11.2. Log of Core Hole in Entry 5A

About 50 ft northeast of array 5

Depth Below Floor (ft)	Description[a]
0–1.5	Salt with some shale
1.5–1.8	Salt with heavier shale
1.8–2.7	Heavy shale, little salt
2.7–2.9	Shale with some salt
2.9–3.2	Shale with some salt
3.2–4.0	Shale
4.0–4.6	Salt with heavy shale
4.6–5.2	Shale
5.2–5.5	Salt with heavy shale
5.5–5.6	Clear salt
5.6–5.8	Shale
5.8–6.3	Salt with some shale
6.3–6.5	Salt with heavy shale
6.5–7.1	Salt with little shale
7.1–8.1	Shale
8.1–9.4	Salt with varying shale
9.4–10.0	Clear salt
10.0–10.2	Salt with little shale
10.2–10.6	Good salt
10.6–11.2	Clear salt
11.2–11.7	Good salt
11.7–12.6	Clear salt
12.6–13.7	Good salt
13.7–15.1	Salt with shale
15.1–15.95	Salt with light shale
15.95–16.65	Good salt
16.65–17.55	Good salt
17.55–18.20	Clear salt
18.20–18.45	Salt with light shale
18.45–18.55	Good salt
18.55–18.85	Shale
18.85–19.15	Salt with heavy shale
19.15–19.45	Salt with light shale
19.45–19.65	Shale or anhydrite
19.65–19.90	Salt with shale
19.90–20.65	Salt with heavy shale

[a]Core described as shale may also contain anhydrite in some instances.

In the room 1 and room 4 arrays a roughly circular ellipsoidal volume of salt about 15 ft in diameter by 12 ft high was raised to temperatures in excess of 100°C. A roughly spherical volume of salt 25 to 30 ft in diameter was raised above 50°C. Room 5 volumes were slightly larger.

11.3.2.2 Salt Temperatures vs Time. – Figures 11.15–11.17 show the temperature-vs-time data for each of the three arrays at a distance of 8 ft from the centers of the arrays. Data shown on each of the graphs are for depths of 1, 5, 9, 13, and 17 ft. (The 17-ft-depth thermocouples were read with a portable pyrometer, and the data are thus likely to be less accurate than for

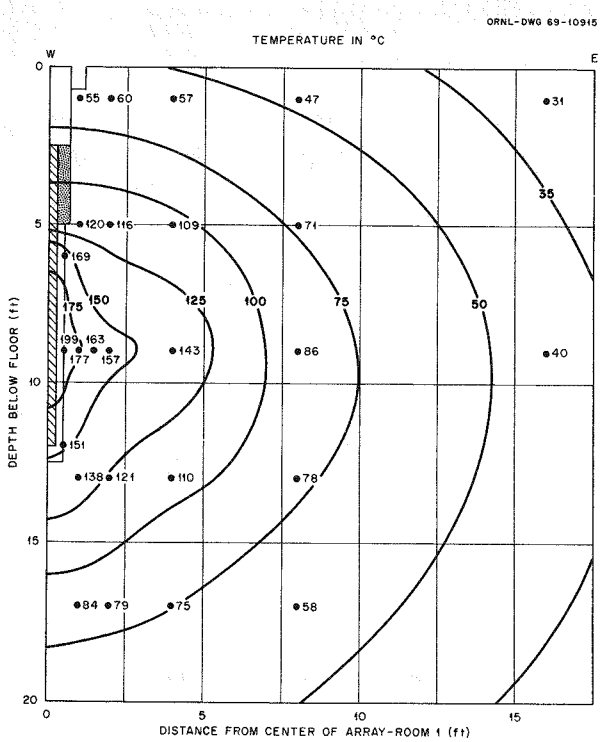


Fig. 11.13. Temperature Contours in Vertical Plane – East-West Direction, Room 1.

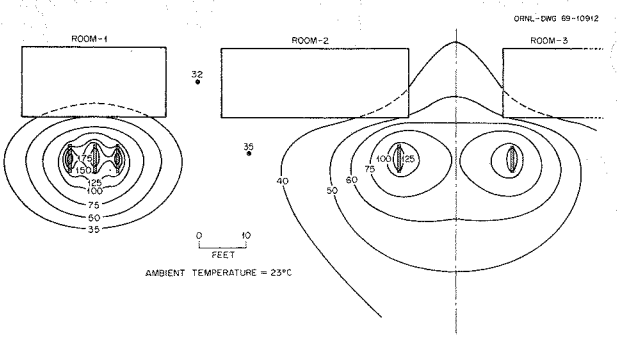


Fig. 11.14. Temperature Contours (at Maximum Values) in North-South Vertical Plane Through Center of Experimental Area.

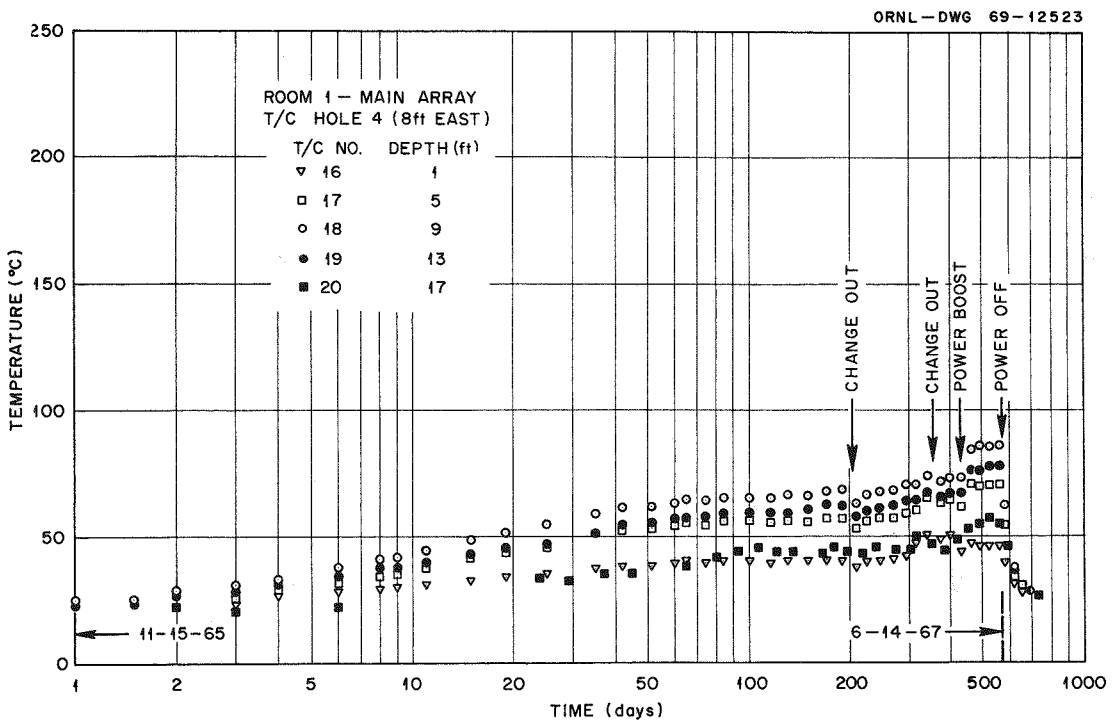


Fig. 11.15. Temperatures vs Time at Various Depths – 8 ft East of Center of Room 1.

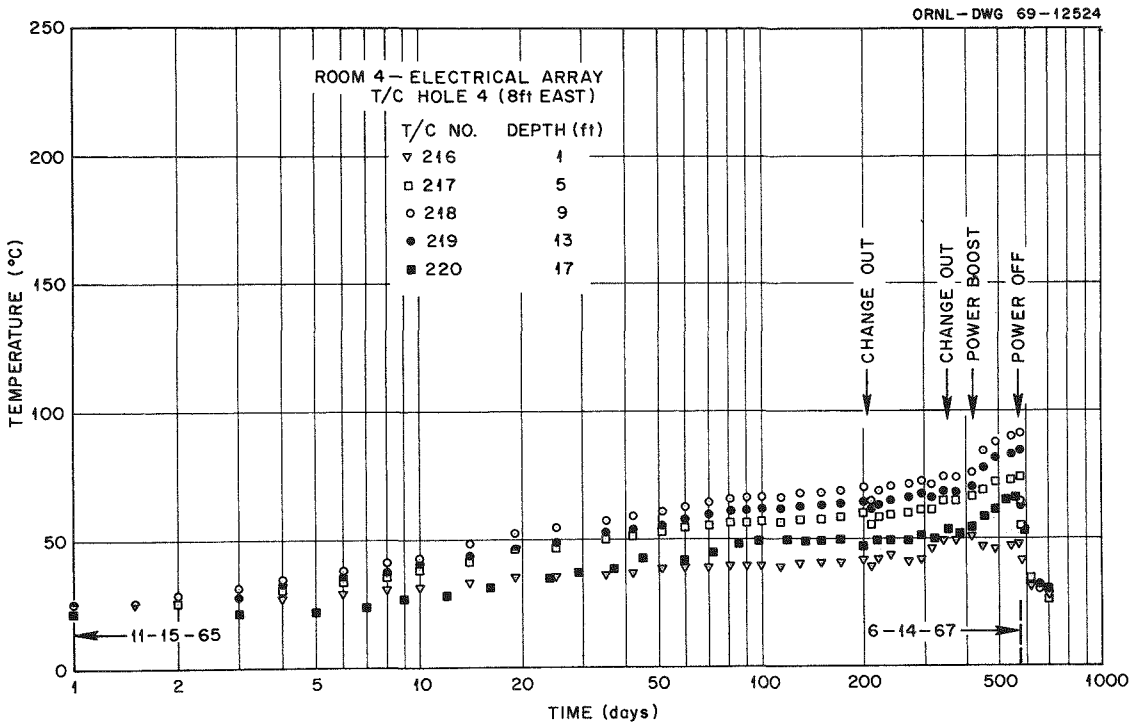


Fig. 11.16. Temperatures vs Time at Various Depths – 8 ft East of Center of Room 4.

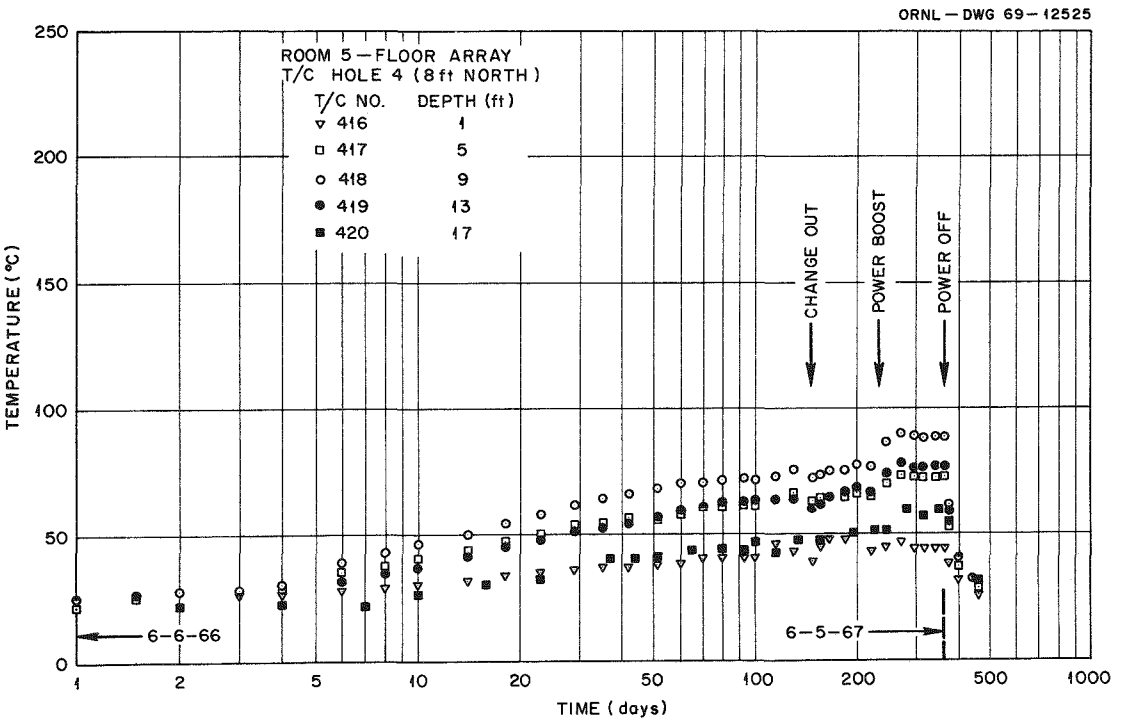


Fig. 11.17. Temperatures vs Time at Various Depths – 8 ft North of Center of Room 5.

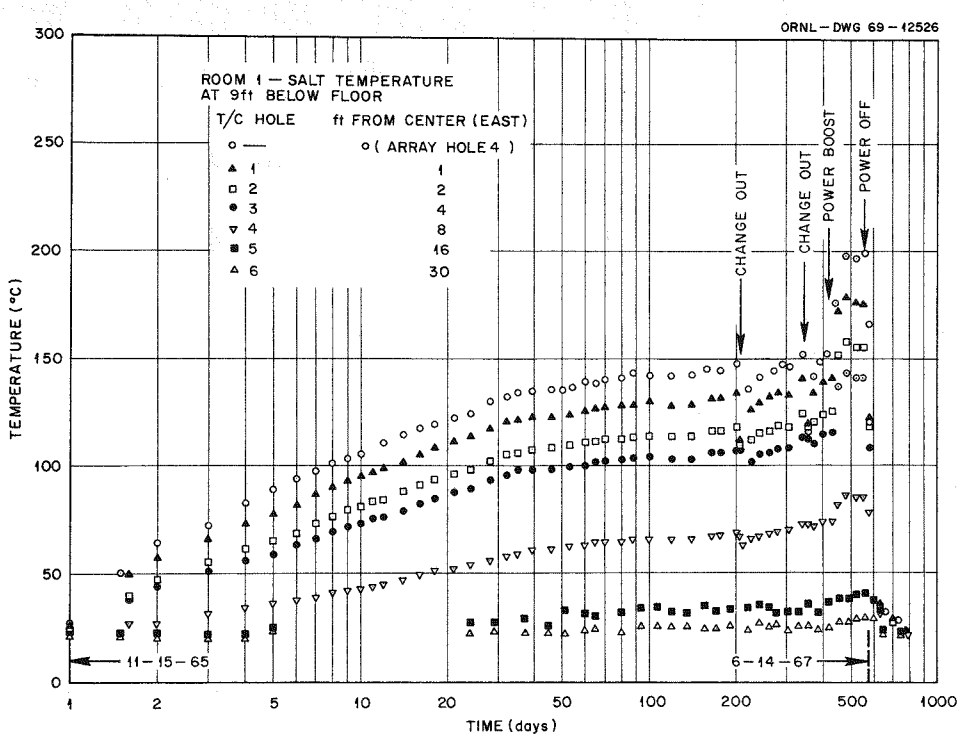


Fig. 11.18. Temperatures vs Time at 9 ft Depth and Various Distances from Center of Room 1.

the other depths.) Note that the time is in terms of days after startup, and thus the dates are the same for rooms 1 and 4, but different for room 5. This also causes the changeouts and power boost to occur at different elapsed times in room 5. The times are not marked on the curves, but the insulating boards were on the room 1 and 4 arrays from about 306 to 413 days and on room 5 from about 108 to 215 days.

[The 9-ft-depth curve for room 1 (Fig. 11.15) may also be seen in Fig. 11.18, which is discussed below.]

A comparison of the data in the three rooms does not show any trends which have not been noted previously.

Figure 11.18 shows the temperature vs time plots in room 1, at a depth of 9 ft, along a line running east from the center of the array (that is, between array holes VI and VII). Effects of the fuel assembly changeouts (temporary drops in temperature) may be seen, as well as the effect of the power boost after about 430 days of operation. The maximum temperature is that at the wall of the center hole of the array (No. IV), while the minimum is 30 ft from the center of the array. The other two arrays are similar, with minor differences as might be expected.

A comparison of the theoretical curve and the temperature rise data from the so-called "control temperatures" in the next figure (Fig. 11.19) gives an indication of how constant the power inputs to the radioactive and electrical arrays were maintained. (Notice that this theoretical curve was calculated using the 20°C thermal properties of salt, rather than the 100° properties used for previous calculations.) These

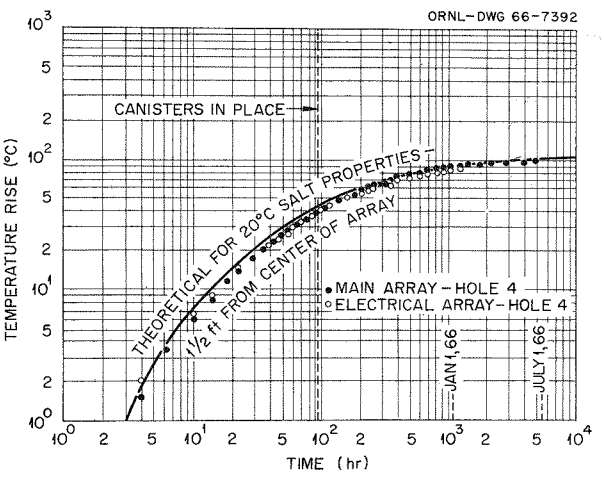


Fig. 11.19. Comparison of Theroretical and Measured Temperature Rises in Rooms 1 and 4.

control temperatures were located 1½ ft from the centers of the array holes (beyond the range of most of the gamma radiation) and were used to monitor the adjustment of total power input, as explained here. When the fuel canisters were placed in the main array (room 1), there was essentially no change in the agreement with the electrical array (room 4) temperature rise. If there had been any significant error in calculating the power output of the fuel assemblies, the main array temperature curve would have been expected to shift. After about 1300 hr elapsed time, both arrays had essentially the same temperature rises, so only the main array was plotted beyond that point. The plot stops at about 4900 hr, the time of the first fuel assembly changeout. Comparisons between other array hole control-point temperatures were about the same, and remained so after the changeout. Comparison of the room 5 temperature rises with the electrical array (room 4), on the same elapsed time basis, showed room 5 running hotter, as would be expected.

The 9-ft-depth temperature vs time plots running north through the center array hole (No. IV) and the peripheral hole (No. V) are shown in Fig. 11.20. Thermocouple hole 29 (16 ft north of center) is just at the base of pillar 1-2. Also shown is the pillar temperature halfway between floor and ceiling at horizontal distances into the pillar of 1, 5, and 15 ft (the center). Generally the same considerations apply as in the discussion of Fig. 11.18. It may be noted that the pillar at midheight did not experience any appreciable temperature rise for about a month or so, and then the maximum rise (occurring later) was not more than about 5°C until after the power boost.

Not shown are the temperatures on a line from the center out through array hole VI, but they are similar to those in Fig. 11.20, as would be expected.

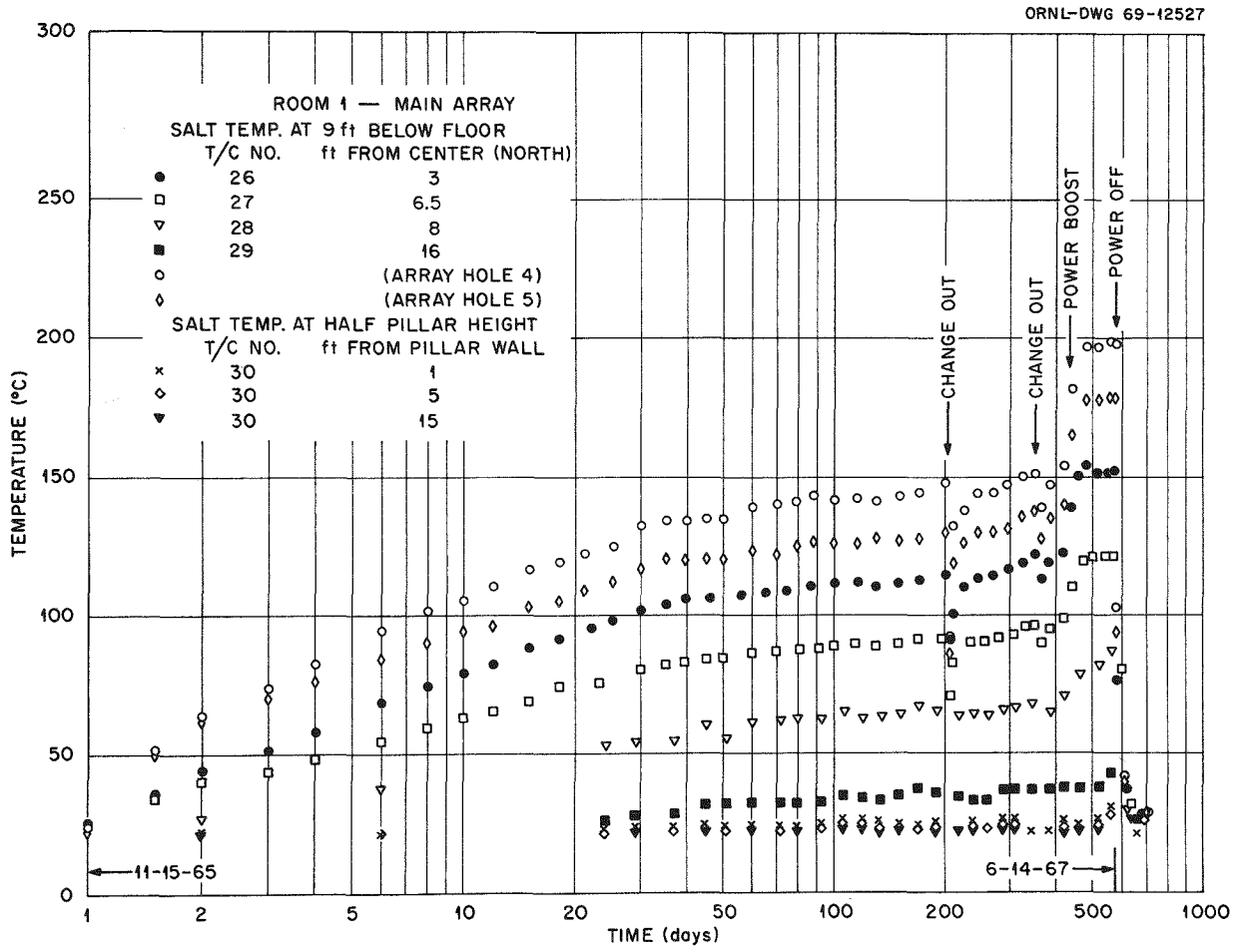


Fig. 11.20. Temperatures vs Time at 9 ft Depth and Various Distances from Center of Room 1 and in Pillar.

11.3.2.3 Other Array Temperatures. – Temperatures in the air annuli of three array holes in rooms 1 and 4 are shown in Figs. 11.21 and 11.22. In room 4 the temperatures are around 25°C lower than those in room 1. This is probably due to the fact that room 4 heaters are inside the hole liners (and the hole liners themselves are smaller in diameter), whereas in room 1 the supplementary heaters are in the air annuli. Room 5 temperatures are closer to room 1 than to room 4, which tends to support this reasoning.

Temperatures at the top, middle, and bottom of lower sections of the center array hole liners themselves in rooms 1 and 4 are shown in Figs. 11.23 and 11.24. It will be noticed that when the fuel assemblies were installed in room 1 (and the electrical power cut back accordingly) there was a marked increase in the liner temperature, as would be expected. The room 4 liner was somewhat hotter, on the average, due to the fact that all of the power was inside the liner. The room 5 liner temperatures were similar to those of room 1.

Temperatures measured between plates of the fuel assemblies in the center array holes are shown in Fig. 11.25. E- numbers identify the ETR fuel assemblies; U and L indicate the assembly occupying the upper or lower position in the canister. From the two previous figures it may be seen that the hole liners had reached maximum temperature (before the power boost) after about 30 days. The fuel assembly temperatures were also at their peak then at about 250°C. With the second and third sets of fuel, the fuel temperature was initially at about 300°C, dropping to about 270 to 280°C after 30 days. This is consistent with the fact that the second and third sets of fuel had higher heat generation rates when they were placed in the mine. It may be seen that when the fuel assemblies were transferred from room 1 to room 5, the lower assembly temperatures remained about the same, but the upper assembly temperatures increased a few degrees. This was probably due to the fact that the zone from 6 to 9 ft depth had considerably more shale than did the 9-to-12-ft zone (see Table 11.2). The effect of the power increase on fuel temperatures may also be seen in Fig. 11.25.

11.3.3 Heated Pillar

The center pillar of the experimental area was heated by 11 heaters each on the south and north sides of the pillar. The heaters were in the floor, with the heated

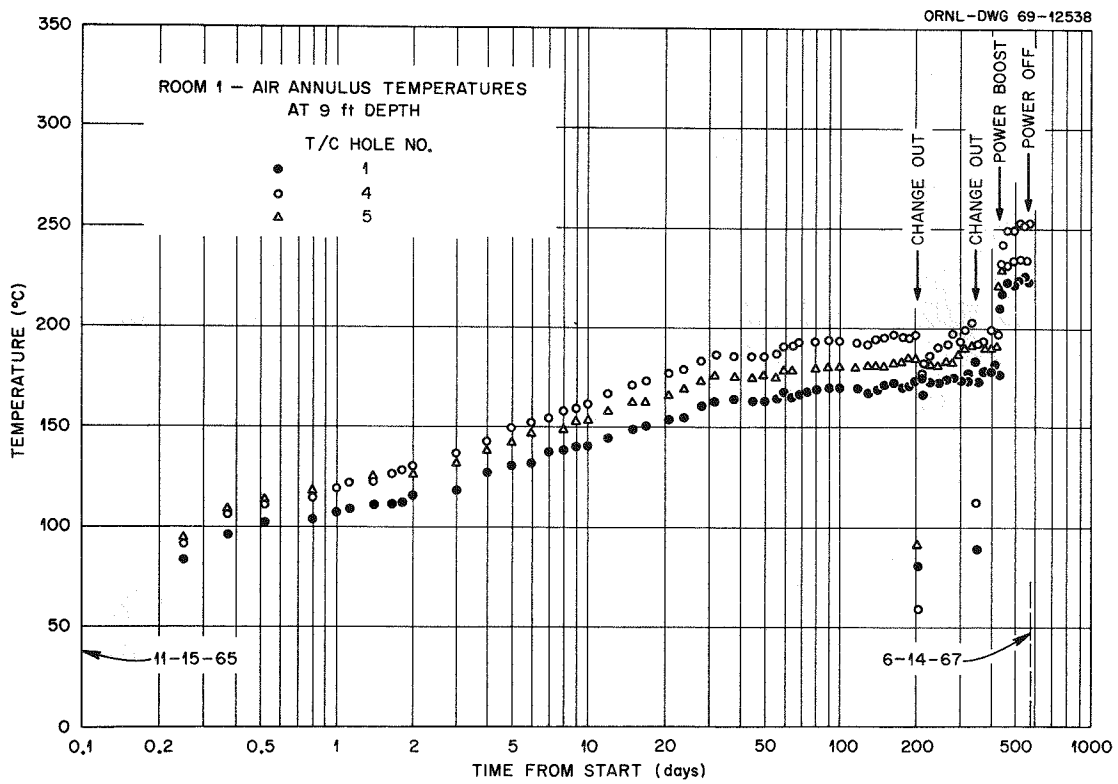


Fig. 11.21. Air Annuli Temperatures – Room 1.

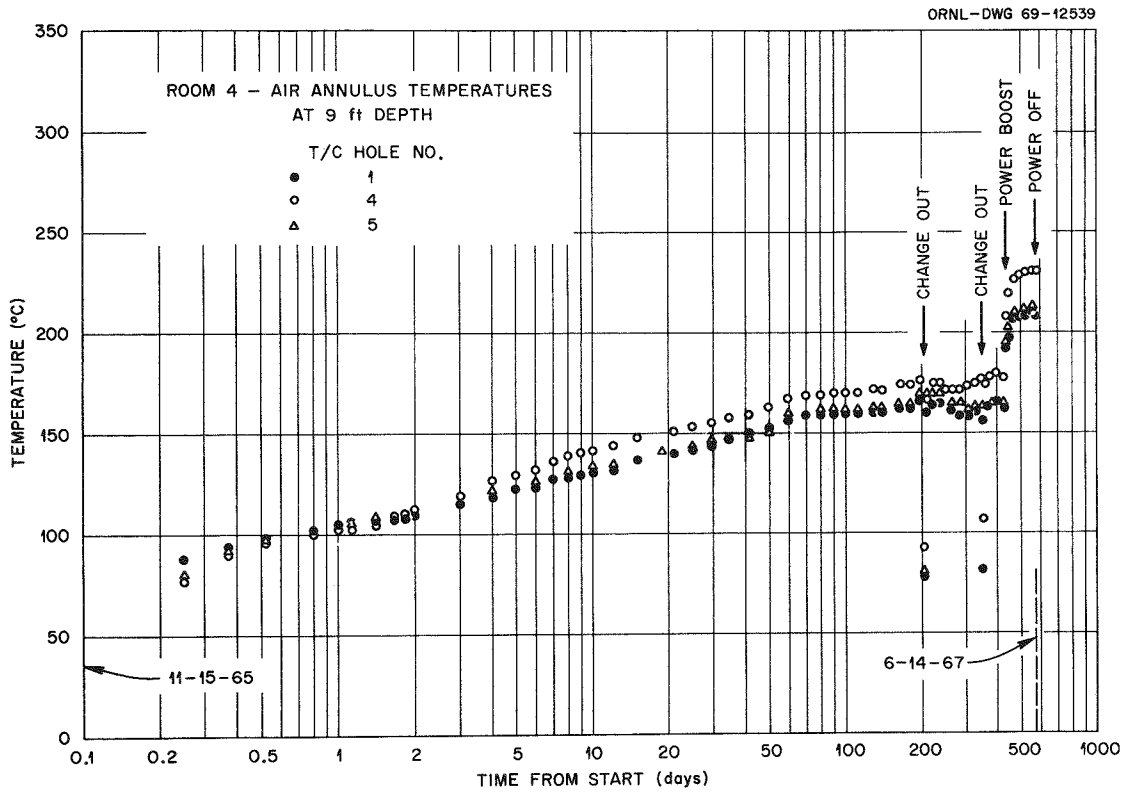


Fig. 11.22. Air Annuli Temperatures – Room 4.

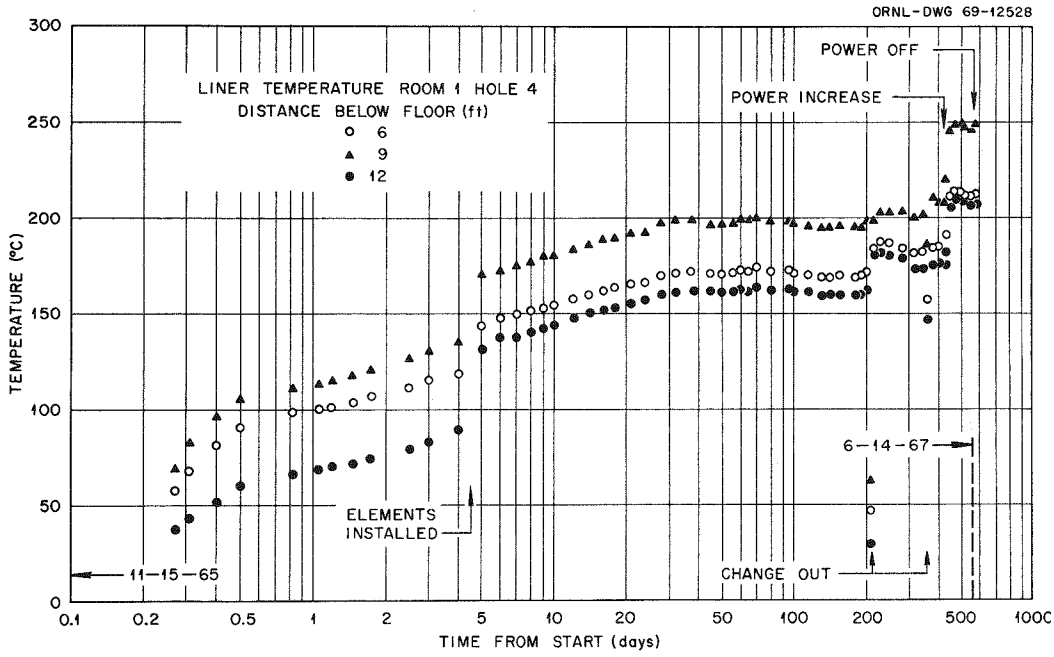


Fig. 11.23. Hole 4 Liner Temperature – Room 1.

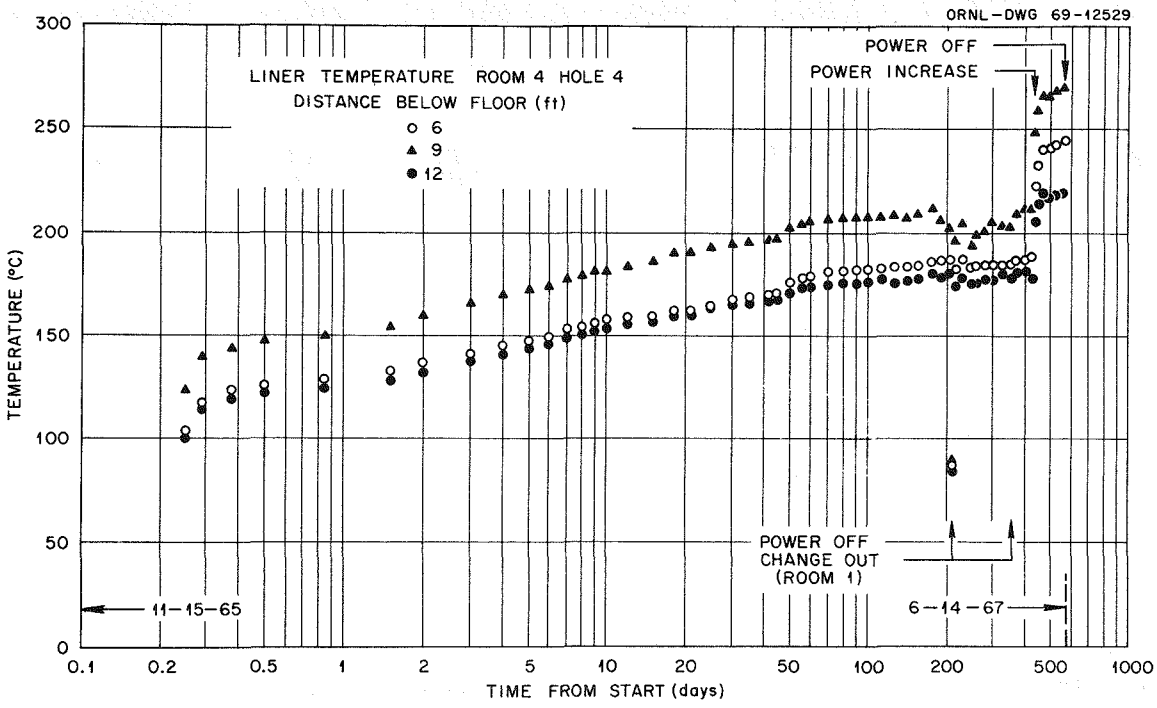


Fig. 11.24. Hole 4 Liner Temperature – Room 4.

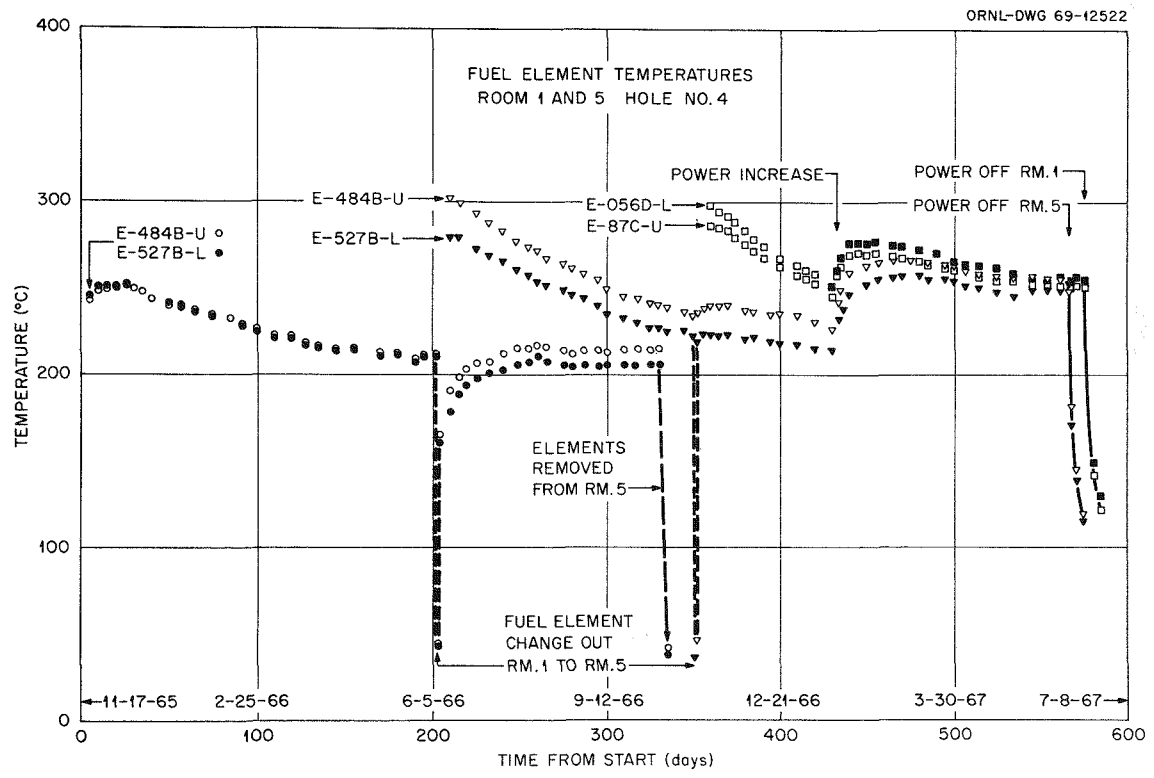


Fig. 11.25. Fuel Element Temperatures.

zone starting at 6 ft below floor level and extending to 12 ft depth. Heaters in each room were numbered from 1 to 11, starting at the back of the room. Spacing was 5 ft, so the No. 6 heater was at the center of the pillar. Power inputs are described in Sect. 11.3.1. Heaters were made of 6-in. sched 40 pipe and placed in 6-in.-diam holes, except the No. 6 heaters, which are described in Sect. 11.3.4.

11.3.3.1 Temperature Profiles. – At the end of the test (early October 1967) temperature contours in the floor of room 2 and under half of the pillar (at a depth of 9 ft) were as shown in Fig. 11.26. The other half of the pillar and room 3 presented essentially a mirror image of this figure. Ambient temperature was about 23°C. The maximum temperature under the exact center of the pillar 9 ft below the floor was 73°C.

Temperature contours in a vertical plane along the east-west center line of the pillar are shown in Fig. 11.27. Vertical maximum temperature contours at the center of the pillar in the north-south direction may be seen in Fig. 11.14.

Very roughly, a volume of salt beneath the pillar and rooms 2 and 3 about 40 ft wide (north to south), 20 ft high, and 50 ft long was raised to a temperature above

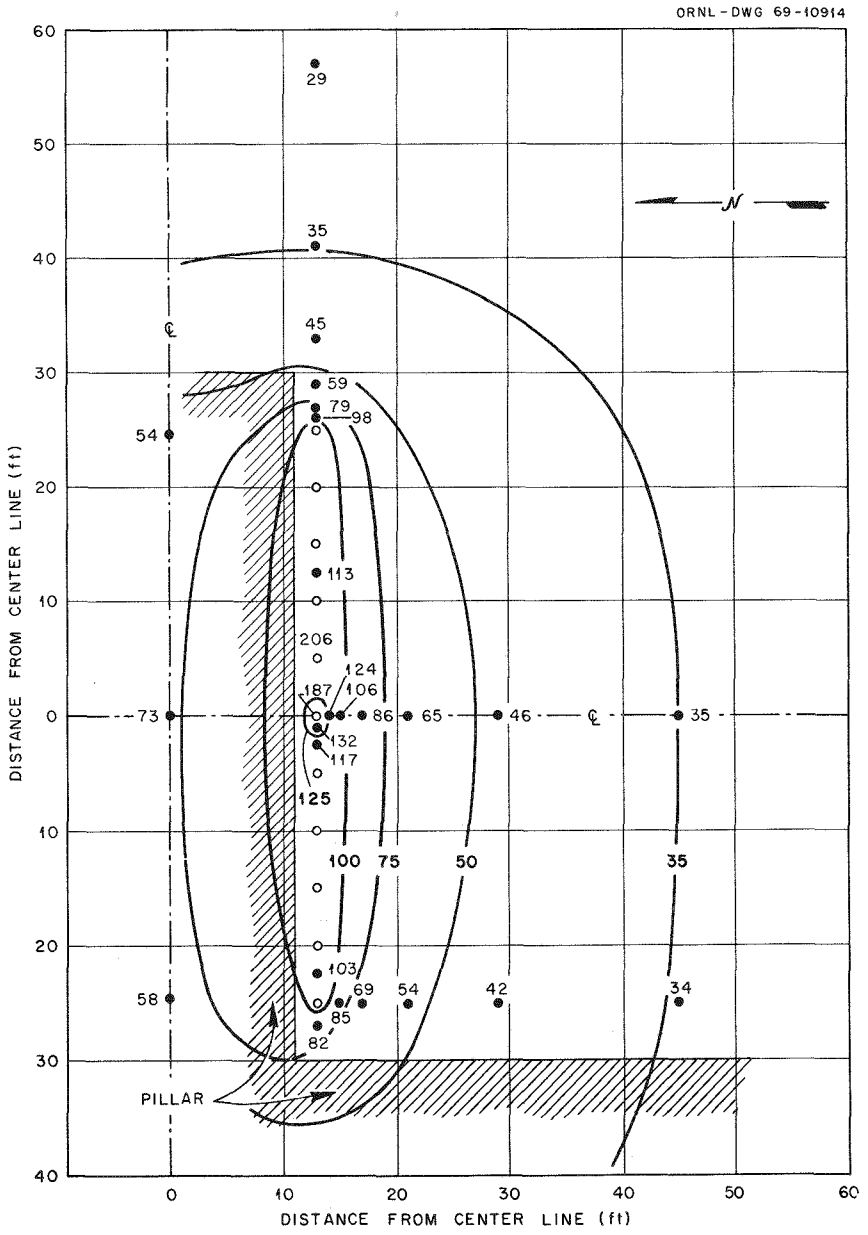


Fig. 11.26. Temperature Contours (°C) in Horizontal Plane at 9 ft Depth Below Floor – Room 2 and Pillar 2-3.

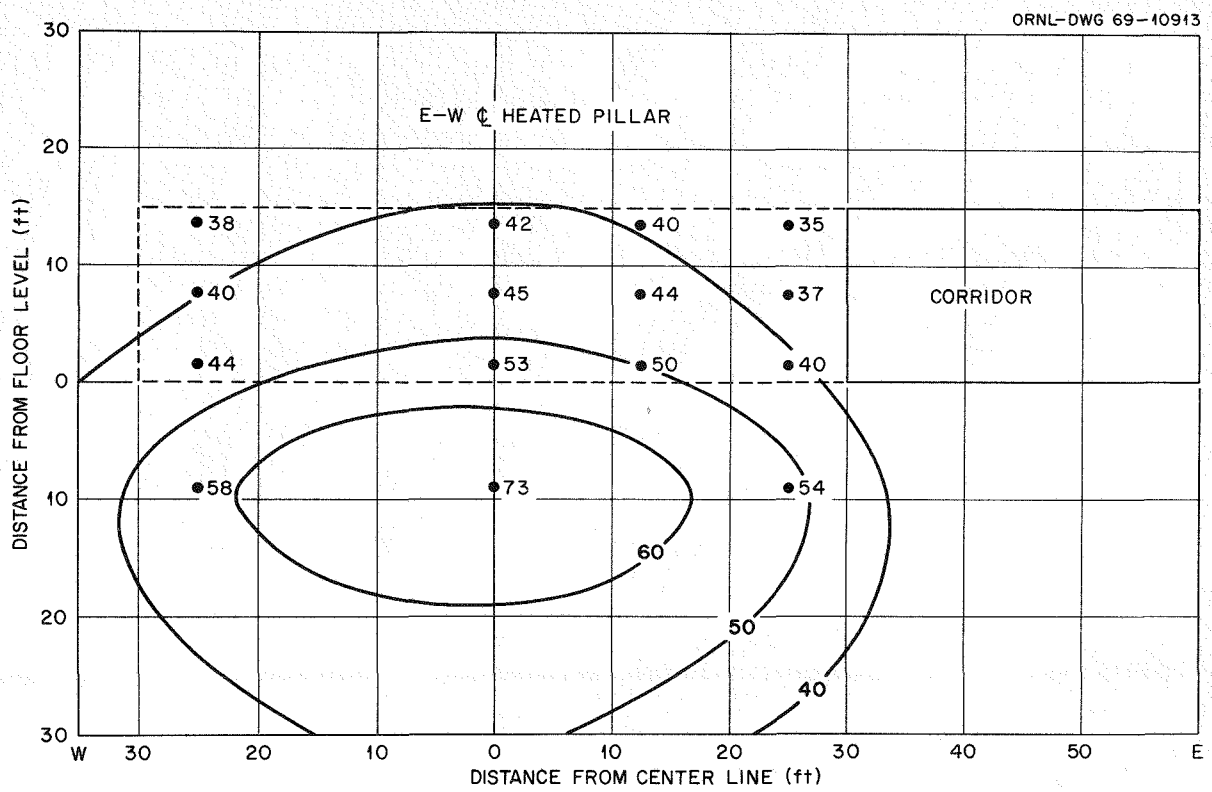


Fig. 11.27. Temperature Contours (°C) in Vertical Plane on Long Axis at Center of Pillar 2-3.

60°C. Under each side of the pillar and rooms 2 and 3 a roughly ellipsoidal volume of salt with axis dimensions of about 17 ft in the north-south direction, 14 ft high, and 57 ft long was raised to above 75°C. A similar volume with dimensions of about 7 ft wide, 8 ft high, and 50 ft long was raised to above 100°C. The 125°C temperature contours close around each individual heater. The dimensions of the above-125°C volumes were about 2 ft wide, 7 ft high, and 3 ft long, except for the heaters at each end of the pillar, where the volumes would be smaller.

11.3.3.2 Salt Temperatures vs Time. – Temperatures as a function of time at the 9-ft depth on the north-south center line through room 2 are shown in Fig. 11.28. These temperature points are in line with the center heater (No. 6) and run from 1 to 30 ft south of the heater. Also shown is the temperature under the center of the pillar. It will be noticed that several of the temperatures started above ambient. This is because heater 6 (a modified pillar heater) had been operated by itself for about five months and shut down only three days prior to the start of the main test (see Sect. 11.3.4).

Temperatures in the above figure may be compared with those in Fig. 11.29, which are on a line running out to the east from the end of the row of heaters. As would be expected, temperatures out from the end of the pillar are lower than those out from the center of the long axis.

Temperatures at different depths below floor level at a point 8 ft south of the center heater are shown in Fig. 11.30. (The 9-ft-depth curve was also shown in Fig. 11.28.) The effects of the greater heat loss to the room (than would be the case if it were solid salt) may be seen in this figure. If it were not for this effect, the 1-ft-depth and 17-ft-depth curves would be the same, as would the 5-ft- and 13-ft-depth curves.

Temperatures in and beneath the pillar itself (at the center of the long axis) are seen in Fig. 11.31. The temperatures 11 ft from the edge are at the approximate center of the pillar. Notice that it took about 10 to 15 days for the center of the pillar (at midheight) to experience a detectable temperature rise.

For a discussion of heater temperatures, see Sects. 11.3.4 and 11.3.5.

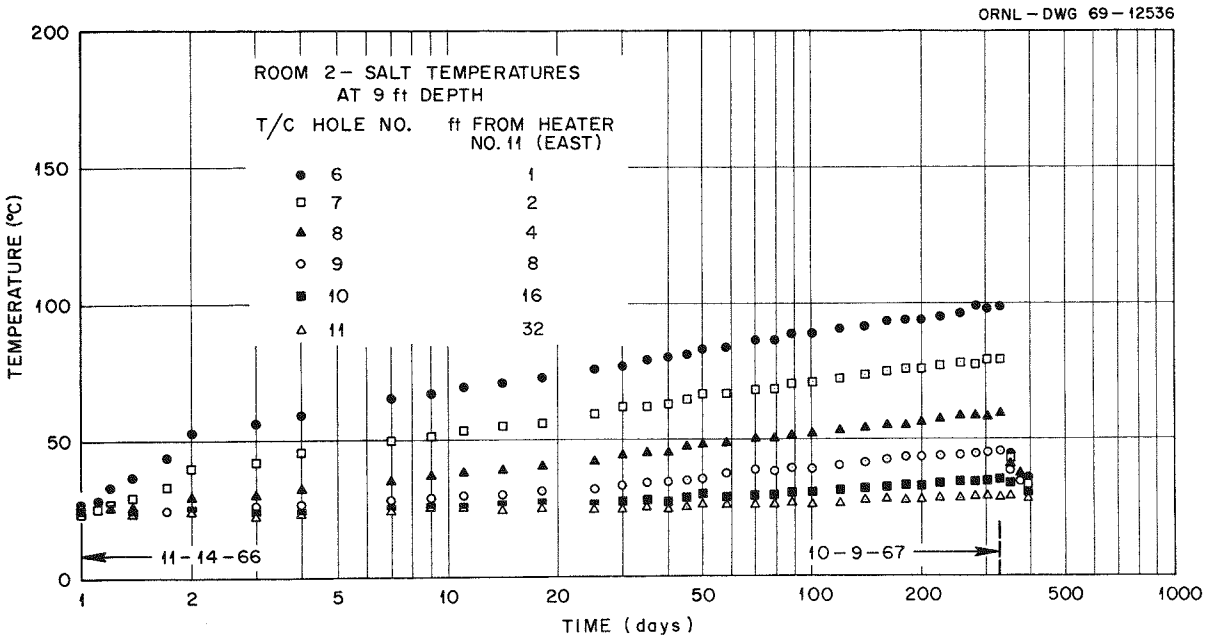


Fig. 11.28. Salt Temperatures vs Time at 9 ft Below Floor at Various Distances South of Heater No. 6 – Room 2.

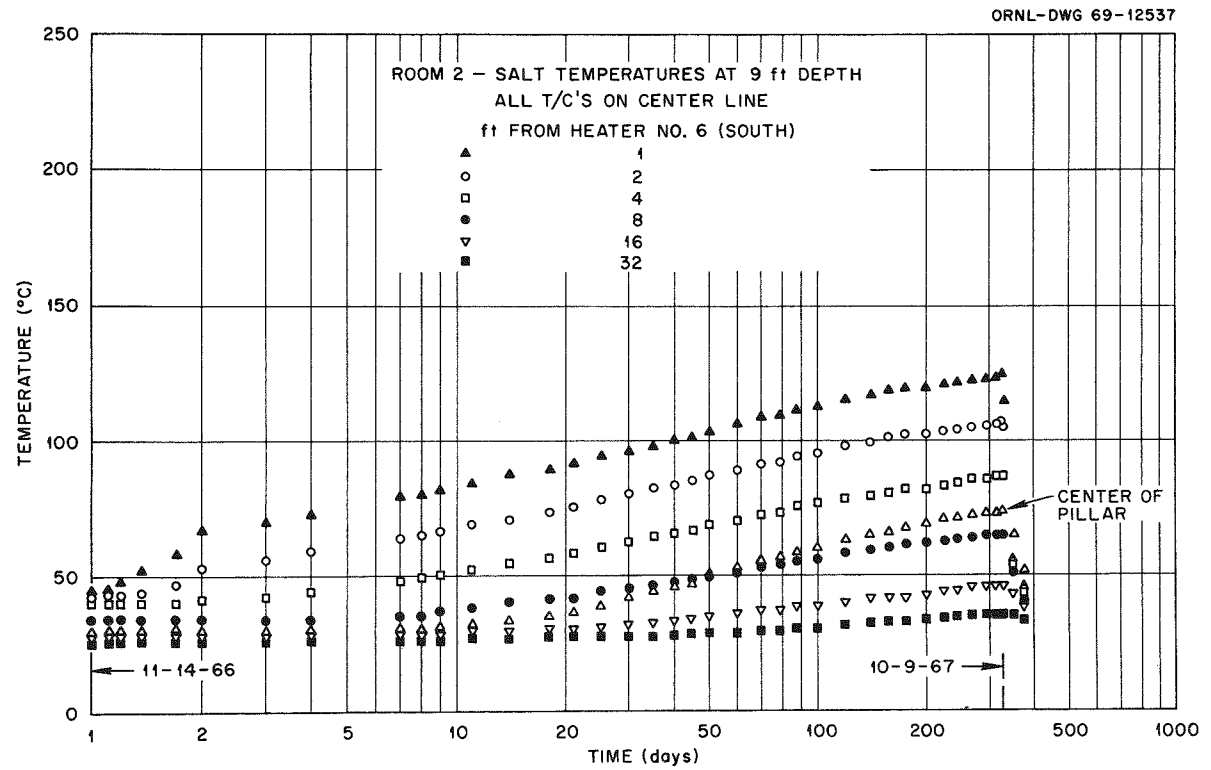


Fig. 11.29. Salt Temperatures vs Time at 9 ft Below Floor at Various Distances South of Heater No. 6 – Room 2.

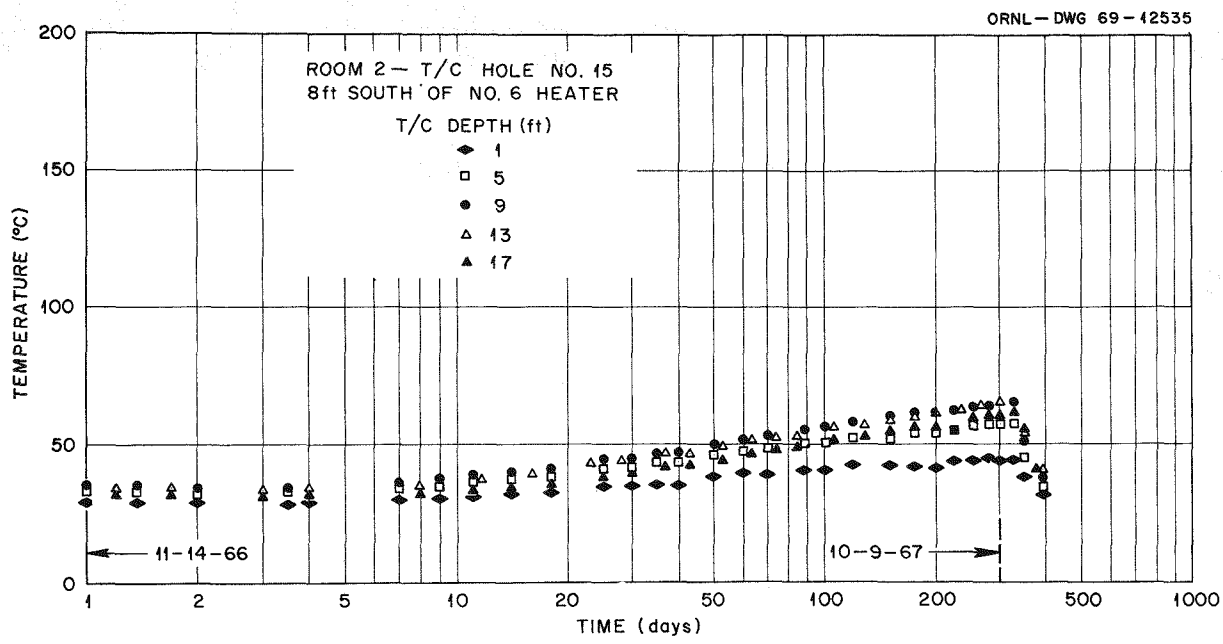


Fig. 11.30. Temperatures vs Time at Various Depths, 8 ft South of Heater No. 6 – Room 2.

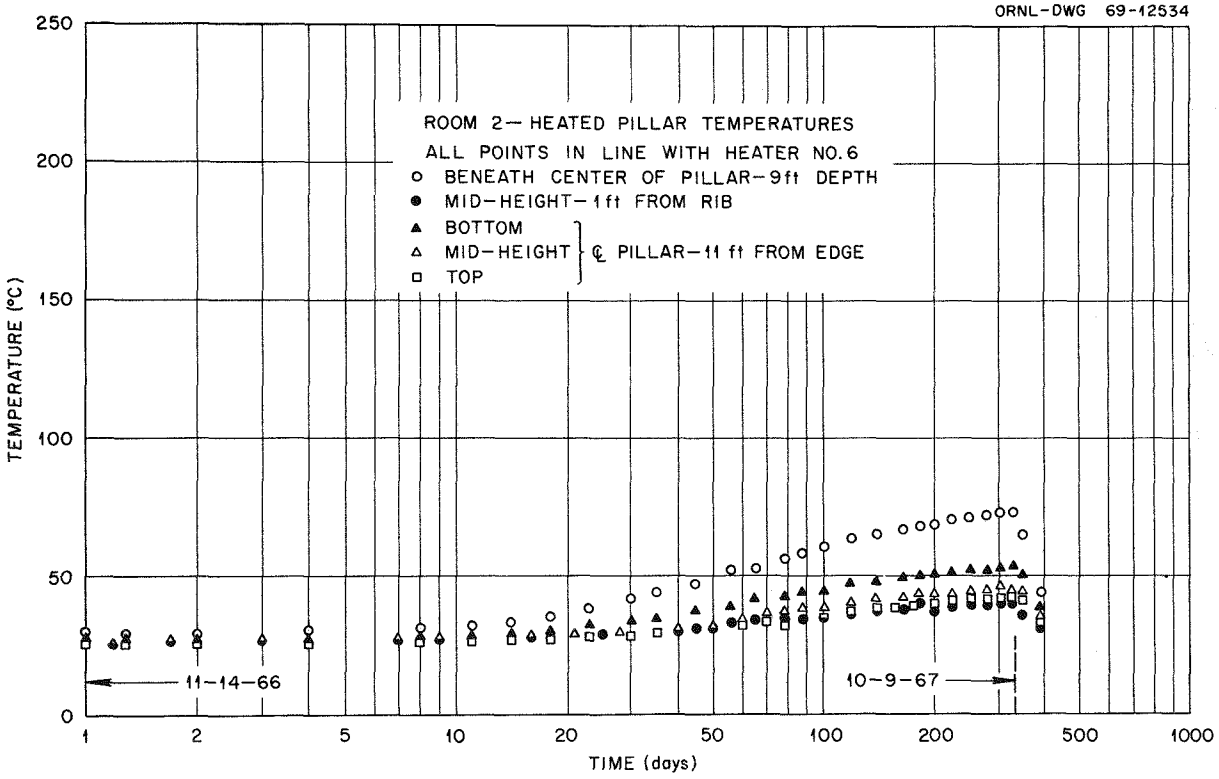


Fig. 11.31. Heated Pillar Temperatures – Room 2.

11.3.4 Modified Pillar Heaters

The modified pillar heaters occupied No. 6 positions in rooms 2 and 3. These heaters differed from the others, as described in Sects. 7.6.1 and 7.6.2. They were made from 4-in. sched 40 pipe, as were the regular heaters, but were placed in 8-in.-diam holes rather than the 6-in. holes for the regular heaters.

The room 2 heater was started on June 22, 1966, and operated until November 11 at an average power input of about 2.8 kW. Heater pipe temperatures at the top, middle, and bottom (6, 9, and 12 ft depth below the floor) during this period are shown in Fig. 11.32. It should be pointed out that the time scale at the beginning of this graph has been modified. Power was turned on at time 1 day as indicated on the scale. The first four points are actually at 0.05 day, 0.15 day, 0.35 day, and 1 day after startup. Thus "1 day" on the scale is really zero days elapsed time, and "2 days" is actually 1 day. The point at 5 days (and all points thereafter) is plotted at the correct elapsed time. Thus the peak temperature appears to have occurred at about the middle of the first day of operation, and then continued to decrease with time thereafter. This decrease in can temperature was anticipated due to the flow of salt into the hole at elevated temperature, with consequent compaction and recrystallization of the crushed salt. The drop in temperature *rise* was about 14% for the top of the can and about 21% at the middle. (The 12-ft-depth temperature appears to be an exception, perhaps because the bottom of the hole acted to restrain the salt flow. However, this thermocouple was read with a portable potentiometer, and only one reading was obtained during the first day.)

A pressure gage connected to the inside of the heater pipe read 0 psig at the start, reached a maximum of about 27½ psig about the time the pipe temperature peaked, and then fell with pipe temperature to a minimum of about 23 psig.

Flow in the 3-, 6-, 9-, and 12-ft-depth flow tubes started at about 0.5 to 0.7 cfm when approximately 1 psig pressure was applied to their inlets. The 6-, 9-, and 12-ft depths dropped to about 0.1 to 0.2 cfm by the end of the test, while the 3-ft-depth probe was showing about 0.9 cfm.

The drop in temperature (without a drop in power) indicates that salt around the heater can was being recompacted and thus producing better heat transfer properties between the can and the solid salt. The

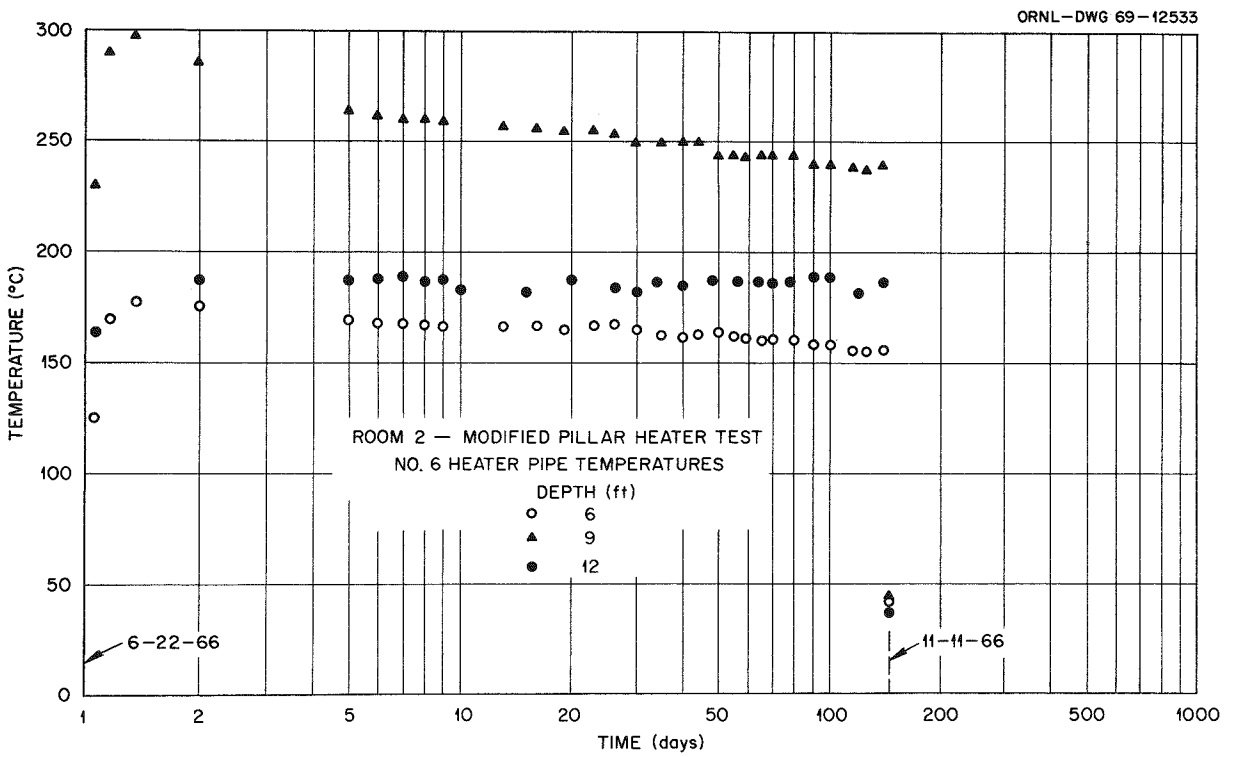


Fig. 11.32. Modified Pillar Heater Test Temperature vs Time – Room 2.

reduction in pressure inside the can merely confirms the fact that the temperature inside the can was reduced. Decreased flow rates through the 6-, 9-, and 12-ft flow tubes also indicate compaction around the can, but the 3-ft-depth tube indicates little compaction several feet above the can. This would be expected. (Not too much significance should be attributed to the flow readings, however, since they were difficult to make. This was primarily because of difficulty in maintaining the pump pressure and in reading the flow gage at low flows.)

After a three-day shutdown of the room 2 heater, all pillar heaters were started on November 14, 1966, at a nominal 1.5-kW input each (including the modified heaters in rooms 2 and 3). The No. 6 heater pipe temperatures are shown in Figs. 11.33 and 11.34. The room 2 heater did not get as hot as the one in room 3, probably because of the better heat transfer of the room 2 heater due to prior recompaction and recrystallization of salt around the pipe.

After about a week of operation, the pressure in heater 6, room 2, was up to about 15 psig, and No. 6 in room 3 was at about 11 psig. Over the course of operation, heater 6 in room 2 built up to a pressure of about 19½ psig. The modified heater in room 3 reached 11.8 psig by February 9, 1967, and then the pressure started to fall due to a tiny leak in the standpipe caused by corrosion. By May 4 the pressure had slowly fallen to below 3 psig (room 2 pressure was 18 psig at this time). On May 4 it was repressurized to 18 psig, and it again fell to below 3 psig in about 2½ weeks, thus indicating a larger leak.

Flow-tube readings were somewhat erratic during operation of the pillar heaters, but, in general, the 9-ft-depth tubes in both rooms showed no flow, the 6- and 12-ft-depth tubes showed about 0 to 0.1 cfm, and the 3-ft tubes about 0.2 to 0.7 cfm.

11.3.5 Effects of Salt, Sand, and Air Backfill

The effects of backfill material (in the annulus around the heater pipes) on the regular pillar heater temperatures are shown in Fig. 11.35. (The regular heaters differed from the modified heaters in that their pipes extended the full length of the hole, although the heating elements were confined to the bottom 6 ft and had some insulation above them.) The two top curves show the upper and lower limits of pipe temperatures at the 9-ft depth on various heaters in rooms 2 and 3 that

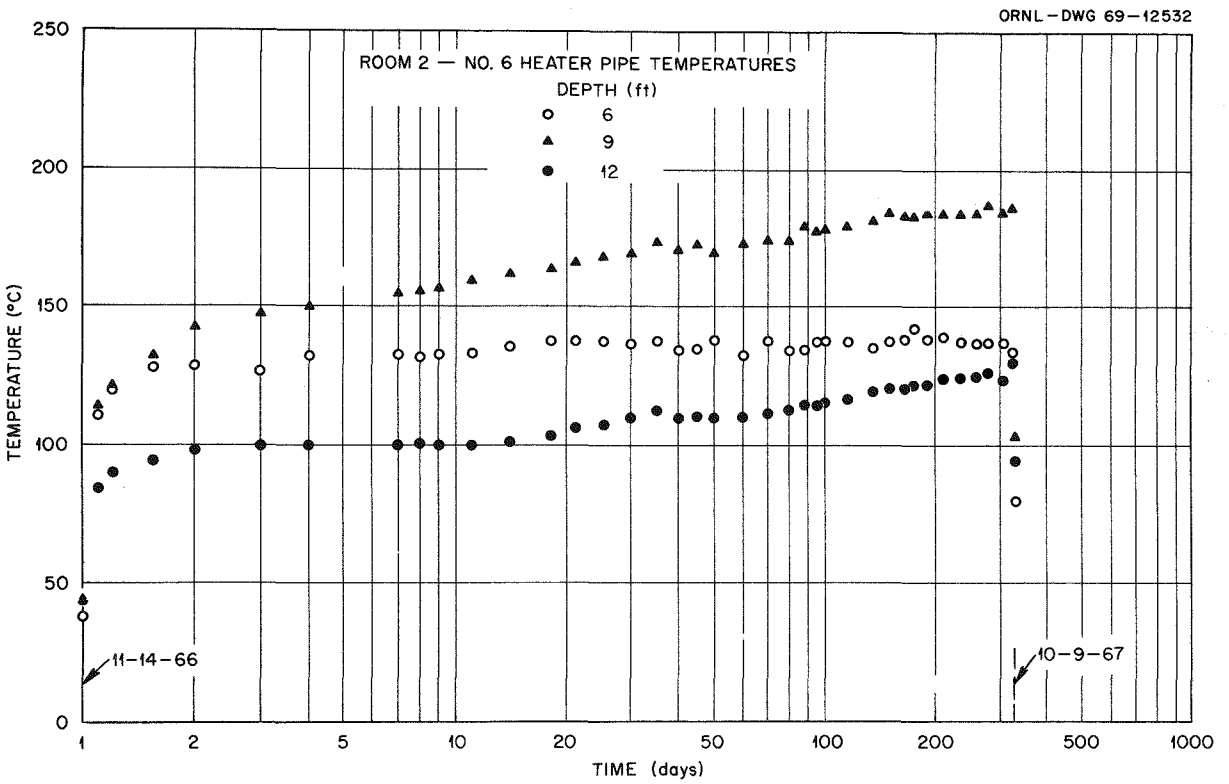


Fig. 11.33. No. 6 Heater Temperature vs Time – Room 2.

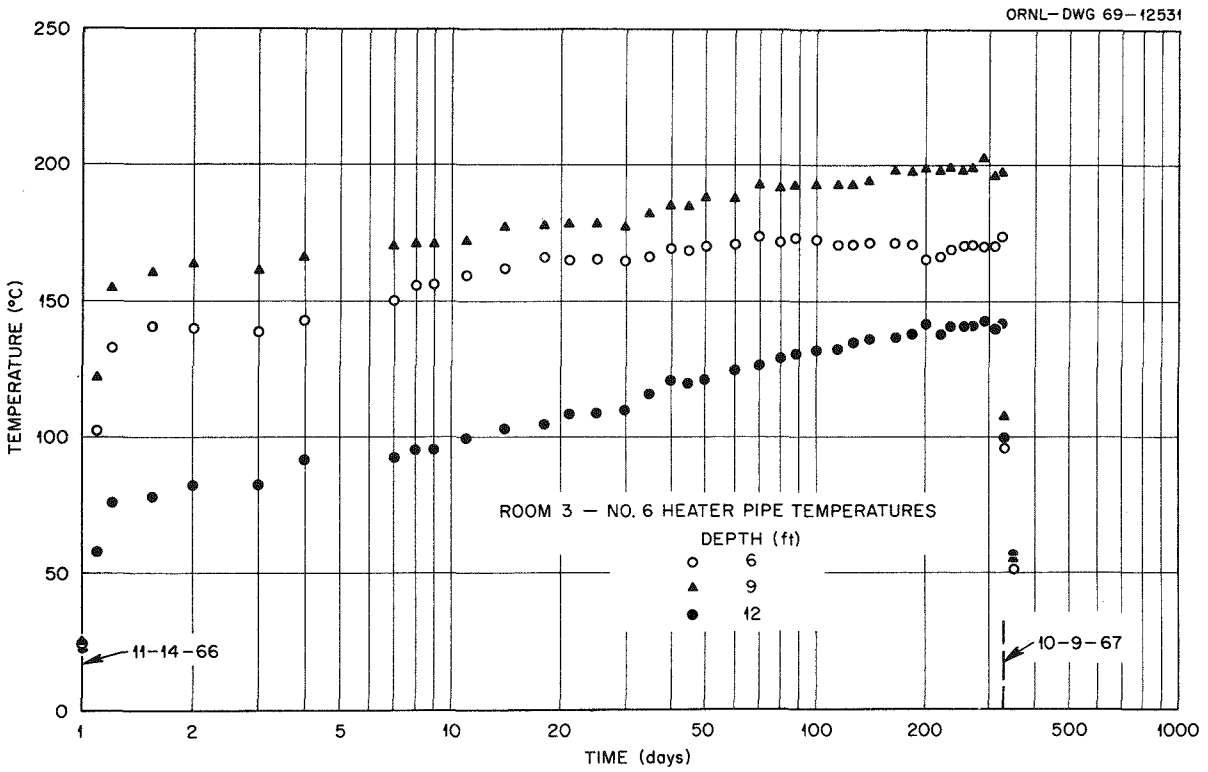


Fig. 11.34. No. 6 Heater Temperature vs Time – Room 3.

were equipped with thermocouples and that had no backfill material (that is, an air gap) around the pipes. There were three other instrumented heaters with air gaps (Nos. 1, 9, and 11) in room 2, and their temperature curves fell within this range.

Only one heater was backfilled with sand (No. 7 in room 2), and its temperature was lower than those with no backfill material. One heater (No. 8 in room 3) was backfilled with salt, and its temperature was lower than the one with sand. The temperature rise for salt backfill was about 20% lower than the coldest of the air-gap heaters and about 30% lower than the hottest one.

Comparing the salt-backfilled regular pillar heater temperature (Fig. 11.34) with that of the modified heaters, it is seen that the modified heaters operated a few degrees hotter. This was probably due to greater heat transfer up the pipe walls in the regular heaters, coupled with the fact that the regular heaters had only a $\frac{3}{4}$-in. annulus of salt backfill, while the modified heaters had a $1\frac{3}{4}$-in. annulus.

11.3.6 Simulated Waste Container Test

SWCT heaters were 6-in. sched 40 pipe in holes 10 in. in diameter by 12 ft deep. In addition to trouble with the power in SWCT heaters (discussed in Sects. 10.5.4.2 and 11.3.1) considerable difficulty was also experienced with thermocouples. On heater 1 (mild steel) in the Experimental Entry, all three thermocouples on the heater pipe did not appear to be reliable. However, the salt temperatures at the wall of the hole and 18 in. from the center of the hole appeared to be reasonable. The wall of the hole reached about 205°C by 100 hr after startup, then fell, and rose again to about 180°C when the power input was 3.3 kW. At 1.6 kW it dropped to about 115°C. At 18 in. out, the temperature reached about 100°C by 100 hr, fell and recovered to about 100°C at 3.3 kW, and fell to about 65°C at 1.6 kW.

No. 2 heater (stainless steel) in the Experimental Entry reached about 190°C at the top and bottom and 290°C at the center by the end of 100 hr. Temperature at the center of the pipe actually peaked at about 320°C after about 5 hr. At 3.1 kW the pipe center temperature was about 220°C. The wall of the hole was about 220°C at 100 hr, reached 240° by 550 hr, and continued at about 190°C during the period of 3.1 kW input. The 18-in.-out temperature reached about 100°C by 100 hr and 120°C by 550 hr. At 3.1 kW it continued about 100°C.

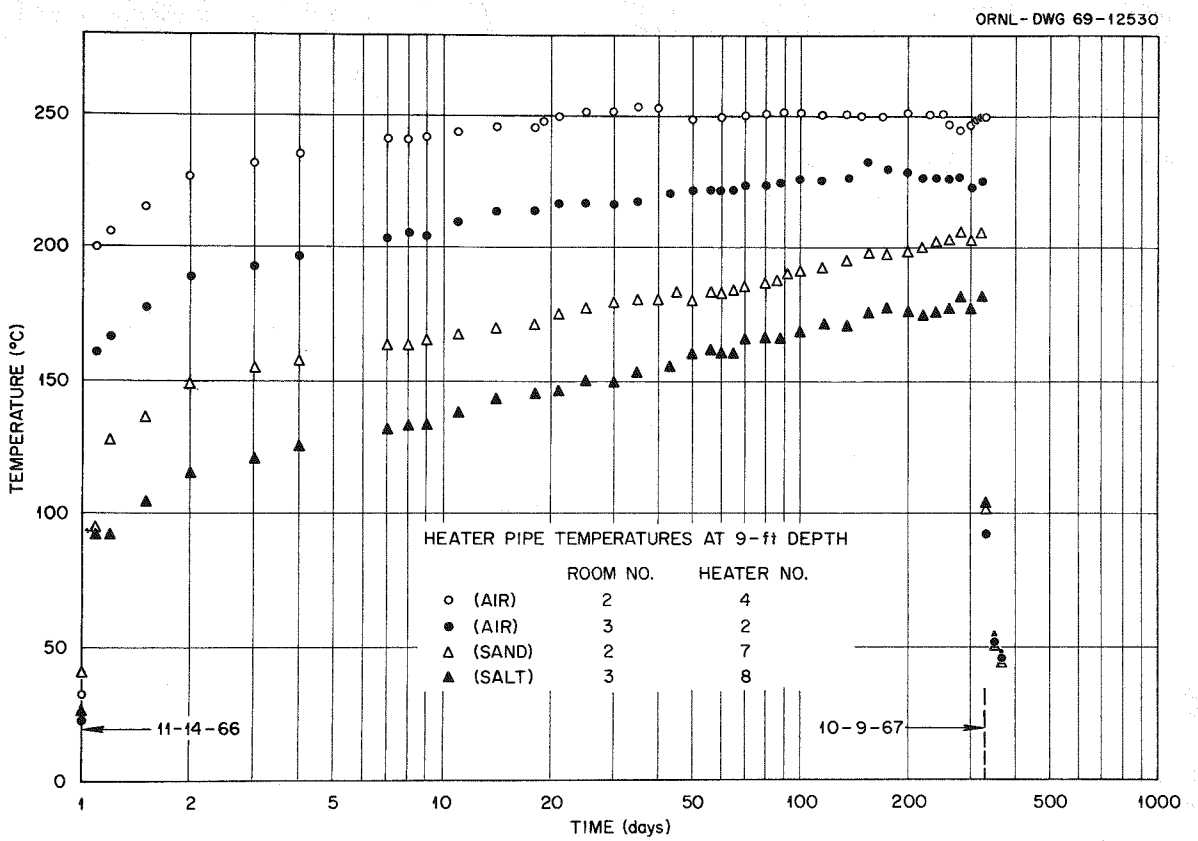


Fig. 11.35. Comparison of Heater Temperatures with Salt, Sand, and Air Backfill.

The entry 5A No. 1 heater pipe (mild steel) reached about 255°C at center, 170°C at top, and 190°C at bottom by 50 hr at 3.2 kW. At 4.3 kW the center temperature reached about 360°C by 95 hr. At 1.6 kW the center temperature was about 200°, the top 125°, and the bottom 150°C. Corresponding wall-of-the-hole temperatures were 150, 245, and 165°C. At 18 in. the corresponding temperatures were about 85, 140, and 115°C. At the center of the four-can array, temperatures at the same times were about 65, 105, and 105°C.

Entry 5A heater 2 (stainless steel) reached about 370°C at the center by 100 hr, while the wall of the hole reached 200°C and the 18-in.-in temperature (toward the center of the four-can array) reached 135°C. On restart, the pipe reached at least 400°C, and the wall of the hole to at least 250°C.

Heater 3 (stainless steel) in entry 5A reached 400°C at the center by 100 hr, the wall of the hole reached 280°C, and the 18-in.-in temperature (toward the center of the array) 145°C. Can couples were erratic at 1.6 kW but indicated a peak temperature around 250°C at the center. The wall of the hole went to about 150°C, and the 18-in.-in temperature to about 115°C.

The can thermocouples on heater 4 (mild steel) were erratic. The wall of the hole reached about 260°C by 100 hr, while the 18-in.-out temperature reached 115°C and the 18-in.-in temperature reached 145°C. On the restart at 4.8 kW, the wall reached 300°C, the 18-in.-out temperature to 150°C, and the 18-in.-in temperature to 175°C. At 3.2 kW the wall-of-the-hole thermocouple failed, the 18-in.-out temperature went to 135°C, and the 18-in.-in temperature went to 150°C.

It is obvious from this temperature history that limited information was gained in the SWCT test. Metallurgical examination results are given in Sect. 10.6.2.

11.4 ROCK DEFORMATION AND MINE STABILITY

Although previous chapters mention the rock mechanics gages, their installation and the results, these references are at best superficial. This section discusses the rock mechanics gages in detail, including (1) a description of the various gage types used in the Lyons mine; (2) discussion of the design of the gage layout, both in the experimental area and throughout the rest of the mine; and (3) presentation of the data, including interpretation and preliminary analysis, for all phases of the experiment.

11.4.1 Description of Gage Types

A wide variety of rock mechanics gages were used in the experimental phases of Project Salt Vault. Some of these were designed and fabricated by ORNL; other more or less standard rock mechanics instruments were purchased from various suppliers. The following description of these instruments is divided into subsections based essentially on the type of deformation measured.

11.4.1.1 Internal Strain Gages. – This type gage consists of a number of wires anchored by expanding-shell roof-bolt anchors at various distances along a borehole in the rock. The collar of the hole is filled with another roof-bolt anchor to which is attached a 12-in. length of pipe and a threaded boss. Stainless steel wires come through this boss and terminate with a small brass nipple clamped to the wire by a set screw. Nipples also carry the wire length identification by filed notches.

This type gage is read using the extensometer shown in Fig. 11.36 (ref. 13). The instrument is screwed onto the threaded boss of the collar anchor by means of the capstan head. The facing surfaces on the collar anchor boss and the base of the instrument provide a reference position for reproducible readings. The wire nipples are next attached to the tensioning spring by means of an adapter (shown in Fig. 11.36). A reading is then obtained by tensioning the wire to a standard value (18 lb) by retracting the micrometer screw and measuring the spring deflection on the dial gage. When the proper tension is achieved, the micrometer on the barrel and handle of the instrument is read. The instrument has a range of 6 in. and a reading accuracy of 0.001 in. Any change in a series of readings over a period of time represents the relative movement between the collar anchor and the point down the borehole where the wire is anchored.

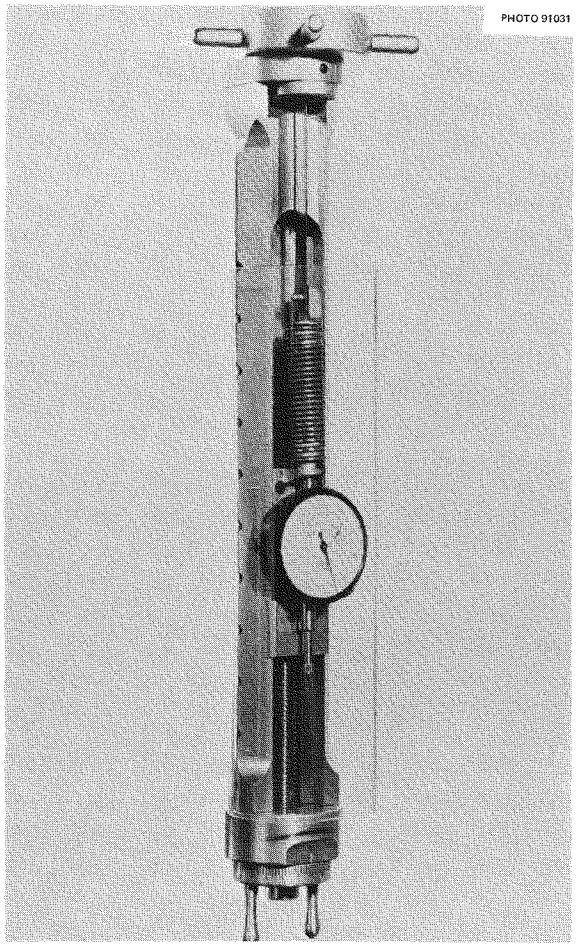


Fig. 11.36. Extensometer for Reading Internal Strain Gage Wires.

This type gage, designated "type A" in our nomenclature, can be installed horizontally, up into the roof, or down into the floor. The vertical stations, both up and down, were limited to 25-ft lengths in this experiment because it was felt that this distance, even in the center of the rooms, would cover most, if not all, of the zone of detectable deformations. The length of horizontal wires was limited to about 50 ft because of practical difficulties in installation. The installation consists in pushing the roof-bolt anchor (with wire firmly attached) down the borehole to the proper point with a set of segmented, locking tubes. The anchor is

[13] E. L. J. Potts, "The 'in Situ' Measurement of Rock Stresses Based on Deformation Measurements," *Proc. Intern. Conf. on State of Stress in the Earth's Crust, Santa Monica, Calif., June 13–14, 1963,* Rand Corp. memorandum RM-3583, pp. 11-1 to 11-17.

then set by expanding the shell against the sides of the hole by screwing the short bolt into the shell using the tubes. When the anchor is firmly seated, the tubes are removed, and subsequent anchors are installed by threading the previously installed wires through the drilled centers of later anchors.

In old workings of the Lyons mine, some internal strain stations were installed in horizontal holes up to 150 ft. For these longer-wire stations, the installation system involved hydraulically expanded anchors.[14] This system avoided the necessity of twisting the installation rods in order to expand the anchor. Also, on these long-wire stations a different type of collar anchor was employed. This collar anchor, shown in Fig. 11.37, was bolted to the face of the rock and had a system of pulleys and springs for maintaining tension on the individual wires between readings, thus avoiding fouling of the wires.

Although the extensometer used with this type station can be read to 0.001 in., accuracy of the measurement is not quite that good. The largest error in the reading is due to friction of the wire along the wall of the borehole and the seating of the brass nipple into the instrument. The magnitude of the error due to friction is a function of the length of the wire; in general, the longer the wire, the less accurate the reading. Errors due to seating of the brass nipple and other random errors were reduced by adopting the following procedure at each wire:

1. The reading was obtained by overtensioning the wire by approximately 2 lb and approaching the proper tension from this higher value.
2. The wire was then released, and the reading process was repeated two more times.
3. If a group of three readings was within a range of 0.003 in. and all readings did not vary in the same direction (for example, each larger than the previous), the average of the three was taken as the reading.
4. If a group of readings did not meet the above test, the reading was repeated until three consecutive readings did meet the test.

The quality of the installation also influences the accuracy of measurements. Some stations perform very well, while others of equal length produce results with

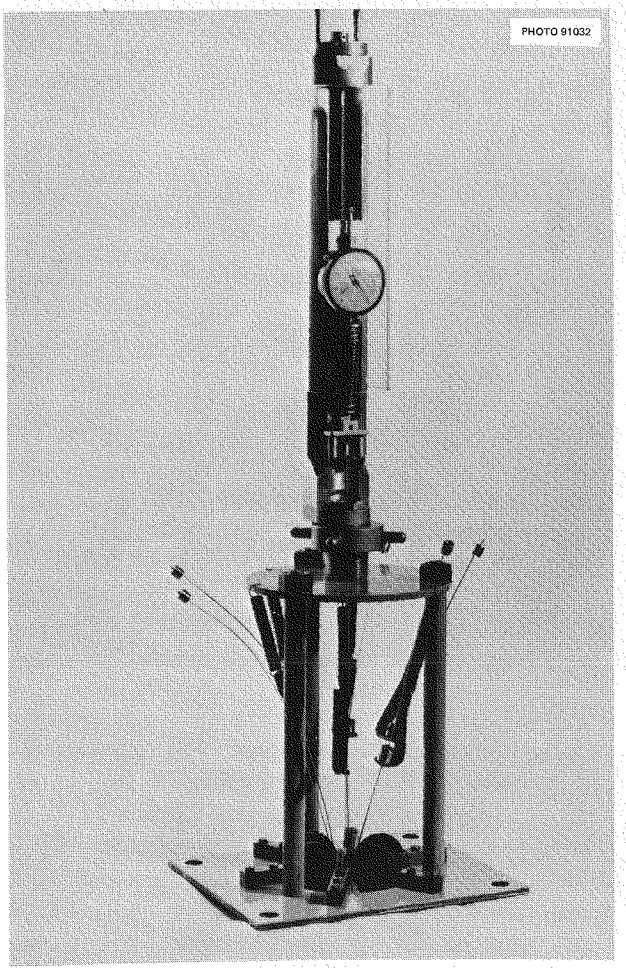


Fig. 11.37. Internal Strain Gage Extensometer Mounted on Special Long Hole Collar Bracket.

an unexplained amount of scatter. Since it is not possible to see 30 to 40 ft down the borehole, past three or four anchors, it is not possible to explain this difference, but it is undoubtedly related to the hardware installation. In general, considering all stations, including the long ones, the standard deviation of the error of this type gage is estimated to be about 0.002 in. (ref. 15).

The extensometers, anchors, and all installation equipment for these internal strain gages were purchased from Professor E. L. J. Potts, Department of Mining Engineering, University of Newcastle-upon-Tyne, England.

[14] E. L. J. Potts, *Proposed Borehole Measurement Network Around and In the Experimental Area,* consultant's report to Health Physics Division, Oak Ridge National Laboratory, Aug. 24, 1963.

[15] W. C. McClain, *A Study of the Strata Movement in the Partial Extraction of Potash,* Ph.D. Thesis, University of Newcastle-upon-Tyne, 1963.

11.4.1.2 Convergence Gages. – In this report the term *convergence* is used only to denote *vertical* closure of the roof and floor in a mined-out room. The most numerous of the several types of instruments employed to measure this convergence was the type F gage, or more simply "pipe type." This gage consists of a long piece of $\frac{1}{2}$-in. pipe anchored vertically in a shallow hole in the roof by a roof-bolt anchor, with a much shorter piece of pipe anchored by a roof-bolt anchor in the floor directly beneath it.[16] A gap of about 8 in. is left between the two abutting ends of the pipe, which are fitted with stainless steel plugs having conical seats milled into their faces. To obtain a reading a standard dial gage, fitted with an extension anvil, is inserted between the steel plugs and seated as shown in Fig. 11.38. Lateral bracing of the pipes is supplied by the wooden tripod seen in the figure and by packing the mouth of the hole around the pipe with lead wool.

[16] F. M. Empson *et al.*, "Demonstration of Disposal of High-Level Radioactive Solids in Salt," *Proc. Second Symp. on Salt, May 3–5, 1965*, vol. 1, pp. 431–43.

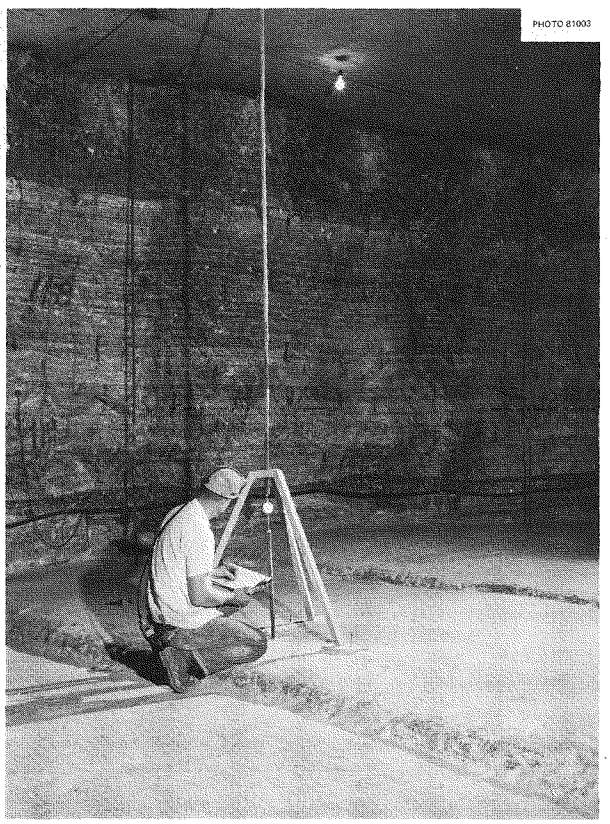


Fig. 11.38. Vertical Convergence Gage (Type F) Being Read in the Lyons Mine.

When the convergence gage is placed very close to the pillar edge, as was frequently the case, lateral support for the long roof pipe is provided by a block and guy-wire arrangement seen in the background of Fig. 11.38. In both cases, the supports do not restrict the vertical movement of the pipe. The bottom part of the gage is usually anchored about 2 ft deep into the floor so as to be below, and hence not to measure, any possible floor heaves. The top pipe is usually anchored about $1\frac{1}{2}$ ft into the roof so that it would be sensitive to the movement of the immediate roof.

The dial gage was read to the nearest 0.0005 in. and calibrated with every use against a constant reference. The accuracy of the measurement is estimated to be 0.001 in. The range of the dial gage is 1 in., but the range of the convergence gage is unlimited, since it is always possible to cut a short segment of pipe off and rethread it without grossly disturbing the installation. This type gage provided the most consistent measurements of all the rock mechanics instruments used.

Early in the program of rock mechanics instrumentation of the original mine workings, a modification of this pipe-type gage was attempted at sites near the edge of the pillar. In order to alleviate certain problems with hole drilling, the pipes were anchored in horizontal holes located vertically above and parallel to one another. These pipes were then turned into vertical alignment with 90° elbows. This type gage, denoted "type B" or "pillar squeeze," produced very erratic and inconsistent results, probably due to angular deformations of the two horizontal pipe segments, which would be magnified at the pipe ends by an amount depending upon the length of the horizontal segment. A normal type F gage was subsequently installed adjacent to most of the pillar squeeze stations. Both these vertical pipe-type gages were designed at ORNL and, except for the expanding roof-bolt anchors, were fabricated in the field by mine personnel.

At the locations where vertical internal strain gages (type A) were installed in roof and floor, a different type of convergence instrument was employed which utilized the existing collar anchors. In this case an adapter was screwed onto the threaded boss of the roof anchor, and a $\frac{3}{8}$-in.-wide stainless steel tape was stretched between it and an extensometer mounted on the threaded boss of the floor anchor. This tape extensometer, shown in Fig. 11.39, and its auxiliary equipment were obtained from Professor Potts; it operates on the same principle as the wire extensometer. The tape is tensioned by screwing a micrometer barrel against a spring, the deflection of which is measured with a small dial gage. Although the microm-

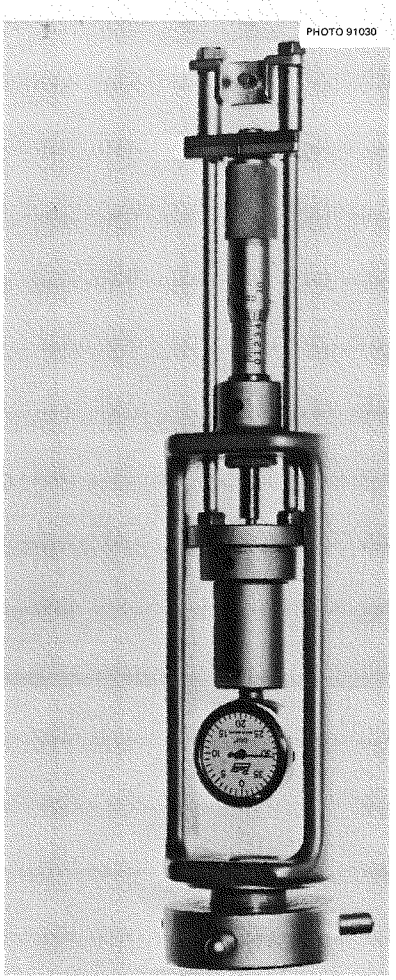


Fig. 11.39. Extensometer for Measuring Vertical Convergence Between Vertical Internal Strain Gage Stations (Type E).

eter has a range of only 1 in., the range of convergence can be extended simply by punching a new hole in the tape. The micrometer can be read to 0.001 in., and the gage has an accuracy approaching that value. This type convergence gage, denoted "type E," has the advantage that there is no permanent obstruction in the room, since the tape can be removed between readings.

In addition to the convergence instruments, a few "post type" convergence indicators were installed at selected points in those areas of the mine where work was under way. These gages consisted of a wooden 4-in. by 4-in. post with one end rounded and fitted into a short length of 3-in. pipe. This assembly is then tightly wedged between the roof and floor. Convergence causes the post to be pushed into the pipe, and movement can be readily observed by a system of pencil marks on the post. The purpose of these gages was to provide a quick on-the-spot evaluation of the condition of the roof before work in an area was commenced. They performed admirably.

11.4.1.3 Horizontal Room Closure. – The horizontal movement of the walls of a room toward each other was measured on both pipe-type gages and tape gages. In both cases, the instruments are identical in every respect, except orientation, to the equivalent vertical convergence gages. The horizontal-closure pipe-type gages are denoted "type D," and the horizontal tape gages are identified as "type C."

11.4.1.4 Diametral Borehole Gages. – All the instruments described in this section have the common attribute of measuring some property of the material in a direction perpendicular to the axis of a borehole. This is opposed to the internal strain gages, which measure deformations along the borehole axis. Since all the boreholes for these instruments were drilled horizontally, their diametral deformation provides a measure of the vertical load or the change in load being supported by the solid material.

A total of 17 instruments called "stressmeters" were obtained from Professor E. L. J. Potts[17] and installed throughout the Lyons mine, 6 of them in the experimental area. One of these instruments and its associated installation and reading equipment is shown in Fig. 11.40. The sensing head, located inside the sleeve (No. 5 on Fig. 11.40), has two tapered keyways milled on opposite sides to receive the movable wedges of the sleeve. Perpendicular to the keyways, and hence to the direction of loading, is a thin slot filled with hydraulic fluid. This hydraulic system terminates in a diaphragm in another (stress free) part of the head. The flexure of this diaphragm, resulting from changes in the load on the instrument, is sensed by an electrical resistance strain gage connected in a bridge circuit with a temperature-compensating gage, also located in the head.

The instrument is installed by inserting the head-and-sleeve assembly and hydraulic ram (No. 3 in Fig. 11.40) into a 2-in.-diam hole using the segmented rods (No. 1). When the instrument is properly located and oriented, the ram is extended, driving the head into the sleeve and expanding the sleeve wedges against the top and bottom of the hole. This is continued until the instrument develops an appreciable "prestress." The ram can then be removed from the borehole by unlocking the quadrant threads (No. 4). Readings are

[17] E. L. J. Potts, "Underground Instrumentation," *Colorado School of Mines Quart.* **52**, 137–81 (1957).

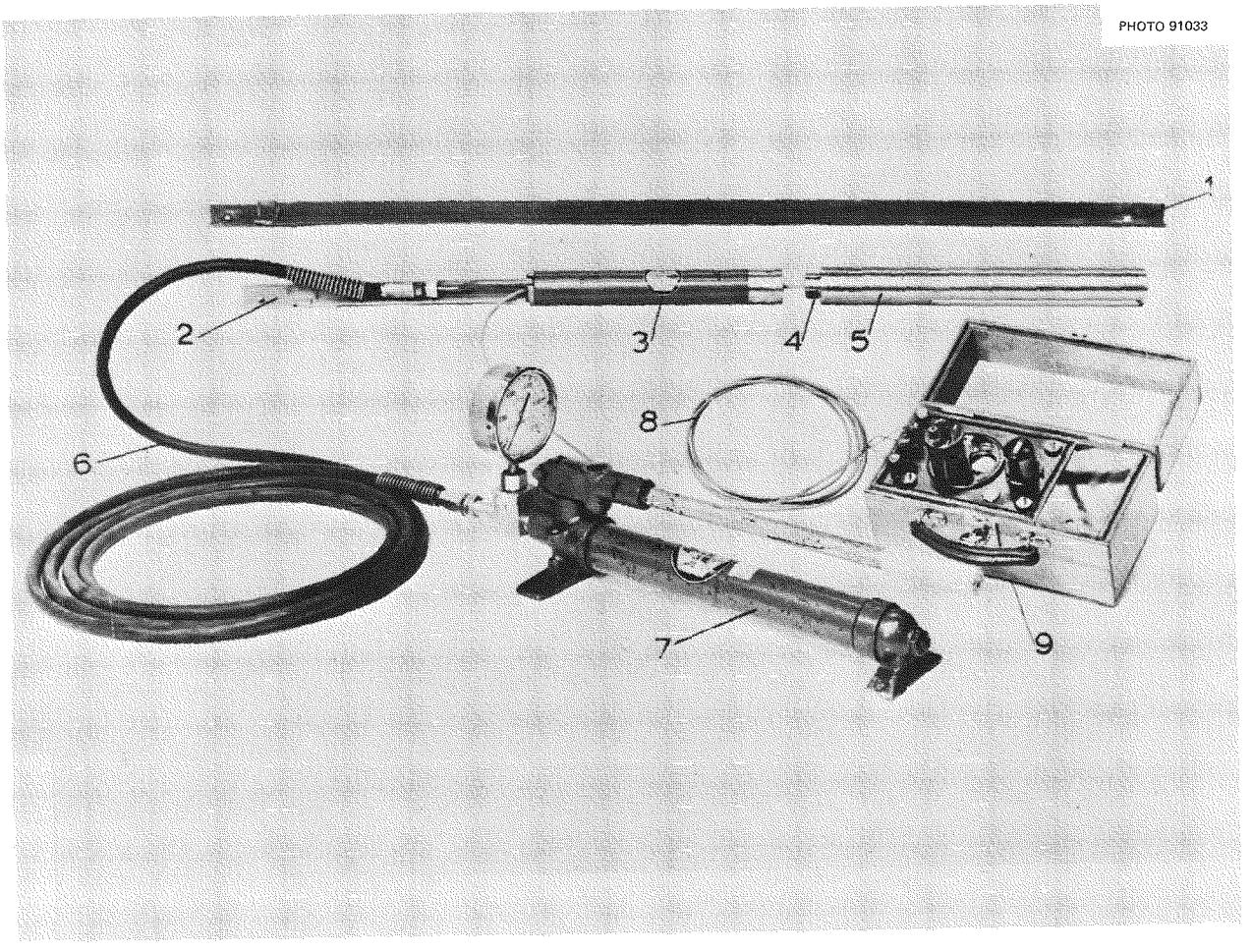


Fig. 11.40. Potts "Stressmeter" with Its Readout and Installation Equipment.

obtained using the readout box (No. 9), which contains the remaining components of a simple bridge, a dry-cell power supply, a null-reading galvanometer, and a direct-reading potentiometer.

Two types of diametral borehole gages were installed in the old mine workings by the U.S. Bureau of Mines. These were the low-modulus borehole deformation gage, developed by Leonard E. Obert, and the borehole pressure cell, developed by L. Panek. The borehole deformation gage senses a change in the diameter of the borehole by the deflection of a strain gaged cantilever.[18] This instrument is read in strain units on a standard SR-4 bridge. The calibration constant is 7 μin. μin.$^{-1}$ in.; that is, a strain-gage reading of 1 μin./in. corresponds to a borehole deformation of 7 μin. The borehole pressure cell[19] is a flat metallic bladder grouted into the borehole. This small "flat jack," as such devices are usually called, is then pressurized using a small pump at the mouth of the hole which is connected to the horizontally oriented flat jack by a small tube. The hydraulic pressure in the system, which should be equivalent to the vertical stress on the gage after a period of time for stabilization, can then be read by means of a simple pressure gage.

11.4.1.5 Floor Leveling. – The floor of each experimental room was covered by a network of leveling stations designed to measure the uplift of the floor due to thermal expansion of the salt. These stations con-

[18] L. Obert, R. H. Merrill, and T. Morgan, *Borehole Deformation Gauge for Determining the Stress in Mine Rock,* USBM R. I. 5978 (1962).

[19] L. A. Panek, "Measurement of Rock Pressure with a Hydraulic Cell," *Trans. AIME* **222**, 287–90 (1961).

sisted of ¼-in. roundheaded stainless steel rivets, 1½ in. long. These rivets were installed by drilling a ¼-in. hole in the salt, filling it with water, and driving the rivet in. The water acts as a lubricant, and most of it is squeezed out during installation. When the remaining moisture evaporates, the recrystallized salt tightly binds the rivet, making it almost impossible to accidentally disturb the station. The rounded head of the rivet serves as an ideal seat for a leveling rod.

The elevations of these floor points relative to an assumed stable point were determined periodically. It is extremely difficult to establish a perfectly stable point in a mine, especially a mine where the rock deforms as easily as salt. For these leveling operations, bench marks were established in entry 5 at a minimum distance of 475 ft from the experimental area. The bench marks were anchored 25 to 30 ft below the level of the floor using the ½-in. pipe and roof-bolt anchor system similar to the pipe-type convergence instruments. It is felt that these base points, if not truly stable, were at least sufficient for the purpose.

The leveling was carried out with a Zeiss model NI-2 autoset (self-leveling) engineer's level and a standard leveling rod fitted with a vernier target. All readings were to the nearest 0.001 ft, and inspection of both the traverse closure errors and the scatter in the data suggests that an accuracy of ±0.002 ft was maintained. The autoset level was found to be relatively sensitive to the usual underground rough handling. It was necessary to check and readjust the instrument before every usage. During the course of the experiment it was also necessary to return the instrument to the supplier on two occasions for more extensive adjustment and repair. Despite this lack of ruggedness, it is doubtful that the number, frequency, and accuracy of leveling results could have been obtained with the personnel available with an ordinary engineer's level.

11.4.1.6 Borehole Leveling. – The self-leveling capabilities of the instrument level described in the previous section permitted a set of measurements to be made which would have been impossible otherwise. These were measurements of the gross vertical deformation of the pillars in the experimental area at various distances into the pillar, including its center line. These measurements were accomplished by drilling horizontal 2-in.-diam holes into the pillars and installing illuminated leveling targets in the holes. These targets, fabricated from 1¼-in. pipe, cut to about 5-in. length and fitted with a translucent plastic front screen and a 6-V light bulb, were installed by wedging them into the back of the holes. Readings were obtained by adjusting the height of the instrument level until the line of sight coincided with the cross hairs scribed on the target screen and then reading the elevation of the target from a vertical tape suspended in the room. These targets were installed in pairs, one above the other. The measurements, therefore, represent the vertical deformation taking place between the two targets.

Although this borehole leveling concept was not originated by us, the installation in the Kansas mine was the first known attempt to apply it. The installation was consequently experimental in nature, and high resolution and accuracy were not attempted. The relative elevation of the targets was established only to the nearest 1/16 in. Difficulties with the adjustment of the height of the instrument and the problems of working on relatively unstable platforms produced a further scattering of the data. In spite of these factors, the results were most interesting and useful.

11.4.1.7 Roof Sag Monitoring Transducers. – The roof of the experimental area consists of a 2-ft-thick layer of salt known to have separated from the overlying material and to be sagging into the experimental area. For a warning against the possibility of an abrupt acceleration in the rate of movement of this bed as a consequence of, for instance, the application of heat, 12 remote-reading roof-sag monitors were installed throughout the experimental area. These instruments consisted of a short piece of wire anchored in the strata above the sagging bed and connected to a potentiometric displacement transducer mounted on the sagging bed. The instruments were read from an indicator unit installed in one of the panels in the control room. The accuracy of this readout was only 0.05 in., but this was considered adequate for the purpose. In addition to permitting the condition of the roof to be ascertained from a remote location prior to entering the experimental rooms, two of the roof sag transducers were tied into the alarm system. This tie-in meant that the roof of the experimental area was under constant surveillance with respect to gross movements (for example, 0.25 in.).

11.4.1.8 Special Roof Bed Gages. – Following analysis of the behavior of the 2-ft-thick roof bed under the influence of the array heating (see Sect. 11.4.5.6) and the decision to embark on a program of roof bolting in the entire experimental area, several special gages were installed to enable a more detailed analysis to be made of the behavior of this roof bed. The first of these special gages consisted in augmenting the vertical internal strain gages (type A) already installed in the roof. The shortest existing wires in the roof at this time were 6 ft long, which would detect a certain amount of deformational strain in addition to the sag of the roof

bed. Therefore several additional stations were installed with the wires anchored just above the separated parting. These stations were sensitive only to the actual sag of the roof bed.

The horizontal slip of the pillars on the shale parting of the roof bed was measured by a modification of the pipe-type gages. In this case, very short pieces of $\frac{1}{2}$-in. pipe were anchored in the pillar wall near the roof and in the roof bed with roof bolt anchors. These were brought into horizontal alignment with appropriate pipe fittings and the measurement was taken between the ends of the pipe in the usual way.

The success of the roof-bolt test and the subsequent roof-bolting program depended upon reliable monitoring of the loads being supported by the roof bolts over a long period of time. This was because the very limited previous experience with roof bolts in Kansas salt mines had indicated that it might not be possible to maintain adequate anchorage of the bolts in the rapidly yielding salt. Roof-bolt load cells are a standard readily obtainable rock mechanics instrument, but these cells are highly sophisticated, ultra-accurate units costing about $500 each. Since the roof-bolting program required a large number of cells to operate over a long period of time at a fairly low sensitivity, these commercially available cells did not seem appropriate. An extremely simple cell was therefore designed and a prototype fabricated at ORNL. This cell consisted of a 2-in.-long piece of $1\frac{1}{2}$-in. heavy-wall stainless steel pipe, tack welded to $\frac{1}{4}$-in.-thick end plates. Three SR-4 electrical resistance strain gages, oriented axially and spaced at 120° around the pipe, provided the sensing element. Laboratory tests and calibration of this cell indicated that it would perform satisfactorily after being cycled to a 50,000-lb load a few times. The sensitivity of this cell was approximately 40 lb-in./μin. when the three strain gages were connected in series and read (in microinch per inch strain units) on a standard bridge.

Thirty-five roof-bolt load cells were fabricated at a cost of approximately $30 each and installed on selected roof bolts during the roof-bolting program. For reading purposes these cells were divided into five groups corresponding to the four experimental rooms plus the corridor. The average load of a given group was then calculated, and this average load was interpreted as being representative of the behavior of the room rather than the loads of the individual cells. This averaging process tends to reduce the influence of erratic behavior of a few of the cells. Operated in this way, these simple load cells were quite adequate in their task of indicating the general level of load supported by the roof bolts and the variation of that load with time.

11.4.2 Design of Gage Layouts

Participation in Project Salt Vault presented a unique opportunity to the rock mechanics researcher. Most underground rock mechanics investigations must be carried out without interfering with production operations and must compete, from this disadvantageous position, for space, equipment (especially drills), and labor. Furthermore, since the cost of the research is usually charged to production, the researcher must usually be able to demonstrate that his results will produce a saving at least equal to the cost. In PSV these considerations were essentially reversed. One of the primary objectives of the experiment (but not the only one) was to investigate the deformational behavior of salt, while certain other objectives were secondary, including the excavation of the experimental area – the usual "production" operation. This reversal of priorities meant that the resources which could be expended on research were larger than normal, that all the desired instrumentation was installed when it was needed, and that the instrumentation was properly read and maintained.

In practice, it was possible to schedule the drilling, gage installation, and instrument reading programs so there was little or no interference with other operations. Furthermore, although the rock mechanics investigation was in a more favorable position vis-a-vis the other operations, available resources were not unlimited. The entire PSV project as well as the rock mechanics research had to be carried out within a fairly strict budget. For this reason design of the gage layouts was given lengthy and serious consideration, both by ORNL personnel and by the various consultants.[14] This consideration included careful detailing of the objectives of the rock mechanics program and repeated examinations of each of the individual measurement points. These examinations were made by asking, Was this particular gage point (there were over 800 such points) necessary? Would it contribute its increment to the overall program? Was it in the best location? Was it sufficient to characterize the deformation at that point? Would a different type gage be more appropriate? Because of this attention to instrumentation design, there were few places where a desirable measurement was not obtained, and there were practically no superfluous gages anywhere throughout the mine. This is in spite of the fact that the experimental area and immediately adjacent areas represented one of the most extensively instrumented underground rock mechanics investigations in existence.

11.4.2.1 Gages in Old Workings. – The rock mechanics instrumentation in the old mine workings was

installed to meet several objectives. These "old workings" included the area immediately around the bottom of the existing shaft, the main entry ways from the shaft to the experimental area, and the previously mined rooms which adjoined the experimental area. The primary objective of the gage installation was to assure the safety of these areas so that continued access to the experimental area could be maintained. The old mine areas adjacent to PSV provided an opportunity to observe the entire sequence of rock deformation from a static, undisturbed condition, through the effect of excavating a new, fairly large area, the influence of the application of a large quantity of heat over an extended period of time, and return of the salt to static conditions. In addition to measurements close in to the experimental area, the extent of these disturbances over a wide portion of the old mined area could be established. Because of this unique property of the Lyons mine, it was expected that some new and useful data on the stability of salt mines in general, and this mine in particular, would be forthcoming from the rock mechanics investigation in the old workings.

In addition to these general objectives related to the experiment, one specific study was undertaken in the old workings. This was an examination and comparison of three different diametral borehole deformation gages. The performance of these gages in relatively homogeneous and elastic rocks is reported to be good.[20] Using theoretical solutions for a cylindrical inclusion in an infinite elastic medium, a realistic and fairly reliable measure of the stress and/or change in stress can be obtained. As the material properties depart from ideally elastic, the performance of these gages is less than satisfactory. In a material as plastic as rock salt, it is frequently impossible to interpret a change in the gage reading (or change in the rate of change of the reading) in any more detail than that "something happened." A comparison of the behavior of three different gage types, having widely differing properties, at the same location and under controlled conditions was, therefore, of some academic interest. However, the principal objective was to ascertain which, if any, of the three gages yielded definitive data on the stress in salt so that the gage could be extensively used in the experimental area in conjunction with the heating tests.

These objectives were met with the gage layout shown in Fig. 11.41. The gages installed around the shaft bottom and along the main east and MOP entries and entry 5 were intended primarily to monitor the safety of these access ways. The extensive instrumentation in "entry 2 south" and in the "west room," projecting toward the experimental area, and also that in entry 5 located beyond the ramp were installed several months before excavation of the experimental area started. Notice that some of the gages (stations 42, 44, 45, 47, and 54) extend under the experimental area proper. This was possible because the level of the floor in the experimental area was stratigraphically some 14 ft above the level of the old mine floor. These gages were not destroyed by the excavation. They provided the basic data concerning the situation prior to mining and the effect of excavating the experimental area, as well as the additional data on the effect of heating during the experiment. The extent of the effect of the mining and later heating in the experimental area on the existing mine was provided by the remainder of the instruments shown on Fig. 11.41, which were arranged along lines radiating out from the experimental area. These radiating lines were:

1. to the south, incorporating gage stations 32, 33, 25, and 26,
2. to the east, including the gages along entry 5 and stations 14 and 15,
3. to the northeast, along stations 51, 59, 12, 11, and those at the shaft bottom.

The comparison of diametral borehole deformation gages was carried out at three locations denoted as "sites 1, 2, and 3." Each site consisted of a Potts stressmeter and a USBM borehole deformation gage installed as close as possible to each other. Considering the length of the holes and the probable hole deviation, the distance between the two gages at each site was probably less than 5 ft. A USBM borehole pressure cell was also installed at each site, as close to the other instruments as permitted by the 12-ft-long pressure tube.

All gage holes were drilled with a diamond drill (Sprague and Henwood model 325) using solid plug-type diamond bits and air flushing of the cuttings. Only in a few cases was the drill located and oriented with surveying instruments. In most cases it was felt that location to within ±3 ft of design by visual orientation was sufficient because of the subsequent uncontrollable deviation of the borehole. This deviation could be estimated from two items of evidence obtained in the experimental area:

1. Gage 47 was intersected by the floor cut at the northwest corner of room 4. This would indicate

[20] E. R. Leeman, "The Measurement of Stress in Rock," *J. S. African Inst. Mining Met.* **65**, 45–114, 254–84 (1964).

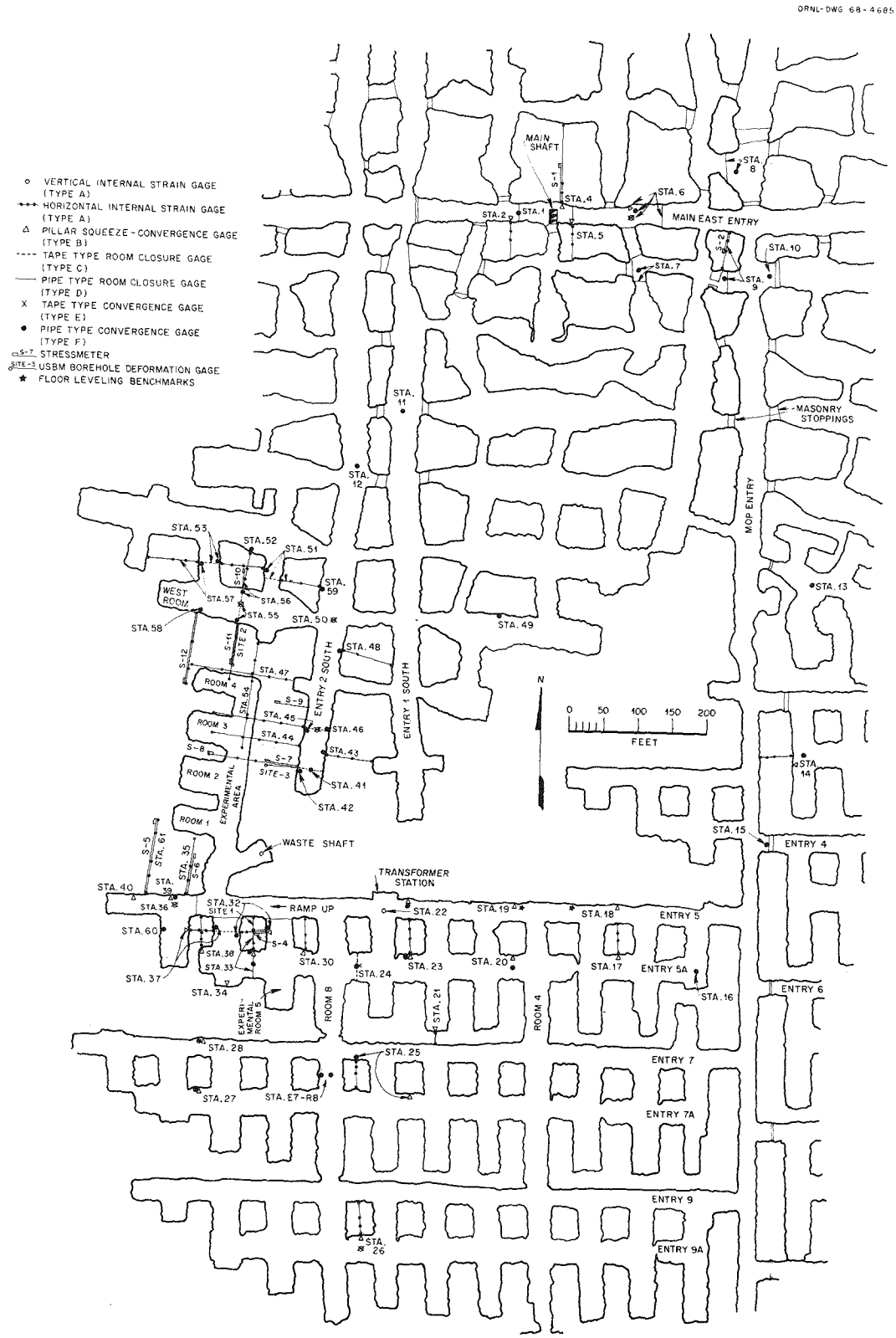


Fig. 11.41. Plan of Instrumented Portion of Old Workings Area of the Lyons Mine.

that at a distance of 140 ft, this hole had deviated upward 10 ft and to the left about 8 ft from its design location.

2. Stressmeter 8 was designed to be 9 ft below the floor of the experimental area on the exact center line of the center pillar. A short hole drilled from the experimental area to the same spot for thermocouple placement intersected this stressmeter hole and cut its lead cable. This would indicate that the 110-ft hole was within 1 ft of its design location.

11.4.2.2 Gages in Experimental Area. – The principal objective of the rock mechanics instrumentation in the experimental area was the complete and detailed characterization of salt deformation in and around the area as a function of time, overburden stresses, radiation fields, elevated temperature, and thermal gradients. This information constituted the basic input required to develop a capability of designing an actual disposal facility in a salt mine. A second objective was to monitor the behavior of the salt continuously in order to guarantee the safety of the mine personnel and to protect the large radiation sources present. This objective was met in two ways: first, by special instrumentation which provided a quick but coarse impression of salt movements. This impression was augmented by an equally quick and cursory examination of all gage readings in the mine at the same time. The second examination of gage results was carried out at ORNL. This examination involved plotting all results and interpreting their significance in terms of mine safety at frequent intervals. Although this examination was necessarily somewhat delayed, the detail provided in instrumentation design and the sensitivity of instrumentation measurements would permit the detection of a possibly hazardous condition long before the hazard would become real.

The rock mechanics instrumentation actually installed in the experimental area is shown in Figs. 11.42–11.44. Figure 11.42 shows the location and identification of all gages of type A, C, E, F, and stressmeters. All vertical internal strain gage wires were installed at depths of 25, 12, and 6 ft up into the roof and down into the floor. The layout of floor leveling pins in experimental rooms 1, 2, and 3 is shown in Fig. 11.43. The floor leveling pins in experimental room 5 were the same as in room 1, and the layout in room 4 was a mirror image of that in room 1. The remaining gages, specifically the borehole leveling points, roof sag monitoring transducers, roof-slip gages, and roof-bolt load cells, are shown in Fig. 11.44.

The design of these gage layouts was based on the experience and judgment of project personnel and consultants concerning the type and magnitude of movements to be expected and the limited previous work on salt deformation carried out in the Hutchinson mine and at the Prototype Hole Liner Experiment (see Chap. 4). Because deformations in the experimental area resulting from the application of heat could not be predicted, a gage was placed at each point where it was felt that a measurement might be desirable rather than just at those points where measurements would be absolutely necessary for proper understanding of the deformation. This approach may have resulted in some redundancy, but it was justified because a complete and detailed representation of the deformation was needed and because we had to be prepared for unexpected movements.

Drilling for gage installation in the experimental area commenced as soon as excavation of the first room was completed. However, since it took longer to complete the gage drilling in a room than the excavation, gage installation lagged ever further behind excavation in the subsequent rooms. Accurate location and orientation of the gage holes were maintained throughout the drilling program. In the case of station 115, this accuracy resulted in the intersection of this hole with the holes drilled perpendicular to it (stations 116 and 118). This intersection resulted in some installation problems which subsequently caused considerable difficulties with the readings at station 115. All other stations were installed without difficulty.

Although some problems associated with corrosion of the stainless steel internal strain gage wire were anticipated, these failed to materialize generally, except at the floor stations near the heat sources. In these cases, the migration of water into gage holes due to the adjacent heating undoubtedly caused accelerated corrosion. All other gages performed satisfactorily throughout the course of the experiment.

11.4.3 Movements Resulting from Experiment Area Excavation

One objective of rock mechanics instrumentation in the old workings was to monitor the deformations caused by excavation of the experimental area. The results obtained from this phase of the experiment are presented here and interpreted. For the following discussions, reference should be made to Fig. 11.41, which shows the location of various gages relative to the existing openings and the newly mined area, and to Fig. 6.3, which shows mining rates in the experimental area by showing the position of the working face in terms of both the actual date and the "standard day." All rock

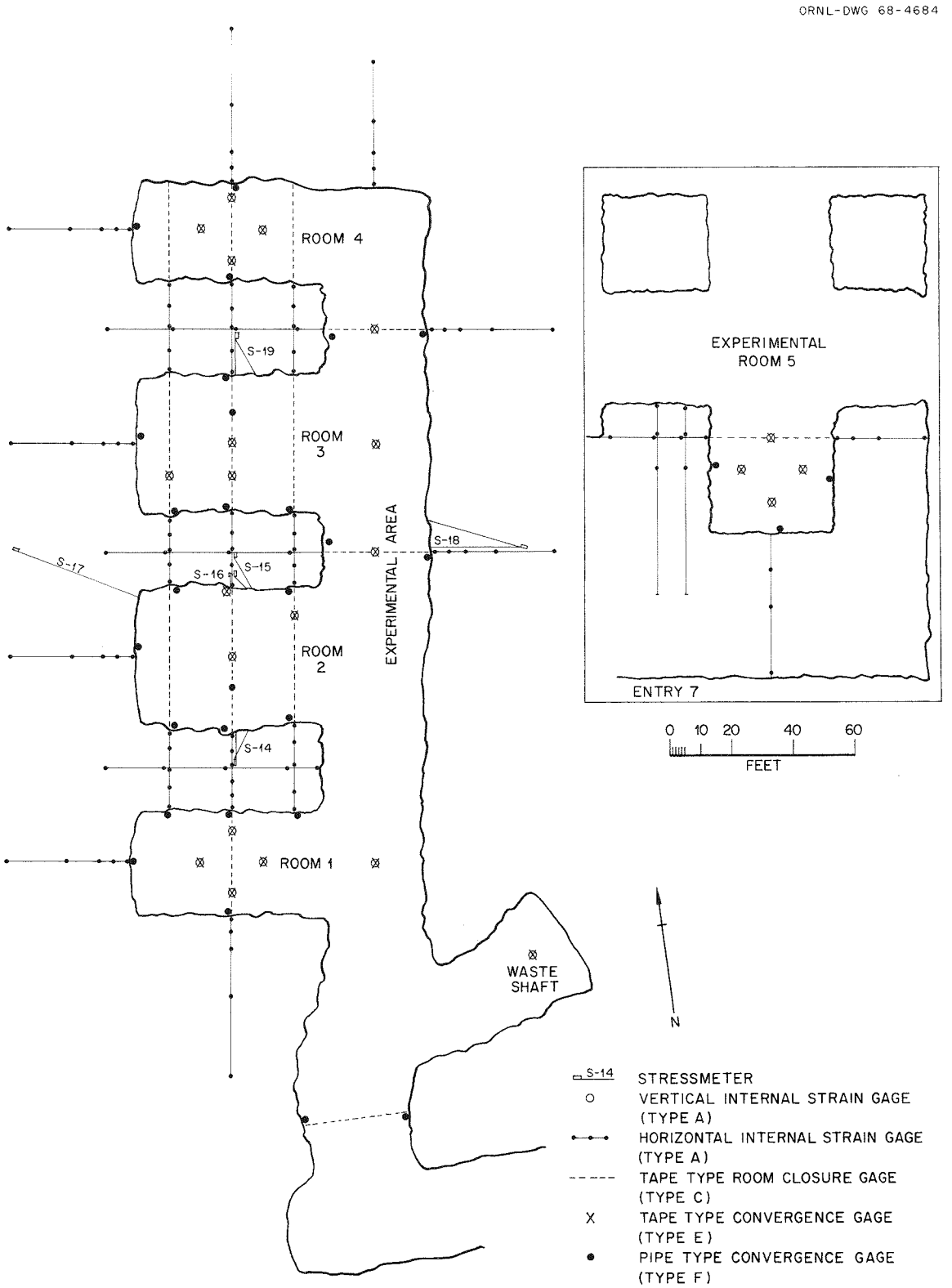


Fig. 11.42. Plan of Experimental Area Showing Rock Mechanics Gages and Their Identification. Gage types A, C, E, F, and stressmeters only.

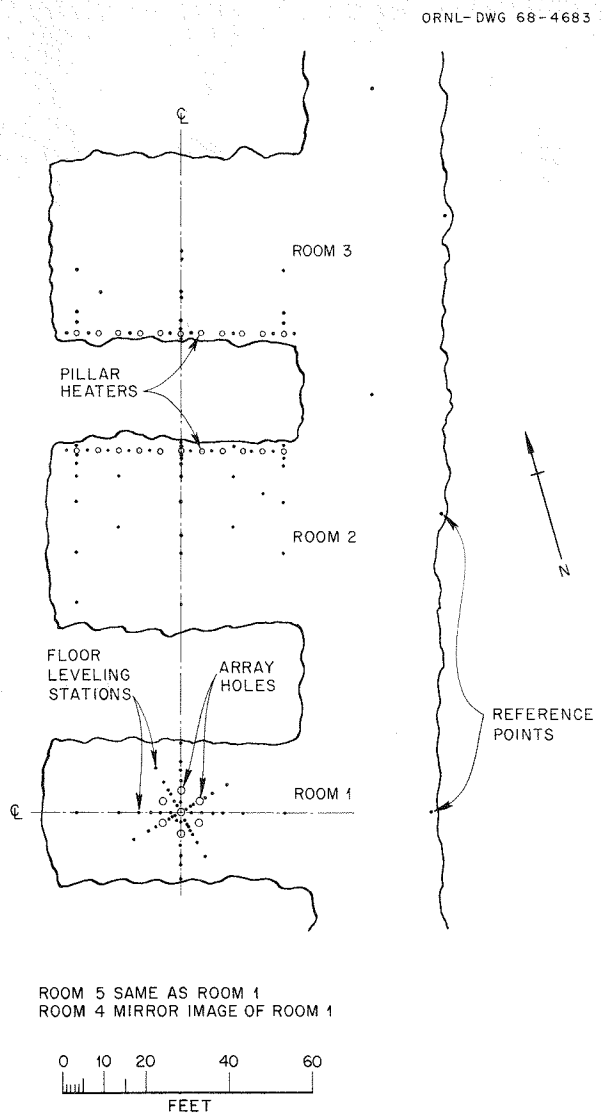


Fig. 11.43. Plan of Experimental Area Showing Floor Leveling Station Layout.

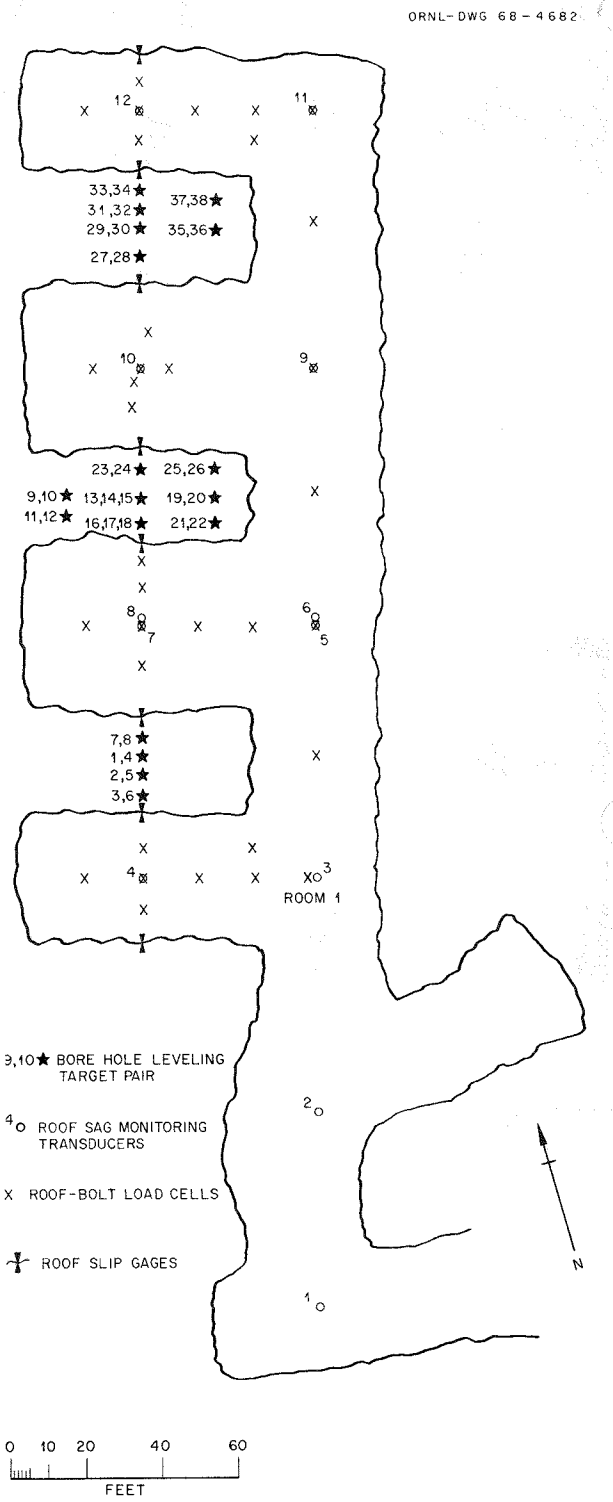


Fig. 11.44. Plan of Experimental Area Showing Special Gage Installations (Borehole Leveling Targets, Roof Sag Monitors, Roof-Bolt Load Cells, and Roof Slip Gages).

mechanics data are presented as a function of this arbitrary time scale which originated on September 1, 1963. This "standard day" procedure was adopted for its convenience and as an aid in plotting the myriad of results obtained in PSV.

11.4.3.1 Results and Interpretation. — Figures 11.45–11.48 show the results obtained from gages 42, 44, 45, and 54 respectively.[21] These plots represent the

[21] W. C. McClain and R. L. Bradshaw, "Stress Redistribution in Room and Pillar Salt Mines," *Intern. J. Rock Mech. Min. Sci.* 4, 245–55 (1967).

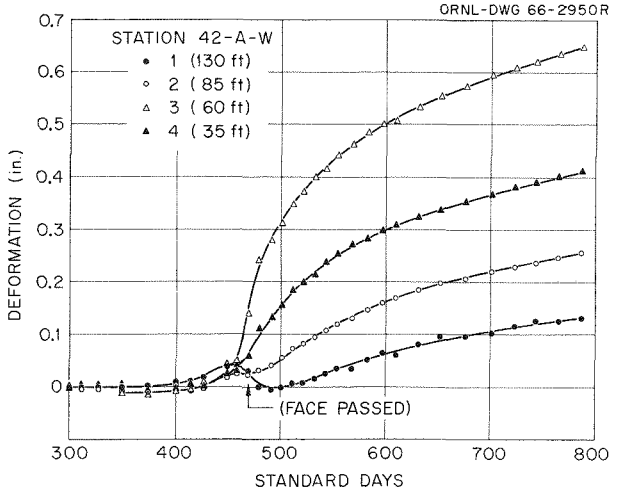


Fig. 11.45. Measured Deformation at Gage 42-A.

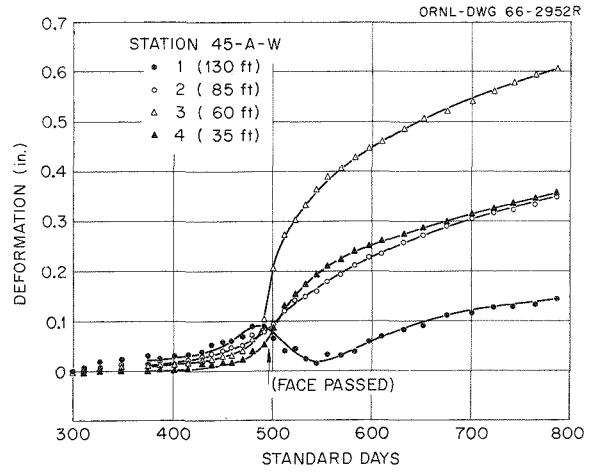


Fig. 11.47. Measured Deformation at Gage 45-A.

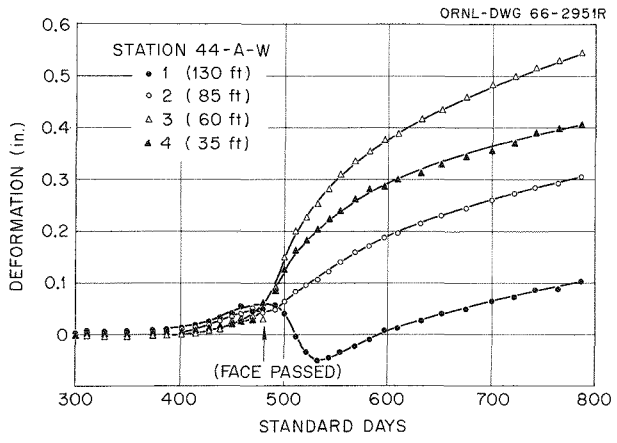


Fig. 11.46. Measured Deformation at Gage 44-A.

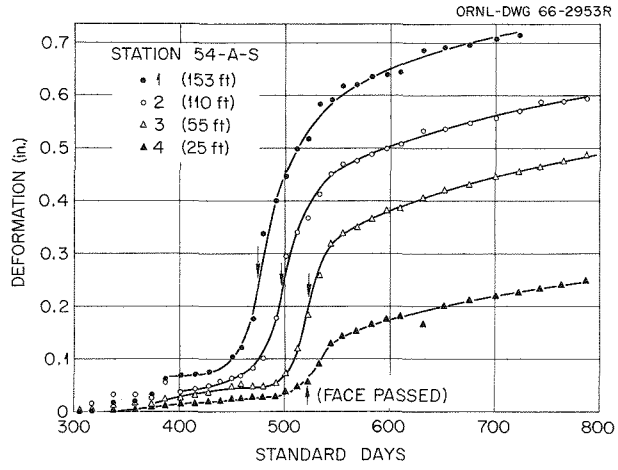


Fig. 11.48. Measured Deformation at Gage 54-A.

cumulative movement as a function of time of each wire in the borehole relative to the collar of the hole. The points on the graphs are actual readings and indicate the sensitivity and accuracy of the instrument. In this form the measured deformation appears to be very complex and difficult to interpret, especially with respect to those wires which show a reversal.

Since these gages pass through a pillar between two rooms, there should be a point somewhere along the borehole which is relatively stationary; that is, the point should not move toward either room. If the anchor of wire 4 of each gage, located 35 ft from the rib of room 2d south, is assumed to coincide with this stationary point, the gross movements of all other anchors relative to anchor 4 can be plotted. These plots are shown in Figs. 11.49 and 11.50; they were constructed using the smoothed curves of Figs. 11.45, 11.46, and 11.48.

Examining first the plots for gages 42 and 45 in Fig. 11.49 (gage 44 has been omitted from these plots, because it is nearly identical with gages 42 and 45 and does not therefore present any new information), which pass beneath the corridor connecting the experimental rooms, it can be seen that the wall of room 2d south, represented by the collar anchor, moves toward the center of the room as expected. It moves slowly in the beginning, undergoes a period of acceleration as the excavation passes opposite it, and then slows down and continues to move into the room at a decreasing rate.

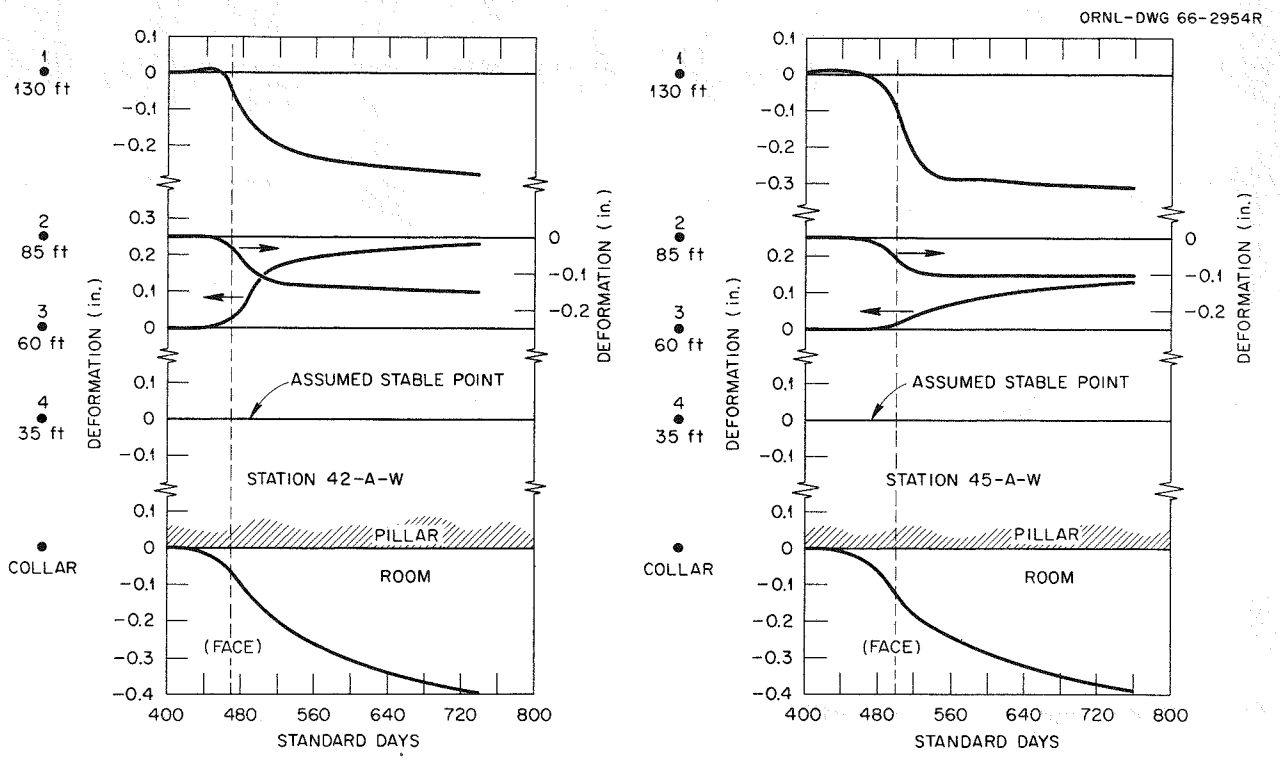


Fig. 11.49. Relative Displacements, Gages 42 and 45.

The wires identified as No. 3 at these three gages were anchored in every case at a distance of 60 ft from the wall of the 2d south room, approximately 10 ft inside the rib of the corridor of the experimental area. Additionally, since the holes were drilled from 2d south, they were 10 to 15 ft below the floor of the experimental area. Movement of these anchors is nearly identical to that of the collar anchor, but in the opposite direction; that is, toward the newly mined area (Fig. 11.49). This means that the effect of the pillar extends a considerable distance into the floor under it and that the material above and below a pillar must be considered to be an integral part of the pillar. This result was also confirmed in laboratory tests on model pillars[22] (see Sect. 12.2.3).

Wires No. 2 were anchored beneath the center of the experimental corridor. These wires exhibit a small movement toward the older workings (2d south). This movement represents the cumulative effects of the asymmetry of the experimental area, directional errors in the borehole, and the error in the original assumption that anchor 4 exactly coincided with the stationary point in the pillar.

Movement shown on the wires anchored beyond the experimental corridor and beneath the experimental rooms and pillars is again toward the experimental entry as expected.

Results obtained from gage 54 are perhaps the most interesting of all. This gage was beneath the experimental entry, and its axis lay alongside the axis of the entry. As the working face approached and passed over anchor 1 (Fig. 11.50), it began to move rapidly toward the newly excavated opening. During this period all the other anchor points indicated relatively little displacement. The face then approached and passed over anchor 2, and it behaved in an identical manner, moving rapidly toward the new opening. Movements detected on anchor 3 are not a further duplication of the previous two, because the excavation did not pass over and beyond this anchor. Notice, however, that movement at the collar anchor away from the new excavation was delayed.

[22] R. L. Bradshaw, T. F. Lomenick, W. C. McClain, and F. M. Empson, "Model and Underground Studies of the Influence of Stress, Temperature, and Radiation on Flow and Stability in Rock Salt Mines," *Proc. First Congr. Intern. Soc. Rock Mechanics, Lisbon, September 25 to October 1, 1966,* pp. 429–33 (1966).

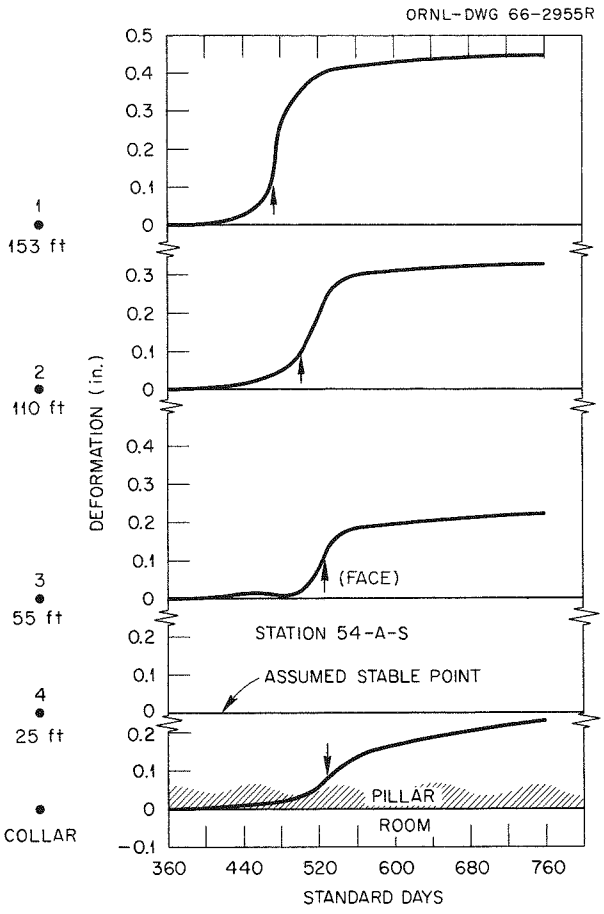


Fig. 11.50. Relative Displacement, Gage 54.

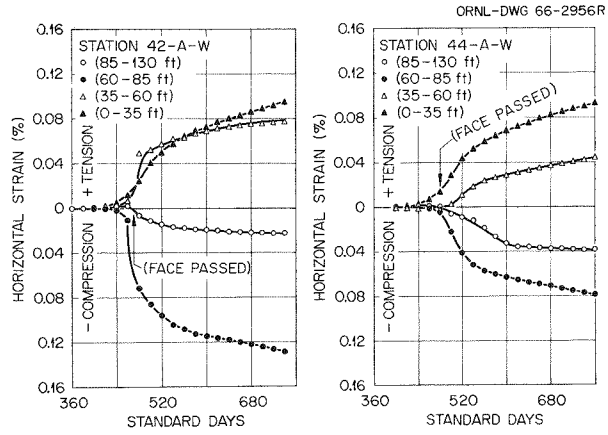


Fig. 11.51. Development of Strain at Gages 42 and 44.

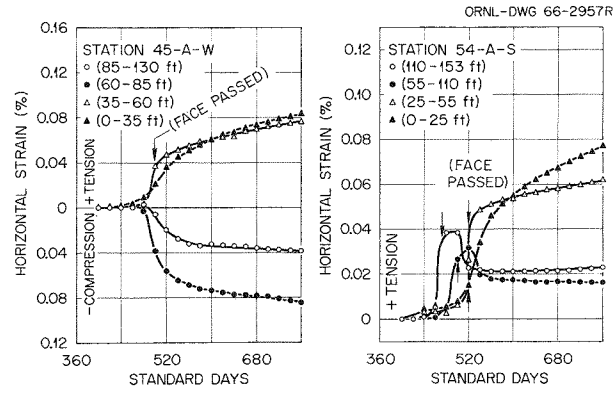


Fig. 11.52. Development of Strain at Gages 45 and 54.

The next logical development of movements defined by these gages is to calculate the strain between each pair of anchor points. These strain curves are plotted against time in Figs. 11.51 and 11.52. Continuing with the discussion of gage 54, the strain curves (Fig. 11.52) show that a maximum tensional strain of 0.03 to 0.04% is developed in the floor under the advancing face, but that this is reduced to a net tensional strain of about 0.02% by compression behind the face. The residual and permanent tensional strain between these two points must be a consequence of the room and pillar configuration of the experimental area, since for a single entry the longitudinal strain should return to zero after passage of the face.

These results, in general, confirm the presence of a wave of compressive stress traveling with the advancing face and suggest that the peak stress in the wave is fairly close to the face even when it is advancing slowly and in a highly plastic material. They also confirm that when the face stops, this traveling compression wave continues to move out away from the face to its equilibrium position at some depth into the rock. Although the highly plastic nature of rock salt makes these effects much more visible, all rocks exhibit a certain amount of plasticity, and the conclusions should be applicable to any rock material.

The strain-time curves for those gages installed transverse to the experimental entry (gages 42, 44, 45, Figs. 11.51 and 11.52) illustrate the strains resulting from the gross movements discussed above. Large tensional strains develop in the pillar separating the new experimental entry from the older workings, and compressional strains of about the same magnitude develop in the floor across the experimental entry. All of these strains are increasing, but at a constantly decreasing rate. This behavior reflects the usually observed effect of creating a new opening in plastic material.[23]

[23] W. C. McClain, "Time-Dependent Behavior of Pillars in the Alsace Potash Mines," *Proc. Sixth Symp. on Rock Mechanics, Rolla, Missouri, 1964*, pp. 480–500.

Redistribution of the load from the newly mined opening over a considerable area can be observed from the results of the convergence gages installed throughout the old workings. Figure 11.53 shows the measured convergence at several points where the effect of mining in the experimental area is indicated by the step in the curve. Figure 11.54 highlights this increased convergence, plotting strain rate as a function of time. Strain and strain rate increase as vertical stress in the vicinity of the gage increases due to load transference from the mining area. It is interesting to note that, in general, the peak strain rate occurs after the working face has passed a point closest to the gage. It is also of interest to note that peak strain rates at points beyond the experimental area (gages 53 and 56) occur at even later times.

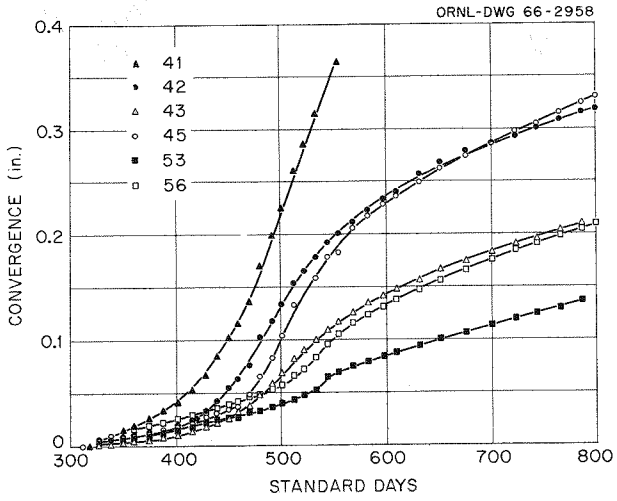


Fig. 11.53. Convergence in Room 2d South.

11.4.3.2 Borehole Deformation Gages. – The quantitative interpretation of results obtained from stressmeters installed in salt or other highly plastic materials is extremely complex. However, the results are useful in a qualitative manner. The readings obtained from four stressmeters installed around the experimental area are shown in Fig. 11.55. The curves show the effect of the new excavation as an increase in indication, which can be interpreted as an increase in stress. This increase proceeds from one instrument to the next in sequence as the mining progresses. It is significant that in every case the maximum rate of change detected by the three different gages at a particular location (horizontal wire, convergence, and stressmeter) is coincident in time.

One reason for employing three different types of borehole deformation gages was to make a comparison of their performance in rock salt. In order to facilitate this comparison, the three different types of gages were installed in a close array at three different locations in the mine.

Results obtained from the three sets of gages are given in Fig. 11.56. At site 1, south of the ramp, the borehole deformation gage (BDG) and the S-4 stressmeter (SM) were installed at the center of an isolated 40-ft pillar in

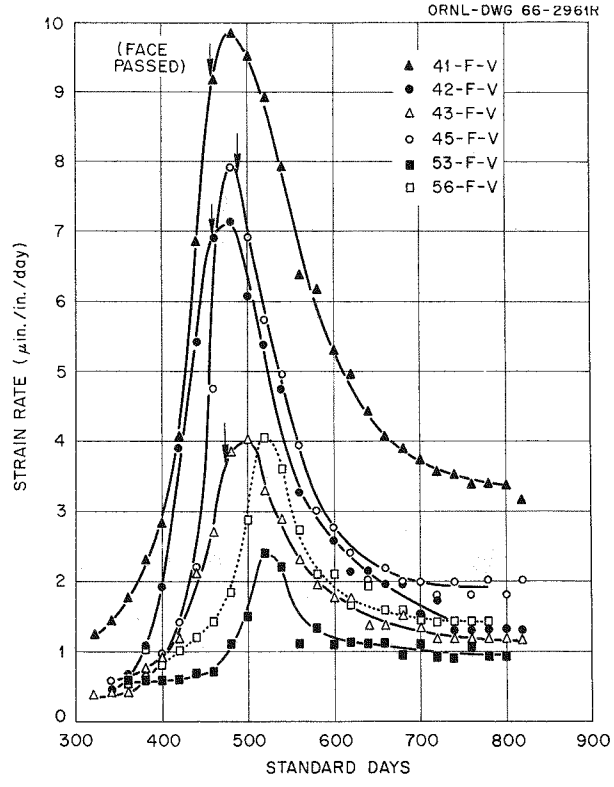


Fig. 11.54. Convergence Strain Rates.

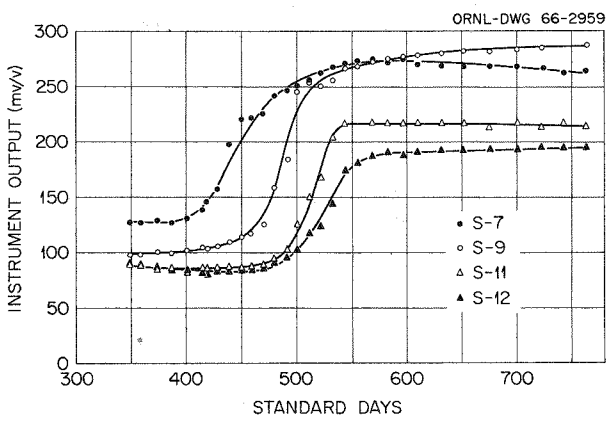


Fig. 11.55. Stressmeter Results.

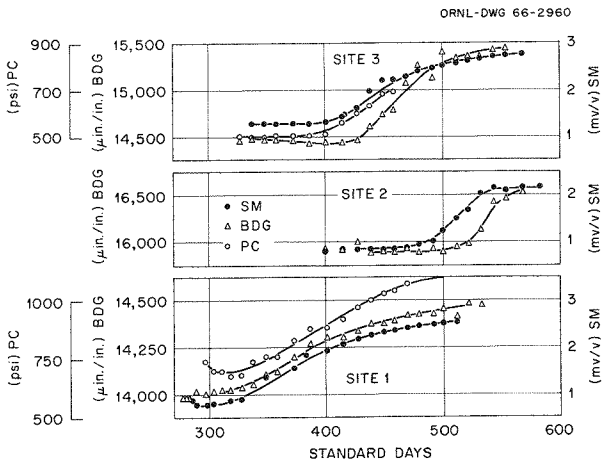


Fig. 11.56. Comparison of Diametral Borehole Deformation Gages.

the old workings (Fig. 11.41). The pressure cell (PC) was installed at its maximum depth of 12 ft. This pillar was affected primarily by construction of the ramp leading up to the higher level of the experimental area. This construction work raised the ceiling on one side of the pillar and thus effectively increased its height-to-width ratio. The shape of the response of these three instruments was very similar, as is shown in Fig. 11.56, even though the three gages varied widely in modulus.

At site 3 the SM (S-7) and BDG were installed at a distance of 50 ft from the wall of room 2d south, while the PC was at only 12 ft. Here there was a net increase in stress, arising from excavation of the experimental area. At site 3 the three instruments again responded in similar fashion, although there appeared to be some delay in the BDG response.

At site 2 the BDG and SM (S-11) were installed at a depth of 60 ft from the wall of the old workings. Here the pressure cell (PC) failed before any results could be obtained because of corrosion. At site 2 the BDG and the SM again performed in similar fashion. In this case the BDG response was delayed approximately 20 days. The reason for this delay is not known, but it is possibly caused by deviations in alignment of the boreholes.

This comparison of three different diametral borehole deformation gages was carried out partially to select the type of gage to be used in the experimental area. The results indicated that none of the gages performed well in highly plastic salt and that there was essentially no difference in the character of the information obtained. As a result, the high-modulus stressmeter was selected on the basis of its availability. Six of these instruments were installed in the experimental area, and these represented the only diametral borehole deformation gages used there.

11.4.3.3 Extent of the Effect of the Excavation. – In addition to deformations of the rock adjacent to the experimental area measured on the gages in the west room and entry 2d south, the extent of the effects of excavating the experimental area on the existing mined-out space was determined. This was done by closely examining the results obtained on those gages located throughout the old workings for any slight change in slope of the deformation curves during the period when the excavating was carried out. Convergence (type F) gages at stations 49, 11, and 12, located at distances of 360, 435, and 335 ft, respectively, all showed a slight increase in slope (convergence rate) about standard day 495. This was the time when the excavation passed nearest these gages, and the inference is that the stress redistribution resulting from the mining operations extended at least 400 ft from the newly mined area.

Gages at stations 27 and R8-E7 showed a slight change in curve slope during the construction of the ramp in entry 5 leading to the experimental area. There was no detectable influence related to the actual excavation of the experimental area. Both of these gages were about 200 ft from the ramp and a little more than 300 ft from the rooms of the experimental area. These results are most interesting, since they imply that the overall disturbance caused by modifying the shape of the supporting pillars is nearly as great as the excavation of new space. During construction of the ramp, the area of salt supporting the overlying material was not changed. The height of the pillars adjacent to the ramp was changed from 14 ft to about 27 ft on one side. This change in shape must have caused these pillars to "shed" load to surrounding areas in much the same way that the load is redistributed when part of the salt supporting that load is removed.

It can be further concluded that there is a slight difference in the stability of the irregular old workings to the northeast of the experimental area and the more recent checkerboard area of square pillars to the southeast (Fig. 11.41). This is deduced from the fact that the effect of mining was transmitted about 400 ft to station 11 but not to stations 26 and 27 about 300 ft away. This is to be expected since the area to the north of the experimental area was mined at a higher extraction ratio and at a much earlier date. Both factors would contribute to making this area more sensitive to an increment of load.

There was no detectable effect of the excavation work at any place around the area of the main shaft or along the main east and MOP entries (Fig. 11.41). These areas were apparently beyond the reach of the disturbance resulting from the mining operations in PSV.

11.4.4 Situation in Experimental Area Prior to Heating

The nature of rock movements in the experimental area immediately prior to startup of the array experiments in rooms 1 and 4 on November 15, 1965 (standard day 806), is described in the next section, including the movements occurring before heating and those after. However, in order to fully understand the analysis and discussion associated with the data, and to complete the interpretation of the influence of the excavation process begun in the previous section, it is advantageous to examine the results obtained during the period immediately prior to heating.

A preliminary analysis[24] of these data was undertaken while the mining operations were in progress. The objective was primarily to confirm the safety of the roof conditions in the experimental area immediately after excavation. Since interpretation of the data obtained during mining operations is complicated by stress redistributions resulting from these operations, as demonstrated in the preliminary analysis, this section deals only with the period between completion of the excavation and the start of the first heating experiments, that is, from standard days 571 to 806.

In general deformations which occur around newly excavated space result from transferral of the overburden load formerly supported by the material which was removed onto the remaining pillars and abutments at the edge of the excavation area and from relief of horizontal restraint at the free surfaces. Such deformations are strongly influenced by the excavated space available as a stress-free area into which the remaining rock can move. If the total excavated area is large enough, the load (stress) on the pillars in the center can be calculated from the weight of the overlying material and the total area supported by these central pillars. In the experimental area the total area excavated was too small for this calculation to be meaningful, and a fairly large proportion of the weight of overlying material formerly supported by the rock which was removed was supported by rock surrounding the experimental area and not by the three rib pillars within it. Although it is impossible to estimate the absolute value of the average load on the pillars, one can draw some qualitative impression of stress distribution based on the geometry of the experimental area. This would be that the average stress on the center pillar was more than on the other two because of its central location, smaller width, and the large adjacent rooms. Although pillar 1-2 is the same size as pillar 3-4, it should have a higher average stress because the corridor does not pass beyond room 4 and because of the influence of the room at the bottom of the waste-charging shaft. These gross geometrical relationships should be altered slightly by second-order geometrical effects. For example, although the nominal dimensions of rooms 1 and 4 and their adjacent pillars are the same, room 1 is slightly wider than room 4, and pillar 1-2 is slightly narrower than pillar 3-4. These second-order effects should tend to increase the difference in behavior of the two rooms.

In addition to geometrical differences, there should be a considerable difference in the behavior of rooms 1 and 4 as observed at any given time (such as at the start of the array experiments) because of differences in their respective ages since mining. These differences are found in all mines but are especially pronounced in salt, potash, and other soft rock mines because of their highly time-dependent deformational properties. When openings are first excavated, the highest stress zone is at the wall of a supporting pillar or abutment, and the stress decreases rapidly with distance from the wall. In addition to the instantaneous elastic response of salt to these stresses, the material at the side of the opening begins immediately to deform plastically. As this yielding deformation takes place, the peak loads are transferred from the pillar edge deeper into the salt and spread over a wider area, with the result that the *rate* of deformation decreases with time because of the decreasing stress. In salt, under conditions similar to those at the Lyons mine, this transient period, with its significant stress redistributions, lasts for several years, perhaps even several decades. Eventually a condition similar to a dynamic equilibrium is approached (as an asymptote) where the stress distribution is more or less stable and the mined space closes at a more or less constant rate. This constant rate of closure is the reason for calling the situation dynamic rather than static equilibrium.

In the experimental area, excavation of room 1 was completed on November 10, 1964, and room 4 was completed on March 18, 1965, some four months later. The array experiments in these rooms were started on November 15, 1965. In other words, not only did the

[24] R. L. Bradshaw, *Analysis of Data from Plastic Flow Gages in Experimental Area of Lyons, Kansas, Salt Mine with Special Consideration of Roof Stability*, ORNL-CF-65-4-56 (1965).

experiments start early in the transient phase of both rooms, but there was sufficient difference in the ages of these rooms (room 1 was one year old, room 4 only eight months) that they were at appreciably different stages in their approach to dynamic equilibrium.

Some of the differences in behavior of rooms 1 and 4 prior to the start of the array experiments on standard day 806 are illustrated in Fig. 11.57. Here the rate of vertical convergence on both sides of each room is plotted against the age of the opening (time since mining) on log-log scales. The higher convergence rates on the pillar sides of the rooms ($109 > 106, 159 > 162$) reflect the fact that stresses are higher in the pillars than in the solid abutments. The higher stresses in the area of room 1 are indicated by the higher convergence rates (for equivalent ages) around room 1 than those in room 4. The difference in slope of the curves representing the two rooms may be due partially to the different stress levels, but, more importantly, it suggests that there may be a more fundamental (and as yet undetermined) difference between the two rooms.

It should be noted that the convergence rates in rooms 1 and 4 at the time of the startup of the array experiments were almost identical. (The last points on the curves of Fig. 11.57 are data points taken immediately prior to startup.) This similarity was purely fortuitous, resulting from the higher stress in room 1, acting for a longer time (since mining), producing convergence rates which just happen to coincide with those in room 4 resulting from lower stresses acting over a shorter period. Although convergence rates in the two experimental array rooms were nearly identical, their "behavior," as discussed earlier in this section and illustrated by the relationships in Fig. 11.57, was somewhat different and could be expected to remain different throughout the course of the experiment.

11.4.5 Movements Induced by Heat in Array Experiment – Rooms 1 and 4

Only the rock movements in and around the two rooms (i.e., rooms 1 and 4) are described in this section. Following sections describe the results obtained in room 5, the heated pillar experiment, and the combined effects of heat on the rest of the mine. The remainder of this chapter is largely devoted to the presentation and interpretation of results. Some analysis is included as necessary, but the detailed analysis is included in Chap. 13.

In order to fully appreciate the inferences drawn from a comparison of the rock mechanics results in the two experimental rooms, it is necessary to recognize both the initial differences between the two rooms, as discussed in the previous section, and the chronology of events influencing rock deformation generally. Excavation of room 1 preceded that of room 4 by about four months; therefore, it had a longer period in which to approach dynamic equilibrium before the heaters were turned on. Geometrical differences between the two rooms included the lack of symmetry with respect to the corridor and waste shaft room, the slightly narrower pillar adjacent to room 1, and the difference in stratigraphic elevation of the floor level (see Sect. 6.4.3). The events which had an effect on the rock deformation are summarized in Table 11.3 in terms of both standard days and date. The following results are presented in terms of standard days.

11.4.5.1 Hole Closure. – The closing of array holes due to flowage of the salt at elevated temperatures was expected to provide some information. Accordingly, an effort was made to monitor the annular space between the hole liner and the wall with a caliper during the course of the experiment. The caliper was not accurate enough to provide a hole closure profile, although it was capable of showing when there was danger of salt freezing the liner into the hole. After termination of the experiment and removal of the liners, the holes were measured with a dial gage. However, by this time deterioration of the surface of the hole seriously reduced the accuracy of these measurements. (The deterioration resulted from the growth of salt crystals left as residue when migrating brine inclusions broke into the hole and the moisture vaporized.) For this reason it is not possible to use the results to draw a hole closure profile with depth. However, the maximum hole closure amounted to approximately 0.5 in.

Table 11.3. Chronology of Events – Rooms 1 and 4

Standard Day	Date	Event
806	Nov. 15, 1965	Start of experiment; power to heaters turned on
~1000	~May 23, 1966	Roof bolts installed
1117	Sept. 22, 1966	Insulation installed on floor around array heaters
1170	Nov. 14, 1966	Heated pillar experiment commenced
1223	Jan. 6, 1967	Insulation removed from floor around array heaters
1240	Jan. 23, 1967	Heat input to arrays increased by 40%
1382	June 14, 1967	Heat off; radiation sources removed; experiment terminated
1499	Oct. 9, 1967	Heated pillar off

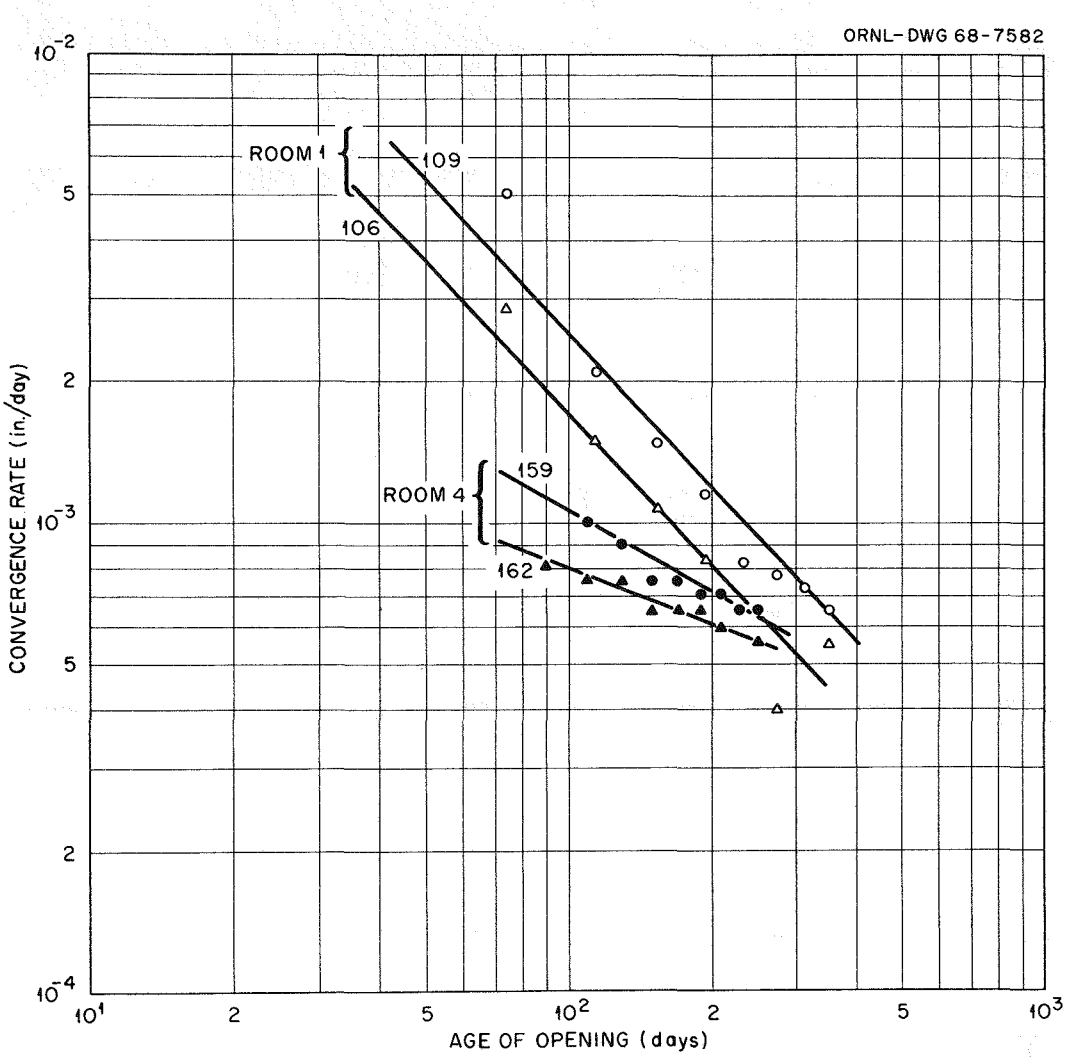


Fig. 11.57. Vertical Convergence Rate as a Function of Time for Rooms 1 and 4 (Prior to Heating).

11.4.5.2 Floor Lift. – Thermal expansion of the floor around the arrays, as measured on the network of leveling pins, is shown in Figs. 11.58 and 11.59. Figure 11.58 illustrates floor uplift as a function of time at selected points around the rooms. As can be seen, response of the floor was immediate to changes in the rate of heat input (standard days 806, 1240, and 1382). When the heaters were turned on (standard day 806), the floor lifted very rapidly at first, then slowed to a nearly constant rate. The same behavior occurred when the heat input was increased by 40% (standard day 1240). The curves in Fig. 11.58 were drawn to disregard the very slight effects of the installation and removal of the floor insulation on standard days 1117 and 1223 respectively. This insulation did not alter the rate of heat input, but it did change slightly the temperature distribution in the floor by reducing heat losses to the room. The data points in Fig. 11.58 indicate a very slight increase in floor uplift following installation of the insulation and a slight recovery (lowering) of the floor after its removal. The recovery of the floor uplift after standard day 1382, which coincides with the cooling of the salt, indicates that the mechanism of floor lift is more complicated than the mere thermal expansion of salt around the heaters. Recovery of the floor uplift appears to be nearly complete in Fig. 11.58 but amounts to only a fraction of the total floor uplift – about 16% in room 1 and about 11% in room 4. Salt in the center of the rooms around the arrays is confined in horizontal directions by the stresses resulting from pillar loading, but it is free to expand vertically up into the rooms. When the salt is heated, thermal expansion

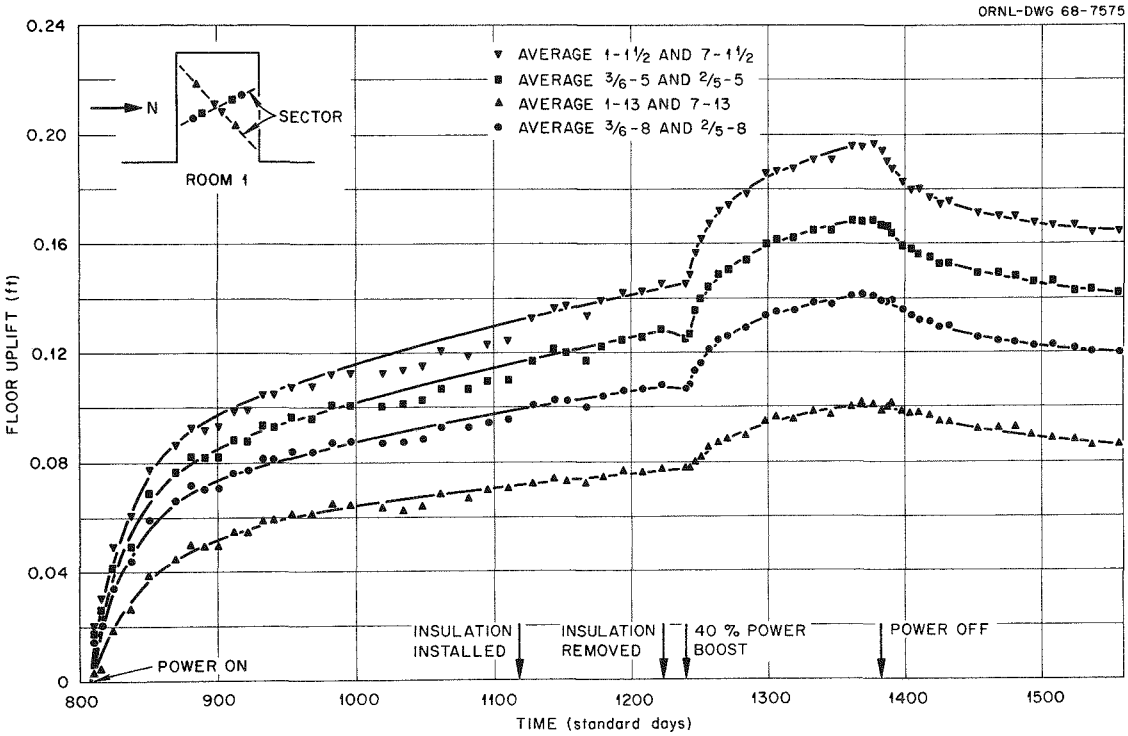


Fig. 11.58*a*. **Floor Uplift as a Function of Time.** Room 1.

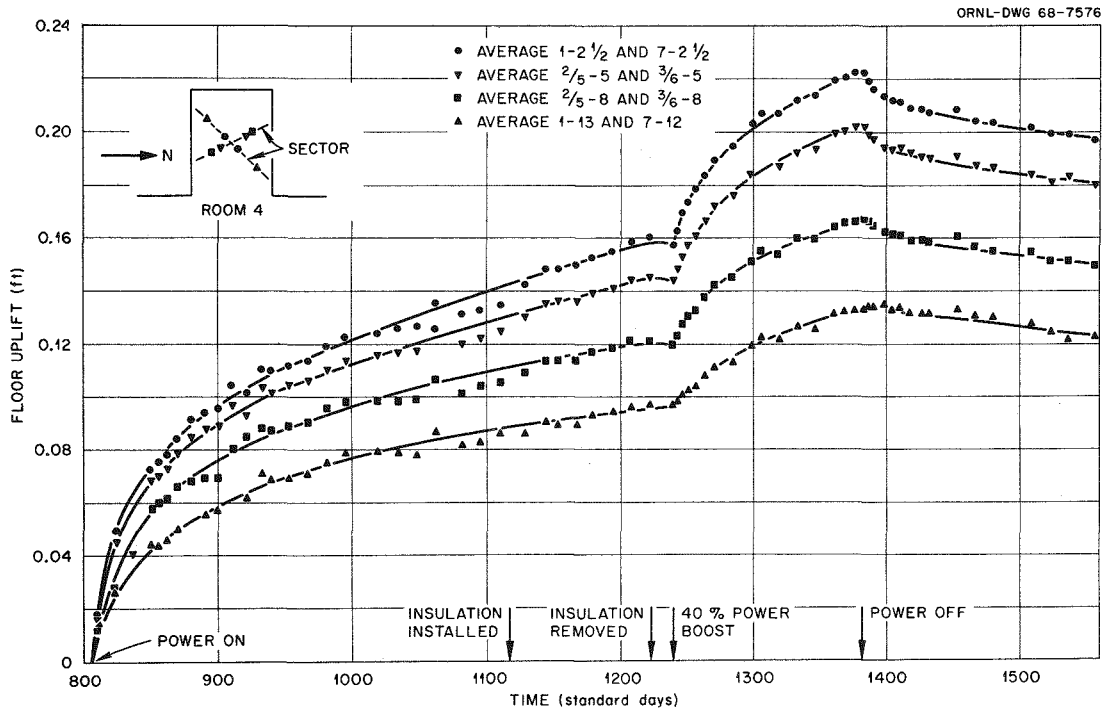


Fig. 11.58*b*. **Floor Uplift as a Function of Time.** Room 4.

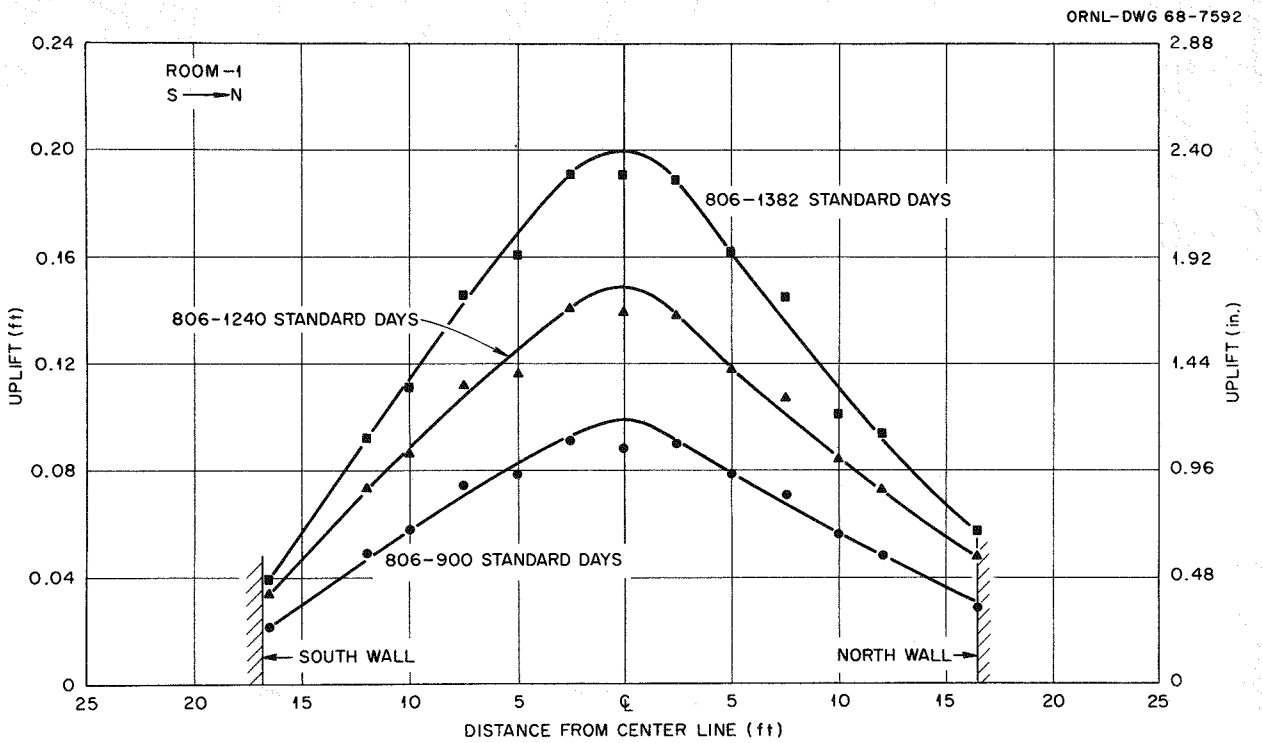


Fig. 11.59*a*. Floor Uplift Profiles at Selected Times. Room 1, north-south.

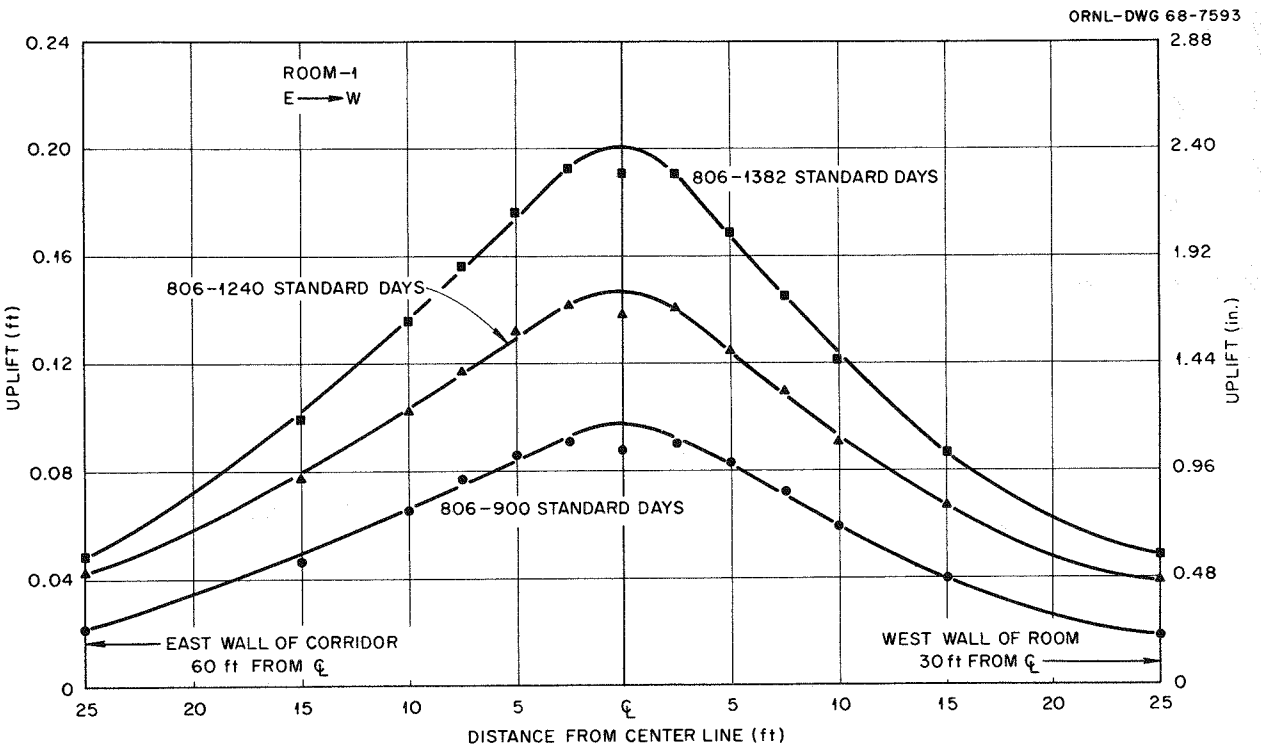


Fig. 11.59*b*. Floor Uplift Profiles at Selected Times. Room 1, east-west.

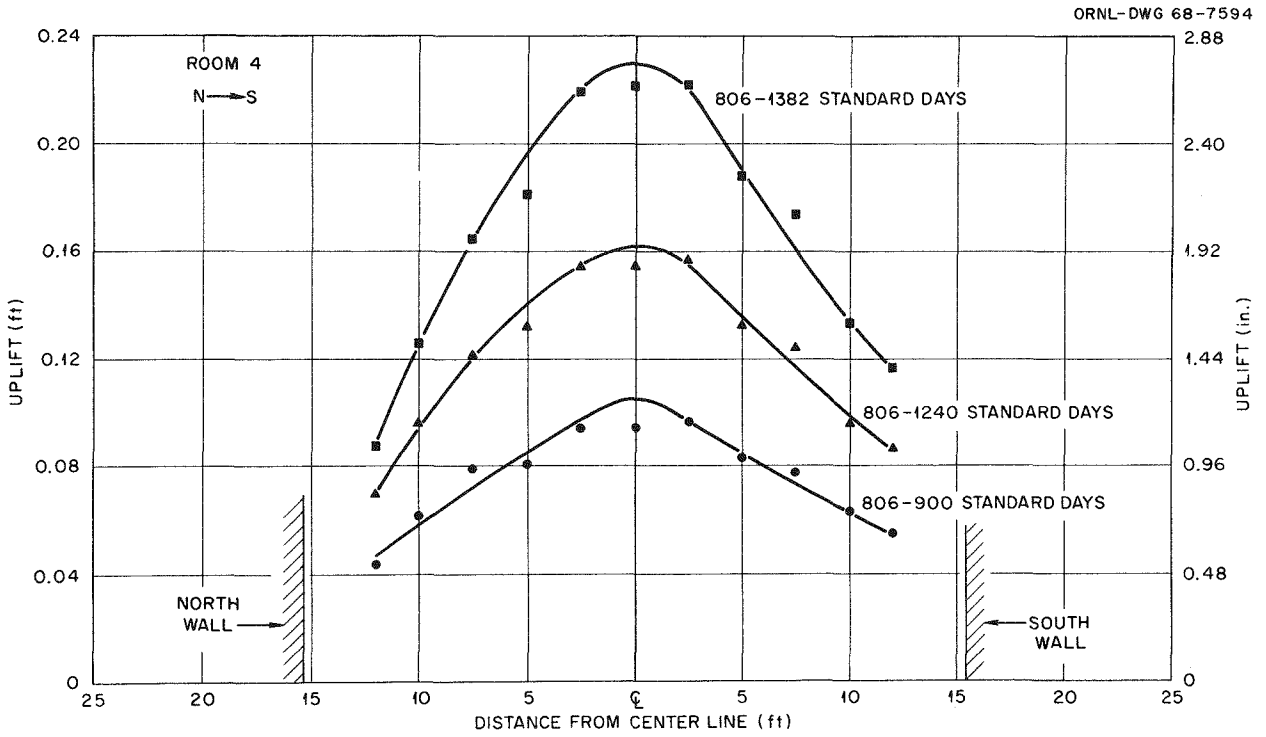


Fig. 11.59*c*. Floor Uplift Profiles at Selected Times. Room 4, north-south.

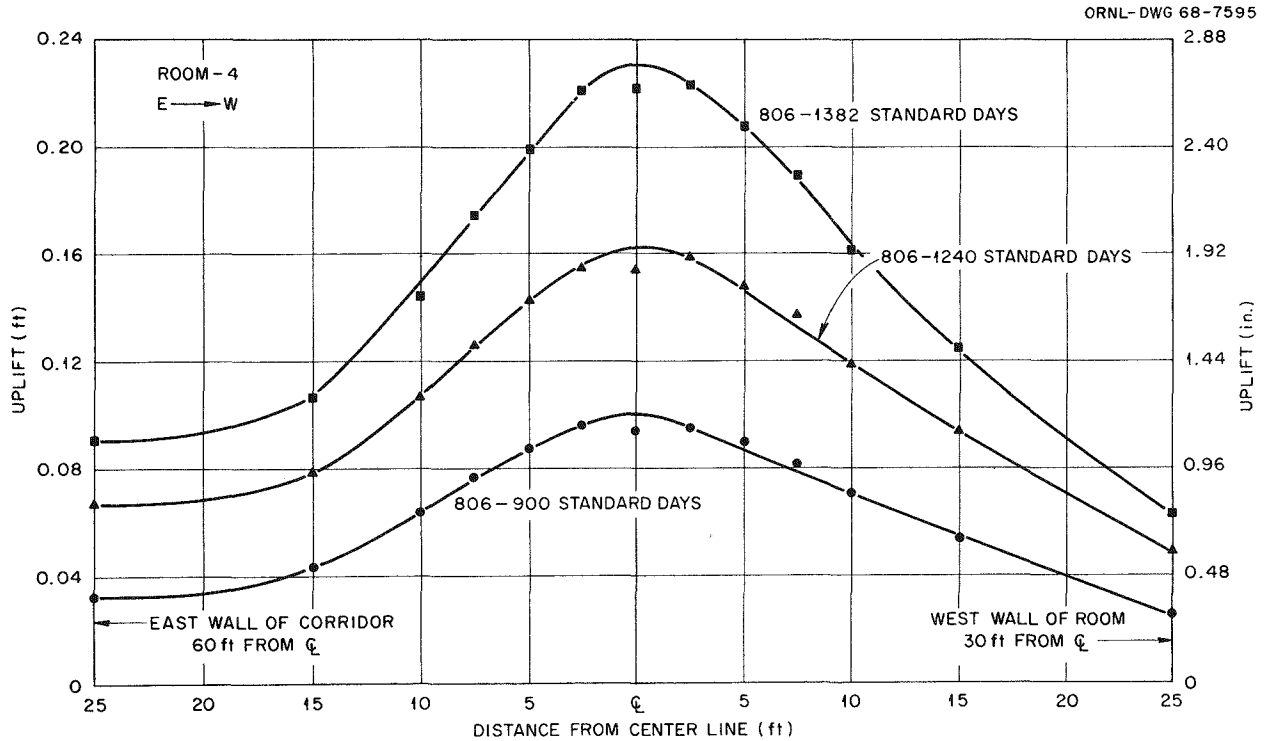


Fig. 11.59*d*. Floor Uplift Profiles at Selected Times. Room 4, east-west.

in the vertical direction will result in uplift of the floor. This component of total floor uplift should be recoverable upon cooling. Direct thermal expansion in the horizontal directions is not possible because of the constraining stress. Therefore, there is an appreciable thermal stress induced in the horizontal direction. Salt in the floor will creep upward (the only direction available to it) under the influence of this horizontal thermal stress, thus providing a second and apparently sizable component of floor uplift which would not be recoverable. The difference in the amount of recoverable floor uplift in the two rooms is probably primarily a function of age. Room 1, having had a longer period in which to relieve the horizontal stresses resulting from pillar loading, should have a smaller component of nonrecoverable floor lift. The stratigraphic difference in elevation of the floor in the two rooms may also have contributed slightly to this difference in recoverable floor uplift. There is no reason to believe that floor uplift is related in any way to absorbed radiation dose in room 1.

The profiles of floor uplift (Fig. 11.59) were drawn for the north-south and east-west lines of symmetry through the arrays in both rooms. The three curves on each plot represent the floor uplift taking place between the start of the experiment (standard day 806) and (1) standard day 900, approximately 100 days; (2) standard day 1240, just prior to the 40% power boost; and (3) standard day 1382, the maximum uplift at the time of power shutdown. These profiles show that the uplift is elongated along the long axis (east-west) of both rooms in response to vertical restraint of the pillars. The uplift in room 1 is quite symmetrical, whereas in room 4 it is skewed slightly to the northwest. This asymmetry of room 4 profiles is apparently related to floor irregularities and differences in the floor elevation in room 4. The floor uplift in room 4 was also influenced by a separation and heaving of the floor beds over part of the room. This floor heave phenomenon is discussed in more detail in Sect. 11.4.7.

In general, in spite of the slight differences discussed above, floor uplift in the two rooms was almost identical in magnitude, shape, rate, and response to the heating.

11.4.5.3 Rib-Side Convergence. – Vertical convergence of the two experimental rooms, as measured on the pipe-type (type F) gages located around the walls (rib sides) of the rooms (five gages in room 1, three in room 4), is shown in Fig. 11.60 as a function of time. Data are included for a period of nearly a year prior to start of the experiment. Since the results from room 1 (Fig. 11.60*a*) cover a longer period and are more detailed, they are discussed in some depth.

The initial portions of the convergence curves, prior to standard day 806, represent the normal creep of salt in the pillars in response to the load increases resulting from mining. The initially high rate of convergence is due both to the excavation of room 1 itself (completed on standard day 436) and to the mining in room 2 (completed on standard day 494). The convergence rate then decreased with time at a decreasing rate and would have continued to do so if the approach to equilibrium had not been disturbed by heating the salt. During this period, three gages along the side of pillar 1-2 (gages 108, 109, 110) indicate a higher rate of convergence than at gage 106, which is also greater than at gage 107. Furthermore, the convergence is greater at the front of the pillar (gage 110) than at the back (gage 108). This ranking reflects the load distribution on the rib side adjacent to the pillar, which should be greater at the front of pillar 1-2 than at the back, greater on the small pillar than on the gage 106 side of the room, and least at the back of the room.

The influence of heat, commencing on standard day 806, on the convergence rates at all gages can be seen in Fig. 11.60. These convergence gages were installed in such a manner that a portion of the thermal stress floor uplift, examined in the previous section, is included in the measured convergence. However, since the convergence gages were anchored $1\frac{1}{2}$ to 2 ft below the floor, only that portion of the floor uplift occurring below this point is included. When this component is estimated and deducted from the total convergence, it is obvious that the entire height of the pillar has experienced an accelerated vertical deformation in response to the heating in the center of the rooms. A ranking of the gages according to average measured convergence rate for the period standard day 806 to 1240 indicates that gage 109 has the highest convergence rate, followed by gages 110, 106, 108, and 107 in decreasing order. This ranking results from the addition of the effects of heating (largest at gages 109 and 106, smallest at gage 107) to the before-heat deformation rates. Therefore, the total convergence during this period (Fig. 11.60) can be interpreted as the sum of components due to (1) overburden and mining stresses, which would have continued along the curve prior to day 806 if heating had not been initiated, (2) uplift of the floor, which at this distance from the heat sources is almost entirely due to horizontal thermal stresses, and (3) an increase in the vertical loading of the pillar due to thermal stresses. This picture of the deformations will be further complicated at some later date by the variation of salt

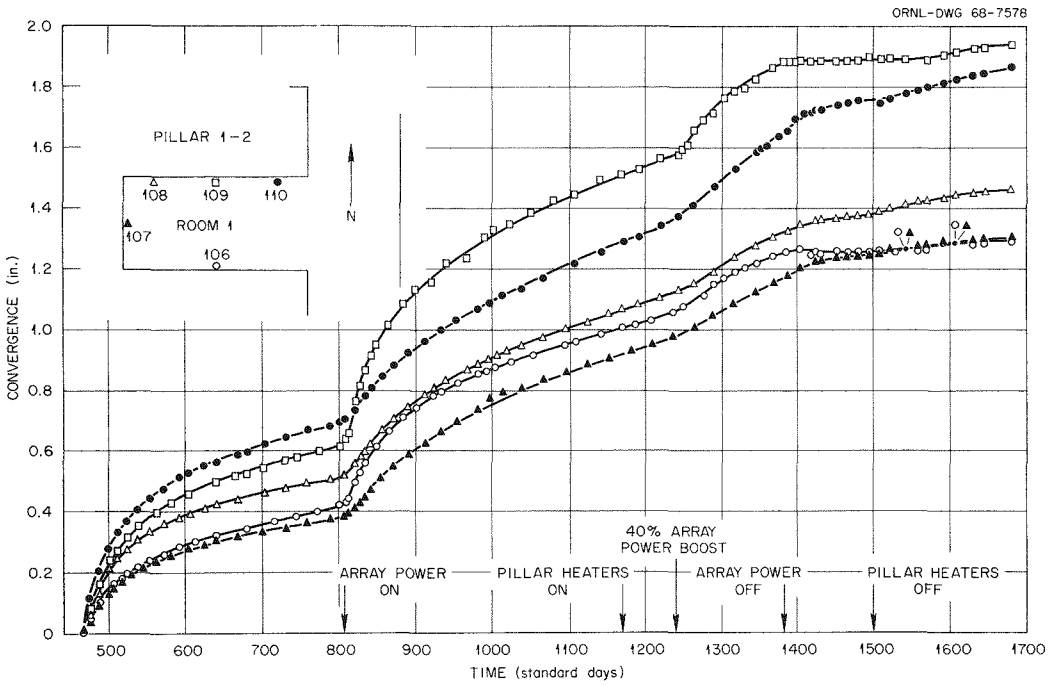


Fig. 11.60*a*. Vertical Convergence as a Function of Time (Pipe-Type Gage). Room 1.

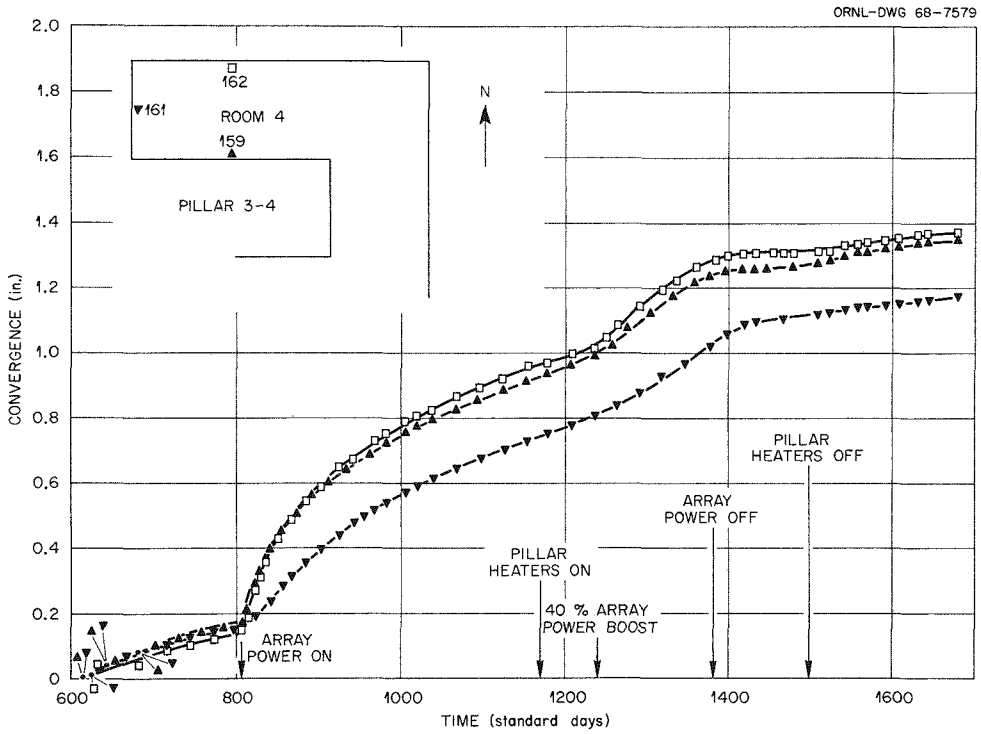


Fig. 11.60*b*. Vertical Convergence as a Function of Time (Pipe-Type Gage). Room 4.

creep properties as a function of temperature. However, even by standard day 1240 there was not yet an appreciable heating of salt in the pillars (see Sect. 11.3). Further insight into these relative effects can be obtained from examination of the convergence curves during the cooling period (that is, after standard day 1382). At gages 106 and 109, where the effects of heating were greatest, the recoverable components were large enough to compensate for the continuing components (viz., mining and overburden stress-induced deformation) and produce a period of essentially zero convergence. At gages 107 and 108, recovery of a part of the floor uplift flattened the slope of the curves noticeably but was not sufficient to completely counteract the overburden loading creep. At gage 110 recovery is still less apparent because of the higher loads and higher rate of convergence around the end of the pillar.

The convergence curves for two of the three gages in room 4 (Fig. 11.60*b*) are almost identical with those of room 1, if comparable gages are started from equivalent points on standard day 806. The effects of heat in the two rooms, of course, should be nearly identical. Apparently the increased deformation rate resulting from the younger age and slightly greater height of the pillar was compensated for by the decreased overburden loading and deformation rate resulting from the difference in geometry, thus producing conditions in room 4 which made the response to heating appear to be nearly identical with that in room 1.

11.4.5.4 Horizontal Deformation of Pillars and Rib Sides. – Horizontal internal strain gages (type A; see Sect. 11.4.1.1) were installed in three sides of the two experimental rooms as shown in Fig. 11.42. A typical example of the raw data obtained from these instruments is shown in Fig. 11.61, which is a plot for the four wires of station 119-A-S. This figure illustrates the nature of the data obtained from this type gage and provides a graphic indication of the accuracy of the measurements. As can be seen from Fig. 11.61, interpretation of the results in this (raw) form is difficult. This figure is included for illustration purposes only.

A much more informative presentation of the horizontal strain gage data is to calculate the movement of each of the wire anchors in a given borehole, relative to some (assumed) fixed point, and plot the displacements as a function of time. Figures 11.62 and 11.63 are such plots for some of the gage stations installed around rooms 1 and 4. All these stations are contained in the horizontal plane located at the midheight of the pillars. Also, the results of the five gages shown for room 1 are equivalent to (mirror image of) the gage results in

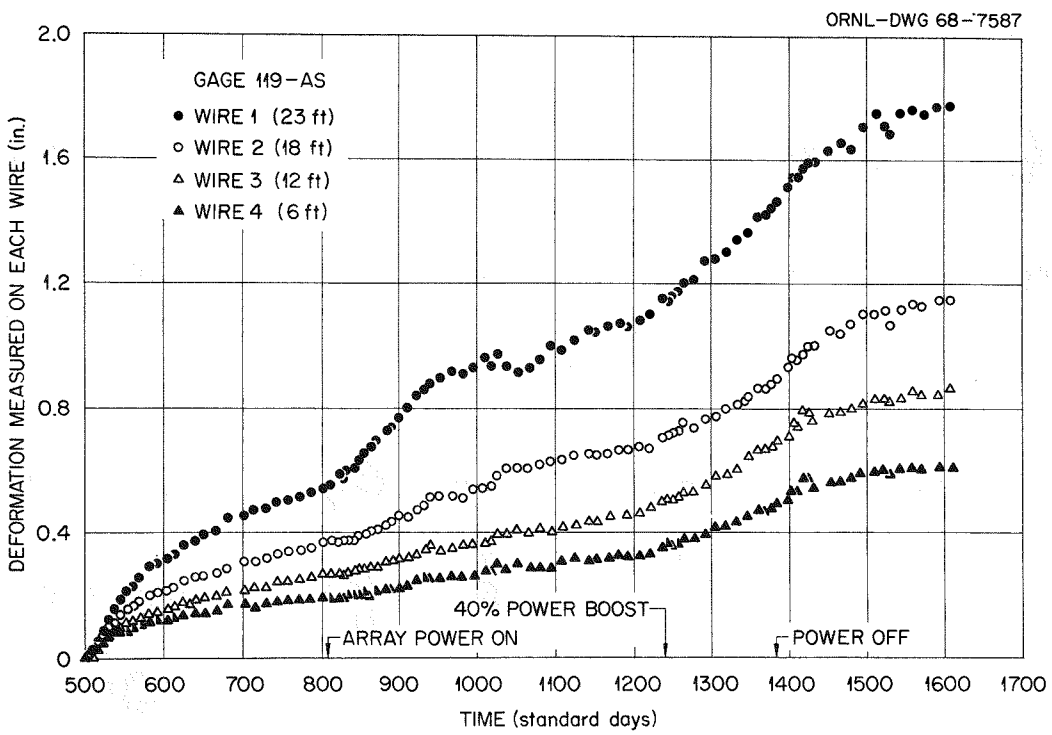


Fig. 11.61. Raw Data Plot of Results from Gage 119-A-S.

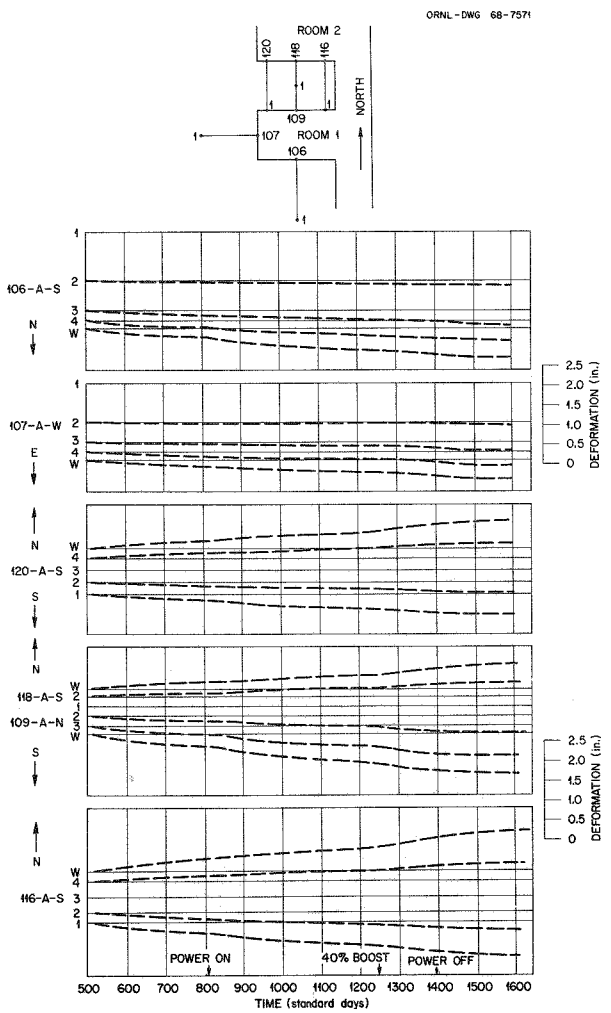


Fig. 11.62. Deformation as a Function of Time for Selected Points Around Room 1 (Gages 106, 107, 120, 118 and 109, 116).

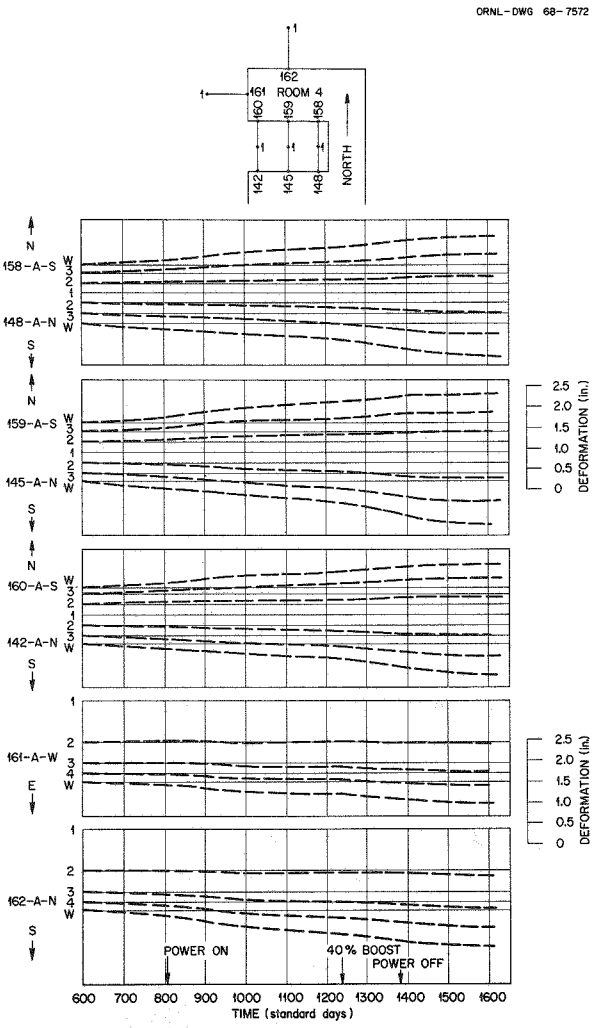


Fig. 11.63. Horizontal Deformation as a Function of Time for Selected Points Around Room 4 (158 and 148, 159 and 145, 160 and 142, 161, 162).

room 4. For the gages passing through the narrow pillars, the point at or nearest the center of the pillar was assumed to be stationary, while for the solid rib-side stations (106, 107 in room 1 and 161, 162 in room 4) the wire anchor located furthest from the wall of the room was assumed to be fixed.

The acceleration of horizontal deformation in response to the heating at standard days 806 and 1240 can be seen clearly on all three walls of rooms 1 and 4. Note also that this effect extends completely through the narrow pillars but is reduced at the walls of rooms 2 and 3. At the walls of these rooms, the changes in deformation rate are also affected by the heating of the center pillar, commencing on standard day 1170.

A comparison of Figs. 11.62 and 11.63 indicates that the deformations around room 4 are approximately equivalent to those in room 1. Even more impressive is the nearly identical correspondence between the horizontal deformations (transverse expansion) measured at pillar 1-2 and pillar 3-4. However, it is obvious that this time plot is not particularly sensitive to small differences in deformation or suitable for illuminating the finer details of deformation.

Deformation of the pillars adjacent to rooms 1 and 4 can be examined in more detail by constructing strain plots of the type shown in Fig. 11.64. The results from all horizontal gages through these two pillars (five gages in pillar 1-2, nine in pillar 3-4) are given. The results

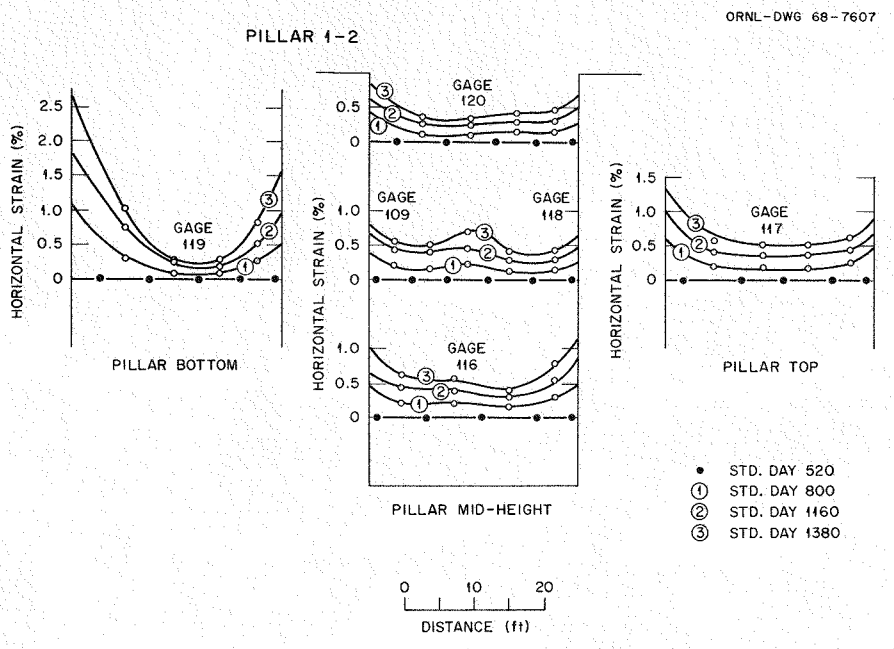


Fig. 11.64*a*. Horizontal Strain as a Function of Distance into the Pillar at Selected Times. Pillar 1-2.

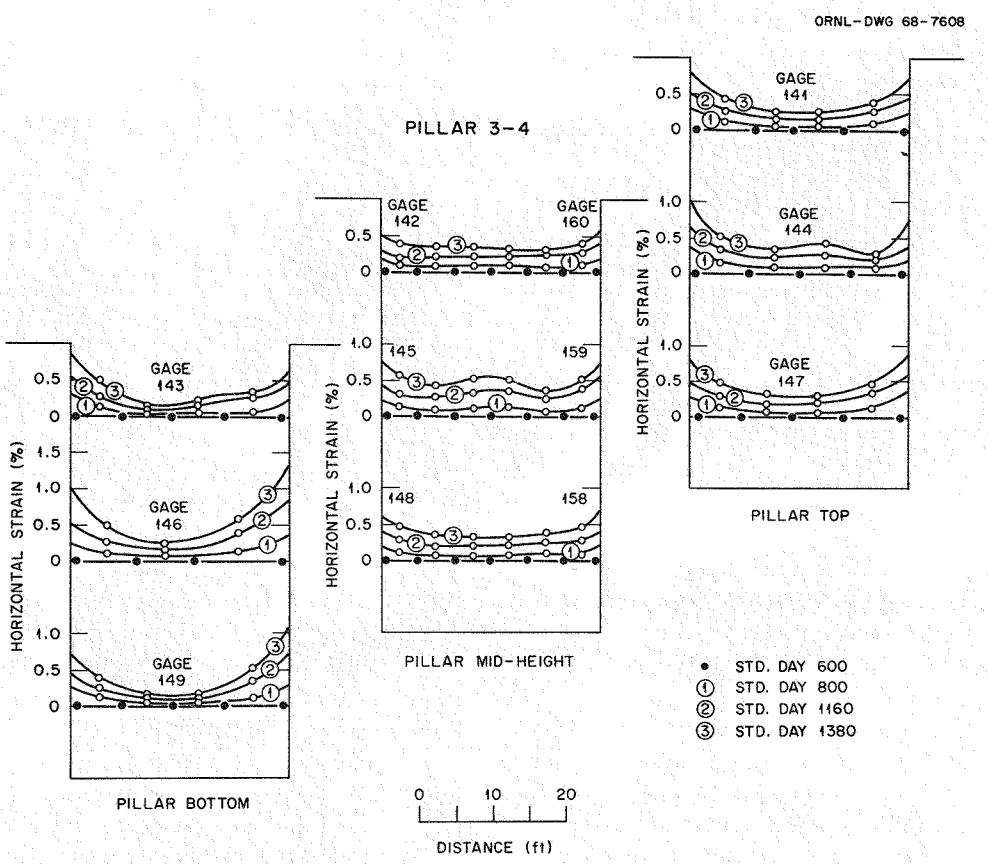


Fig. 11.64*b*. Horizontal Strain as a Function of Distance into the Pillar at Selected Times. Pillar 3-4.

from gages located at the pillar midheight are the same data as shown in the two previous figures. Gages at the top and bottom of the pillars were located about 2 ft from the roof and floor respectively. Points on the curves represent the total horizontal strain accumulated between two adjacent wire anchors at the times indicated. These times are (1) standard day 800, just before starting the heating experiment; (2) standard day 1160, before any effects from either the heated pillar test (at 1170) or the power boost (at 1240); and (3) standard day 1380, two days before turning off the heat. Zero times were taken as standard day 520 for pillar 1-2 and standard day 600 for pillar 3-4. Although this type of plot looks strange at first, it is quite easy to interpret. The U-shaped form of the strain curves indicates that the cumulative horizontal strain nearest the edges of the pillars is greater than that at the center of the pillar. In general strain on the side of the pillar closest to the heated array is greater than on the other side, but by an amount less than would have been anticipated from the deformation plots. The transverse horizontal strain is also greater at the front (corridor) end of the pillars than at the back. This is, of course, a consequence of the total lack of restraint at the front of the pillar and the slight confining effect of the solid walls at the back of the rooms, and the fact that the front ends of the pillars are more highly stressed. The variation of strain with height is even more noticeable – being much greater near the bottom of the pillars than at the top. This is a consequence of the heat and floor uplift at the lower levels. The difference between gages 119 and 146 is a result of the lower level of the floor in room 4 and its relationship to the location of the gage.

The most significant information revealed by this type plot is the increased strain observed at the center of the pillars, specifically at gages 109–118, 145–159, and 144. The implication is that the horizontal strain at the center of the pillar is greater than it is at points located one-third the distance from the rib sides. Since the horizontal constraint should be highest and therefore the horizontal deformation lowest at the center of the pillar, this result is contrary to the expected behavior and cannot be explained at this time.

These strain plots indicate that there is no gross difference between the deformational behavior of the two experimental rooms or their adjacent pillars which could be ascribed to the effects of radiation. Rock mechanics results from mining operations in plastic materials such as salt are usually[25] more descriptive when plotted with the strain rate as a function of time. In this case strain rate vs time plots were found to be practically useless because of the almost instantaneous jump in strain rate due to heating. Since the strain rate is very sensitive to distance from the heat source and the computed value of strain rate is sensitive to reading frequency, it was not possible to make a meaningful comparison of the maximum strain rates. The thermally induced strain rate, after an initial peak, decreases fairly rapidly in a manner similar to the normal creep curve, but it is still high enough to completely mask any of the more fundamental differences in the behavior of the various gages. For these reasons, strain-rate plots are not used in the presentation of our results.

11.4.5.5 Vertical Deformation – Roof Sag. – Vertical deformation in the floor and roof in the vicinity of the heater arrays was measured on the vertical internal strain gages located at positions shown in Fig. 11.42. Since these stations were tied into the leveling network, it was possible to calculate the displacement of each of the wire anchors relative to what should be an absolute base line. This vertical deformation, measured at two of the gages in each of the rooms, was plotted as a function of time in a manner similar to Figs. 11.62 and 11.63 and is shown in Figs. 11.65 and 11.66. The two gages are typical for the rooms and are comparable. As is the case with our horizontal deformation plots, this type of data presentation is somewhat insensitive to the finer details of rock movement. For reasons which will become apparent shortly, it was impractical to compute the vertical strain taking place between adjacent anchors; therefore, these plots of vertical deformations as a function of time are perhaps the best form for presentation of these data.

Since the movement at each point was calculated with respect to a stationary point, the curves representing "floor" stations are equivalent to the floor uplift curves discussed earlier. The effects of heating at standard days 806 and 1240, cooling commencing at day 1382, and the shape of the curves between these points are identical to the floor uplift vs time curves. The deformation of points deeper in the floor, down to a depth of 25 ft, also show an uplift of the same type, which diminishes with increasing depth. The immediate response to the initial heating evidenced by the anchors 25 ft below the floor (13 ft below the heater zone) and the magnitude of that movement (amounting to several tenths of an inch) are somewhat surprising even though the mechanism of that movement is the same as the floor uplifts. The loss of data on the 25-ft-deep floor

[25] W. C. McClain, "The Effect of Nonelastic Behavior of Rocks," *Proc. Eighth Symp. on Rock Mechanics, September 15–17, 1966, Minneapolis,* pp. 204–16; in *Failure and Breakage of Rock,* ed. by C. Fairhurst, AIME, 1967.

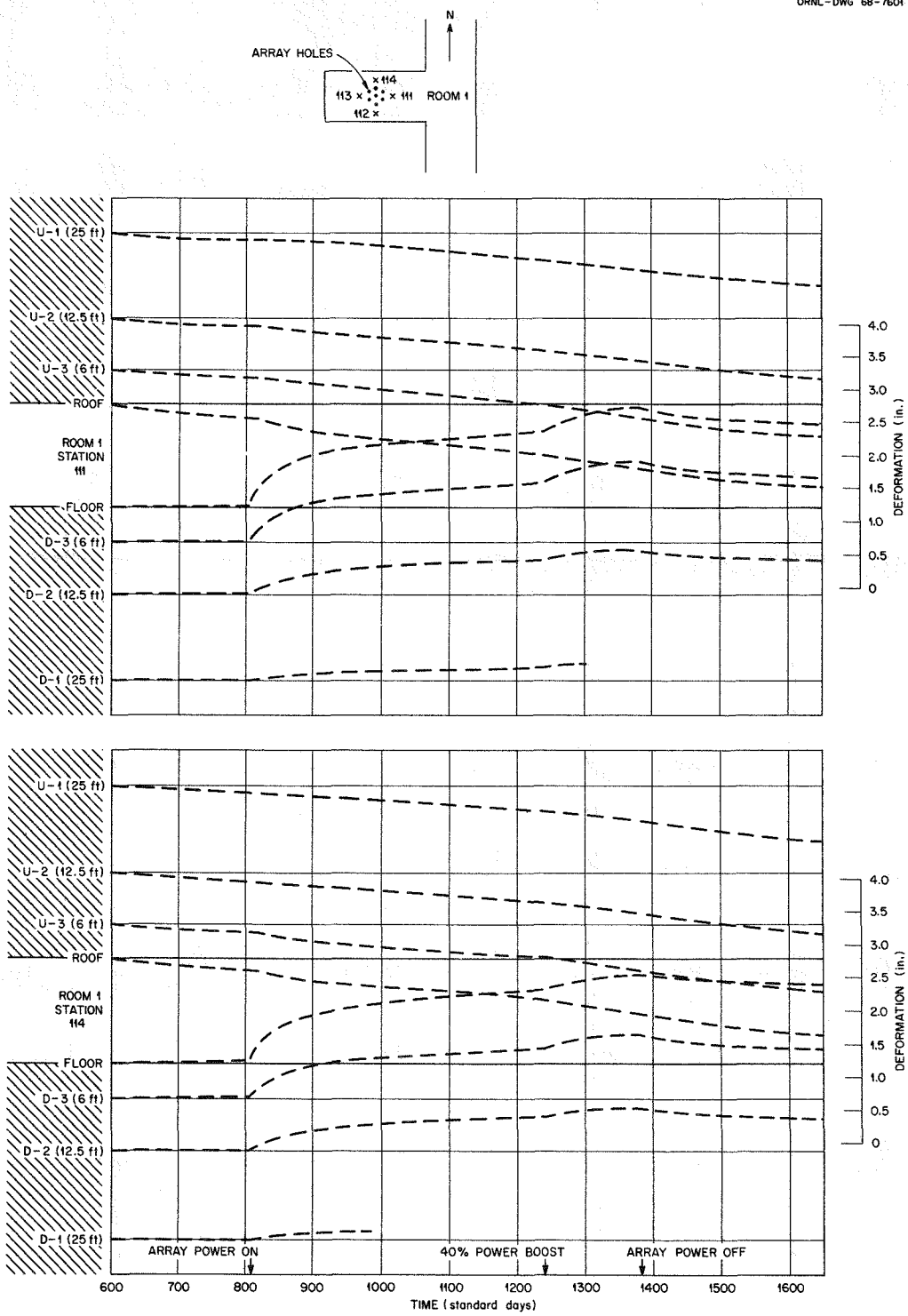


Fig. 11.65. Vertical Deformation as a Function of Time – Room 1 (Gages 111 and 114).

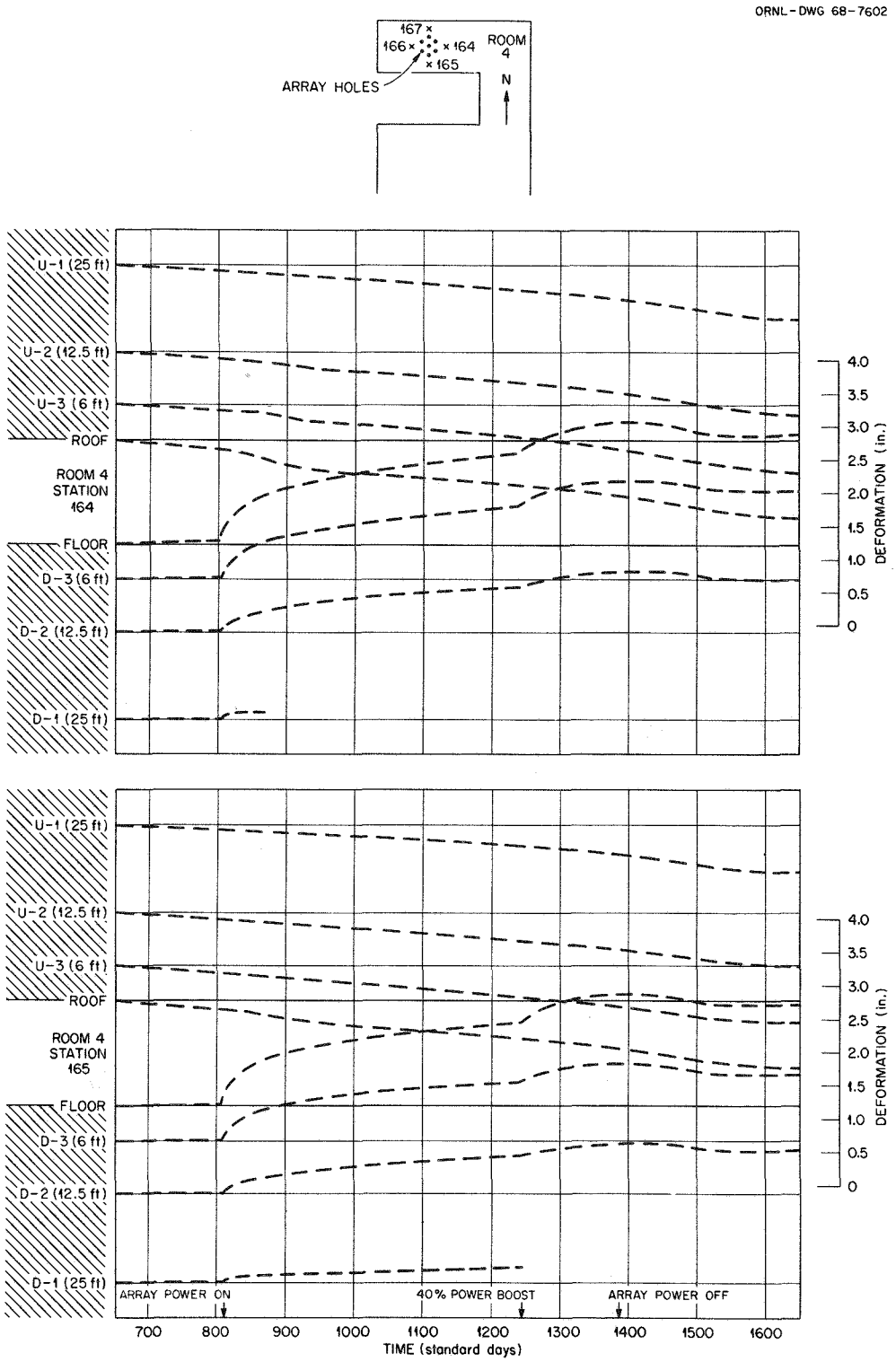


Fig. 11.66. Vertical Deformation as a Function of Time – Room 4 (Gages 164 and 165).

wires at about 60 to 500 days after the start of heating was a consequence of corrosion in the heated zone.

The results obtained for the deformation of the roof over the arrays were perhaps the most interesting of all the rock mechanics data. First, it is seen that the points 25 ft above the ceiling of the rooms have lowered appreciably during the approximately three-year period covered on the figures. A small part of this movement, which amounts to about ¾ in., may be due to local deformation of the roof strata toward the rooms, but at this height above the room ceilings, local effects can hardly account for more than a small fraction of the total. The inference is that the pillars supporting the experimental area have squeezed enough to allow the entire overlying rock mass, including the ground surface, to subside (but not by the whole amount).[26]

Notice that the effects of heating at standard days 806 and 1240, although very slight, can still be seen at the 25-ft level as an acceleration in the rate of lowering. However, there is no evidence of recovery when the power to the heaters was turned off standard day 1382. This is not inconsistent with the previous discussion, since the accelerated deformation of the pillars due to thermal stress loading should be reflected throughout the roof strata. The pillar deformation results (Figs. 11.62 and 11.63) showed no significant response at standard day 1382 other than a very gradual return to preheating deformation rates.

The lines representing the wire anchors at 25 ft (U-1), 12 ft (U-2), and 6 ft (U-3) diverge only very slightly, indicating that this part of the roof material moves as a unit with only a small amount of vertical strain. The curves for the anchors at 6 ft depth (U-3) and at roof level show a divergence prior to standard day 806 and an increasing divergence immediately following start of the experiment. This divergence represents the sagging of a 2-ft-thick bed of salt in the immediate roof of the rooms which had separated from the overlying material along a thin shale parting. The existence of this sagging bed had been detected prior to start of the experiment on a preliminary examination of the gage results and the separation had been defined by probing with a feeler-type instrument. The presence of a thin shale parting 2 ft above the ceiling was, of course, known from the preliminary geological work (Sect. 5.1.3). Although some precautions had been taken in the installation of remote and continuous-reading transducer gages, the rate of sag of this bed prior to heating was considered normal and safe. Similar phenomena are not unusual in most mines in bedded salt and are commonplace in other salt mines in the vicinity. However, acceleration of the sag, by a factor of approximately 5, immediately after the heat was turned on was unexpected, and it was felt that some remedial action should be taken to prevent the development of unsafe conditions in the roof, especially during the heated pillar test.

The mechanism by which the roof in the center of the experimental rooms was deformed by the heating beneath the center of the floor can be determined by a closer examination of some of the deformations occurring around the room immediately after the heaters were turned on. The pertinent deformations are shown as a function of time in Fig. 11.67. As was seen from the floor uplift data, the thermal stresses induced in the salt when the power was turned on produce an immediate uplift of the floor throughout the entire room by the creep resulting from these stresses – not by the thermal alteration of the plastic flow properties of the salt. This floor uplift extends under the edges of the pillars, causing an increase in the vertical stress, especially near the edges of the pillars. The effects of this increased pillar loading can be seen on the F-type convergence gages 106, 109, 159, and 162. The pillar responds to this increased vertical stress, in part, by accelerating the rate of horizontal deformation throughout the entire height of the pillar. This increase in horizontal deformation can be seen on the internal strain gages (A-type) at the pillar midheight at stations 106, 109, 159, and 162-A and at gages near the roof at 117 and 144-A. As the two walls of the room move inward, they exert a horizontal load on the roof bed because of the frictional resistance of the small shale parting separating the roof and the pillar. Since the 2-ft-thick sagging roof bed is an independently acting, self-supporting beam (or more exactly, plate), it will react to this induced "axial" load with a buckling type of deformation or sag. A comparison of the strain rates for 100-day periods preceding and following the application of heat in the array holes dramatizes this acceleration and is given in Table 11.4. The accelerated sag of the roof bed is seen as a result of the disturbed *stress* field caused by the superimposition of thermal stresses onto the preexisting overburden and mining stresses. The effects of this disturbance were amplified in the roof because of its configuration as a beam deflecting under axial loads (see Fig. 11.68).

11.4.5.6 Roof Bolting. – Although the rate of sag of the 2-ft-thick ceiling bed was decreasing with time and was not considered to be potentially hazardous, it did

[26] W. C. McClain, "Surface Subsidence Associated with Longwall Mining," *Trans. AIME* **238**, 231–36 (September 1966).

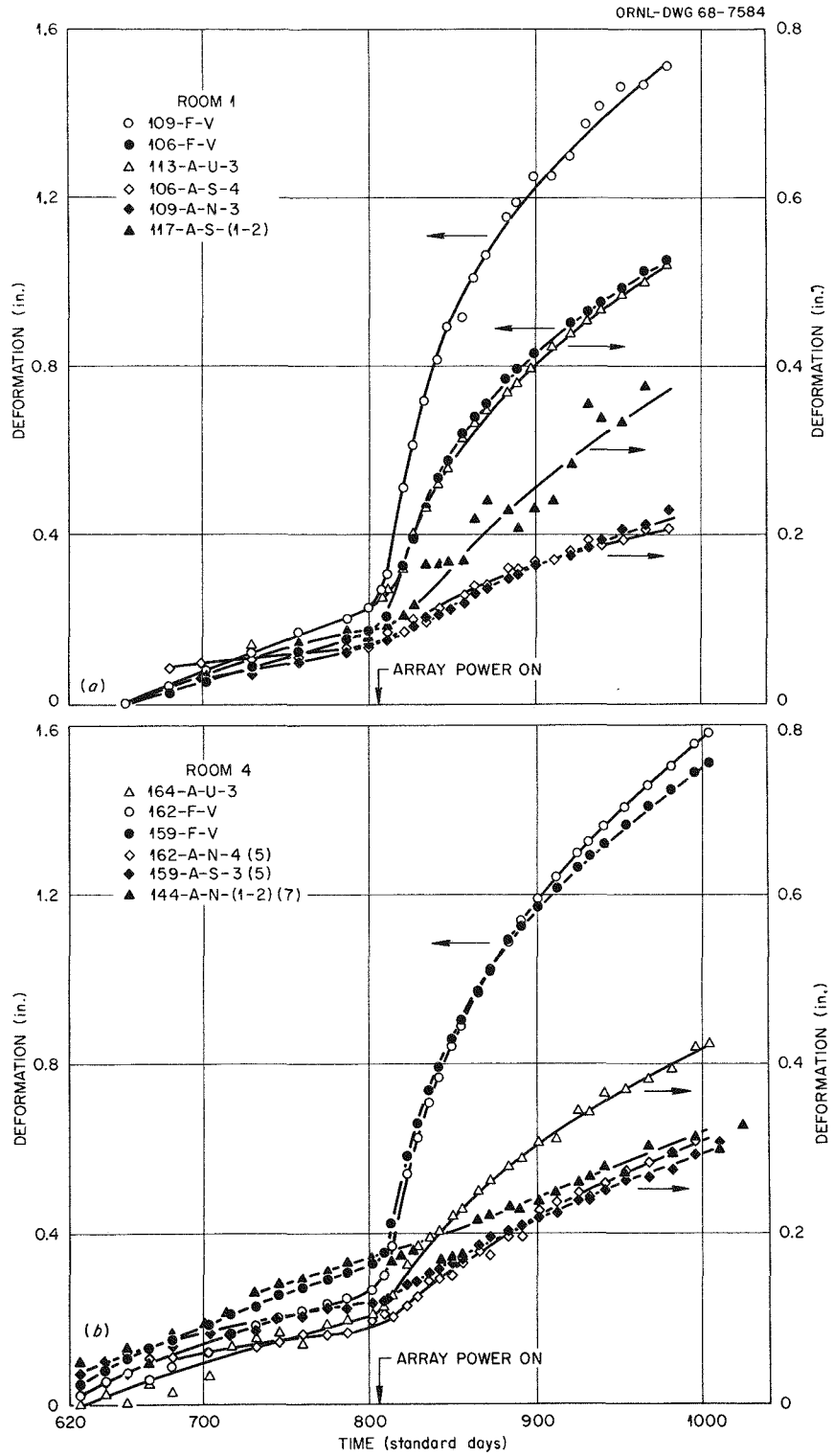


Fig. 11.67. Selected Deformations Around Experimental Rooms as a Function of Time. (*a*) Room 1, (*b*) room 4.

Table 11.4. Comparison of Strain Rates Preceding and Following Heating

See Fig. 11.68

Gage	$\dot{\epsilon}$, Strain Rate (μin. in.$^{-1}$ day^{-1})		Acceleration Factor
	Standard Days 700–800	Standard Days 808–900	
Room 1			
106-F-V	2.55	16.25	6.4
109-F-V	3.35	24.66	7.3
106-A-S-4	1.49	8.38	5.6
109-A-N-3	4.04	10.65	2.6
117-A-S-(1-2)β	3.26	10.56	3.2
Av	2.94	14.10	4.8
Room 4			
159-F-V	3.42	19.79	5.8
162-F-V	3.6	21.70	6.1
159-A-S-3	2.89	8.33	2.9
162-A-N-4	3.23	10.67	3.3
144-A-N-(1-2)	3.40	4.05	1.2
Av	3.31	12.91	3.9

Gage	Roof Bed Sag Rate (10^{-4} in./day)		Acceleration Factor
	Standard Days 700–800	Standard Days 808–900	
Room 1			
111-A-U-3	2.75	11.74	4.3
112-A-U-3	1.22	7.17	5.9
113-A-U-3	3.88	14.78	3.8
114-A-U-3	1.22	5.00	4.1
Av	2.27	9.67	4.3
Room 4			
164-A-U-3	3.57	10.10	2.8
165-A-U-3	0.94	4.90	5.2
166-A-U-3	2.47	7.90	3.2
167-A-U-3	1.29	5.70	4.4
Av	2.07	7.15	3.5

raise several questions relating to continued operation of the experiment. Would the roof sag in the wider rooms 2 and 3 create problems when a large amount of heat was applied at the base of the small center pillar? Since the effect of heat in the arrays was detected in rooms 2 and 3 (but at a much reduced magnitude), would startup of the heated pillar experiment jeopardize the operations in rooms 1 and 4? For these reasons, it was decided that some measures should be taken to prevent an excessive amount of roof sag in the experimental area.

Roof bolts were considered first, but there seemed to be a dearth of information concerning anchorage capacities which could be developed in rock salt. A few bolts had been used in other mines in the area, but apparently[27] without success. Furthermore, it was felt that a certain amount of data on movement of the roof resulting from subsequent heating experiments would be lost if roof bolts were installed to support the 2-ft-thick bed. Several alternative protection systems[28] were examined in some detail: these included a network of chain-link fence material supported on yielding steel cables laced through holes in the pillars, to catch the roof bed, and a tracked vehicle armored with a suitable superstructure to offer temporary protection during periods of activity in a room. Both methods would have been fairly expensive, would have required considerable fabrication and installation time, and, in general, were rather unsatisfactory solutions to the problem. The rock mechanics gage results were then critically reexamined, and it was concluded that the behavior of the 2-ft-thick roof bed was already so well understood that very little additional information would be lost if the sagging bed were successfully bolted to the 3-ft-thick bed immediately above it. Furthermore, the sacrificed data would be compensated at least partially by new data on the behavior of roof bolts in salt. Since the installation of roof bolts throughout the experimental area would provide the most economical and the most satisfactory type of roof support, it was decided that a test area should be established in room 3 with a trial pattern of bolts.

Although this test area was not in the array rooms, necessity for the test was founded upon results obtained in rooms 1 and 4. Furthermore, the subsequent extensive installation of roof bolts influenced the data from rooms 1 and 4, as well as elsewhere in the entire experimental area. These data are presented in later sections of this chapter. Therefore, this seems like an appropriate place to discuss the roof bolt program.

Thirty-seven roof bolts, 4 ft long, were installed in the center of room 3 in the pattern shown in Fig. 11.69. The length of the bolts was selected so that the lower bed would be supported only from the overlying 3-ft-thick bed and the bolt holes would not perforate the shale parting at the top of the 3-ft bed, causing the

[27] R. L. Bradshaw and W. C. McClain, *Roof Bolt Test Analysis and Recommendations,* ORNL-CF-66-4-66.

[28] R. F. Denkins and A. Matthews, *Designs for a Protective Shield for the Salt Vault Project,* ORNL-CF-66-7-66.

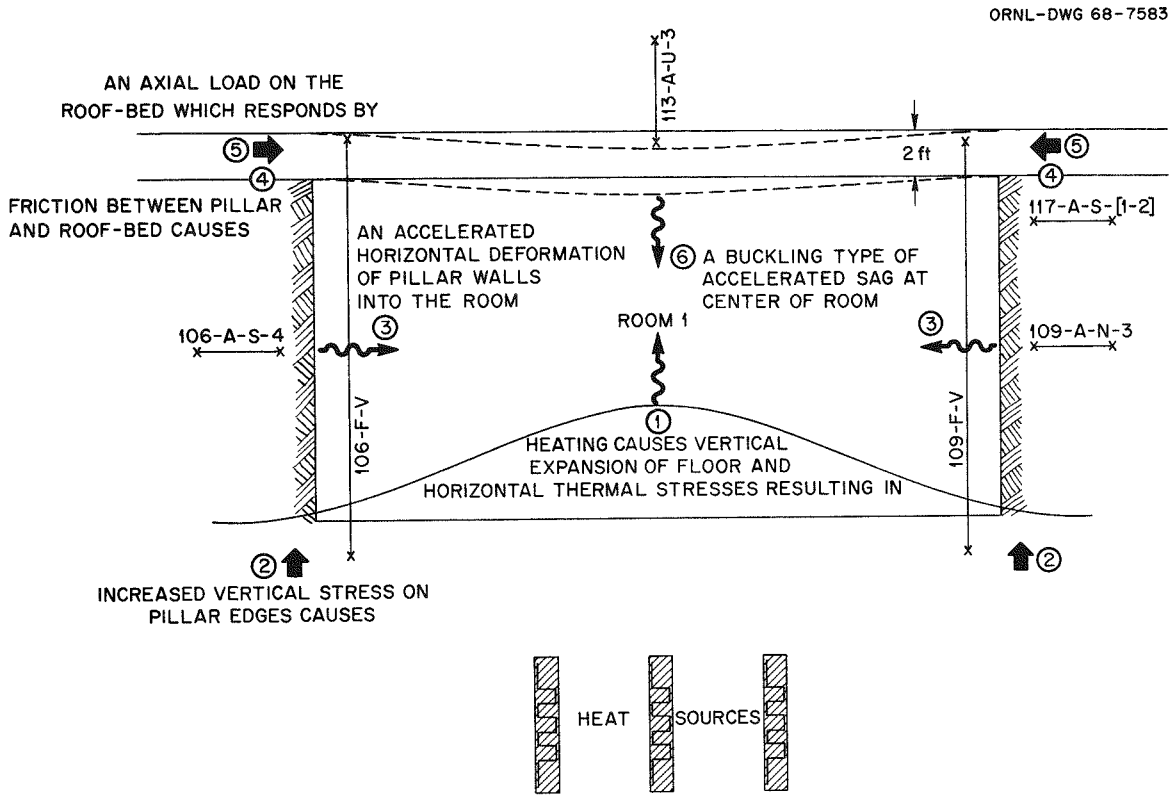


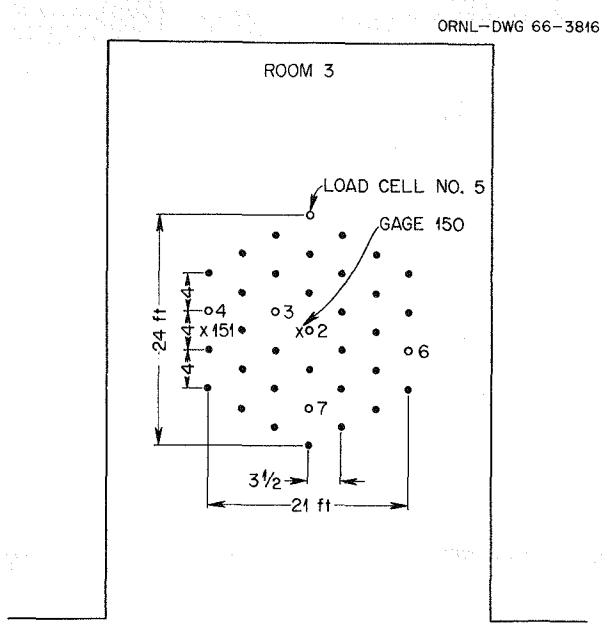
Fig. 11.68. Mechanism of Accelerated Roof Bed Sag.

shale to weather. The 4-ft spacing of bolts was based on a minimum estimate of the anchorage capacity which might be developed in salt by the expanding-shell–bail-type anchors (5 to 6 tons), which would support at least twice the actual dead weight of the sagging bed (when the entire area was bolted). This test pattern, which was considered to be the minimum for a valid test, was installed on March 8, 1966 (standard day 919), and the bolts were torqued to 175 ft-lb (see Table 11.5). This torque produced a load of about 8000 lb on each bolt, as predicted by standard pseudo torque-tension relationships[29] and confirmed by the roof bolt load cells. The bolts were then retorqued the following day to 190 ft-lb. It was felt that this procedure would allow the anchors to become properly seated in the salt before any attempts were made to develop their full anchorage capacity. The final load on the bolts of about 12,000 lb was nearly three times the dead weight of the 2-ft-thick roof bed over the area covered by the bolts. (This decreased to about 9000 lb over a period of about 30 days.) Gage results indicated that the roof in the test area was lifted by about 0.08 in., actually reducing the accumulated sag. The roof bolt test was observed for about a month, during which period it was seen that the roof bolts reduced the rate of sag to essentially zero and that more than sufficient anchor capacity was developed in the salt to enable the bolts to support the sagging bed (if the bolts are retorqued occasionally). As a result, a decision was made to roof bolt the entire experimental area using the same pattern and procedure.

The performance of these bolts was monitored throughout the course of the experiment on roof bolt load cells and on special short-wire roof-sag extensometer stations (see Sect. 11.4.1) located in the center of each room. The results are shown in Figs. 11.70 and 11.71. The sag gage results in rooms 2 and 3 reflect the initial lifting of the roof bed when the bolts were installed and a lesser amount of lifting on subsequent retorquings. After the roof slab had settled down following startup of the heated pillar experiment (on standard day 1170), the sag rate in both rooms was

[29] W. W. Callender, *Pseudotorque-Tension Relationships*, H. K. Porter Co., Inc., publication.

essentially zero, and the total sag accumulated since installation of the gages (standard day 541 for gage 132, standard day 578 for gage 150) was almost identical in both rooms, about 0.100 in. The load-cell data for the two rooms, computed as the average for the cells in a given room, also reflect the retorquings as steep spikes. The narrowness of these spikes is a function of the high modulus of the bolts; a small amount of upward deflection of the bed due to retorquing the bolts relieves a sizable portion of the load on the bolts because of their elasticity. Therefore, the load cell results without regard to the retorquing reflect the "equilibrium" load on the bolts fairly well. Notice especially the gradual increase in the load with time on the bolts in room 3. Since the yield strength of the bolts was supposed to be 22,000 lb, the indicated loads after about 1400 days appear abnormally high and are probably the result of some abnormality in the room 3 cell readings (see Sect. 11.4.1.8). The real load was more likely about 20,000 lb, as indicated from standard day 1520 to 1575. That the anchors are capable of developing even this amount of strength in salt is quite impressive. It is postulated that this amount of anchorage strength is a result of the retorquing procedure employed. If the bolts are tightened only when installed, the salt around the anchor shells will creep away from it, and subsequent load on the bolts will simply slip the anchor along the sides of the holes. However, if the bolts are retorqued several times as the salt creeps away from the expanded anchors, it will soon be opened to a size much larger than the drill hole, and the load-bearing capacity will be greatly increased. The results for rooms 1 and 4 (Fig. 11.71) indicate that although the roof bed was not lifted as much as in rooms 2 and 3, the rate of roof sag was reduced



BOLTS TO BE 4 ft LONG, HOLES TO BE NOT LESS THAN 4 ft−2 in. DEEP AND NOT MORE THAN 4 ft−6 in. (37 BOLTS IN ALL)

IF NECESSARY, MOVE THE LOCATION OF ANY INDIVIDUAL BOLT SO THAT IT COMES NO CLOSER THAN 1 ft TO ANY GAGE HOLE

DIAMETER OF HOLES TO BE DETERMINED BY ACTUAL BOLT AND ANCHOR USED

Fig. 11.69. Roof Bolt Test Pattern.

Table 11.5. Schedule of Roof Bolt Installation and Retorquing

Room No.	Date Installation Started	Date Installation Finished	Amount of Torque (ft-lb)	Date Retorqued	Amount of Torque (ft-lb)	Comments
3	3/8/66	3/8/66	175	3/9/66	190–200	First 37 bolts
				3/19/66	190–200	
3	5/13/66	5/13/66	190–200			Remainder of bolts
1	5/19/66	5/24/66	190–200	5/25/66	125–130	Loosened, greased, and retorqued
				12/5/66	150	
Waste shaft room	5/27/66	6/1/66	125–130	11/18/66	150	Greased head at installation
4	6/2/66	6/2/66	125–130	6/7/66	125–130	Greased head at installation; 19 bolts in center of room
	6/7/66	6/7/66	125–130	7/18/66	150	Installed remainder, retorqued all
2	6/21/66	6/21/66	125–130	7/19/66	150	Greased head at installation
				11/11/66	150	
Corridor	6/23/66	7/11/66	125–130	9/19–21/66	125–130	Greased head at installation
				10/6–7/66	150	
				10/13–14/66		
Ramp	7/11/66	7/15/66	125–130	11/22/66	150	Greased head at installation

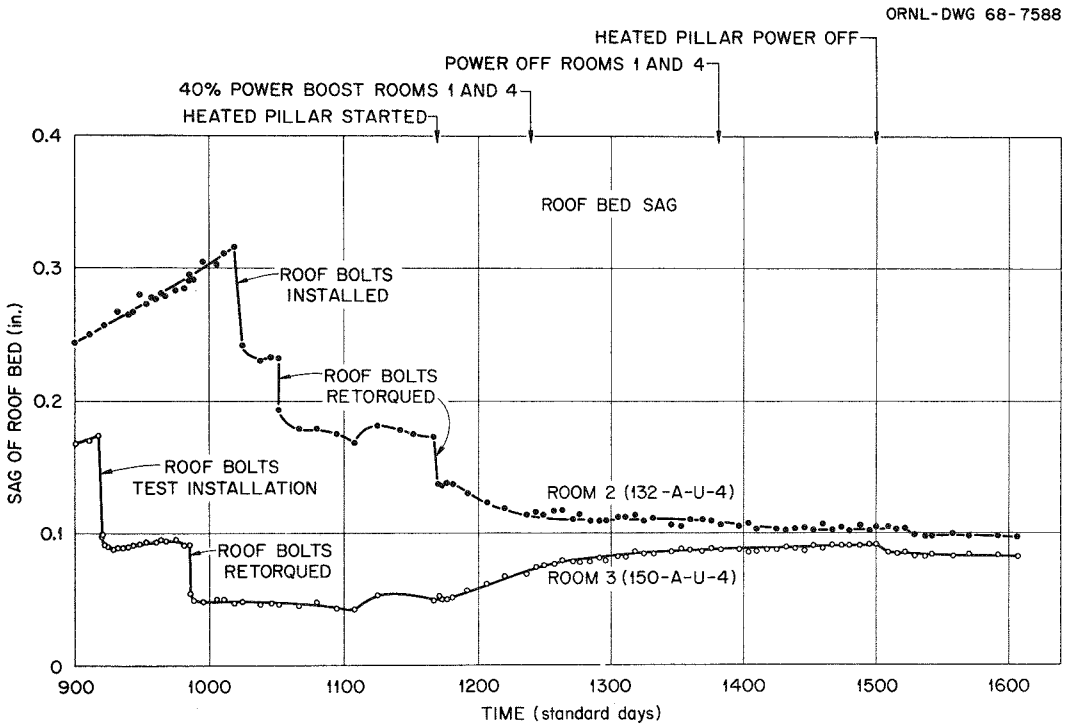


Fig. 11.70*a*. Roof Bolt Results – Rooms 2 and 3. Roof bed sag.

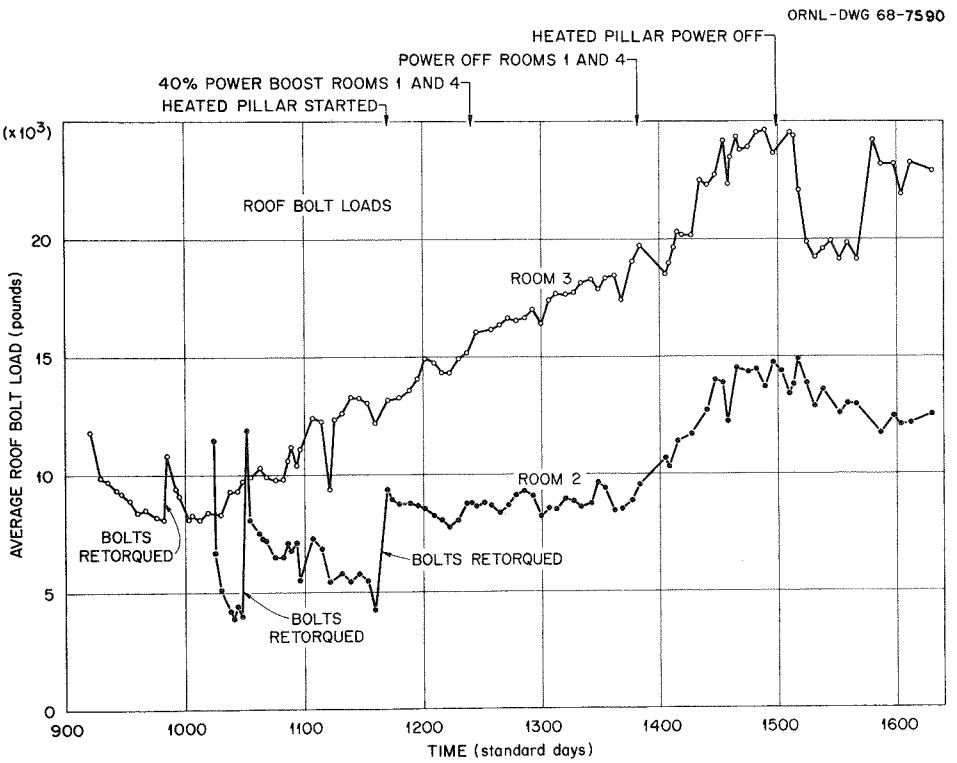


Fig. 11.70*b*. Roof Bolt Results – Rooms 2 and 3. Roof bolt loads.

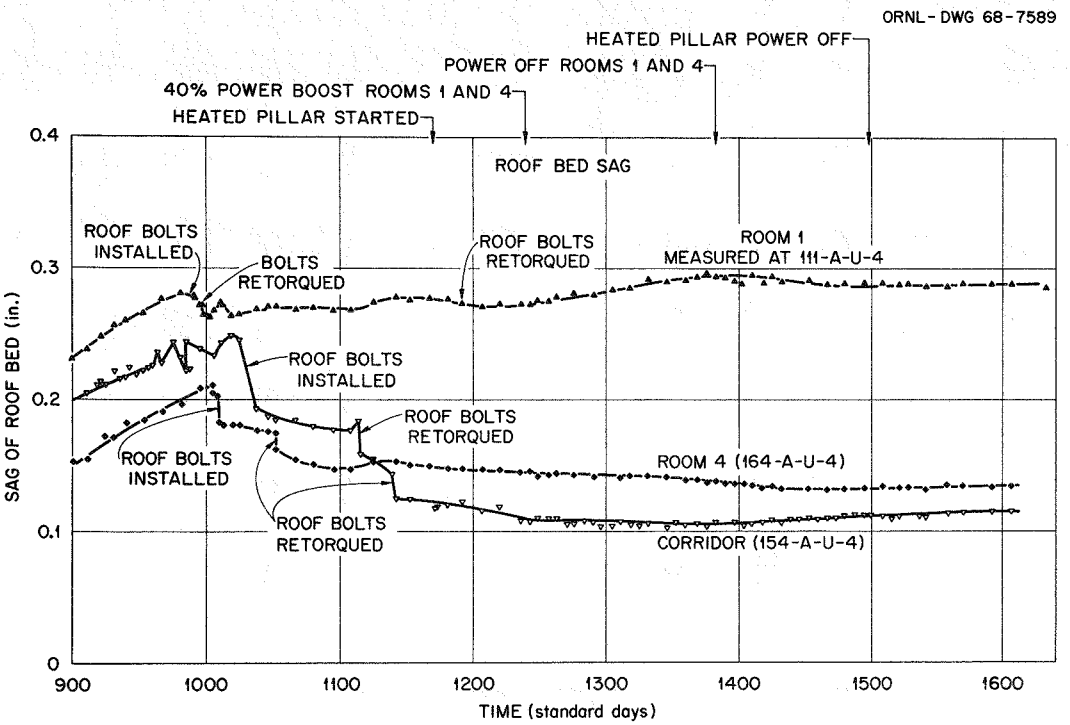


Fig. 11.71*a*. Roof Bolt Results – Rooms 1 and 4 and Corridor. Roof bed sag.

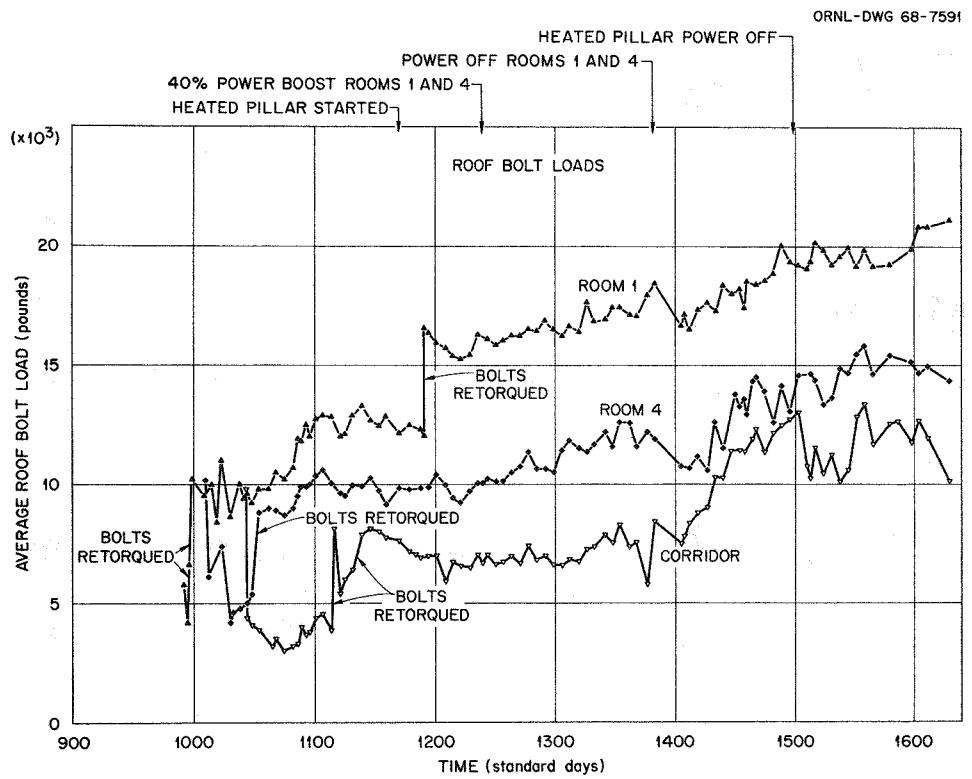


Fig. 11.71*b*. Roof Bolt Results – Rooms 1 and 4 and Corridor. Roof bolt loads.

essentially to zero for the entire period of the experiment. Results for the roof bolts in the corridor are similar to those for rooms 2 and 3. The gradual increase in load on the bolts, as measured by the load cells throughout the experimental area, suggests that the roof bed was "trying" to sag into the rooms but was prevented from doing so by the bolts. Furthermore, the driving force behind that sag must have been something more than the mere dead weight of the beam, since that alone should have produced a constant load on the bolts; that is, the sag throughout the experimental area should have been accelerated by the buckling deflection resulting from the axial loads had the roof bolts not been there to support and restrain the bed. Data for more than a year beyond the period shown in Figs. 11.70 and 11.71 indicate that the roof-bed sag rates in all four rooms and the corridor were essentially zero. The indicated average bolt loads had dropped about 3000 to 4000 lb, except in room 3, where the average was still nearly 25,000 lb.

11.4.5.7 Summary. – The various deformations occurring around the array rooms 1 and 4 and their adjacent pillars, which are considered individually in previous sections, can be combined to show the movements which took place in the vertical north-south plane through the array centers during the heating period. (For convenience, standard days 805 to 1380 are used.) These summary plots are shown in Figs. 11.72 and 11.73. Significant features of these deformations are:

1. Total deformations are primarily the result of creep of the salt under the influence of overburden and thermal stresses.
2. Deformation resulting from alteration of the physical properties of salt (especially creep rate) due to elevated temperatures for the most part was not seen around the array rooms because of the location of the heat sources. Significant portions of structural, load-bearing salt were not heated fast enough or high enough to produce an observable effect.
3. Effects of the transfer of stresses resulting from thermal expansion of salt in the floor around the array heaters were unexpectedly widespread. Accelerated deformation rates resulting from this increased stress were observed at points 25 ft into the floor and roof and on the walls of pillars in the adjacent rooms.

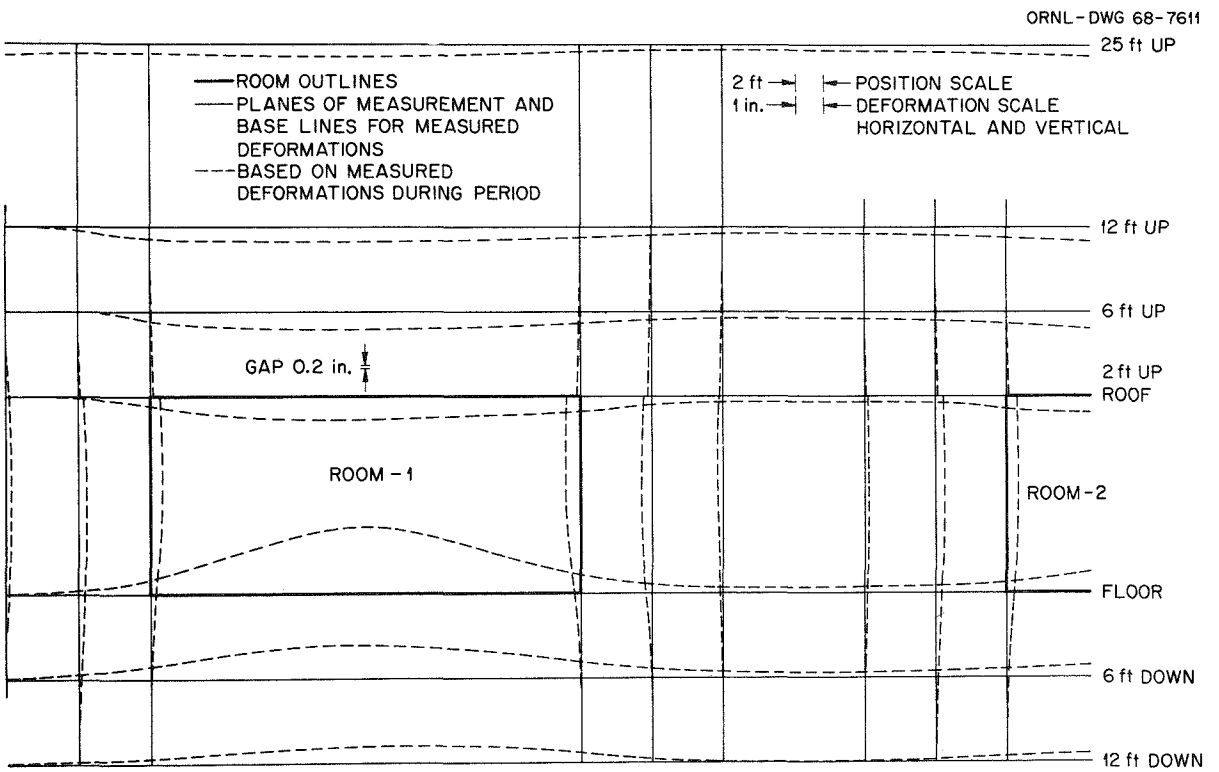


Fig. 11.72. Summary of Deformations Around Room 1.

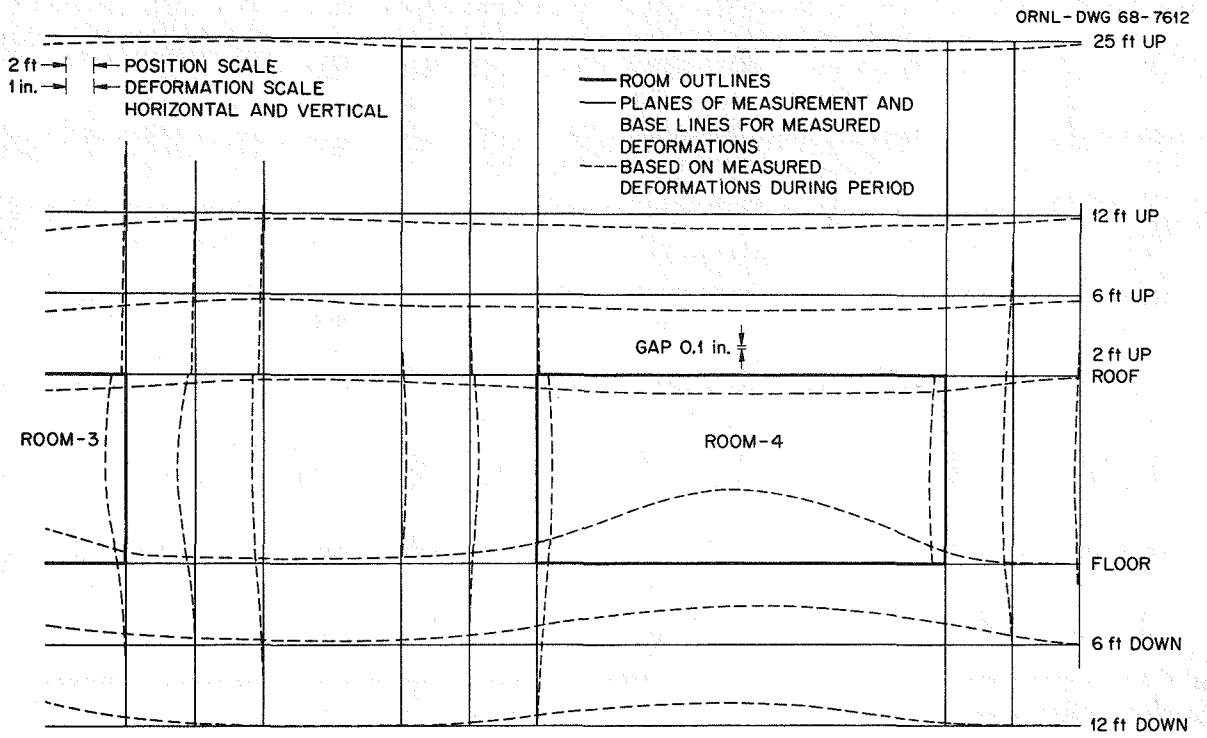


Fig. 11.73. Summary of Deformations Around Room 4.

4. This same mechanism, aided by a buckling-type deflection, was responsible for a drastic acceleration in the sag of the immediate roof over the array.
5. The roof bolt experiment and subsequent installation probably produced more important and useful results than were lost by restricting deformation of the roof.
6. The deformations were so similar in rooms 1 and 4 that it can be stated categorically that there was no significant structural effect produced in the salt by the intense radiation field. Similarities between the two rooms were greater than expected because of the counteracting effects of slight differences in age and geometry.

11.4.6 Movements Induced by Room 5 Experiment

As discussed earlier, the objective of the experiment carried out in room 5 of the existing mine was to investigate the possibility of using previously mined space for disposal rather than newly mined space. The principal differences between room 5 and room 1 (or room 4) were the much larger quantity of shale in the floor within the heated zone, the height of the room, the somewhat different room size, and the absence of significant shale partings in the immediate roof. This section of the report presents the rock mechanics results obtained in the room 5 area and compares them with the results obtained in room 1.

The experiment in room 5 was started on June 6, 1966 (standard day 1009), approximately six months after the start of room 1 and room 4 experiments. Thereafter, significant events occurred more or less simultaneously. Floor insulation in all three rooms was installed (standard day 1117) and removed (standard day 1223) at the same time. The 40% power boost took place on January 23, 1967 (standard day 1240) for all three experiments, and the heater power was turned off on June 5, 1967 (standard day 1373) in room 5, only one week prior to shutdown in rooms 1 and 4. The duration of the heating part of the experiment in room 5, therefore, was only one year as opposed to approximately 19 months in the experimental area. Because of the difference in stratigraphic elevations of room 5 and the experimental area, there was no sagging roof bed in room 5, and, therefore, roof bolts were not installed even though the ceiling height was several feet higher (see Sect. 5.1).

As was the case for rooms 1 and 4, there were no usable hole closure data obtained from room 5. In fact, measurements were even more difficult in room 5 because shale beds in the floor became very soft and friable when dried by the heat. The conclusions from these data are the same as those from rooms 1 and 4; that is, some hole closures did occur, which were monitored during the experiment as a precaution against sealing the liners into the hole, but these closures could not be measured accurately enough to provide salt flow data.

11.4.6.1 Floor Lift. – Floor lift profiles in the east-west and north-south directions through the center of the room 5 array are shown in Fig. 11.74. Since orientation of the room and the layout of the array holes is rotated 90° with respect to the arrays in rooms 1 and 4, the profiles should be compared with their opposite counterparts. (That is, east-west in room 5 is comparable with north-south in rooms 1 and 4.) The maximum total uplift in room 5 was somewhat less than in the experimental area, primarily because the total heat input was about one-third less in the shorter operating period. However, for a given elapsed time, the uplift in room 5 was slightly greater than that in rooms 1 and 4. This may be due to the presence of considerable quantities of shale in the floor of room 5, causing the temperatures to be slightly higher. The floor uplift profiles show a nearly circular deformation extended slightly toward the entrance to the room (to the north). Since the center of the array in room 5 was approximately equidistant from all three pillar edges, this was to be expected and also served to confirm the restraining influence of pillars as discussed in Sect. 11.4.5.2.

For equivalent time periods, the time-uplift plot (Fig. 11.75) of selected points in room 5 shows a slightly greater uplift than those in the experimental area. Recovery of the floor uplift after the heaters were turned off is slightly greater (17.1%) in room 5 than in the other rooms. This difference is probably not significant, but it may be because more of the thermal expansion in shale is recoverable than in pure salt.

11.4.6.2 Convergence. – Vertical convergence as a function of time measured on the pipe-type gages (type F) at the edges of the pillars around room 5 is shown in Fig. 11.76. As can be seen, the rate of convergence prior to heating was very small – almost zero. This is a consequence of the stability which the area had attained since it was mined some 30 years ago. If the amount of convergence resulting only from the heating in rooms 1 and 4 (Fig. 11.60) is calculated by subtracting the extrapolated preheating convergence

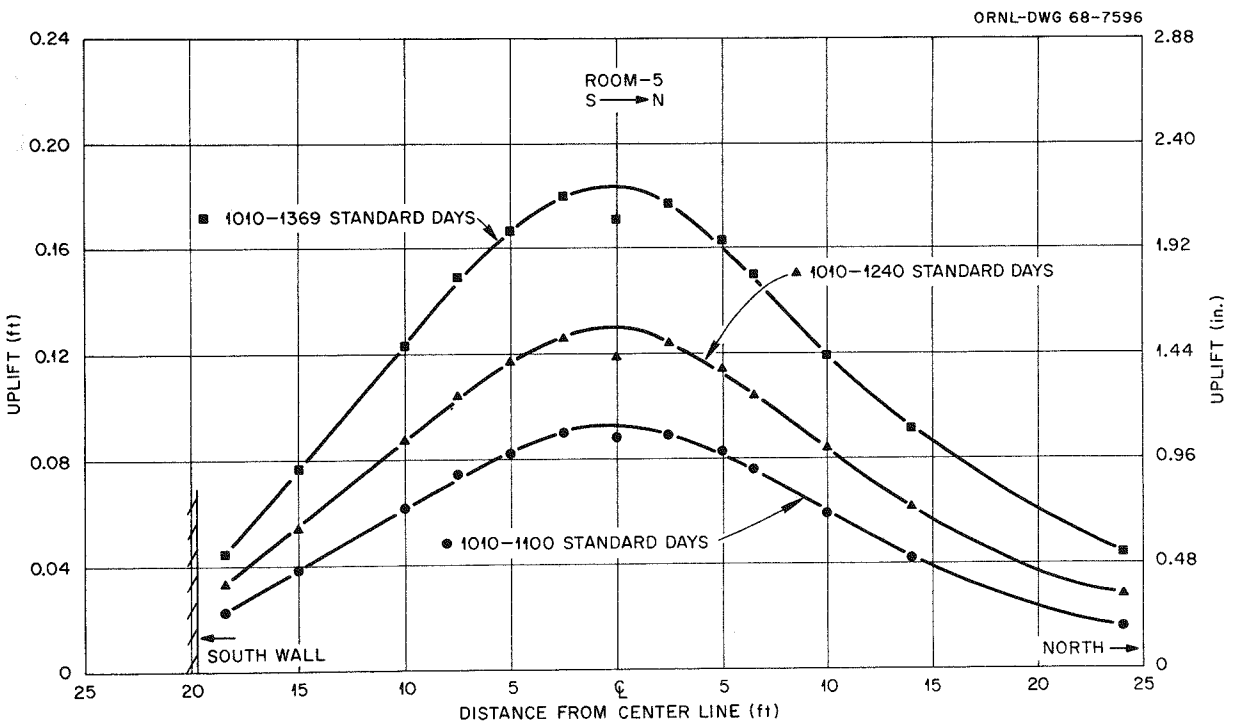


Fig. 11.74*a*. Floor Uplift Profiles at Selected Times – Room 5. North-south.

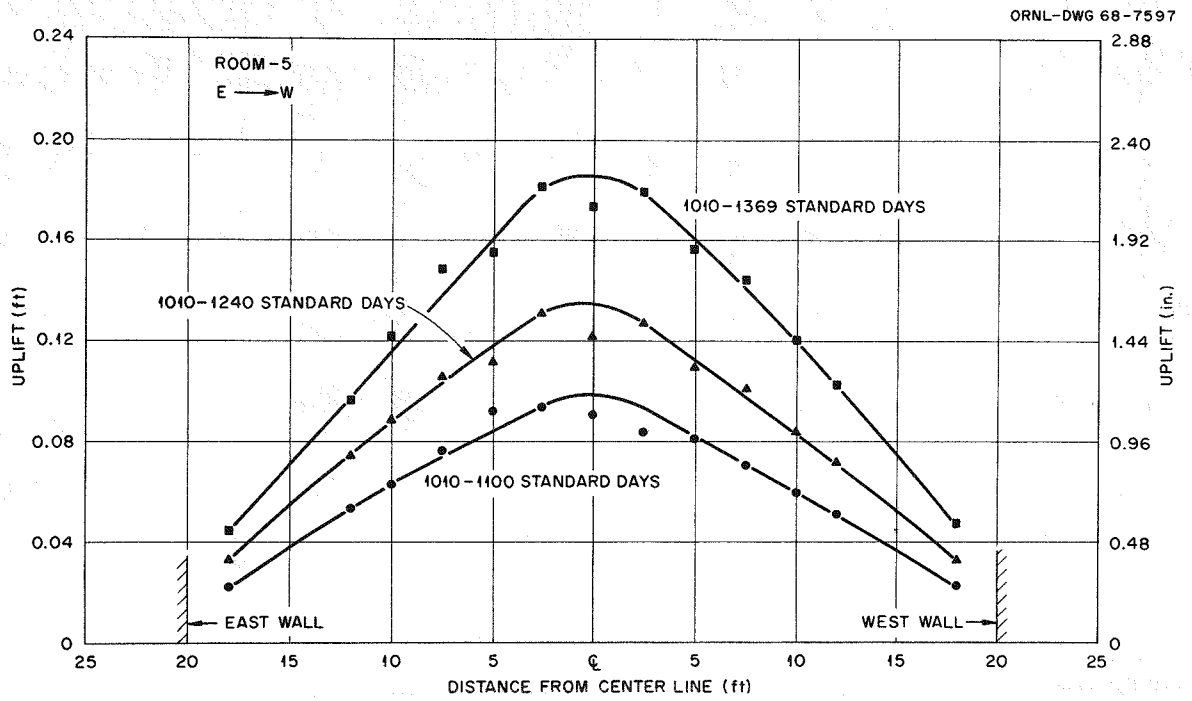


Fig. 11.74*b*. Floor Uplift Profiles at Selected Times – Room 5. East-west.

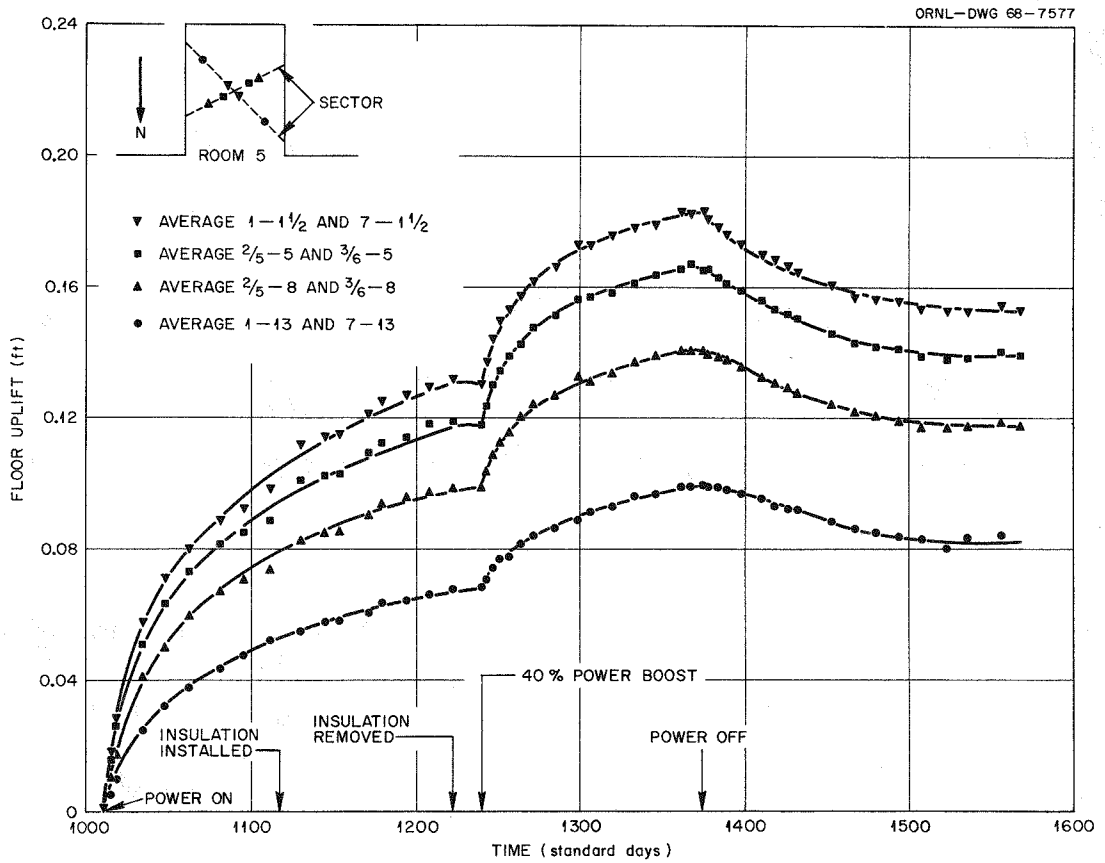


Fig. 11.75. Floor Uplift as a Function of Time – Room 5.

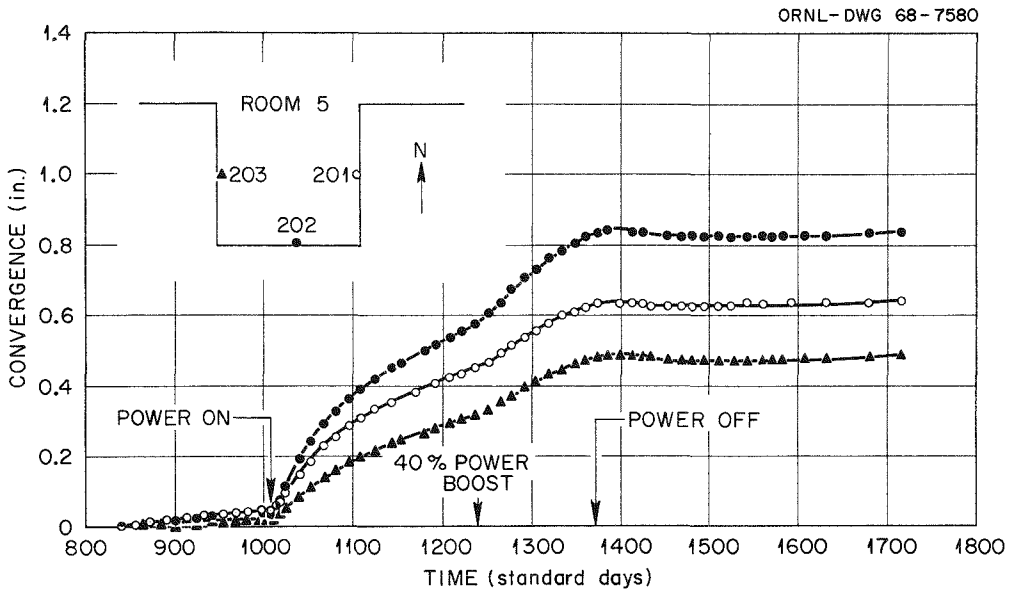


Fig. 11.76. Vertical Convergence as a Function of Time (Pipe-Type Gages) – Room 5.

from the total, it is found that the convergence is very nearly the same as in room 5. This is rather amazing, considering the difference in geometry of the two areas, and it may be more fortuitous than significant.

The ranking of convergence gages in room 5 (202 > 201 > 203) is not what would be expected from considerations of geometry and floor uplift alone. The heater array in room 5 was centered in the almost perfectly square room. Therefore, the direct effect of heating, actually the amount of floor uplift occurring at the edges of the pillars (since a portion of this is included in the convergence measurements), should be about the same at all three stations. Based on thicknesses of the pillars and the extent of excavation beyond them, it would seem that the largest convergence should have been measured on gage 201, followed by gage 202, then gage 203. The reason for the anomalous behavior is not known at the present time but is probably related to some local perturbation in the geological situation.

Notice that the convergence rate after the heaters were turned off returned to the preheating rate by about 1600 standard days. Since the rate of convergence prior to heating was very small, this implies that the rate of recovery of thermal expansion for the flat portion of the curves (from about 1450 to 1600 days) is almost exactly the same as the thermal stress convergence rate prevailing at that time.

11.4.6.3 Pillar Deformation. – Horizontal deformation of the pillars as a function of time on the three sides of room 5 is shown in Fig. 11.77. These curves represent the same type of deformations shown in Figs. 11.62 and 11.63 for rooms 1 and 4, respectively, and are generally comparable with those figures. The accelerated rate of deformation occurring in response to the heat beginning on standard day 1009 and the increase in power beginning on standard day 1240 can be seen. Also, these heat-induced deformations occurred on both sides of these pillars. The deformations are quite similar in shape to their counterparts in rooms 1 and 4 but generally much smaller. This is probably a result of both the difference in geometry and the added stability in room 5 due to its age. (The break in the curve for gage 202-S-1 at about 1370 days coincides with power shutdown, but the reason is not understood.)

11.4.6.4 Deformations in Roof and Floor. – Vertical deformations of points into the roof and floor as a function of time and relative to a fixed elevation are shown in Fig. 11.78. These plots are equivalent to Figs. 11.65 and 11.66, which show the same information for rooms 1 and 4. Uplift of the "floor" point is equivalent to the curves shown in Fig. 11.75. For the wires anchored deeper in the floor at depths of 6, 12½, and 25 ft), the immediate response to heating is almost identical to that in rooms 1 and 4. The behavior of the roof, however, is markedly different. First, the total amount of roof lowering, including that at a height of 25 ft above the ceiling, is considerably less than in the experimental area. The overall lowering of the roof mass results from the effective shortening of pillars by

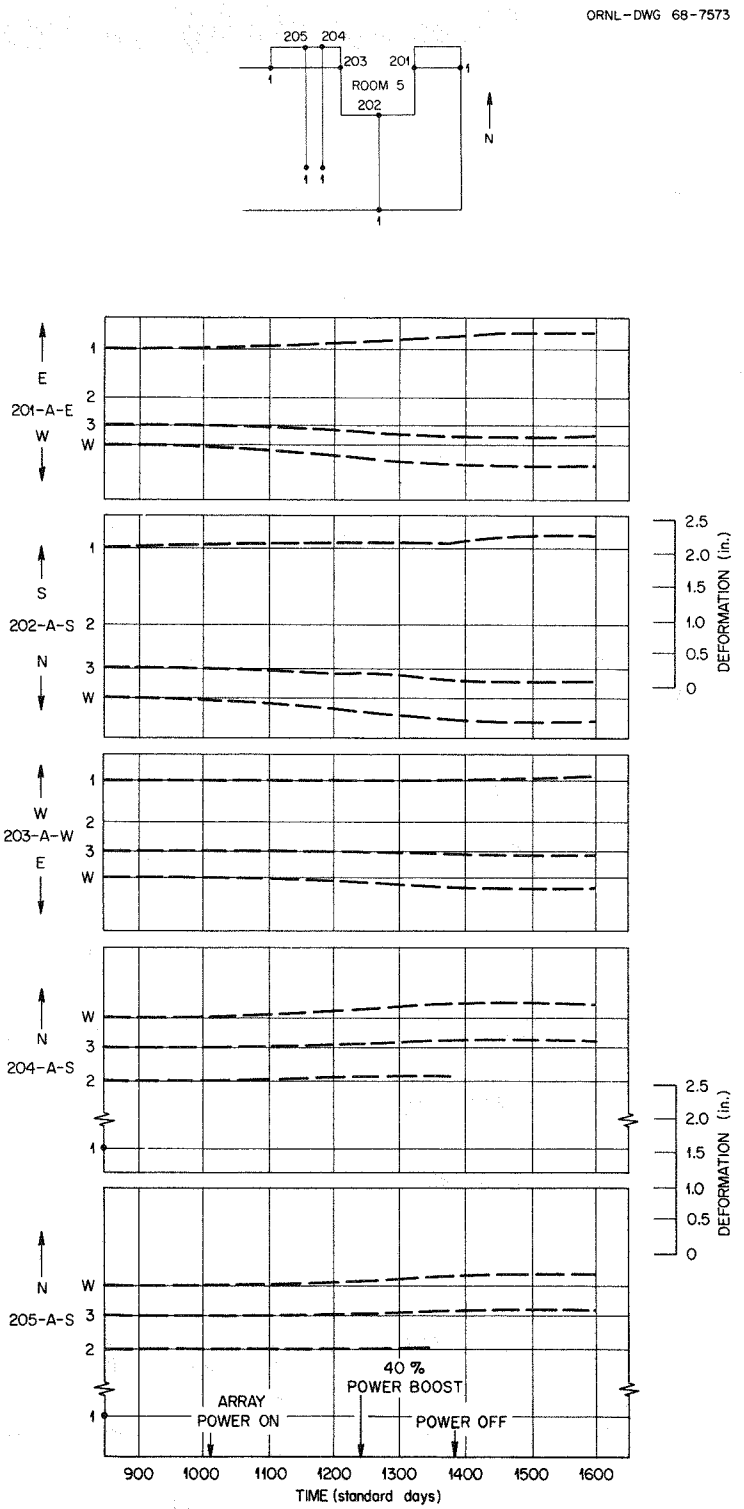


Fig. 11.77. Horizontal Deformation as a Function of Time for Gages Around Room 5.

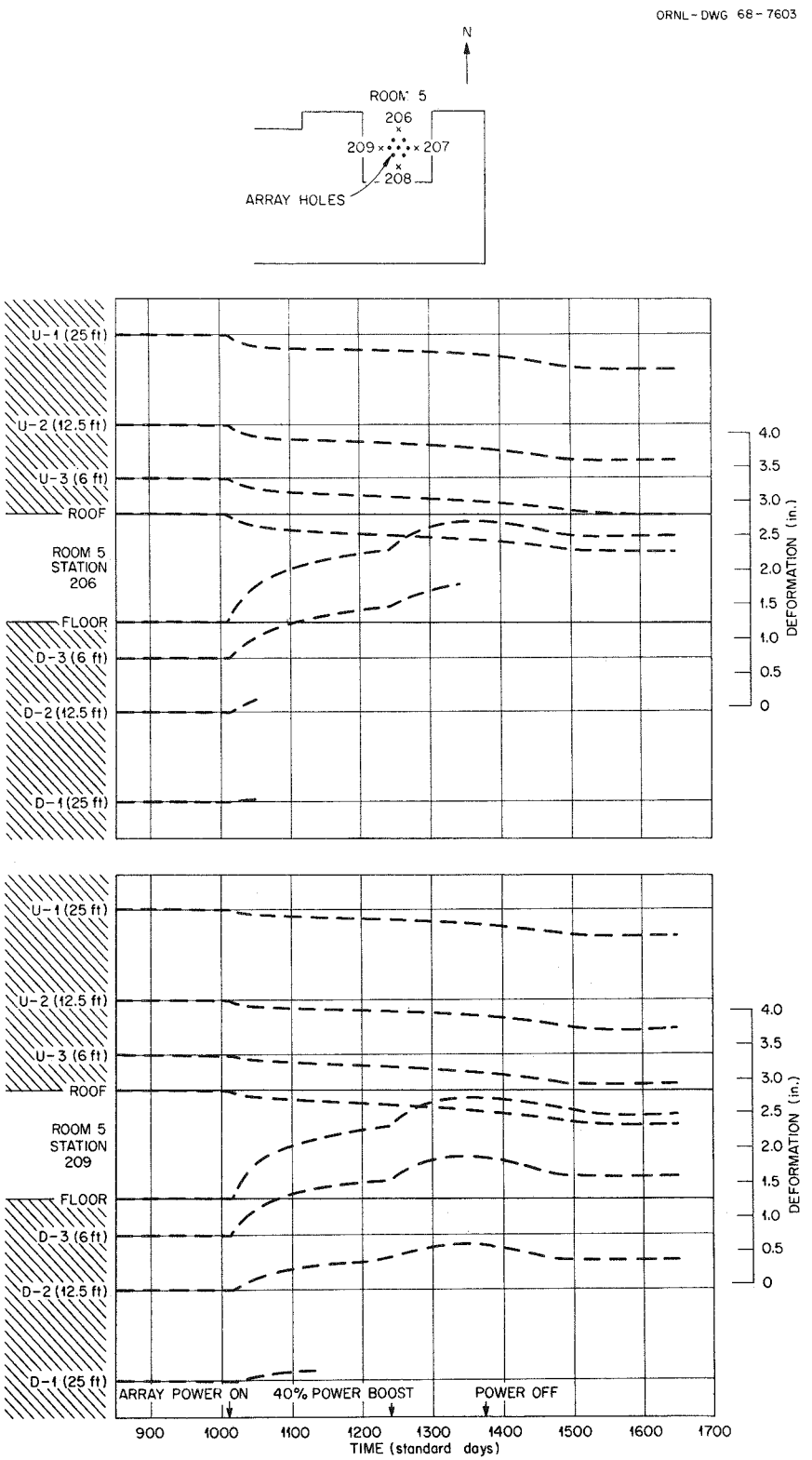


Fig. 11.78. Vertical Deformation as a Function of Time – Room 5 (Gages 206 and 209).

the normal overburden plus the accelerating effect of heating. This shortening is less in room 5 than in the experimental area, primarily because of the much smaller normal rate of closure due to overburden loading and time since excavation.

Perhaps the most significant aspect of the results seen in Fig. 11.78 is that the deformation of all points in the roof is very nearly the same, decreasing only slightly with increased height. This means that the entire roof over this area behaves as a continuous mass and that there has been no separation of relatively thin roof beds as there was in the experimental area. Inspection of the detailed stratigraphy at this horizon (Sect. 5.1) indicates that there are no significant shale partings in this roof along which a bed separation could occur up to a height of 10 ft.

11.4.6.5 Summary. – The deformations which took place around room 5 during the heating portion of that experiment (standard days 1009–1373) are summarized in Fig. 11.79. These deformations are shown on a vertical plane through the center of the heater array in the east-west direction. Because of the 90° rotation in the layout of room 5, Fig. 11.79 is exactly equivalent to Figs. 11.72 and 11.73, which show the same information for rooms 1 and 4. Two major conclusions can be drawn from the rock mechanics results obtained from the room 5 experiment:

1. With one exception (noted in item 2 below), deformations occurring around the heated array in the floor of the existing mine are of the same type and are even quantitatively similar to the deformations around the arrays in the experimental area. Some slight differences due to geometry and, more importantly, from differences in creep rates acquired with age were found.
2. Because of the approximately 15-ft difference in stratigraphic elevation between the experimental area and the existing mine, the roof in room 5 did not contain thin shale partings and, consequently, did not separate and sag into the room. Therefore, from this point of view, the existing mine space would be preferable to newly mined space if the floor did not contain shale layers. However, room 5 was the last room in the entry and thus was probably not typical of the behavior which might be expected in most of the old mine rooms.

11.4.7 Movements Induced by Heated Pillar Experiment

The heated pillar experiment took place in rooms 2 and 3 of the experimental area and around the rib pillar separating those rooms. This pillar is 20 ft wide (nominal), and the two adjacent rooms are 44 ft wide

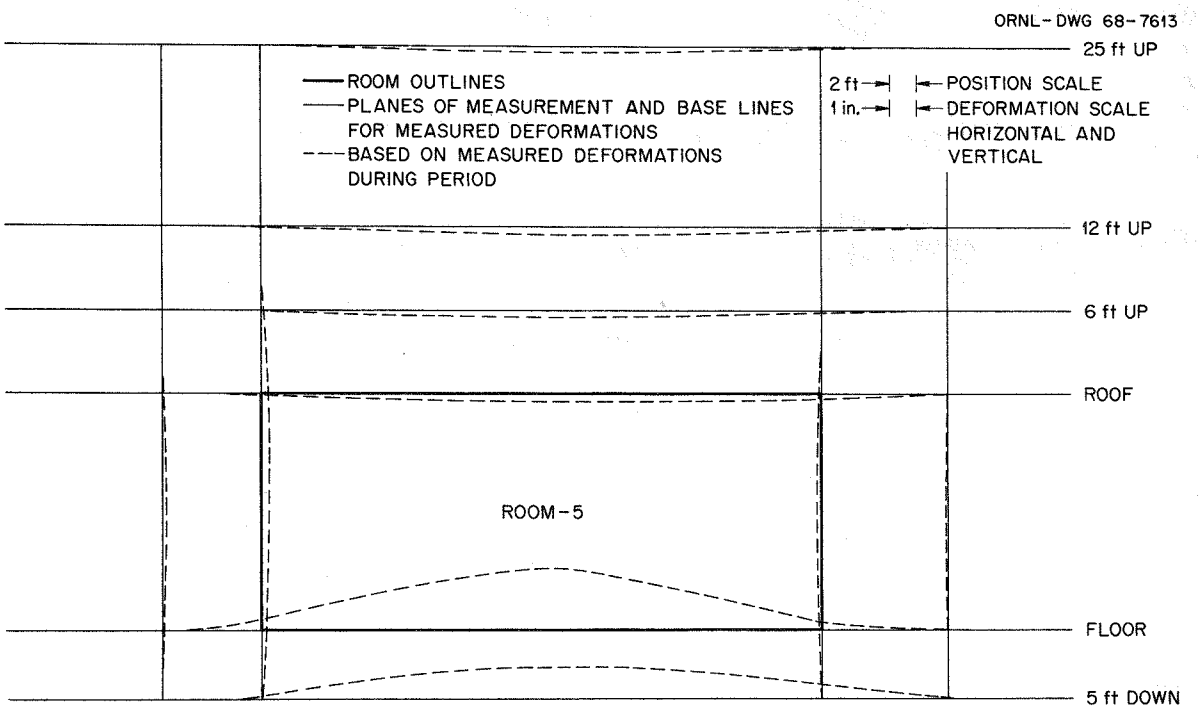


Fig. 11.79. Summary of Deformations Around Room 5.

(see Fig. 11.42). The objective of this experiment was to obtain data on the behavior and properties of a large mass of salt in the floor and beneath a pillar heated to a higher temperature than was possible in the array experiments. Eleven heaters were placed in the floor along each side of this pillar, and a total of 33 kW was applied continuously for a period of nearly a year. The temperature results, which are presented in Sect. 11.3, indicate the extent of the heated zone and its temperature.

The significant dates of the heated pillar experiment were: June 22, 1966 (standard day 1025), when the center heater only (a "modified" pillar heater) in room 2 was turned on (primarily as a materials test); November 14, 1966 (standard day 1170), when all of the pillar heaters were turned on at the "start" of the experiment; and October 9, 1967 (standard day 1499), when the heaters were turned off.

It is necessary here to digress briefly for a discussion of the effect which the thermal expansion of gage wires has on the measurements. This point was passed over in the previous discussion because, with one exception, the gages were installed at locations which did not experience an appreciable temperature rise. That exception was the four vertical holes in the floor at 10 ft from the center of the arrays in rooms 1, 4, and 5. A number of the wires at these stations were broken due to corrosion at various times after the experiment was initiated, and the results were not generally used for quantitative analysis. Therefore, prior to this point it was not necessary to consider thermal expansion of the wires. However, in the heated pillar experiment some of the gage wires were located in areas where the temperature rise was appreciable.

Comparison of Figs. 11.14, 11.26, and 11.27, which illustrate the maximum temperature profiles in the center pillar, and Fig. 11.42, which shows the gage locations, suggests that horizontal internal strain gage 126 should have experienced the highest temperatures. The longest wire at this station was 20 ft, and the maximum temperature, averaged along the borehole, should have been about 50°C (a temperature rise of 27°C). Using a coefficient of linear thermal expansion of stainless steel of $18 \times 10^{-6}/°C$ gives a total change in length of 0.1166 in. Figure 11.83 shows that the deformation at this station during heating amounted to about 2.3 in. Therefore, thermal expansion of the wire results in a 5% error for this severely affected station. Furthermore, expansion of the wire will always be in a direction such that the observed rock deformation is less than the actual deformation. Since the effect of thermal expansion of the wires introduces an error which is never more than 5% and is always in a direction such that the true rock deformation is underestimated, it was decided that this effect could be neglected in interpretation of the results presented in this section.

11.4.7.1 Floor Lift. – Floor lift profiles in the north-south direction at three positions across the heated pillar and both of the adjacent rooms are shown in Fig. 11.80. The three curves on each figure represent the uplift on standard day 1167 (three days before initiation of the experiment), standard day 1240 (approximately two months after the start of the experiment), and standard day 1501 (maximum). The base line in all cases was standard day 1020.

The floor uplift curves in every case show there was more deformation in room 3 than in room 2. This difference was the result of a "floor heave" on the room 3 side of the pillar which did not occur in room 2. A floor heave is distinguished from pure thermal expansion of the floor by its mechanism – a mechanism similar to the roof sag discussed in Sect. 11.4.5.5. A bed of salt, in this case about 5 ft thick, had separated from the underlying material and was buckling upward into the room under the influence of axial (horizontal) stresses on it. The resulting gap was confirmed by drilling into the floor in room 3.

This incident also provides a good illustration of the degree of control offered by the rock mechanics instruments. All of the rock deformation results were plotted and examined continuously during the experiment. Shortly after the start of the heated pillar experiment, preliminary interpretation of these data indicated that there must have been a floor heave in room 3, and instructions were sent to the mine to find its depth by test drilling. A few such holes were drilled to depths of 2 to 3 ft, which is usually the maximum depth for floor heaving and buckling. These holes found nothing. Reexamination of the data confirmed that there must be a floor heave and separation amounting to approximately ¼ in. The test holes were therefore deepened, and the gap was found about 5 ft below the floor.

The pattern of floor uplift seen in Fig. 11.80 also illustrates the restraining influence of the pillar. Although the heaters were located 2 ft from the edge of the pillar and maximum temperatures occurred at that point, the point of maximum floor uplift is 7 to 10 ft from the edge of the pillar.

Displacement of the maximum floor uplift from the maximum temperature was a direct consequence of the vertical restraint supplied by the pillar. Salt under the pillar was prevented from expanding upward by the

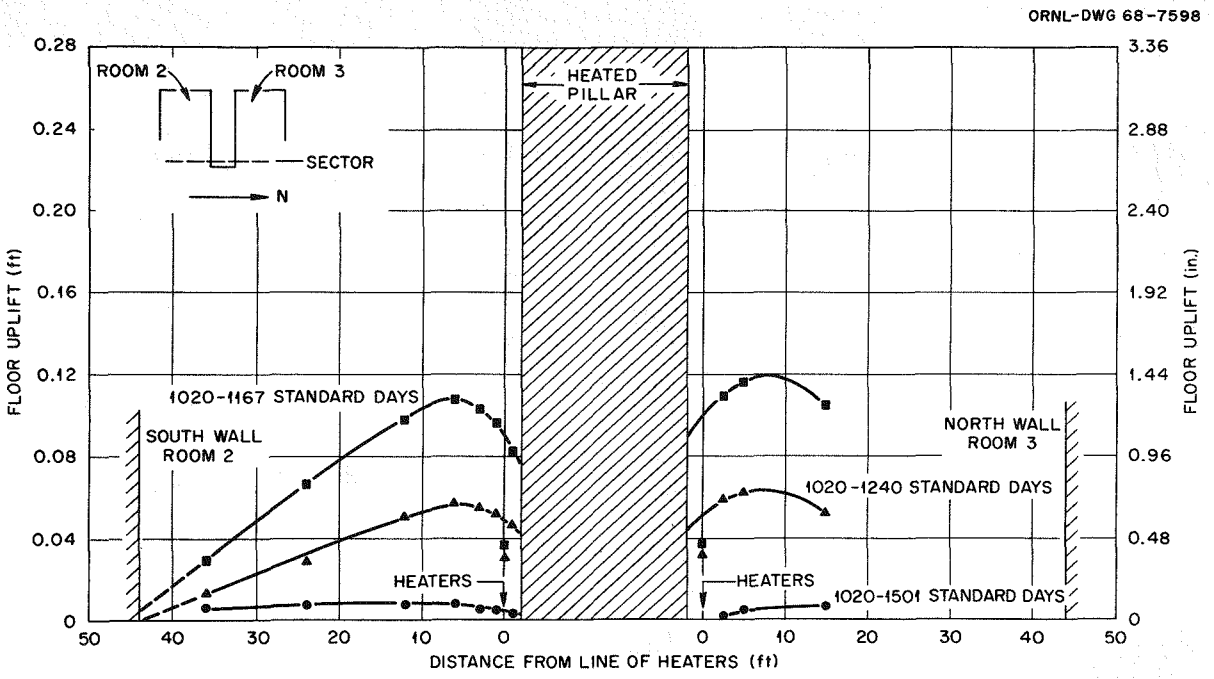


Fig. 11.80*a*. Floor Uplift Profiles, Rooms 2 and 3, Across the Heated Pillar. Front of pillar.

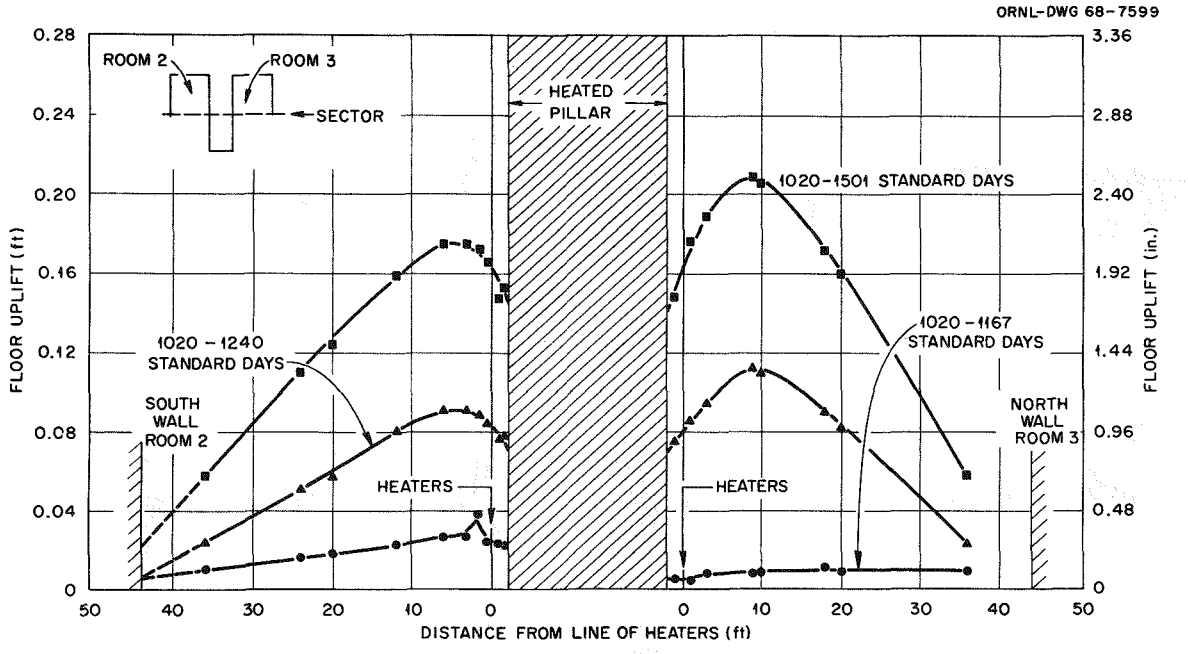


Fig. 11.80*b*. Floor Uplift Profiles, Rooms 2 and 3, Across the Heated Pillar. Middle of pillar.

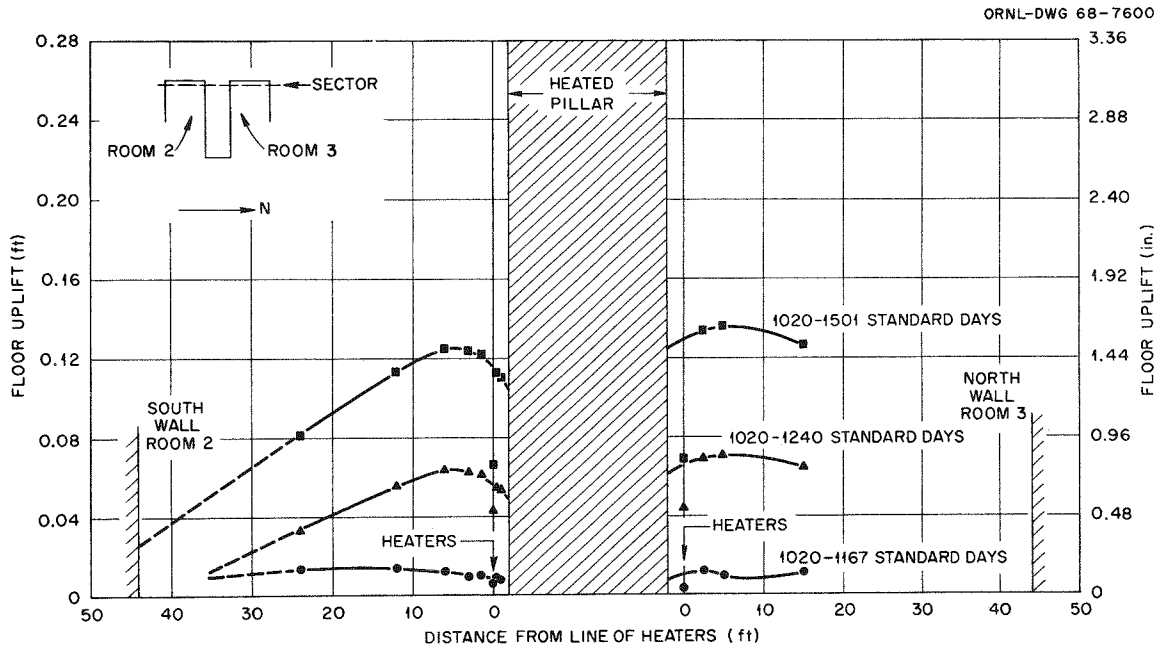


Fig. 11.80c. Floor Uplift Profiles, Rooms 2 and 3, Across the Heated Pillar. Back of pillar.

vertical stress already existing at that point. Note that this effect occurs in spite of the fact that the temperature of the salt is higher under the pillar than at an equal distance from the heaters in the room (see Fig. 11.14). The temperature is higher under the pillar because of both the interaction of the heaters on the two sides of the pillars and the heat loss to the air in the rooms. Based on this examination of floor lift profiles, a very complex situation must have developed under and in this heated pillar. The thermal stresses, which produced most of the motion around rooms 1 and 4, were much higher and more concentrated around this pillar, because there was less room for expansion. Furthermore, a large portion of this pillar was eventually (but not immediately) heated to a temperature high enough to significantly affect its creep properties.

11.4.7.2 Convergence. – Vertical deformation of the heated pillar as a function of time as measured at seven convergence stations (pipe-type gages except for gage 125) around the pillar is shown in Fig. 11.81. The most obvious feature of this deformation is the very rapid acceleration when heat was applied on standard day 1170. It should be noted that this accelerated convergence includes a component resulting from uplift of the floor.

The effect of the modified pillar heater, which was installed adjacent to gage 125 and turned on standard day 1025, can be easily seen on the convergence at that gage. This deformation is probably largely floor uplift due to thermal expansion. However, the effect of this single heater, operating at a power level of 3 kW, can also be seen at all other convergence stations around the pillar as a slight upturning of the convergence-time curves for the period from standard day 1025 to standard day 1170. This implies that the operation of one heater alone disturbed the stress in the pillar sufficiently to accelerate the deformation of the entire pillar, albeit only slightly.

Before comparing the rates of movement at these gages, mention should be made of the strange behavior of gage 128 between days 1320 and 1380. The "wrinkle" in the convergence curve here is due to the effect of a slab of salt on the side of the pillar and its removal (in the interest of safety) which physically disturbed the gage. The wrinkle in the curve could have been removed by interpolating between the data at both ends of the disturbance period, since the reason for it was known, but it was left in to provide an added touch of realism and to illustrate the type of behavior which could take place in some instances for reasons unknown.

The average convergence rates for these seven gages are shown in Table 11.6 for the periods of (1) no heating (standard days 900 to 1000), (2) full heating

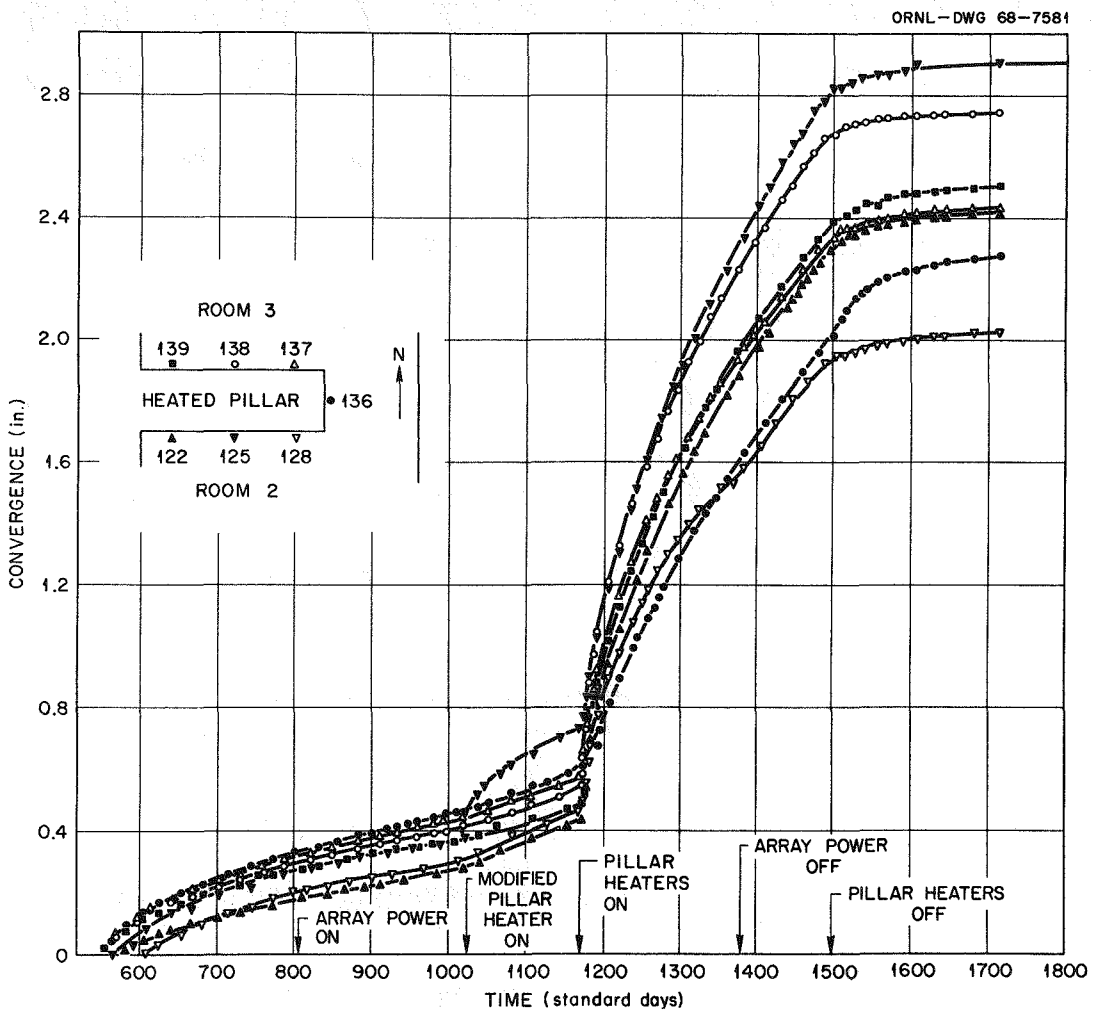


Fig. 11.81. Vertical Deformation (Convergence) of Heated Pillar as a Function of Time.

power (standard days 1180 to 1280), and (3) after 60 days of cooling (standard days 1560 to 1660). Prior to heating, that is, for the period between standard days 900 and 1000, the gages indicate their expected order in rates of convergence: The gages in room 3 are slightly higher than their counterparts in room 2, because room 3 was excavated at a later date, and the rate of convergence increases from the back of the room toward the corridor, reflecting the increased loading on the open end of the rib pillar. For the heating period (standard days 1180 to 1280) the highest convergence rate occurs at the center section of the pillar, since this is the hottest area. The lowest convergence rate during heating is seen at the open end of the pillar (gage 136), because there was a smaller floor lift component in the convergence at this point than at all other points. After the heaters had been off for about 60 days (standard days 1560 to 1660), all the convergence rates except at

Table 11.6. Average Convergence Rates Around the Heated Pillar

Gage No.	Convergence Rate (10^{-4} in./day)		
	Standard Days 900 to 1000	Standard Days 1180 to 1280	Standard Days 1560 to 1660
122	4.2	74.5	3.0
139	4.3	85.0	3.5
125	4.3	92.5	3.5
138	5.1	91.0	2.0
128	5.0	59.5	3.6
137	5.9	79.0	2.6
136	6.0	57.3	6.3

gage 136 were reduced to values below the preheat rates. In the interpretation of these data, the total convergence rate is visualized as being made up of three parts: (1) the convergence rate due to overburden load on the pillar, which occurred along the continuation of the curves prior to standard day 1025, (2) the component resulting from a change in physical properties (for example, increased plasticity) of the salt due to elevated temperatures, and (3) the component resulting from thermal stresses, a small fraction of which is available as "negative" stress due to recovery during the cooling period.

Although the gage results are not given, an accelerated convergence was detected at all convergence gages located around rooms 2 and 3, including those on the far sides of the rooms, a little more than 40 ft from the heaters.

11.4.7.3 Horizontal Deformation of Heated Pillar. – Nine horizontal internal strain gages were installed through the heated pillar. The collar anchors on these stations – on both sides of the pillars – were located approximately 1 ft from the actual edge of the pillar. Thus the true deformation of the pillar could be determined without including in the measurements the effects of superficial cracking and slabbing of the pillar surfaces due to accelerated deformation produced by the heating.

The deformation of points at various positions along the holes of these stations is shown in Figs. 11.82–11.84. These figures indicate that prior to heating (before standard day 1170) the center pillar was deforming at a rate somewhat higher than that of the pillars adjacent to rooms 1 and 4. This was expected because the center pillar is one-third smaller than the other pillars, the adjacent rooms are one-fourth larger than rooms 1 and 4, and it is at the center of the experimental area and therefore a lesser percentage of its load could be transferred to the solid abutments. The acceleration of this horizontal deformation at all points in the pillar is apparent, beginning on standard day 1170. The rapidity of this response indicates once again that it is almost entirely due to thermal stresses rather than changes in physical properties resulting from elevated temperatures. Notice that an acceleration in horizontal deformation resulting from operation of the modified pillar heater (standard day 1025) is seen at gage 126 but not at any of the other gages, even though it was seen throughout the pillar on the convergence curves. This is partly a consequence of the relative insensitivity of this way of plotting horizontal deformation data.

The horizontal strain between adjacent anchors was computed for (1) standard day 1020, prior to the modified pillar heater test, (2) standard day 1170, just prior to the start of heating, (3) standard day 1260, three months after heating, and (4) standard day 1500, maximum temperature condition; standard day 600 was used as a base line for all strains. These strain curves are shown in Fig. 11.85. Recalling the discussion of similar curves for the pillars adjacent to rooms 1 and 4, this type plot produces a U-shaped curve, indicating greater horizontal strain at the edges of the pillars than in the center. Figure 11.85 reveals that the U shape is achieved at all stations except 125 and 122. This anomaly may be related to gage malfunction or local geology.

High strains at the edges of the pillars, as shown by the gages at the bottom of the pillar (Fig. 11.85, gages 123, 126, and 129), are undoubtedly due to the higher rate of deformation resulting both from the high temperature and high thermal stresses at those points. Horizontal strain at the top of the pillar (Fig. 11.85, gages 121, 124, and 127) is more evenly distributed across the pillar and, in fact, is slightly greater at the center section of the pillar than at the center section of the pillar near the floor level. Since this lower center section is at a higher temperature than elsewhere in the pillar, including the lower edges of the pillar, this observation can be explained as follows:

Previous discussion of the stratigraphy of the experimental area demonstrated that the tops of the pillars are relatively free to move on the ceiling bed because of the lubrication offered by the thin shale parting at that point, whereas the bottoms of the pillars are tightly keyed into the floor up to heights of 2 to 3 ft at least. Therefore, even though the bottom edges of the pillar were deforming rapidly because of their proximity to the heaters, they still provided a considerable horizontal restraint to the lower center sections of the pillar. Along the top of the pillar, the outer edges deform easily; and, because of their slip along the shale parting, much less horizontal restraint is transferred to the upper center of the pillar. Therefore it deforms at a rate more nearly equal to that at the edges.

11.4.7.4 Vertical Movements. – The vertical movements which occurred at two stations in rooms 2 and 3 are shown in Figs. 11.86 and 11.87. These figures were constructed in the same way as the plots for rooms 1, 4, and 5 (see Figs. 11.65, 11.66, and 11.78) and show the vertical movement of points on and into the roof and floor to depths of 25 ft. Curves for the "floor" points in each case represent the time function of floor uplift. Discontinuities in the "roof" curves which occur on standard day 925 in room 3 and on standard day 1025

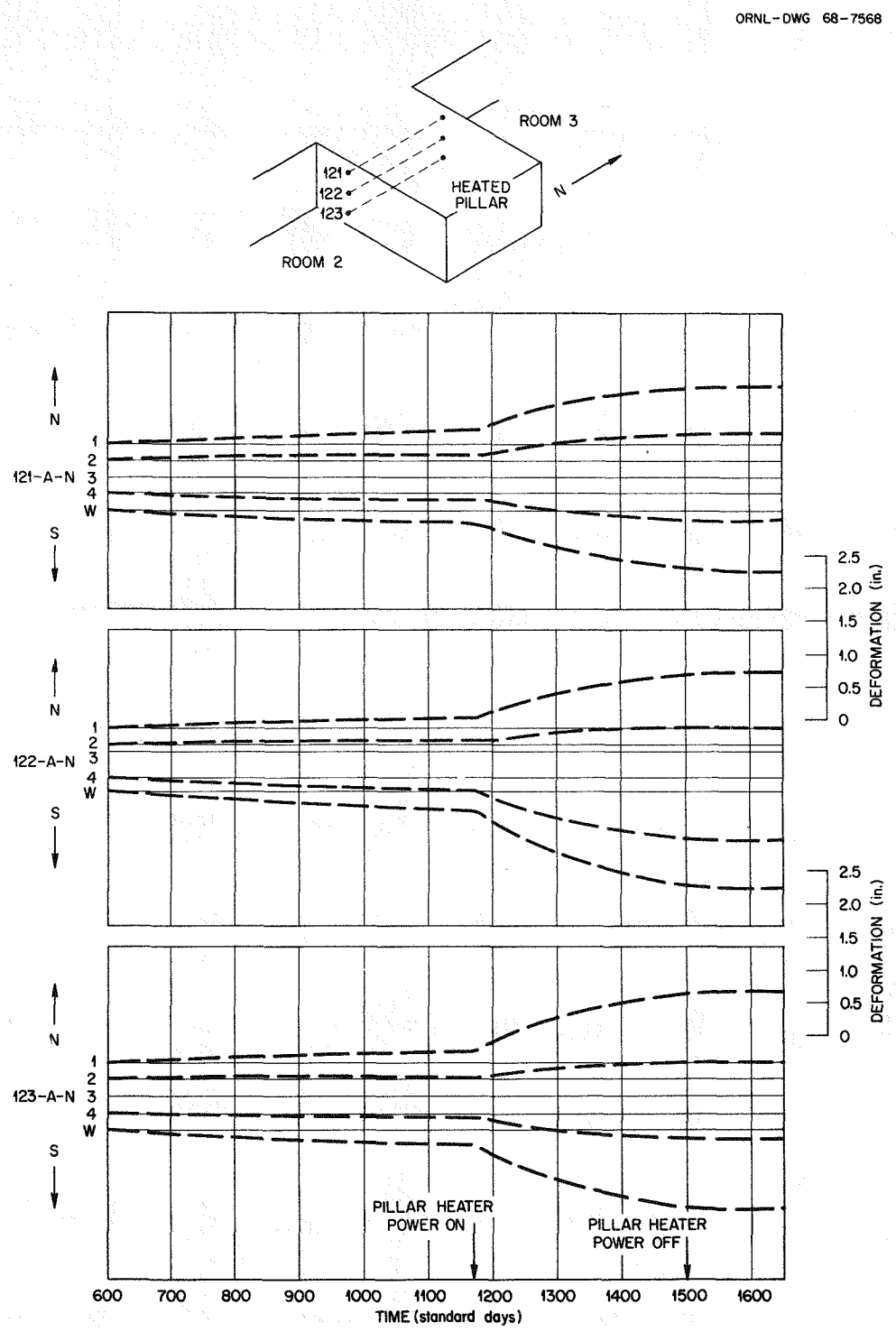


Fig. 11.82. Horizontal Deformation as a Function of Time. Center pillar, gages 121, 122, and 123.

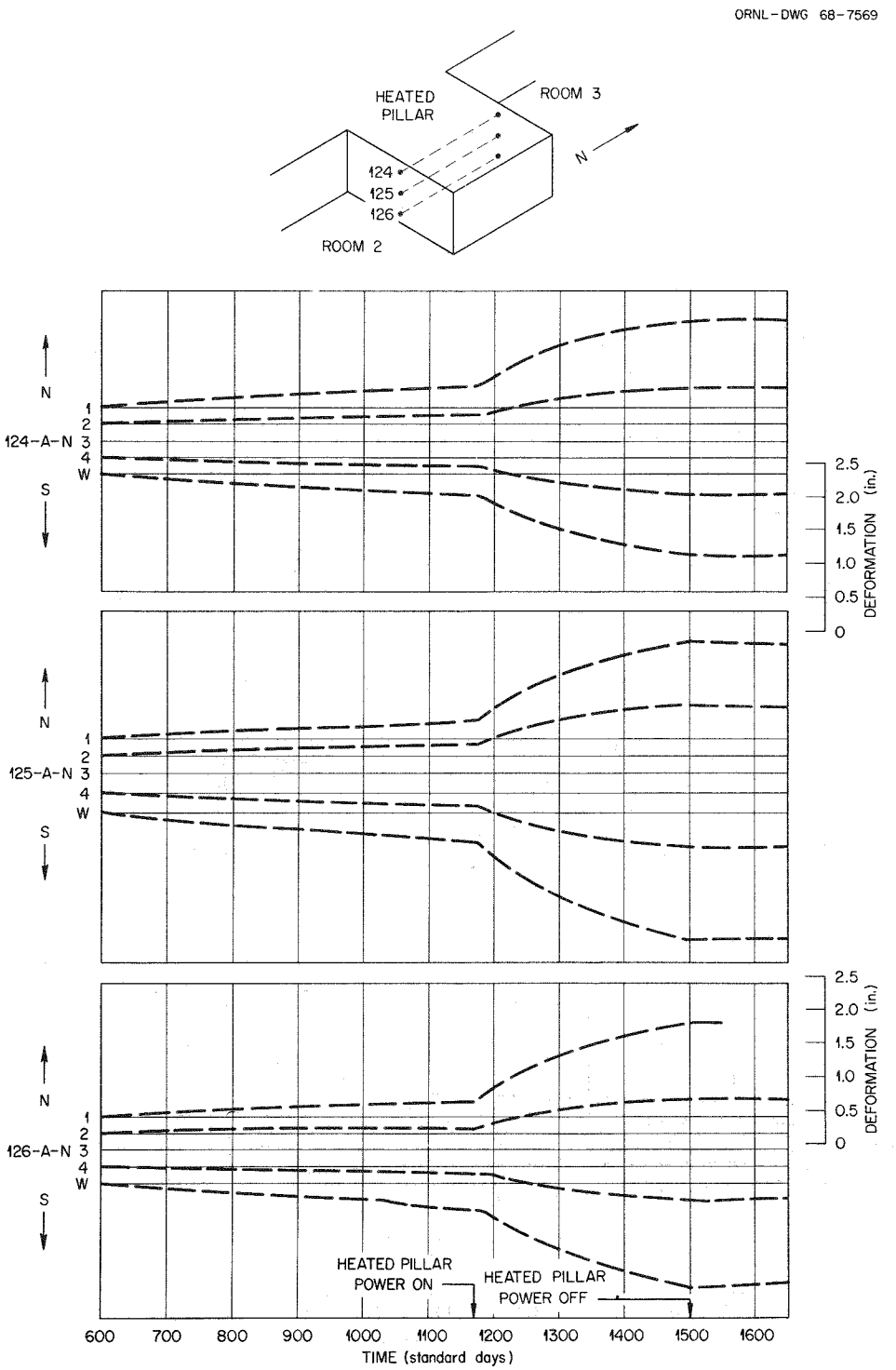


Fig. 11.83. Horizontal Deformation as a Function of Time. Center pillar, gages 124, 125, and 126.

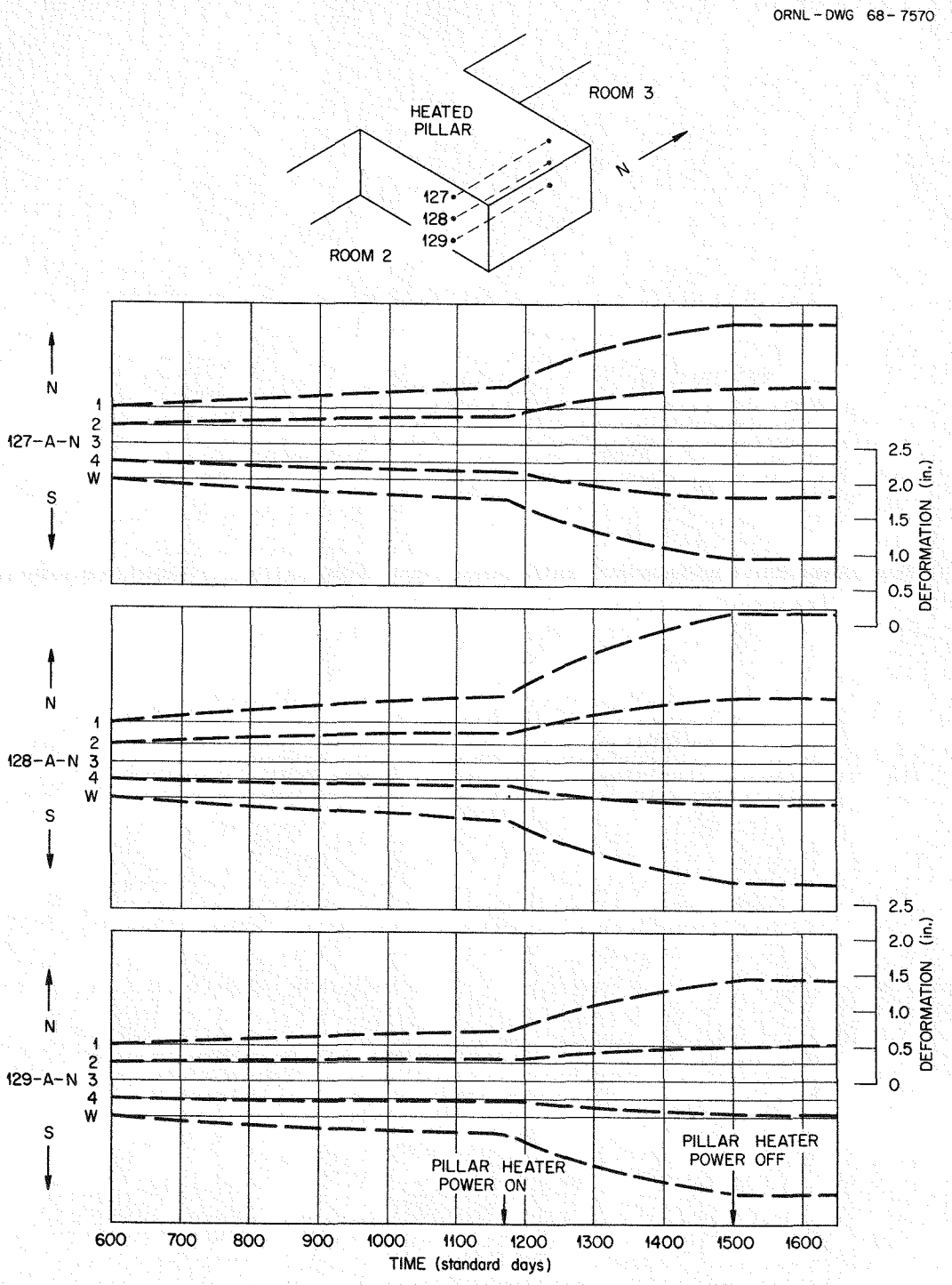


Fig. 11.84. Horizontal Deformation as a Function of Time. Center pillar, gages 127, 128, and 129.

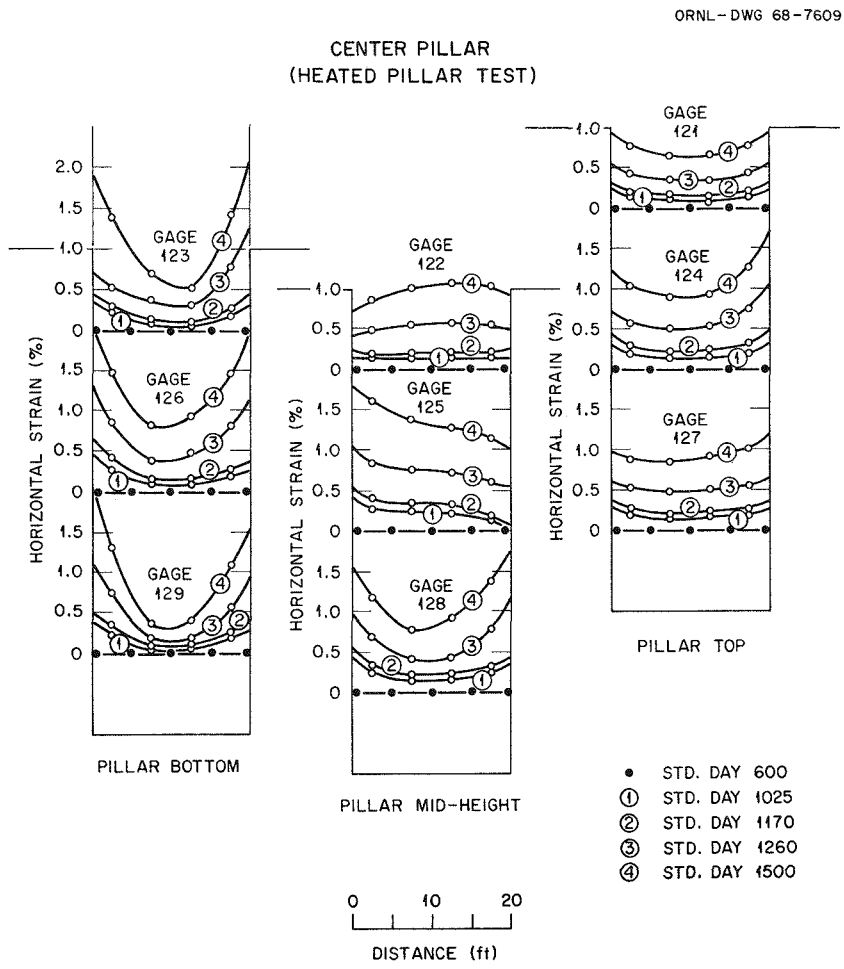


Fig. 11.85. Horizontal Strain as a Function of Distance into (Heated) Pillar at Selected Times.

in room 2 are real, having been caused by the lifting of the sagging roof bed when the roof bolts were installed. Note that after the roof bolts were installed, the curves for the roof point and the U-3 point (located 6 ft up) are parallel or slightly converging, indicating that the sag of the roof bed has been arrested and the bed is deforming as though it were an integral part of the entire roof unit.

The effect of the modified pillar heater, commencing on standard day 1025, can be seen on two gages in room 2 (130 and 132), even though the power to this single heater was only 3 kW and both gages were more than 20 ft distant from the heater. Once again, this indicates the extent of the thermal stress transfer to points distant from the heat source, far beyond the limits of the heated zone. Also note the considerable upward movement of points located 25 ft below the floor level (approximately 0.5 in. in each case). This *movement is greater than the estimated movement* 25 ft below the floor in the center of rooms 1 and 4 (see Fig. 11.65), even though the array heaters were much closer to the gages in those rooms. The amount of movement 25 ft below the floor in rooms 2 and 3 was somewhat surprising, since it was thought that these anchors would be outside the zone of appreciable deformation. This movement was underestimated, because the interrelationships between a loaded pillar and the adjoining rock rigidly keyed together were inadequately understood at the time the gages were installed. Subsequent laboratory pillar-model tests (see next chapter) illuminated these interrelationships.

True "convergence" of the area (as opposed to vertical deformation of the pillar) will be approximated by closure of the points located 25 ft above the ceiling and 25 ft below the floor. Prior to heating, this convergence was proceeding at a nearly constant

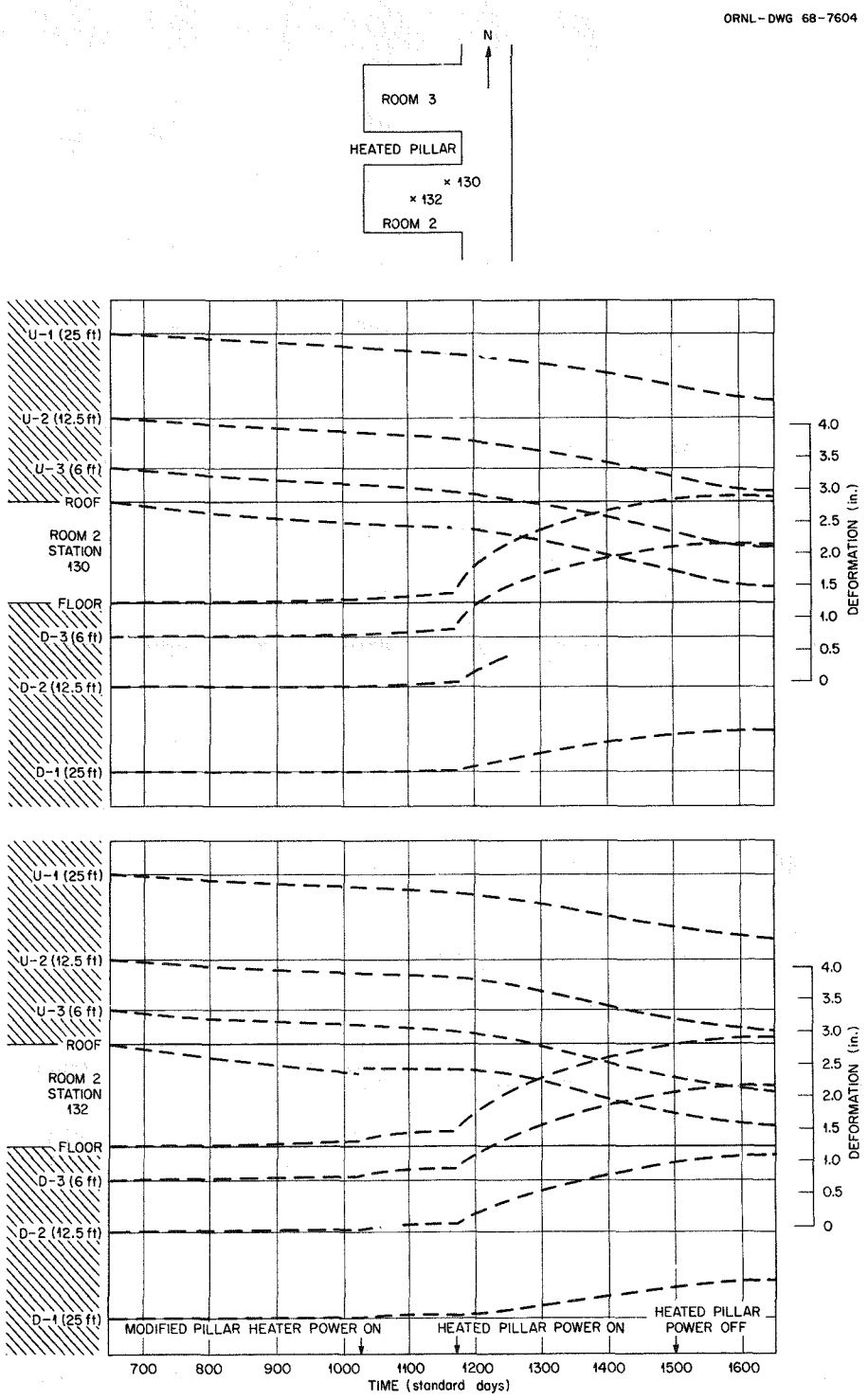


Fig. 11.86. Vertical Deformation as a Function of Time. Room 2, gages 130 and 132.

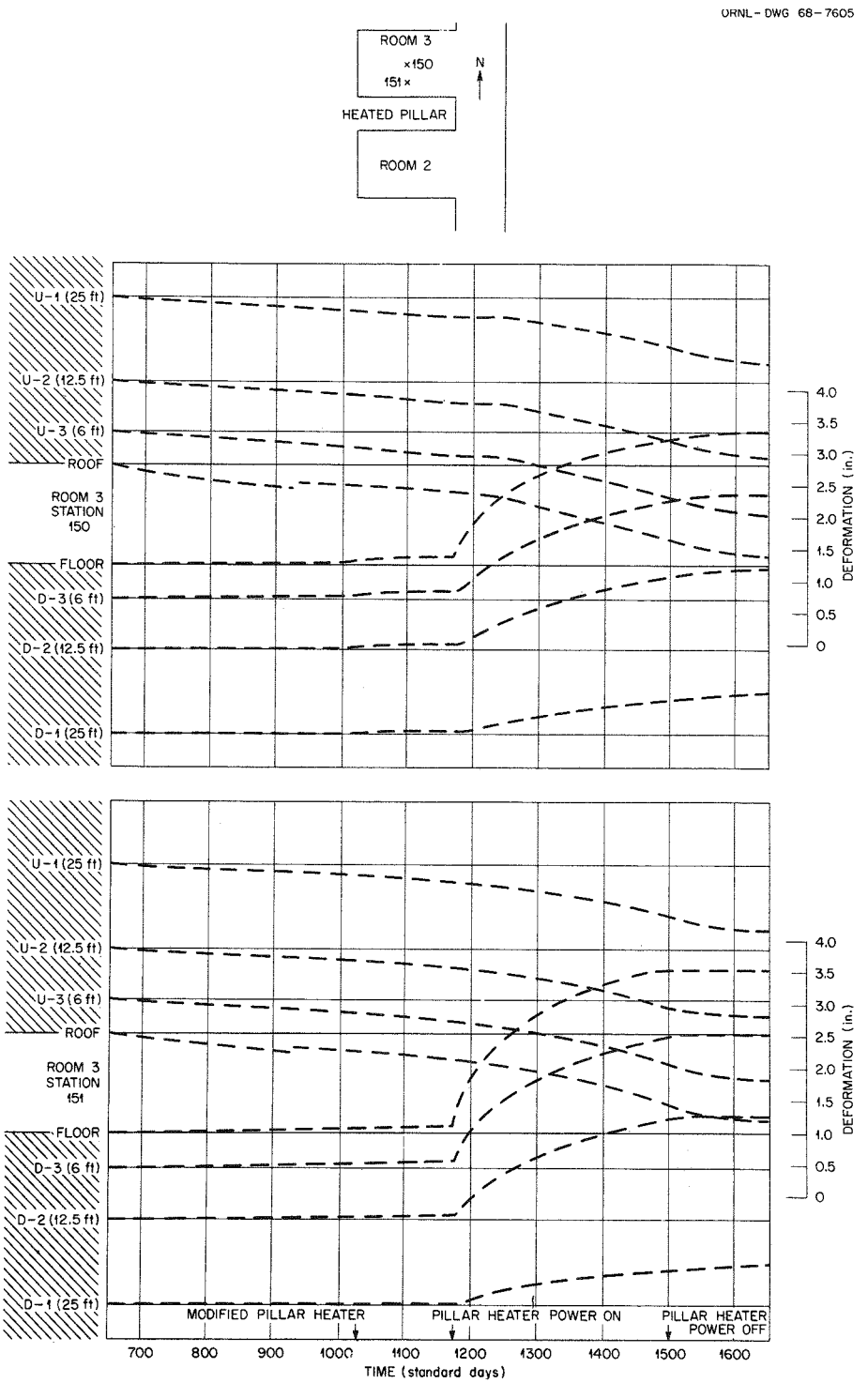


Fig. 11.87. Vertical Deformation as a Function of Time. Room 3, gages 150 and 151.

(slightly decreasing) rate of about ¼ in./year. This is seen on the U-1 point 25 ft above the ceiling. During the first year of heating, this convergence amounted to about 1 in., distributed approximately equally between the roof and the floor (each at 25 ft). However, while the entire roof was lowered more or less as a unit, the uplift of the floor strata decreased appreciably with increasing depth. This is a consequence of gradients of both the overburden and thermal stresses in the floor, stemming from the fact that the pillar is keyed into the floor, and the reduced level of these gradients in the roof material because of the lubricating shale parting at the ceiling level, which reduces the keying effect at the roof.

11.4.7.5 Summary. – This gross difference in behavior of the roof and the floor can be seen more easily in Fig. 11.88, where deformations around the heated pillar are summarized. This figure shows the vertical and horizontal movements during heating (standard days 1170–1500) in the vertical north-south plane through the center of the pillar and the adjacent rooms. The figure was constructed with measurements from the borehole leveling instruments, roof slip gages, and roof bed sag monitors (see Sect. 11.4.1). All vertical movements were calculated relative to the absolute level brought in from outside the experimental area, and the horizontal movements were plotted on the assumption that the vertical center line of the pillar remains undeformed.

Although most of the significant conclusions based on rock mechanics results from the heated pillar experiment are drawn from a detailed analysis in Chap. 13 of the interactions of stress-temperature-strain and time, a few conclusions based on the above interpretation of the data are summarized here:

1. The quantity and quality of instrumentation in and around the heated pillar was adequate to provide the information required to perform a detailed analysis. At the same time it was certainly not excessive, as evidenced by the extent of interpolation needed to construct Fig. 11.88. However, since it may not be apparent to those unfamiliar with rock mechanics literature, it should be pointed out that the data shown in Fig. 11.88 and the inferences which can be drawn from them represent a significant advance in understanding the deformational behavior of support pillars on the basis of in situ measurements.

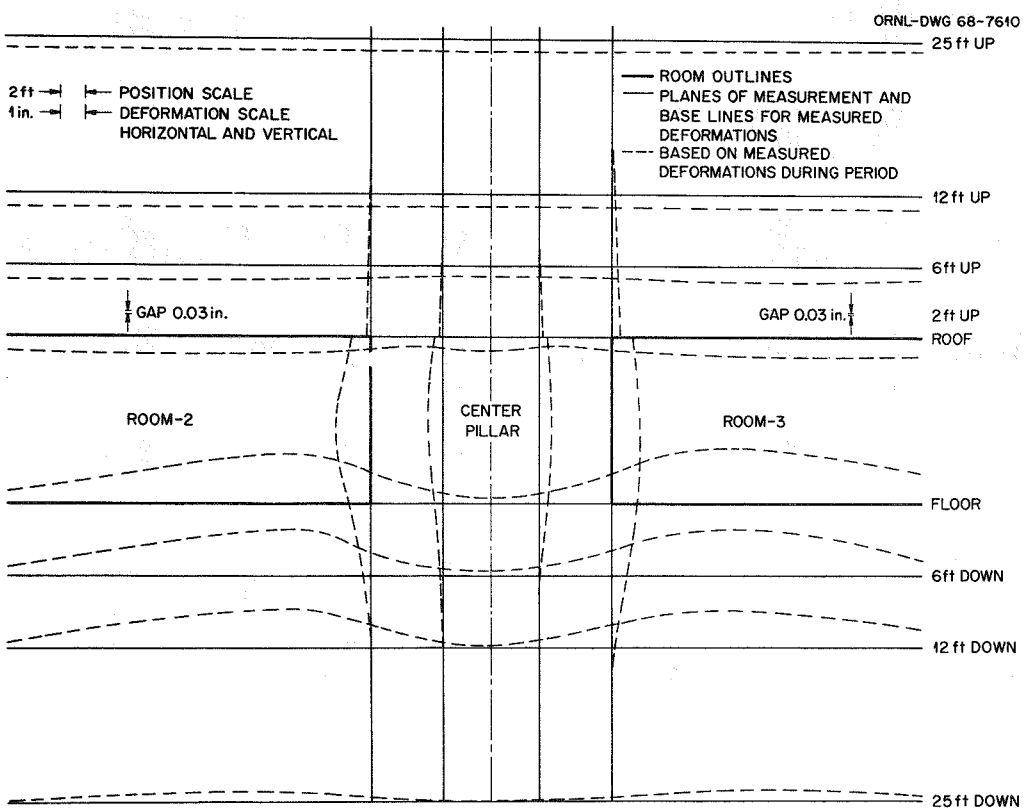


Fig. 11.88. Summary of Deformations Around Heated Pillar and Rooms 2 and 3.

Also, it is significant that the observed behavior in the mine correlates well with that observed in laboratory pillar models (Chap. 12).

2. In the heated pillar experiment, where a large volume of salt was heated appreciably, the deformations resulting from thermal stresses and their transfer to remote points were clearly much larger and more dominant than the deformations resulting from increased creep properties of salt at elevated temperatures. However, heating of the pillar took place over a much shorter time than would be the case in an actual waste disposal operation, and the situation might be somewhat different where the temperature rise is considerably slower.
3. The effect of local geology (stratigraphy) on the deformations, especially the presence of thin shale partings capable of providing lubricated surfaces, was larger than anticipated. This influence may limit the applicability of this analysis to other geological environments. However, the fortuitous circumstances of having a shale parting at the roof and of having the pillar bottom keyed into the floor in this experimental installation, coupled with the pillar-model tests, will allow some limits to be placed on the variability to expect from different geological configurations.

11.4.8 Deformation of Entire Experimental Area and the Rest of the Mine

Previous sections discuss the rock mechanics results obtained from the three major experiments: (1) the radioactive and control array experiments in rooms 1 and 4, (2) the array experiment in the floor of the existing mine in room 5, and (3) the heated pillar experiment. In each case, considerations are confined to the effects of each experiment in its immediate vicinity. This section (1) examines some of the interactions between these individual experiments, including the presentation of some new data where the effects of single experiments could not be separated from the whole; (2) describes the behavior of the experimental area as a whole, including the corridor connecting the rooms, in response to the various experiments being conducted at various times; and (3) explores the effects of these operations on the behavior of the surrounding "old workings" area, especially its stability.

In order to better understand the interactions of the various activities, it is necessary to review the chronology of events in the experimental area. For convenient reference, this chronology is shown in Table 11.7.

Table 11.7. Chronology of Experimental Activities

Standard Day	Date	Event
367	Sept. 2, 1964	Started excavation of experimental area
571	Mar. 25, 1965	Completed mining operations in experimental area
806	Nov. 15, 1965	Started array experiment in rooms 1 and 4
929	Mar. 18, 1966	Roof bolt test – room 3
992	May 20, 1966	Started roof bolt installation program – entire experimental area
1009	June 6, 1966	Started "floor" array experiment in room 5
1025	June 22, 1966	Started modified pillar heater test – room 2
1039	July 6, 1966	Completed roof bolt installation program – entire experimental area
1170	Nov. 14, 1966	Started heated pillar experiment – all heaters
1240	Jan. 23, 1967	Heat input increased by 40% – rooms 1, 4, and 5, simultaneously
1373	June 5, 1967	Stopped heating floor array in room 5 – all power off
1382	June 14, 1967	Stopped heating array experiments in rooms 1 and 4 – all power off
1499	Oct. 9, 1967	Terminated heated phase of heated pillar experiment

11.4.8.1 Deformations Throughout Experimental Area. – A general picture of movements taking place throughout the four rooms of the experimental area could be obtained by superimposing Figs. 11.72, 11.73, and 11.88 in their proper spacial relationship. The mosaic obtained in this way would represent the vertical north-south plane through the center line of the heaters from one end of the experimental area to the other. Apart from illustrating the general downward movement of the roof over the entire area, including those areas supported by pillars, this figure would not provide any new information. Furthermore, since the time basis for constructing movements around the heated pillar was different from that for the heating experiments in rooms 1 and 4, the mosaic would not be very accurate. The true temporal relationships between horizontal movements in this north-south plane are shown in Fig. 11.89. In this figure the movements of all points as a function of time are shown relative to the center of the heated pillar. It is possible to link all measurement points from 50 ft south of room 1 to 50 ft north of room 4 in this manner by using the horizontal room closure gages.

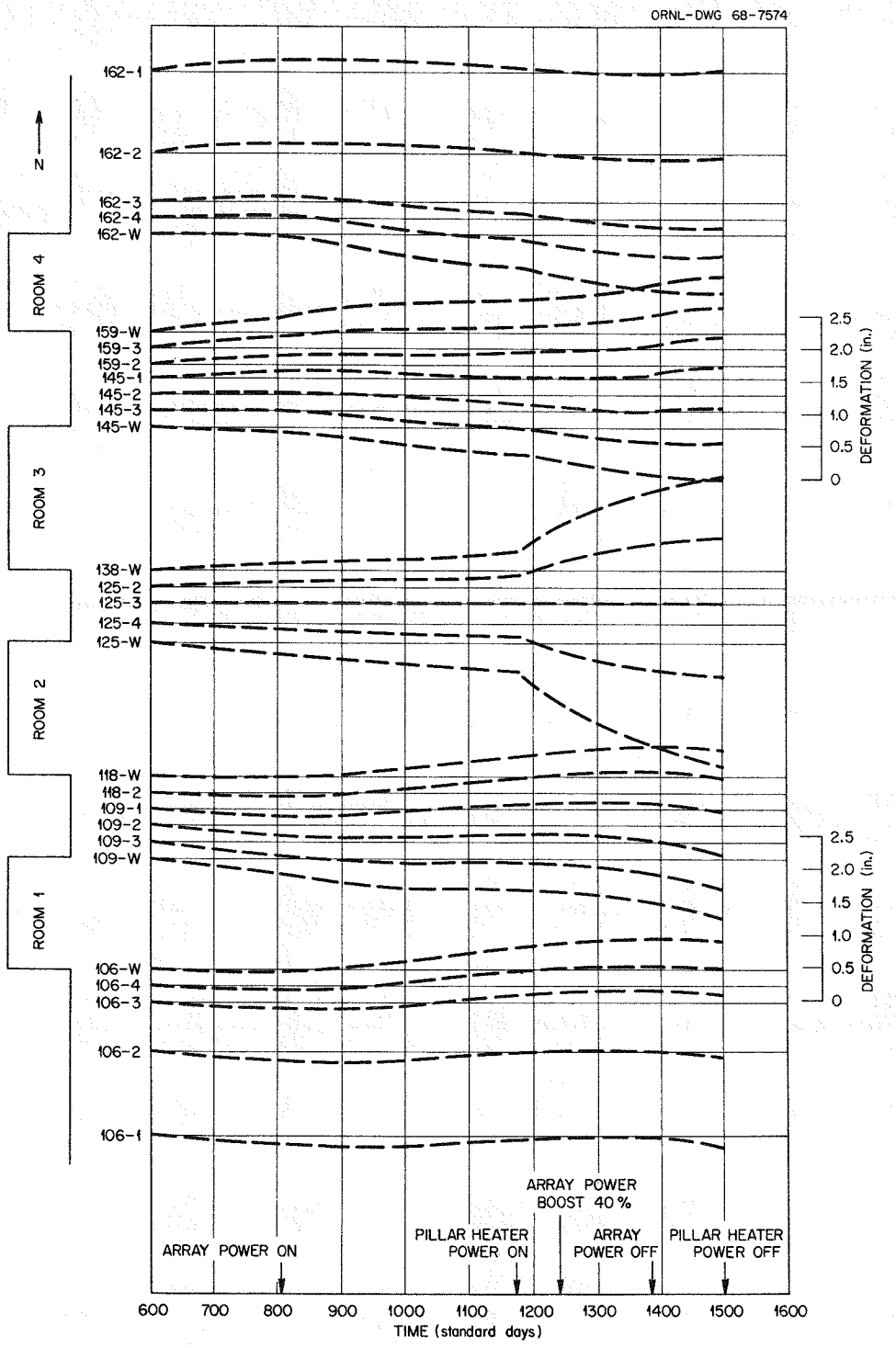


Fig. 11.89. Horizontal Deformation as a Function of Time Throughout Entire Experimental Area.

Deformation (expansion) of the three pillars, especially in response to the heating on standard days 806, 1170, and 1240, can be seen clearly in Fig. 11.89. Deformation of the center pillar is the same as seen on Fig. 11.83 for gage 125-A-N. This deformation appears to be reasonably symmetrical about the pillar center, but, more importantly, deformation of the two end points of the measurement link (106-1 and 162-1) also appears to be reasonably symmetrical. This symmetry tends to justify use of the center of the heated pillar as a reference point. However, some rather unusual deformations result from this type of presentation. Notice that pillar 1-2 (that is, the pillar between rooms 1 and 2), apart from its general expansion, shows a general drift first toward room 1, then (commencing about standard day 850) back toward room 2, then it reverses itself about standard day 1200 and again drifts toward room 1. Pillar 3-4 shows a similar (mirror image) drift but somewhat less well developed. Figure 11.89 indicates that the horizontal closure of room 1 prior to heating is due entirely to the deformation of the pillar 1-2, with no contribution being made by the south (abutment) wall. At the same time, the total horizontal closure of room 2 results from the deformation of the center pillar with no contribution from the south wall of that room. Furthermore, these same relationships hold as a mirror image for rooms 3 and 4. In this type of presentation, errors due to thermal expansion of the wires and steel tapes, instrument malfunctions, and, to a certain extent, even reading errors tend to cumulate. It would seem probable that these errors have contributed to the unusual deformations, especially the drift of pillars 1-2 and 3-4 shown in Fig. 11.89, but it is difficult, if not impossible, to ascribe all these deformations to the effects of cumulative errors.

One explanation could be that the entire experimental area, nearly 400 ft wide, was undergoing a slow extension due to creep towards the extensively excavated portions of the mine both to the north and south. The various heating experiments could then be seen as a perturbation of this gradual extension, causing it to be temporarily reversed. Expansion of the individual pillars, of course, is superimposed on these gradual deformations. Although this explanation would certainly be possible, it is by no means proved, and the deformations shown on Fig. 11.89 must remain largely unexplained.

11.4.8.2 Stressmeter Results from Experimental Area. – Six stressmeter-type diametral borehole deformation gages were installed in the pillars and abutments in and around the experimental area. As seen in Sect. 11.4.3, it was impossible to obtain quantitative data from these instruments because of the plasticity of the salt. However, it is possible to recover significant qualitative information concerning the behavior of salt by interpreting the stressmeter results on the assumption that an abrupt change in slope of the instrument output indicates a change in stress at that point.

The results from the six stressmeters are shown in Fig. 11.90. On all of the instruments there is an initial very rapid falloff of prestress load, representing accommodation of the salt to the stresses applied during installation of the instrument. After this initial period, the slope of the output curve is probably related to stress on the salt at that point but only in a very general way. The flat and level output from stressmeters 17 and 18 would imply a lower stress level than is indicated at the other four locations. However, it is not possible to rank the four instruments installed in the pillars according to their loads.

When the array power was turned on in rooms 1 and 4 (standard day 806), there was a definite increase in the output on stressmeter No. 14. There was also a much smaller but definite increase at stressmeter No. 19. These instruments are located near the centers of pillars 1-2 and 3-4. The increase in the readings following standard day 806 can be interpreted as representing an increase in the vertical stress on those pillars. In view of the previous discussion, that increment of load would be the thermal stresses transferred to that point from the heat sources in the middle of the room. The effect of the modified pillar heater commencing on standard day 1025 can be seen on both stressmeter 16 and 15. On stressmeter 16, the effect is much more abrupt and somewhat larger than at stressmeter 15. Since stressmeter 16 was located only 5 ft from the edge of the pillar, this is the type of response to be expected. When all the pillar heaters were turned on (standard day 1170), both stressmeter 15 and 16 reflect an increase in stress which, once again, represents the thermal stress loading of the pillar. Notice that in this case the effect at the center of the pillar (stressmeter 15) is much greater than at the point only 5 ft from the edge.

Up to this point the stressmeter readings have only confirmed the thermal stress loading of the pillars which had been deduced from the strain measurements. From here on, the stressmeter results become more interesting. First, it is seen that the instruments in the heated pillar show an increasing output for only about the first 60 days of heating. Thereafter, the slope of the readings reverses and becomes negative. Rather than indicating a decreasing stress on the pillar, these readings may represent the situation where the creep

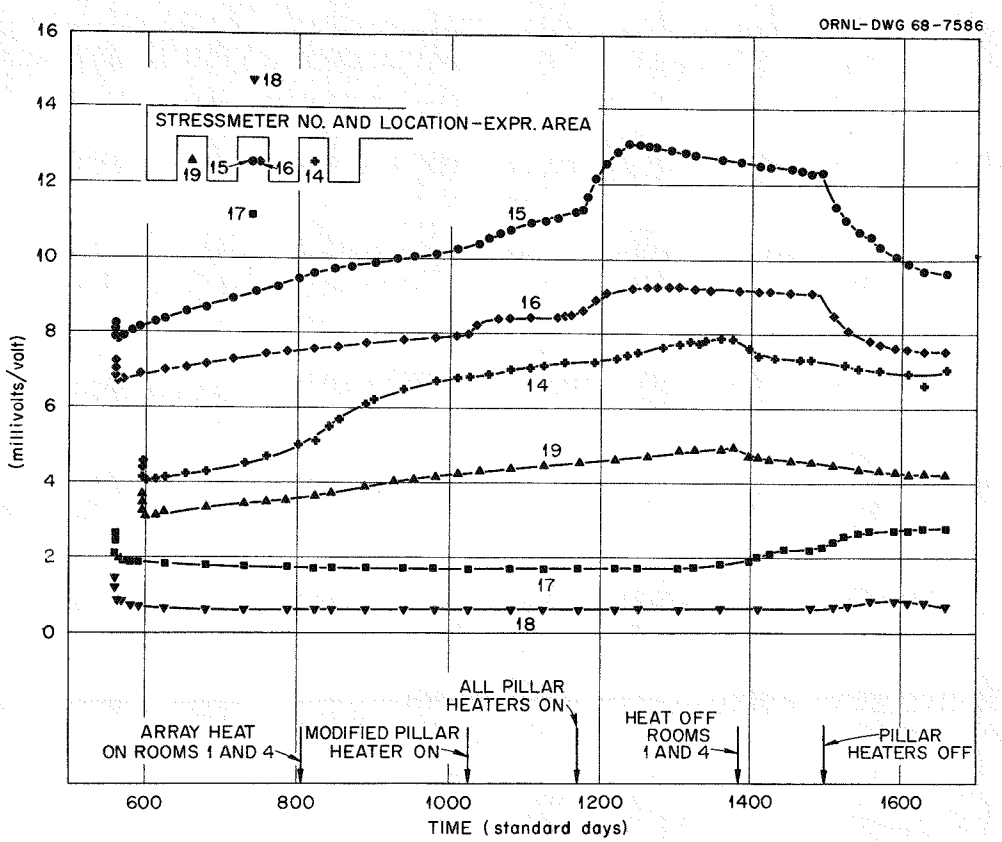


Fig. 11.90. Experimental Area Stressmeter Results.

properties of the salt have been increased by the temperature rise to the point where the salt immediately adjacent to the stressmeters is now creeping away from the instruments at a faster rate than it is creeping toward it. This is possible because of the high modulus of the instruments and the fact that they were installed at a preload stress. (Or there could be a combination of decreasing stress and increased plasticity.)

Now examine the readings obtained as the power to the various heaters was turned off. First, on standard day 1382 the array heaters in rooms 1 and 4 were shut down and both stressmeters 14 and 19 responded immediately by showing a declining output. At the same time, there was another larger increment in the reading on stressmeter 17 and a slight but definite increase in the output on stressmeter 18. These readings can be interpreted as follows:

When the heaters were turned on, an increment of thermal stress was added to the overburden loading on the pillar which disturbed the (dynamic) equilibrium which had been established between the stress distribution and the rates of deformation of the pillars and abutments. During the period of heating, the system accommodated the altered stress pattern by an increase in the rate of deformation at high stress regions, which in turn slowly redistributed the loads until a situation approaching equilibrium was achieved. When the heaters were then turned off, the recoverable portion of the thermal stress (and consequent recoverable thermal expansion) in the pillar was rapidly removed. The ability of the pillar to support overburden load was consequently also very rapidly reduced. In essence, the pillars underwent a sudden contraction, so sudden, in fact, that the roof of the area could not immediately respond, and a portion of overburden load previously supported by the pillar was transferred elsewhere – that is, to the abutments, as indicated by the readings on stressmeters 17 and 18.

This interpretation serves primarily to indicate the very complex interrelationships between the pillar deformations and the stress distributions, both on the pillars and the abutments, and to suggest its sensitivity to the disturbances created by heating. The stressmeter

readings certainly shed some light on the events taking place; but the difficulty of obtaining valid "stress" measurements in any material, and especially in salt, added to the complex and rapidly changing stress pattern suggested by these results, makes the detailed analysis of these results exceedingly difficult.

11.4.8.3 Deformations in Experimental Area Corridor. – Horizontal deformations on the east side of the corridor connecting the four rooms of the experimental area are very small when compared with the pillar deformations. However, the vertical movements taking place at the center of this corridor, especially the roof deformations, are of the same magnitude as the vertical movements occurring elsewhere in the experimental area. The vertical deformations at gage stations 105, 134, and 154 are shown as a function of time in Fig. 11.91. These figures are the same type as the other vertical-movement-vs-time plots seen previously in this chapter. These three gages are located at the front of room 1, at the end of the heated pillar, and at the front of room 3, respectively, and it is instructive to compare the movements at these three different locations.

First, the uplift of the floor at gage 134 is both larger and more abrupt following initiation of heating at pillar 2-3 than at the other two stations. This should be expected because this gage was closer to the heat sources than the others. Sagging of the 2-ft-thick roof bed can be seen at all three stations and especially at gage 105. There, the divergence of the two curves marked "roof" and "U-3" is apparent, even before the start of the experiment. The total sag accumulated at this gage before the roof bolts were installed was approximately 0.4 in. – much more than was seen at other gages. This was because of the span at the front of room 1, the age of the opening, and the fact that gage 105 was installed much closer to the working face than the other stations – therefore a smaller amount of movement was lost before readings commenced. Notice that although the roof bolts did arrest the sag of the roof bed at this gage, the amount of roof bed lifting was smaller than elsewhere in the experimental area. This reduced roof lift was probably because a higher amount of sag had occurred. This illustrates one of the basic tenets of roof bolting practices, which is: If you are going to install roof bolts, do it as soon after excavation as possible.

11.4.8.4 Effect of the Heating Experiments on the Existing Mine Area. – Effects which the heat experiments had on the "old workings" of the existing mine were most visible in rooms adjacent to the experimental area. Figures 11.92 and 11.93 show vertical convergence as a function of time at stations in the west room and entry 2 south (see Fig. 11.41 for locations). There are two rather significant conclusions which can be drawn from these results: (1) the application of heat in the experimental area had very little influence on movements and deformations taking place in the old workings compared with the effect of excavating the experimental area, and this effect was opposite to that caused by excavating; that is, the convergence rates in the old workings decreased more rapidly than normal, and (2) the old workings gages responded to the cooling in the experimental area by an increase in their rate of deformation, returning to a rate approximately equal to what would have been expected had heating not taken place.

In view of the foregoing discussions of the effects of heating on the pillars in the experimental area, this response may appear confusing. However, the two situations are not comparable; in the experimental area, the deformations were due to the heating of either the pillar itself or the adjacent floor, whereas the old workings deformations are in response to the deformations and loadings of the experimental area pillars. During the heating phase, the experimental area pillars tended to carry increased stress because of the thermal expansion of the salt. However, this increase of stress was limited by an accelerated creep rate resulting from both the elevated temperature and the increased stress itself. The net effect which the heating had over the larger area was therefore slight when compared with the effects of excavation, even though the pillar deformations were considerably altered, but it resulted in the heated pillars supporting more than their normal share of the overburden load, thus reducing the load on the pillars in the old workings. When the heat was turned off, recovery of the thermal expansion significantly reduced the stress on the pillars in the experimental area, but without any compensating mechanism. These pillars were no longer capable of supporting even their share of the overburden load, and that portion of the load was transferred to the surrounding areas in the form of an increased pillar stress in those areas. This increase in stress was the cause of the accelerated deformation in the old workings during the cooling phase.

The horizontal gages in the old workings adjacent to the experimental area confirm the reduced deformation rates during heating in the experimental area and the increased deformation rates after termination of heating.

The influence of the heating (and cooling) in the experimental area did not extend much beyond the adjacent rooms in the old workings, that is, beyond 200

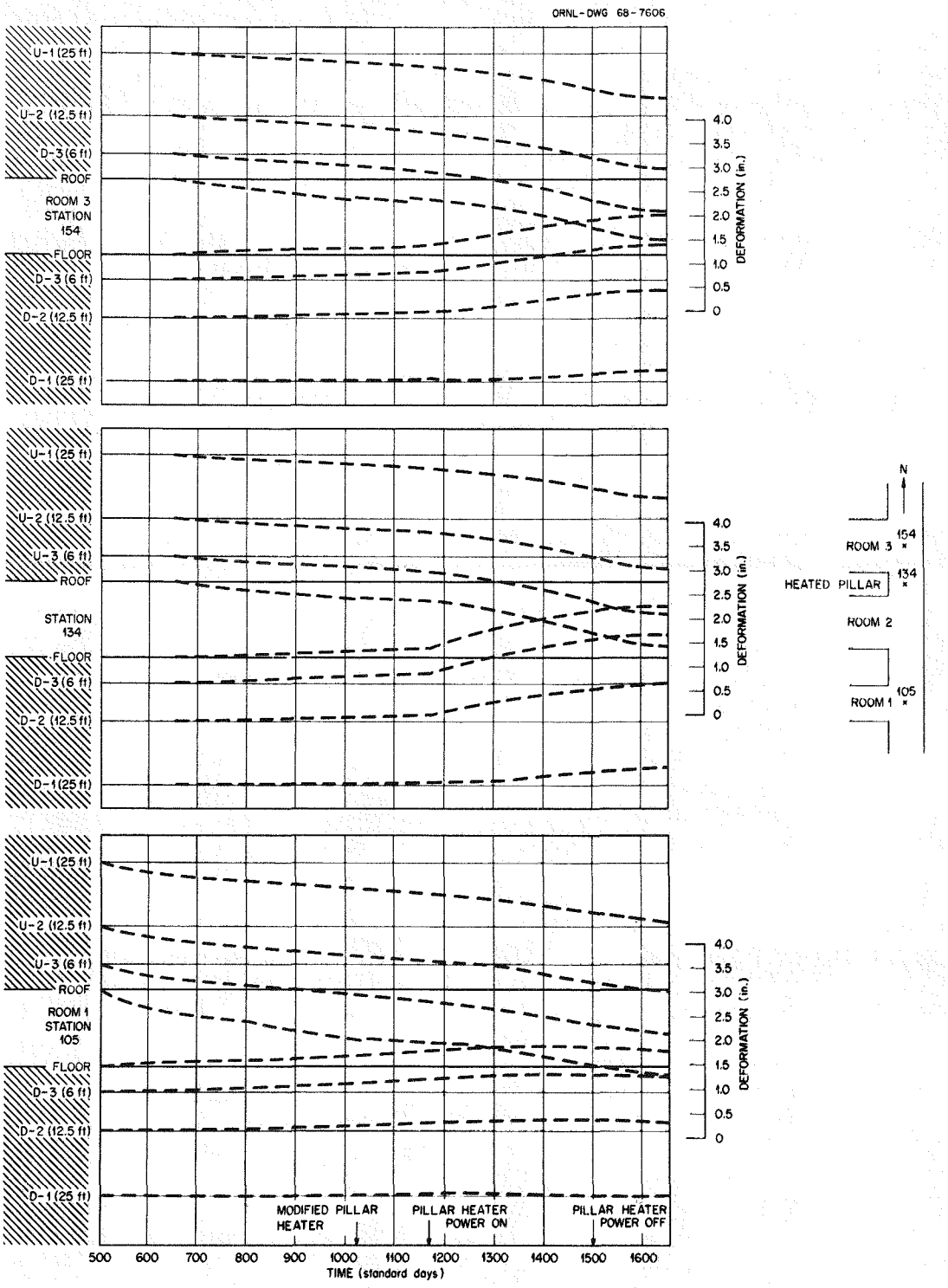


Fig. 11.91. Vertical Deformation as a Function of Time.

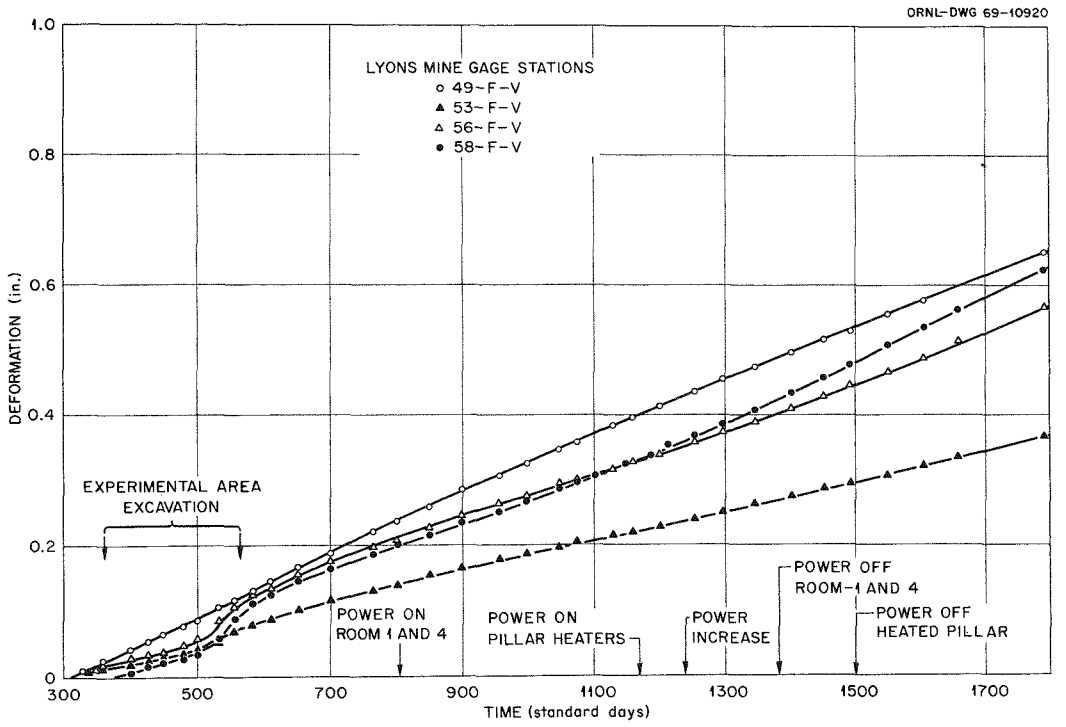


Fig. 11.92. Vertical Convergence as a Function of Time – Old Workings.

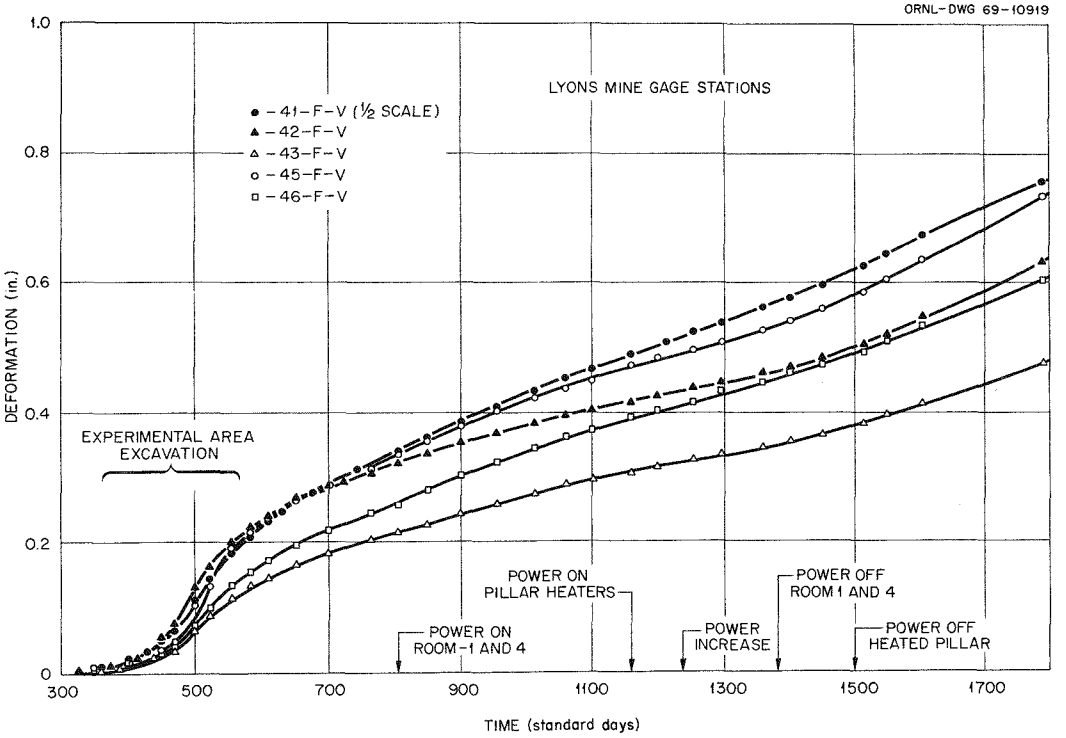


Fig. 11.93. Vertical Convergence as a Function of Time – Old Workings.

Table 11.8. Convergence Rates in Old Mine Area

Gage	Convergence Rates (10^{-3} in./day)		
	Prior to Standard Day 800	Standard Days 800 to 1500	After Standard Day 1500
1-F-V	0.75	0.80	0.72
6-F-V	1.22	1.00	0.94
11-F-V	0.50	0.50	0.41
12-F-V	0.41	0.38	0.35
14-F-V	0.66	0.60	0.58
15-F-V	0.34	0.32	0.31
16-F-V	0.44	0.41	0.43
20-F-V	0.23	0.20	0.20
22-F-V	0.36	0.19	0.17
23-F-V	0.30	0.17	0.18
41-F-V	1.14	0.81	0.94
42-F-V	0.42	0.25	0.46
43-F-V	0.36	0.24	0.34
45-F-V	0.52	0.35	0.53
46-F-V	0.45	0.33	0.38
48-F-V	0.32	0.26	0.29
49-F-V	0.49	0.42	0.40
51-F-V	0.30	0.23	0.27
53-F-V	0.28	0.22	0.25
56-F-V	0.39	0.34	0.40
57-F-V	0.23	0.19	0.22
58-F-V	0.38	0.40	0.48
59-F-V	0.34	0.22	0.35

ft. The effect of cooling is not discernible at gage 49-F-V (Fig. 11.41) and at gages 11-F-V and 12-F-V (Table 11.8). All of the vertical convergence (the most sensitive type) gages from the shaft area down through entry 5 (gages 1 through 23) show only the expected gradual decrease in rate as a function of time (Table 11.8). For comparison, the convergence rates for the gages in the west room and entry 2 south are also given in Table 11.8 (gages 41 through 59, not including 49). The increase in convergence rate during the cooling period on these gages is apparent.

12. Laboratory Pillar Model Experiments

T. F. Lomenick

The effect of temperature, compressive stress, and time on the deformation of rock salt has been investigated through scale-model specimens of mine pillars. Tests have been performed on samples of bedded salt, as well as on dome salt, from six different mines in the Unites States and from the anticlinal structure of the Asse II salt mine in northeast Germany. Efforts have been made to ascertain the optimum model size for laboratory studies and to determine the effect of pillar shape on deformation. Finally, the effect of stratigraphic discontinuities on the deformational behavior of pillars and the mechanisms of pillar deformation have been investigated.

12.1 SUMMARY OF PREVIOUS WORK

Many workers have performed creep tests on rock salt; but, although some general conclusions concerning deformation of salt could be drawn from them, these experimental data could not be used to predict with any certainty creep rates in multiple openings in salt deposits containing radioactive waste products. A theoretical approach to a solution of the problem did not appear to be practicable either. Thus, through experimentally derived data, an empirical solution to the problem has been sought.

To determine the effect of radiation on the rate of creep of salt, Gunter and Parker[1] tested 2-in. cubes of salt from dome and bedded deposits that were exposed to 5×10^8 R of gamma radiation and unirradiated samples of the same type of salt. Their tests were conducted at room temperature and at a constant load of 2500 psi for a period of 100 min. With the irradiated dome salt specimens and irradiated specimens of bedded salt that were loaded perpendicular to the bedding planes, they found that creep rates were a little less than with their unirradiated counterparts; however, with bedded salt loaded parallel to the bedding planes, a slightly higher rate of strain was observed in irradiated samples than in unirradiated salt. From these studies, they concluded that the radiation effect on creep rates in salt was small and would not prohibit the disposal of radioactive wastes in salt mines, either in domes or in bedded salt deposits.

It has been observed in many investigations of the deformation of specimens of rock salt that the strength is increased by confining pressure. LeComte[2] found that confining pressure, in addition to increasing the strength of salt, also serves to decrease the creep rate. His tests, which were conducted on artificial polycrystalline rock salt cylinders having a length of 1.25 in. and a diameter of 0.5 in., showed that, in tests at 104.5°C and 1000 psi axial stress, the effect of increasing the confining pressure to 14,700 psi was to decrease the creep rate by a factor of 4. Handin,[3] using cylindrical specimens of natural rock salt from the Hockley mine, Texas, also showed that confining pressures increase the strength of salt. His tests were conducted at room temperature and under confining pressures as high as about 75,000 psi.

Serata[4] has reported successful extrapolation of creep data on scale-model specimens of mine pillars of salt to creep rates in salt mines. His models were 5-in. cubes that contained semicylindrical openings midway along the four vertically aligned faces to form the pillar and surrounding rooms. Confinement was provided at the

[1] B. D. Gunter and F. L. Parker, *The Physical Properties of Rock Salt as Influenced by Gamma Rays,* ORNL-3027 (1961).

[2] P. Lecomte, *Creep and Internal Friction in Rock Salt,* Harvard University, unpublished doctoral dissertation, 1960.

[3] J. Handin, "An Application of High Pressure in Geophysics: Experimental Rock Deformation," in *Trans. ASME* 75, 315–24 (1953).

[4] S. Serata, "Continuum Theory and Model of Rock Salt Structures," *Second Symposium on Salt,* Jon L. Rau (ed.), The Northern Ohio Geological Society, Inc., Cleveland, Ohio, 1966, pp. 1–17.

top and bottom of the specimens to restrict the lateral movement of salt in the roof and floor portions. Tests were carried out on two models at room temperature and with pillar width-to-height ratios of 10 and 16.6 and axial loads of 5300 and 4300 psi respectively. The results showed that the creep curves for the specimens were parallel and that the rate of creep continued to decrease with time to about 135 days.

Obert,[5] using a slightly different type of pillar model, has also extrapolated creep data on model tests to mine conditions. His models were cylindrical and used steel confining rings at the top and bottom of the specimens to restrict the lateral flow of salt in the roof and floor. Tests were conducted on samples of rock salt, as well as on trona and potash ore. Axial loads for the tests on pillars having a width-to-height ratio of 4, conducted at room temperature for periods of 1000 hr, ranged from 2000 to 12,000 psi. His creep curves for rock salt showed an initial high rise in deformation with time, followed by a period where the creep rate decreased with time and finally by what appeared to be steady-state creep.

Dreyer and Borchert[6] have used rectangular model specimens to determine the ultimate strength of mine pillars in German rock salt works. In a later work Dreyer fitted an empirical equation giving the pillar breaking strength to a series of tests on models of kieserite-hardsalt.[7] The roof and floor portions of all models were restrained by steel jackets, while the cross-sectional areas of the pillars tested varied from 100 to 225 cm^2, with pillar heights ranging from 2.5 to 10 cm.

12.2 PRELIMINARY INVESTIGATIONS

12.2.1 Sample Preparation and Test Procedure

To simulate pillar, roof, and floor conditions that would exist in mined cavities in rock salt, sample specimens were fabricated to represent scale models of salt pillars and their surrounding rooms. The test specimens used in this work were cylindrical, with a portion of the center ground out to form the pillar and surrounding rooms (Fig. 12.1). By cementing steel rings around the ends of the samples with epoxy resin, effective confining pressure was applied to the roof and floor portions of the models when they were loaded. Constant uniaxial loads were applied to the models by hydraulic compression testers having capacities up to 300,000 lb. Cavity closure was measured by mounting two dial gages 180° apart on the rings. All tests were conducted in a controlled-temperature room, equipped with automatic dehumidifiers to prevent condensation on the samples during extremely damp periods. Elevated-temperature tests were performed with the specimens inside a cylindrical heating jacket and with barrier heaters on top and bottom between the specimen and the platens.

Most tests were performed on model pillars fabricated from $5^{1}1/16$-in.-diam cores of rock salt taken in the mine of the Carey Salt Company, Lyons, Kansas. Similar cores for model tests were recovered from sample cubes of salt, measuring 1 to 2 ft on a side, taken from rock salt mines at Hutchinson, Kansas; Retsof, New York; Detroit, Michigan; Grand Saline, Texas; Cote Blanche, Louisiana; and Asse, Germany. In addition, a few rectangular-shaped models were cut from some of the sample blocks, and, in one case, an $11\frac{1}{2}$-in.-diam core was taken for model testing. For model preparation, all cores were first cut to their approximate desired length by band saw and then finished by machine sanding. Next, steel confining rings (ASTM A-108 grade 1018), which were $\frac{5}{8}$ in. thick and $\frac{1}{16}$ in. greater in inside diameter than the salt cores, were affixed to the tops and bottoms of the cores using

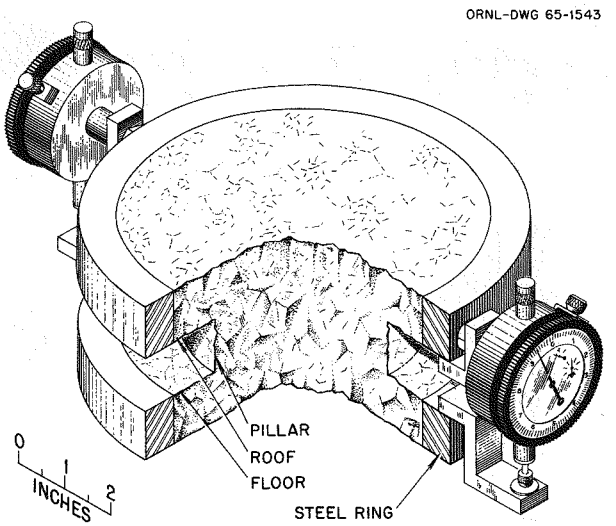


Fig. 12.1. Pillar Model.

[5] L. E. Obert, "Deformational Behavior of Model Pillars Made from Salt, Trona, and Potash Ore," *Proc. Sixth Symp. on Rock Mechanics,* Rolla, Missouri, 1964, pp. 539–60.

[6] Wolfgang Dreyer and Hermann Borchert, "Zur Druckfestigkeit von Salzgesteinen," *Kali und Steinsalz,* Heft 7, 234–41 (1961).

[7] W. Dreyer, "Die Bedeutung von Modellversuchen aus Salzgestein fur die Beurteilung gebirgsmechanischer Probleme im Kalibergbau," *Berkgakademie,* Heft 3, 157–62 (1964).

Ciba Araldite 502 epoxy and Ciba hardener 951 for samples heated up to 100°C. For temperatures in excess of 100°C, Ciba Araldite 6005 epoxy and pyromellitic dianhydride (PMDA) hardener were used. The 1-in.-high unconfined center portion of the sample was then ground out, using a sanding disk attached to a standard drill press, to form the size pillar desired. Sheet Teflon greased with a mixture of silicon grease and graphite was inserted between the tops and bottoms of the samples and the platens of the compression machines to reduce the friction between the salt and the platens to an insignificant amount. The importance of eliminating the friction between the salt specimens and the test machine platens in ascertaining a true measure of the laboratory deformation of rock salt has been investigated by others.[4,5]

To ensure a uniform temperature within the heated model specimens, Chromel-Alumel thermocouples were emplaced in $^1/_{16}$-in.-diam holes drilled into the center of the pillar, as well as at the outer edge. A 12-point strip-chart recorder with a 0-to-350°C range was used to trace the temperature curves. A constant-voltage transformer was used in supplying 118 V ac to adjustable autotransformers which were used as temperature controls for the cylindrical heating jackets, as well as for the heaters in the platens at the top and bottom of the sample. In this manner temperatures were regulated to within 1 to 2% of the desired values.

In general, the same test procedure was used for all specimens to ensure uniformity. This procedure consisted in rapidly applying a compressive load corresponding to 75% of the testing load and releasing it and then applying a load of 85% of the test load, which was also immediately released. A base reading for the dial gages was then taken. These initial loadings served to seat the dial gages, used to measure deformation, and to set the platens firmly on the sample. The full test load was then applied to the specimen within a few seconds, and deformation was recorded, first at intervals of seconds, then minutes, and then at progressively longer intervals. Figure 12.2 shows a model being tested at room temperature in a compression machine.

Most tests were conducted at temperatures of 22.5, 60, 100, and 200°C for axial loads of 2000, 4000, 6000, 8000, and 10,000 psi. In addition, a few special tests were conducted on salt samples at loads as high as 15,000 psi. Duration of the tests varied from a few minutes for those specimens where the deformation rate was exceedingly fast to a single case where the sample was allowed to deform over a period of about $3^1/_3$ years. The most common test periods were about 500 to 1000 hr. For certain temperature and load combinations, duplicate or triplicate tests were run in order to obtain an approximate measure of variation from sample to sample. A total of about 110 pillar models were tested in these studies.

12.2.2 Simulation of Mine Pillars in Scale Models

The deformation characteristics of the rock are an extremely important consideration in the simulation of mine conditions in scale-model tests. For example, to determine the stability of mine pillars composed of plastic materials like rock salt, it is absolutely necessary to simulate in the models not only the mine pillar but also the roof and floor conditions. However, for brittle rocks like dolomite, the roof and floor apparently do not greatly affect the deformation of the pillar.

This has been illustrated in uniaxial tests of model mine pillars of rock salt and dolomite. In both cases the models were fabricated from $5^1{}^1/_{16}$-in.-diam cores. After cutting the cores to a length of 5 in., a portion of the center of the specimens was ground out as described earlier to form the pillar (1 in. high by 4 in. in diameter) and the surrounding roof and floor. Steel rings were then epoxied to the top and bottom portion of the samples to restrain laterally the rock in the roof and floor (as would be the case in actual mine workings). Type SR-4 wire strain gages were used in conjunction with a Baldwin-Lima-Hamilton type N strain indicator to determine radial stress on the rings. As seen in Fig. 12.2, three wire gages are attached at equidistant locations to the outside portion of each ring. Upon the application of axial stress, the deformation of the steel rings is measured by the strain indicator. The radial stress exerted by the rocks on the inner portion of the rings was calculated by use of the equation[5]

$$p = \frac{E\epsilon(b^2 - a^2)}{2a^2}, \tag{12.1}$$

where

p = internal pressure applied to the inside part of the ring,

ϵ = measured strain on the outside part of the ring,

a = inside radius of the ring,

b = outside radius of the ring, and

E = Young's modulus of elasticity for steel.

For rock salt samples tested at room temperatures, it was found that the radial stress exerted on the rings increased with increasing axial loads up to approxi-

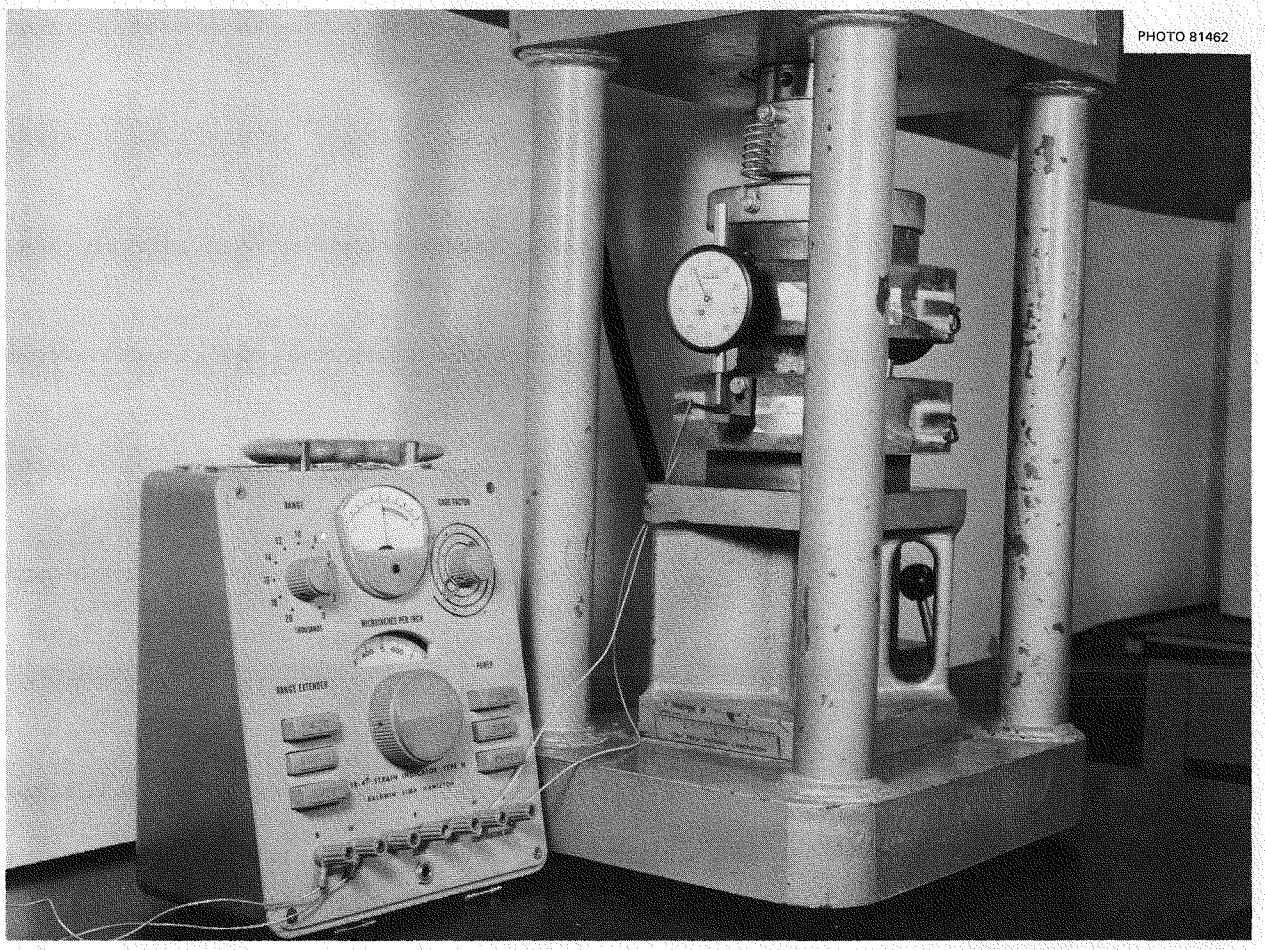


Fig. 12.2. Pillar Model in Compression Machine.

mately 75% (11,250 psi) of the axial load at 15,000 psi (see Fig. 12.3). However, for the dolomite samples, it was observed that the radial stress did not exceed about 5% of the axial stress of the pillar load, even at loads as high as 23,000 psi. These data indicate that for materials that deform plastically like rock salt, actual mine conditions are simulated best when the roof and floor portions of the models are constrained laterally. This allows confining stress in the roof and floor to be transmitted into the pillar (at least for samples having a width-to-height ratio of 4), thereby making the pillar stronger. For dolomite the relatively small values of radial stress measured on the confining rings of the models indicate that the roof and floor have less influence on the strength of the pillars; and, thus, the simulation of the roof and floor in models used to define mine pillar deformation in rocks of this type are not as critical as for rocks that deform plastically under the same conditions. (The reasons for the difference in loading rates on the salt and dolomite samples in Fig. 12.3 were the creep properties of salt and convenience in testing.)

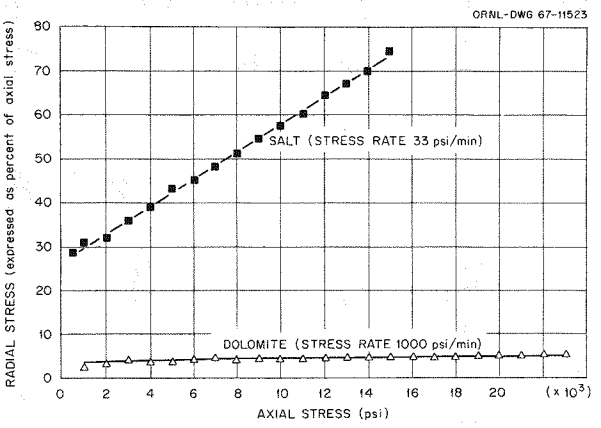


Fig. 12.3. Radial Stress in Rock Salt and Dolomite Pillar Models.

12.2.3 Size of Model Specimens

The scaling of mine works to a convenient size for laboratory testing is a matter of great concern in model studies of rock deformation, since all geologic features may not be adequately represented in scaled-down laboratory specimens. Perhaps the most important scaling considerations in regard to the salt mine structures are the size of the test specimens with respect to the grain size of the rock salt and the amount of salt above and below the mine pillars. Obert[8] has stated that reproducible results can be obtained when the pillars of the test specimens have a diameter of about 8 to 10 grains. Serata[9] has reported that specimens containing about 500 grains should be adequate for test purposes. Both of these conditions are met in the "standard test specimen" ($5\,^1/_{16}$-in.-diam core cut to 5 in. in length that includes a 1-in.-high by 4-in.-diam pillar).

To evaluate the effects of various salt thicknesses in the roof and floor of test models, several samples were tested having the same pillar dimensions of 4 in. in diameter by 1 in. in height, but with different thicknesses of salt ($^7/_8$, 2, 3, and 4 in.) above and below the pillar (see Fig. 12.4). In Fig. 12.5, which shows pillar deformation with time, it is observed that there is little difference in the deformation curves of the samples with 2 in. or more of salt above and below the pillar; however, in the specimen having only a $^7/_8$-in. layer of salt in the roof and floor, the amount and rate of deformation is markedly greater. It is concluded from these data, along with the measured values of radial stress in the roof and floor of model salt pillars as discussed above, that salt at least twice the height of the pillar should lie above and below any given pillar to approximate the true strength of actual mine pillars.

In addition to the tests discussed above, one specimen having dimensions twice that of the "standard model specimen," that is, an 8-in.-diam pillar 2 in. high with a roof and floor thickness of 4 in., was tested at a load of 4000 psi at 22.5°C. The deformation curve for this sample is seen in Fig. 12.6 to be essentially the same as that for the smaller "standard model" for the same type of rock salt. It is thus concluded that a $5\,^1/_{16}$-in.-diam core of rock salt 5 in. long, which is ground out in the center for a 4-in.-diam 1-in.-high pillar and therefore, contains 2 in. of salt in the roof and floor above and below the pillar, adequately simulates mine conditions where the pillar, roof, and floor are essentially all rock salt.

12.3 RESULTS OF MODEL PILLAR TESTS

In order to obtain data on the deformation of rock salt under temperature and pressure conditions that would be expected in an actual disposal operation, a series of model pillars, fabricated from rock salt from

[8]L. E. Obert, Applied Physics Laboratory, U.S. Bureau of Mines, College Park, Md., personal communication, 1964.

[9]S. Serata, Serata Geomechanics, Berkeley, Calif., personal communication, 1964.

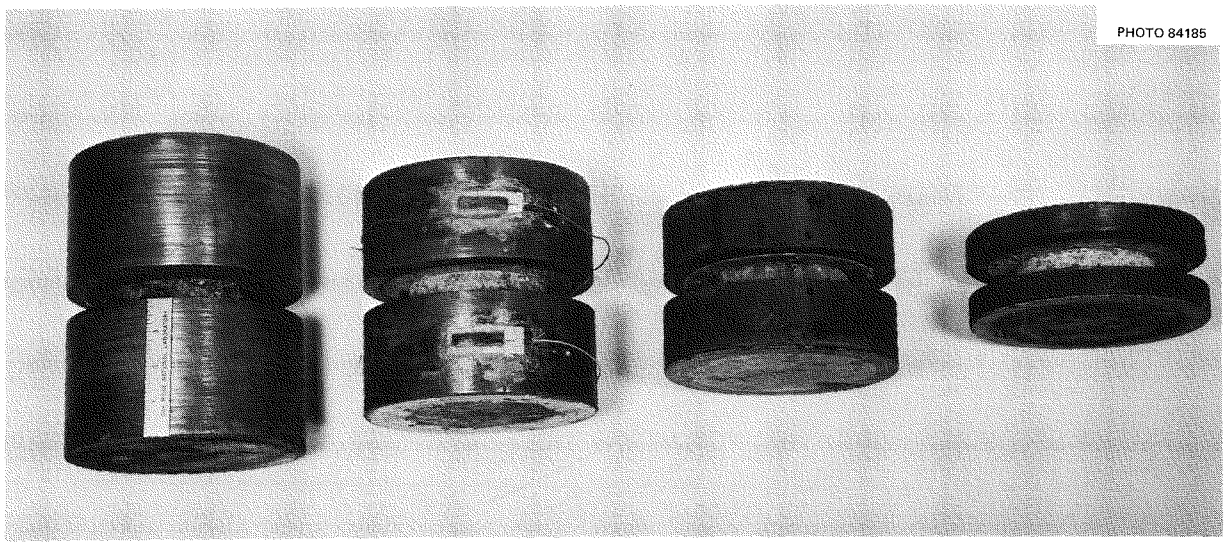


Fig. 12.4. Photograph of Pillar Models with $^7/_8$, 2, 3, and 4 in. of Salt in the Roof and Floor.

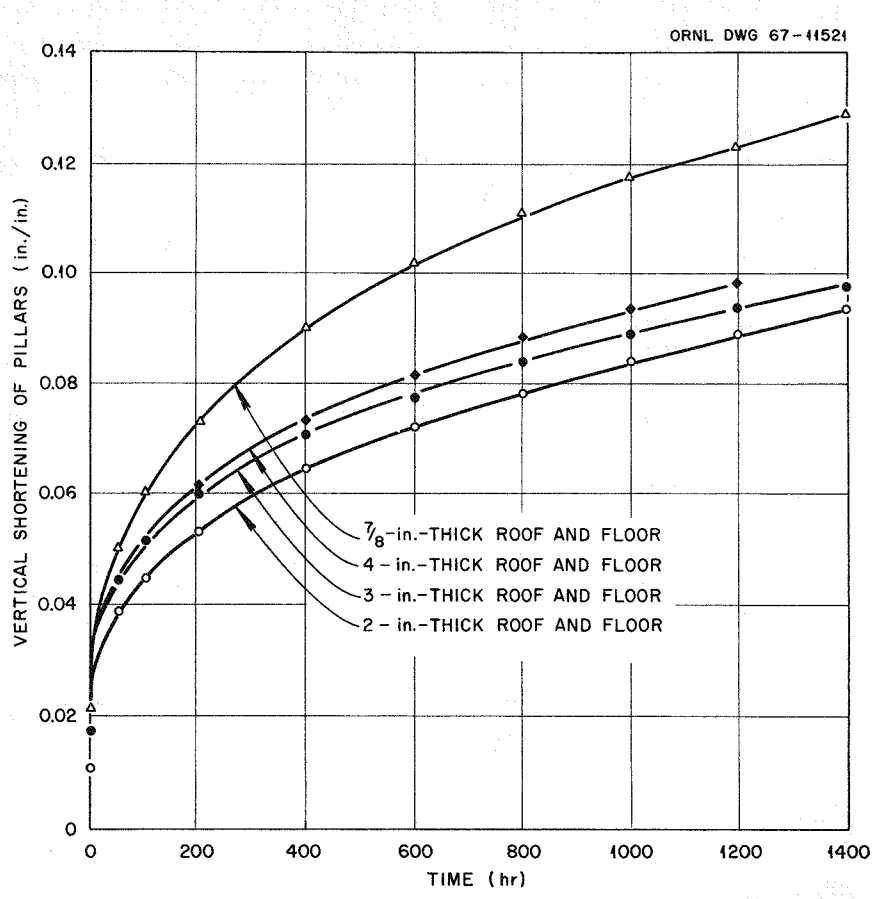


Fig. 12.5. Deformation of Pillar Models at 22.5°C and 6000 psi with 7/8, 2, 3, and 4 in. of Salt in the Roof and Floor.

the Lyons, Kansas, mine, were tested at all combinations of axial loads of 2000, 4000, 6000, 8000, and 10,000 psi and temperatures of 22.5, 60, 100, and 200°C. In addition, data on the effects of shale partings and pillar shapes on the deformation of rock salt, which must also be considered in an actual disposal operation, have been obtained from model tests. These data, along with field data from the Lyons mine, form the basis for predicting pillar behavior in salt cavities used for the disposal of radioactive wastes. Since the occurrence of rock salt in the United States is rather widespread, it is conceivable that many sites could be used for waste disposal operations. In order to make gross comparisons of the deformation of salt from one mine to another, model pillars fabricated from rock salt from five other mines in the United States and one German mine were tested at temperatures of 22.5 and 100°C for an axial load of 4000 psi. For the following tests the observed deformations are for salt samples from the Lyons, Kansas, mine unless otherwise stated.

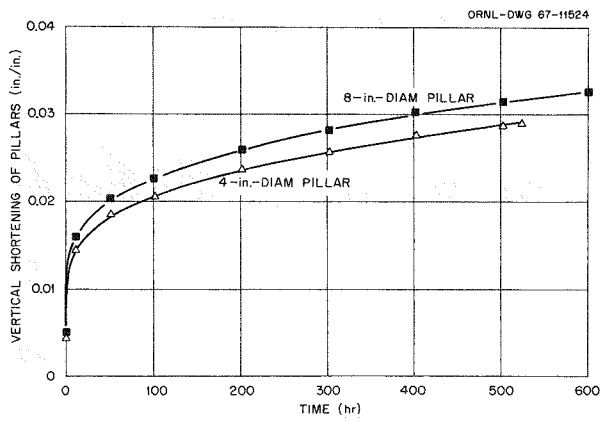


Fig. 12.6. Deformation of 4- and 8-in.-diam Pillar Models.

12.3.1 Effect of Load

Figure 12.7 shows deformation curves for model pillars of rock salt that have been tested at ambient temperature and at various stresses. All the curves show

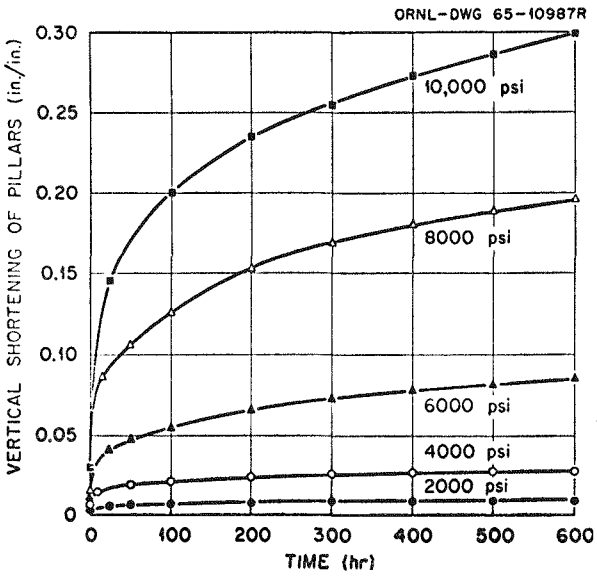


Fig. 12.7. Deformation of Pillar Models at 22.5°C.

some similarities, even though the stress for each curve is different. In each curve there is initially a high rate of deformation that decreases with time. This decrease in deformation rates is shown to continue to 600 hr. However, in longer-duration model tests, which will be discussed in more detail later, it has been observed that rates continue to decrease even after more than 29,000 hr ($3\frac{1}{3}$ years). It should be added here, too, that this is in agreement with measurements that have been made in salt mines which show that deformation rates are still decreasing with time in openings up to 12 years old.[10] In the figure it is also observed that the deformation of the pillars increases markedly with higher stresses. For the 2000-psi model the total deformation is 0.01 in. after 600 hr. Since the pillar was only 1 in. high before deformation, the pillar deformation is about 1%. It is also noted that for the sample tested at 6000 psi the deformation is 0.09 in. (9% deformed), while for the 10,000-psi sample the pillar has deformed 0.3 in. (30%) after 600 hr of testing.

12.3.2 Effect of Temperature

Perhaps even more significant than the increased pillar deformation with higher stress is the greatly accelerated deformation at elevated temperatures. In Figs. 12.8 through 12.12 pillar deformations with time for models tested at 2000, 4000, 6000, 8000, and 10,000 psi and at various temperatures are shown. Generally, in all cases, it is noted that there is initially a high creep rate that decreases with time, as in the case with models

[10] R. L. Bradshaw, W. J. Boegly, Jr., and F. M. Empson, "Correlation of Convergence Measurements in Salt Mines with Laboratory Creep Test Data," *Proc. Sixth Symp. on Rock Mechanics*, Rolla, Missouri, 1964, pp. 501–14.

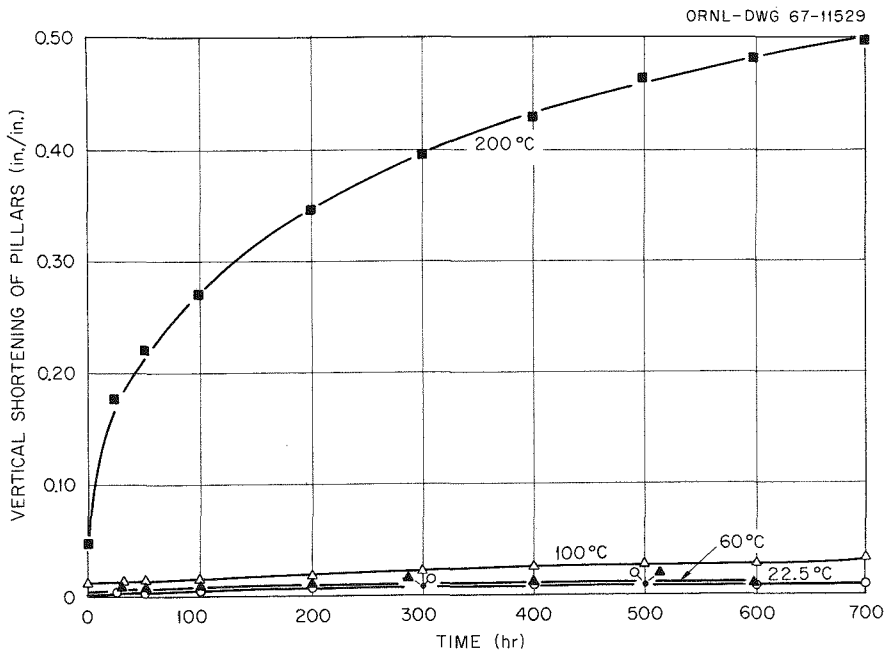


Fig. 12.8. Deformation of Pillar Models at 2000 psi.

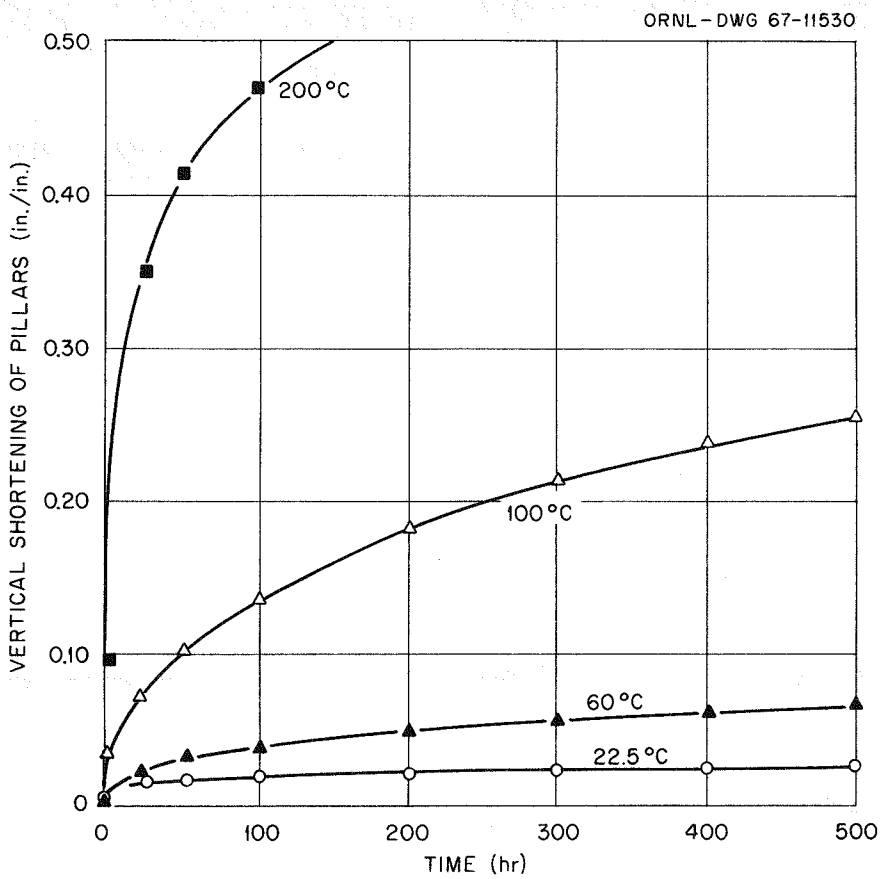


Fig. 12.9. Deformation of Pillar Models at 4000 psi.

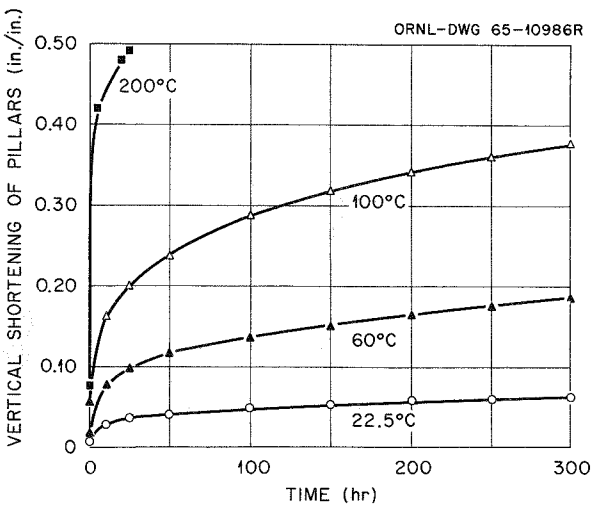


Fig. 12.10. Deformation of Pillar Models at 6000 psi.

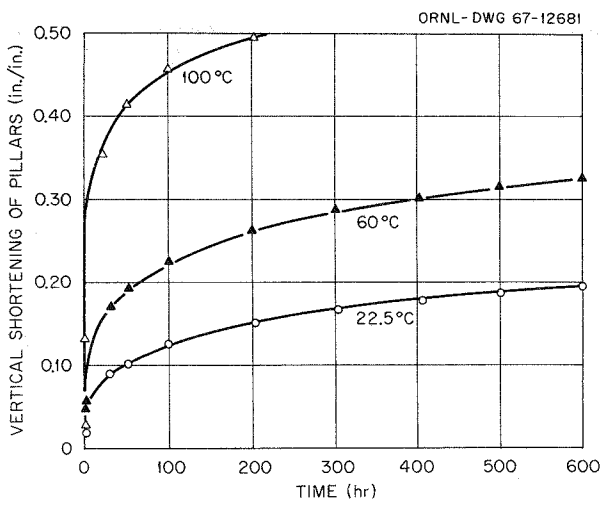


Fig. 12.11. Deformation of Pillar Models at 8000 psi.

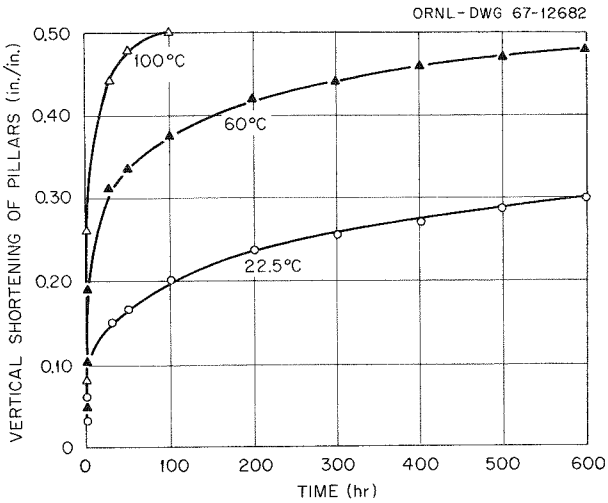


Fig. 12.12. Deformation of Pillar Models at 10,000 psi.

tested at room temperature. In the tests at 2000 psi (Fig. 12.8) it is observed that the effect on pillar shortening by raising the temperature to 60 and 100°C is not nearly so pronounced as at 200°C. At the latter temperature the pillar had deformed 50% after 700 hr, while the deformation at 60°C was less than 5% during the same period of time. In general, cavity closure is complete after about 0.5 to 0.6 in. (50 to 60%) of pillar shortening in models deformed at elevated temperatures. This is due to the lateral flowage of salt into the room opening from the pillar, as well as more or less vertical movement into the opening from the roof and floor, and will be discussed in more detail later. In the 4000-psi model (Fig. 12.9), it is noted that the same general pattern of increased deformation at higher temperatures is apparent, but the pillar shortening at 60 and 100°C is considerably more pronounced than that in the 2000-psi tests (Fig. 12.8). From the curves for the models loaded to 6000 psi (Fig. 12.10), it is noted that in the specimen tested at 22.5°C the 1-in.-high pillar has deformed about 0.06 in. (6%) after 300 hr, while the model tested at 60°C has deformed about 0.19 in. (19%), and at 100°C about 0.38 in. (38%). At 200°C the model deformed more than half an inch (50%) in less than 30 hr. In the 8000- and 10,000-psi tests (Figs. 12.11 and 12.12), it is seen that exceedingly large deformations occur in relatively short periods of time, even at salt temperatures of 60 and 100°C. The deformation at 200°C was so rapid that the desired load of 8000 psi could not be reached before complete cavity closure. The model tests thus confirm the belief that closure rates for actual mine openings used for disposal of radioactive wastes will be greatly accelerated with the increase in temperature of the salt.

Further examination of the effect of loading at elevated temperatures can be made in Figs. 12.13 to 12.15. At 60°C (Fig. 12.13), it is seen that the deformation of the model loaded to 10,000 psi after 600 hr is about 50 times greater than the model loaded to 2000 psi, but only about twice that of the model loaded to 6000 psi. With the models tested at 100 and 200°C (Figs. 12.14 and 12.15), the deformations at the various loads are not easily comparable, since flowage and thus cavity closures at these temperatures for all loads are very rapid.

These data clearly show that at 200°C pillar temperatures severe structural stability problems could occur in subsurface salt excavations, even at superincumbent loads as low as 2000 psi. However, heat transfer studies have shown that it will take years for pillars to approach this temperature, and by that time the rooms will have long since been backfilled with crushed salt.

Salt pillars subjected to elevated temperatures apparently behave like pillars under higher stresses. This is illustrated in Fig. 12.16, which shows the deformation with time of models at various temperatures and stresses. It is of interest that the deformational behavior of the salt pillar tested at 4000 psi at 60°C is approximately the same as the behavior of the sample tested at 6000 psi and 22.5°C. Also, the curve for the 4000-psi model at 100°C shows behavior similar to that of the 6000-psi sample at 60°C. This strongly suggests that the net effect of elevated temperature is essentially the same as that of increased pillar stress.

12.3.3 Effect of Temperature Elevation After Initial Loading

The general effect of heat on the deformation of rock salt is discussed above. In the tests described here, which were carried out to establish empirical relations between temperature, pressure, and time, the samples were first heated and then loaded. However, under actual disposal conditions the mine pillar would be loaded first, and then the salt would be heated as the rooms are filled with waste. To define pillar deformation under the latter conditions, a model specimen was loaded to 4000 psi at room temperature of 22.5°C for about 800 hr; then the temperature was increased to 100°C. In the case of both initial loading and elevation of the temperature, it is observed in Fig. 12.17 that the deformation curve rises sharply initially and then continues to rise, but at a decreasing rate; however, in

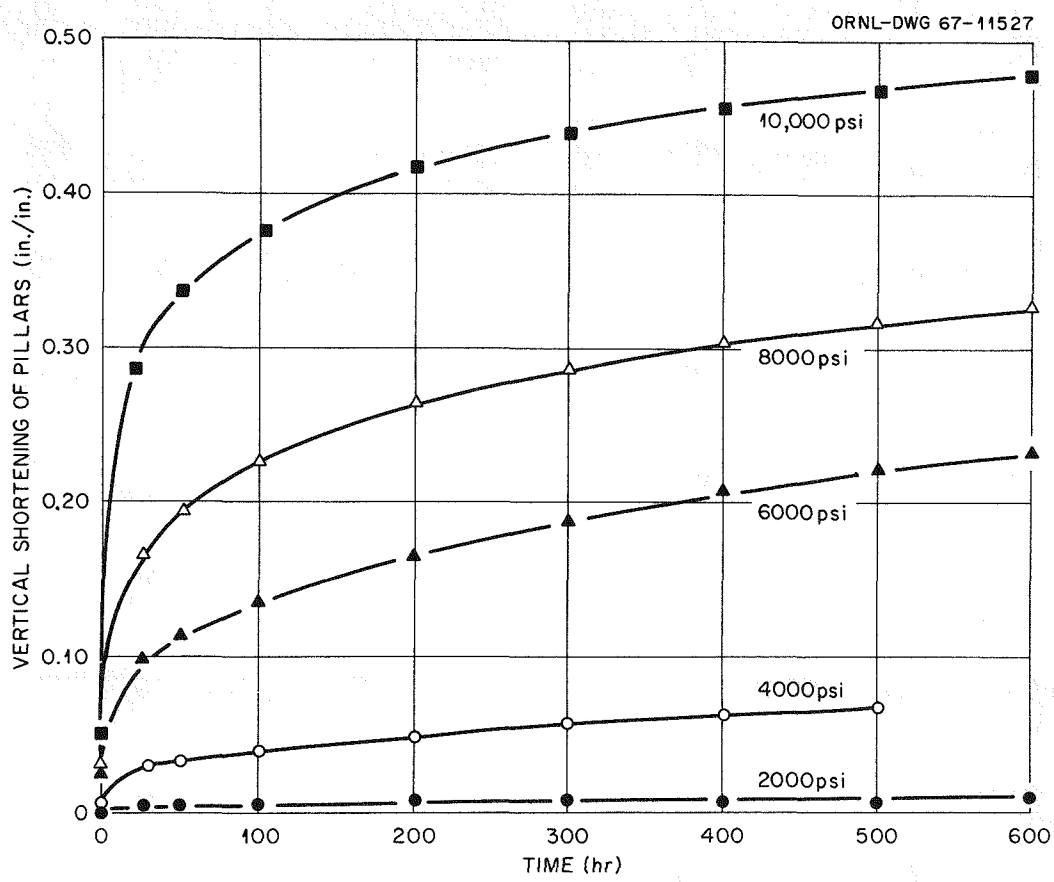


Fig. 12.13. Deformation of Pillar Models at 60°C.

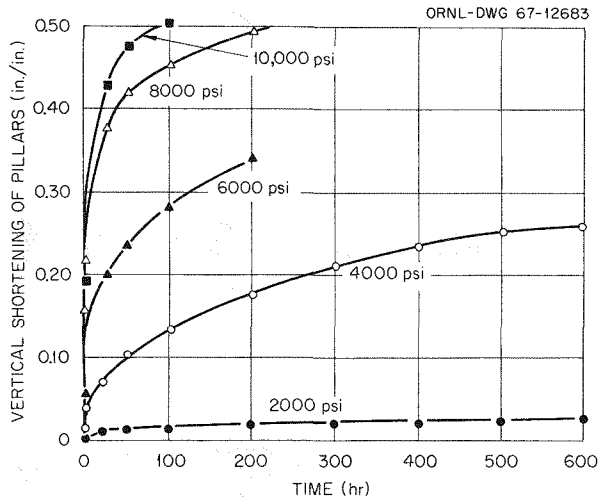


Fig. 12.14. Deformation of Pillar Models at 100°C.

the latter case the total deformation is significantly greater. It is also of interest that upon the application of heat (the temperature of the salt was raised from 22.5 to 100°C over a period of about 4 hr), there was a corresponding increase in the load on the sample. This increase of load, which was due undoubtedly to thermal expansion of the salt, attained a peak value of 4640 psi (a 16% increase) after the salt had reached a temperature of about 80°C, approximately 2 hr after the initial temperature rise. The linear coefficient of thermal expansion of salt is about 40×10^{-6}. Thus for a temperature rise of about 77.5°C, the linear expansion for a 5-in.-high salt cylinder would be about 0.0155 in. Furthermore, since four-fifths of the length of the model salt cylinder was confined by steel rings, which reduced the expansion in a radial direction, it is apparent that the vertical expansion of the salt speci-

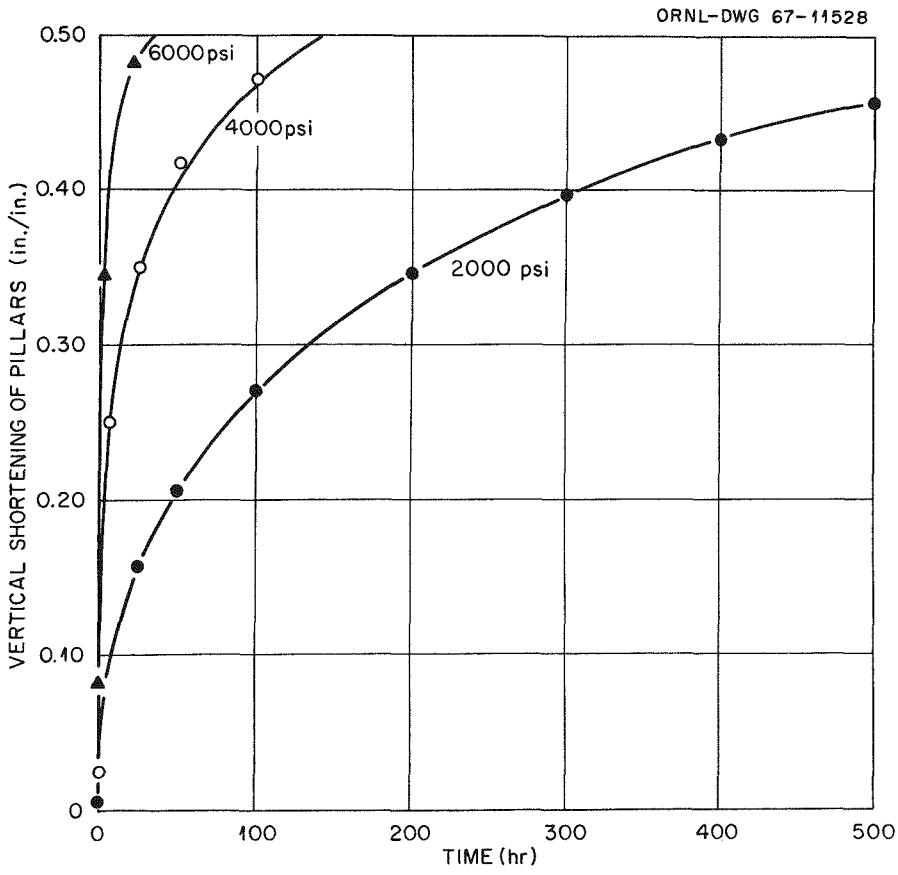


Fig. 12.15. Deformation of Pillar Models at 200°C.

men would be somewhat greater than the linear expansion. (The volumetric or cubic expansion of salt is approximately three times the linear expansion, since sodium chloride is isometric.) It is unlikely that the increase in load was due to any increase in the temperature of the hydraulic fluid which drives the ram in the test machine, since 2-in.-thick blocks of a solid insulation material (Transite) were placed between the heated specimen and the platens of the test device. Thus no significant amount of heat would be expected to reach the hydraulic fluid during the 4-hr period of the temperature rise. It is also significant that by the time the salt temperature had reached its maximum value of 100°C, the load had decreased to a static value of 4000 psi. This test shows that some increase in the load on salt pillars will occur with a significant rise in temperature; however, because of the accelerated flow of salt at elevated temperatures, the load is rather quickly relieved. Since the temperature rise in the salt in an actual mine disposal facility will rise very slowly (probably over periods of many months to years), it is difficult to state precisely, based on laboratory tests of pillar models that are uniformly heated within a few hours, the nature of the increase in pillar loading and the relief of this excess load through salt flow.

In general the net effect of elevating the temperature of model pillar specimens that have undergone deformation at lower temperatures is a renewed cycle of accelerated deformation that is very similar to the deformation of samples that have been tested only at the higher temperatures. This is visible in Fig. 12.18, which shows the deformation curve for a model that was deformed at a load of 6000 psi and at a temperature of 22.5°C for 115 hr, after which the temperature was increased to 100°C and the sample tested for several hundred more hours. Also shown is the deformation curve for a model pillar that was tested only at a load of 6000 psi and 100°C. By originating the latter curve at the point where the temperature is increased to 100°C for the former, it is seen that the

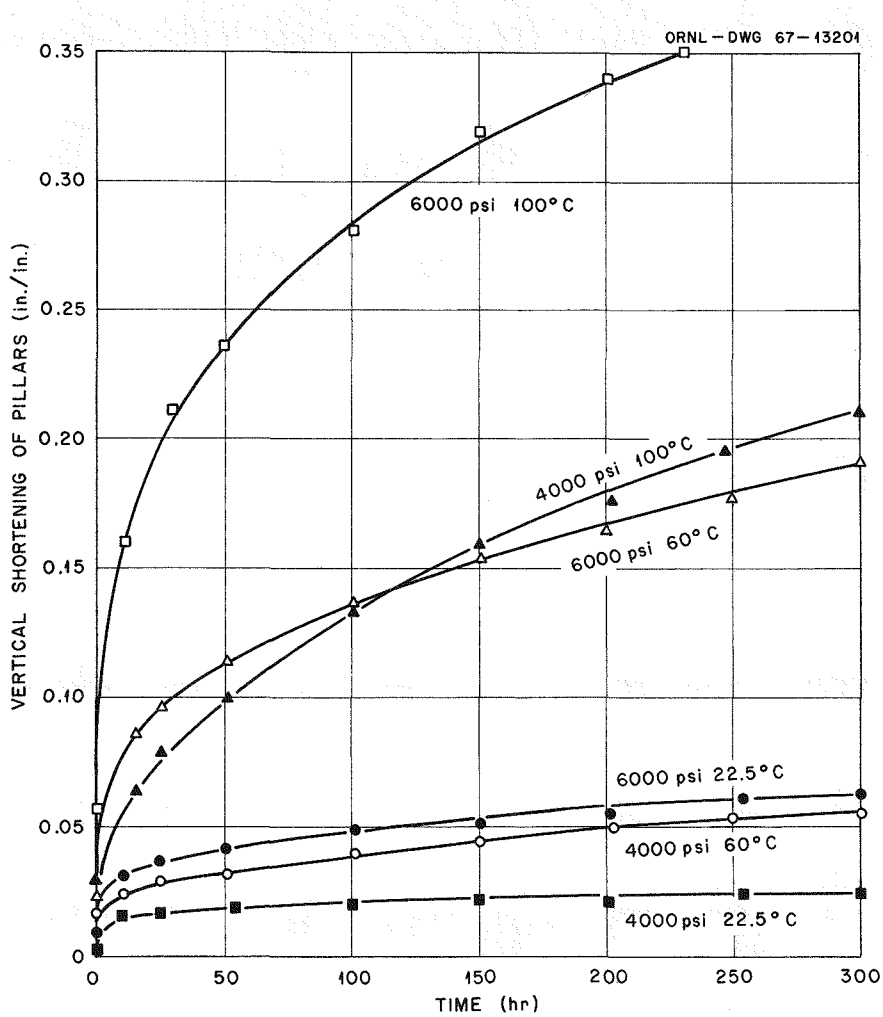


Fig. 12.16. Deformation of Pillar Models at Various Temperatures and Pressures.

two curves for 100°C and 6000 psi are almost identical. Since the total deformation for the ambient-temperature portion of the sample is relatively small, only about 0.05 in. in 115 hr, in comparison with that occurring after the elevation in temperature, it is not surprising that the initial deformation does not appreciably affect that part of the curve where the temperature is increased to 100°C.

A second illustration showing the effect on deformation of increasing the temperature of a model specimen that has been deformed at a lower temperature is seen in Fig. 12.19. Here it is observed that one specimen was deformed at a load of 6000 psi and at a temperature of 64°C for about 1000 hr before the temperature was increased to 100°C. It is seen that the acceleration in deformation is not as great as that of the test described previously, even though the deformation is conspicuous. This is probably due to the smaller temperature rise differential in the latter case. It is also observed that the deformation curve of the sample tested only at 6000 psi and 100°C approaches the former curve, even though it does not do so as rapidly as in the previous example. The test was terminated before the total pillar shortening for both samples was identical.

These tests strongly suggest that the total pillar shortening for model specimens that have been deformed under one temperature and then elevated to another will be about the same as that which models with no previous history of laboratory deformation would experience in a relatively short period of time if they were tested only at the same elevated temperature and load.

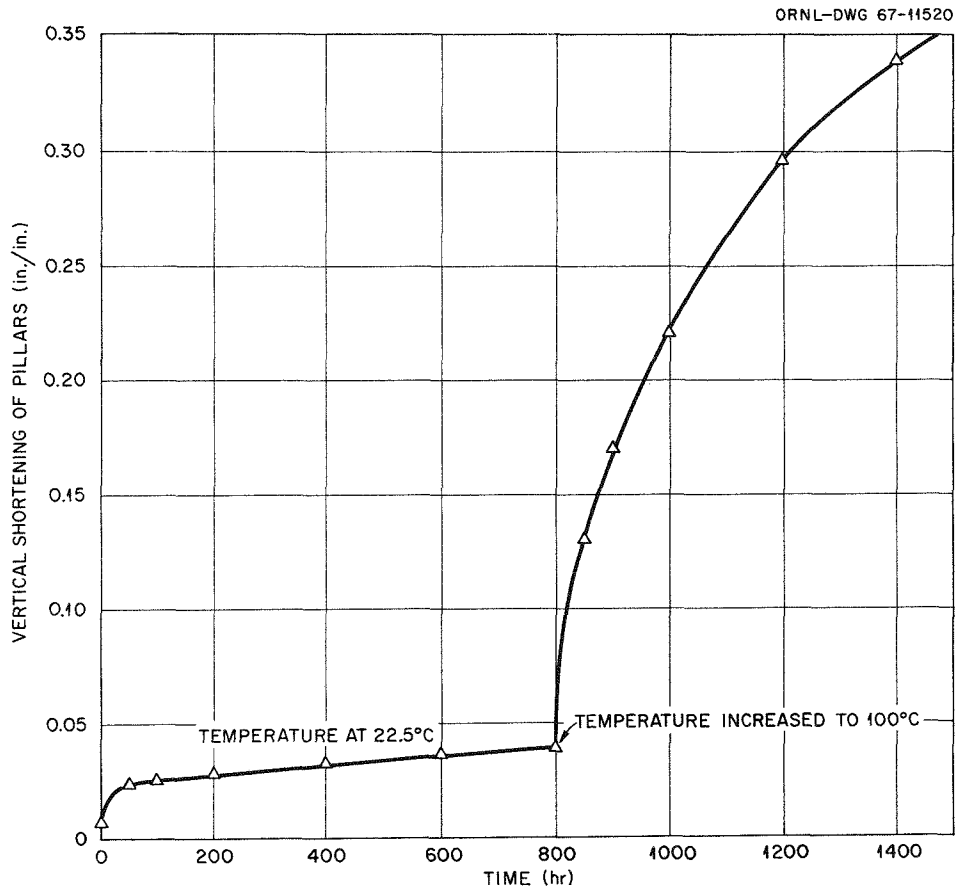


Fig. 12.17. Deformation of Pillar Model at 4000 psi and 22.5 and 100°C.

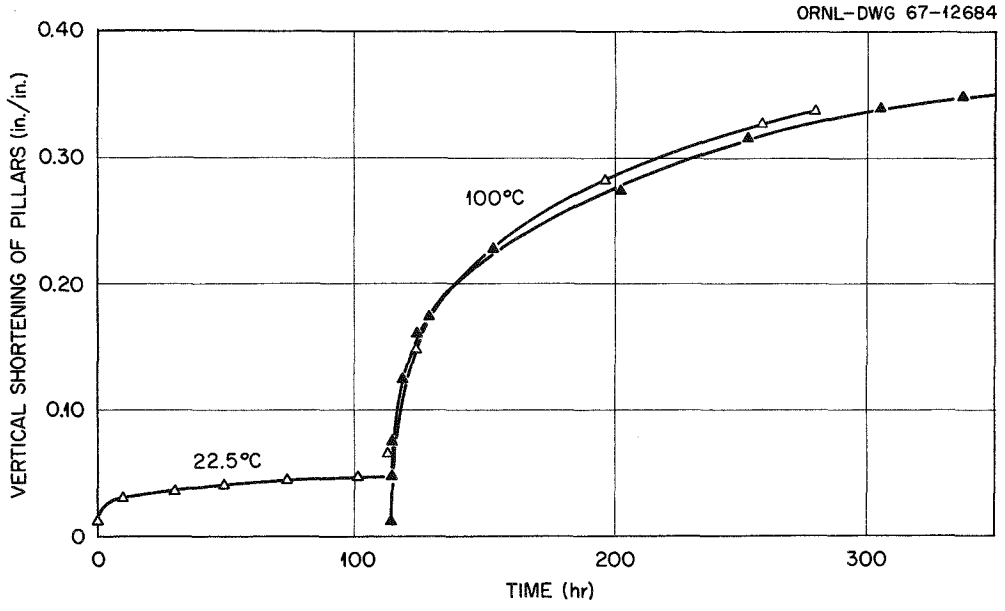


Fig. 12.18. Deformation of Pillar Models at 6000 psi and 22.5 and 100°C.

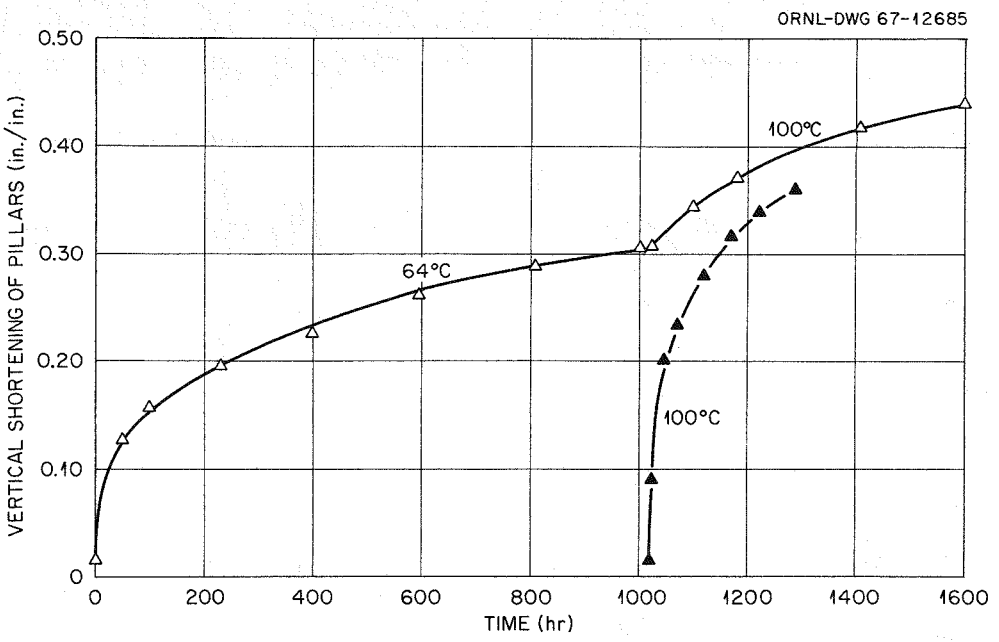


Fig. 12.19. Deformation of Pillar Models at 6000 psi and 64 and 100°C.

12.3.4 Effect of Shale Partings

Even though some salt deposits, such as salt domes, are essentially free of other intercalated rocks, most bedded deposits contain lithologic discontinuities of dolomite, shale, anhydrite, and other materials. For instance, the 300-ft-thick salt sequence at Lyons, Kansas, is only about 60% NaCl, with the other 40% being mostly shale and anhydrite. In many cases these other materials may form a part of the roof, floor, or even the pillars in a mine and thus enter into the deformation of the openings. In Fig. 12.20 the occurrence of thin shale beds in salt mines is depicted. In the one case, thin shales are shown at the top and bottom

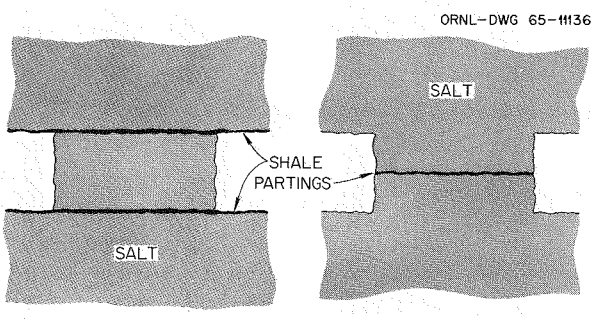


Fig. 12.20. Sketch Showing Lithologic Discontinuities in Salt Mines.

of a mine pillar, thus separating the pillar from the floor and ceiling. Shale beds such as this are common in bedded salt, and in many cases the salt is mined or falls to these partings, since they serve as effective friction reducers. In the other case a single shale bed occurs in the center of the pillar, with salt continuing uninterrupted from the pillar into the areas above and below. The presence of these partings, even though they are quite thin, can have a significant effect on the rate of cavity deformation, depending on whether the shale is at the top and bottom of the pillar or in the center. This is shown in Fig. 12.21, where deformation curves are presented for model salt pillars that have been deformed (*a*) without any simulated shale partings, (*b*) with simulated shale partings at the top and bottom of a pillar, and (*c*) with a simulated shale parting in the center of the pillar. Thin sheets of Teflon lubricated with grease and graphite serve as friction reducers and thus simulate shale partings. Analysis of data and observations from the Kansas mines indicate that the shale partings do have a lubricating effect, but not so marked an effect as do the Teflon sheets. Therefore, the actual effects to be expected in a mine would be somewhere between these two extremes shown in Fig. 12.21. With the model having no simulated shale partings and the model where the shale parting is in the center of the pillar, the deformational curves are almost identical, both showing about 0.03 in. (3%) deforma-

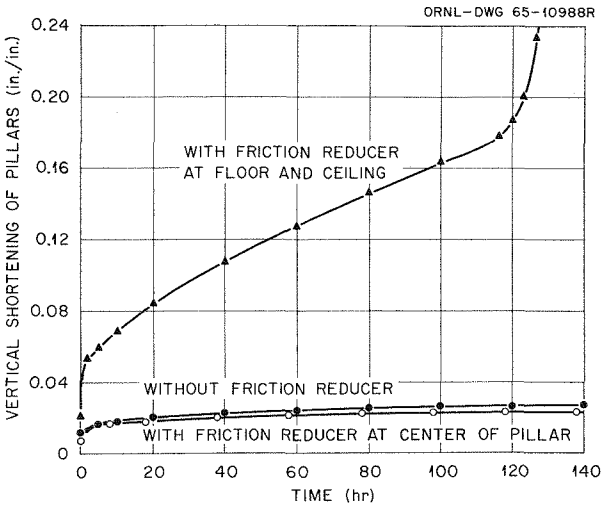


Fig. 12.21. Deformation of Pillar Models at 4000 psi and 22.5°C With and Without Simulated Shale Partings.

tion after 140 hr of testing. However, in the model with friction reducers at the top and bottom of the pillar, the deformation proceeds initially at a very fast rate before it begins to decrease with time. The model appears to then deform at a constant rate for a short time and then at an increasing rate, resulting in sudden failure after less than 130 hr. It is also of interest that in models with no simulated shale partings, sudden or catastrophic pillar failure could not be induced even under stresses as high as 15,000 psi.

Excavations in bedded salt deposits may sometimes contain shale beds only at the top or only at the bottom of pillars. In Fig. 12.22 the behavior of model pillars with natural shale beds at the tops of the pillars is compared with the deformation of a model having a simulated shale parting and a model without shale partings. All of the specimens with shale partings show, as expected, greater deformation than the specimen without shale. In the specimen with the Teflon simulated shale parting, the deformation rate is initially lower than the models with the natural shales, but the deformation rates in the latter samples decrease at a more rapid rate than in the specimen with the simulated shale. The thickness of the natural shale parting is approximately $\frac{1}{8}$ in. in the model showing the lower deformation curve, while the remaining one is composed essentially of a shale roof and a rock salt pillar and floor. This difference in thickness of the shale section in the models probably accounts for the variation in deformational behavior.

The accelerated deformation rate of the models when simulated shale partings occur at the top and bottom of

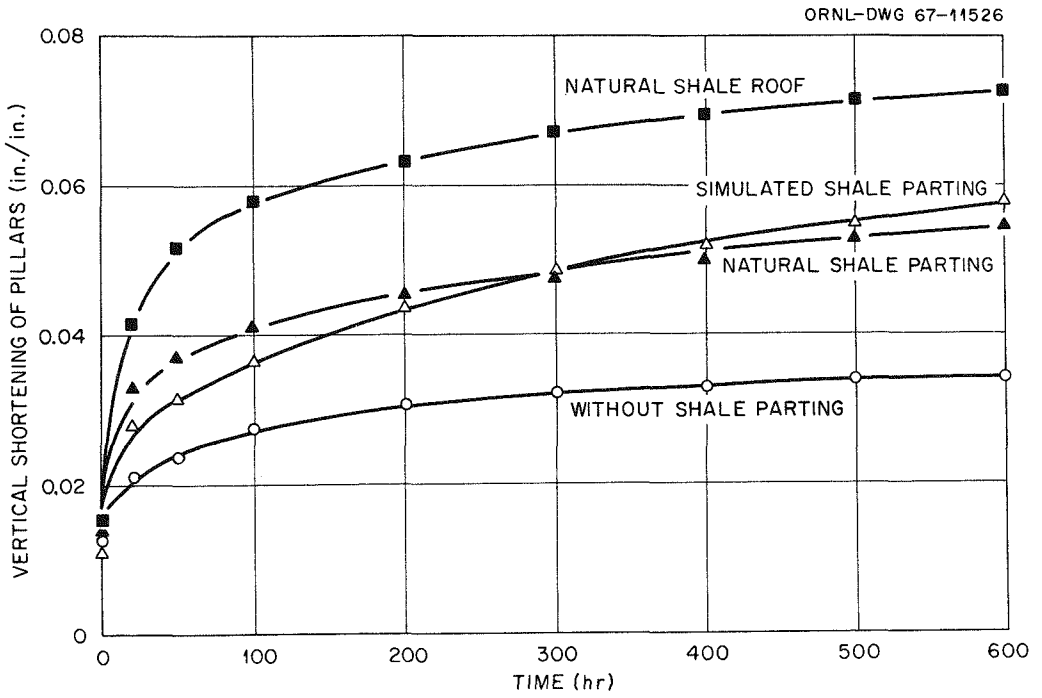


Fig. 12.22. Deformation of Pillar Models at 4000 psi and 22.5°C With Natural and Simulated Shale Partings and Without Shale Partings.

the pillars apparently results from the more or less independent deformation of the pillar. When there are no partings at the top and bottom of the pillar, or even if the parting is in the center of the pillar, there is an interlocking effect of salt crystals from the pillar to the roof and floor which serves to allow the pillar, roof, and floor to deform more or less as a single unit. However, when partings exist between the pillar and the roof and floor, they serve as effective friction reducers which consequently allow the pillar to deform more independently of the roof and floor, so horizontal confining pressures in the roof and floor are not completely transmitted into the pillar.

In addition to the occurrence of interbedded shale partings in the salt comprising the mine pillars, it is also recognized that thin shale beds occur in the roof and floor of the excavations at various distances above and below the mine pillars. To determine the effect of these shales on pillar deformation, a model was fabricated with simulated shale partings in the roof and floor of the sample 1 in. from the top and bottom of the pillar. The deformation curves for this sample, for a model with no shale partings, and for a model with only $\frac{7}{8}$ in. of salt above and below the pillar are shown in Fig. 12.23. It is observed that the deformation of the model with simulated shale partings is somewhat greater than the "standard" model with no shale partings but is about the same as the model with only $\frac{7}{8}$ in. of salt above and below the pillar. (The "standard" models contain 2 in. of salt above and below the pillar.) From this test it is concluded that shale partings in the roof and floor portions of scale models of mine pillars can cause a slightly accelerated rate of deformation. Presumably, the effect of these shale partings at various distances above and below the pillar could be produced by simply testing models having various thicknesses of salt above and below the pillar. Even though this has not been verified in model tests, it appears that the nearer the shale parting lies to the pillar, the greater the deformation. Also, it would seem from the previously discussed tests for determining the optimum model size that when the shale partings lie as much as two pillar heights from the top or bottom of the pillar, they will not significantly affect the deformation of the pillar.

A cross-sectional view (model was sawed in half) of the model with simulated shale partings (after deformation) is shown in Fig. 12.24. Note that the simulated shale parting is no longer horizontal but that the salt outward from the center has flowed toward the cavity opening. This behavior is in agreement with the deformational behavior of other models discussed later.

12.3.5 Effect of Pillar Shapes

The width-to-height ratio of salt pillars is an important consideration in predicting mine closure. This is

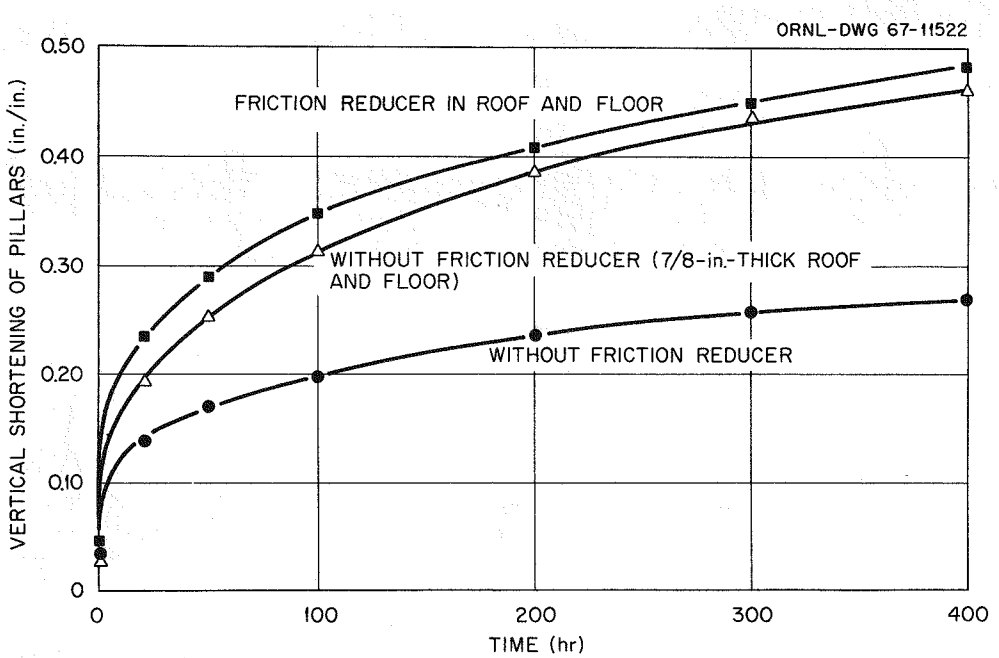


Fig. 12.23. Deformation of Pillar Models at 10,000 psi and 22.5°C With and Without Simulated Shale Partings.



Fig. 12.24. Photograph of Deformed Pillar Model with Simulated Partings in the Roof and Floor.

illustrated in Fig. 12.25, which shows pillar deformation with time for models for which the ratios of width (diameter) to height were 2, 3, and 4. All pillars were originally 1 in. in height, while their widths were 2, 3, and 4 in. From the curves it is seen that pillar shortening proceeds at a faster rate with the models having smaller diameter-to-height ratios. Thus pillar strength increases with increasing width-to-height (w/h) ratios. For instance, after 800 hr of testing, it is observed that the $w/h = 3$ sample had deformed about 0.0435 in., approximately 43% more than the $w/h = 4$ specimen, which had deformed only about 0.0305 in. The $w/h = 2$ pillar showed an even greater deformation of 0.0525 in.; this is 73% more pillar shortening than the $w/h = 4$ sample after the same period of testing.

In addition to the tests discussed above, a few models having rectangular pillars were deformed. (All previously deformed model pillars were cylindrical.) These models had overall dimensions of 6.45 by 3.94 in., with pillar dimensions of 5.01 and 2.51 in. The lengths of the pillars were, therefore, approximately twice their widths, and the salt extraction was about 50% (roughly the same as that for the cylindrical samples). Under these conditions, as shown in Figs. 12.26 and 12.27, significant differences in pillar deformation are apparent when the rectangular specimens are compared with the cylindrical specimens having the same horizontal cross-sectional areas. In Fig. 12.26, which shows the deformational curves for a rectangular specimen and a cylindrical specimen tested at 4000 psi and 22.5°C, it is apparent that the rectangular pillar is weaker than its cylindrical counterpart. After 1000 hr of testing, the former had deformed approximately 40% more than the latter. Both samples were fabricated from salt taken

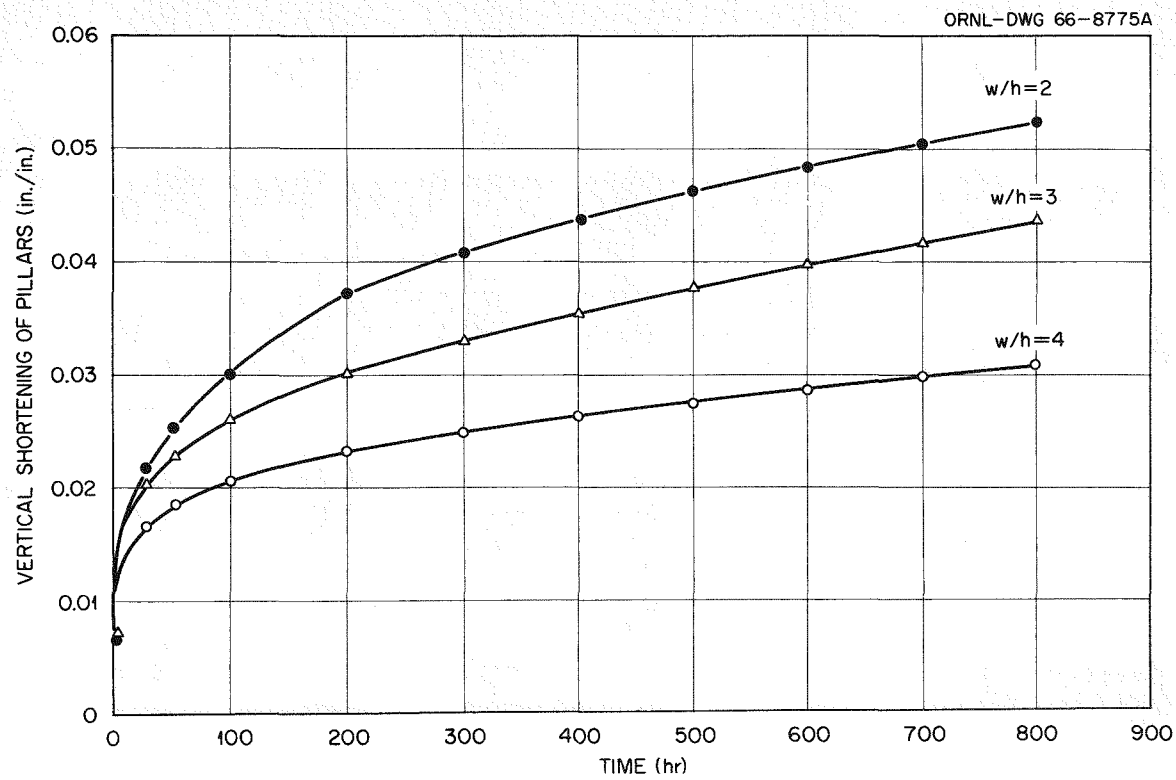


Fig. 12.25. Deformation of Pillar Models at 4000 psi and 22.5°C with Width-to-Height Ratios of 2, 3, and 4.

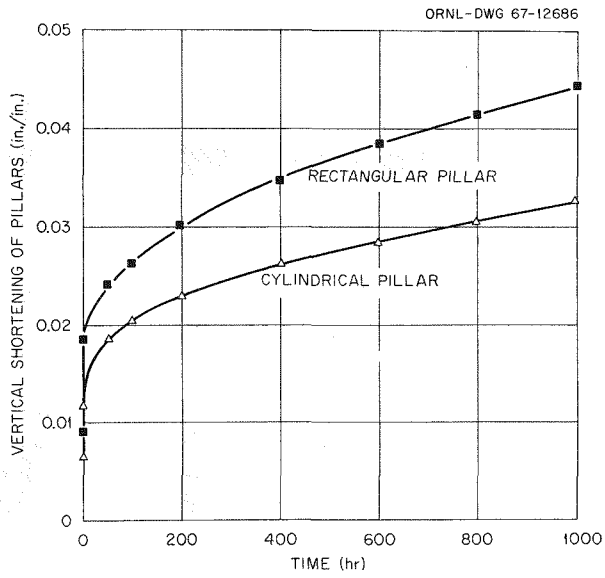


Fig. 12.26. Deformation of Cylindrical and Rectangular-Shaped Pillar Models at 4000 psi and 22.5°C.

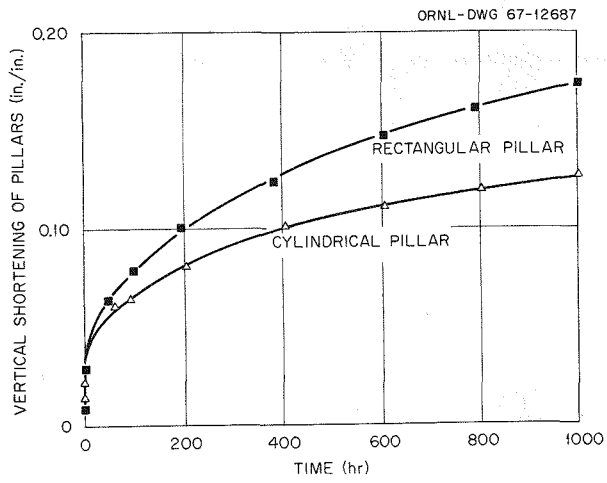


Fig. 12.27. Deformation of Cylindrical and Rectangular-Shaped Pillar Models at 6000 psi and 22.5°C.

from the mine at Lyons, Kansas. The same pattern of deformation is observed in Fig. 12.27, which shows the deformation of dome salt (Grand Saline, Texas) at an axial load of 6000 psi and at a temperature of 22.5°C. The deformation in this case is also about 40% more for the rectangular specimen than for the cylindrical one after about 1000 hr.

The greater strength of cylindrical pillars may be explained, in part, by the apparently high concentrations of stress at the corners of the rectangular pillars, which lead to spalling of the salt at these locations and, thus, to reductions in the cross-sectional area over which the loads are distributed. Also, it would appear that as the lengths of rectangular pillars increase in relation to their widths (for the same total cross-sectional area), the pillars will be correspondingly weaker. This is due, presumably, to reductions in the transmission of confining stresses from the roof and floor of the specimens to the pillars, as would also be the case for pillars having width-to-height ratios less than 4. It was shown earlier, in the case of specimens having shale partings at the tops and bottoms of the pillars, that when confining stresses are not transmitted into the pillars from the roofs and floors, the pillars are considerably weaker than when confining stresses are effectively transferred into the pillars.

12.3.6 Comparisons of Salt from Various Localities

In order to make a general comparison of the deformational behavior of rock salt from various localities in the United States, as well as from European deposits, tests were conducted at 4000 psi and at temperatures of 22.5 and 100°C on model pillars fabricated from salt samples taken from mines at Lyons and Hutchinson, Kansas; Retsof, New York; Detroit, Michigan; Grand Saline, Texas; Cote Blanche, Louisiana; and Asse, Germany. The Kansas salt is from a bedded deposit of Permian age, while the New York and Michigan salts are bedded and of Silurian age. The Grand Saline and Cote Blanche mines are situated in dome-type deposits. The Asse salt is mined from an anticlinal structure.

In the tests at 22.5°C, shown in Fig. 12.28, it is observed that the deformation curves for the Lyons, Hutchinson, Michigan, Cote Blanche, and Asse II mine deposits are strikingly similar; however, the Grand Saline mine salt deforms at a greater rate, and the salt from the Retsof mine deforms, at least initially, at an even more accelerated rate.

As seen in Fig. 12.29 for the 100°C tests, there is a rather wide spread in the deformation associated with

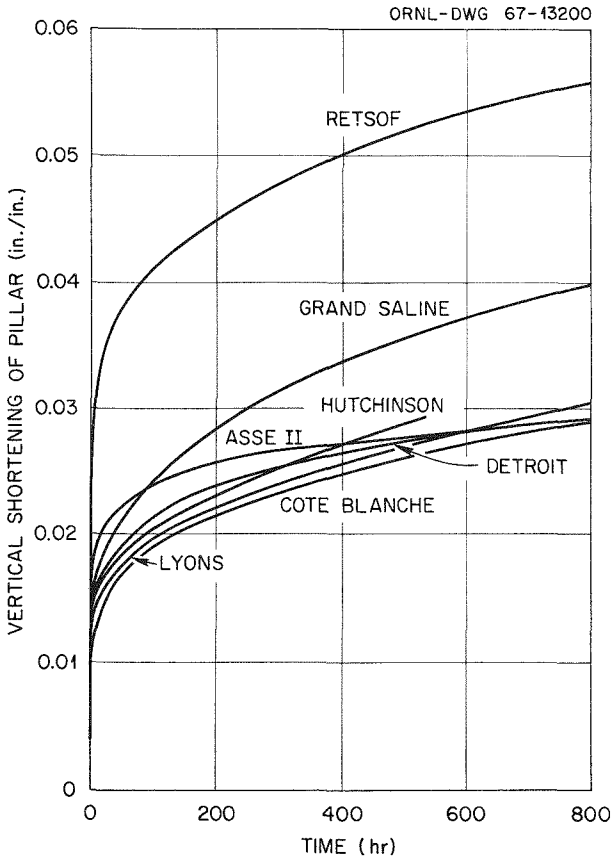


Fig. 12.28. Deformation of Pillar Models from Various Localities at 4000 psi and 22.5°C.

the various types of salt. The Lyons, Hutchinson, Cote Blanche, and Grand Saline curves are similar and show the largest amounts of pillar shortening. The Retsof sample is observed to deform at a markedly slower rate. The curve for the Detroit salt is distinctly different from the others in that the deformation rate is initially slower, but it does not decrease as rapidly with time. Thus from these tests it appears that the total deformation for the Detroit salt will eventually exceed that of the other deposits. The Asse II salt, under these conditions, appears to be stronger than the others.

The reasons for the differences in the behavior of the salts from the various localities as shown in these tests are not fully understood. The depths of the mines do not vary greatly, most being about 1000 ft deep; thus the overburden loads that the salts have been subjected to in Recent geologic time and the resulting prestrained conditions (before laboratory testing) of the samples would appear to be roughly the same. As shown in Table 12.1, all of the salts are relatively low in

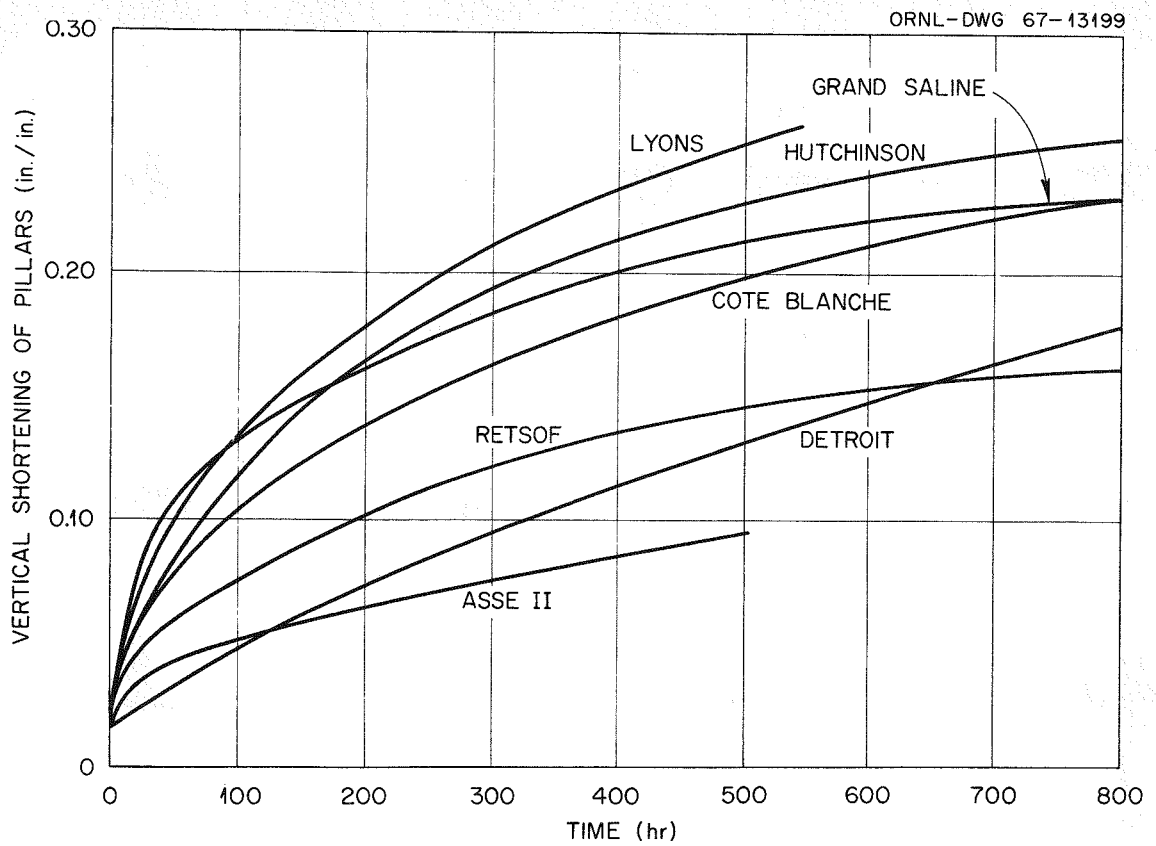


Fig. 12.29. Deformation of Pillar Models from Various Localities at 4000 psi and 100°C.

Table 12.1. Water Insolubles of Rock Salt[a]

Mine Location	Percent by Weight
Lyons, Kansas	0.88
Hutchinson, Kansas	2.27
Retsof, New York	2.00
Detroit, Michigan	0.78
Grand Saline, Texas	1.13
Cote Blanche, Louisiana	1.12
Asse, Germany	2.45

[a]Dale W. Kaufman (ed.), *Sodium Chloride,* pp. 603–4, Am. Chem. Soc. Monograph Ser. 145, Reinhold, New York, 1960.

insolubles; therefore the differences in deformation behavior would not appear to be due to the presence of large quantities of impurities in some deposits. However, it is noted that the Retsof and Asse II salts, which appear to deform after the initial deformation at a slower rate than the other salts, contain about twice as much material that is insoluble in water as the samples from the other localities, with the exception of the Hutchinson salt. Using x-ray diffraction techniques, it was found that anhydrite was the principal water-insoluble impurity for all samples except the Asse II salt, which contained polyhalite as its major impurity. Table 12.2 gives the average chemical composition of salt from three of the mines. In general the water-insoluble fraction is about the same as that present in the samples analyzed for this study.

There do not appear to be any consistent differences in behavior related solely to the three structural types of deposits, namely, domal, anticlinal, or bedded. Differences in grain size may account for some of the variations in deformation; however, all samples are extremely coarse grained with the exception of the Retsof and Asse II salts. The Retsof salt is unique in that there is a pronounced lack of grain intergrowth, and the grains are apparently not firmly cemented together; thus the texture of the salt is somewhat friable. This may account for the high initial defor-

Table 12.2. Chemical Composition of Rock Salt[a]

	Location		
	Retsof, New York	Detroit, Michigan	Hutchinson, Kansas
NaCl	98.262	98.181	96.970
Na_2SO_4			
$MgCl_2$	0.002	0.024	0.066
$MgSO_4$			
$CaCl_2$	0.006	0.053	0.034
$CaSO_4$	0.743	0.872	0.875
H_2O	0.015	0.114	0.670
H_2O insoluble	0.962	0.756	1.407
HCl			
	99.990	100.000	100.022

[a]"Salt," p. 68 in *Interscience Encyclopedia of Chemical Technology*, vol. 12, Interscience, New York, 1964.

mation rate of the Retsof salt, since some compaction and reorientation of grains would be expected to occur when the salt is loaded initially. Perhaps the thermal expansion of the salt was instrumental in reducing the intergranular voids for the 100°C test, which did not experience the extremely rapid initial deformation shown by the sample tested at 22.5°C.

12.3.7 Reproducibility of Results

In order quantitatively to evaluate the effects of temperature, axial load, and time on the deformation of salt, it is important that the samples tested be, as nearly as possible, the same type of salt, including similar grain size, impurities, bedding, etc. With the salt from the Lyons mine, all specimens, with the exception of a few special samples, were fabricated from a series of 5-ft-long cores taken in the roof immediately above the thick shale bed in entry 5 of the old mine workings near the experimental site (see Fig. 5.2). This part of the salt section in the mine, which also comprises the lower part of the pillars and walls in the experimental area, consists, for the most part, of coarse-grained crystals of clear halite that range from 1/4 to 3/4 in. Finely divided blebs of clay are concentrated in the salt at intervals of about 1 to 6 in. along bedding, giving the salt a characteristic banded appearance. A few stringers of anhydrite and an occasional pod of clay are also found in the salt. More rarely, polyhalite blebs can be identified. Specimens from the other localities were prepared from single blocks that appeared to be about the same type of salt throughout.

To obtain an approximate measure of the variation in deformational behavior of model specimens of the same type of salt in the Lyons mine tested under the same conditions, duplicate and triplicate samples were run at several combinations of pressure and temperature. In Fig. 12.30 the deformation curves for three samples, each tested at 6000 psi and 22.5°C, are shown. The curves for these samples are essentially the same. Good agreement is also shown for the duplicate samples tested at 4000 psi and 22.5°C (see Fig. 12.31). It is evident in Fig. 12.32, which shows the deformation of two samples heated to 200°C and loaded to 2000 psi, that reproducible results can also be obtained for samples tested at elevated temperatures.

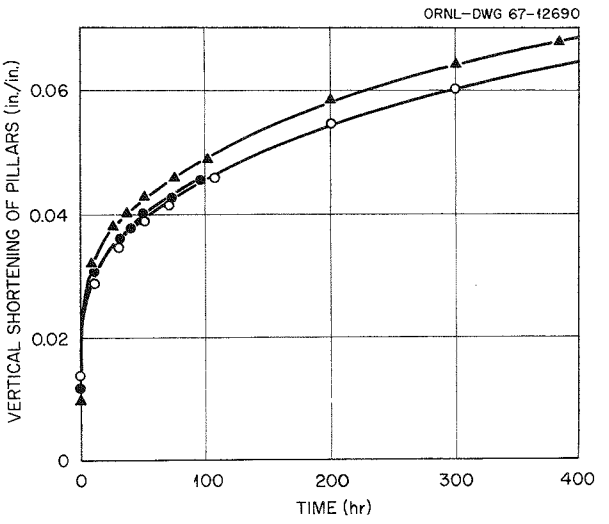


Fig. 12.30. Deformation of Pillar Models at 6000 psi and 22.5°C.

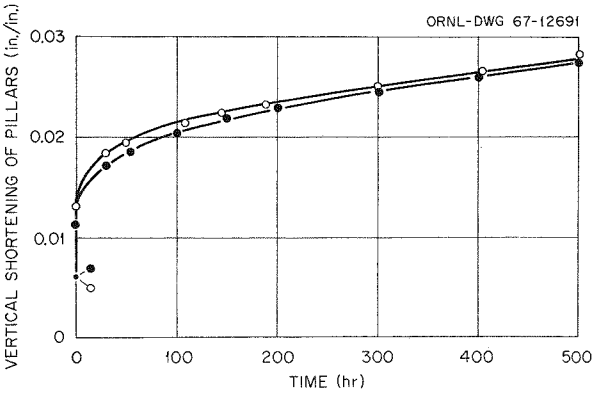


Fig. 12.31. Deformation of Pillar Models at 4000 psi and 22.5°C.

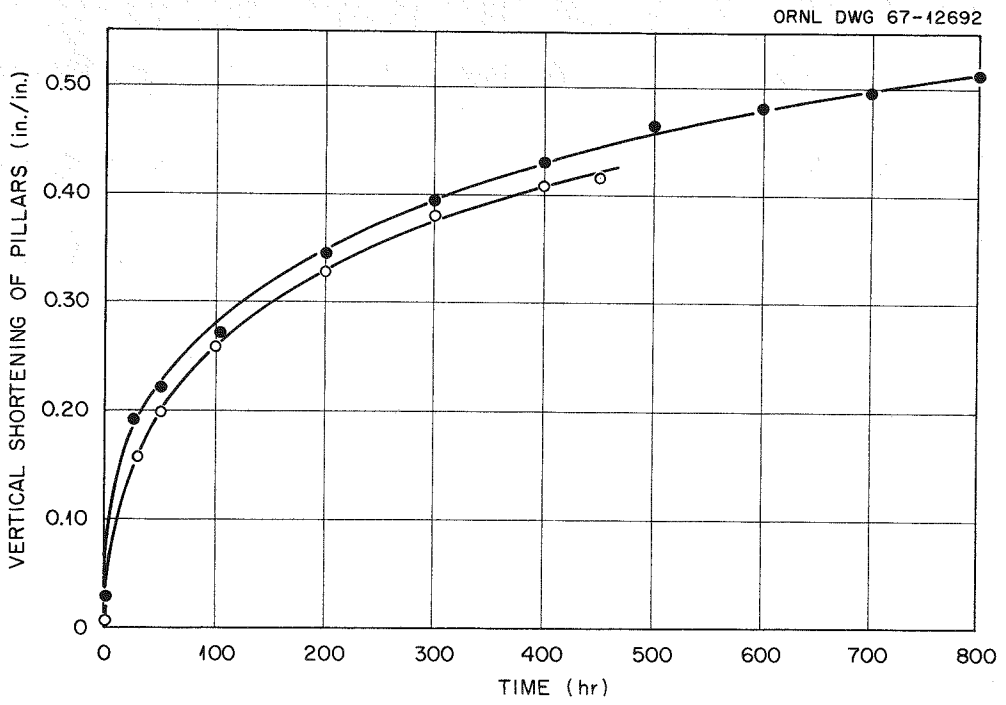


Fig. 12.32. Deformation of Pillar Models at 2000 psi and 200°C.

12.3.8 Ultimate Strength

The ultimate strength of support systems is of fundamental importance in all underground openings. To determine the ultimate or breaking strength of mine pillars in salt, two models, one having a width-to-height ratio of 3 and the other a width-to-height ratio of 4, were loaded at rates of 33 psi/min until failure or extensive deformation occurred. The deformation curves for these samples are shown in Fig. 12.33. In both cases it is seen that sudden or brittle pillar failure did not occur even under loads as high as 14,000 psi; however, considerably more deformation did occur in the smaller-diameter pillar than in the larger one. This verifies the conclusion drawn from other tests, described above, that pillars having a width-to-height ratio of 4 are stronger than those having a width-to-height ratio of 3. Although 100% pillar shortening was not attained in either sample, both were deformed to the extent that accumulation of spall or small pieces of broken salt from the pillars had filled a part of the cavity opening. Thus the effective pillar diameter of the smaller-diameter pillar had increased to the point that it extended almost the entire width of the excavated cavity. The combined effects of pillar shortening and pillar spall on cavity closure are discussed in more detail later; however, it is evident that the smaller the width-to-height ratio of the pillars (assuming a greater excavation ratio), the greater will be the amount of pillar shortening prior to complete cavity closure. The results of these tests also suggest that sudden or brittle pillar failure will not occur in salt pillars having width-to-height ratios of 3 and 4 at loads up to 14,000 psi, and perhaps even at any higher loads, although deformation of the pillars through creep of the salt would occur at a very high rate. The ultimate strength or breaking strength of pillars of these types thus cannot be determined, since the salt under these conditions will flow very rapidly but will not fail in a brittle manner regardless of the load.

12.3.9 Mechanisms of Deformation

Although the exact mechanisms of the deformation within salt pillars are not fully understood, some generalizations can be formulated from observations of deformed specimens. Figure 12.34 shows cross-sectional views of two model pillars that were cut vertically in half after deformation. Before deformation, the pillars were 4 in. in diameter and 1 in. high. In these specimens an attempt was made to define the principal movement by observing the relation of the pillar and the material

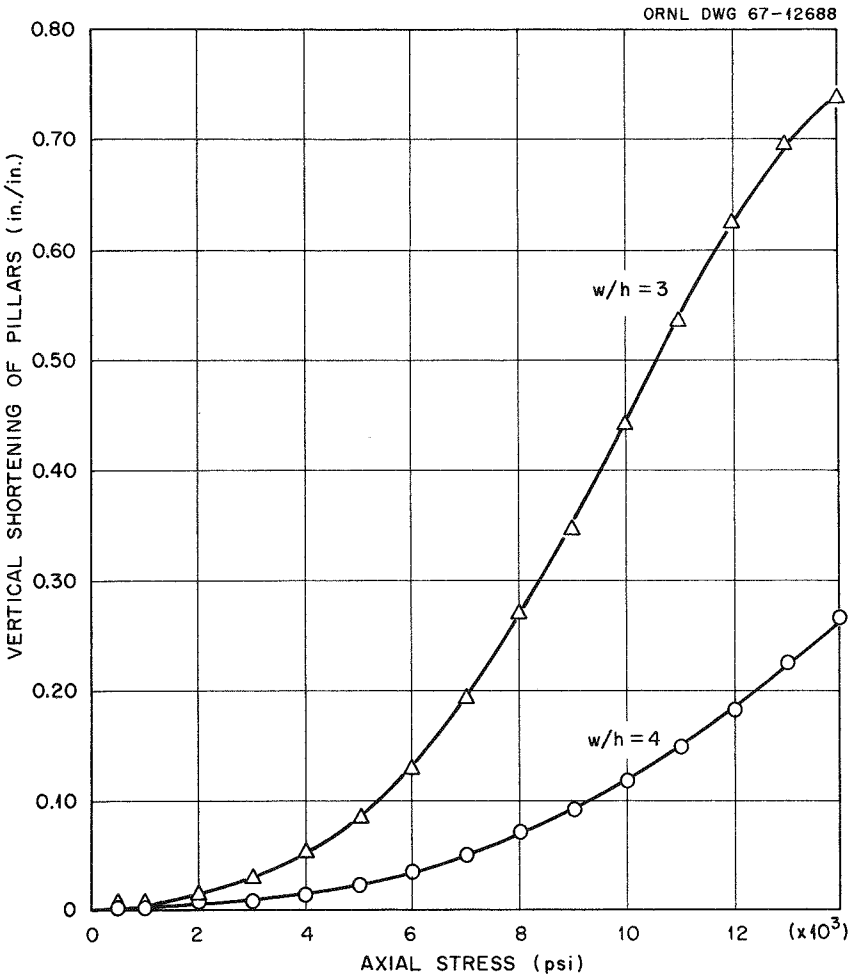


Fig. 12.33. Ultimate Strength of Pillar Models at 22.5°C and with Width-to-Height Ratios of 3 and 4.

above and below it after deformation. The dark horizontal lines seen in the salt specimens are $\frac{1}{16}$-in.-diam holes that were bored horizontally through the tops and bottoms of the pillars and filled with colored salt before the specimens were deformed. In the model pillar deformed at 22.5°C, it is seen that the pillar is only slightly more than 4 in. in diameter. However, a considerable amount of loose salt from the outermost portion of the pillar had accumulated in the surrounding cavity opening and was subsequently removed. The cross-sectional view shows that the pillar did not deform independently of the roof and floor but that all three parts of the model entered into closure of the cavity. Note especially how the roof and floor have flowed into the cavity opening. The most resistance to deformation in the model is believed to be in the center of the pillar (due to confining pressure) and immediately above and below the pillar in the roof and floor. Thus, movement here is at a minimum. This is shown in the photograph by the greater distance between the lines in the center of the pillar than at the edges. Toward the outside of the pillar, there is less resistance to deformation; thus salt from the pillar tends to move horizontally into the opening, while material from above and below also moves in to fill the cavity.

In the model pillar deformed at 100°C, the overall deformational pattern is similar to that of the sample tested at room temperature; but instead of the outermost portion of the pillar deforming through spalling, it stayed intact and deformed more plastically. The pillar diameter in this case increased from 4 to $4\frac{1}{2}$ in. as a result of the deformation.

The deformational behavior of salt pillars is illustrated further in Fig. 12.35. In this "standard size" model

PHOTO 81465

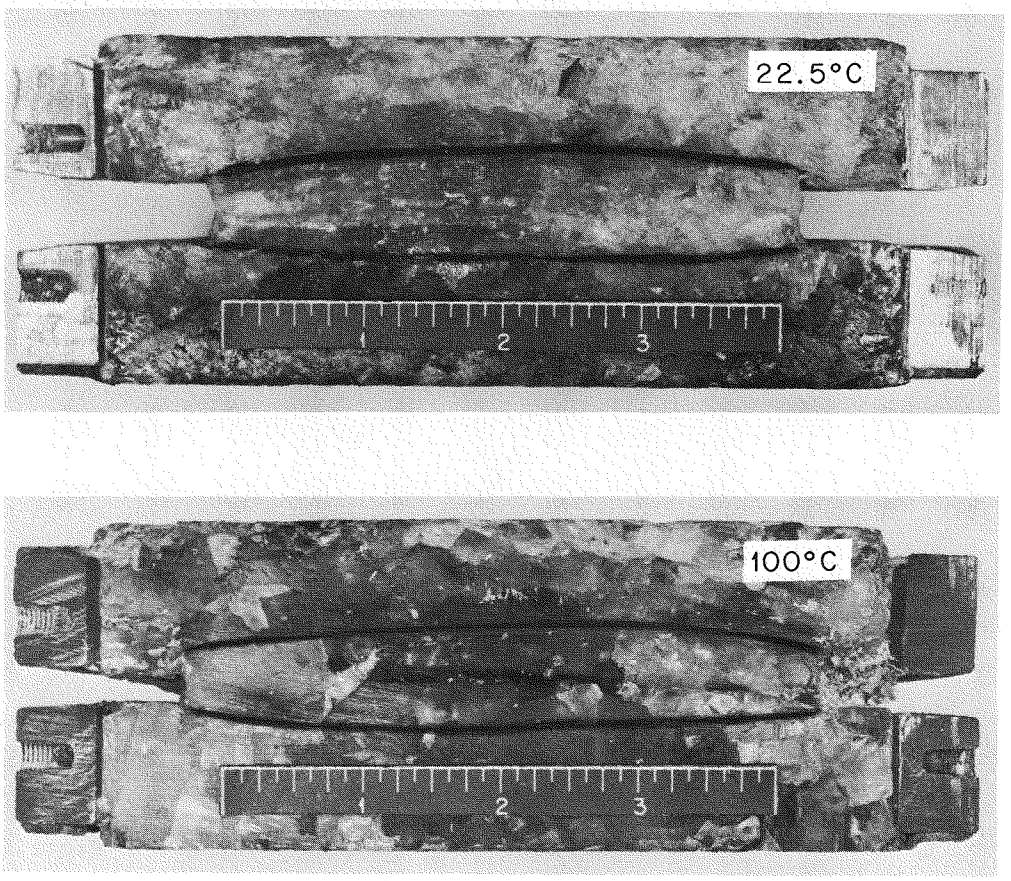


Fig. 12.34. Photograph of Pillar Models Showing Vertical Deformation at 22.5 and 100°C.

specimen, which has been cut in half, $^1/_{16}$-in.-diam holes were drilled vertically through the center of the specimen and at a distance of 1 and $1^3/_4$ in. from the center and then filled with colored salt before testing at a load of 6000 psi and a temperature of 100°C. The lateral movement of salt is illustrated by the bending of the colored salt lines toward the cavity opening. Close observation of the specimen reveals that the curved portions of the lines extend beyond the original pillar height (1 in.) and into the roof and floor. Thus salt in the roof and floor also moves outward from the center line of the specimen and down (or up in the floor) toward the cavity opening. This outward and downward (or upward) movement of salt from the roof and floor continues all the way to the top and bottom of the sample. This is illustrated by noting that the vertical holes that were originally 1 and $1^3/_4$ in. from the center of the specimen were found after deformation to be $1^1/_{16}$ and $1^{13}/_{16}$ in. distant respectively. The original 4-in. diameter of the pillar increased to a little over 5 in. as a result of the deformation, and the original cavity height of 1 in. was reduced to about $^1/_2$ in. at the edge of the ring and to about $^3/_8$ in. at the pillar face. Essentially no pillar spall accompanied the deformation of the model. This was obviously due to the temperature (100°C) at which the test was performed.

In the two preceding figures it is observed that cavity closure is due to the lateral flowage of salt from the pillar into the opening, as well as to the more or less vertical movement of salt into the cavity from the roof and floor. In general this type of deformation prevails at ambient temperature as well as at elevated temperatures; however, in the case of the former, the effective width of the pillar remains about constant, since the amount of pillar spall approximates the lateral flow of salt from the pillar, while at elevated temperatures there



Fig. 12.35. Photograph of Pillar Model Showing Horizontal Deformation at 6000 psi and 100°C.

is a progressive increase of pillar width with deformation, since there is little or no pillar spall and the salt flows en masse. This increase in pillar width, which results in a lower pillar stress, undoubtedly accounts, in part, for the marked decrease in rate of cavity closure with time, especially when the total deformation exceeds about 50%. This is illustrated in Fig. 12.36, which shows the deformation curve for a model pillar specimen heated to 100°C and loaded to 8000 psi. Note the marked flattening of the curve after about 150 hr and about 0.50 in. of pillar shortening. An examination of the specimen after 900 hr of testing showed that cavity closure was essentially complete. Thus when the salt is heated, it is apparent that initially there will be a rapid increase in pillar shortening, the rate being dependent, of course, on the temperature and load. Then as the pillar width increases and the cavity becomes filled, there is another pronounced decrease in the rate of cavity closure, which continues until all of the void space is filled with salt from the pillar and from the roof and floor. For the model salt pillars tested at 22.5°C, and even for those tested at temperatures of 60°C and at loads no greater than 4000 psi, the deformation proceeded at such a low rate that it was not possible to observe total cavity closure for the duration of the tests in the laboratory. However, it is presumed that, since there is no effective increase in the pillar width due to pillar spall at ambient temperatures, there would be no decrease in axial load on the pillar and, thus, no flattening of the deformation curve until the accumulation of salt in the cavity from pillar spall is sufficient to fill essentially the entire cavity. Figure 12.37 shows a photograph of a model pillar taken after 1000 hr of testing at 22.5°C and 10,000 psi. The pillar shortening of this specimen totaled about 0.35 in.; and although there is considerable spall from the pillar in

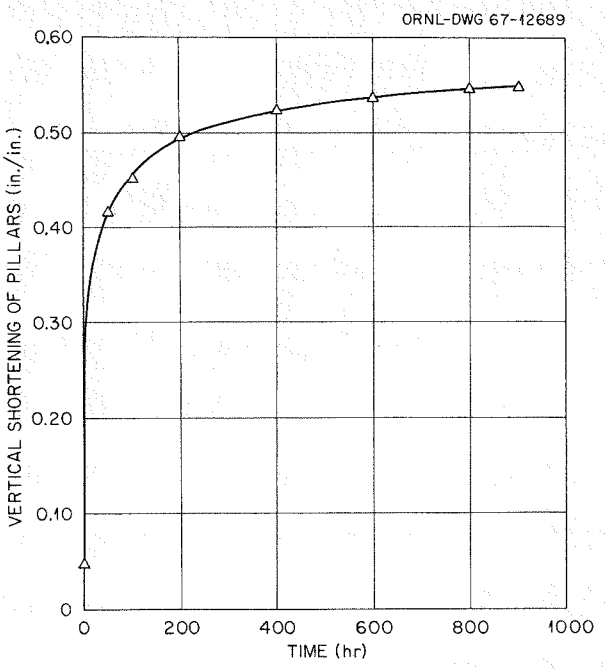


Fig. 12.36. Deformation of Pillar Model at 8000 psi and 100°C.

the cavity, it has not completely filled the opening. Pillar spall commonly occurs as thin and somewhat elongated fragments that separate along nearly vertical tension cracks that develop on the pillar walls as a result of the outward flow of salt.

12.3.10 Long-Term Creep

In order to ascertain whether or not creep rates continue to decrease with time for periods in excess of a few thousand hours, creep rates were recorded over a period of $3\frac{1}{3}$ years on a model that was loaded to 6000 psi at 22.5°C and over a period of 1 year on a model loaded to 4000 psi at 22.5°C. Plots of the cumulative deformation with time are shown in Fig. 12.38. In both cases it is observed that the rate of deformation continues to decrease with time to the extent of the test periods. This decrease in creep rate with time has also been studied in actual mine workings.[10] In this study, observations in the Lyons mine show that in mine openings up to 12 years old there is a continual decrease in the rate of floor-to-ceiling convergence.

12.4 DISCUSSION OF RESULTS

12.4.1 Relationship of Load, Temperature, and Time

In order to predict the effects of load, temperature, and time on underground openings in salt deposits, empirical equations have been developed that fit the results of the model pillar tests of rock salt from the Lyons mine having a pillar width-to-height ratio of 4. These equations are expressed as

$$\dot{\epsilon} = 0.39 \times 10^{-37} T^{9.5} \sigma^{3.0} t^{-0.70} ,$$
$$\epsilon = 1.30 \times 10^{-37} T^{9.5} \sigma^{3.0} t^{0.30} , \qquad (12.2)$$

where

$\dot{\epsilon}$ = strain rate or vertical shortening of pillars (in. in.$^{-1}$ hr^{-1}),

ϵ = cumulative deformation (in./in.),

T = absolute temperature (°K),

σ = average pillar stress (psi), and

t = time (hr).

In Fig. 12.39 the cumulative deformation of a series of samples tested at a temperature of 22.5°C and at loads ranging from 2000 to 10,000 psi are shown as logarithmic plots of cumulative deformation and time. It is observed that the data can be fitted by a series of straight-line plots after 1 hr, having a slope of 0.30. In general, the straight-line plots fit the data remarkably well over most of the range of the tests. In these plots zero cumulative deformation is taken to be that which existed after 2 min of test time. This method of expression eliminates most of the effects of extraneous variation in the initial deformation from sample to sample. In an actual mine operation, it is not possible to measure the early deformation phase; thus, the rate of deformation, which is the time derivative of cumulative deformation, is a more important variable than perhaps an extremely precise measure of the total cumulative deformation.

Figure 12.40 shows plots of the same type as above for samples tested at 60°C. The cumulative deformation with time for each load can also be fitted by a straight line having a slope of 0.30, as can the plots of samples tested at 100 and 200°C. Thus the exponent of time in the equation for ϵ, Eq. (12.2), is 0.30.

Data on cumulative deformation in excess of about 0.30 in./in. are not included, since at these high values the effects of lateral pillar expansion due to plastic flow, and perhaps even pillar spall, which can only be measured qualitatively, markedly influence the deformational behavior of the models. Thus, the deformational behavior of mine pillars above about 30% of pillar shortening is not predictable with the Eqs. (12.2). In an actual disposal operation, it is planned to backfill the rooms with crushed salt excavated from other parts

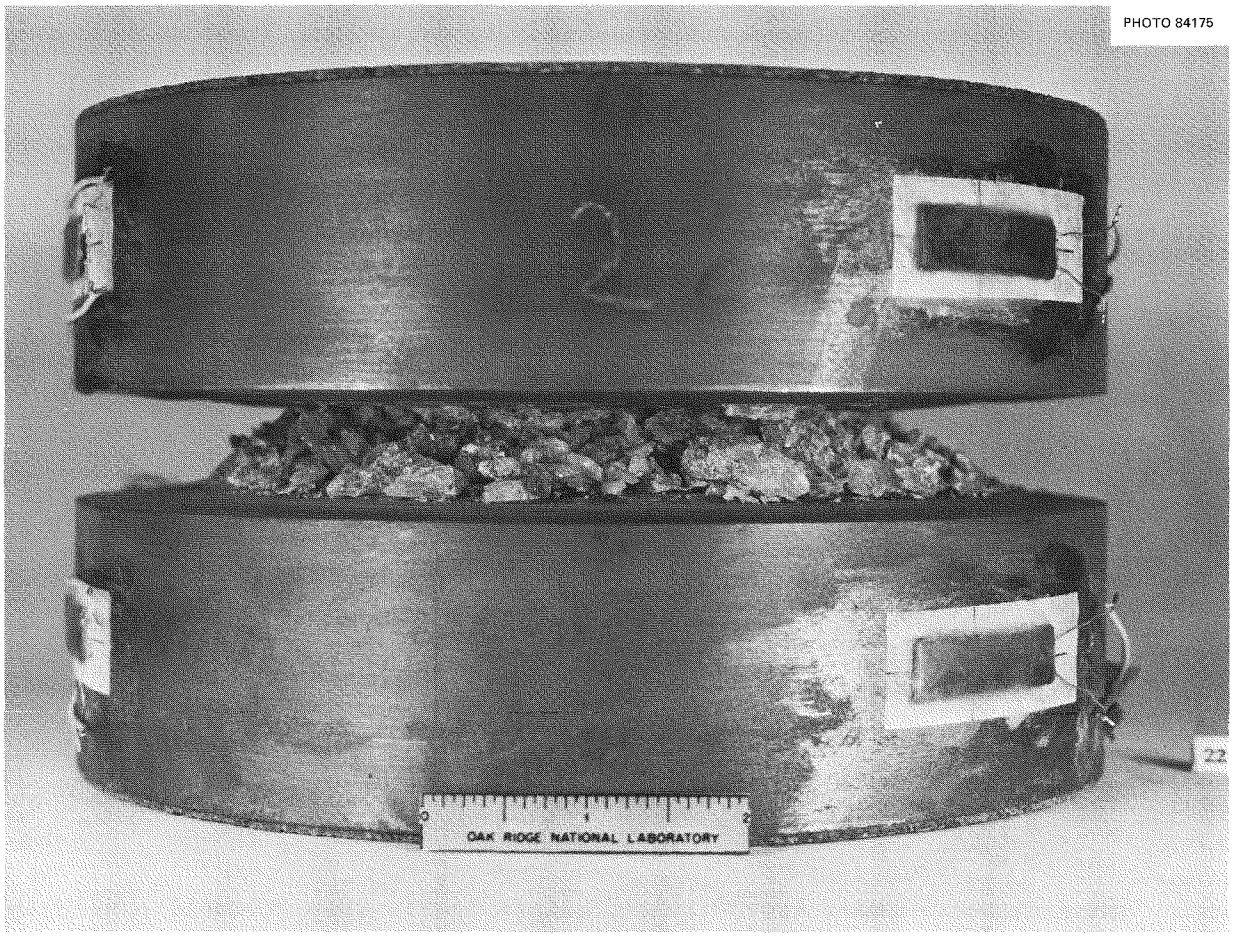


Fig. 12.37. Photograph of Pillar Model After 1000 hr of Testing at 10,000 psi and 22.5°C.

of the mine as containers of waste are disposed in the mine floors. Under these conditions, it is unlikely that deformation would exceed about 30% anyway.

The exponent on stress in Eqs. (12.2) was determined by plotting cumulative deformation logarithmically for various stresses at a selected time (see Fig. 12.41). The resulting points for a selected time of 100 hr were then fitted with a straight line having a slope of 3.0. Plots of the several stresses and cumulative deformation at elevated temperatures show about the same average value as that at ambient temperature for the effect of stress on pillar deformation.

To determine the temperature exponent in the equations, logarithmic plots of cumulative deformation vs temperature for various sample specimens were made and then fitted with a straight line having a slope of 9.5 (see Fig. 12.42). This steep slope or high value for the exponent of temperature indicates that temperature is the single most important parameter that affects cavity closure in salt mines.

Figures 12.43–12.46 show comparisons of the actual deformation curves for model specimens and calculated curves for the same conditions of temperature, time, and load, using the equations given above, at temperatures of 22.5, 60, 100, and 200° respectively. For the curves at 22.5°C (Fig. 12.43), it is seen that the calculated curves are similar to the actual ones at 2000, 4000, and 6000 psi; even at the higher loads, there is good agreement between the two plots. In general the calculated curves show a closer similarity to the actual ones at lower stresses and temperatures than at higher loads and temperatures, especially at the upper ends of the curves, where deformation is greatest. These deviations at higher loads and temperatures are believed to be due to the effects of pillar spall and lateral pillar expansion in the heated samples, which undoubtedly

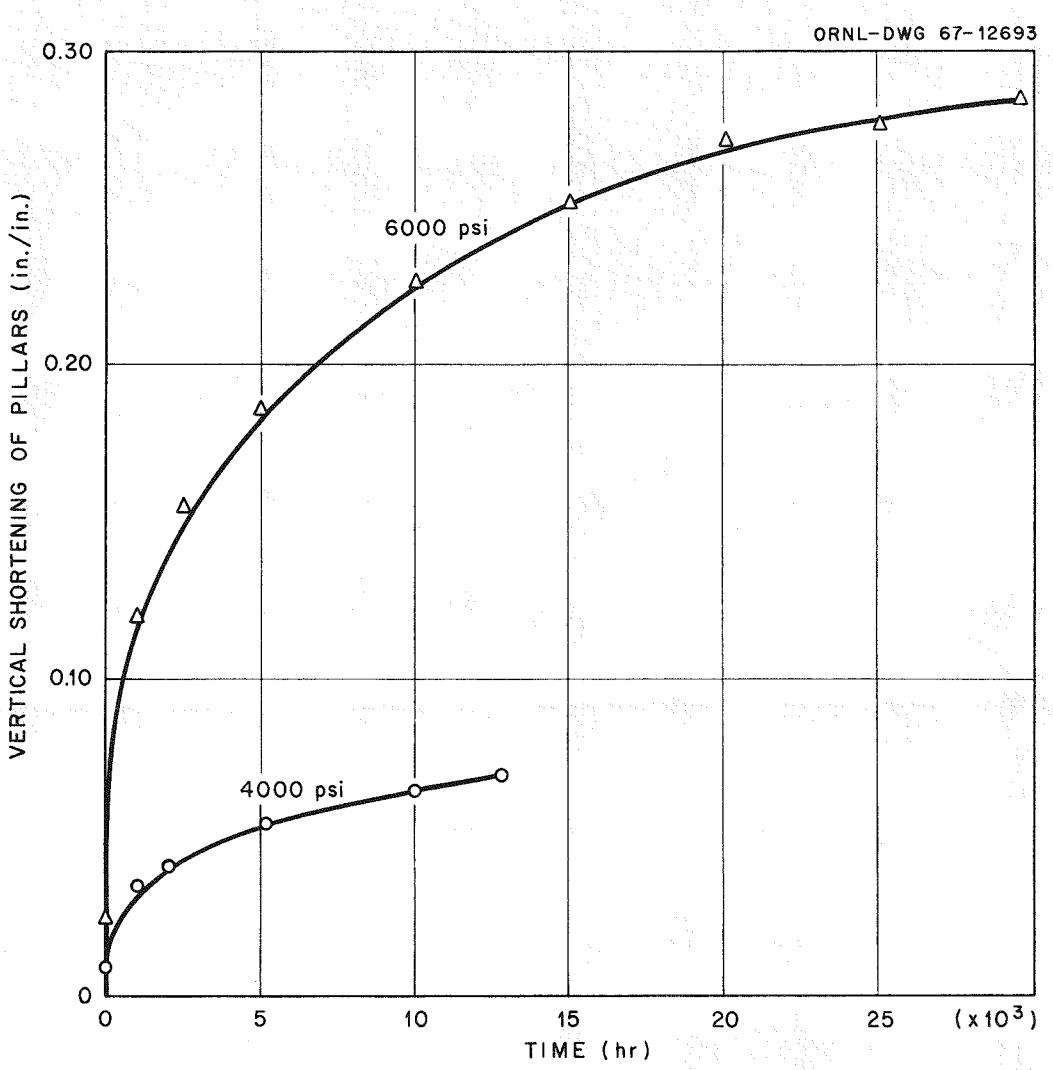


Fig. 12.38. Deformation of Pillar Models at 6000 and 4000 psi and 22.5°C.

affect deformation under high load and temperature conditions and which have not been taken into account in the equation.

12.4.2 Relationship to Actual Mine Conditions

Since the model pillar specimens of salt from Lyons that were used in tests to develop the equation were essentially all salt and did not contain shale beds or other rocks in the roof, floor, and/or pillars, predictions using the equations are valid, strictly speaking, only for that type of salt. However, the closure rates of excavations in bedded, as well as dome, salt deposits that do not contain shale partings or other rock types in critical areas could also be approximated by these equations. The expressions would be expected to be least effective in predicting deformation in mine openings where shale beds occur at both the tops and bottoms of pillars. Since the shales serve as effective friction reducers, confining stresses in the roof and floor of the mines are not transmitted into the pillars; thus mine pillars under these conditions will deform more nearly as if they were simply squeezed between two rigid plates. The strength of actual mine pillars based on the model study would perhaps be expected to be several times less under conditions where shale partings occur at the tops and bottoms of pillars than where salt continues uninterrupted from the pillars into the roof and floor. Also, the effect on deformation would not be expected to be nearly so pronounced

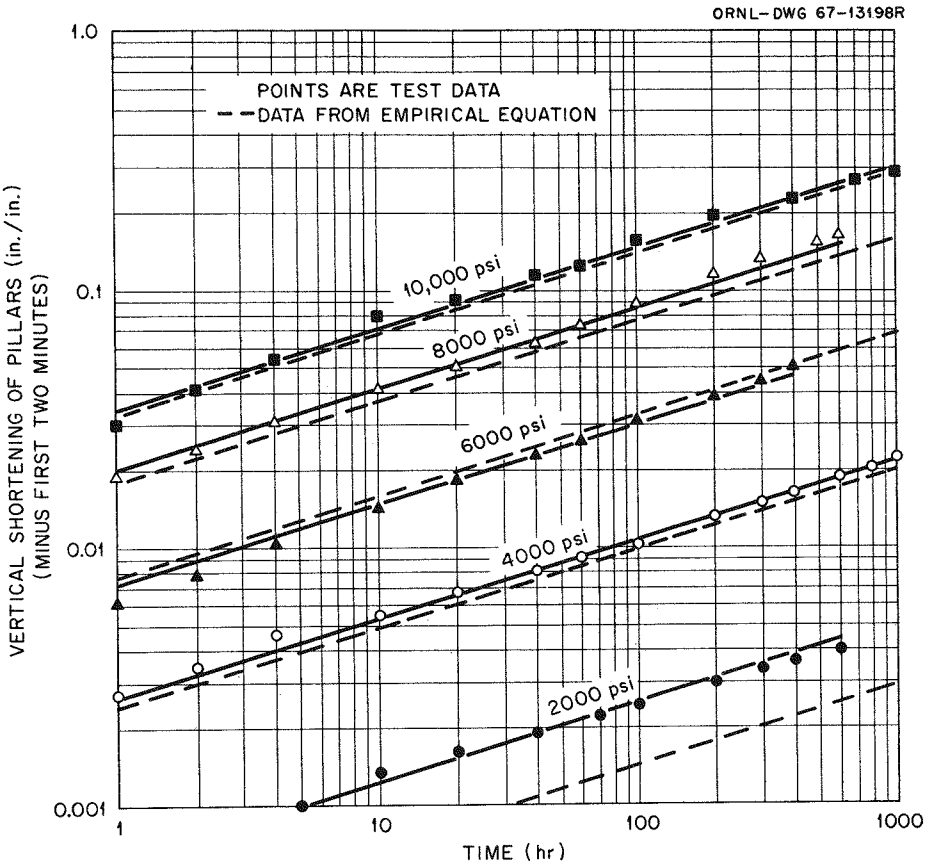


Fig. 12.39. Logarithmic Plots of Cumulative Deformation of Pillar Models at 22.5°C.

where the shale occurs only at the top or bottom of the pillar. If salt deposits contain shale partings that cannot be avoided in mining, it is better that the openings be made so that the shales are located in the center part of the pillar. The center of the pillar apparently is a more or less neutral plane, and, therefore, shale partings at this location will not influence the rate of deformation; however, as the location of the shales approaches the top or bottom of the pillar, they cause an increasingly greater increase in the rate of cavity closure. In general a similar pattern of deformation occurs with shale beds in the floor and ceiling of salt mines. The nearer the shale parting in the ceiling and/or floor to the pillar, the weaker is the pillar. This is because as the thickness of the uninterrupted salt section that lies in the roof and floor above and below the pillar is reduced, there is a corresponding reduction in the confining stress in the roof and floor which can be transmitted into the pillar. When shale partings lie only a few inches above and/or below the pillars in mines, it is common for buckling of the roof and/or heaving of the floor to occur. This phenomenon is well illustrated in Fig. 12.47, a photograph showing floor heaving and downwarping of the ceiling (the center section of the ceiling slab has fallen) in an old part of the Lyons mine. This type of deformation not only results in more rapid closure of the mined opening but creates mine safety problems, since ceiling slabs commonly sag to a considerable extent and then fail and fall suddenly.

Even though there are some variations in the creep rates of salt from one mine to another and even within a single mine where such factors as impurities, grain size, texture, etc., may cause slight differences in behavior, it is apparent that the general creep behavior of salt is the same regardless of the origin and/or location of the deposit. The principal difference then is the magnitude of the creep rate. (The rate of creep was found to decrease with time in the model tests, and this has also been verified in mine openings that are up to 12 years old.) Furthermore, it is apparent that the most important parameters that affect cavity closure in salt deposits that might be used for the disposal of

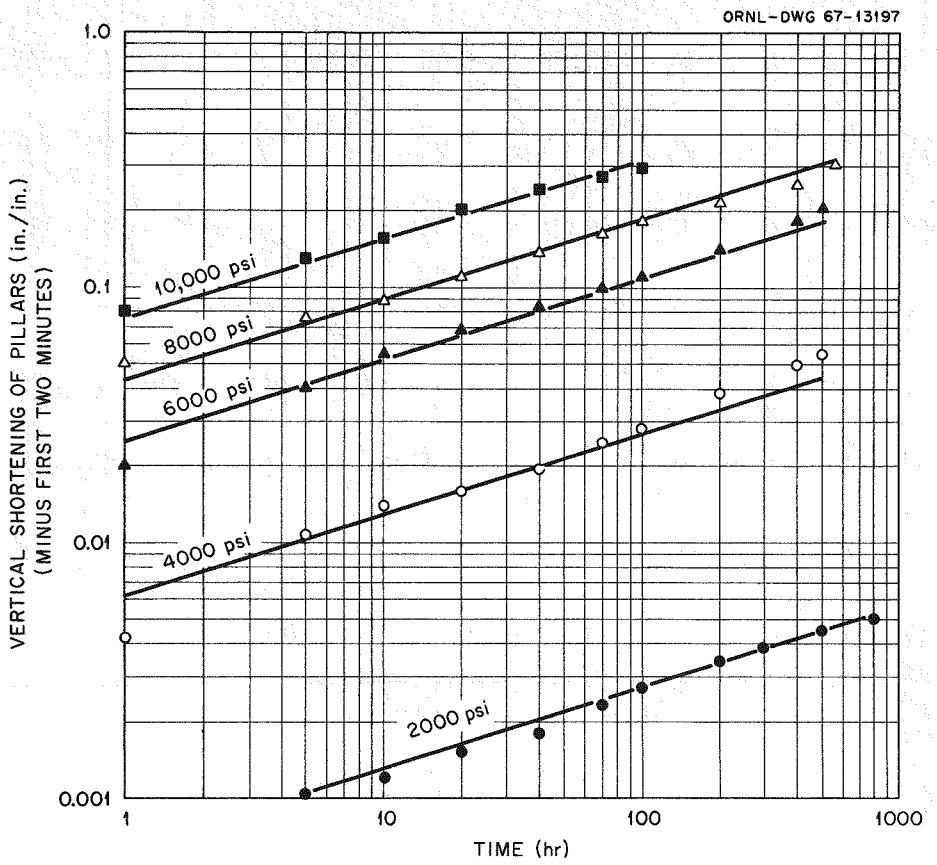


Fig. 12.40. Logarithmic Plots of Cumulative Deformation of Pillar Models at 60°C.

high-level wastes are not those of location and genetic type of deposit, grain size, impurity content, texture, etc., but the presence of shale partings at or near the pillar-floor and/or pillar-ceiling contacts, the width-to-height ratios of the pillars, and the effects of temperature, load, and time.

Based on the results of model tests, mine pillars having width-to-height ratios of 2 and 3 will deform approximately 75 to 45% faster, respectively, than pillars having a width-to-height ratio of 4. For pillars with width-to-height ratios less than 2, it would appear that the rate of deformation will be even greater. It is also apparent that with mine pillars having width-to-height ratios of 3 or 4, catastrophic pillar failure will not occur at ambient temperature, even at loads as high as 14,000 psi, which is well beyond the upper limit of loading that would be expected in any salt mine used for the disposal of wastes. Pillars having widths about four times their heights appear to be most common in the Carey salt mines at Lyons and Hutchinson, Kansas. Also, the widths of rooms between the pillars in these mines appear to be about one-half the width of the pillars.

It is apparent that the greater the percentage of extraction of salt from underground workings, the greater will be the superincumbent load on the salt remaining in the pillars. Also, in general, for a given room height, the higher the percentage salt extraction, the smaller will be the width-to-height ratio of the supporting pillars. For larger cavity openings and slimmer pillars, correspondingly greater floor-to-ceiling convergences will occur in mines prior to complete cavity closure.

Cylindrical model pillars were used for the tests to develop the empirical equations given above; however, in actuality, mine pillars may vary from nearly cylindrical to rectangular. For rectangular pillars having lengths about twice their widths and containing the same cross-sectional area and height as cylindrical pillars with width-to-height ratios of 4, it is assumed, from model tests, that they will deform about 40% faster than their cyclindrical counterparts. Rectangular pillars

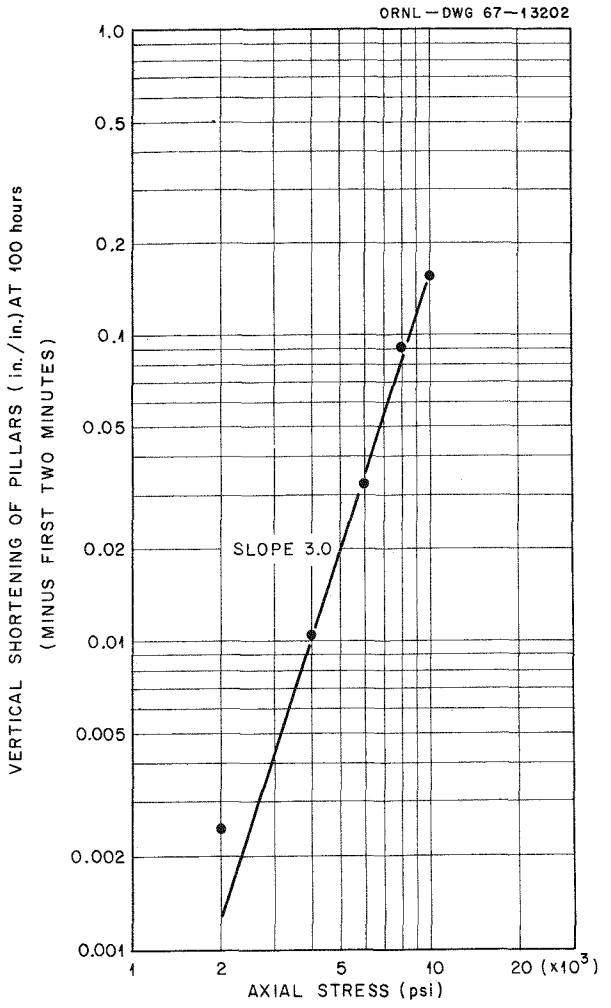


Fig. 12.41. Determination of Stress Function of Pillar Models at 22.5°C.

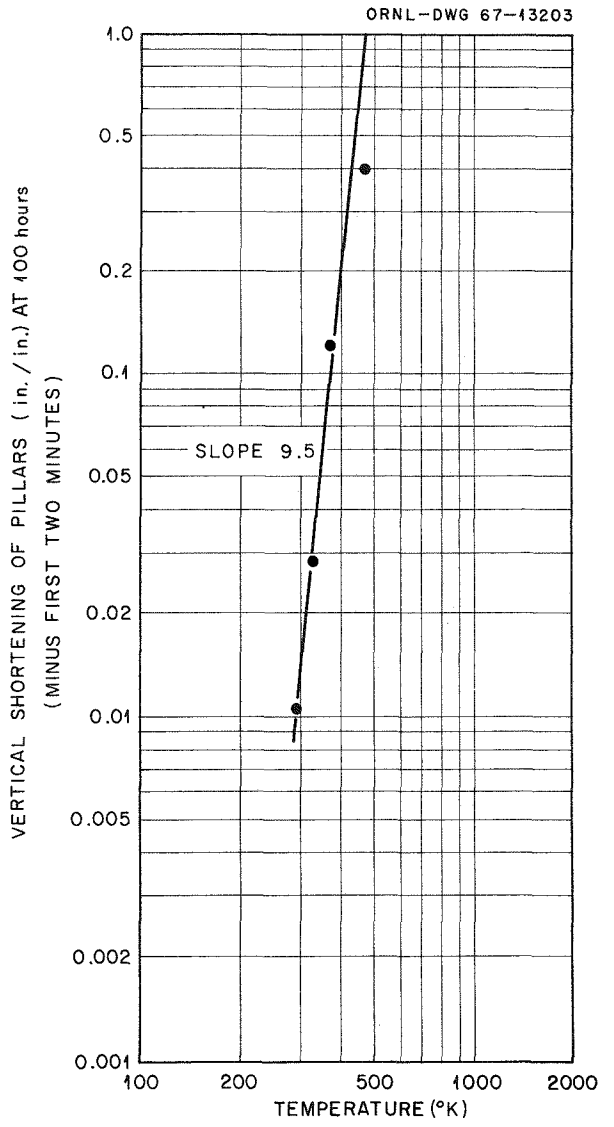


Fig. 12.42. Determination of Temperature Function of Pillar Models at 4000 psi.

with lengths several times their widths may be used for specially mined excavations in salt used for the disposal of high-level radioactive wastes. However, it is assumed that width-to-height ratios less than 2 would not be used.

12.5 SUMMARY AND CONCLUSIONS

In order to properly design actual disposal facilities in salt, it is necessary that the effects of temperature, load, time, and stratigraphic relations on structural openings be determined. To investigate the deformational behavior of rock salt in mined openings, scale models of salt pillars and their surrounding rooms were fabricated and tested under conditions that might be expected in actual operations. It was determined that a $5\frac{11}{16}$-in.-diam core of rock salt 5 in. long and ground out in the center to form a 4-in.-diam, 1-in.-high pillar adequately simulates mine conditions where pillar width-to-height ratios are about 4.

Laboratory tests of samples from the Lyons mine were conducted at temperatures of 22.5, 60, 100, and 200°C for axial loads of 2000, 4000, 6000, 8000, and 10,000 psi at each temperature. From these tests it is concluded that deformation of the pillars increases markedly with increasing loads. However, even more significant is the greatly accelerated creep rate of the salt at elevated temperatures. An empirical relationship

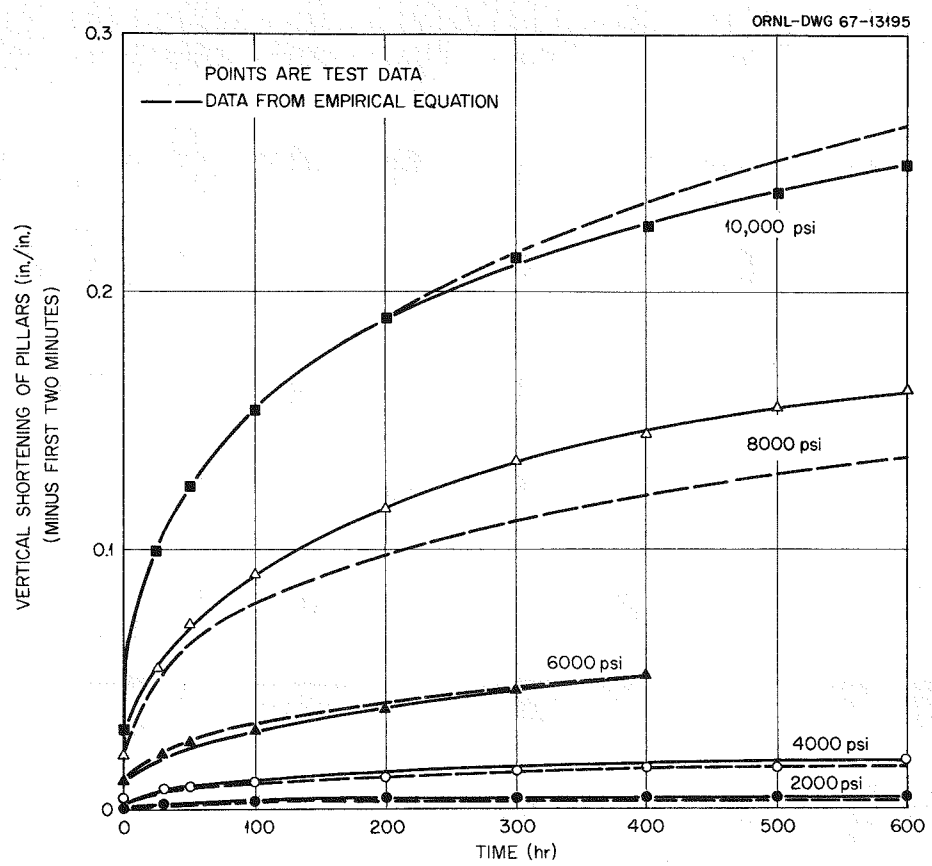


Fig. 12.43. Comparisons of Deformation from Tests of Pillar Models at 22.5°C and from Empirical Equation.

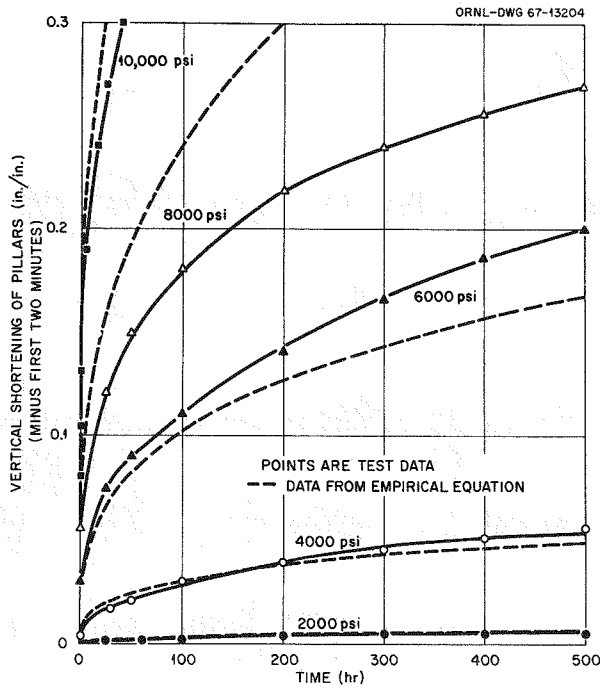


Fig. 12.44. Comparisons of Deformation from Tests of Pillar Models at 60°C and from Empirical Equation.

between creep, stress, temperature, and time has been developed from the tests and is given as

$$\dot{\epsilon} = 0.39 \times 10^{-37} T^{9.5} \sigma^{3.0} t^{-0.70} ,$$
$$\epsilon = 1.30 \times 10^{-37} T^{9.5} \sigma^{3.0} t^{0.30} , \qquad (12.2)$$

where

$\dot{\epsilon}$ = strain rate or vertical shortening of pillars (in. in.$^{-1}$ hr^{-1}),

ϵ = cumulative deformation (in./in.),

T = absolute temperature (°K),

σ = average pillar stress (psi), and

t = time (hr).

At all axial loads and constant temperatures, there is initially a high creep rate that decreases with time. Creep rates are observed to continue to decline even after more than 3 years of testing. This agrees with measurements that have been made in salt mines, which show that deformation rates continue to decrease with time, at least in openings up to 12 years old.

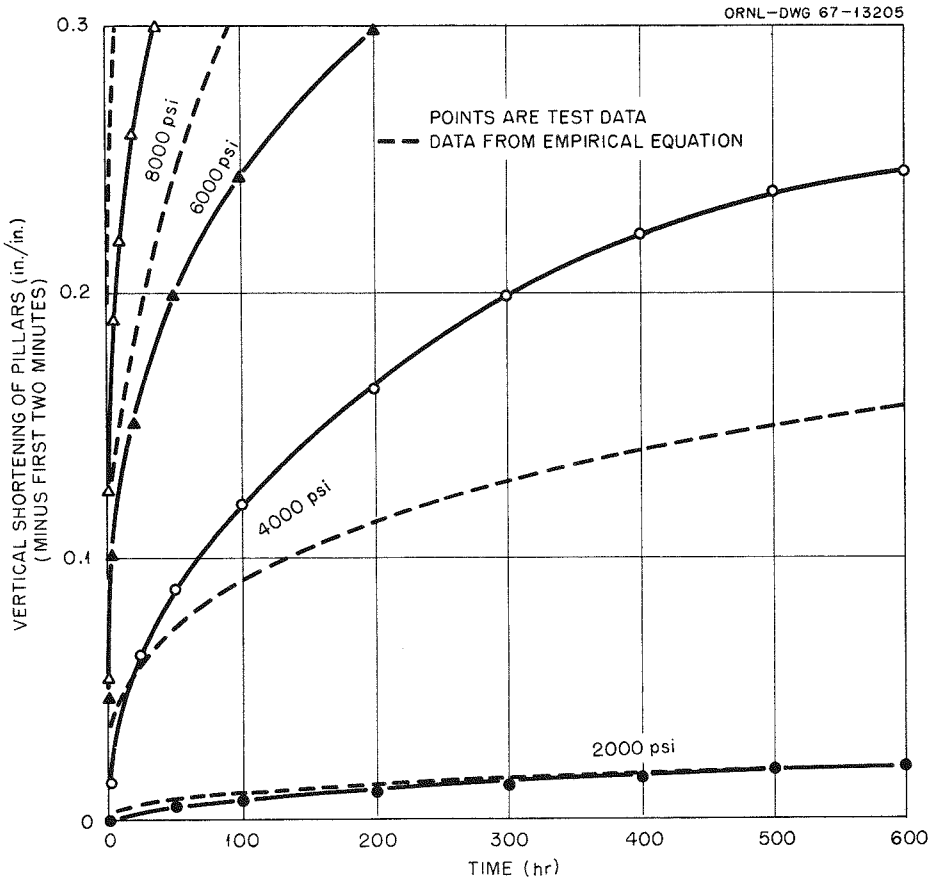


Fig. 12.45. Comparisons of Deformation from Tests of Pillar Models at 100°C and from Empirical Equation.

Model tests, verified by measurements in salt mines, show that thin shale beds, which commonly occur with bedded salt deposits, cause greatly accelerated rates of deformation in excavated cavities when they occur in the pillars at roof and floor interfaces. Under these conditions the shales, which are effective friction reducers, serve to reduce significantly the transfer of lateral confining stresses from the roof and floor of the openings into the pillars. Thus the pillars deform more nearly as if they were squeezed between two rigid plates and not as pillars without shale partings, where cavity closure is due to the lateral flowage of salt from the pillars into the openings as well as the more or less vertical movement of salt into the cavity from the roof and floor.

Tests were made with salt from mines at Lyons and Hutchinson, Kansas; Retsof, New York; Detroit, Michigan; Grand Saline, Texas; Cote Blanche, Louisiana; and Asse, Germany. It was found that the general deformational behavior is the same; however, some variations in the rates of deformation were observed. Creep rates were also found to vary with the width-to-height ratios of pillars as well as with pillar shapes.

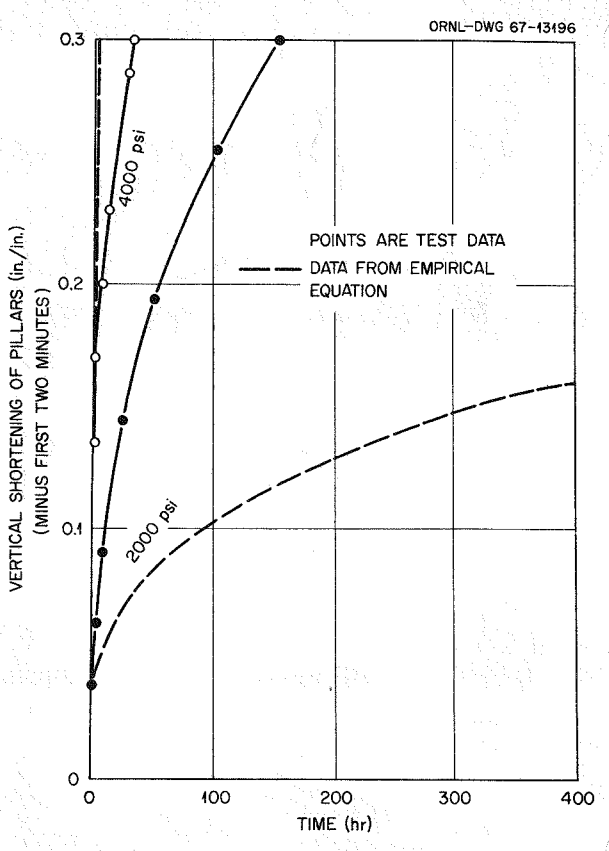


Fig. 12.46. Comparisons of Deformation from Tests of Pillar Models at 200°C and from Empirical Equation.

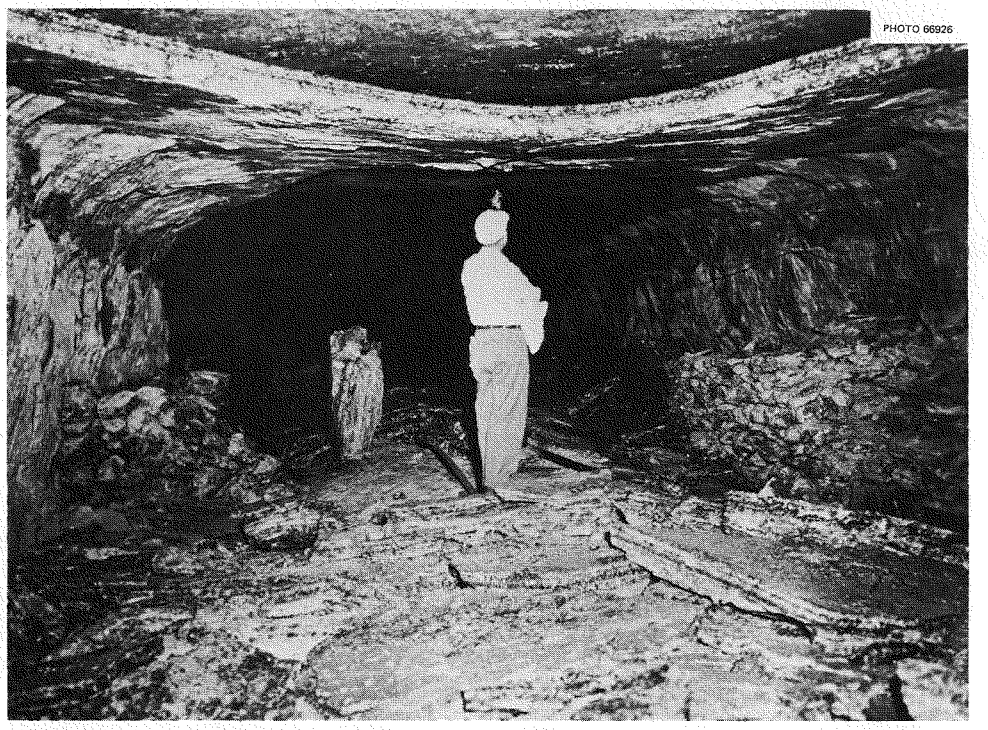


Fig. 12.47. Photograph Showing Roof Buckling and Floor Heaving in Carey Salt Mine, Lyons, Kansas.

13. Analysis of Combined Effects

W. C. McClain A. M. Starfield[1]

In this chapter the analysis of the deformational behavior of the entire experimental area under the combined influence of stress, stress history, heat, thermal gradients, and time is presented. This analysis is quantitative in the sense that numerical values are used for the various physical property parameters and that both the deformations and stresses and their relationships and variations are evaluated in numerical terms. This is in contrast to the qualitative interpretation of the deformation results presented in Sect. 11.4. Although the analysis was carried out primarily to provide the background information and technical reference for a future study of the effect of various design parameters on the long-term deformation of an actual waste disposal facility, it also resulted in an improved understanding of the behavior of the entire experimental area, especially with regard to the interdependence of the various parameters.

The organization of this chapter reflects the general approach to the investigation. First, a theoretical analysis was carried out to determine the feasibility of using computer modeling techniques. When this analysis indicated that all of the effects could be simulated, a computer program was written which combined the various influences over an area broad enough to include the entire four-room experimental area. These two steps, which are discussed in detail in the first two sections of this chapter, were carried out by A. M. Starfield. As anticipated, it was then necessary to search for the proper physical property values and to make several modifications in the program in order to reproduce the deformation results actually measured in the field during the PSV experiment. This was accomplished by making repeated computer runs using different values and observing the effects. Results of this investigation and the influence of some of the parameters are discussed in Sect. 13.3.

[1] Consultant, School of Mineral and Metallurgical Engineering, University of Minnesota, Minneapolis; now at Department of Applied Mathematics, University of Witwatersrand, Johannesburg, South Africa.

13.1 THEORETICAL ANALYSIS

In this analysis the laboratory measurements of creep in model salt pillars (see Chap. 12) are interpreted as providing a phenomenological or qualitative, though not necessarily quantitative, understanding of creep in actual mine pillars. The qualitative relationships obtained from the laboratory measurements are developed into a model of the deformations occurring in and near a mined excavation, and quantitative values for the various parameters of the model are then obtainable from comparisons with in situ measurements. At the same time the consistency of agreement between the model and in situ measurements will indicate whether or not the model gives a reasonable reflection of the physical processes contributing to the deformation of the rock salt.

Deformations will occur in the pillars and surrounding salt as a result of three interrelated phenomena:

1. the redistribution of stress as a result of mining operations in the salt,
2. the action of thermal stresses induced by temperature increases in the salt surrounding the radioactive waste,
3. the redistribution of stress as a result of changes in the creep characteristics of the pillars with temperature.

Condition 1 is common to all mining operations, while conditions 2 and 3 are peculiar to situations where heat sources are placed in the mine. Therefore, it would appear reasonable to first consider existing analyses of rock movements near underground mine excavations and then to extend these to include the thermal effects of conditions 2 and 3.

Methods for calculating ground movements and stress redistribution near flat-lying, partly excavated tabular deposits, except for the most simple of geometries, have only recently been developed. Salamon[2] in 1963 suggested a "face element" technique for calculating strata movements near excavations in linearly elastic rocks once the vertical closure and relative movements between the roof and floor of the excavation are known. In order to predict these relative movements within the excavation, an electric resistance analog was devised by the Mining Research Laboratory of the South African Chamber of Mines.[3] It appears to be very difficult, if not impossible, to extend the application of this analog technique to include the nonlinear temperature effects and time-dependent behavior of salt required for this analysis. However, the original "face element" concept has recently been adapted to digital computing methods for calculating both the relative movements between roof and floor in a tabular excavation and the deformation of the surrounding strata. Details of this method have not yet been published, but some of the results which have been obtained using it are given in a paper by Starfield and Fairhurst.[4] The digital computer method is far more flexible than the analog, and it should be possible to extend it to the unusual heating conditions of interest. The following analysis was therefore carried out with this as the primary objective.

13.1.1 Rheological Properties of Rock Salt

The rheological properties of rock salt depend very strongly on the temperature and stress fields to which the salt is subjected. Under completely triaxial hydrostatic loading, salt would be expected to behave perfectly elastically,[5] and this behavior would be far less dependent on temperature and pressure than is the creep rate under uniaxial loading. Between the two extremes of hydrostatic and uniaxial loading, the transition from elastic to time-dependent behavior and the creep rate must depend on an invariant of the stress field which reflects the deviation from hydrostatic conditions. The octahedral shear stress,

$$\tau_{oct} = \tfrac{1}{3}[(\sigma_1 - \sigma_2)^2 + (\sigma_2 - \sigma_3)^2 + (\sigma_1 - \sigma_3)^2]^{1/2}, \quad (13.1)$$

is just such an invariant, changing from $\tau_{oct} = 0$ for hydrostatic conditions to $\tau_{oct} = \sigma_1\sqrt{2}/3$ for uniaxial loading.

Dimensional analysis requires that the relationship between stress and strain be a function not only of a stress invariant but also of a dimensionless invariant. If τ_{lim} represents the octahedral shear stress at which the transition from elastic to time-dependent behavior takes place, then in a general form the relationship between strain e and stress σ is of the form

$$e = f(\tau_{oct}/\tau_{lim}) \cdot \sigma . \quad (13.2)$$

The stress-strain relationship obtained for model salt pillars[6] may be written in the form

$$e = (\text{constant} \times T^{9.5} \times t^{0.3} \times \sigma^{2.0})\,\sigma , \quad (13.3)$$

where t is the time and T the absolute temperature. This expression suggests that $f(\tau_{oct}/\tau_{lim})$ depends on $(\tau_{oct}/\tau_{lim})^{2.0}$. The creep and creep rate functions are thus apparently proportional to the ratio τ_{oct}/τ_{lim} to a power of about 2.

This argument leads to a justification of the first assumption to be made in this analysis. An unconfined salt pillar will be subjected to a much higher ratio of τ_{oct}/τ_{lim} than any other part of the salt mass. Since the creep rate function depends on something like the square of this ratio, the creep rate will be considerably higher in the pillar than anywhere else in the surrounding salt. The first assumption to be made will thus be that the creep rate in the surrounding rock can be neglected in comparison with the creep rate in the pillars. This assumption should be a valid approximation except for the immediate vicinity of the roof and floor of a mined-out room. Since these areas must be excluded from the analysis anyway, because of the bed separation and viscoelastic buckling which undoubtedly occur (see Sect. 11.4.5.6) but which cannot be conveniently incorporated into the computer model, this exception is probably not serious. Therefore the partly confined salt above and below the mining

[2] M. D. G. Salamon, "An Elastic Analysis of Displacements and Stresses Induced by Mining of Seam or Reef Deposits," *J. S. African Inst. Mining Met.* **64**, 128 (1964).

[3] N. G. W. Cook, "The Design of Underground Excavations," *Failure and Breakage of Rock,* ed. by C. Fairhurst, p. 174, 1967.

[4] A. M. Starfield and C. Fairhurst, "How High Speed Computers Advance Design of Practical Mine Pillar Systems," *Eng. Mining J.*, May 1968, p. 78.

[5] S. Serata, "Theory and Model of Underground Opening and Support System," *Proc. Sixth Symp. on Rock Mechanics,* 1964.

[6] J. F. Lomenick and R. L. Bradshaw, "Deformation of Rock Salt in Openings Mined for the Disposal of Radioactive Wastes," *Rock Mech.* **1**, 15–29 (1969).

horizon will be treated as an elastic material with modulus and Poisson's ratio independent of stress and temperature, while the supporting pillars will be allowed to deform in a much more complicated way.

13.1.2 Creep in Salt Pillars

Compression tests on model pillars under constant vertical load σ_0 (psi) at constant absolute temperature T_0 (see Chap. 12) have led[6] to the following formula for the strain (in microinches per inch) after time t (in hours):

$$e = 1.3 \times 10^{-37} T_0^{9.5} t^{0.3} \sigma_0^{3.0} . \tag{13.4}$$

This empirical expression excludes the first 2 min of loading, but it will be assumed to be valid from time zero.

If a full-size pillar underground deforms qualitatively in the same way as a model pillar in the laboratory, then under constant load and temperature the strain in the pillar will be given by

$$e = A T_0^b t^a \sigma_0^c , \tag{13.5}$$

where A, a, b, and c are constants. It is possible that the exponents a, b, and c will not change significantly with the size and shape of the pillar, and their numerical values may thus be similar to the exponents in Eq. (13.4). However, the constant A will almost certainly depend on the shape, size, and the composition (such as the distribution of shale partings in the pillar) of the pillar.

In the underground situation a pillar will in fact be subjected to changing stresses and temperatures. Suppose that the temperature is constant but the compressive load is a function of time $\sigma(t)$. Then at time τ the load will be $\sigma(\tau)$, and if a small change in load $d\sigma(\tau)$ occurs at that time, the resulting change in strain, $de(t)$, at any subsequent time t, will by analogy with Eq. (13.5) be given by

$$de(t) = cA T_0^b (t - \tau)^a [\sigma(\tau)]^{c-1} d\sigma(\tau) . \tag{13.6}$$

Integration of this expression for all stress increments between zero time (at which the strain was assumed to be zero) and time t gives the total strain at time t,

$$e(t) = cA T_0^b \int_0^t (t - \tau)^a \sigma(\tau)^{c-1} \frac{\partial \sigma(\tau)}{\partial \tau} d\tau . \tag{13.7}$$

Equation (13.7) reduces to (13.5) if $\sigma(\tau) = \sigma_0$ for all $\tau > 0$.

The effect of temperature changes may be included in Eq. (13.7) by using an equivalence between temperature and time which was first noted by Leaderman.[7] From Eq. (13.5) it can be confirmed that the strain in a pillar at temperature T_1 and time t_1 is the same as the strain in the pillar at temperature T_0 and t_0 if

$$t_0 = (T_1/T_0)^{b/a} \cdot t_1 . \tag{13.8}$$

The change in temperature is thus equivalent to a change in the time scale. This equivalence was used by Morland and Lee[8] to calculate the influence of time-dependent temperature fields by replacing the temperature and times in part of Eq. (13.7) by a temperature-time equivalent. In our case this would mean that for a changing temperature $T(t)$, Eq. (13.7) becomes:

$$e(t) = cA \int_0^t \left[\int_0^t T^{b/a}(u)\, du - \int_0^\tau T^{b/a}(u)\, du \right]^a \sigma^{c-1}(\tau) \frac{\partial \sigma}{\partial \tau} d\tau ,$$

or

$$e(t) = cA \int_0^t \left[\int_\tau^t T^{b/a}(u)\, du \right]^a \sigma^{c-1}(\tau) \frac{\partial \sigma}{\partial \tau} d\tau . \tag{13.9}$$

Equation (13.9) thus expresses in a completely general form for a salt pillar the relationship between stress and strain at any time and temperature.

For computational purposes the integral with respect to τ is reduced to a sum. Suppose that the time 0 to t is divided into N intervals each of length δt, and let e_n denote the strain at time $n\,\delta t$. Then Eq. (13.9) may be written

$$e_N = cA \sum_{n=1}^{N} \int_{(n-1)\delta t}^{n\,\delta t} \left[\int_\tau^{N\,\delta t} T^{b/a}(u)\, du \right]^a \sigma^{c-1}(\tau) \frac{\partial \sigma}{\partial \tau} d\tau . \tag{13.10}$$

Now suppose that the intervals δt are so small that the term

$$\left[\int_\tau^{N\,\delta t} T^{b/a}(u)\, du \right]^a$$

[7] H. Leaderman, chap. I in *Rheology*, vol. II, ed. by F. R. Eirich, Academic, 1956.

[8] L. W. Morland and E. H. Lee, "Stress Analysis for Linear Visco-Elastic Materials with Temperature Variation," *Trans. Soc. Rheol.* 4, 233 (1960).

is very nearly linear over each of the intervals. Then as an approximation:

$$e_N = \frac{1}{2} cA \sum_{n=1}^{N} \left\{ \left[\int_{n\,\delta t}^{N\,\delta t} T^{b/a}(u)\,du \right]^a + \left[\int_{(n-1)\delta t}^{N\,\delta t} T^{b/a}(u)\,du \right]^a \right\} \int_{(n-1)\delta t}^{n\,\delta t} \sigma^{c-1}(\tau) \frac{\partial \sigma}{\partial \tau} d\tau$$

$$= \frac{1}{2} A \sum_{n=1}^{N} \left\{ \left[\int_{n\,\delta t}^{N\,\delta t} T^{b/a}(u)\,du \right]^a + \left[\int_{(n-1)\delta t}^{N\,\delta t} T(u)^{b/a}\,du \right]^a \right\} \{\sigma^c(n\,\sigma t) - \sigma^c(\overline{n-1}\,\delta t)\} \ . \quad (13.11)$$

If $\sigma(n\,\delta t)$ is denoted by σ_n and the integral

$$\left[\int_{n\,\delta t}^{N\,\delta t} T^{b/a}(u)\,du \right]^a$$

by ψ_{N-n}, then

$$e_N = \frac{1}{2} A \sum_{n=1}^{N} (\psi_{N-n} + \psi_{N-n+1})(\sigma_n^c - \sigma_{n-1}^c) , \quad (13.12)$$

which can be rewritten

$$e_N = E_0 \sigma_N^c + B_N , \quad (13.13)$$

where

$$E_0 = \frac{1}{2} A(\psi_0 + \psi_1)$$

and

$$B_N = \frac{1}{2} A \sum_{n=1}^{N-1} (\psi_{N-n+1} - \psi_{N-n-1})\sigma_n^c - \frac{1}{2} A(\psi_N + \psi_{N-1})\sigma_0^c$$

and thus depends on the loads at each of the previous time steps, that is, the loading history of the pillar.

Since the deformations in a salt mine will be calculated in sequential time steps, at any time $N\,\delta t$ the loads σ_0, σ_1, σ_2, ..., σ_{N-1} will have been calculated, and once the pillar temperature is specified as a function of time, the functions ψ_0, ψ_1, ψ_2, ..., ψ_{N-1}, ψ_N can also be calculated. Thus, at any instant, σ_N and B_N will be known, and Eq. (13.13) can thus be considered as the instantaneous relationship between the stress and strain in the salt pillar.

In the next section the interaction of the deformation of the salt pillars, defined by Eq. (13.13), along with the movements in the surrounding mass of salt, will be considered.

13.1.3 The Mining Horizon as an Incompatibility in an Infinite Elastic Body

Since the height of the rooms and pillars in the mine is negligible as compared with the depth of the mining horizon below the surface, two simplifying assumptions can be made:

1. that the rock mass surrounding the excavation tends to infinity in all directions,
2. that both the roof and floor of the excavation can be considered as part of the same plane – the mining horizon. If a Cartesian axis system with the x and y axes in the plane of the excavation and the z axis pointing downward is then introduced, the roof of the excavation is the plane $z = 0$ (approached from the negative z direction), and the footwall is the plane $z = 0$ (approached from the positive z direction).

However, once mining operations begin, the roof and floor of the excavation will, of course, converge. This convergence can be represented as a displacement anomaly on the plane $z = 0$, and the mining horizon can be considered as an incompatibility in an infinite rock salt mass. According to the assumption discussed in Sect. 13.1.1, this rock salt mass will be assumed to be linear and elastic with modulus E and Poisson's ratio ν independent of stress and temperature.

The equations of equilibrium in this elastic mass can be expressed in terms of the displacements u, v, and w (in the x, y, and z directions respectively) which are induced in the mass as a result of mining:

$$\frac{\partial e}{\partial x} + (1 - 2\nu)\,\nabla^2 u = 0 ,$$

$$\frac{\partial e}{\partial y} + (1 - 2\nu)\,\nabla^2 \mathrm{v} = 0 , \quad (13.14)$$

$$\frac{\partial e}{\partial z} + (1 - 2\nu)\,\nabla^2 w = 0 ,$$

where

$$e = \frac{\partial u}{\partial x} + \frac{\partial v}{\partial y} + \frac{\partial w}{\partial z}.$$

The solution to these equations in the infinite mass can be expressed[9] in terms of three harmonic functions ϕ_1, ϕ_2, and ϕ_3:

$$u = 2(1-\nu)\frac{\partial \phi_1}{\partial z} - (1-2\nu)\frac{\partial \phi_3}{\partial x} - z\frac{\partial \phi}{\partial x},$$

$$v = 2(1-\nu)\frac{\partial \phi_2}{\partial z} - (1-2\nu)\frac{\partial \phi_3}{\partial y} - z\frac{\partial \phi}{\partial y}, \qquad (13.15)$$

$$w = 2(1-\nu)\frac{\partial \phi_3}{\partial z} + (1-2\nu)\left(\frac{\partial \phi_1}{\partial x} + \frac{\partial \phi_2}{\partial y}\right) - z\frac{\partial \phi}{\partial z},$$

where

$$\phi = \frac{\partial \phi_1}{\partial x} + \frac{\partial \phi_2}{\partial y} + \frac{\partial \phi_3}{\partial z}.$$

Solutions of the form

$$\begin{aligned} \phi_1 &= -U/r, \\ \phi_2 &= -V/r, \\ \phi_3 &= -W/r, \end{aligned} \qquad (13.16)$$

where

$$r^2 = x^2 + y^2 + z^2,$$

are of particular interest in this case. On the plane $z = 0$,

$$\begin{aligned} u &= -(1-2\nu)\, Wx/(x^2+y^2)^{1/2}, \\ v &= -(1-2\nu)\, Wy/(x^2+y^2)^{1/2}, \\ w &= (1-2\nu)\,(Ux+Vy)/(x^2+y^2)^{1/2} \end{aligned} \qquad (13.17)$$

at all points of the plane except the origin, where the displacements are indeterminate. However, if a small rectangle of length $2\,\Delta x$ and width $2\,\Delta y$ surrounding the origin is considered, the *average* displacements over the area of the rectangle near the plane $z = 0$ can be calculated. For example, for small z, the average vertical displacement W will be

$$\overline{W} = \frac{1}{4\,\Delta x\,\Delta y}\int_{-\Delta x}^{\Delta x}\int_{-\Delta y}^{\Delta y} W\,dy\,dx$$

$$= \frac{1}{4\,\Delta x\,\Delta y}\cdot 4W(1-\nu)\left[\arctan\left(\frac{\Delta x}{z}\right) - \arctan\left(\frac{-\Delta x}{z}\right)\right].$$

If z approaches 0 from the positive z direction, that is, from below the floor,

$$\overline{W} \to W\pi(1-\nu)/\Delta x\,\Delta y,$$

and if z approaches 0 from the negative direction, that is, from above the roof,

$$\overline{W} \to W\pi(1-\nu)/\Delta x\,\Delta y.$$

The relative vertical movement between roof and floor in the rectangle is thus $-2W\pi(1-\nu)/\Delta x\,\Delta y$. If this vertical closure between roof and floor is denoted by W_∞, then

$$W_\infty = -2W\pi(1-\nu)/\Delta x\,\Delta y,$$

and similarly

$$\begin{aligned} U_\infty &= -2U\pi(1-\nu)/\Delta x\,\Delta y, \\ V_\infty &= -2V\pi(1-\nu)/\Delta x\,\Delta y, \end{aligned} \qquad (13.18)$$

where U_∞ and V_∞ are the relative movements between roof and floor or "ride components" in the x and y directions respectively. It follows from Eq. (13.17) that the closure and ride components anywhere in the horizon outside of the rectangle surrounding the origin are zero.

The stresses induced by these closures and ride components will now be considered. The stresses corresponding to harmonic solutions ϕ_1, ϕ_2, and ϕ_3 in general are given by[9]

$$\sigma_x = 2G\left[\frac{\partial^2 \phi_3}{\partial z^2} + 2\frac{\partial^2 \phi_1}{\partial x\,\partial z} + 2\nu\frac{\partial^2 \phi_2}{\partial y\,\partial z} + (1-2\nu)\frac{\partial^2 \phi_3}{\partial y^2} - z\frac{\partial^2 \phi}{\partial x^2}\right],$$

[9] N. G. W. Cook *et al.*, "Rock Mechanics Applied to the Study of Rockbursts," *J. S. African Inst. Mining Met.* **66**, 485–86 (1966).

$$\sigma_y = 2G\left[\frac{\partial^2\phi_3}{\partial z^2} + 2\frac{\partial^2\phi_2}{\partial y\,\partial z} + 2\nu\frac{\partial^2\phi_1}{\partial x\,\partial z} + (1-2\nu)\frac{\partial^2\phi_3}{\partial x^2} - z\frac{\partial^2\phi}{\partial y^2}\right],$$

$$\sigma_z = 2G\left[\frac{\partial^2\phi_3}{\partial z^2} - z\frac{\partial^2\phi}{\partial z^2}\right], \qquad (13.19)$$

$$\tau_{xz} = 2G\left[\frac{\partial^2\phi_1}{\partial z^2} + \nu\frac{\partial}{\partial y}\left(\frac{\partial\phi_1}{\partial y} - \frac{\partial\phi_2}{\partial x}\right) - z\frac{\partial^2\phi}{\partial x\,\partial z}\right],$$

$$\tau_{yz} = 2G\left[\frac{\partial^2\phi_2}{\partial z^2} - \nu\frac{\partial}{\partial x}\left(\frac{\partial\phi_1}{\partial y} - \frac{\partial\phi_2}{\partial x}\right) - z\frac{\partial^2\phi}{\partial y\,\partial z}\right],$$

$$\tau_{yx} = 2G\left[(1-\nu)\frac{\partial}{\partial z}\left(\frac{\partial\phi_1}{\partial y} + \frac{\partial\phi_2}{\partial x}\right) - (1-2\nu)\frac{\partial^2\phi_3}{\partial x\,\partial y} - z\frac{\partial^2\phi}{\partial x\,\partial y}\right],$$

where the shear modulus $G = E/2(1+\nu)$.

Substituting for ϕ_1, ϕ_2, and ϕ_3 from Eq. (13.16), the three stresses having components in the z direction are found to be

$$\sigma_z = 2GW/(x^2+y^2)^{3/2},$$
$$\tau_{xz} = 2G[(1+\nu)\,U/(x^2+y^2)^{3/2} + 3\nu(Vxy - Uy^2)/(x^2+y^2)^{5/2}], \qquad (13.20)$$
$$\tau_{yz} = 2G[(1+\nu)\,V(x^2+y^2)^{3/2} + 3\nu(Uxy - Vx^2)/(x^2+y^2)^{5/2}]$$

on the plane $z = 0$.

The plane $z = 0$ can now be divided into a number of rectangles each of length $2\,\Delta x$ and width $2\,\Delta y$ so that the coordinates of the center of the $(m-n)$th rectangle will be $(2m\,\Delta x,\ 2n\,\Delta y)$. If the average normal stress over the $(m-n)$th rectangle is denoted by $(\bar{\sigma}_z)_{mn}$, then, by definition,

$$(\bar{\sigma}_z)_{mn} = \frac{1}{4\,\Delta x\,\Delta y}\int_{(2m-1)\Delta x}^{(2m+1)\Delta x}\int_{(2n-1)\Delta y}^{(2n+1)\Delta y}\sigma_z\,dy\,dx. \qquad (13.21)$$

If two sets of "point" functions are now defined as

$$f_1(m,n) = (m^2\Delta x^2 + n^2\Delta y^2)^{1/2}/mn,$$
$$f_2(m,n) = (m^2\Delta x^2 + n^2\Delta y^2)^{-1/2}, \qquad (13.22)$$

it can be shown that the average normal stress will be given by

$$(\bar{\sigma}_z)_{mn} = \frac{GW}{2\,\Delta x^2\,\Delta y^2}[f_1(2m+1, 2n-1) + f_1(2m-1, 2n+1) - f_1(2m+1, 2n+1) - f_1(2m-1, 2n-1)] \qquad (13.23a)$$

and the average shear stresses by

$$(\bar{\tau}_{xz})_{mn} = \frac{U}{W}(\bar{\sigma}_z)_{mn} + \frac{\nu GU}{2\,\Delta y^2}\left[\frac{2m+1}{2n+1}f_2(2m+1, 2n+1) + \frac{2m-1}{2n-1}f_2(2m-1, 2n-1) - \frac{2m+1}{2n-1}f_2(2m+1, 2n-1) - \frac{2m-1}{2n+1}f_2(2m-1, 2n+1)\right]$$
$$+ \frac{\nu GV}{2\,\Delta x\,\Delta y}[f_2(2m+1, 2n+1) + f_2(2m-1, 2n-1) - f_2(2m+1, 2n-1) - f_2(2n-1, 2n+1)], \qquad (13.23b)$$

$$(\bar{\tau}_{yz})_{mn} = \frac{V}{W}(\bar{\sigma}_z)_{mn} + \frac{\nu GV}{2\,\Delta x^2}\left[\frac{2n+1}{2m+1}f_2(2m+1, 2n+1) + \frac{2n-1}{2m-1}f_2(2m-1, 2n-1) - \frac{2n-1}{2m+1}f_2(2m+1, 2n-1) - \frac{2n+1}{2m-1}f_2(2m-1, 2n+1)\right]$$
$$+ \frac{\nu GU}{2\,\Delta x\,\Delta y}[f_2(2m+1, 2n+1) + f_2(2m-1, 2n-1) - f_2(2m+1, 2n-1) - f_2(2m-1, 2n+1)].$$

The average stress components at the $i - j$th element due to closure components U_{kl}, V_{kl}, and W_{kl} at the $k - l$th element will be given by Eqs. (13.23) provided that

$$m = i - k ,$$

$$n = j - l ,$$

and, by Eq. (13.18),

$$U = -U_{kl}\, \Delta x\, \Delta y/2\pi(1 - \nu) ,$$

$$V = -V_{kl}\, \Delta x\, \Delta y/2\pi(1 - \nu) , \qquad (13.24)$$

$$W = -W_{kl}\, \Delta x\, \Delta y/2\pi(1 - \nu) .$$

A more general form of Eq. (13.23) would be

$$(\bar{\sigma}_z)_{ijkl} = a_{ijkl}\, W_{kl} ,$$

$$(\bar{\tau}_{xz})_{ijkl} = (a_{ijkl} + b_{ijkl})U_{kl} + c_{ijkl}\, V_{kl} , \qquad (13.25)$$

$$(\bar{\tau}_{yz})_{ijkl} = (a_{ijkl} + d_{ijkl})V_{kl} + c_{ijkl}\, U_{kl} ,$$

where the coefficients a_{ijkl}, etc., can be determined by comparison with Eqs. (13.23).

Finally, the total stresses at the $i - j$th rectangle, $(S_z)_{ij}$, are obtained by adding the contributions from the closure components at each of the elementary rectangles in the mining plane to the primitive stresses P_z, P_{xz}, and P_{yz} which were acting on the mining horizon before mining operations were started:

$$(S_z)_{ij} = P_z + \sum_k \sum_l (\sigma_z)_{ijkl} ,$$

$$(S_{xz})_{ij} = P_{xz} + \sum_k \sum_l (\bar{\tau}_{xz})_{ijkl} , \qquad (13.26)$$

$$(S_{yz})_{ij} = P_{yz} + \sum_k \sum_l (\bar{\tau}_{yz})_{ijkl} .$$

Equations (13.26) and (13.25) express the total stresses acting in the plane of the excavation as linear functions of the closure components at all points in the plane. In particular the normal stress is a linear function of only the vertical closure components in the plane, while the shear stresses depend on both ride components.

Equations (13.25) and (13.26) can be solved for all the components of closure and ride in the plane of the excavation by specifying the stresses S_z, S_{xz}, and S_{yz} at each of the rectangles in the plane in the following manner: If the $i - j$th rectangle represents a *mined* portion of the horizon, then

$$(S_z)_{ij} = (S_{xz})_{ij} = (S_{yz})_{ij} = 0 . \qquad (13.27)$$

If the $i - j$th rectangle represents an *unmined* portion of the horizon (i.e., part of a pillar, a remnant, or an abutment), then two cases arise:

1. If the $i - j$th rectangle is sufficiently far from any excavation that it must be considered relatively confined, then using the same arguments as in Sect. 13.1.1, it can be assumed to deform elastically. It follows that

$$(S_z)_{ij} = EW_{ij}/h ,$$

$$(S_{xz})_{ij} = GU_{ij}/h , \qquad (13.28)$$

$$(S_{yz})_{ij} = GV_{ij}/h ,$$

where h is the pillar height, so that W_{ij}/h will be the vertical pillar strain, etc.

2. If this rectangle is part of a pillar or part of a remnant or abutment which is sufficiently close to a room to be considered relatively unconfined, the salt between the roof and floor will creep, and at a time $N\ \delta t$ after mining operations were started, the stress-strain relationship will be given by Eq. (13.13), namely

$$e_N = E_0 \sigma_N^c + B_N .$$

Instantaneously at time $N\ \delta t$ the stress on the pillar σ_N will be $(S_z)_{ij}$, and the vertical strain e_N will be W_{ij}/h. Thus at each time interval the stress $(S_z)_{ij}$ is related to the vertical closure by an expression of the form

$$(S_z)_{ij} = \left[\frac{1}{E_0}(W_{ij}/h - B_N)\right]^{1/c} . \qquad (13.29)$$

The shear stresses must also be related to the shear strains in the salt by some form of shear-creep relationship. In the absence of any information on this relationship, one can only suggest that the creep in shear will be similar in form to creep in uniaxial compression and that some sort of equation similar to Eq. (13.29) should relate $(S_{xz})_{ij}$ to U_{ij}/h and $(S_{yz})_{ij}$ to V_{ij}/h.

13.1.4 Temperature Changes and Thermal Stresses

To complete the analysis, the temperature changes and the resulting thermal stresses in the salt due to heat sources in the floor of the mine must be considered. The influence of the temperature changes within the pillar on its creep characteristics has already been included in Eq. (13.9). Although sophisticated heat transfer[10] programs are now available for calculating the temperature rises in the salt at any distance from heat sources buried in the floor of the mine, these are neither necessary nor particularly desirable for inclusion in this analysis. For this purpose, a simplified calculation starting with an instantaneous heat source at some point in the infinite rock mass is sufficient. An instantaneous heat source is defined as a source which liberates a finite quantity of heat in a very short time. The strength of the source, Q, is the temperature to which this finite amount of heat would raise a unit volume of the salt.[11] If the instantaneous source liberates its heat at time τ, then the temperature in the rock at a radial distance r from the source at a subsequent time t is given by[11]

$$T(r, t) = T_0 + \frac{Q}{(\pi\theta)^{3/2}} \cdot e^{-r^2/\theta} , \qquad (13.30)$$

where $\theta = 4K(t - \tau)$ and K = thermal diffusivity of the rock salt.

As a result of the attempted expansion of the salt with increasing temperature, thermal stresses are induced in the rock surrounding the source. The thermal stress components F_z, F_{xz}, and F_{yz} at a point (x, y) on the plane $z = 0$ as a result of an instantaneous point source located at $(0, 0, d)$ in the infinite mass can be obtained from Nowacki:[12]

$$F_z = \frac{mQG}{2\pi r^3} \left\{ \left[2 - \frac{3(x^2 + y^2)}{r^2} \right] erf\left(\frac{r}{\sqrt{\theta}} \right) - \frac{2r}{\sqrt{\pi\theta}} \left[2 - \frac{3(x^2 + y^2)}{r^2} \left(1 + \frac{2r^2}{3\theta} \right) \right] e^{-r^2/\theta} \right\} , \qquad (13.31)$$

$$F_{xz} = \pm F_{yz} = \pm \frac{3mQGd}{2\pi r^5} (x^2 + y^2)^{1/2} \times \left[erf\left(\frac{r}{\sqrt{\theta}} \right) - \frac{2r}{\sqrt{\pi\theta}} (1 + 2r^2/3\theta)\, e^{-r^2/\theta} \right] ,$$

where

$r^2 = x^2 + y^2 + d^2$,

$m = \alpha(1 + \nu)/(1 - \nu)$,

α = coefficient of thermal expansion of the rock salt,

and the sign of the shear stress will depend on the quadrant of (x, y).

If the heat source is a continuous function of time $Q(\tau)$, then the stresses at time t are given by integrals of Eq. (13.31),

$$F_z(t) = \int_0^t Q(\tau)\, F_z(\theta)\, d\tau$$

and

$$F_{xz}(t) = \pm F_{yz}(t) = \int_0^t Q(\tau)\, F_{xz}(\theta)\, d\tau . \qquad (13.32)$$

The temperature at a distance r from the source is given by

$$T(r, t) = T_0 + \pi^{-3/2} \int_0^t Q(\tau)\, \theta^{-3/2}\, e^{-r^2/\theta}\, d\tau . \qquad (13.33)$$

Once $Q(\tau)$ is specified, the integrals in (13.32) and (13.33) can be evaluated mathematically or calculated numerically using a summation scheme in the same way as the approximation to Eq. (13.9).

A number of assumptions are implicit in the application of Eqs. (13.32) and (13.33) to the problem at hand:

1. It is assumed that the thermal diffusivity K and coefficient of expansion α are independent of the temperature of the salt. Mean values of K and α over the expected range of temperatures must thus be selected.
2. An inconsistency has been introduced in the scale of the problem. While it is reasonable to neglect the height of the rooms and pillars in comparison with the depth of the mine below the surface, this height is directly comparable with the depth of burial of

[10] W. D. Turner and J. S. Crowell, *Notes on Heating – an IBM 360 Heat Conduction Program,* CTC-INF-980 (November 1969).

[11] H. S. Carslaw and J. C. Jaeger, *Conduction of Heat in Solids,* 2d ed., Oxford, p. 260, 1959.

[12] W. Nowacki, *Thermoelasticity,* p. 201, Pergamon, 1962.

the heat sources in the floor of the mine. Since the roof and floor of the mine are being considered as two sides of the same plane $z = 0$, the best compromise is to measure the depth of burial d of the heat sources from a point halfway between the roof and floor of the rooms in which the sources are buried.

3. The thermal stresses are calculated on the assumption that the pillars are unable to expand laterally into the rooms. Since the lateral deformation of the pillars has so far been ignored, this assumption is no worse than assumptions that are already implicit in our analysis.

Within these limitations, Eqs. (13.32) and (13.33) probably give a reasonably good description of the thermal effects of the waste in the footwalls. The pattern of heat sources in a room can be simulated by one or more point sources, and the resultant thermal stresses in the plane of the excavation and the temperatures in the pillars can be obtained by superimposing the stresses and temperatures from all of the heat sources in the mine.

13.2 DESCRIPTION OF THE COMPUTER PROGRAM

The computer program which was written to provide a simulation of the deformational behavior of the experimental area is essentially a synthesis of the various components discussed in the previous section in such a way so as to include their interactions. A listing of the program (in FORTRAN language) is included as Appendix 13.A, and reference can be made to it during the following discussion. Also, a description of some of the program parameters is given in Table 13.1.

The objectives of the program are to calculate the stresses in the pillars and abutments, the vertical deformation at any point in these pillars and abutments, and the movements and stresses at any point in the elastic zones above and below the mining horizon.

13.2.1 Basic Setup

Although the analysis was carried out for a general three-dimensional geometry, the program was written for the case of plane strain, that is, assuming no displacements will occur in the y direction. This assumption led to a considerable simplification, and it should be applicable to a full-scale room and rib pillar design. While the four-room experimental area is obviously not in plane strain, it should be possible to test the program against the results obtained at the north-south center line of the pillars.

The ride components in the x direction were also ignored. It is unlikely that primitive shear stresses exist, so that the "effective" primitive shear stress results only from thermal shear stress components F_{xz} and F_{yz}. Since the heat sources were symmetrically distributed through the experimental area, the shear components tend to cancel out. Therefore, the effective shear stresses should be negligible and the ride components very nearly zero. In actual waste disposal operations, the heat sources will be evenly distributed throughout the mine but will be placed sequentially, which will lead to at least some asymmetry. If this leads to significant shear stresses, then some modification of Eq. (13.29) may be required to incorporate the creep of the pillars in shear.

The plane of the excavation (in the x direction only) is divided into a number NX of segments each of width 2DX. The origin is placed well to the left of the excavated area, and the region $0 \leqslant x \leqslant 2NX$ embraces the entire area over which significant relative movement between the roof and floor may occur. The order of mining operations is simulated by defining, at each time step, the "status" of each segment, that is, whether it represents an excavated portion of the mine, as in Eq. (13.27), or an unexcavated portion. In the analysis of Sect. 13.1 and in the first version of the program, it was necessary to specify whether a particular segment was a confined portion of an abutment behaving elastically as in Eq. (13.28) or was near enough to a pillar edge to be creeping according to Eq. (13.29). This distinction was found to require considerable judgment on the part of the programmer and to produce unacceptably distorted stress distributions. Therefore, the program was modified to define the relative proportions of elastic and creep behavior at each segment according to its distance from the nearest excavated segment. This was accomplished by defining an arbitrary factor which reduces the total stress on a segment to a "creep effective stress" for use in Eq. (13.5) according to

$$\sigma_0 = \sigma_T[1 - e^{-\bar{\omega}\lambda/h}] \quad , \tag{13.34}$$

where $\bar{\omega}$ represents the distance of the segment from the nearest excavation, h is the pillar height, and λ is an arbitrary coefficient representing the effectiveness of distance in providing confinement. These conditions imposed on the average vertical stress at each of the NX segments lead by the first of Eq. (13.25) to a set of NX equations which can be solved for the closure

components W_{kl}. In this plane strain problem, Eq. (13.25) reduces to

$$\sigma_i = \sum_{k=1}^{n} \alpha_{ik} W_k , \qquad (13.35)$$

where the "influence coefficients" α_{ik} are the plane strain equivalents of the coefficients α_{ijkl} in Eq. (13.25).

13.2.2 Computation at Each Time Step

13.2.2.1 Temperatures. – Since the solution was carried out for plane strain, a row of individual heat sources parallel to the y axis was simulated by a single line source located at a depth (called DPQ) below the floor. The actual vertical cylindrical shape of each heat source was thus ignored, and the depth was taken to be the mid height of the individual cylinders. The strength of this line source was obtained by "smearing" the heat along the distance between the discrete sources. Depending both on the location and time of installation of each of these line sources (obviously some time after the excavation of the room), the average temperature of an unexcavated segment affected by the heat sources at each time step can be calculated from Eq. (13.33). This *average* temperature was approximated by the temperature at the center of the segment and the mid height of the pillar. These temperatures can be printed out for comparison with the more elaborate heat transfer calculations and adjusted if necessary by moving the point which is taken as representative of the average segment temperature. The time-temperature creep functions ψ_{N-n} which are used in the calculation of E_0 and B_N in Eq. (13.13) are then calculated for each creeping element at each time step.

13.2.2.2 Thermal Stresses. – The thermal stresses associated with each line heat source can be simulated in two different ways:

1. The thermal response of the salt surrounding the source is assumed to be viscous in nature. The viscous response to a continuous heat source is then, by the correspondence principle, directly proportional to the elastic response to an instantaneous heat source. The radial and tangential thermal stresses are thus (see Eq. 13.31):

$$\sigma_{rr} = (QV/\pi)(1 - e^{-u})/r^2 ,$$
$$\sigma_{\theta\theta} = (QV/\pi)\,[(1 + 2u)e^{-u} - 1]/r^2 , \qquad (13.36)$$

where

$u = r^2/4kt$ and

V = the product of the coefficient of expansion and the coefficient of viscosity.

By analogy with Eq. (13.5) the coefficient of viscosity would be expected to be extremely sensitive to temperature, probably varying as $1/T^c$.

2. The thermal response of the rock surrounding the line source is assumed to be elastic. The effect of a continuous heat source is then the superposed effect of a number of instantaneous sources, and the thermal stresses are obtained by adding the stresses in Eq. (13.36) at each time step of the solution. The constant V will then be given by

$$V = \alpha(\mathrm{DT})\,\frac{E}{2(1 - \nu)} , \qquad (13.37)$$

where α = coefficient of linear thermal expansion and DT = time step (hr) (in the program; see Appendix 13.A). In either case, the normal components of the thermal stresses in the plane, $F_z(t)$, are calculated at each time step for all heat sources and added together to obtain the total thermal stress normal to each segment. This value is added to the primitive stress P_z [see Eq. (13.26)] to obtain an "effective primitive stress"

$$P_z(t) = P_z + \sum_{\text{heat sources}} F_z(t) , \qquad (13.38)$$

which varies with time and includes the thermal stress effects in the mine.

Preliminary runs with the computer program indicated that neither of these methods of handling the thermal stress was adequate. The viscous thermal stress method did not produce nearly enough of a perturbation to simulate the extensive thermal stress effects discussed in Sect. 11.4. Furthermore, the character of the simulated deformations, especially at the time the heat sources were turned off, differed markedly from that actually observed. The elastic thermal stress method produced simulated deformations which appeared to have a much more realistic shape, but the effects of a single room of heaters strongly influenced the entire experimental area rather than being confined fairly close to the heat sources. The reason for this was that the computer program considers thermal stresses as a local concentration of the primitive stress. The segment subjected to the maximum thermal stress for each heat source is, obviously, the one containing the heat source. Since this segment must be an excavated

one, the program causes all of that maximum thermal stress to be transferred to the supporting pillars. This, in turn, causes abnormal stress concentrations in the pillars, which consequently adjust by shedding the load to the other portions of the mine, thereby spreading the effect over a wide area.

Apparently the salt in the floor was actually behaving like something between purely elastical and purely viscous, transmitting the thermal stresses nearly elastically but responding at least partially viscously by flowing up into the room. The initial program was therefore modified to reduce the value of the thermal stresses induced in mined-out segments by a constant factor ξ representing the relief of these thermal stresses by flowage while leaving the remainder of the thermal stress response as calculated by the elastic method.

13.2.2.3 Solution of Closure Equations. – From the total primitive stresses on each segment at each time step, $P_z(t)$, the first of Eq. (13.26) can be solved for the vertical closures in the plane $z = 0$ at each time interval with the aid of conditions (13.27), (13.28), and (13.29). Once the convergences are known, the normal stresses can be calculated from (13.26). These must be stored at each time step in order to calculate B_N of Eq. (13.13) for the following time step.

The solution of Eqs. (13.26) with (13.27), (13.28), and (13.29) at each time step can now be obtained by an iterative method. The equations constitute a set of NX equations in NX unknowns and are linear except for the nonlinear term introduced by (13.29) for each element that creeps. The linear equations are solved by Gauss-Seidel iteration, which is modified to a successive application of Newton's method of tangents for the nonlinear equations.[13] The solution of these equations is convergent.

13.2.2.4 Calculation of Off-Seam Displacements and Stresses. – Since the material in the roof and floor is assumed to be linearly elastic, the calculation of displacements and stresses at any point not in the plane of the mining horizon is a straightforward process based on the already determined displacement at the $z = 0$ plane as a boundary condition.

13.2.3 Input Data

In this section the input data which are required by the program will be discussed. These data consist of both physical property values and various operational parameters. The discussion of these input data will provide additional description of how the program works, but the main purpose of including it was to illustrate the wide variety of means available for modifying the simulated deformations produced for comparison with the actual underground measurements.

The input parameters are listed in the first column of Table 13.1 along with a brief definition. The first five of these parameters (E through PRIM) are concerned with the properties of the salt above and below the mining horizon. The next six (ES through W) define the properties of the pillars and remnants in the seam. The next seven parameters in the list (DX through MQ) are primarily concerned with the operation of the program. For all of these, the definitions given in Table 13.1 should be adequate. The next parameter, FLAM, is the λ in Eq. (13.34) and is the coefficient relating the distance of the segment being considered from the nearest mined segment to the amount of confinement and therefore the tendency toward elastic rather than creep behavior. The factor ξ, which establishes the portion of the thermal stress in a mined segment which is transferred to the pillars, is applied directly in statement 89 of the program (see "Thermal Stress" section of program listing, Appendix 13A). The parameter KI (statement following statement 4 in program listing) is used to limit the number of segments on either side of the segment containing a particular heat source which must be examined for temperature and thermal stress effects. Although this parameter is related to both the depth of burial of the heat sources and the segment width, it is largely under the control of the programmer. Depending on the geometry and time span of the problem, it was necessary to adjust this parameter over a fairly broad range.

The strength of each heat source (Q) can be obtained from the expression:

$$Q = \frac{Q_0}{c}, \tag{13.39}$$

where

Q_0 = constant heat generation rate per unit length of the line source (units such as kW/m or Btu hr^{-1} ft^{-1}),

c = heat capacity of salt (mean value = 28.2 Btu ft^{-3} $°F^{-1}$),

by converting it to the required units of °C ft^2 hr^{-1}. In order to turn off a heat source, simply add a source at the same location having a negative strength. For calculation of thermal stresses by the elastic method, the parameter EQ (or V in equation 13.37) should be as defined in Eq. (13.37). However, for reasons which will

[13] J. Todd, *A Survey of Numerical Analysis*, pp. 230 and 259, McGraw-Hill, 1962.

Table 13.1. Description of Program Parameters

Parameter Name[a]	Value Used for Comparison with Experimental Area	Definition of Parameter
E	10^6 psi	Elastic modulus of roof and floor rock
PR	0.4	Poisson's ratio of roof and floor
TEMP	300°K	Initial ambient temperature in vicinity of mining horizon
DIFF	0.1 ft^2/hr	Mean thermal diffusivity in vicinity of heat sources
PRIM	1000 psi	Pre-mining vertical stress
ES	1.5×10^6 psi	Elastic modulus of pillar
ALF	0.65×10^{-36}	Creep constants equivalent to A, a, c, b, respectively, in Eq. (13.5)
BET	0.37	
GAM	3.0	
PWR	9.5	
W	14.0 ft	Pillar height
DX	2.5 ft	Half width of each segment
NX	80	Total number of segments
DT	120 hr	Length of time step
NT	500	Total number of time steps
NCR	30	Maximum number of segments allowed to creep
DPQ	9 ft	Depth of heat source center below floor
MQ	16	Maximum number of line heat sources
FLAM	0.4	Confinement-distance coefficient, λ, in Eq. (13.34)
ξ	0.5	Thermal stress transference factor
KI	5	Number of segments to calculate thermal effects on either side of each heat source
		For Each of the MQ Heat Sources
Q	°C ft^2 hr^{-1}	Strength of the heat source
EQ	psi hr °C^{-1}	The coefficient V in Eqs. (13.37)
XQ	ft	The x coordinate of the heat source
NQ		The number of time steps before introducing the heat source
		For Each Change in Mining Pattern
NDT		Number of time steps at which the mining pattern is *next* changed
KK(I)		Code for status of each of NX segments: 0 = mined out, positive = creeping, negative = elastic
		For Each of the NCR Creeping Segments
NAC		The number of time steps elapsed before the segment is first permitted to creep

[a]Used in computer program, Appendix 13.A.

be discussed in the next section, this parameter was considered to be purely arbitrary.

13.3 COMPARISON OF COMPUTER MODEL WITH EXPERIMENTAL AREA

Following the initial preparation of the computer program, a number of preliminary runs[14] were carried out using simplified mining patterns and conditions (e.g., completely elastic media). These preliminary runs served to demonstrate that the program performed the calculations in the proper manner, provided some background on the response produced by changes in the input data, and most importantly, led to the major modifications mentioned in the previous section. Following this period of program testing, an extended series of computer runs was undertaken to establish the mix of physical property values and other parameters which would best reproduce the movements and deformations actually measured in the experimental area.

13.3.1 Basis of Comparison

13.3.1.1 Mine Layout and Mining Sequence. – The first problem in modeling the experimental area in the computer simulation was the departure from the

[14]Translation of the original program for compatibility with ORNL computing systems and most of these preliminary runs were carried out by R. E. Richert under the ORAU Summer Student Trainee Program.

assumed plane strain situation. Since heat sources were located in all four rooms of the experimental area and interactions between the rooms were of primary interest, the vertical north-south section through the area was chosen as the *xz* plane. This plane was placed at the midpoint between the corridor and the back of the room, so that it went through the center line of the circular arrays in rooms 1 and 4 and was highly instrumented (see composite results in Figs. 11.72, 11.73, and 11.88). Although the computer model considered the four rooms to be infinitely long, thus ignoring the presence of both the connecting corridor to the east and the solid unexcavated salt to the west, the effects of these departures from plane strain should be a minimum at the point midway between them. Examination of the differences in the behavior at the front and back of the pillars (Figs. 11.60, 11.64, 11.81, and 11.85) suggests that the effects of the corridor and solid salt become significant only very close to the two ends of the pillar. Therefore, it appears that the plane strain assumption is reasonable and that modeling of the experimental area along the north-south center line would be valid.

The selection of a segment width is primarily a compromise between the amount of detail desired in the results and the difficulties (and computer time) of handling a large number of segments. Preliminary runs indicated that a segment width of 5 ft would provide adequate detail, thus permitting coverage of the entire area with a total of 80 segments. Rooms 1 and 4 and pillars 1-2 and 3-4 were modeled at six segments, or 30 ft wide, exactly equal to their nominal widths. Rooms 2 and 3 were modeled at nine segments, or 45 ft wide, whereas their nominal width was 44 ft. This slight departure would not be expected to introduce a significant error. The center pillar (pillar 2-3) was also modeled at its nominal width of 20 ft, or four segments. The layout of the modeled experimental areas is shown at the bottom of Fig. 13.5.

The computer model assumes that each (infinitely long) room is excavated instantaneously. In order to simulate this excavation, the average date of excavation of each room was determined from Fig. 6.3, and this date was taken to represent the instantaneous excavation of the entire room. These dates are shown in Table 13.2.

The length of the time step in the computer simulation is, once again, primarily a compromise between the amount of detail desired and the computing time required. Since all previous time steps are considered in the calculation at each successive time step, computer time increases rapidly with the number of time steps.

Table 13.2. Computer Model Mining Sequence

Room	Date	Standard Day	Computer Model Day
1	10-30-64	426	0
2	12-22-64	480	55
3	2-03-65	517	90
4	2-22-65	538	115

Based on the preliminary runs, a time-step length of five days was chosen and found to provide adequate detail in all computations related to the experimental area, while not requiring excessive computer time.

13.3.1.2 Point of Comparison. – As noted above, the computer program does not provide any information on the lateral deformation of the pillars, and the simulated room convergences will not be comparable with the actual measured convergences because the model does not consider bed separation or viscoelastic buckling of the roof and floor. The computer simulation does, however, yield an estimate of the vertical pillar deformation. This deformation was measured in the experimental area on convergence gages (type F) located at the edge of the pillar. The anchors for these gages were located about 18 in. away from the pillar edges and from $1\frac{1}{2}$ to 2 ft into the roof and floor. The relative motions of these two anchor points could have been determined by using the "off-seam point" portion of the program, but it was found in trial runs that the "closure" of the room segment adjacent to the pillar edge was only about 2% greater than the convergence of the off-seam points. This was because the segment closure is taken to be that at the segment midpoint (i.e., $2\frac{1}{2}$ ft from the pillar edge, whereas the gage anchors are located $1\frac{1}{2}$ ft from the edge) and because the roof and floor are assumed to be elastic.

Therefore, the closures calculated from these segments were compared directly with the measured pillar edge convergences. In this way the closure at segment 18 (see Fig. 13.1) corresponds to convergence gage 106 and segment 23 to gage 109 in room 1; segment 30 to gage 118 and segment 38 to gage 125 in room 2 (Fig. 13.2); segment 43 to gage 138 and segment 51 to gage 145 in room 3 (Fig. 13.3); and segment 58 to gage 159 and segment 63 to gage 162 in room 4 (Fig. 13.4).

13.3.1.3 Simulation of Heat Sources. – The computer program simulates the heat sources by a line source parallel to the *y* direction buried under the floor of the mine. For the row of heaters along the sides of the center pillar, this simulation presents no problems, and the strength of the line source can be obtained from Eq.

(13.39) using 1.5 kw power input per 5 ft of distance for Q_0. This gives the strength of the heat source (Q) as 20°C ft^2 hr^{-1}.

The simulation of the circular arrays of the heat sources in rooms 1 and 4 by infinite line sources presented more of a problem. A number of geometrical arrangements of line sources having different strengths, all at 9 ft below the floor, were tried in trial runs, and the resulting temperatures in the salt at the north-south center-line plane were compared with actual temperature measurements. These actual temperatures were best simulated by two line sources at the center of each room, 5 ft apart, with initial strengths of 2.5°C ft^2 hr^{-1} each. These heat sources were turned on, increased by 40%, and turned off (by adding a negative source at the same location) according to the schedule shown in the first part of Table 13.3 (see also Table 11.3).

In the trial runs for determining the strength of the heat sources in rooms 2 and 3, it was discovered that the theoretically determined strength of 20°C ft^2 hr^{-1} for the rows of pillar heaters produced temperatures in the salt somewhat higher than actually observed. The difference was probably due to the heat lost to the ventilation air. This could have been corrected by adding heat sinks, but a reduction in the strength of the line sources (to 15°C ft^2 hr^{-1}) also resulted in an acceptable temperature distribution. The strengths of the rows of heaters at the center pillar and their schedule of operation are shown in the second part of Table 13.3.

13.3.2 Computer Simulation of Experimental Area

13.3.2.1 Procedure. – After establishing the value of some of the parameters as discussed in the previous section, the series of computer runs to determine the values of the remaining physical properties and parameters was undertaken. The general procedure used was as follows:

1. First, only the deformations due to the excavation of the experimental area and prior to any heating were considered. A set of values was selected by trial and error for those physical properties which are not concerned with thermal effects (in general, the first ten items in Table 13.1) which would produce a computer-simulated closure comparable with the measured convergences. Since the initial portion of the measured convergence data was missing because of the necessary delay after mining before installation of the gages, this comparison was based on the convergence *rate* just prior to heating and the fit of the general shape of the curves. Once a comparison was established on this basis, the amount of deformation, the curve shape, and the deformation rate could be compared at all later times.
2. Next, the simulated deformations during the heating periods were made to correspond to the equivalent actual deformations. This was accomplished by (again) trial-and-error manipulation of the parameters related to thermal effects, especially PWR [the exponent on temperature in Eq. (13.5)], ξ, and EQ or V, the coefficient in Eq. (13.37). Comparison of the computer-simulated closures with the measured convergences was again based on rates of deformation at some characteristic point, shape of the curves, and the amount of deformation, in that order. In this comparison, it was discovered that several different sets of values determined in step 1 above would equally satisfy the preheating deformations but result in drastically different closures during the heating period. Therefore, it was necessary to return to step 1 many times before arriving at the final values.
3. After completing step 2, the deformations during the cooling period were calculated and compared with the measured convergences. This comparison was made almost solely on the basis of deformation rates, and the criterion of acceptance was considerably more liberal.

Table 13.3. Heat Source Schedule in Computer Model of Experimental Area

Condition	Heat Strength (°C ft^2 hr^{-1})	On at Program Day	Equivalent Standard Day	V in Eq. (13.37)
Rooms 1 and 4 Arrays				
Initial	2.5	380	806	9500
40% increase	1.0	815	1241	2500
Off	−3.5	955	1381	5500
Center Pillar Heaters				
On	15.0	745	1171	3500
Off	−15.0	1075	1501	3500

13.3.2.2 Comparison of Convergence and Closure Curves. – The values of the various physical properties and other parameters which were used in the computer run producing an acceptable fit with the observed deformations are given in Tables 13.1 and 13.3. Figs. 13.1–13.4 show the comparisons of the computer-simulated closure with the measured convergences in the four experimental rooms. First, notice that in all four rooms, the general shape of the closure curves

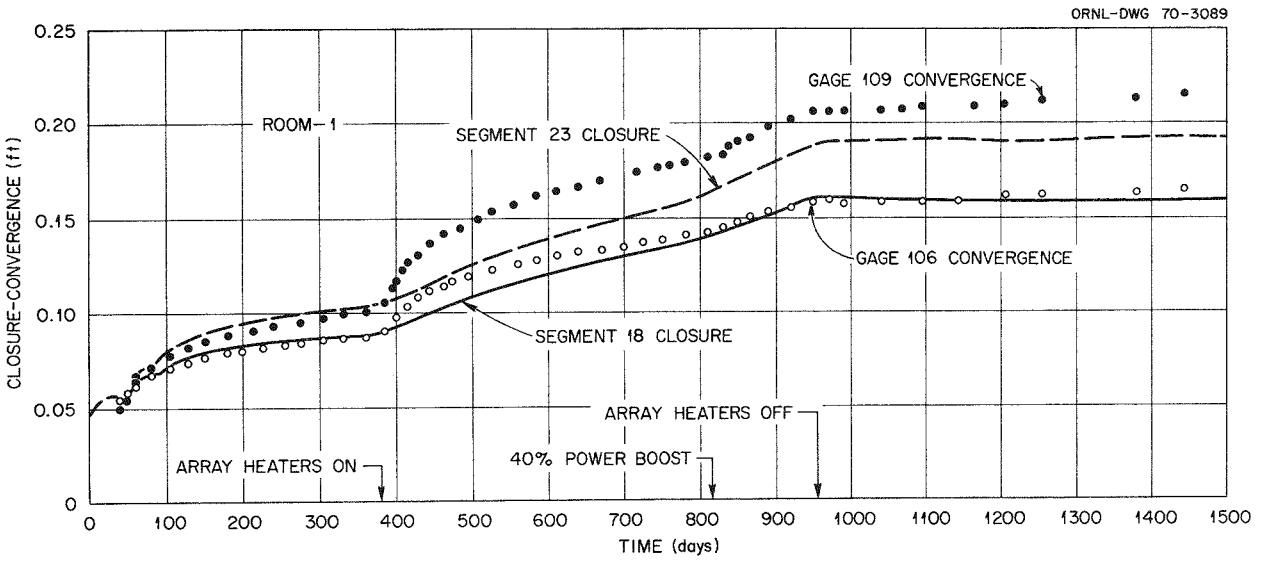


Fig. 13.1. Comparison of Computer Model Closures with Measured Convergences in Room 1.

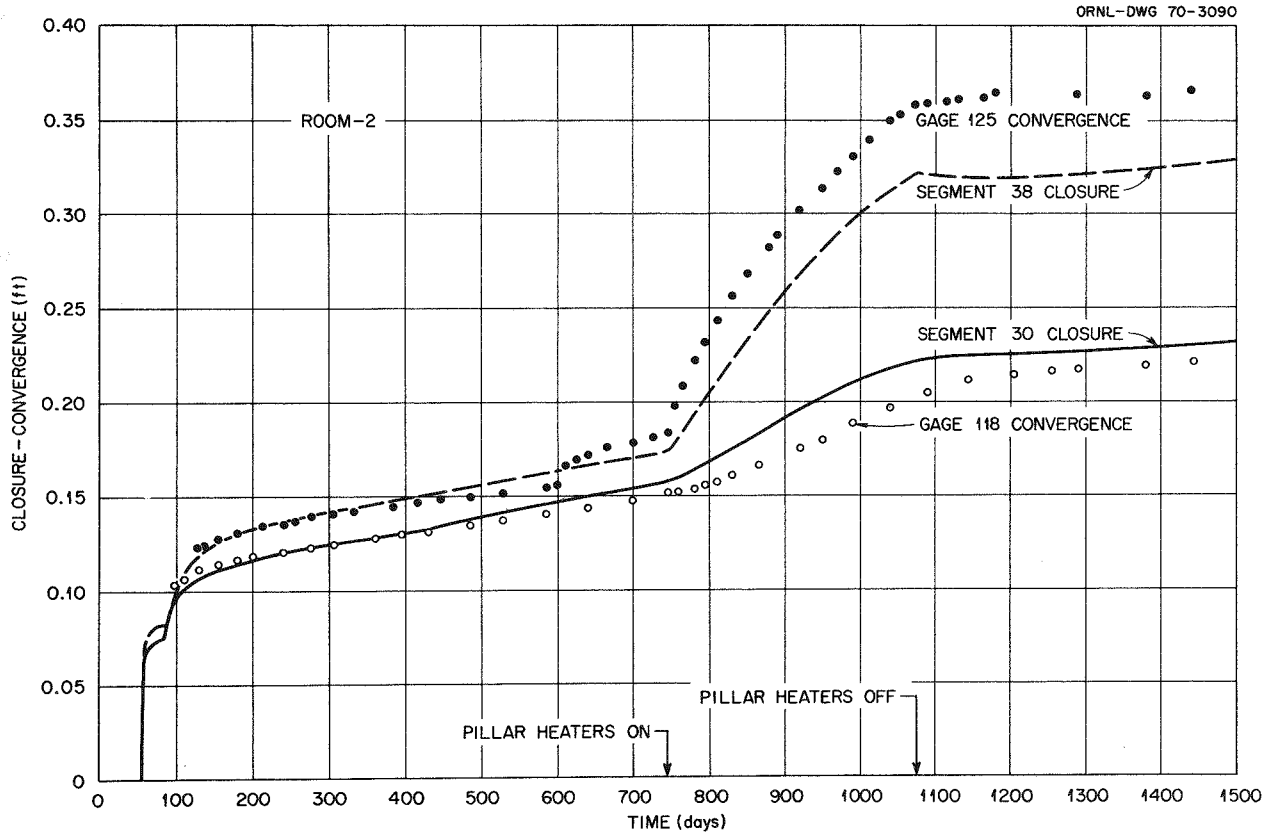


Fig. 13.2. Comparison of Computer Model Closures with Measured Convergences in Room 2.

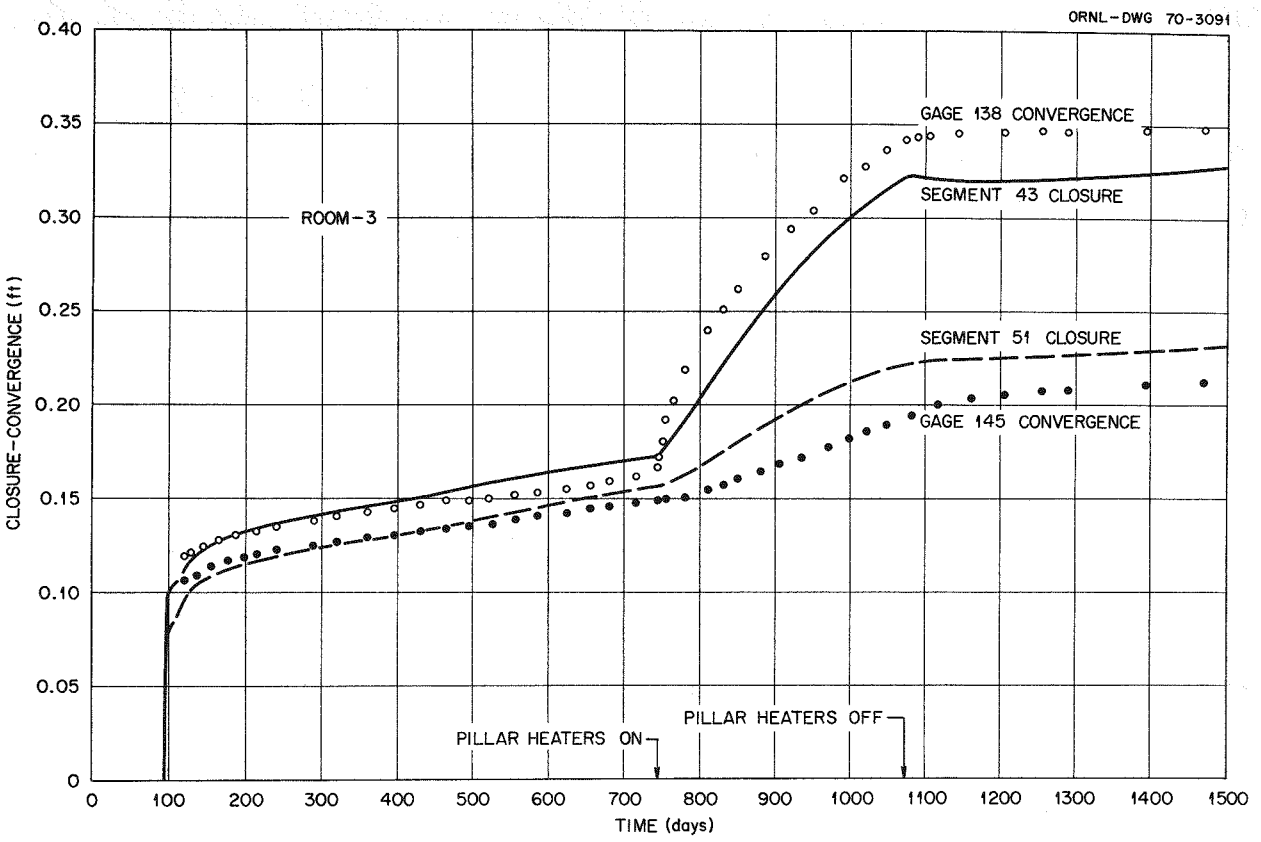


Fig. 13.3. Comparison of Computer Model Closures with Measured Convergences in Room 3.

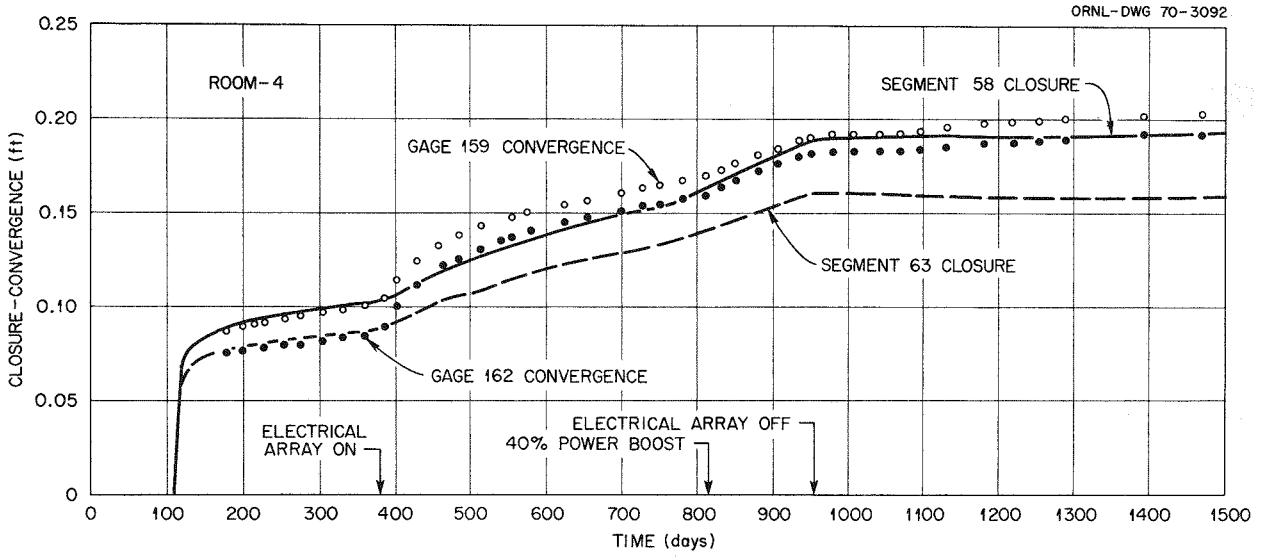


Fig. 13.4. Comparison of Computer Model Closures with Measured Convergences in Room 4.

obtained from the computer simulation is very close to the measured convergence curves and that the rates (except as noted below) are very nearly identical. The amount of closure compares somewhat less closely with the value of the convergence, but even this is within about 10%.

The maximum departure of the calculated curves from the experimental results occurs immediately after the heaters were turned on. In rooms 1 and 4, the observed convergence rate was much higher than the calculated closure rate for approximately 100 days following day 380 (standard day 806), when the array heating was initiated. The same situation (though somewhat less pronounced) can be seen at gages 125 and 138 (segments 38 and 43) following startup of the pillar heaters on day 745 (standard day 1171). However, at greater distances from the heat sources, the opposite effect occurs; that is, the measured convergence rates were less than the calculated closure rates. This can be seen at gages 118 and 145 following commencement of the pillar heater experiment and at all points in rooms 2 and 3 following the initiation of the heating at the arrays in rooms 1 and 4. These departures were interpreted as resulting primarily from inaccurate computer modeling of the thermal stresses. If the physical properties are changed to more closely reproduce the response of the gages close to the heaters, closures at more distant points become so large that they no longer resemble the actual convergences. Likewise, when the properties are changed to exactly reproduce the deformations at the distant points, the closures near the heat sources are very large. The physical properties used for the comparison represent a compromise between these two extremes. With this compromise the closure rates at all times except immediately after initiation of the heating compare favorably, and even the difference between the values of closure and convergence are not excessively large. Therefore, the error, which is apparently in the modeling of the thermal stresses, can be considered acceptable.

The calculated vertical closures at each of the segments across the entire experimental area at various selected times are shown in Fig. 13.5, along with the layout of the excavated rooms and "unexcavated" segments. At day 90 only rooms 1 and 2 have been mined out. Day 380 represents the closures which have occurred prior to any heating. Between day 380 and day 745, only the array heaters in rooms 1 and 4 were operating. The curve for day 1075 shows primarily the effects of heating at the center pillar. After day 1075, all heaters were off.

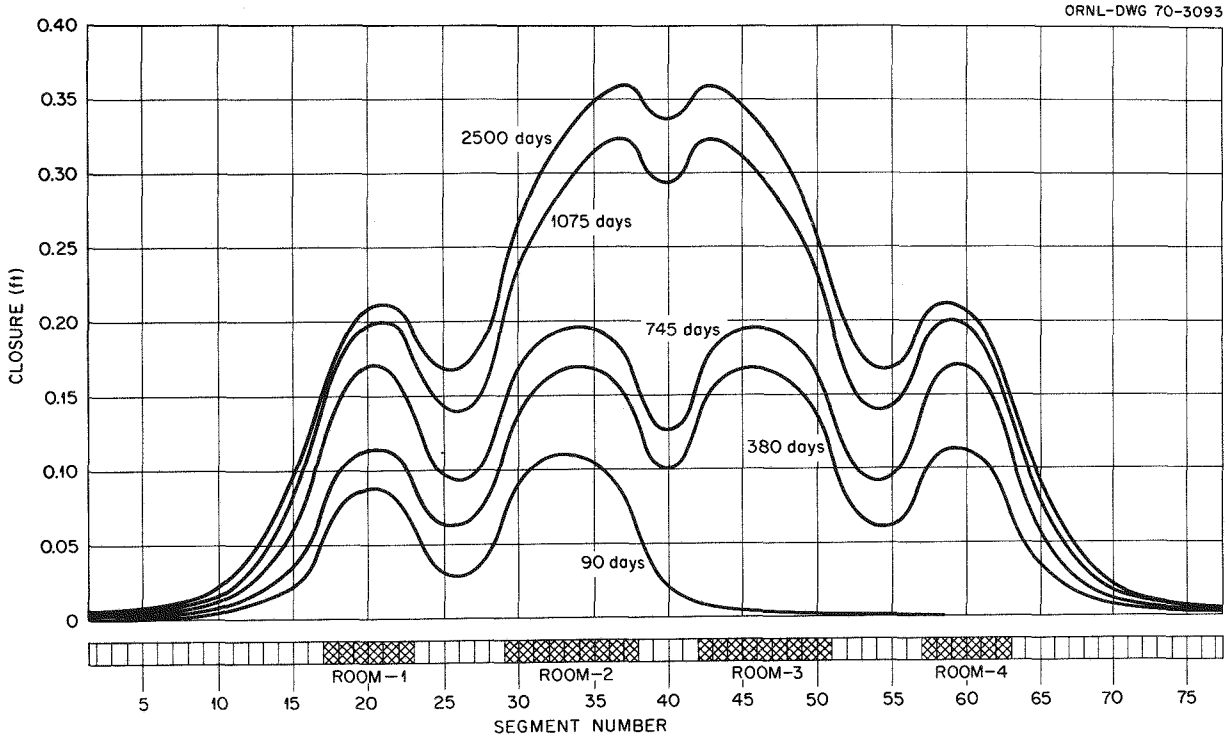


Fig. 13.5. Computer Model Closure Distribution Across Entire Experimental Area at Selected Times.

13.3.2.3 Comparison of Stresses. – Confirmation that the closure results presented in Figs. 13.1–13.4 represent a reasonable simulation of the behavior of the entire experimental area under the combined influences of stress, elevated temperatures, thermal stresses, and time, and are not simply the consequence of a fortuitous selection of variables, can be obtained from comparison of calculated pillar stresses with the results obtained on the "stressmeters" (see Sect. 11.4.8.2) installed in the experimental area. Before making that comparison, however, it is necessary again to emphasize that the interpretation of the results of these diametral borehole deformation gages installed in strongly plastic materials such as salt is not a straightforward process and that quantitative interpretation is impossible. Changes in the stresses applied to the pillars, especially abrupt stress changes, are nevertheless indicated qualitatively by a change in the stressmeter reading. The stress at segment 26 at the center of the pillar between rooms 1 and 2 as calculated for the computer model is shown as the solid curve in Fig. 13.6 as a function of time. The calculated stress at the center of pillar 3-4 is essentially identical for the portion of the curve shown. The stressmeter results from gage S-14 (pillar 1-2; see Fig. 11.42) and S-19 (pillar 3-4) are plotted below the calculated stresses. Figure 13.7 shows the computer model stresses at the center of pillar 2-3 (segment 40) and the results from stressmeters S-15 and S-16 (see Fig. 11.42). On this plot the increase in stressmeter output starting at day 599 (standard day 1025) represents the thermal stress loading caused by the single pillar heater adjacent to gage 125, which was turned on early as a part of a materials test (see Sect. 11.4.7). This heating was not included in the computer simulation.

During the heating period at the center pillar, the stress curves obtained from the computer model show almost exactly the same shape as the results from S-15 and S-16. The comparison at S-14 was almost as good, while at S-19 a comparison with the simulator stresses was more difficult because of the reduced sensitivity of the stressmeter (probably because of a lower installation prestress). These results again show the slight discrepancy between the model and the experimental area in the effects of the thermal stresses at some distance from the heat sources. For example, the fairly abrupt flattening of the stress curve at segment 40 (Fig. 13.7) at about day 400 is seen as (in part at least) an effect of the array heaters in rooms 1 and 4. No effect can be seen at this time on the stressmeter results. Similarly, the calculated stresses at segment 26 (Fig. 13.6) show a considerable increase resulting from the

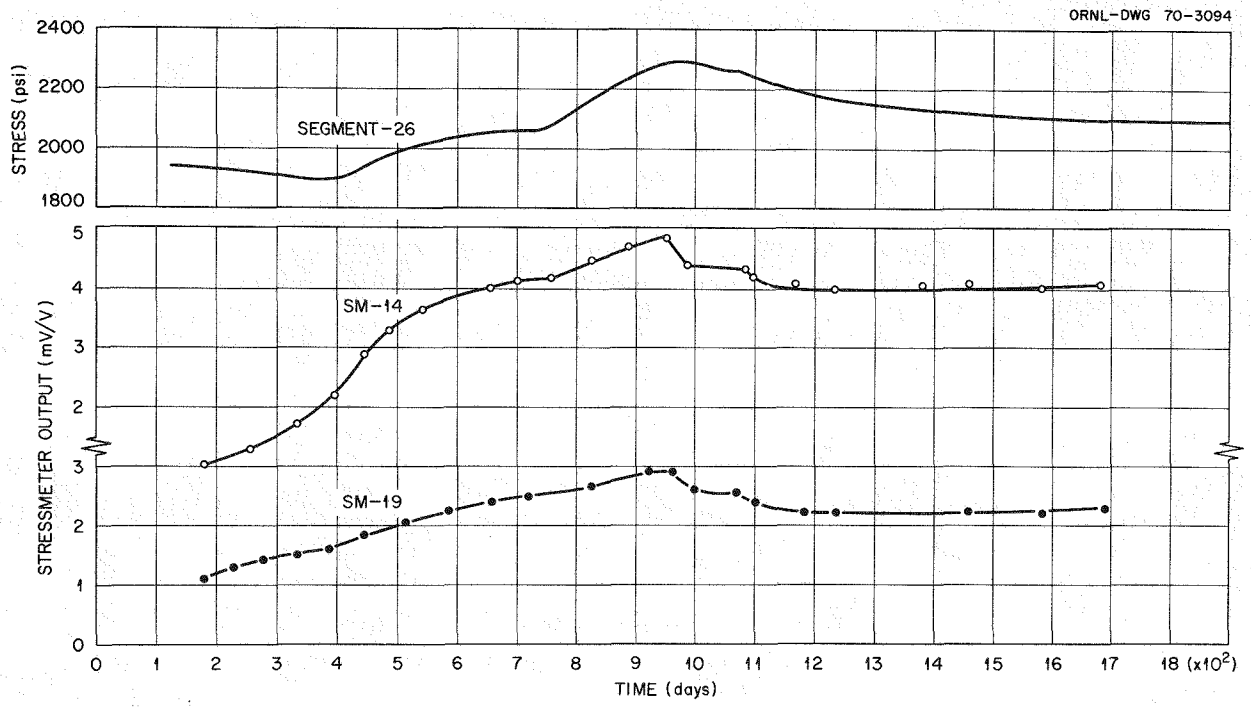


Fig. 13.6. Comparison of Computer Model Pillar Stresses with Stressmeter Outputs – Pillars 1-2 and 3-4.

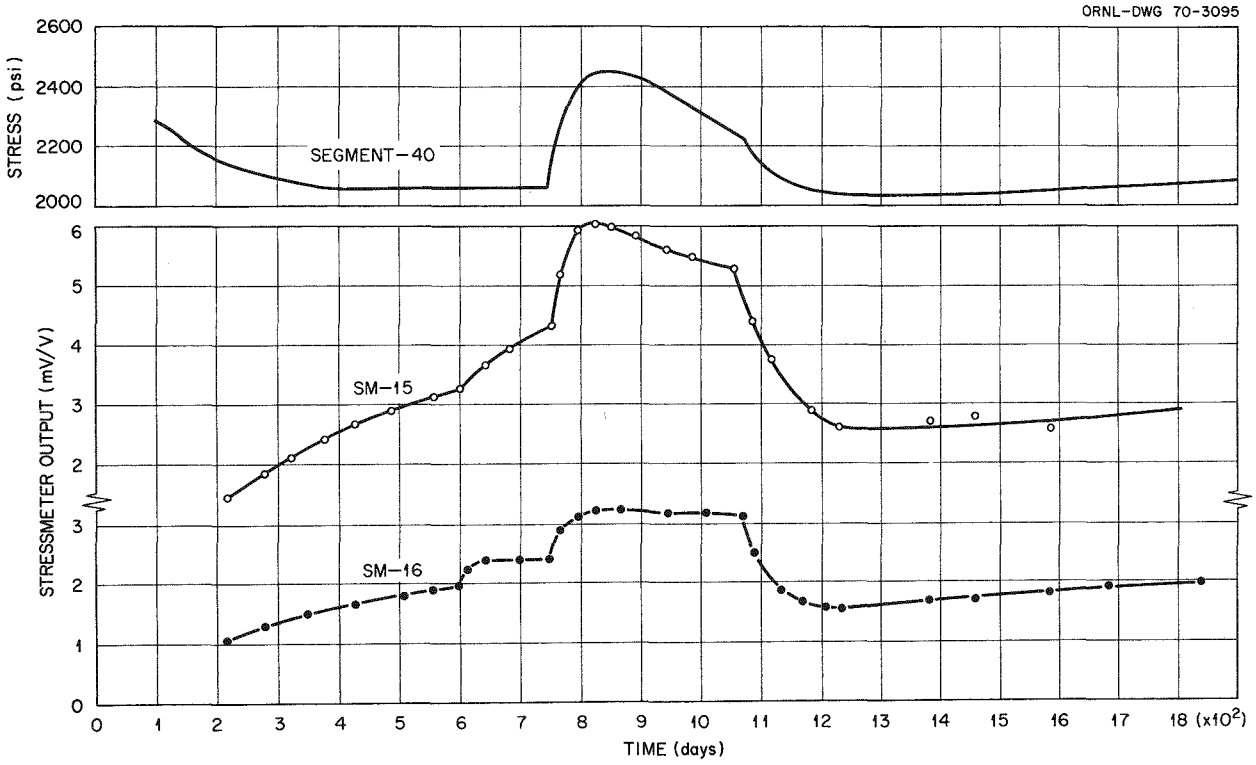


Fig. 13.7. Comparison of Computer Model Pillar Stresses with Stressmeter Outputs – Center Pillar.

initiating of heating at the center pillar (at day 745). Although a change can be detected in the S-14 results, it is proportionally less than indicated from the model.

This comparison between the stresses calculated from the computer model and the stressmeter results, especially during the periods of heating, indicates that the behavior of the experimental area is being adequately simulated by the model.

13.3.3 Discussion

As explained above, the fit of the computer model with the experimental results was obtained by trial and error using various sets of physical property parameters. This procedure permitted an evaluation of the effects which variations in some of the parameters had on the resulting deformations of the model and therefore provided some insight into the behavior of the underground experimental area.

The first and most significant of these findings was the relationship between the rigidity of the (elastic) roof and the effective stiffness of the support pillars. In the set of parameters used for the comparison (Table 13.1), the behavior of the model is quite sensitive to this relationship. For example, a slight change in the modulus of the roof and floor material (E in Table 13.1) produces a relatively large change in the amount of pillar deformation. An increase in E, increasing the rigidity of the roof "plate" spanning the entire experimental area, causes much of the vertical stresses which should be borne by the pillars to be transferred into the abutments at the two ends of the experimental area. If the rigidity of the roof is decreased, the roof plate can deflect more, which increases the load on the pillars and therefore their deformation. This sensitivity to the rigidity of the roof implies that the four-room experimental area is at least slightly subcritical in horizontal extent; the pillar loads are somewhat less than those which would be experienced in an infinitely large area having the same relative extraction.

The pillar stiffness is simply the stress-strain relation of the pillar as a whole, which in this case is also a function of time and temperature according to Eq. (13.5) and is further complicated by the constraint and the interaction of the several segments which are built into the computer program. If the pillars are made a little "softer" by increasing the coefficients in Eq. (13.5), the pillar deforms more rapidly – as would be expected. However, at some point, further softening of the pillar has very little influence on pillar deformation

because it deforms so much that the pillar stress is once again transferred into the abutments via the rigidity of the roof. Likewise, stiffening of the pillars reduces their deformation, but not as much as would be expected, since the load on the pillar also increases as a consequence of its greater stiffness.

The roof rigidity and pillar stiffness used for the comparison between the model and the experimental area would appear to be a fairly good selection based on the behavior of the model using slightly different values and based on the behavior of the experimental area. For example, at the time of design, the experimental area was estimated to be somewhat subcritical in horizontal extent based on previous underground results (see Sect. 13.3.3). The values of the coefficients from Eq. (13.5) used in the comparison run (see ALF, BET, GAM, and PWR in Table 13.1) are only slightly different from those obtained from the laboratory experiments [Eq. (13.4)]. In fact, they are well within the experimental accuracy of values determined from the laboratory pillar models. This was somewhat surprising and may have been fortuitous. Since the laboratory coefficients were obtained on small-scale models and described the deformation of the entire (model) pillar rather than only a segment of it, a much wider difference in the coefficients would have been tolerated and, indeed, was expected.

A second significant finding from the searching computer runs was the relative insensitivity of the coefficient V in Eq. (13.36), defined by Eq. (13.37). For a truly elastic material, this should be fixed and constant. Even though the floor was assumed to be elastic, it was realized that its response, especially to thermal stresses, would not be strictly elastic. An approximation of its true behavior was therefore attempted by using (1) values different from that theoretically defined (4000 psi hr $^{\circ}C^{-1}$) and (2) different values both for the initial heating, subsequent power increase, and cooling at the arrays and at the center pillar heaters. The differences in the values of V at the different times and locations can be interpreted as differences in the portion of thermal stress which is lost by viscous deformation. The insensitivity of this coefficient in influencing the behavior of the model helps to explain the wide differences which were required in order to obtain a fit with the experimental data (see Table 13.3).

13.3.4 Extrapolation of Computer Model to Waste Disposal Facility Design Problems

The computer model described in this chapter can be applied to the examination of the closure distributions to be expected in an operating facility disposing of real radioactive wastes simply by establishing the desired geometry and extending the time span to 50–100 years. For such an extrapolation, it is suggested that the strength of the heat sources be adjusted to yield a true temperature distribution consistent with that given by the more sophisticated heat transfer codes for the waste characteristics and filling schedule being considered. The physical property parameters given in Table 13.1 and the heating coefficients from Table 13.3 (for the array rooms) could then be used. The real question is not whether such an extrapolation can be done, nor how to do it, but how valid is it?

A design study of this type probably would be formulated as a comparison between mining geometries (widths of rooms and pillars), depth, heat load from the waste, and/or other variables. The comparison between the different cases would almost certainly be based on closure, either volumetric room closure or convergence at the center of the room, and the examination of that closure could be phrased in either of two ways:

1. At what time after filling with waste will the closure reach a value such that the backfill salt in the room can be considered to be completely reconsolidated and recrystallized, thus assuring permanent containment of the waste?
2. What is the value of the closure (possibly as a percentage of that desired) at some specified point in time, such as when the access shafts are filled and sealed or 25 years after completion of operations?

This discussion implies that exact answers are really not required in a design study of this type. If a desired closure should be achieved at, say, 25 years after filling, an error of ±5 years (±20%) or even more would be immaterial. Furthermore, the principal objective of such a design study would be to establish the limits on the range of the various operational parameters (room width, for example) between which other considerations (such as the maximum allowable salt temperature) will control. Therefore, once again, extreme accuracy is not required in the predictions.

As mentioned earlier, the calculated closures fitted the measured convergence to within a maximum error of about 10% with an average error of much less (see Figs. 13.1–13.4). The fit of the closure *rates,* which becomes more important in long-time-span extrapolations, was considerably better, except for the brief period immediately following initiation of the heating. The fit of the computer model with the experimental results and the verification of the model behavior from the stress comparisons can be used as a basis for

estimating the accuracy of predictions of closures under different conditions. These estimates are, of course, purely subjective and include a considerable intangible factor based on judgment and experience with the rock mechanics of evaporite deposits.

1. If an experimental area having some features similar to the PSV demonstration area, but others considerably different, were to be established at the Lyons mine, the computer model using the same physical property parameters would probably predict convergences to within the same accuracy as found in the comparison after a similar period of operation. For example, this hypothetical experimental area might involve five 30-ft-wide rooms separated by 20-ft-wide pillars (giving nearly the same overall dimension as in PSV), with heat sources located throughout the floor areas.
2. At much greater time spans, say 30 to 50 years, the computer model predictions would probably still be within an average of ±20% of actual measurements. For predictions involving only a short period following heating (a few years), the major factor influencing the behavior of the salt is the thermal stresses. These are also a major uncertainty in the computer model. At longer times (a few tens of years) the thermal stresses have an almost insignificant effect on the total deformations. Therefore, it is felt that longer time estimates can be made without some of the increases in error usually associated with such extrapolations.
3. If an actual waste disposal facility were to be established at or near the Lyons mine, the present concept[15] would call for rows of equally sized rooms and pillars with a total span of several thousands of feet. Under these conditions it is felt that the computer model would predict closures to about ±20%. This seemingly highly overoptimistic estimate is based on consideration of the differences in the behavior of a small span like the experimental area and a much larger area. The four-room experimental area was apparently somewhat subcritical, and therefore the calculated closures were particularly sensitive to the rigidity of the roof strata and the *relationship* between this and the pillar stiffness. In a disposal operation the overall span would be much larger than critical; therefore the closure of most of the rooms (all except those within a few hundred feet of the abutments) would be independent of the roof rigidity, and no sensitive relationship between roof rigidity and the pillar stiffness will exist. Since it is (largely subjectively) felt that the structural behavior of the pillars is one of the features which is most accurately reproduced in the computer model, it follows that predictions in this case should be reasonably accurate.
4. For design studies of waste disposal operations at locations other than near the Lyons mine, and especially those in other salt deposits (but at the same depth), the computer model should be able to predict closures to within about ±35%, *provided* that the coefficients in Eq. (13.5) are available from pillar scale-model testing of samples obtained from the site. This estimate of accuracy is based on the close correlation between the coefficients used in the comparison run of the computer model and those obtained from the laboratory pillar model tests.
5. The accuracy of predictions made for waste disposal operations at different depths (and, of necessity, with different pillar deformation coefficients) is somewhat harder to estimate. For depths in the range of 500 to 2000 ft, the predictions should still be within ±35%, provided that the salt continues to deform in the normal manner up to the maximum stresses expected, as would be determined from the required laboratory testing program. This rather tentative estimate is based on the fact that the depth influences the behavior of the computer model only by changing the pillar stress (σ_0) in Eq. (13.5).

Based on these estimates of the accuracy of the computer model and the reasoning which went into them, it would appear that the primary objective of both the underground rock deformation measurement program and the analysis presented in this chapter has been achieved: the combined effects of stress, elevated temperatures, thermal gradients, and time on the deformation of salt are sufficiently well understood that rational design of actual waste disposal facilities can be undertaken.

[15] R. L. Bradshaw, J. J. Perona, J. O. Blomeke, and W. J. Boegly, Jr., *Evaluation of Ultimate Disposal Methods for Liquid and Solid Radioactive Wastes: VI. Disposal of Solid Wastes in Salt Formations,* ORNL-3358 (Rev.) (March 1969).

Appendix 13.A. FORTRAN LISTING OF COMPUTER PROGRAM

```
      PROGRAM SALT
C
C        CREEP PROGRAM FOR A ROOM-AND-PILLAR SALT MINE WITH
C        HEAT SOURCES IN THE FOOTWALL  (PLANE STRAIN)
C        ------------------------------------------
C
C
C
      DIMENSIONX(80),P(80),A(80),KK(80),TP(80),STR(80)
      DIMENSION SA(40,500),T(40,500),NSG(40),BB(40),FB(40)
      DIMENSION  NAC(40),SAC(12)
      DIMENSION C(25),NQ(25),XQ(25),EQ(25),TS(10),XZ(30),YZ(30)
      READ(08,NUM
      DO(01)NYM=1,NUM
C
C        INPUT OF DATA CARDS
C
      READ(02,E,PR,TEMP,DIFF,PRIM
      PRINT(03,NYM,E,PR,TEMP,DIFF,PRIM
      READ(04, ES,ALF,BET,GAM,PWR,W
      PRINT(05,ES,ALF,BET,GAM,PWR,W
      READ(06,DX,NX,DT,NT,NPT,NCR,DPQ,MQ
      PRINT(07,DX,DT,DPQ
      READ(08,I1,I2,I3,I4,I5
      DTA=0.5*ALF*(DT**BET)
      PWR=PWR/BET
      GM1=GAM-1.
      FLAM=0.4
      DO201J=1,12
      TM=2.*(J-1)
  201 SAC(J)=1.2445*EXPF(-TM*FLAM*DX/W)
      INT=0
      TYM=0
      DT1=DT/24.
      DQS=DPQ*DPQ
      DQT=(DPQ+0.5*W)**2
      ACC=0.004*PRIM
      CON=E/(6.283*(1.-PR*PR)*DX)
      CS=0.25*DX*CON
      CD=-0.125/(3.1416*(1.-PR)*CS)
      IF(MQ)2,2,3
    3 READ(09, (C(I),EQ(I),XQ(I),NQ(I),I=1,MQ)
      PRINT(10,(C(I),EQ(I),XQ(I),NQ(I),I=1,MQ)
      DO4I=1,MQ
      XQ(I)=XQ(I)/(2.*DX)
    4 EQ(I)=EQ(I)*Q(I)/3.142
      KI=4.+DPQ/(2.*DX)
    2 READ(11,(NSG(I),I=1,NCR)
      IF(I4)7,7,8
    8 READ(12,(XZ(I),YZ(I),I=1,I5)
```

```
      7 READ(1,1)NDT, (KK(I),I=1,NX)
        READ (1,1)(NAC(I),I=1,NCR)
        PRINT(12,INT,(KK(I),I=1,NX)
C
C          CALCULATION OF INFLUENCE COEFFICIENTS
C
        DO6I=1,NX
        XA=2*(I-1)
        A(I)=CAN/(XA*XA-1.)
        P(I)=PRIM
      6 X(I)=0
        AA=A(1)
        AS=AA-0.75*ES/W
        DO5I=1,NCR
      5 T(I,1)=0
C
C          BEGINNING OF LOOP FOR SUCCESSIVE TIME STEPS
C
        D020N=1,NT
        INT=INT+1
        TYM=TYM+DT1
        D021I=1,NX
     21 TP(I)=TEMP
        IF(MQ)22,22,23
     23 D024I=1,MQ
        TA=N-NQ(I)
        IF(TA)24,24,25
     25 TA=4.*DIFF*DT*(TA-.5)
        IF(DQS/TA-.001)28,28,19
     19 IX=XQ(I)
        YX=IX-KI
        JX=YX
        XA=2.*DX*(YX-XQ(I))
        KJ=2*KI+2
C
C          CALCULATION OF THERMAL STRESSES
C
        D026J=1,KJ
        R=DQS+XA*XA
        TM=EXPF(-R/TA)
        TS(J)=((DQS-XA*XA)*(1.-TM)/R+2.*XA*XA*TM/TA)/R
        IF(J-1)26,26,27
     27 JX=JX+1
        IF(KK(JX))202,89,202
    202 P(JX)=P(JX)+EQ(I)*0.5*(TS(J)+TS(J-1))
        GO TO 26
     89 P(JX)=P(JX)+EQ(I)*0.5*(TS(J)+TS(J-1)) *0.5
     26 XA=XA+2.*DX
     28 KJ=2*KI+5
        XA=(2.*(YX-XQ(I))-3.)*DX
        JX=YX-2.
C
```

```
C          CALCULATION OF PILLAR TEMPERATURES
C
      DO29J=1,KJ
      JX=JX+1
      IF(KK(JX))30,29,30
   30 XB=(DQT+XA*XA)/TA
      IF(XB-2.5)31,31,29
   31 TM=XB*(1.-XB*(.25-XB*(.0555556-XB*(.010417-XB/60.))))
      TP(JX)=TP(JX)+Q(I)*(TM-.5772-LOGF(XB))/(12.56*DIF)
   29 XA=XA+2.*DX
   24 CONTINUE
   22 DO37L=1,NX
      IF(KK(L))37,37,38
   38 KA=KK(L)
C
C          CALCULATION OF INSTANTANEOUS CREEP VARIABLES
C
      NB=N-NSG(KA)+1
      SUM=0
      IF(NB)42,40,40
   40 TN = TP(L)**PWR + T(KA,NB+1)
      T(KA,NB+2)=TN
      IF(NB)42,42,41
   41 NKC=NAC(KA)
      SA(KA,NB)=DTA*(STR(L)**GAM)*(SAC(NKC)**GM1)
      DO43I=1,NB
   43 SUM=SUM+SA(KA,I)*((TN-T(KA,I))**BET-(TN-T(KA,I+2))**BET)
   42 FB(KA)=DTA*((TN-T(KA,NB+1))**BET)
      BB(KA)=SUM
   37 CONTINUE
C
C          SOLUTION OF CLOSURE EQUATIONS
C
      DO950NZ=1,20
      IND=1/NZ
      DO951I=1,NX
      TM=P(I)
      DO952J=1,NX
      JA=J-I
      IF(JA)48,52,52
   48 JA=-JA
   52 TM=TM+A(JA+1)*X(J)
      STR(I)=TM
      XA=X(I)
      IF(KK(I))53,54,55
   54 X(I)=XA-1.3*TM/AA
      IF(ABSF(TM)-ACC)951,951,56
   56 IND=IND+1
      GOTO951
   53 X(I)=1.3*(PRIM-TM+AA*XA)/AS
      GOTO951
```

```
   55 KA=KK(I)
      Z=FB(KA)
      NKC=NAC(KA)
      CGEL=0.6028*SAC(NKC)/ES
      CGCR=Z*TM*((TM*SAC(NKC))**GM1)
      DEN=AA*(CGEL+GAM*CGCR/TM)-1./W
      X(I)=XA-(BB(KA)+CGCR+CGEL*TM-XA/W)/DEN
   51 CONTINUE
      IF(IND)60,60,50
   50 CONTINUE
      PRINT113,IND
   60 IF(INT-NPT)90,62,62
   62 INT=0
C
C        OUTPUT OF RESULTS
C
   59 PRINT114,TYM,(X(I),I=1,NX)
   61 IF(I1)64,64,65
   65 PRINT 115,(STR(I),I=1,NX)
   64 IF(I2)69,69,70
   70 PRINT116,(P(I),I=1,NX)
   69 IF(I3)71,71,72
   72 PRINT117,(TP(I),I=1,NX)
   71 IF(I4)90,90,73
C
C        CALCULATION OF OFF-SEAM DISPLACEMENTS AND STRESSES
C
   73 DO741Z=1,15
      DO751=1,5
   75 TS(I)=0
      YA=YZ(IZ)
      YB=YA*YA
      XB=XZ(IZ)+DX
      DAD=CS+CS
      DO78MZ=1,2
      DO791=1,NX
      D=DAD*X(I)
      XC=2*I-1
      XC=XB-XC*DX
      XD=XC*XC
      TM=XD+YB
      TMA=D/(TM*TM)
      TS(1)=TS(1)-D*CD*(YB/TM+(.5-PR)*LOGF(TM))
      TS(2)=TS(2)+D*CD*(XC*YA/TM+2.*(1.-PR)*ATANF(XC/YA))
      IF(I4-2)79,79,80
   80 TS(3)=TS(3)-XC*TMA*(XD+3.*YB)
      TS(4)=TS(4)+XC*TMA*(YB-XD)
      TS(5)=TS(5)+YA*TMA*(3.*YB-XD)
   79 CONTINUE
      XB=XB-2.*DX
   78 DAD=-DAD
```

```
      PRINT 118,XZ(IZ),YZ(IZ),TS(1),TS(2)
      IF(I4-2)74,74,81
   81 PRINT 119,TS(3),TS(4),TS(5)
   74 CONTINUE
   90 IF(N-NDT)20,91,91
C
C          CHANGE OF MINING PATTERN
C
   91 READ 111,NDT,(KK(I),I=1,NX)
      READ 111,(NAC(I),I=1,NCR)
      PRINT 112,N,(KK(I),I=1,NX)
   20 CONTINUE
  101 CONTINUE
C
C          FORMAT STATEMENTS
C
  102 FORMAT(E9.2,F4.2,3F7.1)
  104 FORMAT(5E9.2,F5.2)
  106 FORMAT(F5.2,I3,F5.2,3I3,F5.2,I3)
  108 FORMAT(5I2)
  109 FORMAT(2E9.2,F5.2,I3,2E9.2,F5.2,I3,2E9.2,F5.2,I3)
  111 FORMAT(25I3)
  103 FORMAT(//////6X,7HPROBLEM,I4////2X,9HHOST ROCK,3X,2HYM,E10.2,4X,
     22HPR,F5.2,5X,4HTEMP,F7.0,4X,11HDIFFUSIVITY,F6.2,12H (SQ.FT/HR.)/
     32X,16HPRIMITIVE STRESS,F7.0,4H PSI)
  105 FORMAT(2X,7HPILLARS,3X,2HYM,E10.2,5X,15HCREEP CONSTANTS,E12.3,3F8.
     22.5X,6HHEIGHT,F6.1,3H FT)
  107 FORMAT(/2X,2HDX,F8.3,3H FT,6X,2HDT,F6.1,5H HRS.,5X,
     215HDEPTH OF BURIAL,F6.1,3H FT)
  110 FORMAT(//12X,16HHEAT SOURCE DATA,2X/2X,8HSTRENGTH,9X,5HVISC.,3X,
     28HPOSITION,4X,5HSON AT,20(/E14.3,E14.3,F11.3,I8))
  112 FORMAT(//12X,23HMINING PATTERN  AT STEP,I3/2514/2514/2514/2514)
  113 FORMAT(//2X,23HLOSS OF ACCURACY   IND=,I3/)
  114 FORMAT(//2X,5HTIME=,F8.1,5H DAYS/12X,12HCLOSURE (FT),8(/10E12.4))
  115 FORMAT(/12X,14HSTRESSES (PSI),8(/10F10.1))
  116 FORMAT(/12X,16HPRIMITIVE STRESSES,8(/10F10.1))
  117 FORMAT(/12X,12HTEMPERATURES,4(/14F8.1))
  118 FORMAT(/2X,4HAT (,2F7.1,30H )   INDUCED DISPLACEMENTS ARE,2E13.3)
  119 FORMAT(19X,20HINDUCED STRESSES ARE,3E14.4)
  120 FORMAT(12F6.1)
      END SALT
/*
```

14. Summary and Conclusions

W. C. McClain R. L. Bradshaw

Project Salt Vault was the culmination of about ten years of study and testing at ORNL aimed at establishing the feasibility, safety, and techniques for disposing of high-level power reactor wastes in natural salt formations. This report documents the background and early studies, the design, installation, and operation of PSV, and the conclusions derived from the project in as complete detail as possible. This summary chapter follows the general organization of the body of the report: each section summarizes the material and conclusions in the corresponding chapter of the report.

14.1 BACKGROUND

The problem of disposing of large quantities of highly radioactive fission products resulting from the reprocessing of spent fuel was considered during the early stages of reactor development, and it was recognized that unless satisfactory solutions were forthcoming, the use of nuclear power as a source of energy could be significantly impeded. The longevity of the hazard associated with these waste materials implies that any "disposal" system must achieve isolation from the biological environment for periods of at least several tens of thousands of years without prime reliance on a high degree of surveillance and extensive environmental monitoring programs. Anything short of this objective can only be considered "temporary storage."

In September 1955, at the request of the U.S. Atomic Energy Commission (AEC), a committee of geologists and geophysicists was established by the National Academy of Sciences–National Research Council (NAS-NRC) to consider possible disposal of radiologic wastes in geologic structures within the continental United States. This committee concluded that natural salt formations at sufficient depth are the most promising possible disposal sites. The advantages of salt for this purpose are:

1. Salt deposits are essentially impermeable and completely isolated from circulating groundwater. Furthermore, any fractures tend to heal due to the plastic properties of salt. This means that materials deposited in salt formations are unlikely to come into contact with leaching solutions over very extended periods of time.
2. Salt deposits are relatively abundant in the United States. Utilization of salt formations for this purpose will consume only a very small fraction of the available salt resources.
3. Salt formations, in general, are located in regions of low seismicity, thus reducing further the probability of environmental disturbances dislocating the waste.
4. The technology of excavation in salt is well developed, and excavation is a relatively low-cost operation.
5. Salt has good thermal properties for removing heat from the radioactive material and has approximately the same structural and shielding properties as concrete.

As a result of the recommendations of this NAS-NRC committee, the Health Physics Division began studies of the disposal of high-activity liquid waste. Liquid waste was considered first because, under the fuel-reprocessing technology existing at the time, most of the fission products were contained in a relatively large volume of liquid. Processes for solidification had been proposed but were in early stages of development. Related studies were carried out in other institutions, and the results of these were drawn upon liberally in the ORNL work.

The ORNL program indicated that liquid wastes probably could be safely deposited in natural salt formations but that a number of problems would require rather detailed examination. At about the time this conclusion was reached, the AEC began an ac-

celerated program aimed at developing waste-solidification processes. Therefore, the ORNL program shifted to studies of ultimate disposal of packaged solidified wastes. This shift in approach eliminated most of the problems associated with liquid wastes.

14.2 PREVIOUS STUDIES

Investigations completed prior to the design of the Project Salt Vault demonstration included: (1) heat transfer properties of salt, (2) effects of radiation on the structural properties of salt, (3) salt as a gamma radiation shield, (4) some of the effects of small quantities of moisture usually found trapped in bedded salt deposits, (5) prediction of mine stability, and (6) the economics of disposal of radioactive solids in a salt mine facility based on a preliminary conceptual design.

The following major conclusions were drawn from these studies:

1. In situ heat transfer properties of salt were sufficiently close to the values determined in the laboratory that confidence could be placed in theoretical heat transfer calculations.
2. Most bedded salt contains a fraction of a percent of trapped moisture which is released at temperatures above about 250°C.
3. Radiation exposure doses of 5×10^8 R produce some change in structural properties, but the effect on mine stability should be negligible.
4. Rock salt is approximately equivalent to concrete as a gamma radiation shield.
5. Stability of a waste-disposal mine at ambient temperature could be predicted approximately from observed conditions in existing salt mines.
6. Elevated temperatures would cause accelerated creep, but the exact effects on structural stability could not yet be predicted accurately.
7. Preliminary estimates of the cost of a large-scale disposal operation in salt [about 0.01 mill/kWhr(electrical)] showed that such an operation was economically compatible with competitive nuclear power.

In order to determine the optimum modes of operation of an actual waste disposal facility in a salt mine, and to evaluate variables significantly contributing to the cost of such a facility, a preliminary conceptual design was developed. The design of the field-scale demonstration experiment, Project Salt Vault, was based largely on this conceptual design and was intended to verify certain aspects of it.

14.3 PRELIMINARY DESIGN OF PROJECT SALT VAULT

The engineering and scientific objectives of the PSV demonstration experiment were: (1) demonstration of waste-handling equipment and techniques; (2) determination of possible gross effects of radiation (up to 10^9 rads) on hole closure, floor uplift, salt shattering temperature, etc., in an area where salt temperatures were in the range of 100 to 200°C; (3) determination of possible radiolytic production of chlorine; and (4) collection of information, especially on creep and plastic flow of salt at elevated temperatures, which could be used later in the design of an actual disposal facility.

The demonstration was to be carried out in the Lyons, Kansas, mine of the Carey Salt Company using 14 irradiated Engineering Test Reactor (ETR) fuel assemblies contained in seven cans. These cans were to be placed in a circular array of holes in the floor, with one can in the center and the other six cans located peripherally on 5-ft centers. To increase the radiation dose received by the salt, the assemblies were to be exchanged for freshly irradiated assemblies at six-month intervals over the course of two years. All fuel assemblies were to be returned to the Idaho Chemical Processing Plant (ICPP) for recovery of the unfissioned fuel.

An identical array using electrical heaters only was to be operated as a control to determine the combined effect of radiation and heat on the salt characteristics. In addition, one rib pillar was to be heated by a number of electrical heaters placed in the floor around its base to yield information on the creep and plastic flow of salt at elevated temperatures.

As originally conceived the reactor fuel assemblies, after canning in Idaho, would be shipped by rail in an existing cask especially modified for this purpose. At Lyons, the cask would be removed from a rail car standing on an existing spur and up-ended over a cased vertical shaft extending to the mine working area, approximately 1000 ft below. The assemblies would then be lowered, one at a time, through the shaft and into a movable shielded cask mounted on a fuel assembly transporter. The transporter would move to the experimental area, where the cask would be positioned and lowered over the designated hole in the floor of the mine. The can would then be lowered through the bottom of the cask into place. The holes, approximately 10 in. in diameter by 12 ft deep, would have suitable liners. Lead or uranium shields placed in the tops of the holes would serve as biological shielding while the cans were in place.

To meet the objectives of the experiment, it was necessary to expose a reasonably large mass of salt to radiation dosages and temperatures comparable with those anticipated in an actual disposal operation. The particular geometrical configuration chosen for this experiment would expose a circular area about 12 to 14 ft in diameter to the desired temperatures and radiation dosages.

The decision to use irradiated reactor fuel assemblies in this experiment rather than actual calcined wastes or separated fission product sources was based on considerations of availability, cost, and radiation characteristics. Selection of the ETR fuel was made from considerations of the operating cycle of the reactor, the number of assemblies which would be required to charge seven holes in the demonstration, and the dimensions of the assemblies. From the standpoint of allowable element temperature, power reactor elements would have been preferable, but uncertainties in availability led to the selection of the ETR fuel assembly as the best overall choice.

The final salt-dose calculations could not be made until the irradiation history of the actual assemblies was known; but based on preliminary calculations, it appeared that the peak salt dose with two 90-day-decayed ETR assemblies in a can would be about 3×10^8 rads, accumulated over a two-year period. Since laboratory tests had indicated little change in physical properties at 10^8 rads but a significant (about 10%) drop in compressive strength at 5×10^8 rads, it was desirable to achieve doses near 10^9 rads in this experiment, if practical. Changing the assemblies three times during the course of the two-year test (four sets of assemblies total) should increase the peak dose to about 8×10^8 rads. At the same time, this would give additional experience with the operation of the handling equipment.

Several different layouts were considered for the experimental area. The one finally chosen was very similar to the pattern envisioned in the conceptual design for an actual waste disposal mine. In this plan there would be four experiment rooms, two 30 ft wide and two 40 ft wide. All rooms would be 60 ft long and connected by a corridor. The center pillar would be 20 ft wide and the other two would be 30 ft wide. The radioactive and duplicate arrays would be in the end rooms, and the center pillar would be heated by means of 22 heaters to yield the salt flow data. According to the theoretical heat calculations, the major portion of the pillar base would experience temperature rises in excess of 70°C. The temperature rise in the center of the floor in the end rooms due to the heating of the center pillar would be negligible. The arrays in the end rooms, however, would contribute to heating of the two 30-ft-wide pillars.

On the opposite side of the corridor, before reaching the four experiment rooms, a fifth room was to be excavated for the bottom end of the waste charging shaft from the surface. All five of these rooms and the corridor were to be excavated above the roof of the original mined area, so that the arrays could be located in the relatively pure stratum which was originally mined.

A third seven-can heater array was to be installed in the existing floor of the mine. The fuel assemblies which were to be removed from the main test array at the end of each six-month period would be placed in this array so that a dose of the order of 10^8 rads could be delivered to the salt-shale mixture in the floor. In this way the possibility of using existing mine space rather than new excavations for waste disposal could be investigated.

Details of the instrumentation had not been completely worked out at this time, but experimental measurements which were to be made included salt temperatures, salt radiation dose, radiolytic gas production, thermal expansions of floor and pillars, and stress and stress changes in pillars and other parts of the formation.

It appeared desirable to have a total of about 400 thermocouples, based on 13 thermocouple holes each containing five thermocouples located in and around each of the seven-can arrays plus 40 thermocouple holes associated with the center pillar. These 40 holes would be located in the center pillar, in the floor around and beneath the pillar, and in the formation at the back of the room. Thermal expansion of the floor in and near the arrays would be measured by means of leveling points related to a bench mark located elsewhere in the mine. Floor-to-ceiling movement would be measured by a portable strain gage. In addition, thermal expansion, along with creep and plastic flow of the pillars, floor, roof, and end walls, would be measured by both surface and internal strain gages. These gages would be installed as soon as possible after excavation so that background creep rates could be obtained. A first approximation of the number of strain gages required was 300 external and 150 internal gages.

It was theoretically possible that some radiolytically produced chlorine would be released into the array holes, although laboratory results indicated that the amount would be very small. Thus it was planned to sample and analyze the gas from the annulus between the salt and the outer can in some of the radioactive

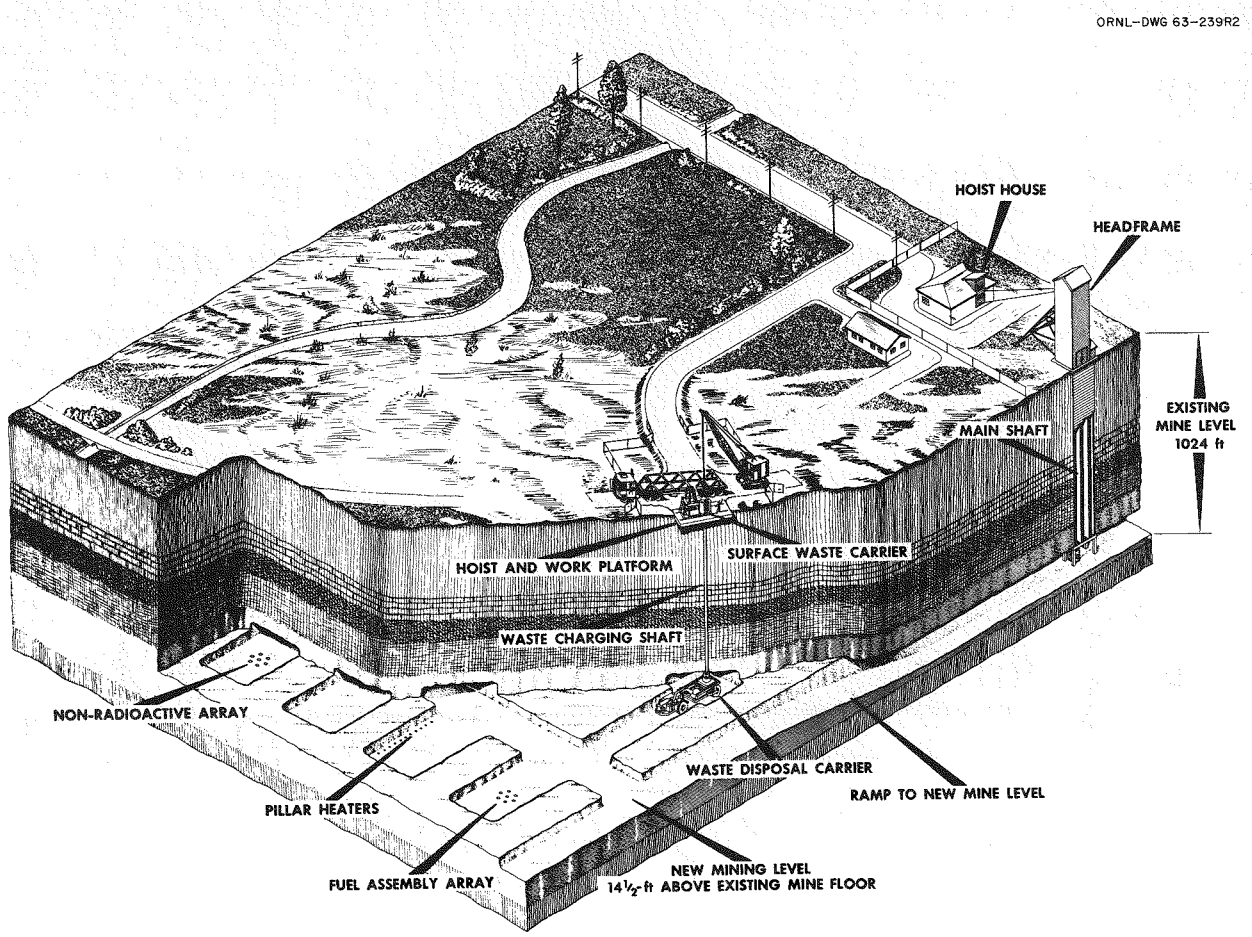


Fig. 14.1. Pictorial Cutaway View of the Project Salt Vault Experiment.

array holes. Gas from some of the holes in the duplicate array would also be sampled as a control.

A pictorial cutaway view of the entire experiment, including certain fairly minor modifications from the description just presented, is given in Fig. 14.1.

14.4 STUDIES PRELIMINARY TO MAIN EXPERIMENT

Several studies which were pertinent to the demonstration were either already under way prior to, or were initiated and run concurrently with, the design and preparation phases of the demonstration. First, it was expected that holes in the floors of mined openings would be used for ultimate disposal of high-level radioactive solids in salt. Therefore, it was anticipated that the effect of elevated temperatures on the deformational properties of salt would significantly affect the structural behavior of the mine rooms. To study this effect, an opening 8 ft wide by $9\frac{1}{2}$ ft deep by 2 ft high was created in the face of a very large pillar in the Carey Salt Company mine in Hutchinson, Kansas. Immediately after the opening was created, electrical transducer-type strain gages were installed to measure floor-to-ceiling convergence, movement of the floor, and convergence of the side walls. Background creep-closure data were collected for a period of 214 days. The gages were then temporarily removed to permit the installation of heaters. Heater power was controlled by a thermostat (exposed to the cavity air but shielded from radiant heat) set for 170°C.

The heating phase showed that elevating the wall temperature of an isolated cavity by about 120°C (about 20°C rise at a distance of 9 ft from the cavity) resulted in a rapid reduction of about 5% in cavity dimensions followed by a rapid decrease in closure rate.

However, after more than a year at elevated temperature, the rate was still 10 times higher than at ambient temperature. The effect appeared to be approximately equivalent to that which would be obtained by doubling the load on the salt pillar.

The power was turned off after 511 days of heated operation, but transducer readings were taken for about $2\frac{1}{2}$ years more. All temperatures were back to within about 10°C of ambient by three weeks after shutdown, and to within 2 to 3°C of ambient after about four months. After the salt temperature had returned to ambient, the transducer readings indicated little or no movement taking place inside the cavity. However, by this time the readings were becoming somewhat erratic, perhaps due to the length of time the transducers and readout unit had been exposed to the salt environment. About the only conclusion that could be drawn was that cavity closure rates after the termination of heating were probably less than they were immediately prior to heating.

The second area of preliminary investigations related to rock deformation instrumentation. The Applied Physics Laboratory of the U.S. Bureau of Mines carried out considerable development work in connection with the Disposal in Salt Project on stress gages for use in salt to measure the magnitude and direction of the principal stresses. Several types of gages were studied, and four of these gages or measurement methods were tested simultaneously by APL at the Carey mine, Hutchinson, Kansas. Additional tests were carried out using a Potts-type stressmeter, internal strain wire gages, and pipe-type convergence or closure gages. The general conclusions drawn from these studies were that none of the stress instruments were capable of directly indicating quantitative stress levels but that most of them did qualitatively indicate changes in stress satisfactorily. The pipe-type convergence gage was easiest and cheapest to install and gave the most precise readings. On the other hand, it can be used only external to pillars, whereas the other types can provide information on internal behavior of pillars and ribsides.

The next area investigated concerned the ability to predict the effects of elevated temperature on creep and mine stability. S. Serata in 1959 suggested that creep rates (or closure rates) of mined openings at ambient temperatures always decrease with time. In 1959 both ORNL and Serata installed several vertical and horizontal convergence measuring stations in the Carey Salt Company's mine at Hutchinson, Kansas. Since that time ORNL has added additional stations at the Carey mines in both Hutchinson and Lyons, Kansas. Data from these stations indicated that Serata's hypothesis of steadily decreasing vertical convergence was correct, at least for the pillar stress levels encountered in the Kansas mines. In March 1963 Serata indicated that he had successfully extrapolated creep data from laboratory pillar models to creep rates in mined openings.

L. Obert, of the Applied Physics Laboratory of the U.S. Bureau of Mines, developed a somewhat different technique for performing creep tests on pillar models. At our request the Applied Physics Laboratory carried out 1000-hr creep tests on model pillars machined from 6-in.-diam. cores of Lyons mine salt. These tests, run at several different values of average pillar stress, appeared to be sufficient to allow the development of an empirical equation which can be used to predict vertical closure rates in salt mine openings up to several years old.

Preliminary testing of the hole liner design and fabrication materials was carried out in a prototype test in the existing mine floor of the Lyons mine. The floor-leveling part of this test also indicated that standard leveling techniques would provide sufficient accuracy in the demonstration.

The storage of high-level wastes in salt formations will expose the surrounding salt to radiation, and the dose in the immediate proximity of the packaged wastes is expected to be as high as 10^{10} rads. While it was known that radiation could cause some damage to alkali halides, there had been no definitive work to prove or disprove the release of free halogen from sodium chloride. Therefore, a number of studies were carried out on this effect using natural salt (both ground and chunk), reagent-grade salt, and artificially grown crystals. All of these samples would produce some oxidizing power (presumably due to chlorine) when dissolved after being irradiated. However, no release of chlorine from the solid samples could be detected under any of the laboratory test conditions, and it would not be expected that any appreciable chlorine would be released under field conditions in a waste disposal operation.

For the demonstration disposal of high-level radioactive wastes in a salt mine, dosimetry was required to measure the gamma dose being delivered to the salt surrounding the radioactive material. No readily available dosimeters had ever been used or tested under the extremely severe conditions expected in the mine. Upon investigation, both silver-activated metaphosphate glass rods with a postirradiation heat treatment and glass-encapsulated deaerated ferrous sulfate solution were found to be satisfactory, and both were used in the experiment.

14.5 GEOLOGY AND DESCRIPTION OF LYONS MINE

The Lyons mine of the Carey Salt Company, located in Rice County, Kansas, near the city of Lyons, was selected as the site for the PSV demonstration experiment. The mine was opened originally in 1890, and production had terminated in 1948. During this period approximately 200 acres were mined out. The salt was mined by the room-and-pillar method, with salt extraction varying from about 60 to 70%. The floor of the mine lies a little over 1000 ft below the land surface, which is about 1700 ft above sea level.

The excavated horizon is in the lower part of the Hutchinson salt member of the Wellington formation which underlies central and south-central Kansas and extends southward into Oklahoma. This member is an integral part of the gently westward-dipping Permian-Pennsylvanian sedimentary rocks that underlie much of Kansas and crop out in the eastern one-third of the state. The salt is not present along this outcrop, probably because it has been dissolved by groundwater and surface water; however, it is present down the dip to the west. The eastern edge of the salt body lies approximately 400 ft below the land surface, but near its western edge in Kansas it is found at a depth of more than 1500 ft. Thicknesses of the unit range up to as much as 400 ft in Kansas. In general the Hutchinson consists of a complex mixture of salt, anhydrite, and shale, with salt being the predominant fraction throughout most of its extent in Kansas. At the Lyons mine the Hutchinson salt member consists of about 300 ft of nearly flat-lying beds of salt, shale, and anhydrite, with salt comprising about 60% of the sequence.

The salt unit that has been mined in the Lyons mine consists of relatively pure salt that contains minor inclusions of clay and shale. The first 115 to 135 in. of the section below the floor in the westernmost portion of entries 7 and 9 (near the experimental area) contains between 20 and 40% shale. The shale is present in beds that vary greatly in thickness over relatively short distances and may grade vertically and laterally into zones of salt that contain many pods and irregularly shaped lenses of shale and anhydrite. A second shaly zone approximately 40 to 50 in. thick is present, generally from about 220 to 235 in. below the floor. Four separate shaly zones occur in the first 250 in. of section above the mine roof. The thickest shale bed lies at a minimum distance of about 20 in. above the ceiling of the mine, while the other less prominent zones of shale lie between about 130 to 230 in. above the roof. These zones are usually only a few inches thick and contain, in addition to shale, lenses and stringers of anhydrite and salt.

The newly mined area for the experiment lies at a level of about 14½ ft above the preexisting mine floor and extends upward a distance of about 15½ ft to a thin shale parting at the roof. The floor of the newly mined area is composed predominantly of rock salt. A prominent shale bed that varies from a few inches to more than 1 ft in thickness lies approximately 2½ ft above the new floor. Two easily distinguishable shale beds that are about ⅛ to ¼ in. in thickness are also observed in the test area at distances of about 12 ft above the floor. The salt in the excavated area contains numerous blebs of polyhalite that are commonly concentrated along bedding, giving the salt a banded appearance.

Because of the importance of the ceiling within the experimental area in maintaining mine stability, a series of ten cores ranging from 3.5 to 11 ft in length were taken in the roof of the experimental area of the mine to define more specifically the lithology of the salt section. From the cores, a generalized cross section of the first 11 ft of roof in the experimental area was prepared. The first prominent shale bed above the ceiling in the experimental area lies about 2 ft above the roof, and, from the core drilling, it was observed that a separation has developed at that point. It was expected that eventually separations might occur at the 5-, 8½-, and 9-ft shale beds and perhaps at some of the marginal shale partings between the 2- and 5-ft sections.

The Lyons mine was in relatively good condition, considering its age and history, at the time preparations for Project Salt Vault began in 1963. Access to the mine is through a single rectangular shaft approximately 8 by 16 ft divided into two hoisting compartments 5 ft 9 in. by 6 ft 9 in. and a ventilating compartment 3 ft 0 in. by 6 ft 9 in. Except for a few feet at the collar, the shaft is lined for its full depth of 1024 ft with 4-in.-thick longleaf yellow pine which has required only slight repair since installation when the shaft was sunk in 1890. Shaft condition was generally good, with only minor repairs to guides, corner strips, the water rings, and inspection openings considered necessary. The shaft collar was of unknown competence, and replacement was considered desirable.

The headframe, installed in 1955 following the dismantling of the timber mill and headframe, was fabricated of steel pipe. External corrosion was obvious, and it was suspected that corrosion was also present on the inner surfaces. The headframe was not considered suitable for further use.

The electrical components of the hoist drive were in good condition. The 350-rpm, 150-hp wound-rotor induction motor in use at Lyons since 1949 was in good condition. The drum controller was in good shape, and the secondary grid resistors were in satisfactory condition. The reversing contactor, while old, was serviceable and required only minor repair.

The conditions of the underground workings varied with their age and with the mining practice at the time various sections were mined.

In general, areas near the shaft and to the north, west, and immediately south of the shaft were mined during the early years of operation. During this period, extraction was undesirably high and an arched roof was used. The high extraction ratio resulted in rapid movement, and a thin section of salt remaining at the top of the arch fell away from the shale parting above. In large areas the floor was covered with the roof slab.

In later years the mining practice was changed to open entries and rooms which are rectangular in section and about 10 ft in height. This left a roof slab about 7 ft thick below the first major shale parting at 17 ft above the floor. Areas mined in this way have been exceptionally stable.

Although the Lyons mine was considered to be in good condition and probably the best readily available site for the demonstration experiment, a considerable amount of repair, replacement, renovation, and cleanup were required before beginning installation of the experimental equipment proper.

14.6 MINE RENOVATION AND PREPARATION

The primary purpose of this section is to describe the renovations and preparatory work at the Lyons mine which does not fit under the heading of "installation of experimental equipment." Table 14.1 gives a brief outline of this work and when it was performed. The distinction between preparation and installation is somewhat arbitrary and based largely on whether hardware described in the next section (Design and Fabrication of Equipment) was involved or not.

One of the first jobs to be undertaken was the construction of a new shaft collar and headframe to replace the existing inadequate temporary structure. Both the shaft collar and the headframe were constructed to a design and specifications supplied by Stearns-Roger Corporation. The collar work included a concrete pad and foundations and a new poured concrete collar on the shaft to a depth of 12 ft. The new 14,000-lb-capacity structural steel headframe was of fairly typical design, 60 ft high overall with dual 8-ft-diam sheave wheels. Although no provisions were made for hoisting salt to the surface, the dual sheave wheels would permit hoisting in both compartments or the use of a counterweight in one compartment.

In design of the special shaft and other facilities for lowering the fuel element canisters underground, it was desirable to have the maximum diameter available within the limitations imposed by project financing. While the canisters to be handled in the demonstration were only about 6 in. in diameter, it was considered advantageous to have a larger-diameter shaft in case it should become possible to dispose of actual pots of calcined waste. Standard oil field casing 20 in. OD and 0.438-in. wall thickness with inside diameter of 19.1 in. was chosen on the basis of availability of casing and cost of the completed shaft.

The second important factor in the design of the shaft was double casing at the top to assure sealing of the casings into the structure in such a way that groundwater would not reach the salt formation. This was accomplished by first drilling a 32-in.-diam hole to 300

Table 14.1. Schedule of Mine Renovation and Experimental Preparation

June 15, 1963, to Nov. 7, 1963	Preliminary work both underground and around shaft at topside.
Nov. 7, 1963, to Mar. 23, 1964	Construction of new shaft collar and headframe and renovation of mine hoist. All access to underground areas denied.
Mar. 23, 1964, to June 17, 1964	Limited underground work (mostly surveying, gage hole drilling, and preparation of prototype hole liner experiment). Mining equipment disassembled.
May 25, 1964, to June 17, 1964	Transfer mining equipment underground and reassemble.
June 2, 1964	Start of prototype hole liner experiment.
June 17, 1964, to July 9, 1964	Installation of 19-in.-diam waste shaft.
June 17, 1964, to July 31, 1964	Cleanup of entries and access ways in mine.
July 9, 1964, to Oct. 13, 1964	Structural and interior renovation of hoist house.
July 15, 1964, to Aug. 29, 1964	Construction of ramp up to experimental area level from mine level.
Sept. 2, 1964, to Mar. 25, 1965	Excavation of experimental area.
Nov. 24, 1964, to Nov. 4, 1965	Drilling in experimental area (including room 5) for gages, thermocouples, heaters, hole liners, etc.

ft and cementing 26-in.-OD surface pipe for the entire 300 ft. No water-bearing formations are present below 300 ft, and the bottom of the 26-in. casing is cemented in an impermeable shale which overlies the salt.

The remainder of the hole was drilled at 24-in. diameter, and the 20-in. casing was cemented from the surface to approximately 1040 ft. By far the most rigorous specification to be met by the drilling contractor was that the shaft must not deviate from vertical at any point by more than 1°. In other words, the entire length of the shaft had to lie within a slender cone described by the starting point at the surface and a circle of 17-ft radius at the mine level. An accurate survey of the completed shaft using gyroscopic instruments indicated a total deviation of 2.53 ft to the northwest.

A very minimum amount of maintenance had been carried on underground during the long period between closing of the mine in 1948 and preparations for Project Salt Vault beginning in 1963. Therefore a substantial part of the effort in preparation for Project Salt Vault consisted in cleaning up the main entries and access ways and restoring the services required for underground operations, especially power and ventilation.

Since all the mining machinery had been removed from the Lyons mine, it was necessary to procure and install underground all the equipment needed for the excavation of the experimental area. The basic elements of this equipment suite consisted of a used loading machine and two used trailing-cable shuttle cars, which were purchased. Other equipment, acquired on a rental basis, consisted of post-mounted drills for blast hole drilling, a short-wall undercutter, and a three-drum tugger hoist for stacking the salt underground. All this mining machinery was electrically powered with 480-V three-phase alternating current, except for the shuttle cars, which used 250-V direct current. Since no cleanup of the underground workings had been done for many years, the first task after reassembly of the mining machinery underground was the removal of spalling walls, sagging roofs, and floor heaves along the access route from the main shaft to the experimental area.

The procedure used for excavating the experimental area was similar to that used in the Carey operations at the Hutchinson mine and throughout the industry. In this procedure the face is first undercut to a depth of approximately 10 ft and a straight pattern of blast holes drilled to an equivalent depth in the material above. The holes are then charged with explosive (40% dynamite in this case) and detonated electrically using time-delay caps in such a way that progressively higher layers of salt are broken loose. The broken salt is then loaded onto the shuttle cars using the gathering-arm-type loader.

The cleanup and experimental area excavation work represented a significant portion of the total effort in the Project Salt Vault even though none of it was directly associated with the hardware aspects of the equipment. During this preliminary period about 20,000 tons of salt were excavated from the experimental area in addition to the many thousands of tons moved in the mine cleanup operations, 7000 ft of small-diameter (less than 6 in.) hole was drilled for instrumentation, most of it under rigorous directional control, and about 1600 ft of large-diameter hole (6 in. and greater), including the waste shaft, was completed. In addition, a large amount of support work (both for the mining operations and the experimental), such as temporary installation and later removal of power, compressed air, and lighting services, was completed.

14.7 DESIGN AND FABRICATION OF EQUIPMENT

The major components of special equipment in the Project Salt Vault experiment which required design and fabrication are described below.

14.7.1 Fuel Assembly Canisters

The special containers for the ETR fuel assemblies were approximately 5 in. in diameter by about $7\frac{1}{2}$ ft long. They were designed to hold two ETR fuel assemblies end-to-end in a shock-resistant and hermetically sealed container. Shipping and storage specifications required that the containers for the assemblies be hermetically sealed. The walls of the containers needed to be as thin as practical to maximize the radiation dose to the salt, yet strong enough to withstand the pressure buildup that might occur as a result of (1) release of fission product gases from a leaky assembly or (2) an increase in the temperature of the gases in the event of loss of coolant during loading and shipment. The body of the canister was fabricated of $4\frac{3}{4}$-in.-OD, 0.120-in.-wall 304L stainless steel tubing. The closures and other subassemblies of all units were tested by helium leak-check methods at various stages during fabrication to ensure the integrity of the system. The end closure was contained in one unit to simplify hot-cell procedures. Just before the closure was installed, the canister was purged with helium. The assembly was seated by using an impact wrench. After seal welding, the canister was tested by a helium leak detector before it was loaded into the shipping cask.

14.7.2 Shipping Cask

The shielded cask for shipping the fuel assembly canisters between Idaho Falls, Idaho, and Lyons, Kansas, contained a rotatable magazine which served a dual purpose: as an indexing mechanism to allow loading or unloading of one canister at a time, and as a heat exchanger to remove the decay heat, amounting to approximately 23,000 Btu/hr, from the cask. The structural framework of the magazine was constructed, for the most part, from pipes terminating in headers at both ends. Cooling water entered and left through concentric pipes at one end of the magazine. Heat was removed mainly by radiation from the canister to the pipe walls; water circulating through the pipes carried the heat to an external radiator. The clearance between the magazine and the internal cavity of the cask, as well as between the canister shield plug and the cavity, was approximately $^1/_{16}$ in. The total shielding was 10 in. lead equivalent, and the shipping weight of the cask was 28 tons. A 35-ton mobile crane was used to lift the cask from the shipping trailer at Kansas.

14.7.3 Waste-Charging Facility

The waste-charging facility provided biological shielding during unloading and a means of erecting the cask (from its horizontal shipping position to the vertical position) for unloading the canisters into the mine. This facility was located at the top of the 19.1-in.-ID waste shaft and consisted of a concrete work platform and biological shield, a ventilation system, headframe, hoist, and protective enclosure. To prevent contamination of the mine air in the access tunnels should an accidental release of radioactivity occur from a canister, arrangements were made for a special air flow pattern. A fan powered by a 10-hp electric motor was installed at the surface to exhaust all air entering the experimental area up the waste shaft. In case of an accident to the main shaft or hoist, or a fire in the mine, the topside facility and hoist were designed to provide safe emergency hoisting of personnel in the waste-charging shaft. An auxiliary emergency cage was stored at the topside facility for this purpose. This cage could be connected to the hoist cable and would allow one man at a time to be removed from the mine.

14.7.4 Underground Transporter

To provide the flexibility necessary for an actual disposal operation, a highly maneuverable transporter was developed. A number of alternate transportation systems were considered, including overhead rail and trolleys and rail-type transportation. Rough cost estimates indicated that it would be cheaper to use a self-powered vehicle to provide flexibility within the mine. The procurement specification for this machine included the design, fabrication, and testing of a standard two-wheel rubber-tired trailer with a power-positioned, steel-cased lead shield. The specifications required that the unit negotiate a 10% grade at a speed of at least 1 mph with a fully loaded trailer. The vehicle also had to be able to turn in a 25-ft-wide corridor without backing or scraping the walls. The complete assembly, including the tractor, weighs about 100,000 lb. The shield itself weighed approximately 50,000 lb.

14.7.5 Storage Holes

The array holes (storage holes) contained a number of auxiliaries, including the hole liners themselves, which would not be required for an actual disposal operation. Since the Lyons mine was only leased from the Carey Salt Company, it was necessary to provide additional features to guarantee that the canned fuel assemblies could be withdrawn from the mine at the end of the experiment. The upper part of the storage hole consisted of a 16-in. hole drilled to a depth of 5 ft 3 in., followed by a 12-in. hole drilled to a total depth of 12 ft 8 in. Into this hole was inserted the metal liner used to provide containment and to ensure that the canisters could be removed. The liner was made in two sections: the upper liner was carbon steel well casing, 14 in. OD, which was grouted into the salt. The lower liner section, which was bolted to the fixed upper section and was removable, was fabricated of 304L stainless steel tubing, 6-in. OD by $^1/_4$-in. wall, for maximum corrosion resistance. To avoid the problem of collapse pressure, an annular space was provided between the salt and the lower liner section. Auxiliary heaters were provided to supplement the heat lost as the radioactive decay heat rate of the fuel assemblies diminished.

The major components of experimental equipment described in the preceding sections and their position in the sequence of operations for transferring the fuel assemblies from Idaho to the salt mine are shown in Fig. 14.2.

14.7.6 Heated Pillar Equipment

The heated pillar test was designed to obtain additional information on the thermomechanical properties of in situ salt under transient temperature conditions. In this test a nominally 20-ft-wide pillar between the two center rooms of the experimental area was extensively heated by a total of 33 kW of electrical power

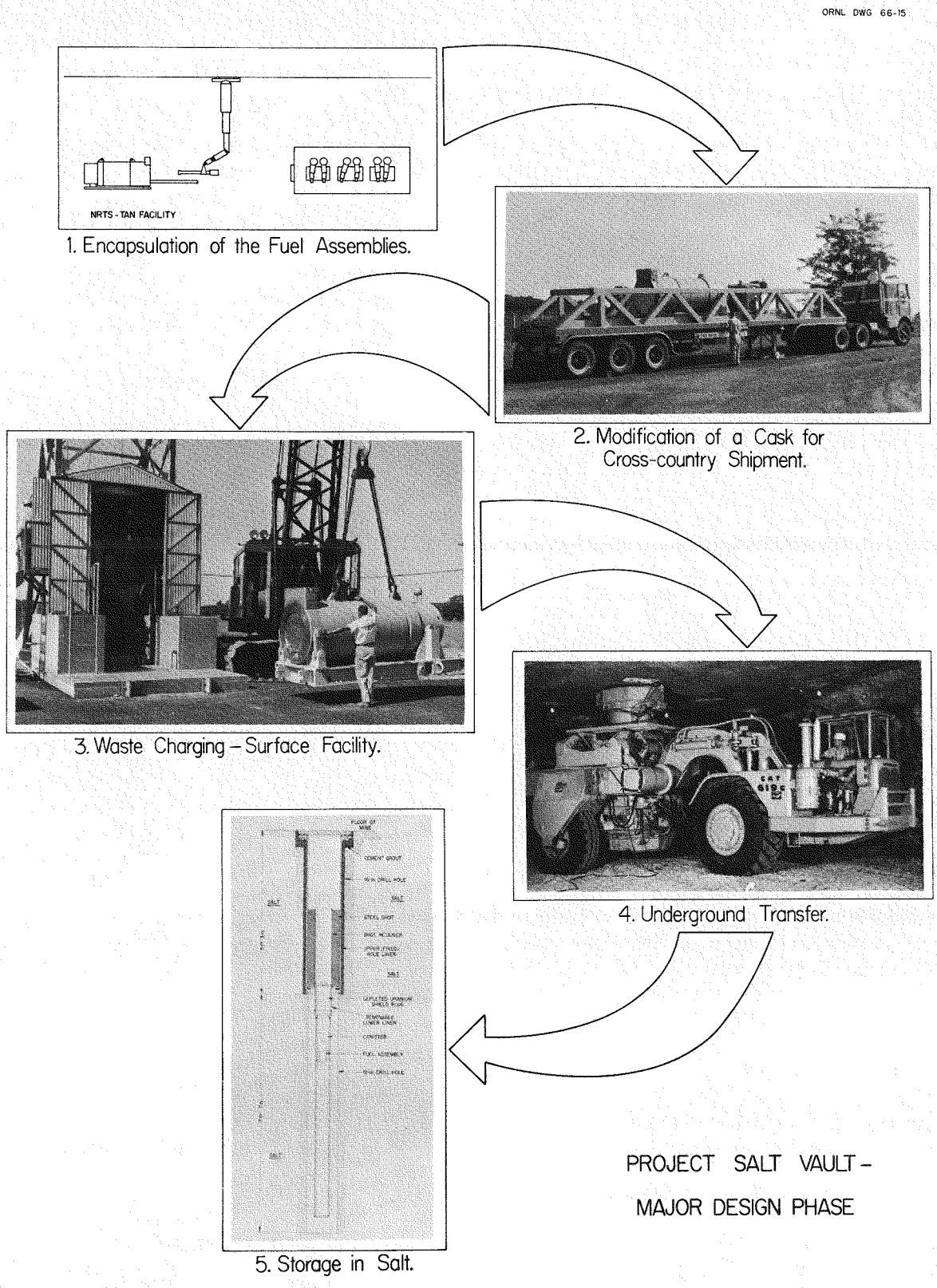


Fig. 14.2. Major Components of Experimental Equipment Specially Designed for Project Salt Vault.

applied to 22 heaters in the floor along the sides of the pillar. The heaters were located at a distance of approximately 2 ft from the base of the pillar.

Twenty of the twenty-two heaters were of the same design, and two were known as "modified pillar heaters." The regular heaters were contained in a 13-ft-long, 4-in.-diam sched 40 carbon steel pipe with three 2-in.-long, ½-in.-diam legs on the bottom. Each of the standard pipes contained an assembly of two U-shaped heater elements with Incoloy sheaths. The upper region of the pipes was filled with fiber-glass insulation to minimize convective heat transfer up the pipe. The two modified heaters were designed to yield additional information about the durability of carbon steel and 304L stainless steel in the salt environment at elevated temperatures. One was made of 4-in. sched 40 carbon steel pipe and the other of 304L steel, but the overall length was only 7 ft instead of 13 ft as for the regular heaters. The tops of these heaters were welded shut, and the electrical leads were brought up through a standpipe. The sealed portions of these heaters were flushed with dry nitrogen at ambient temperature before welding, so that as the temperature went up, a pressure would build up, and leaks in the heater pipe could be detected by a pressure loss. Three ⅛-in.-diam nickel tubes were strapped on the outside of each of the modified heater pipes. By pressurizing these tubes and measuring the flow, information could be obtained about the degree to which the salt had sealed around the pipe.

14.7.7 Instrumentation

In the PSV demonstration there were 393 thermocouples which were automatically recorded at regular intervals. To accomplish this, several multipoint recorders were used: one 12-, five 24-, and two 144-point loggers. In addition to the recorded thermocouples, there were others which were read with a portable potentiometer called a Minimite. The total number of thermocouples was about 545.

Figure 14.3 is a simplified block diagram of the power circuit for the array and pillar heaters and is largely self-explanatory. The main electric supply came in at 2400 V three-phase, and the experiment was operated from a 150-kVA transformer bank. Each of the radioactive array hole liners had two sets of three heater elements installed on the outside to supplement the radioactive decay heat and to allow the total power input to be maintained at a constant level as the radioactive heat decreased with time. The electrical array heater elements were located inside the liners and were identical to the pillar heater elements described earlier.

The off-gas system was used only on the arrays and was designed primarily to detect chlorine or other reaction products which might be produced by irradia-

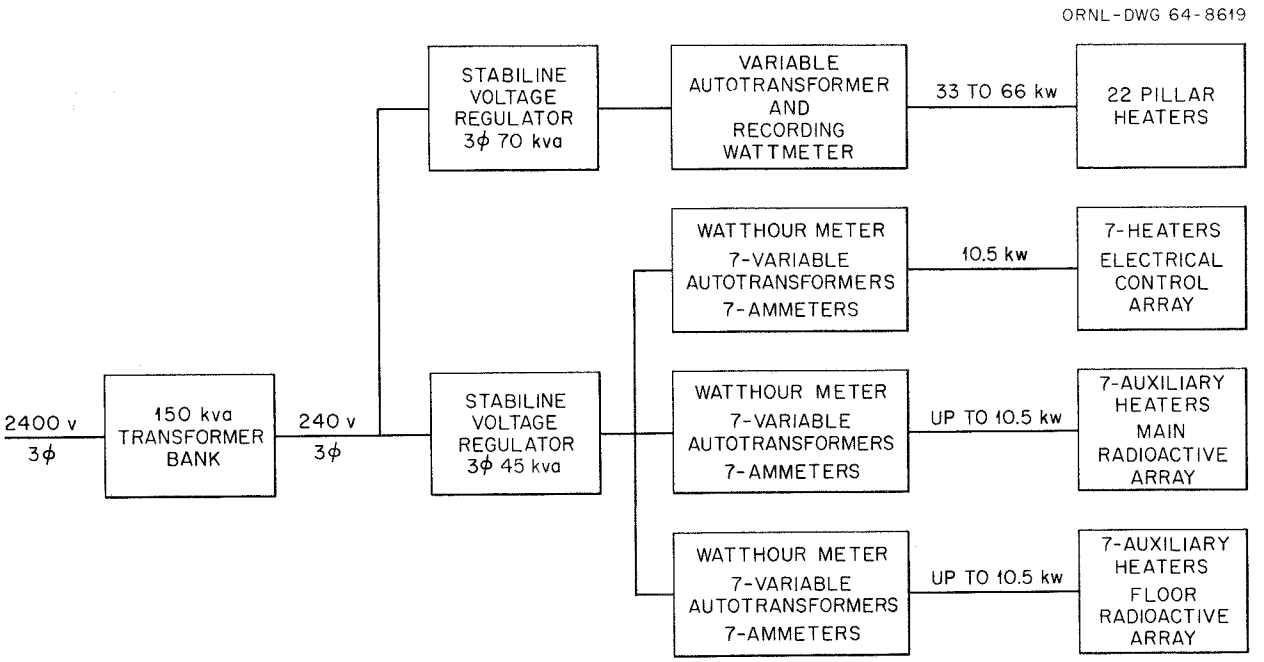


Fig. 14.3. Simplified Block Diagram of Power Circuit for Array and Pillar Heaters.

tion and/or elevated temperatures. An off-gas inlet and outlet to the annulus between the lower liner and the salt was provided on each array hole.

The radiation detection system (also called the purge system) was primarily designed to detect and contain any possible leaks in the fuel assembly canisters. In each radioactive array hole, the upper liner, which was in communication with the canister, contained an inlet port and an outlet port. The outlet ports were connected to an activated coconut-charcoal trap which contained two thin-wall G-M tubes inside a modified lead counter pig. From there the line led into a second counter pig containing a chamber with an end-window G-M tube. A purge pump, rotameter, and valve system was adjusted to draw about 1 liter/min through each of the hole liners and into the trap and counter system. Normally, the G-M tubes in the charcoal traps were read periodically with a portable G-M survey meter. The end-window tube was connected to an alarming-type count-rate meter in the underground control room which would cut off the purge pump, close the port solenoids on the hole liners, cut off all auxiliary electrical heater power, and transmit an alarm to the appropriate places if the reading exceeded the alarm point.

There were four conditions which were of prime importance to the experiment and which were included in an extensive monitoring and alarm system: (1) radioactivity leakage from one of the fuel assembly containers, (2) excessive fuel element temperatures, (3) rapid sag of a layer of salt in the roof of the experimental area, and (4) auxiliary electrical power failure to one of the arrays. If any instrument monitoring these four conditions exceeded preestablished limits, the interlocking system would shut off the electrical power to all arrays and during off-duty hours transmit an alarm signal to the operators' home.

Each radioactive array had two holes drilled tangent to the storage holes at an angle of 25° from the vertical for insertion of rods containing the dosimeters. These dosimeter holes were associated with array holes I and IV. The rod design allowed the insertion of six chemical dosimeters and 18 glass fluorods in each dosimeter hole so that the incident dose at various distances into the salt could be measured simultaneously.

14.8 INSTALLATION OF EXPERIMENTAL EQUIPMENT

The installation of the experimental equipment at and in the mine was carried out between June 1, 1965, and the start of the experiment in November 1965.

The facility at the top of the waste-charging shaft for handling the shipping cask and lowering the canisters into the mine was constructed primarily by subcontractors. The largest contract was for grading and leveling the area around the shaft and construction of the shielding, headframe, shelter, paving, and security fence. Following this basic work, the installation of various services and auxiliary equipment was undertaken.

The contract for the underground transporter specified that it be delivered underground at the Lyons mine. Therefore, the disassembly and transfer into the mine and reassembly of the unit were the responsibilities of the contractor. The unit was received at the mine fully assembled (except for the lead shield rings) on a railroad flat car. Since size and weight limitations of the main shaft at Lyons had been incorporated in the design of the various components of the machine, no particular difficulties were experienced in this phase of the operation. The disassembly-reassembly job, including installation of the lead rings, occupied a three-man crew for a total of five weeks. Performance of the transporter in the underground workings exceeded expectations. The 10% grade could be negotiated with ease. The transporter with its 25-ton shield was found to be nimble, responsive to the controls, and stable.

Incoming power was received from Kansas Power and Light Company at 2300 V and divided into four separate circuits – three on the surface and the fourth feeding the underground operations. One surface power circuit supplied the waste-charging facility for the winch, hydraulic system, and lighting through a three-phase bank of three 15-kVA 2300/400-V transformers at the site. The other three circuits went through the new switchgear in the hoist house. One of these three circuits supplied power to the 150-hp hoist motor at 2300 V. A second circuit fed a bank of three 37.5-kVA transformers connected 2300/440 V. The third circuit supplied the underground power system at 2300 V by a feeder cable, three-conductor No. 4 with 5-kV insulation and an integral ground, installed in the counterweight (north) compartment of the main shaft. The 2300-V three-phase system terminated at a substation in entry 5 and room 7. Three 50-kVA 2400/480/240-V dry-type transformers were installed as a source of power for mining operations, for experiment requirements, and for lighting.

The upper sections of the array hole liners were grouted into the 5-ft-3-in.-deep, 16-in.-diam upper portion of the hole using "salt-crete" grout. This portland cement grout was made in the ordinary way except that crushed and graded salt was used instead of

the sand and that brine was used instead of fresh water. The most important part of the hole liner installation was to assure that the liners were plumb and concentric in the hole and even with the floor. The remainder of the hole liner installation consisted in attaching the various connections, bolting the lower section in place, and assembling the steel shot shield above it.

The 22 heaters for the pillar heater experiment were installed in the holes along the base of the pillar between rooms 2 and 3. In each room the row of 11 heaters, spaced at 5-ft intervals, was placed 2 ft out from a "nominal" pillar edge location. These pillar heaters were therefore on two parallel lines 27 ft apart. The holes were numbered from the back of each room, and the two "modified" pillar heaters were placed in hole 6. The heaters were installed so that they would all be at the same elevation. The annular space around one of these heaters was backfilled with dry quartz sand, and three others were backfilled with crushed salt. All other heaters were not backfilled, but fiber-glass insulation was placed in the upper portion of the annulus between the heater and the hole to prevent excessive convective heat losses.

A major part of equipment installation effort, especially by the mine personnel, was involved in what may be classed as instrumentation. All of this work will be summarized in the following paragraphs except for the rock mechanics gages, which are discussed elsewhere. Much of the instrumentation, especially for power control, temperature recording, and the alarm system, was centrally located at two points: (1) the control room, a 12 X 20 ft wooden frame building constructed at the top of the ramp opposite the experimental entry specifically to house the instruments, and (2) the power control panel, located in the experimental entry between rooms 2 and 3.

All thermocouples were fabricated before delivery to the mine; that is, they were received with male connector plugs attached and with the junctions formed at the proper lengths. Those thermocouples which were attached directly to the heater or otherwise exposed to temperatures in excess of 150°C (for example, the wall-of-hole thermocouples) were sheathed in swaged stainless steel. All other thermocouples were unsheathed and insulated with fiber-glass fabric. All of the thermocouples to be installed in holes in the salt were first encased in ¼-in. plastic tubes of either Teflon or polyethylene depending on the maximum temperature expected.

For those thermocouples which were to be read manually with the portable Minimite instrument, the male connector plug was left exposed. The connections between the recorded thermocouples and the appropriate recorder or logger were completed by running duplex leads from the thermocouple connector plug to junction boxes mounted on the walls of the rooms. From the junction boxes, 12- and 24-pair cables carried the signals to the recorders. The cables, junction boxes, and leads were all cut to length, wired, and assembled when received at the mine.

The equipment and instruments for the control of the power to the heaters in the three main arrays and the pillar heater experiment were mounted in modular steel panels, each prewired and preassembled before delivery to the mine. Installation therefore consisted in mounting the panels and making the necessary connections to the power distribution system and between the various panels.

The major components of the off-gas system were also preassembled prior to delivery to the mine. Installation consisted in mounting the various parts (rotameter box, vacuum pump, condenser, etc.) at convenient places and hooking them together. In all three array rooms the bundle of Teflon off-gas tubes was placed in a small trench, along with the heater power leads, and covered with steel plate.

The radiation detection system was installed in rooms 1 and 5 only. Again, the installation was primarily a matter of locating, mounting, and connecting the prefabricated components. The common plastic tube and the solenoid control lead wires leading from the hole liners were placed in the steel-plate-covered trench with the off-gas tube bundle. A continuous air monitor (CAM) was also used to continuously sample the air at the top of the ramp throughout the operation of the experiment. An extension hose permitted the use of this instrument at more remote and specific points during the canister handling operations.

The various components of the alarm system had also been fabricated in preassembled panels, and installation at the mine was therefore largely a matter of connecting and checking the system. The various alarm signals were carried from the experimental area to the unit in the hoist house through a 25-pair telephone cable installed by Southwestern Bell Company down the main shaft and to the control room. The alarm system signals were transmitted from the hoist house alarm unit to the three remote signaling units located at the operators' houses and the sheriff's office on existing telephone lines.

Two periods of intensive testing of all equipment and systems were scheduled which would duplicate, as nearly as possible, the actual fuel element canister handling operations. These two tests were called "cold

checkout," which was intended to check and debug the mechanical functioning of the equipment, and the "cobalt checkout," which would provide additional testing and experience with the mechanical equipment and check all of the shielding facilities. For the cold checkout, several empty canisters were shipped to the mine in the shielded shipping cask. The cask was erected over the waste shaft, and the various handling operations were carried out. At first the various subprocedures, such as moving a canister in and out of an array hole or in and out of the shipping cask, were run through several times. Finally, these procedures were put together and several complete canister handling cycles, from shipping cask to array hole and return, were carried out. No basic deficiencies in the equipment or its design were encountered in this check, but normal and expected mechanical "bugs" were turned up.

In the cobalt checkout, two canisters were loaded with 500 Ci of ^{60}Co each in the form of five 100-Ci capsules distributed along the length of the canister. These were then loaded into the shipping cask and sent by truck to Lyons using the procedures planned for the fuel-element shipments. The detailed procedural checklist to be used for the change-outs was followed, and a close examination of the radiation field was made at every stage as a check on the shielding. Only a few very minor mechanical "bugs" were discovered, and these were quickly corrected. However, three significant shielding deficiencies were revealed and corrected by making relatively minor modifications in the equipment.

The work described in this section covered a period of about six months and involved a mine crew of nine men, in addition to the ORNL personnel permanently at the site and those temporarily assigned to direct a particular aspect of the installation. This total, of course, does not include the effort devoted to the shop fabrication of the experimental equipment or the work supplied under subcontract.

14.9 HAZARDS ANALYSIS

The 14 fuel assemblies (at from 60 to 75 days out-of-reactor) would be transferred from the ETR canal to the hot-cell facilities, where the fuel would be loaded into the canisters. After loading, mechanical sealing, seal welding, and helium leak testing, the fuel canisters would be loaded into the shipping carrier and the carrier and its shipping rack transferred to a special heavy-duty trailer. When this operation was complete, the truck would be routed to Lyons, Kansas. Responsibility for the fuel canning, seal welding, carrier loading, and shipping was assumed by the Phillips Petroleum Company.

A detailed structural analysis of the cask, magazine, shipping frame, and canister was made. This analysis indicated that the units and assembly would meet the structural criteria cited in Sects. 72.32, 72.33, and 72.34 of the Code of Federal Regulations, Title 10, Part 72.

Two methods were used for calculating the ability of the cask to withstand the effects of a fire [Sects. 72.31(c) and 72.34(b)]. The cask was coated with intumescent paint before use, because of the excellent fire-retardant properties and low cost of application. Based on the calculations, paint test data, and engineering judgment, it was estimated that the cask should be able to withstand a fire of from 45 to 60 min without serious shield damage and certainly without release of any radioactive materials to the environment.

Fission product gamma-activity calculations for the ETR fuel assemblies were made with the PHOEBE code, which provides a machine method of calculation for beta and gamma activities from ^{235}U-produced fission products for any given set of irradiation and decay-time conditions. The activities obtained were then used as the source strengths for the shielding calculations (Sect. 72.35). The calculations indicated that the ICC regulations could be met without difficulty.

It was necessary that the fuel element array be subcritical in the normal condition, even if the sealed canisters became filled with water (Sect. 72.37). Furthermore, it was necessary that the configuration be subcritical in the event of a collision that might involve loss of all the cooling water, dislodgement of the canisters such that they could be located anywhere within a 5-in.-ID by 19½-in.-OD by 7.5-ft-long annular cylinder within the cask, or loss of coolant and fuel meltdown in the event of a fire. An analysis showed that the material in the seven canisters would be subcritical under all possible conditions.

During normal shipping conditions the bulk of the decay heat would be removed by the circulating cooling water in the canister magazine (Sect. 72.38). The cooling water was supplied by a system consisting of a radiator, fan, and circulating pump, on a diesel engine. This system was selected because it was simple, reliable, and economical. A diesel motor fitted with an oversize radiator and dual inlet and outlet nozzles to provide a net cooling capacity of 1900 Btu/min at 125°F maximum ambient air temperature was specified based on data obtained from equipment manufacturers. The

unit purchased had greater cooling capacity than specified; it should have a cooling capability of at least 4350 Btu/min when running at 1800 rpm under full load. The diesel was equipped with an auxiliary water pump which was used solely for circulating the water between the cask and the radiator. The magazine inlet cooling water temperature was not known at this time; for the purposes of heat calculations it was assumed to be 150°F. Heat transfer calculations were made to obtain estimates of the temperatures which might be reached in strategic locations in the cask under the following conditions: (1) without coolant circulating, (2) with forced cooling, (3) including the maximum effect of solar heating. Calculated temperatures were within acceptable limits, but the validity of some of the assumptions used in the calculations was not known. Therefore, a series of tests were carried out using electrically heated dummy canisters in the shipping cask. In one of these tests, the loss-of-coolant-circulation condition was simulated. After 24 hr the fuel assembly canisters had reached a temperature of 752°F; it was therefore concluded that the melting point of the cladding of the assemblies would not be exceeded under these conditions.

The analyses of the cask showed that structural integrity was guaranteed under normal shipping and severe collision conditions, that the external exposure would be reduced to less than 10 millirems/hr at 1 m from the surface, that a configuration which would allow a critical mass to develop was not possible, that the cooling system would remove sufficient decay heat to prevent melting of the fuel elements under normal operating conditions, and that release of radioactivity to the environment in any credible accident was highly improbable.

The containment design was unusual for shipping casks in that complete radioactive material containment was assured by a hermetically sealed fuel element container design. Only sound fuel elements were canned for use in the demonstration, and, under normal conditions, fission gases would be retained by the fuel element cladding. In a severe collision, when the integrity of the cladding could be lost by impact damage or high temperature, the canister would retain gaseous as well as volatile fission products. The maximum credible accident was considered to be one in which the cask was involved in a sustained fire, and loss of shielding resulted from a rupture in the steel shell of the cask and the release of molten lead. Engineering design was used to prevent the maximum credible accident from occurring.

Design of the fuel assembly canister for this experiment was based on the necessity for providing secondary containment by the canister. The canister as designed provided containment by means of both a mechanical closure and a seal weld. If, during any portion of the shipment from Idaho to Lyons or the experiment, the fuel assembly cladding temperature should exceed its melting point, the canisters would still provide containment. Thus, during the fuel shipments and whenever the canisters were being moved from the surface into the mine, two containment barriers were provided. When the canister was inserted into the array storage hole, a third containment barrier was provided by the gasketed upper flange. However, due to the large number of penetrations in the upper liner section (for thermocouple leads, power leads, and off-gas lines), 100% tertiary containment for the entire storage period could not be guaranteed. Therefore, a gas purge system which pulled air into the upper liner and vented it through a charcoal trap, filter, and monitoring system before release was installed.

Engineering safeguards were designed into the waste-handling equipment to reduce the probability of any accident occurring. However, even with the engineering safeguards and detailed checklists, there still remained the possibility that a mishap could occur that would ultimately lead to a release of radioactivity from the fuel assembly canister. This release could occur due to a number of unrelated occurrences (such as a cladding failure in the ETR assembly followed by a subsequent leak in the canister) or to one event such as a drop or impact to the canister. In general, because the ETR fuel assemblies were fabricated from an aluminum-uranium alloy completely clad with aluminum, the amount of radioactivity released would depend on the number of plates which were ruptured or damaged. Fuel assembly meltdown was not possible while a single canister was being transferred in the experiment, and the only possible place where meltdown could occur was in the storage hole in the mine floor, where additional heat was supplied by electrical heaters. Because of this possibility, the storage holes were made leak-tight, and the purge system was installed to detect and contain any potential activity released. As a further safeguard, control systems were provided to shut down electrical power to the auxiliary heaters should the fuel assembly temperature exceed a safe level.

The types of accident which could occur are defined as:

I. Type I accident – an accident or release due to cladding failure on one fuel plate.

II. Type II accident – an accident or release due to impact or dropping of the canister. This accident category is assumed to result in the breakage of up to 19 fuel plates (one ETR assembly).

In addition to the number of plates which are broken, the two categories of accidents can be described by the location in which they might occur. A type I accident could occur anywhere in the handling or storage operation, since it is the result of an initial cladding failure of the fuel assembly followed by a failure of the canister and would not necessarily require impact. A type II accident, however, was not possible during the handling operations at mine level. The movements of the canister during these stages of the experiment were slow, and there were no possibilities of long drops or severe impact that would result in this amount of damage. This type of accident would occur in the waste shaft and would result in the release of activity up the waste shaft to the atmosphere.

A type I accident, or a "leaky fuel assembly," could not occur unless the integrity of the canister was also lost. The exact causative agent for producing such a failure in the canister cannot be predicted; however, such things as corrosion, minor physical damage, or inadequate welds are possible. The canisters were constructed of 304 stainless steel and were protected from direct exposure to the salt by the hole liner; the air inlet to the liner (for the fission product detection system) had a filter to exclude salt dust. Because of these precautions, the probability of a failure in the canister integrity during the early stages of the experiment was small, but it increased with length of time in the mine. As a result, the only gaseous fission product of concern would be the ^{85}Kr, since the ^{131}I would have decayed to less than 1 Ci per canister after 150 days out of the reactor. The degree of severity of a canister leak would depend on the position of the canister when the leak occurred. If a leak occurred while the canister was located in the storage holes, the release would be detected by the hole liner purge system, and corrective action could be taken without the release of any activity to the mine atmosphere. If the leak were to occur when the canister was in the underground transporter, it would be detected by the air monitoring equipment, and the canister and the transporter could be stored until corrective action could be taken. The same is true for a leak occurring when the canister was in the waste shaft. In this case the air flow in the shaft would be essentially zero, and the activity could be contained in the shaft. In no case, due to the system employed for ventilating the experimental area, could the activity be released to the main mine air, resulting in contamination of the mine access tunnels or the main access shaft. Remedial actions that would be taken would depend on the location of the canister when the leak occurred, but in general would probably consist in allowing a decay period for shorter-lived fission products if they were present, followed by either a slow and controlled release of the activity up the waste shaft, or the gases could be collected and contained. The activity released by the failure of one fuel plate was assumed to be 100% of the rare gases and 0.1% of the ^{131}I present. Because the failure of the fuel plate would probably not expose all of the core material, and further because the canister leak would probably be from a relatively small hole, it was felt that these assumptions on activity release were conservative. Based on the above assumptions, 0.006 Ci of ^{131}I, 2 Ci of ^{85}Kr, and 1 Ci of ^{131m}Xe could be released into a mine storage room. Assuming the fission products are uniformly distributed throughout the air in the 60-ft by 30-ft by 14-ft storage rooms, their concentrations would be 8.4×10^{-6} μCi/cc ^{131}I, 2.8×10^{-3} μCi/cc ^{85}Kr, and 1.4×10^{-3} μCi/cc ^{131m}Xe. Therefore, the release of activity from a type I accident in the mine would not produce conditions that could not be tolerated. Limits would have to be placed on the amount of time that could be spent in the room, but in the case of ^{131}I, after waiting eight days the exposure time could be doubled due to decay of the radioiodine. The fission gases could be slowly bled out to the waste shaft without causing hazards in the mine or at the surface. If the type I accident were to occur in the waste shaft, the iodine would probably be trapped on the surface of the waste shaft, and the release of 3 Ci of ^{85}Kr and ^{131m}Xe to the atmosphere would not cause any greater hazards than those produced in the mine room.

A type II accident is one in which the canister and the fuel assemblies are both extensively damaged at the same time. The exact causative agent for such an accident was not known, but it could result from dropping or some other type of impact. Due to the handling procedures and equipment design, this type of accident could only occur in the waste-charging shaft. As a result the activity would be released to the atmosphere. Depending on the amount of impact, varying degrees of damage to the fuel assemblies could result. However, it was assumed that the maximum amount of damage would be the rupture of one-half of the total fuel plates in the canister (19 plates ruptured). This assumption was thought to be very conservative because of the design and construction of the ETR assembly and the fact that breaks in the plates would

expose only a relatively small amount of the metallic alloy core material. For this study a release of 0.1% of the ^{131}I and 100% of the fission product gases was assumed. Based on these releases and the amount of fission products available in 19 fuel plates, the following quantities of radioactivity would be released: 39 Ci of ^{85}Kr, 21 Ci of ^{131m}Xe, and 0.11 Ci of ^{131}I. No cesium or strontium would be released since melting would not occur. The hazard associated with the release of the fission product activity to the atmosphere was calculated using Sutton's theory for an instantaneous point source. Weather Bureau information for Wichita, Kansas (nearest station to Lyons, approximately 80 miles to the southeast) indicated that the average wind speed was 13 mph and the prevailing direction was from the south. For this study calculations for atmospheric release were performed using two meteorological categories: condition D (cloudy to partly cloudy with wind speed of 6 m/sec) and condition F (inversion with wind speed 2 m/sec). The results of the calculations of the thyroid dose following inhalation due to the release of 0.11 Ci of ^{131}I to the atmosphere in a type II accident indicate that the release of this activity on a cloudy or partly cloudy day with the average wind speed equal to 13 mph (a type D condition) would produce a thyroid dose of 125 millirems to an individual standing 100 m away. This value is considerably below the permissible dose to the thyroid for a 13-week period. In the case of the inversion, the dose to the thyroid would be 1.6 rems, which is again below the permissible dose to the thyroid for a 13-week period. The calculations of ground contamination resulting from the release of radioiodine indicate that for either of the assumed meteorological conditions there would be no restriction on food production at distances greater than 100 m. If the activity were released during an inversion condition, milk produced on land located less than 1050 m could not be consumed. However, the restriction on land from 100 to 1000 m could be lifted after about 30 days. Doses at 100 m due to immersion in the ^{85}Kr and ^{131m}Xe released from the waste shaft in the worst condition (an inversion) would be 42 millirems due to the ^{85}Kr and 16 millirems due to the ^{131m}Xe. Both of these dosages are within permissible limits.

14.10 OPERATING EXPERIENCE

Although most of the detailed technical results concerning temperature, rock deformation, off-gas, etc., and their analysis will appear in the next section, this section contains some important "results" of the experiment. These are principally related to the performance of and experience with the equipment for handling the fuel element canisters. A schedule of the activities during this period is given in Table 14.2.

Since an initial period of intensive gage reading at the start of the experiment was considered desirable, the array experiments were started and operated for the

Table 14.2. Schedule of Operation of Experiment

Nov. 15, 1965	Official startup; power turned on in rooms 1 and 4.
Nov. 17, 1965–Nov. 19, 1965	Fuel element canisters installed in room 1.
Dec. 1, 1965–Apr. 19, 1966	Room 5 experimental equipment installed, hooked up, and checked out.
Mar. 8, 1966–Apr. 17, 1966	Roof bolt test in room 3.
Apr. 28, 1966–July 19, 1966	Install, torque, and retorque roof bolts throughout entire experimental area.
June 6, 1966	Room 5 startup: power on.
June 8, 1966–June 15, 1966	Change out of fuel element canisters, room 1 to room 5; new canisters from Idaho into room 1.
June 22, 1966–Nov. 11, 1966	Operated modified pillar heater in hole 6, room 2.
Sept. 22, 1966–Jan. 6, 1967	Fiber-glass insulation boards on floors of rooms 1, 4, and 5.
Oct. 11, 1966–Oct. 13, 1966	Fuel element canisters removed from room 5 for shipment to Idaho.
Oct. 31, 1966–Nov. 10, 1966	Changeout of fuel element canisters, room 1 to room 5; new canisters from Idaho into room 1.
Nov. 14, 1966	Start heated pillar experiment, 33-kW power input.
Jan. 23, 1967	Increased power to array heaters in rooms 1, 4, and 5 by 40%.
Mar. 2, 1967–July 14, 1967	Intermittent work on installation and hookup of simulated waste can tests (SWCT).
July 17, 1967–Dec. 20, 1967	Operation of SWCT.
June 5, 1967	Termination of array experiment in room 5 (power off).
June 14, 1967	Termination of array experiments in rooms 1 and 4 (power off).
June 5, 1967–Jan. 31, 1968	Collection of cooldown data; dismantling, inspection, and disposal of experimental equipment.
June 12, 1967–June 14, 1967	Fuel element canisters removed from room 5 for shipment to Idaho.
June 26, 1967–June 27, 1967	Fuel element canisters removed from room 1 for shipment to Idaho.
Oct. 9, 1967	Termination of pillar heater experiment (power off).

first two days using electrical heat only. On the third day following startup, the first fuel element canisters were transferred from the shipping cask to the main radioactive array in room 1. This transfer and all of the others discussed below were carried out using the detailed procedure and checklist. Handling of the canisters required a crew of 8 to 11 people, depending on which phase of the transfer procedures was being carried out.

The changeout of fuel element canisters was carried out in a manner somewhat different than originally planned. Those plans called for receiving the full shipping cask and moving new ones to room 1, those in room 1 to room 5, and those in room 5 back into the shipping cask. Instead, the original canisters, which had been in the mine a year and in the room 5 array for the last six months, were removed and returned to Idaho. Canisters containing new fuel elements were loaded into the shipping cask and returned to Lyons. In the meantime, the canisters in room 1 were moved to the now empty holes in room 5. This procedure eliminated the need for the extra storage hole. When the new canisters were received, they were installed in the array holes in room 1. Minor difficulties were experienced with the hydraulic system of the underground transporter. This was corrected during the period following the changeout.

Although initial plans had called for four sets of fuel element canisters and operation of PSV for two years, the design objectives of 10^9 rads peak dose to the salt in room 1 had been attained with only three sets of canisters and operation for about 19 months. Therefore, it was decided to terminate this portion of the experiment. Electrical power to rooms 1, 4, and 5 was turned off on June 5, 1967. Commencing a week after the power shutoff, the fuel element canisters were removed from room 5, loaded into the shipping cask, and returned to Idaho. The cask was returned to Lyons empty, and the canisters were removed from room 1 on June 26 and 27, 1967. These transfers were completed without incident.

Over the 19-month course of this part of the experiment, 21 canisters containing about 200,000 Ci of activity each (when received at the mine) were handled, 14 of them on three occasions and the other 7 twice. All of the handling operations were completed without incident and with only very minor mechanical problems with the diverse equipment. Quarterly radiation exposures to the mine personnel exceeded 50 mr only for the one period when difficulties were experienced with retrieval of thermocouple leads. This was in spite of the fact that all of the transfers were accomplished without the aid of hot cells, which would, of course, be required in any actual disposal facility. One of the major objectives of the experiment was to demonstrate the techniques and equipment for handling waste containers in an underground environment, and the Project Salt Vault experience toward this objective can be considered an unqualified success.

The second major experiment in Project Salt Vault was the extensive heating of the small pillar between rooms 2 and 3 in the experimental area. This was accomplished by 22 heaters in the floor along the two sides of the pillar. Two of these heaters, the "modified pillar heaters," were also involved in a subsidiary experiment. Startup of the pillar heater experiment (November 14, 1966) was much simpler than for the arrays and consisted in reading all gages, roof-bolt load cells, and thermocouples for background; turning on the power at 1500 W each, a total of 33 kW; and reading those same instruments at fairly frequent intervals during the early period of rapid heating.

Throughout the course of the radioactive portion of the experiment no releases of activity occurred. However, alarms due to malfunction of the system were a regular but unscheduled event. During the 19-month period, a total of 20 alarms occurred which required trips into the mine during off-duty hours, and at least 9 additional alarms required trips to the mine office or sheriff's office. Nearly all of these false alarms were due to one of two main types of malfunction: (1) extreme sensitivity of the system to minor variations in line voltage and (2) failure of a transistorized input module in the count-rate meter.

There were several items of routine servicing which were related to the more unusual aspects of this experiment. The first of these was the servicing of ordinary mine equipment. This included twice monthly checking of the hoisting equipment, and especially its associated safety devices, and weekly servicing of the mine lamps carried by the underground crew. The second was the routine scaling of the room and walls in all regularly traveled portions of the mine. Here it should be mentioned that the thermally accelerated deformation of the center (heated) pillar in the experimental area required extensive scaling of the pillar after about six months of operation – much earlier than would have been expected under ordinary conditions. Third was the monthly servicing and "exercising" of the underground transporter.

The nonroutine items during the operational period included relatively small subsidiary experiments which were either planned or added to the experimental plan in order to elucidate other results or unexpected

activities resulting from the operation of the experiment. The largest of these nonroutine activities was the bolting program, which began with the trial installation of 37 roof bolts in room 3 and which was carried out with the regular mine crew. When the decision was made to proceed with the installation throughout the experimental area, arrangements were made to secure a separate three-man crew for this work. They performed the drilling, bolt installation, and torquing. Approximately 1600 bolts of high-strength steel, 4 ft long by $\frac{3}{4}$ in. nominal diameter, were installed on 4-ft centers in a triangular pattern. It was found to be desirable to grease the surfaces between the bearing plate and the bolt head. This lubrication made it possible to secure the desired bolt loading at a torque of 125 to 150 ft-lb. Bethlehem type K-3 expansion shell anchors were used on all bolts. Three dozen load cells were installed under selected bolt heads with leads run to a central location in each room. Soon after installation and after several load cell readings had been taken, U.S. Bureau of Mines personnel checked the bolts for load-carrying capacities. They reported that the bolts would elongate at 20,000-lb load and pull from the shell anchorage at 24,000 lb.

Several special experiments were carried out in an effort to accurately measure the rate at which moisture was entering the array holes due to the migration of brine inclusions in the salt. The difficulty with these measurements was due to the moisture already in the mine air (40 to 60% relative humidity) and the low rate of moisture production from the salt in the array holes. These special experiments included the use of Drierite columns in the off-gas lines, cold traps using ice and brine, dry ice, and liquid nitrogen, and one series of experiments (the most successful) where dry nitrogen gas was swept through the hole and off-gas system.

One of the objectives of the array experiments was to heat the largest possible volume of salt to a temperature approaching 200°C without running any risk of developing excessive temperatures within the fuel elements. After about six months of operation of the arrays, it was determined that the heat losses from the floor of the array rooms were sufficient to appreciably distort the isotherms. In an effort to reduce these heat losses to the ventilation air and thus perhaps increase the peak salt temperature, the areas around the arrays in rooms 1, 4, and 5 were covered with 1-in.-thick fiber-glass insulation boards beginning September 22, 1966. By December it was obvious that these measures were ineffective in increasing the peak temperature, although temperatures in the upper portion of the salt around the arrays were increased. Therefore, the fiber-glass insulation was removed, and on January 23, 1967, the total power (electrical and decay) to all of the three arrays was increased from 1500 to 2100 W per hole. This power boost achieved the desired effects.

The "modified pillar heater" portion of the experiment was included to comparatively evaluate the qualities of stainless steel and carbon steel as waste container materials when in contact with salt at elevated temperatures. When the stainless steel heater assembly lost pressure after several months operation, this portion of the experiment was expanded by the addition of the Simulated Waste Container Test (SWCT). The design of the two modified pillar heaters was identical except that one was carbon steel while the other was 304L stainless steel. The carbon steel modified pillar heater in room 2 was started on June 22, 1966, at a nominal power of 3 kW and operated until termination of the heated pillar test on October 9, 1967. Power input was reduced to 1.5 kW on November 14, 1966, when the heated pillar test was started. The pressurized system remained tight throughout the test period. The hole was backfilled with crushed salt around and over the heater in the same way as in an actual disposal operation. When the heater was removed from the hole, the surfaces exposed to the salt were covered with a general coating of rust. The second modified pillar heater, fabricated of 304L stainless steel, was started on November 14, 1966, along with the remaining 20 open heaters. The heater lost pressure in about three months, although the heating elements did not fail, and when it was removed from the hole, the pressure loss was found to be due to severe corrosion of the $\frac{1}{2}$-in. sched 40 pipe connected to the pressurized section of the heater. The heater container itself was still pressure tight, although metallurgical examination of the can revealed that stress corrosion cracking had penetrated about half the wall thickness.

The objective of the SWCT test was to secure additional data on the effect of moisture on stainless steel and carbon steel containers in the relatively pure salt of the floor of the experimental entry and in the salt-shale mixture of the original mine floor. The test utilized six heaters, three of 304L stainless steel and three of carbon steel. Two of each were located in the original mine floor in a square array of 10-in.-diam by 12-ft-deep holes about 50 ft from the room 5 (floor) array. The two heaters in the experimental entry were located in similar holes with the bottom 12 ft below the floor. The holes were backfilled with crushed salt after placing the heaters. Due to heater failures, the operation of the SWCT tests was less than satisfactory, and the results were inconclusive.

Dismantling of equipment began as soon as possible after termination of each part of the demonstration. In some cases it was necessary to make modifications in order to continue other experiments. For example, after the array operation ceased, wiring was changed to utilize the regulated power supply and the watt-hour meter from one array to power the SWCT array in the original mine floor. Removal of the heaters and SWCT cans was most difficult. Redrilling around the modified heaters and SWCT cans was necessary, and additional dissolution of salt in the lower section of the holes using fresh water to relieve them from their original test hole was effective.

Examination of the modified pillar heaters and of the SWCT heaters revealed that gross cracking had occurred in both the 304L stainless steel modified pillar heater and in one of the 304L SWCT heaters. Also, the 304L $\frac{3}{4}$- and $\frac{1}{4}$-in. pipes used on the modified pillar heater as electrical conduit and for a pressure connection to the floor were severely corroded. The cracking and most severe corrosion were in those parts of the heaters which were cooler and at which water may have condensed. Metallographic examination of the 304L stainless steel modified pillar heater revealed the cracking to be due to stress corrosion. Transgranular cracks were found in metallographic samples removed from the center of the sealed heated portion as well as in the cool portion of the heater assemblies. Although the sealed heated portion had held air pressure, more than half of the wall thickness was penetrated by the cracks. Metallographic examination of the carbon steel modified pillar heater showed a corroded outer surface but no evidence of penetration. There was apparently little, if any, loss of wall thickness to corrosion.

In general, the operation phase of the Project Salt Vault experiment was successfully completed with only minor problems. The demonstration of the canister handling equipment and techniques was especially successful.

14.11 RESULTS AND ANALYSIS

In this section the technical results and analysis of radiation, moisture, temperature, and rock deformation are summarized. A large quantity of data on these items was obtained from the experiment, typical examples of which, along with detailed analysis and interpretation, were presented in Chap. 11 of this report. Only the major conclusions and a few summary plots are included here.

14.11.1 Radiation

The nominal ETR assembly irradiation history was 23 days (2×10^6 sec) irradiation at a flux of 1.84×10^{14}. Four hundred grams of ^{235}U per assembly was assumed. The calculated earliest age for canning this nominal fuel assembly was 60 days after discharge from the reactor, based on a maximum fuel assembly temperature of about 850°F in the hot cell. This would mean that shipment could be made by 75 days after reactor discharge, and the cans could be in the mine by 90 days after discharge. At 90 days the nominal radioactive heat generation would be about 750 W per canister of two ETR fuel assemblies.

Of the first set of fuel assemblies, five of the seven canisters had calculated heat generation rates of about 620 W at 90 days, while the other two canisters were generating about 590 W. The canisters were not placed in the mine until the assemblies were 107 to 109 days out of the reactor (November 17–19, 1965), so the dose to the salt from the first set of assemblies was somewhat less than nominal. The second set of fuel assemblies was transferred into the main array on June 13–15, 1966, when they were 105 to 107 days out of the reactor. However, due to a higher average burnup, these fuel assemblies were considerably more radioactive than nominal and had a heat generation of about 780 W at the time of placement in the mine. The third (and final) set of canisters was transferred into room 1 on November 7–10, 1966, when the fuel assemblies were 84 to 87 days out of the reactor and canister heat generation rate was about 800 W. This set of assemblies was removed from room 1 on June 26–27, 1967, for return to Idaho. Thus three sets of fuel assemblies were used in room 1, covering a total period of about 19 months. Room 5 was exposed to only the first two sets of assemblies, for a total period of about $11\frac{1}{2}$ months.

The measured peak radiation dose to the salt in the main array (room 1), at the junction between the two ETR fuel assemblies, was about 3.7×10^8 rads as of November 1, 1966. By May 1967 the total was about 5.3×10^8 rads. Generally, the accuracy of the dose measurements themselves is believed to be within about 20%. However, the point at which the measurements of the incident dose to the salt were made (the junction between the assemblies) was such as to produce dose values which were lower than the average incident salt dose over the 6-ft length of the tandem fuel assemblies by about a factor of 1.4 and lower than the peak dose by a factor of about 1.9. If a fourth set of fuel assemblies were assumed to be identical to the third, the total dose at the junction of the assemblies would

have been about 6.8×10^8 rads after two years of operation. On the other hand, the original goal of achieving a peak dose of at least 5×10^8 rads had been met by May of 1967.

In view of the fact that both field and laboratory studies confirmed that the radiation effects on salt do not appear to have any detrimental effects for waste disposal, there did not seem to be any need for bringing in the fourth set of fuel assemblies. The approximately 30% increase in total dose which would accrue with the fourth set of fuel assemblies would be unlikely to produce any new results. Therefore, it was decided to terminate the radioactive tests with the third set of fuel assemblies, and they were removed from the room 1 array at the end of June 1967.

It was expected that because of the buildup factor the peak absorbed dose to the salt would be about 7×10^8 to 8×10^8 rads at a salt depth of $2\frac{1}{2}$ cm. Based on the actual measurements, the absorbed dose after about 19 months of operation in the mine was approximately 5.5×10^8 rads and occurred at the wall of the hole. The estimated average dose to the salt over the length of the hole was about 8×10^8 rads. The estimated peak absorbed dose was about 10^9 rads. The measured dose at the wall of the hole in the array in the old mine floor (room 5), which received the ETR fuel after it had remained about six months in the experimental area, was slightly more than 10^8 rads. The average dose over the length of the hole in room 5 would be somewhat higher.

Dose dropped off very rapidly with distance out into the salt, with doses at 6 in. into the salt being a little less than 10^8 rads. Therefore, in each of the seven main array holes, a volume of about 14 ft^3 of salt was exposed to doses ranging from 10^8 to 10^9 rads. In addition, temperatures at the periphery of the array holes ranged up to about 200°C. Theoretical studies indicate that some free chlorine should be produced within the salt structure at these dose levels; however, the elevated temperatures tend to have the reverse effect, that is, to anneal some of the radiolytic effects. On several occasions the chlorine indicator tubes (which were also sensitive to other substances) indicated the presence in the off-gas of small quantities of some material which reacted with the tubes. The first instance was in early March of 1966 with one hole in room 1 indicating about 0.1 ppm. The next instance was in early February 1967 after the power input to the arrays had been boosted. In this instance, all holes in both rooms 1 and 5 gave indications. The room 1 holes indicated values of around 1 ppm, with the room 5 holes indicating less than 0.5 ppm. Air flow rates were about 7 liters/min per array hole at this time. These indications started after temperatures at the walls of the holes exceeded about 175°C, and it is of interest to note that they were roughly proportional to the fuel assembly dose rates, that is, more in room 1 where the dose rate was much higher. Indications continued until the shutdown of the arrays at the end of June 1967. However, the levels decreased with time to about 0.2 to 0.3 ppm in room 1 and 0 to 0.1 ppm in room 5, again suggesting a dose-rate dependence. When the array-hole off-gas was run through cold traps and the contents of these traps were analyzed for chlorine, the results were negative. When the contents of the cold trap were run over a gas chromatographic column, a relatively strong peak indicative of a hydrocarbon was found. It seems most likely that this organic material was a remnant of an organic peroxide that was formed by radiolysis of material in the shale bands. It was thus concluded that no free chlorine had been released from the salt.

14.11.2 Moisture

No significant effects were expected from the small brine-filled cavities in the salt in rooms 1 and 4, because the salt temperatures would not exceed 250°C. In room 5 considerable water was expected in the off-gas system due to the release of moisture from the appreciable quantities of shale present at temperatures above 100°C. However, it was found that the small quantities of moisture trapped in brine-filled cavities in the salt tend to migrate toward a heat source. This water posed no problem in the demonstration, since it was removed by the off-gas system; but, in order to determine the approximate water inflow rates which might be expected in an actual disposal operation, a theoretical study was made, along with a few experimental measurements. The most important characteristic of the theoretical diffusion model used is that the cavity migration rate is a function of temperature and is directly proportional to temperature gradient, both of which can be measured on NaCl crystals. The main objective of the laboratory experiments was to compare the results with the diffusion model and to attempt to obtain agreement at least within an order of magnitude. Although the experimental work was not done with high precision, and even though the experimental setup was rather simple, the results were considered adequate. The laboratory data agreed with theoretical calculations within the anticipated range.

Using the migration rates indicated by the theory, calculations were then made to determine what might be expected in an actual disposal facility. These were

based on the temperature vs time and distance relationships for a typical high-level future solidified-waste disposal facility. Assuming about ½% by volume of water in the salt, one might expect a total brine inflow per waste container disposal hole of perhaps 2 to 10 liters taking place over a period of 20 to 30 years after burial of the waste. The peak inflow rate would occur at around one year after burial and be somewhere in the range of 200 ml to 1 liter/year per hole. This corresponds to about ½ to 3 ml/day per hole, a range similar to that estimated in the demonstration waste container holes. This water (or brine) inflow rate would be expected to taper off and approach zero after 20 to 30 years. Other considerations indicate that such volumes and inflow rates will be tolerable in a disposal facility.

The effects of the water in the salt on the modified pillar heaters and the simulated waste container (SWCT) heaters have been described earlier. These field tests have indicated that once the migrating brine reaches the crushed salt backfilling the hole, it moves upward and condenses in the colder regions above the waste containers. Under some conditions, since the upper regions of real waste containers may not be full of waste, the upper ends of the containers may temporarily be located in the condensation zone. If this is the case, stress corrosion cracking of these portions of stainless steel containers may occur. If the containers are of mild steel, only generalized rusting would be expected, and container integrity should be maintained for an indefinite period of years. Even if the containers do perforate, this should not produce any problem in a disposal facility, since there should be no gas pressure in the containers; and even if there is, there are other safeguards built in.

14.11.3 Temperature

This section summarizes the temperature distributions measured during all of the various phases of the demonstration, including the three arrays, the heated pillar, and the simulated waste container tests.

In the arrays the total power input was nominally 10½ kW, including both electrical and radioactive decay heat. Both the main radioactive and electrical control arrays (rooms 1 and 4) were started on November 15, 1965. When the fuel assembly cans were inserted, the electrical power was adjusted to maintain a constant total power input as the radioactive power decreased. On January 24, 1967, the power was increased about 40% in order to reach a peak salt temperature of about 200°C. The carbon steel modified pillar heater in room 2 was started on June 22, 1966, at a nominal power input of 3 kW and operated at this level until November 11, 1966. On November 14, 1966, all of the pillar heaters (22, including the modified heaters) were started at a nominal power input of 1.5 kW per heater (33 kW total). The wattmeter indicated that this average level was fairly well maintained until shutdown on October 9, 1967.

Comparison of the maximum temperatures in the horizontal plane achieved in the array rooms indicated that there was essentially no difference between rooms 1 and 4 but that room 5 experienced higher temperatures close to the heaters and lower temperatures further away. The minor differences between rooms 1 and 4 are not considered to be significant, and thus it appears that the radiation in room 1 did not have any appreciable effect on heat transfer in the salt. The higher temperatures in room 5 were almost certainly associated with the poorer heat transfer characteristics of the about 25 to 30% shale and anhydrite interbedded with the salt over the 12-ft depth of the array holes. These measured temperatures were compared with the theoretical calculations in the preliminary design of the experiment. The theoretical calculation assumed an infinite salt medium; that is, the rooms also were filled with solid salt. The heat losses to the room air were considerably greater than if the salt had been solid, and the in-place heat dissipating properties of the salt also appear to have been somewhat better than the 100°C values assumed in the calculations. Consequently, it was necessary to raise the power per array hole from a nominal 1500 W to 2100 W in order to get the peak salt temperature to about 200°C at the center of the arrays.

The maximum temperatures in the vertical plane through the arrays (see left side, Fig. 14.4) show the effect of the greater heat loss to the room than would be the case if the room were filled with solid salt. For example, the 50°C isotherm intersects the floor (9 ft above the center of the heat sources) at about 4 ft from the center of the array, while the corresponding point beneath the array (18 ft depth) is at about 10 ft from the center. The midpoint of the pillar between array rooms 1 and 2 did not experience any appreciable temperature rise for about a month or so following the start of the heaters, and the maximum rise was not more than about 5°C until after the time of the power boost.

The temperature in the air annuli between the salt and the lower liners in room 4 were around 25°C lower than in room 1. This is probably due to the fact that in room 4 the heaters were inside the hole liners and the hole liners themselves were smaller in diameter, whereas

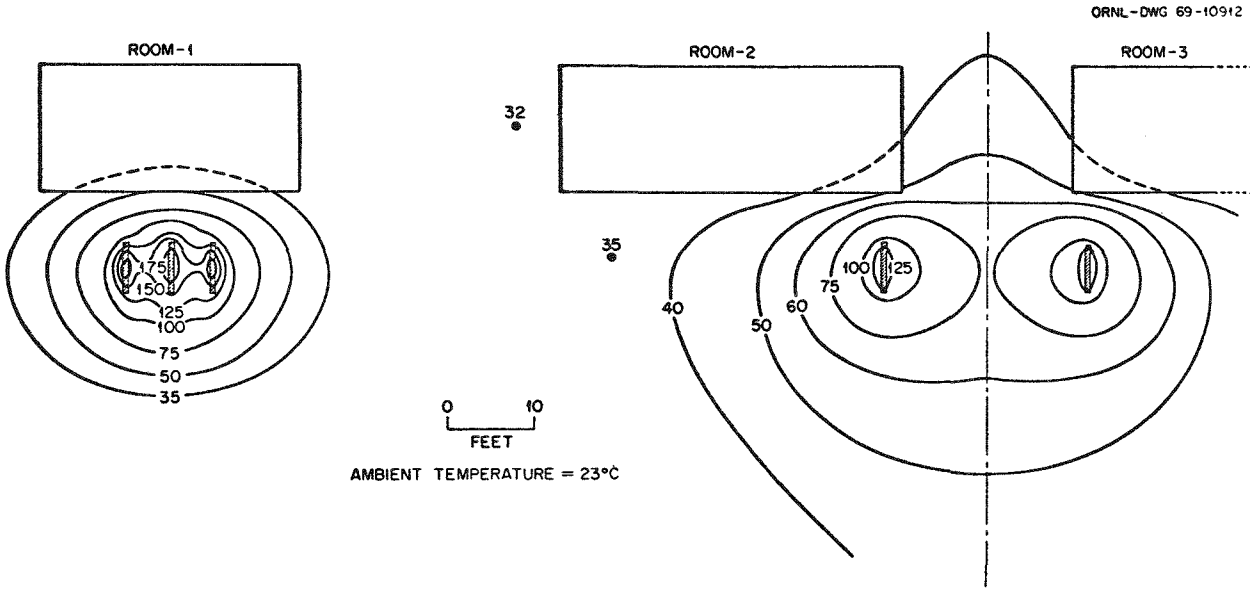


Fig. 14.4. Temperature Contours (at Maximum Values) in the North-South Vertical Plane Through Center of Experimental Area.

in room 1 the supplementary heaters were in the air annuli. Room 5 temperatures were closer to those in room 1 than to room 4, which tends to support this reasoning.

The hole liners had reached maximum temperature (before the power boost) after about 30 days of operation. The fuel assembly temperatures were also at the peak then at about 250°C. With the second and third sets of fuel, the fuel temperature was initially at about 300°C and dropped to about 270 to 280°C after 30 days. This would be expected since the second and third sets of fuel had higher heat generation rates when they were placed in the mine. When the fuel assemblies were transferred from room 1 to room 5, the lower assembly temperatures remained about the same, but the upper assembly temperatures increased a few degrees. This was probably due to the fact that the zone from 6- to 9-ft depth had considerably more shale than did the 9-to-12-ft zone.

The center pillar of the experimental area was heated by 11 heaters each on the south and north sides of the pillar. The heaters were in the floor, with the heated zone starting at 6 ft below floor level and extending to 12-ft depth. At the end of the test the maximum temperature under the exact center of the pillar at 9 ft below the floor was 73°C. Very roughly, a volume of salt beneath the pillar and rooms 2 and 3 about 40 ft wide (north-south), 20 ft high, and 50 ft long was raised to a temperature in excess of 60°C (see right side, Fig. 14.4). Under each side of the pillar and rooms 2 and 3 a roughly ellipsoidal volume of salt with axis dimensions of about 17 ft in the north-south direction, 14 ft high, and 57 ft long was raised to above 75°C. A similar volume with dimensions of about 7 ft wide, 8 ft high, and 50 ft long was raised to above 100°C. The 125°C temperature contours closed around each individual heater. It took about 10 to 15 days for the center of the pillar (at midheight) to experience a detectable temperature rise.

The modified pillar heater in room 2 was started on June 22, 1966, and ran until November 11 at an average power input of about 2.8 kW. The peak heater pipe temperature appears to have occurred at about the middle of the first day of operation, and it then continued to decrease with time thereafter. This decrease in can temperature was anticipated and resulted from the flow of salt into the hole at elevated temperature, with the consequent compaction and recrystallization of the crushed salt backfill, thereby improving its heat transfer properties. The drop in the temperature *rise* was about 14% for the top of the can and about 21% at the middle. A pressure gage connected to the inside of the heater pipe read 0 psig at the start, reached a maximum of about 27½ psig at about the time the pipe temperature peaked, and then fell with the pipe temperature to a minimum of about 23 psig. The reduction in pressure inside the can merely confirms the fact that the temperature inside the can

was reduced. After a three-day shutdown of the room 2 heater, all of the pillar heaters were started on November 14, 1966, at a nominal 1.5 kW input each (including the modified heaters in rooms 2 and 3). After about a week of operation, the pressure in this modified pillar heater was up to about 15 psig and, over the course of operation, reached a pressure of about 19½ psig. The modified heater in room 3 reached about 11.8 psig by February 9, 1967, and then the pressure started to fall due to a tiny leak in the standpipe caused by corrosion. By May 4 the pressure had slowly fallen to below 3 psig. On May 4 it was repressurized to 18 psig, and the pressure again fell to below 3 psig in about 2½ weeks, thus indicating a larger leak.

The effects of the backfill material in the annulus around the heater pipes on the regular pillar heater temperatures were also investigated. Only one heater had quartz sand for backfill material, and its temperature was lower than those with no backfill material. One heater had salt for backfill, and its temperature was lower than the one with sand. The temperature rise for the salt backfill was about 20% lower than the coldest of the air-gap (no backfill) heaters and about 30% lower than the hottest one.

14.11.4 Rock Deformation and Mine Stability

This section summarizes the results obtained from the extensive rock mechanics instrumentation network installed in the experimental area and in the "old workings" part of the mine, especially surrounding the experimental area. A wide variety of gage types were used in the network including:

1. Internal strain gages consisting of wires anchored at various distances along boreholes by expanding-shell roof-bolt anchors and a portable extensometer attached at the mouth of the hole.
2. Vertical convergence gages and horizontal closure gages using a similar instrument with steel tapes stretched across the openings.
3. Vertical convergence gages and horizontal closure gages fabricated from ½-in. pipe, anchored by roof bolts and read with a standard dial gage inserted between abutting ends of the pipe.
4. Diametral borehole deformation gages of three different types: low, intermediate, and high modulus.
5. Floor leveling networks consisting of roundhead stainless steel rivets driven into the floor and read using precision techniques by a self-leveling engineer's level from a base point outside the disturbed area.
6. Borehole leveling stations where the elevations of illuminated targets mounted at the back of horizontal holes drilled into the pillars were determined.
7. Special remote-reading roof sag indicators, simplified roof-bolt load cells, and roof-bed slip gages.

Some of these were designed and fabricated by ORNL for their specific application. Others were more or less standard rock mechanics instruments which were purchased or otherwise obtained from various suppliers. A detailed description of each of these gage types and the design of the rock deformation measurement network utilizing them is given in Sect. 11.4 of the report.

The rock mechanics instrumentation in the "old workings" portion of the Lyons mine included the area immediately around the bottom of the shaft, the entry ways from the shaft to the experimental area, and the previously mined rooms adjacent to the experimental area. The primary objective of this gage installation was to assure the safety of these areas so that continued access to the experimental area could be maintained. The old mine areas adjacent to the experiment also provided an opportunity to observe the entire sequence of rock deformation from a static undisturbed condition, through the effect of excavating a fairly large area, the influence of the application of a large quantity of heat over an extended period of time, and the return to static conditions. In addition to measurements close to the experimental area, the extent of these disturbances on a wider portion of the old mined area could be established.

The first major disturbance measured on the rock deformation gages was that resulting from the excavation of the experimental area, primarily as a consequence of the overburden load transferred from the newly mined openings. This redistribution of load was observed over a considerable area of the old workings, primarily on the convergence gages. In this case both the strain and the strain rate increased as the vertical stress in the vicinity of the gage increased. It is interesting to note that, in general, the peak strain rate occurred after the working face had passed its closest point to the gage. It is also of interest to note that the peak strain rates at points beyond the experimental area occurred at even later times.

The quantitative interpretation of results obtained from diametral borehole deformation installed in salt or other highly plastic materials is extremely complex. However, it is valid to make use of the results in a

qualitative manner. The results from this type of instrument installed in the existing mine show the effect of the new excavation as an increase in indication which can be interpreted as an increase in stress. This increase proceeds from one instrument to the next in sequence as the mining progresses. It is significant that in every case the maximum rate of change as detected by the three different types of gages at a particular location (horizontal wire, convergence, and diametral borehole deformation gage) was coincident in time. A comparison of three different types of diametral borehole deformation gages was also carried out at this time, partially to select the type of gage to be used in the experimental area. The results indicated that none of the gages perform really well in the highly plastic salt and that there was essentially no difference in the character of the information obtained.

In addition to the deformations of the rock adjacent to the experimental area, the extent of the effects of excavating the experimental area on the entire existing mined-out space was determined. This was done by closely examining the results obtained on those gages located throughout the old workings for any slight change in slope of the deformation curves during the period when the excavating was being carried out. Convergence gages located at distances of up to 435 ft showed a slight increase in convergence rate at about the time the excavation was passing nearest the gages; the inference is that the stress redistribution resulting from the mining operations extends at least 400 ft from the newly mined area. Gages to the south of the experimental area showed a slight change in curve slope during the construction of the ramp in entry 5 leading to the experimental area, but there was no detectable influence related to the actual excavation of the experimental area. These gages were located about 200 ft from the ramp and a little more than 300 ft from the rooms of the experimental area. These results are most interesting, since they imply that the overall disturbance caused by modifying the shape of the supporting pillars is nearly as great as the excavation of new space. During the construction of the ramp, the area of salt supporting the overlying material was not changed, but the height of the pillars adjacent to the ramp was changed from 14 ft to about 27 ft on one side. This change in shape must have caused these pillars to "shed" load to surrounding areas in much the same way that the load is redistributed when part of the salt supporting that load is removed. It can be concluded further that there is a slight difference in the stability of the irregular "old workings" to the northeast of the experimental area and the more recent checkerboard area of square pillars to the southeast. This is to be expected, since the area to the north of the experimental area was mined at a higher extraction ratio and at a much earlier date. Both of these factors would contribute to making this area more sensitive to an increment of load. There was no detectable effect of the excavation work at any place around the area of the main shaft or along the main access roads. These areas were apparently beyond the reach of the disturbance resulting from the mining operations in the experimental area.

The principal objective of the rock mechanics instrumentation in the experimental areas was the complete and detailed characterization of the deformation of salt in and around the area as a function of time under the influence of the overburden stresses, radiation fields, elevated temperature, and thermal gradients. This information constitutes the basic input toward one of the fundamental program objectives of developing a capability of designing an actual solidified high-level waste disposal facility in a salt mine. A second objective of the instrumentation was to continuously monitor the behavior of the salt in order to guarantee the safety of the mine personnel and to protect the large radiation sources present.

To complete the interpretation of the influence of the excavation process and to more fully appreciate the deformations which occurred during the heating phases of the experiment, it is advantageous to more closely examine the results obtained during the period between the completion of the excavation and the beginning of the first heating experiments. In general, the deformations which occur around newly excavated underground space result from the transferral of the overburden load formerly supported by the material which was removed onto the remaining pillars and the abutments at the edge of the excavation area, and from the relief of horizontal restraint at the free surfaces. If the total area excavated is large enough, the load (stress) on the pillars in the central portion can be calculated from the weight of the overlying material and the total area supported by each pillar. In the PSV experimental area, the total area of excavation was too small for this type of calculation, and it must be anticipated that a fairly large proportion of the weight of overlying material formerly supported by the material which was removed would be supported by the solid material surrounding the experimental area and not by the three rib pillars within the experimental area. Although it is impossible to estimate the absolute value of the average load on the pillars, it is possible to draw some qualitative impression of the stress distribution based on the geometry of the

experimental area. This impression would be that the average stress on the center pillar would be more than on the other two, because of its central location, smaller width, and large adjacent rooms. Although pillar 1-2 is the same size as pillar 3-4, it would have a somewhat higher average stress because the corridor does not pass beyond room 4 and because of the influence of the shaft room. These gross geometrical relationships will be altered slightly by second-order geometrical effects. For example, although the nominal dimensions of rooms 1 and 4 and their adjacent pillars are the same, room 1 is actually slightly wider than room 4 and pillar 1-2 is slightly narrower than pillar 3-4. These second-order effects would tend to increase the difference in the behavior of the two rooms.

In addition to geometrical differences, there will be a considerable difference in the behavior of rooms 1 and 4 as observed at any given time (such as at the start of the array experiments) because of the differences in their respective ages since mining. These differences can be found in all mines, but they are especially pronounced in salt, potash, and other soft materials because of their highly time-dependent deformational properties. When the openings are first excavated, the highest stress zone is at the wall of the supporting pillar or abutment, and the stress decreases rapidly with increasing distance from the wall. In addition to the instantaneous elastic response of the salt to these stresses, the material at the side of the opening will immediately begin to deform plastically. As this yielding type of deformation takes place, the peak loads will be transferred from the pillar edge deeper into the salt and spread over a wider area, with the result that the *rate* of deformation will decrease with time because of the decreasing stress. In salt, under conditions similar to those at the Lyons mine, this transient period with its significant stress redistributions lasts for several years, perhaps even several decades. Eventually a condition similar to a dynamic equilibrium is approached (as an asymptote) where the stress distribution is more or less stable and the mined space is closing at a more or less constant rate. This constant rate of closure is the reason for calling the situation dynamic rather than static equilibrium. In the experimental area, the excavation of room 1 was completed four months before the excavation of room 4. The array experiments in these two rooms were started eight months after room 4 was excavated. Not only did the experiments start early in the transient phase of both rooms, but they were at appreciably different stages in their approach to equilibrium. Most of these differences in the behavior of rooms 1 and 4 prior to the start of the array experiments were apparent in the gage data.

The results obtained from rock mechanics instrumentation during the heating phases of the experiment are summarized in the following paragraphs. Considering first the array rooms 1 and 4, it was seen that the floor area around the array holes was immediately uplifted very rapidly when the heaters were turned on but that this uplift soon slowed to a nearly constant rate. The same behavior was found when the heat input was increased by 40%. The recovery of the floor uplift after the heaters were turned off indicates that the mechanism of this floor lift was more complicated than simply thermal expansion of the salt around the heaters. The recovery of the floor uplift amounted to only a fraction of the total floor uplift – about 16% in room 1 and about 11% in room 4. The salt at the center of the rooms around the arrays was confined in the horizontal directions by the stresses resulting from the pillar loading but was free to expand vertically up into the rooms. When the salt was heated, elastic thermal expansion in the vertical direction resulted in a lift of the floor. This component of the total floor uplift should be recoverable upon cooling. Direct thermal expansion in the horizontal directions was not possible because of the constraining stress. Therefore, there is an appreciable thermal stress induced in the horizontal direction. The salt in the floor will creep upward (the only direction available to it) under the influence of this horizontal thermal stress, thus providing a second and apparently sizable component of the floor uplift which would *not* be recoverable. The difference in the amount of recoverable floor uplift between the two rooms was probably primarily a function of their different ages. Room 1, having had a longer period in which to relieve the horizontal stresses resulting from pillar loading, would be expected to have a smaller component of nonrecoverable floor lift. In general, and in spite of the slight differences discussed above, the floor uplift in the two rooms would appear to be almost identical in both magnitude, shape, rate, and response to the heating.

The vertical convergence gages around the edges of these two rooms were constructed in such a way as to include a component of floor uplift. However, when this component was estimated and deducted from the total convergence, it was obvious that the entire height of the pillar had experienced an accelerated vertical deformation in response to the heating at the center of the rooms. The total convergence during the heating period can be interpreted as the sum of components due to: (1) the overburden and mining stresses, (2) the uplift of floor, which at this distance from the heat sources is almost entirely due to horizontal thermal stresses, and (3) an increase in the vertical loading of

the pillar due to thermal stresses. This picture of the deformations will be further conplicated by the variation of salt creep properties as a function of temperature at some later date. However, this effect did not become significant in the array rooms. Further insight into the relative magnitudes of these three effects can be obtained from examinating the convergence curves during the cooling period. At those gages where the effects of heating were greatest, the recoverable components were large enough to compensate the continuing (viz., mining and overburden stress-induced deformation) components and to produce a period of essentially zero convergence. The convergence curves for two of the three gages in room 4 were almost identical with those of room 1 if comparable gages were started from equivalent points on standard day 806. The effects of heat in the two rooms would, of course, be expected to be nearly identical. Apparently the increased deformation rate resulting from the younger age and slightly greater height of the pillar was compensated by the decreased overburden loading and deformation rate resulting from the difference in geometry, thus producing conditions in room 4 which made the response to heating appear to be nearly identical with room 1.

Horizontal internal strain gages were installed in three sides of the two experimental rooms. The acceleration of the horizontal deformation in response to the heating could be clearly seen at all gage locations. This effect extended completely through the narrow pillars and could be detected, but much reduced, at the walls of rooms 2 and 3. The deformations around room 4 were approximately equivalent to those in room 1. The deformations of the pillars adjacent to rooms 1 and 4 were examined in much more detail. This examination indicated that there is no gross difference between the deformational behavior of the two experimental rooms or their adjacent pillars which could be ascribed to the effects of radiation.

The vertical deformation in the floor and roof in the vicinity of the heater arrays was measured on the vertical internal strain gages. Since these stations were tied into the leveling network, it was possible to calculate displacement of each of the wire anchors relative to what should be an absolute base line.

The movement of points on and near the floor was, of course, identical to the floor uplift results. However, the deformation of points deeper in the floor, down to a depth of 25 ft, also shows an uplift of the same type, which diminishes with increasing depth. The immediate response to the initial heating of the anchors at a distance of 25 ft below the floor (i.e., 13 ft below the heater zone) and the magnitude of that movement, amounting to several tenths of an inch, is somewhat surprising even though the mechanism of that movement is the same as was discussed with respect to the floor uplifts. The results obtained for the deformation of the roof over the arrays were perhaps the most interesting of all the rock mechanics data. First, it was seen that the points 25 ft above the ceiling of the rooms had lowered appreciably during the approximately three-year period examined in detail. A small part of this movement, which amounts to about $^{3}/_{4}$ in., may be due to local deformation of the roof strata toward the rooms, but at this height above the room ceilings, local effects can hardly account for more than a small fraction of the total. The inference is that the pillars supporting the experimental area had squeezed enough to allow the entire overlying rock mass, including the ground surface, to subside (but not by the whole amount). The effects of heating could still be seen at the 25-ft level as a very slight acceleration in the rate of lowering. However, there was no evidence of recovery when the power to the heaters was turned off. This is not inconsistent with the previous discussion, since the accelerated deformation of the pillars due to thermal stress loading would be expected to be reflected throughout the roof strata. Another aspect of the roof gages was the clear definition of the sagging of a 2-ft-thick bed of salt at the immediate roof of the rooms. The existence of this sagging bed had been detected prior to the start of the experiment on a preliminary examination of the gage results and the separation defined by probing with a feeler-type instrument. The presence of the thin shale parting at 2 ft above the ceiling was, of course, known from the early geologic work. Although some precautions in the form of the installation of remote and continuous-reading transducer gages had been taken, the rate of sag of this bed prior to heating was considered normal and harmless. Similar phenomena are not unusual in most mines in bedded salt and are commonplace in other salt mines in the vicinity. However, the acceleration of the sag, by a factor of approximately 5, immediately after the array heater power was turned on was unexpected, and it was felt that some remedial action would be required to prevent the development of hazardous conditions when the heated pillar test was started.

The mechanism by which the roof at the center of the experimental rooms is deformed by the heating beneath the center of the floor can be determined by a closer examination of some of the deformations occurring around the room immediately after the heaters were turned on; this is summarized in Fig. 14.5. As was seen

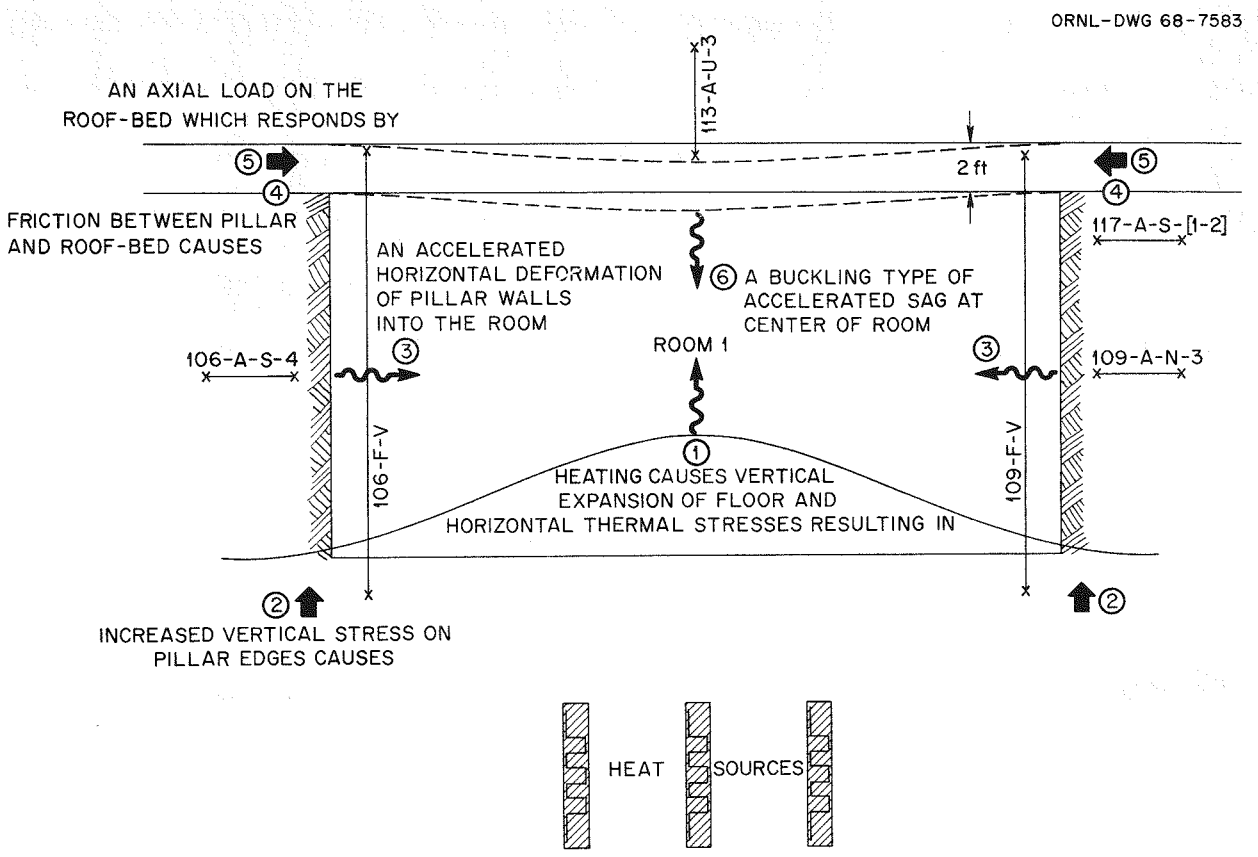


Fig. 14.5. Mechanism of Stress Transference from Floor to Ceiling.

from the floor uplift data, the thermal stresses induced in the salt when the array power was turned on produce an immediate uplift of the floor throughout the entire room by the creep resulting from these stresses – not by the thermal alteration of the plastic flow properties of the salt. This floor uplift extends under the edges of the pillars, causing an increase in the vertical stress, especially near the edges of the pillars. The pillar responds to this increased vertical stress, in part, by an acceleration of the rate of horizontal deformation throughout the entire height of the pillar, as was seen on the horizontal deformation gages. As the two walls of the room move inward, they exert a horizontal load on the roof bed because of the frictional resistance of the small shale parting separating the roof and the pillar. Since the 2-ft-thick sagging roof bed is an independently acting, self-supporting beam (or more exactly, plate), it will react to this induced "axial" load with a buckling type of deformation which is detected as a sag. The accelerated sag of the roof bed is, therefore, seen as a result of the disturbed *stress* field caused by the superimposition of thermal stresses onto the preexisting overburden and mining stresses, which was amplified in the roof because of its configuration as a beam deflecting under axial loads.

Although the rate of sag of the 2-ft-thick ceiling bed was decreasing with time and was not in itself considered to be even potentially hazardous, the phenomenon did raise several questions relating to the continued operation of the experiment, especially in view of the plan to extensively heat the center pillar of the experimental area. Therefore, it was decided to try to support this bed with roof bolts, and a test area was established in room 3 of the experimental area and a trial pattern of bolts installed. This test area consisted of 37 roof bolts, 4 ft long, installed at the center of room 3. The length of the bolts was selected so that the lower bed would be supported from only the overlying 3-ft-thick bed and so that the bolt holes would not perforate the shale parting at the top of the 3-ft bed. The 4-ft spacing of the bolts was determined based on a minimum estimate of the anchorage capacity which

might be developed in salt by the expanding-shell–bail-type anchors which would support at least twice the actual weight of the sagging bed when the entire area was bolted. A special torquing procedure was developed which succeeded in improving the anchorage capacity to the place where the final load on the bolts was about 12,000 lb, nearly three times the dead weight of the 2-ft-thick roof bed over the area. Gage results indicated that the roof in the test area was lifted by about 0.08 in., actually reducing the accumulated sag. The roof bolt test was observed for about a month, during which period it was seen that the roof bolts reduced the rate of sag to essentially zero and that more than sufficient anchor capacity would be developed in the salt to enable the bolts to continue to support the sagging bed. Based on this evidence, the decision was made to roof bolt the entire experimental area using the same pattern and procedure, even though it was obviously overdesigned. The performance of these bolts was monitored on the roof bolt load cells and on special short-wire roof-sag extensometer stations, located at the center of each room, throughout the course of the experiment. The results from these gages for rooms 1 and 4 indicate that although the roof bed was not lifted as much as was the case in rooms 2 and 3, the rate of roof sag was reduced to essentially zero for the entire period covered by the experimental results. The results with the roof bolts in the corridor were similar to those in rooms 2 and 3. The gradual increase in the load on the bolts, as measured by the load cells throughout the experimental area, suggests that the roof bed was "trying" to sag into the rooms but was prevented by the bolts. Furthermore, the driving force behind that sag must have been something more than the mere dead weight of the beam, since that alone would have produced a constant load on the bolts; that is, the sag throughout the experimental area would have been accelerated by the buckling deflection resulting from the axial loads had the roof bolts not been there to support and restrain the bed.

The various deformations occurring around the array rooms 1 and 4 and their adjacent pillars were combined in Fig. 14.6 to show the movements which took place in the vertical north-south plane through the array centers during the heating period. The significant features of these deformations are:

1. The total deformations were primarily the result of creep of the salt under the influence of overburden and thermal stresses.
2. Deformation resulting from the alteration of the physical properties of the salt (especially creep rate) due to an elevated temperature, for the most part, was not seen around the array rooms because of the location of the heat sources. Significant portions of structural load-bearing salt were not heated fast enough or high enough to produce an observable effect.
3. The effects of the transference of stresses resulting from the thermal expansion of the salt in the floor around the array heaters were unexpectedly widespread. Accelerated deformation rates resulting from this increased stress were observed at points 25 ft into the floor and roof and on the walls of the pillars in the adjacent rooms.
4. This same mechanism, aided by a buckling type of deflection, was responsible for a drastic acceleration in the sag of the immediate roof over the array.
5. The roof bolt experiment and subsequent installation probably produced more important and useful results than were lost by restricting the deformation of the roof.
6. The deformations were so similar between rooms 1 and 4 that it can be categorically stated that there were no significant structural effects produced in the salt by the intense radiation fields. The similarity between the two rooms was even better than expected because of the counteracting effects of slight differences in age and geometry.

As discussed earlier, the objective of the experiment carried out in room 5 of the existing mine was to investigate the possibility of using previously mined space for disposal rather than newly mined space. The principal differences between room 5 and room 1 (or room 4) were the much larger quantity of shale in the floor at the heated zone, the height of the room, the somewhat different room size, and the absence of significant shale partings in the immediate roof. Two major conclusions can be drawn from the interpretation of the rock mechanics results obtained from the room 5 experiments:

1. With a single exception noted in item 2 below, the deformations occurring around the heated array installed in the floor of the existing mine were of the same type and could be explained by the same mechanisms and were even quantitatively similar to the deformations around the arrays in the newly mined experimental area. Some slight differences due to geometry and, more importantly, the differences in creep rates acquired with age would be expected and were found.

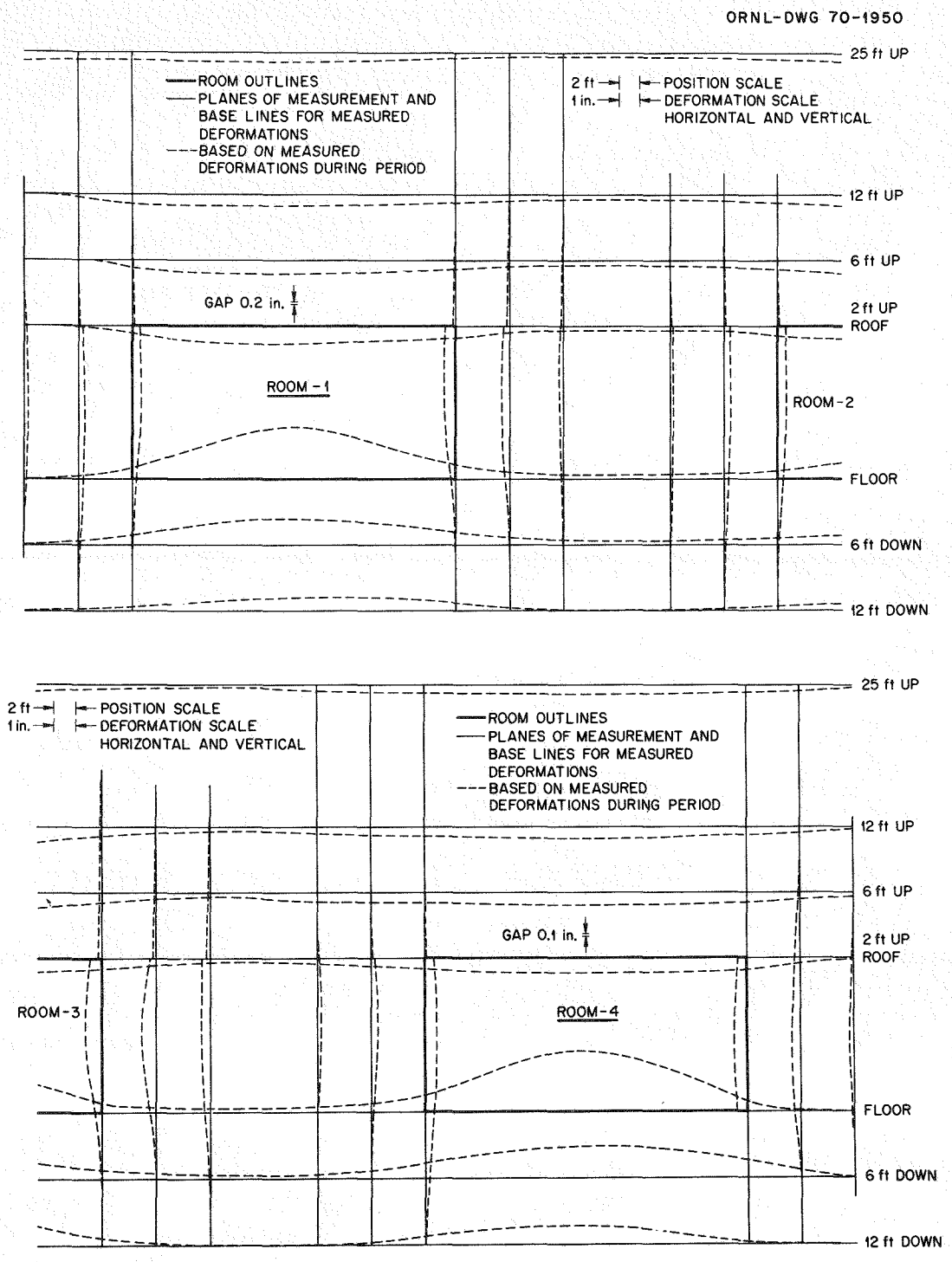


Fig. 14.6. Summary of Deformations Around Rooms 1 and 4 During Heating.

2. Because of the approximately 15-ft difference in stratigraphic elevation between the experimental area and the existing mine, the roof in room 5 did not contain thin shale partings and, consequently, did not separate and sag into the room.

The heated pillar experiment took place in rooms 2 and 3 of the experimental area and around the rib pillar separating those rooms. This pillar is 20 ft wide (nominal), and the two adjacent rooms are 44 ft wide. The objective of this part of the experiment was to obtain data on the behavior and properties of a large mass of salt in the floor and beneath a pillar heated to a much higher temperature than would have been possible in the array experiments. Eleven heaters were placed in the floor along each side of this pillar, and a total of 33 kW was applied continuously for a period of nearly a year.

In general the measured rock deformations around the heated pillar were similar to those around the array rooms but considerably larger, since more heat was being applied, and they included a significant component resulting from the change in the deformational properties of the salt with increased temperature. Figure 14.7 summarizes the vertical and horizontal deformation of the pillar and its adjacent rooms in the same way as Fig. 14.6. Based on the detailed analysis and interpretation of the deformations summarized in Fig. 14.7, the following conclusions can be drawn.

1. The quantity and quality of instrumentation in and around the heated pillar were adequate to provide the information required to perform a detailed analysis and at the same time were certainly not excessive. However, since it may not be apparent to those unacquainted with the rock mechanics litera-

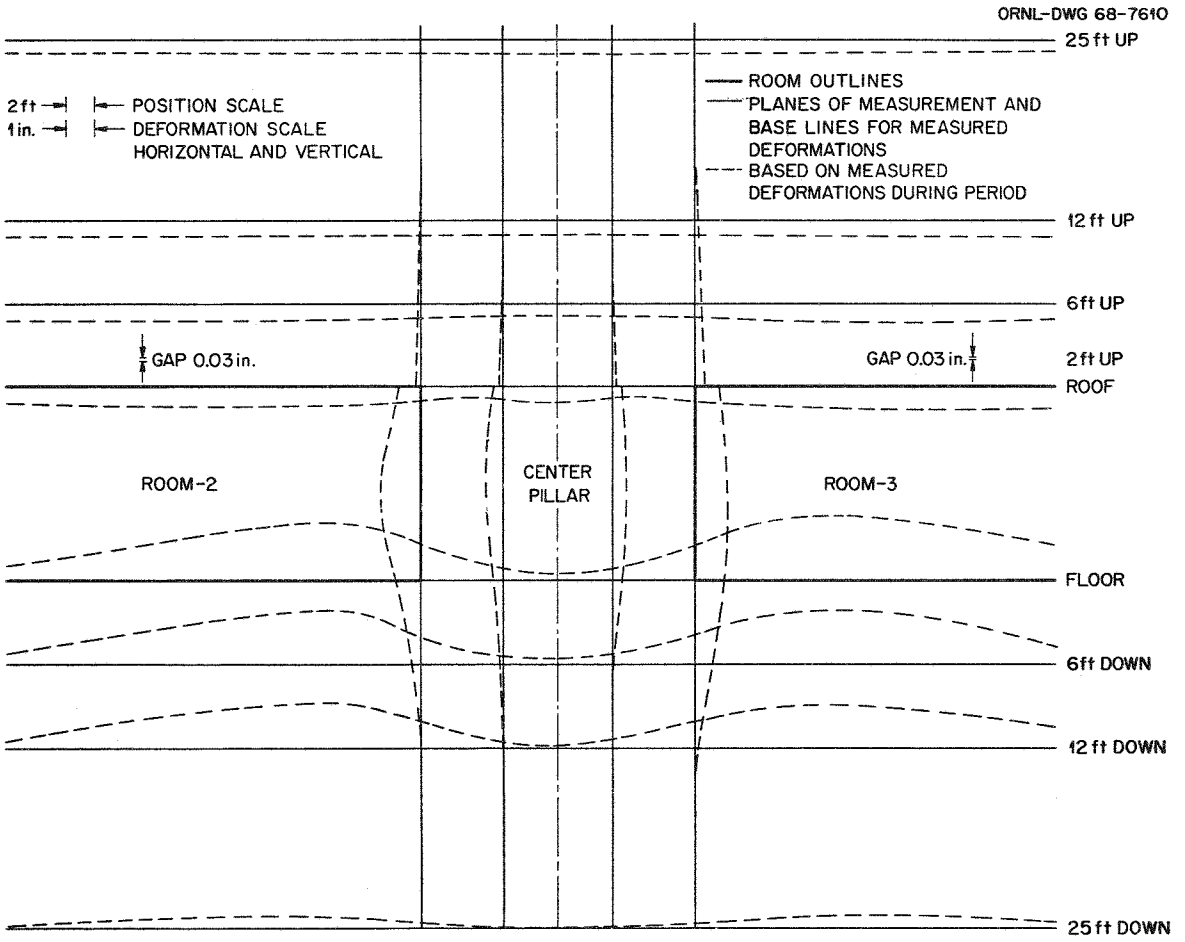


Fig. 14.7. Summary of Deformations Around Center Pillar and Rooms 3 and 4 During Heating.

ture, it should be pointed out that the data and the inferences which can be drawn from Fig. 14.7 represent a significant advance in understanding of the deformational behavior of support pillars based on in situ measurements.

2. Even in this heated pillar experiment where a large volume of salt was heated appreciably, the deformations resulting from the influence of thermal stresses and their transferal to remote points were clearly much larger and more dominant than the deformations resulting from increased creep properties of salt at elevated temperatures. However, the heating of the pillar took place over a much shorter time than would be the case in a typical waste disposal operation, and the situation might be somewhat different where the rate of temperature rise is considerably slower.
3. The effect of the local geological situation, especially the presence and locations of thin shale partings capable of providing a lubricated surface, on the deformations was much larger than initially anticipated. This influence will somewhat limit the applicability of the analysis to different geological environments. However, the fortuitous circumstances of having a shale parting at the roof and the pillar bottom keyed into the floor in this experimental installation, coupled with the laboratory pillar-model tests, will allow some limits to be placed on the variations resulting from different geological configurations.

The effects which the heating experiments had on the old workings area of the existing mine were, of course, most visible in the rooms adjacent to the experimental area. There are two rather significant conclusions which were from the vertical convergence at stations in these areas: (1) The application of heat in the experimental area had very little influence on the movements and deformations taking place in the old workings when compared with the effect of excavating the experimental area, and this effect was opposite to that caused by excavating; that is, the convergence rates in the old workings decreased more rapidly than normal. (2) The old workings gages responded to the cooling in the experimental area by an increase in their rate of deformation, returning to approximately what would have been expected had the heating not taken place. In view of the foregoing discussions of the effects of heating on the pillars in the experimental area, this response may appear contradictory. However, the two situations are not comparable; in the experimental area the deformations were due to heating of either the pillar itself or the adjacent floor salt, whereas the old workings deformations are in response to the deformations and loadings of the experimental area pillars. During the heating phase the experimental area pillars tend to carry increased stress because of the thermal expansion of the salt. However, this increase of stress was limited by an accelerated creep rate resulting from both the elevated temperature and the increased stress itself. The net effect which the heating had over the larger area was therefore slight when compared with the effects of excavation, even though the pillar deformations were considerably greater, but it resulted in the heated pillars supporting more than their normal share of the overburden load, thus reducing the load on the pillars in the old workings. When the heat was turned off, recovery of the thermal expansion significantly reduced the stress on the pillars in the experimental area, but now without any compensating mechanism. These pillars were no longer supporting even their fair share of the overburden load, and that portion of the load was transferred to the surrounding areas in the form of an increased pillar stress in those areas. This increase in stress was the cause of the accelerated deformation in the old workings during the cooling phase. The horizontal gages in the old workings adjacent to the experimental area confirmed the reduced deformation rates during heating in the experimental area and the increased deformation rates after termination of heating. The influence of the heating (and cooling) in the experimental area did not extend much beyond the adjacent rooms in the old workings, that is, beyond 200 ft from the heaters themselves.

14.12 LABORATORY PILLAR MODEL EXPERIMENTS

In this study the effect of temperature, as well as compressive stress and time, on the deformation of rock salt was investigated through scale-model specimens of mine pillars. Tests were performed on samples of bedded salt, as well as on dome salt, from six different mines in the United States and from the anticlinal structure of the Asse II salt mine in Northeast Germany. Experiments were made to ascertain the optimum model size for laboratory studies and to determine the effect of pillar shape on deformation. The effect of stratigraphic discontinuities on the deformational behavior of pillars was also investigated. Finally, some studies on the mechanisms of pillar deformation were carried out.

Many workers have performed creep tests on rock salt, and although some general conclusions concerning deformation of salt could be drawn from them,

previous experimental data were not available that could be used to predict with any great degree of certainty creep rates in multiple openings in salt deposits containing radioactive waste products. A theoretical approach to the solution of the problem did not appear to be practicable. Thus through experimentally derived data an empirical solution to the problem was sought.

To simulate pillar, roof, and floor conditions that would exist in mined cavities in rock salt, sample specimens were fabricated to represent scale models of salt pillars and their surrounding rooms. The test specimens used in this work were cylindrical, with a portion of the center ground out to form the pillar and surrounding rooms. By "epoxying" steel rings around the ends of the samples, effective confining pressure was applied to the roof and floor portions of the models when they were loaded. Constant uniaxial loads were applied to the models by hydraulic compression testers having capacities up to 300,000 lb. Cavity closure was measured by mounting two dial gages 180° apart on the rings. All tests were conducted in a controlled-temperature room equipped with automatic dehumidifiers to prevent condensation on the samples during extremely damp periods. Elevated-temperature tests were performed with the specimens inside a cylindrical heating jacket and with barrier heaters on top and bottom between the specimen and the platens. Most tests were performed on model pillars fabricated from $5^{1}\,{}^{1}/_{16}$-in.-diam cores of rock salt taken in the mine of the Carey Salt Company, Lyons, Kansas. Similar cores for model tests were recovered from sample cubes of salt measuring 1 to 2 ft on a side taken from rock salt mines at Hutchinson, Kansas; Retsof, New York; Detroit, Michigan; Grand Saline, Texas; Cote Blanche, Louisiana; and Asse, Germany. For model preparation, all cores were first cut to their approximate desired length by band saw and then finished by machine sanding. The 1-in.-high unconfined center portion of the sample was ground out, using a sanding disk attached to a standard drill press, to form the size pillar desired. Sheet Teflon coated with a mixture of silicon grease and graphite was inserted between the tops and bottoms of the samples and the platens of the compression machines to reduce the friction between the salt and the platens to an insignificant amount. The importance of eliminating the friction between the salt specimens and the test machine platens in ascertaining a true measure of the laboratory deformation of rock salt has been investigated by others.

In general, the same test procedure was used for all specimens to ensure uniformity. This procedure consisted in rapidly applying a compressive load corresponding to 75% of the testing load and releasing it and then applying a load of 85% of the test load, which was also immediately released. A base reading for the dial gages was then taken. These initial loadings served both to seat the dial gages used to measure deformation and to set the platens firmly on the sample. The full test load was then applied to the specimen within a few seconds, and deformation was recorded, first at intervals of seconds, then minutes, and then at progressively longer intervals.

Most tests were conducted at temperatures of 22.5, 60, 100, and 200°C for axial loads of 2000, 4000, 6000, 8000, and 10,000 psi. In addition, a few special tests were conducted on salt samples at loads as high as 15,000 psi. Duration of the tests varied from a few minutes for those specimens where the deformation rate was exceedingly fast to a single case where the sample was allowed to deform over a period of about $3^{1}/_{3}$ years. The most common test periods were about 500 to 1000 hr. For certain temperature and load combinations, duplicate or triplicate tests were run in order to obtain an approximate measure of variation from sample to sample. A total of about 110 pillar models were tested in these studies.

The deformation characteristics of the rock are an extremely important consideration in the simulation of mine conditions in scale-model tests. For example, to determine the stability of mine pillars composed of plastic materials like rock salt, it is absolutely necessary to simulate in the models not only the mine pillar but also the roof and floor conditions. However, for brittle rocks like dolomite, the roof and floor apparently do not greatly affect the deformation of the pillar. This has been illustrated in uniaxial tests of model mine pillars of rock salt and dolomite. In both cases the models were fabricated from $5^{1}\,{}^{1}/_{16}$-in.-diam cores. Upon the application of axial stress, the deformation of the steel rings was measured by a strain gage indicator. The radial stress exerted by the rocks on the inner portion of the rings was calculated by use of a standard equation. For rock salt samples tested at room temperatures, it was found that the radial stress exerted on the rings increased with increasing axial loads up to approximately 75% (11,250 psi) of the axial load at 15,000 psi. However, for the dolomite samples it was observed that the radial stress did not exceed about 5% of the axial stress of the pillar load, even at loads as high as 23,000 psi. These data indicate that, for materials that deform plastically like rock salt, actual mine conditions are simulated best when the roof and floor portions of the models are constrained laterally. This allows confining stress in the roof and floor to be transmitted into the

pillar (at least for samples having a width-to-height ratio of 4), thereby making the pillar stronger. For dolomite the relatively small values of radial stress measured on the confining rings of the models indicate that the roof and floor in models used to define mine pillar deformation in rocks of this type are not as critical as for rocks that deform plastically under the same conditions.

To evaluate the effects of various salt thicknesses in the roof and floor of test models, several samples were tested having the same pillar dimensions of 4 in. in diameter by 1 in. in height, but with different thicknesses of salt ($\frac{7}{8}$, 2, 3, and 4 in.) above and below the pillar. It was observed that there was little difference in the deformation curves for the samples with 2 in. or more of salt above and below the pillar; however, for the specimen having only a $\frac{7}{8}$-in. layer of salt in the roof and floor, the amount and rate of deformation were markedly greater. It was concluded from these data, along with the measured values of radial stress in the roof and floor of model salt pillars as discussed above, that salt at least twice the height of the pillar should lie above and below any given pillar to approximate the true strength of actual mine pillars. In addition to the tests discussed above, one specimen having dimensions twice that of the "standard model specimen," that is, an 8-in.-diam pillar having a 2-in. height and a roof and floor thickness of 4 in., was tested at a load of 4000 psi at 22.5°C. The deformation curve for this sample was essentially the same as that for the smaller "standard model" for the same type of rock salt. It was thus concluded that a model pillar 4 in. in diameter and 1 in. high, fabricated from $5\frac{1}{16}$-in.-diam core 5 in. long, adequately simulates mine conditions where the pillar, roof, and floor are essentially all rock salt.

In order to obtain data on the deformation of rock salt under temperature and pressure conditions that would be expected in an actual disposal operation, a series of model pillars fabricated from rock salt from the Lyons, Kansas, mine were tested. In addition, data on the effects of shale partings and pillar shapes on the deformation of rock salt, which must also be considered in an actual disposal operation, were obtained from model tests. These data, along with field data from the Lyons mine, form the basis for predicting pillar behavior in salt cavities used for the disposal of radioactive wastes. Since the occurrence of rock salt in the United States is rather widespread, it is conceivable that many sites could be used for waste disposal operations. In order to make gross comparisons of the deformation of salt from one mine to another, model pillars fabricated from rock salt from five other mines in the United States and one German mine were also tested.

Since the model pillar specimens of salt from Lyons, Kansas, that were used in the tests to develop the empirical equations (given in a later paragraph) were essentially all salt and did not contain shale beds or other rocks in the roof, floor, and/or pillars, predictions using the equations are valid, strictly speaking, only for that type of salt. However, the closure rates of excavations in bedded as well as dome salt deposits that do not contain shale partings or other rock types in critical areas could also be approximated by these equations. As the models with shale partings indicated, the expressions would be expected to be least effective in predicting deformation in mine openings where shale beds occur at both the top and bottom of the pillars. Since the shales serve as effective friction reducers, confining stresses in the roof and floor portions of the mines are not transmitted into the pillars; thus mine pillars under these conditions will deform more nearly as if they were simply squeezed between two rigid plates. The strength of actual mine pillars based on the model study would be expected to be perhaps several times less for conditions where shale partings occur at the tops and bottoms of the pillars than where salt continues uninterrupted from the pillars into the roof and floor. Also, the effect on deformation would not be expected to be nearly so pronounced where the shale occurs only at the top or bottom of the pillar. If salt deposits contain shale partings that cannot be avoided in mining, it is better that the openings be made so that the shales are located in the center part of the pillar. The center of the pillar apparently is a more-or-less neutral plane, and therefore shale partings at this location will not influence the rate of deformation; however, as the locations of the shales approach the top or bottom of the pillar, they cause an increasingly greater increase in the rate of cavity closure. In general a similar pattern of deformation occurs for shale beds in the floor and ceiling of salt mines. The nearer the shale parting in the ceiling and/or floor to the pillar, the weaker is the pillar. This is due to the fact that as the thickness of the uninterrupted salt section that lies in the roof and floor above and below the pillar is reduced, there is a corresponding reduction in the confining stress in the roof and floor which can be transmitted into the pillar. When shale partings lie only a few inches above and/or below the pillars in mines, it is common for buckling of the roof and/or heaving of the floor to occur. This type of deformation not only results in a more rapid closure of the mined opening but creates mine safety and operational problems.

Even though there are some variations in the creep rates of salt from one mine to another and even within a single mine where such things as impurities, grain size, texture, etc., may cause slight differences in behavior, it seems apparent that the general creep behavior of salt is the same regardless of the origin and/or location of the deposit. The principal difference is one of the magnitude of the creep rate. Furthermore, it is apparent that the most important parameters that affect cavity closure in salt deposits that might be used for the disposal of radioactive wastes are not those of location and genetic type of deposit, grain size, impurity content, texture, etc., but the presence of shale partings at or near the pillar-floor and/or pillar-ceiling contacts, the width-to-height ratios of the pillars, and the effects of temperature, load, and time.

Based on the results of model tests, mine pillars having width-to-height ratios of 2 and 3 will deform approximately 75 to 45% faster, respectively, than pillars having a width-to-height ratio of 4. For pillars with width-to-height ratios less than 2, it would appear that the rate of deformation will be even greater. It is also apparent that for mine pillars having width-to-height ratios of 3 or 4, catastrophic pillar failure will not occur at ambient temperature, even at loads as high as 14,000 psi, which is well beyond the upper limit of loading that would be expected in any salt mine that would be used for the disposal of wastes.

Cylindrical model pillars were used for the tests to develop the empirical equations given below; however, in actuality, mine pillars may vary from nearly cylindrical to rectangular. It was concluded from model tests that rectangular pillars having lengths about twice their widths and containing the same cross-sectional area and height as cylindrical pillars with width-to-height ratios of 4, will deform about 40% faster than their cylindrical counterparts. Rectangular pillars with lengths several times their widths may be used for specially mined excavations in salt used for the disposal of high-level radioactive wastes. However, it is assumed that width-to-height ratios less than about 2 would not be used.

An empirical relationship between creep, stress, temperature, and time has been developed from the tests and is given as:

$$\dot{\epsilon} = 0.39 \times 10^{-37} T^{9.5} \sigma^{3.0} t^{-0.70},$$
$$\epsilon = 1.30 \times 10^{-37} T^{9.5} \sigma^{3.0} t^{0.30}, \qquad (14.1)$$

where

$\dot{\epsilon}$ = strain rate or vertical shortening of pillars (in./in./hr),

ϵ = cumulative deformation after the first 2 min (in./in.),

T = absolute temperature (°K),

σ = average pillar stress (psi), and

t = time (hr).

At all axial loads and constant temperatures, there is initially a high creep rate that decreases with time. Creep rates were observed to continue to decline even after more than three years of testing. This agrees with measurements that have been made in salt mines which show that deformation rates continue to decrease with time, at least in openings up to 12 years old. Model tests, verified by measurements in salt mines, show that thin shale beds, which commonly occur with bedded salt deposits, cause greatly accelerated rates of deformation in excavated cavities when they occur in the pillars at the roof and floor interfaces. In comparing the deformational behavior of salt from mines at Lyons and Hutchinson, Kansas; Retsof, New York; Detroit, Michigan; Grand Saline, Texas; Cote Blanche, Louisiana; and Asse, Germany, it was found that the general deformational behavior is the same; however, some variations in the rates of deformation were observed. Creep rates were also found to vary with the width-to-height ratios of pillars as well as with pillar shapes.

14.13 ANALYSIS OF COMBINED EFFECTS

In this section the analysis of the deformational behavior of the entire experimental area under the combined influence of stress, stress history, heat, thermal gradients, and time over the entire four-room experimental area of Project Salt Vault is summarized. Although the analysis was carried out primarily to provide the background information and technical reference for a future study of the effect of various design parameters on the long-term deformation of an actual waste disposal facility, it also resulted in an improved understanding of the behavior of the entire experimental area, especially with regard to the interdependence of the various parameters.

The general approach to the investigation was to first carry out a theoretical analysis to determine the feasibility of using computer modeling techniques. When this analysis indicated that all of the effects could be simulated, a computer program was written which combined the various influences over an area broad enough to include the entire four-room experimental area. As anticipated, it was then necessary to search for the proper physical property values and to make several

modifications in the program in order to reproduce the deformation results actually measured during the PSV experiment. This was accomplished largely by making repeated computer runs using different values and observing the effects.

In the theoretical analysis the laboratory measurements of creep in model salt pillars were interpreted as providing a phenomenological or qualitative, though not necessarily quantitative, understanding of creep in actual mine pillars. These relationships were then developed into a model of the deformations occurring in and near a mined excavation using the following logic.

Deformations will occur in the pillars and surrounding salt as a result of three interrelated phenomena:

1. the redistribution of stress as a result of mining operations in the salt,
2. the action of thermal stresses induced by temperature increases in the salt surrounding the radioactive waste, and
3. the redistribution of stress as a result of changes in the creep characteristics of the pillars with temperature.

Condition (1) is common to all mining operations, while conditions (2) and (3) are peculiar to situations where heat sources are placed in the mine. Therefore, it would appear reasonable to first consider existing analyses of rock movements near underground mine excavations and then to extend these to include the thermal effects of conditions (2) and (3).

Methods for calculating ground movements and stress redistribution near flat-lying, partly excavated tabular deposits, except for the most simple of geometries, have only recently been developed and adapted to digital computing methods. It should be possible to extend these to the unusual heating conditions of interest. The following analysis was therefore carried out with this as the primary objective.

The rheological properties of rock salt depend very strongly on the temperature and stress fields to which the salt is subjected. Under completely triaxial hydrostatic loading, salt would be expected to behave perfectly elastically, and this behavior would be far less dependent on temperature and pressure than is the creep rate under uniaxial loading. Between the two extremes of hydrostatic and uniaxial loading, the transition load from elastic to time-dependent behavior and the creep rate must depend on an invariant of the stress field which reflects the deviation from hydrostatic conditions. The octahedral shear stress is just such an invariant.

Dimensional analysis requires that the relationship between stress and strain be a function not only of a stress invariant but also of a dimensionless invariant which can be obtained from the stress-strain relationship for model salt pillars.

This argument leads to a justification of the first assumption to be made in this analysis. An unconfined salt pillar will be subjected to a much higher stress than any other part of the salt mass, and the creep rate will be considerably higher in the pillar than anywhere else in the surrounding salt. The first assumption to be made will thus be that the creep rate in the surrounding rock can be neglected in comparison with the creep rate in the pillars. This assumption should be a valid approximation except for the immediate vicinity of the roof and floor of a mined-out room. Since these areas must be excluded from the analysis anyway, because of the bed separation and viscoelastic buckling which undoubtedly occur but which cannot be conveniently incorporated into the computer model, this exception is probably not serious. Therefore the partly confined salt above and below the mining horizon will be treated as an elastic material with modulus and Poisson's ratio independent of stress and temperature, while the supporting pillars will be allowed to deform in a much more complicated way.

If a full-size pillar underground deforms qualitatively in the same way as a model pillar in the laboratory, then under constant load and temperature the strain in the pillar will be given by an expression of the same form as Eq. (14.1).

Since the height of the rooms and pillars in the mine is negligible as compared with the depth of the mining horizon below the surface, two simplifying assumptions can be made:

1. that the rock mass surrounding the excavation tends to infinity in all directions and
2. that both the roof and floor of the excavation can be considered as part of the same plane – the mining horizon.

However, once mining operations begin, the roof and floor of the excavation will, of course, converge. This convergence can be represented as a displacement anomaly on the plane, and the mining horizon can be considered as an incompatibility in an infinite rock salt mass. According to the assumption discussed previously, this rock salt mass is assumed to be linear and elastic with modulus and Poisson's ratio independent of stress and temperature.

To complete the analysis, the temperature changes and the resulting thermal stresses in the salt due to heat

sources in the floor of the mine must be considered. The influence of the temperature changes within the pillar on its creep characteristics has been included in the equations. Although sophisticated heat transfer programs are now available for calculating the temperature rises in the salt at any distance from heat sources buried in the floor of the mine, these are neither necessary nor particularly desirable for inclusion in this analysis. For this purpose, a simplified calculation starting with an instantaneous heat source at some point in the infinite rock mass is sufficient. A number of assumptions are implicit in the application of this analysis to the problem at hand:

1. It is assumed that the thermal diffusivity and coefficient of expansion are independent of the temperature of the salt. Mean values of these properties over the expected range of temperatures must thus be selected.
2. An inconsistency has been introduced in the scale of the problem. While it is reasonable to neglect the height of the rooms and pillars in comparison with the depth below surface of the mine, this height is directly comparable with the depth of burial of the heat sources in the floor of the mine. Since the roof and floor of the mine are being considered as two sides of the same plane, the best compromise is to measure the depth of burial of the heat sources from a point halfway between the roof and floor of the rooms in which the sources are buried.
3. The thermal stresses are calculated on the assumption that the pillars are unable to expand laterally into the rooms. Since the lateral deformation of the pillars has so far been ignored, this assumption is no worse than assumptions that are already implicit in our analysis.

Within these limitations the equations probably give a reasonably good description of the thermal effects of the waste in the foot walls (floor). The pattern of heat sources in a room can be simulated by one or more sources, and the resultant thermal stresses in the plane of the excavation and the temperatures in the pillars can be obtained by superimposing the stresses and temperatures from all of the heat sources in the mine.

The computer program which was written to provide a simulation of the deformational behavior of the experimental area is essentially a synthesis of the various components summarized above in such a way as to include their interactions. The objectives of the program were to calculate the stresses in the pillars and abutments, the vertical deformation at any point in these pillars and abutments, and the movements and stresses at any point in the elastic zones above and below the mining horizon.

Although the analysis was carried out for a general three-dimensional geometry, the program was written for the case of plane strain, that is, assuming no displacements will occur in the y direction. This assumption led to a considerable simplification, and it should be applicable to a full-scale room and rib-pillar design. While the four-room experimental area is obviously not in plane strain, it should be possible to test the program against the results obtained at the north-south center line of the pillars.

Following the initial preparation of the computer program, a number of preliminary runs were carried out using simplified mining patterns and conditions (e.g., completely elastic media). These preliminary runs served to demonstrate that the program was performing the calculations in the proper manner, provided some background on the response produced by changes in the input data, and most importantly, led to modifications in the program. Following this period of program testing, an extended series of computer runs was undertaken to establish the mix of physical property values and other parameters which would best reproduce the movements and deformations actually measured in the experimental area.

The first problem in modeling the experimental area in the computer simulation was the departure from the assumed plane strain situation. Since heat sources were located in all four rooms of the experimental area and interactions between the rooms was of primary interest, the vertical north-south section through the area was chosen. This highly instrumented plane was placed at the midpoint between the corridor and the back of the room, so that it went through the center line of the circular arrays in rooms 1 and 4. Although the computer model considered the four rooms to be infinitely long, thus ignoring the presence of both the connecting corridor to the east and the solid unexcavated salt to the west, the effects of these departures from plane strain should be a minimum at the point midway between them. Examination of the differences in the behavior at the front and back of the pillars suggests that the effects of the corridor and solid salt become significant only very close to the two ends of the pillar. Therefore, it appears that the plane strain assumption is reasonable and that modeling of the experimental area along the north-south center line would be valid.

The computer program did not provide any information on the lateral deformation of the pillars, and the

simulated room convergences will not be comparable with the actual measured convergences because the model does not consider bed separation or viscoelastic buckling of the roof and floor. The computer simulation did, however, yield an estimate of the vertical pillar deformation. This deformation was measured in the experimental area on convergence gages located at the edge of the pillar, and comparison with the computer simulation was made using these data.

After establishing the value of some of the parameters, the series of computer runs to determine the values of the remaining physical properties and parameters were undertaken. The general procedure used was as follows:

1. First, only the deformations due to the excavation of the experimental area and prior to any heating were considered. A set of values was selected by trial and error for those physical properties which are not concerned with thermal effects which would produce a computer-simulated closure comparable with the measured convergences. Since the initial portion of the measured convergence data was missing because of the necessary delay after mining before installation of the gage, this comparison was based on the convergence *rate* just prior to heating and the fit of the general shape of the curves. Once a comparison was established on this basis, the amount of deformation, the curve shape, and the deformation rate could be compared at all later times.
2. Next, the simulated deformations during the heating periods were made to correspond to the equivalent actual deformations. This was accomplished by (again) trial-and-error manipulation of the parameters related to thermal effects. Comparison of the computer-simulated closures with the measured convergences was again based on rates of deformation at some characteristic point, shape of the curves, and the amount of deformation, in that order. In this comparison it was discovered that several different sets of values determined in step 1 above would equally satisfy the pre-heating deformations but result in drastically different closures during the heating period. Therefore, it was necessary to return to step 1 many times before arriving at the final values in step 2.
3. After completing step 2, the deformations during the cooling period were calculated and compared with the measured convergences. This comparison was made almost solely on the basis of deformation rates, and the criterion of acceptance was considerably more liberal.

In all four rooms the general shape of the closure curves obtained from the computer simulation was very close to the measured convergence curves, and the rates (except as noted below) are very nearly identical. The amount of closure compares somewhat less closely with the value of the convergence, but even this is within about 10%.

The maximum departure of the calculated curves from the experimental results occurred immediately after the heaters were turned on. In rooms 1 and 4 the observed convergence rate was much higher than the calculated closure rate for approximately 100 days following initiation of the array heating. The same situation was seen following startup of the pillar heaters. However, at greater distances from the heat sources, the opposite effect occurs; that is, the measured convergence rates were less than the calculated closure rates. These departures were interpreted as resulting primarily from inaccurate computer modeling of the thermal stresses. If the physical properties are changed to more closely reproduce the responses of the gages close to the heaters, closures at more distant points become so large that they no longer resemble the actual convergences. Likewise, when the properties are changed to exactly reproduce the deformations at the distant points, the closures near the heat sources are very large. The physical properties used for the comparison represent a compromise between these two extremes. With this compromise the convergence rates at all times except immediately after initiation of the heating compare favorably, and even the discrepancies in the amounts of closure convergence are not excessively large. Therefore, the error apparently in the modeling of the thermal stresses can be considered acceptable.

Confirmation that the closure results discussed above represent a reasonable simulation of the behavior of the entire experimental area under the combined influences of stress, elevated temperatures, thermal stresses, and time, and were not simply the consequence of a fortuitous selection of variables, was obtained from a comparison of the calculated pillar stresses with the results obtained on the diametral borehole deformation gages installed in the experimental area.

Considerable insight into the behavior of the underground experimental area was obtained serendipitously from the procedure used to fit the physical property parameters to the computer model in the form of an evaluation of the effects of changes in some of the variables. The most significant of these findings was the relationship between the rigidity of the (elastic) roof and the effective stiffness of the support pillars. In the

set of parameters used for the comparison, the behavior of the model is quite sensitive to this relationship. For example, a slight change in the modulus of the roof and floor material produces a relatively large change in the amount of pillar deformation. An increase in the rigidity of the roof "plate" spanning the entire experimental area causes much of the vertical stresses which should be borne by the pillars to be transferred into the abutments at the two ends of the experimental area. If the rigidity of the roof is decreased, the roof plate can deflect more, which increases the load on the pillars and therefore their deformation.

The pillar stiffness is simply the stress-strain relation of the pillar as a whole, which in this case is also a function of time and temperature and is further complicated by the constraints and the interactions built into the computer program. If the pillars are made a little "softer," the pillar deforms more rapidly – as would be expected. However, at some point further softening of the pillar has very little influence on pillar deformation because it deforms so much that the pillar stress is once again transferred into the abutments via the rigidity of the roof. Likewise, stiffening of the pillars reduces their deformation but not as much as would be expected, since the load on the pillar also increases as a consequence of its greater stiffness.

The roof rigidity and pillar stiffness used for the comparison between the model and the experimental area would appear to be a fairly good selection based on the behavior of the model using slightly different values and based on the observed behavior of the experimental area.

The computer model described in this section can be applied to the examination of the closure distributions to be expected in an operating facility disposing of real radioactive wastes simply by establishing the desired geometry and extending the time span to 50–100 years.

Based on estimates of the accuracy of the computer model, it would appear that the primary objective of both the underground rock deformation measurement program and the analysis summarized here has been achieved: the combined effects of stress, elevated temperatures, thermal gradients, and time on the deformation of salt are sufficiently well understood that rational design of actual waste disposal facilities can be undertaken.

14.14 CONCLUSION

This document and the PSV demonstration experiment it describes represent the culmination of a research and development program spanning more than 10 years. Salient features of this program leading to the Project Salt Vault experiment were outlined in the early chapters of this report. A large portion of the report (Chaps. 5 to 10) was devoted to detailed descriptions of the PSV demonstration itself. Although these descriptions may have seemed tediously detailed in some cases, it was felt that they were necessary to adequately document all aspects of the demonstration and the many peripheral experiments and activities. The remaining chapters present the technical results obtained and a fairly exhaustive interpretation and analysis of their significance. With the completion of this experiment, it can be concluded that most of the major technical problems pertinent to the disposal of highly radioactive wastes in salt have been resolved. Project Salt Vault successfully demonstrated the feasibility and safety of handling highly radioactive materials in an underground environment. The stability of the salt under the effects of heat and radiation has been shown, as well as the capability of solving minor structural problems by standard mining techniques. The data obtained on the deformational characteristics of salt have made it possible to arrive at a suitable design for a mine disposal facility.

From the early beginnings of this program, it was realized that satisfactory solutions to the problem of the final disposition of the fission product wastes formed a very real part of the overall goal of the widespread use of nuclear power in the civilian economy. However, during the initial stages a detached, almost academic attitude prevailed, since there was some question at that time about the ability of nuclear reactors to economically compete with conventional power stations; and even if they could, the disposal of large quantities of highly radioactive waste seemed to be a problem which would not have to be faced for several decades. This situation changed drastically at about the time of the preliminary planning for Project Salt Vault with the construction of the first few nuclear-powered central generating stations in selected areas. Still, the research and development program proceeded with no real sense of urgency. Also, at about this time a preliminary economic analysis[1] of the entire concept of waste solidification and disposal in specially mined chambers in bedded salt deposits was carried out. This analysis indicated that the costs of this method

[1] J. O. Blomeke, R. L. Bradshaw, J. J. Perona, and J. T. Roberts, *Estimated Costs for Management of High-Activity Power Reactor Processing Wastes*, ORNL-TM-559, 21 pp, (1963).

were completely compatible with competitive nuclear power and only slightly more than perpetual tank storage, an interim alternative which could hardly be called a solution to the problem. The total costs for the operation of a salt mine disposal facility were estimated to be only a few thousandths of a mill for each kilowatt-hour of electricity produced.[2]

About the time the field work on the experiment was being completed, utility companies began ordering nuclear reactors at a pace far exceeding all earlier projections. Obviously the waste disposal problem could no longer be deferred indefinitely. Based largely on the highly successful results of the Project Salt Vault demonstration experiment and in view of its stated goals on waste management,[3] the Atomic Energy Commission requested an examination of several questions related to the establishment of a facility for the disposal of radioactive wastes in salt. The results of this examination are embodied in a recent press release which reads, in part:[4]

"The Atomic Energy Commission today announced the tentative selection of a site near Lyons, Kansas, for an initial salt mine repository for the demonstration of long-term storage of solid high-level and long-lived low-level radioactive wastes.

"The Commission will seek authority from the Congress for initiation of the project during FY 1972. The cost to establish the project is estimated at approximately $25,000,000.

"After the project is authorized, it will take about four years to prepare it to start receiving high-level wastes."

This announced intention means that the entire program summarized in this report may soon reach fruition.

[2] R. L. Bradshaw, J. J. Perona, J. O. Blomeke, and W. J. Boegly, Jr., *Evaluation of Ultimate Disposal for Liquid and Solid Radioactive Wastes, Part VI, Disposal of Solid Wastes in Salt Formations,* ORNL-3358, 90 pp. (1969).

[3] Atomic Energy Commission, "Licensing of Production and Utilization Facilities: Siting of Commercial Fuel Reprocessing Plants and Related Waste Management Facilities, Statement of Proposed Policy," *Federal Register* **34**(105), 8712 (June 3, 1969).

[4] Atomic Energy Commission press release N-102, June 17, 1970.

ORNL-4555
UC-70 — Waste Disposal and Processing

INTERNAL DISTRIBUTION

1. Biology Library
2–4. Central Research Library
5. ORNL – Y-12 Technical Library Document Reference Section
6–56. Laboratory Records Department
57. Laboratory Records, ORNL R.C.
58. ORNL Patent Office
59. E. D. Arnold
60. J. A. Auxier
61. S. E. Beall
62. M. Bender
63. D. S. Billington
64. R. E. Blanco
65–66. J. O. Blomeke
67. A. L. Boch
68. W. J. Boegly, Jr.
69. C. J. Borkowski
70. B. F. Bottenfield
71. G. E. Boyd
72. F. N. Browder
73. K. B. Brown
74. F. R. Bruce
75. T. H. J. Burnett
76–85. K. E. Cowser
86. F. L. Culler
87. Roger Dahlman
88. R. S. Dillon
89. Wallace de Laguna
90. F. M. Empson
91. E. J. Frederick
92. D. E. Ferguson
93. J. H. Gibbons
94. J. H. Gillette
95. H. W. Godbee
96. C. R. Guinn
97. M. B. Herskovitz
98. R. F. Hibbs
99. J. M. Holmes
100. B. L. Houser
101. G. S. Hurst
102. D. G. Jacobs
103. W. H. Jordan
104. Hisashi Kubota
105. Eugene Lamb
106. J. L. Liverman
107. T. F. Lomenick
108–132. W. C. McClain
133. K. Z. Morgan
134. D. J. Nelson
135. J. P. Nichols
136. J. J. Perona
137. G. W. Renfro
138. R. H. Ritchie
139. Garland Samuels
140. W. F. Schaffer, Jr.
141. A. H. Snell
142. W. S. Snyder
143. Jim Steed
144–153. E. G. Struxness
154. D. A. Sundberg
155. Tsuneo Tamura
156. D. B. Trauger
157. J. E. Turner
158. W. D. Turner
159. A. M. Weinberg
160. J. C. Frye (consultant)
161. Edward Gerjuoy (consultant)
162. J. B. Hursh (consultant)
163. Jacob Kastner (consultant)

EXTERNAL DISTRIBUTION

USAEC, RDT Site Office (ORNL)

164. D. F. Cope
165. R. L. Phillipone

USAEC, Washington, D.C. 20545

166. C. B. Bartlett
167. R. B. Chitwood
168–172. W. G. Belter
173. J. J. DiNunno
174. J. A. Erlewine
175. L. E. Johnson
176. W. L. Lennemann
177. K. L. Mattern
178. W. H. McVey
179. A. F. Perge
180. A. J. Pressesky
181. R. M. Richardson
182. W. H. Regan
183. Milton Shaw
184. J. R. Totter
185. Henry A. Nowak
186. D. J. Donoghue
187. O. P. Gormley

USAEC-ORO

188. Laboratory and University Division
189. Patent Office
190. S. R. Sapirie
191. L. H. Jackson
192. A. R. Sutliff
193. R. B. Martin
194. H. N. Culver

Battelle Pacific Northwest Laboratory, P.O. Box 999, Richland, Washington 99352

195. H. M. Parker
196. D. W. Pearce
197. A. M. Platt
198. K. J. Schneider
199. A. G. Blasewitz

Atlantic Richfield Hanford Company, Attention: Document Control, P.O. Box 250, Richland, Washington 99352

200. R. E. Tomlinson
201. J. H. Warren

E. I. du Pont de Nemours & Company, Savannah River Laboratory, Aiken, South Carolina 29801

202. C. M. Patterson

AEC-IDO, P.O. Box 2108, Idaho Falls, Idaho 83401

203. K. K. Kennedy

Idaho Nuclear Corporation, P. O. Box 1845, Idaho Falls, Idaho 83401

204. J. A. Buckham
205. G. E. Lohse
206. Cyrus Klingsberg, NAS-NRC, 2101 Constitution Avenue, Washington, D.C., 20418
207. Clark Goodman, Department of Physics, University of Houston, Houston, Texas 77004
208. W. K. Davis, Bechtel Corporation, P.O. Box 3965, San Francisco, California 94119
209. R. D. Evans, Department of Physics, Massachusetts Institute of Technology, Cambridge, Massachusetts 02139
210. J. E. McKee, Division of Engineering and Applied Science, California Institute of Technology, Pasadena, California 91109
211. J. H. Rust, Department of Pharmacology, University of Chicago, 947 E. 58th Street, Chicago, Illinois 60637
212. F. H. Spedding, Ames Laboratory, Iowa State University, Ames, Iowa 50010
213. H. Worthington, Devon Apartments, No. 1512, 2401 Pennsylvania Avenue, Wilmington, Delaware 19806
214. F. L. Parker, Vanderbilt University, Nashville, Tennessee 37203
215. J. A. McBride, E. R. Johnson Assoc., Suite 312, Barr Building, 910 17th Street NW, Washington, D.C. 20006
216. Manson Benedict, Massachusetts Institute of Technology, Cambridge, Massachusetts 02139
217. P. T. Flawn, University Station, Box X, Austin, Texas 78712
218. J. F. Reed, National Science Foundation, 1800 G Street NW, Washington, D.C. 20550
219. H. H. Seliger, Department of Biology, The Johns Hopkins University, Baltimore, Maryland 21218
220. Clarke Williams, Nassau-Suffolk Regional Planning Board, Hauppauge, New York 11787
221. R. H. Burns, AERE, Harwell, Didcot, Berkshire, England
222. H. Krause, Gesellschaft fur Kernforschung m.b.h., Karlsruhe, Germany
223. Robert Schneider, Chief, Office of Radiohydrology, Water Resources Division, USGS, Washington, D.C. 2-242

224–228. W. W. Hambleton, Director, the State Geological Survey, University of Kansas, Lawrence, Kansas 66044

229–231. Robert C. Will, Chief, Radiation Control Section, Kansas State Department of Health, State Office Building, Topeka, Kansas

232. Curtis C. Chezem, Head, Department of Nuclear Engineering, Kansas State University, Manhattan, Kansas 66502
233. E. F. Gloyna, Dean of Engineering, Taylor Hall, Room 167, University of Texas, Austin, Texas 78712
234. C. V. Theis, USGS, P.O. Box 4369, Albuquerque, New Mexico 87106
235. H. J. Carey, Jr., The Carey Salt Company, Hutchinson, Kansas 67501
236. R. W. Rosberg, The Carey Salt Company, Hutchinson, Kansas 67501
237. R. B. Stone, The Carey Salt Company, Hutchinson, Kansas 67501
238. C. Fairhurst, School of Mineral and Metallurgical Engineering, University of Minnesota, Minneapolis, Minnesota 55455
239. L. P. Hatch, Brookhaven National Laboratory, Upton, Long Island, New York 11973
240. H. Borchert, Institut fur Tieflagerung, Bornhardtstr. 22, 3392 Clausthal-Zellerfeld, Germany
241. Klaus Kuhn, Gesellschaft fur Strahlenforschung M.B.H., Institut fur Tieflagerung, Bornhardtstr. 22, 3392 Clausthal-Zellerfeld, Germany
242. A. M. Starfield, Department of Applied Mathematics, University of Witwatersrand, Jan Smuts Avenue, Johannesburg, South Africa
243. E. J. Tuthill, Brookhaven National Laboratory, Upton, Long Island, New York 11973

244–250. Alex L. Lindsay, Kaiser Engineers, Kaiser Center, Oakland, California

251. E. S. Stowers, Jr., Stowers Machinery Corporation, 6301 Rutledge Pike, Knoxville, Tennessee

252. E. L. J. Potts, Department of Mining Engineering, University of Newcastle-upon-Tyne, England
253–254. Lyons Chamber of Commerce, Lyons, Kansas 67554
255. R. Rzekiecki d'Alegron, S.E.S.R., Center d'Etudes Nuclaires de Cadarache, P.O. Box No. 1, St. Paul les Durance 13, France
256. Robert E. Richert, 156 Main Street, Attica, New York 14011
257. Benjamin Friesen, Department of Radiation Biophysics, University of Kansas, Lawrence, Kansas
258. Dale Saffels, Chairman, Kansas Corporation Commission, State Office Building, Topeka, Kansas
259. George Moore, Kansas Game and Fish Commission, Pratt, Kansas
260. Freeman Biery, 2043 E. 35th Street, Topeka, Kansas 66605
261. Richard Walker, Sterling College, Sterling, Kansas
262. Dan Powers, Sterling College, Sterling, Kansas
263. Lloyd C. Hulbert, Kansas State University, Manhattan, Kansas
264. R. H. Gifford, Executive Director, Southern State Nuclear Board, Atlanta, Georgia
265. E. W. Zeltmann, New York State Public Service Commission, 44 Holland Avenue, Albany, New York 12208
266. M. King Hubbert, USGS, Washington, D.C.
267. R. L. Nace, Water Resources Division, USGS, Washington, D.C.
268. W. B. Heroy, Sr., Southern Methodist University, Dallas, Texas
269. J. A. Lieberman, Department of Health, Education, and Welfare, Washington, D.C.
270–445. Given distribution as shown in TID-4500 under Waste Disposal and Processing Category (25 copies – NTIS).